

2
B.S.

AGARD-R-654

AGARD-R-654

AD A 044805

AGARD

ADVISORY GROUP FOR AEROSPACE RESEARCH & DEVELOPMENT

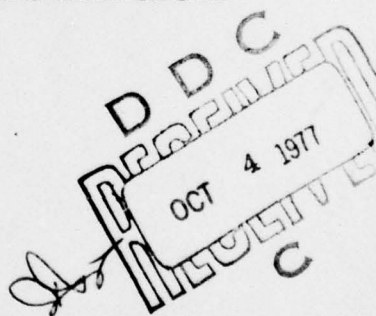
7 RUE ANCELLE 92200 NEUILLY SUR SEINE FRANCE

AGARD REPORT No. 654

Special Course on Concepts for Drag Reduction

DISTRIBUTION STATEMENT A

Approved for public release;
Distribution Unlimited



NORTH ATLANTIC TREATY ORGANIZATION



DISTRIBUTION AND AVAILABILITY
ON BACK COVER

DDC FILE COPY

**Best
Available
Copy**

NORTH ATLANTIC TREATY ORGANIZATION
✓ ADVISORY GROUP FOR AEROSPACE RESEARCH AND DEVELOPMENT
(ORGANISATION DU TRAITE DE L'ATLANTIQUE NORD)

✓ AGARD Report No.654

6 SPECIAL COURSE ON CONCEPTS FOR DRAG REDUCTION.

11 Jun 77

12 297p.



The material assembled in this book was prepared under the combined sponsorship of the Fluid Dynamics Panel, the von Karman Institute and the Consultant and Exchange Program of AGARD and was presented as an AGARD Special Course at the von Karman Institute, Rhode-St-Genese, Belgium on 28 March - 1 April 1977.

400 043

1B

THE MISSION OF AGARD

The mission of AGARD is to bring together the leading personalities of the NATO nations in the fields of science and technology relating to aerospace for the following purposes:

- Exchanging of scientific and technical information;
- Continuously stimulating advances in the aerospace sciences relevant to strengthening the common defence posture;
- Improving the co-operation among member nations in aerospace research and development;
- Providing scientific and technical advice and assistance to the North Atlantic Military Committee in the field of aerospace research and development;
- Rendering scientific and technical assistance, as requested, to other NATO bodies and to member nations in connection with research and development problems in the aerospace field;
- Providing assistance to member nations for the purpose of increasing their scientific and technical potential;
- Recommending effective ways for the member nations to use their research and development capabilities for the common benefit of the NATO community.

The highest authority within AGARD is the National Delegates Board consisting of officially appointed senior representatives from each member nation. The mission of AGARD is carried out through the Panels which are composed of experts appointed by the National Delegates, the Consultant and Exchange Program and the Aerospace Applications Studies Program. The results of AGARD work are reported to the member nations and the NATO Authorities through the AGARD series of publications of which this is one.

Participation in AGARD activities is by invitation only and is normally limited to citizens of the NATO nations.

The content of this publication has been reproduced directly from material supplied by AGARD or the authors.

Published June 1977

Copyright © AGARD 1977
All Rights Reserved

ISBN 92-835-1247-2



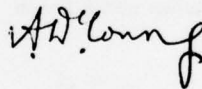
*Printed by Technical Editing and Reproduction Ltd
Harford House, 7-9 Charlotte St, London, W1P 1HD*

PREFACE

The dramatic increases in the cost of oil that have occurred in recent years and the awareness that the world's oil stocks may be largely depleted within a few decades have caused a major upsurge of interest into ways of reducing the drag of aircraft. A growing research effort is being mounted in a number of countries into investigations of ideas for drag reduction, some novel and some that were looked at in the past but were not then pursued to the point of application because the economic facts of life were different from and less pressing than they are now. These ideas include means for reducing skin friction drag (e.g. compliant walls, boundary layer control, etc.), induced drag (e.g. winglets), interference drag, transonic shock wave drag (supercritical wings) and supersonic wave drag. In addition the internal aerodynamics of ducting, especially diffusers is receiving attention to improve the performance of engines.

Already this research effort is bearing fruit and it was thought by the AGARD Fluid Dynamics Panel and the Von Karman Institute that the time was opportune to provide a Special Lecture Course devoted to this work and its potential for the future. The organisers of the course were fortunate in persuading outstanding experts in this field in the USA and in Europe to contribute to the Course.

It is hoped that this survey of current activities and their possibilities will be of particular and timely help to aircraft designers as well as to those concerned with the planning of research.



A.D. YOUNG
Course Director

January 1977

ACCESSION	
NTIS	Y. 18 Section <input checked="" type="checkbox"/>
DDC	B. H. Section <input type="checkbox"/>
NAVY/NO/NO/D	
J S I CATION	
BY	
DISTRIBUTION/AVAILABILITY CODES	
Dist	SP CIAL
A	

CONTENTS

	Page
PREFACE by A.D.Young	iii
	Reference
AN OVERVIEW OF CONCEPTS FOR AIRCRAFT DRAG REDUCTION by J.N.Hefner and D.M.Bushnell	1
METHODS FOR REDUCING SUBSONIC DRAG DUE TO LIFT by R.T.Whitcomb	2
LAMINAR FLOW CONTROL, LAMINARIZATION by W.Pfenninger	3
LAMINAR FLOW CONTROL – CONCEPTS, EXPERIENCES, SPECULATIONS by B.Edwards	4
SLOT INJECTION FOR SKIN-FRICTION DRAG REDUCTION by A.M.Cary, Jr., D.M.Bushnell and J.N.Hefner	5
DIFFUSERS AND THEIR PERFORMANCE IMPROVEMENT BY MEANS OF BOUNDARY LAYER CONTROL by R.C.Adkins	6
DRAG REDUCTION BY COMPLIANT WALLS: THEORY by G.Zimmermann	7
ON THE PROBLEM OF DRAG REDUCTION BY MEANS OF COMPLIANT WALLS by A.Dinkelacker	8
EFFECT OF COMPLIANT WALL MOTION ON TURBULENT BOUNDARY LAYERS by D.M.Bushnell, J.N.Hefner and R.L.Ash	9

AN OVERVIEW OF CONCEPTS FOR AIRCRAFT DRAG REDUCTION

Jerry N. Hefner and Dennis M. Bushnell
 NASA Langley Research Center
 Hampton, Virginia 23665
 U.S.A.

1. INTRODUCTION

An assessment of the future natural petroleum situation, presented recently in Reference 1 and shown in Figure 1, indicates that by the year 2000 almost all of the U.S. petroleum supply will be depleted and less than half of the world's supply will remain. This limited supply of petroleum fuel coupled with ever-increasing energy demands can only be expected to create severe energy shortages and higher fuel prices and will have a potentially dangerous economic impact on the world's airlines. Figure 2 (obtained from Ref. 2) shows that since 1973, commercial jet fuel prices in the U.S. for domestic and international airlines have already increased by approximately 150% and 220%, respectively. Since airplanes that are being designed today will probably still be in service in the year 2000, it is obvious that advanced technologies capable of making significant improvements in aircraft fuel conservation must be developed and implemented as soon as possible. Many recent studies have considered the effect of the energy situation on present aircraft and those of the future¹⁻¹³ and generally conclude that although present transport aircraft are reasonably energy efficient, significant improvements in fuel conservation can still be obtained through advanced design and technology.

The purpose of this paper is to provide a current overview of aerodynamic drag reduction concepts which have potential for reducing aircraft fuel consumption. The discussion will show where the greatest percentages of aircraft fuel is burned and what areas have the greatest potential for fuel conservation. The paper will focus on aerodynamic improvements and will touch only briefly on structural and propulsion improvements. Concepts for reducing pressure drag (i.e., roughness, wave, interference, and separation drag), drag due to lift/induced drag, and skin-friction drag at subsonic and supersonic speeds will be emphasized.

2. WORLD JET FUEL CONSUMPTION

World and U.S. jet fuel consumption for a wide range of stage lengths is shown in Figures 3 and 4.⁶ Both figures show that most of the world's and the U.S.'s jet fuel is consumed for stage lengths less than 1500 statute miles. In fact, 34.5% of the U.S. jet fuel and 29% of the world jet fuel is consumed for stage lengths of 500 statute miles or less. As Figure 4 shows, the largest single fuel consumer in the U.S. by aircraft type is the Boeing 727 which consumes approximately 38% of the jet fuel; the 727 accounts for about 34% of the jets in service in the U.S. fleet. Wide-bodied, long-haul jets, which account for only 13% of the U.S. jet fleet, use approximately 22.5% of the U.S. jet fuel. Thus, two important points are indicated by these figures. First, advanced technology to reduce fuel consumption must address short-haul as well as long-haul transports. Second, based on the makeup of the U.S. jet transportation fleet which represents almost half of the world fleet, it appears that most of the existing world transport fleet is composed of relatively recently produced aircraft. Therefore, advanced technology for aircraft fuel conservation must include improvements to existing aircraft in addition to new energy-efficient aircraft designs.

3. FACTORS INFLUENCING AIRCRAFT PERFORMANCE

The classical theory of aircraft range performance, as reviewed quite well in Reference 14, clearly shows how propulsion, structural, and aerodynamic efficiencies interact to affect aircraft performance. The most general form of these range performance relationships is the simplified "Breguet range equation" for cruising at constant lift coefficient, constant angle of attack, and constant speed (altitude increasing),

$$R = \left(\frac{V}{SFC} \right) \left(\frac{L}{D} \right) \ln \left(\frac{W_i}{W_f} \right)$$

This relationship expressed in terms of the fuel burned is

$$\Delta W = W_i \left(1 - \frac{1}{e^{\frac{R}{(V/SFC)(L/D)}}} \right)$$

where R is the range, V/SFC is the propulsion efficiency, W_i/W_f is the structural efficiency, and L/D is the aerodynamic efficiency. The designer of a particular airplane can use relationships such as these to assess the effects of improvement in the various propulsion, structural, and aerodynamic efficiencies on either fuel consumption or range requirements. Although the present overview is directed at improvements in aerodynamic efficiency, a few comments regarding possible improvements in propulsion and structural efficiencies are germane.

As discussed in Reference 1, propulsion research is underway within NASA to improve the efficiency of existing engines and to provide the technology for improved future engines. The studies have shown that existing engines can be improved significantly by

- (1) reducing the compressor and turbine tip clearance by approximately 10% (this could reduce SFC by about 4%)
- (2) replacing conventional seals with labyrinth seals to provide up to 2% reduction in SFC

- (3) installing low pollution combustors which have high efficiency at idle and low thrust conditions to provide another 1% reduction in SFC
- (4) reducing compressor and turbine end wall pressure losses at hub and tip which could give an additional 1% reduction in SFC and
- (5) improving turbine blade cooling to provide another 1% reduction in SFC.

These improvements, when evaluated as to their economic practicality, suggest that fuel consumption of current engines can be reduced from 5-10%.

For improved new engines, Figure 5 (from Ref. 1) shows the various improvements being considered in current NASA/industry advanced turbofan studies. These improvements include: higher fan efficiency, composite blades and nacelles, advanced compressor design, improved seals and bearings, and reduced emissions combustors. Figure 6 (from Ref. 1) shows results of a recent NASA Lewis study and compares an advanced 1985 turbofan with a current turbofan engine. The 1985 engine has a considerably higher engine thrust-to-weight ratio, its cruise turbine inlet temperature is 278° K higher, its overall pressure ratio has increased from 28 to 40, its fan pressure ratio is somewhat lower, and its bypass ratio increased from 6 to 10.4. (The engines were evaluated with a simplified analysis of a 200-passenger, 3000-nautical-mile transport assuming constant structural weight fraction.) When compared to the current engines, the 1985 engine weight and SFC were lower by 20% and 8%, respectively. Although the combined fuel reduction was a significant 22.3%, it should be cautioned that the level of technology required for this improvement will not be easily obtained and other new engines may provide even greater gains (e.g., the high bypass ratio turbofan, the regenerative turbofan, and the turboprop).

A means of improving aircraft structural efficiency is through the use of advanced composite structures¹⁵ because they possess high strength-to-weight and stiffness-to-weight ratios. The blending of high strength fibers, similar to that illustrated in Figure 7 (from Ref. 1), can produce new reduced-weight structures that can be used directly for fuel savings or can be traded off to gain improved structural lifetimes or lower manufacturing costs. Figure 8 (from Ref. 1) summarizes results from a number of design studies¹⁶ which show the potential weight reductions from composite structures. Note that weight reductions in the range of 40-50% are possible.

A recent fuel-conservative transport study¹⁷ showed that a significant weight savings could be achieved with an all-composite primary aircraft structure. The various types of composite structure (i.e., graphite-epoxy honeycomb, graphite-epoxy integrated acoustics structure, PRD-49 honeycomb, and stiffened graphite-epoxy honeycomb) and their relative weight savings compared to conventional aluminum skin stringer construction are shown in Figure 9 (from Ref. 1). For example, the estimated structural weight savings for using a graphite-epoxy composite primary wing structure is approximately 25%; this would translate into a fuel savings of 10-15%.

Although the advantages of composite structures would appear obvious, thus far composites have not been widely accepted for commercial aircraft. The greatest deterrent for their acceptance have been high costs and a lack of experience with composites under actual service conditions. However, prices for composites are dropping and NASA/DOD programs to use composites for primary and secondary load-carrying structures on military and civil aircraft are providing the needed flight experience. Therefore, composite structures will probably have a significant impact on aircraft fuel conservation in the near future.

4. AERODYNAMIC EFFICIENCY

The aerodynamic efficiency of aircraft configurations can be improved through increases in lift characteristics and/or decreases in total drag. The present review will focus on improving aerodynamic efficiency through drag reduction.

Before discussing concepts for drag reduction, the drag sources which most adversely affect fuel consumption and hence have the greatest potential for reduction must be identified. Figures 10 and 11 (from Refs. 17 and 18, respectively) show that most of the fuel for subsonic and supersonic transports is consumed at cruise conditions. As the length of the mission (stage length) is reduced, increasing amounts of fuel (percentagewise) are used for climb conditions. However, approximately 90% of the fuel consumption by subsonic transports occurs during climb and cruise regardless of stage length. Therefore, it is reasonable to assume that attempts to conserve fuel should focus on the major drag sources corresponding to the aircraft configuration at climb and cruise conditions.

What are the major sources of drag for climb and cruise conditions? Figure 12 shows graphically what the major sources of drag are for a subsonic transport configuration. The sources indicated are skin friction, induced drag/drag due to lift, roughness, afterbody/separation, and interference. Wave or compressibility drag, although not indicated on Figure 12, becomes an important drag source as transonic flight speeds are approached and, as will be shown, is a large portion of the drag for supersonic flight.

Aerodynamicists generally use the conventional drag polar, as illustrated in Figure 13, to account for the components of the total drag. The components of drag indicated on the figure can represent several of the drag sources shown on Figure 12. For example, the profile drag is composed primarily of skin friction, roughness drag, interference drag, and separation drag. The minimum profile drag ($\Delta C_{D_{MIN}}$) is primarily the drag due to skin friction and is defined generally for nonlifting conditions. For the configuration at lifting conditions, an additional increment in profile drag results (C_{D_L}). The induced drag component (C_{D_I}) results primarily from the flow circulation around the wing. Trim drag (C_{D_T}) refers to that drag resulting from changes in the aircraft configuration (e.g., control deflections) to balance the aerodynamic moments on the airplane. Compressibility or wave drag (C_{D_C}) is due to strong compression or shock waves forming on the aircraft configuration as the free stream or local flow velocities approach or exceed sonic conditions.

Another more detailed breakdown of drag sources by configuration component is shown in Figure 14 (from Ref. 19). Although the figure does not suggest the relative severity of each drag source, it does clearly delineate the number of factors influencing the total drag of an aircraft configuration.

The relative magnitudes of the various drag sources for typical subsonic and supersonic aircraft are shown in Figures 15 and 16. Although this representation is based on the authors' evaluation of the available data for the particular classes of aircraft and may not be representative of a specific aircraft configuration in a given class, it does indicate the drag sources identifiable with a particular type of configuration and mission. For example, roughness drag, which represents a small but important source of drag on most aircraft configurations, is the primary drag source for current helicopters. The main point, however, from the two figures is that the skin-friction drag and drag due to lift contribute as much as 85% of the total drag for subsonic and supersonic aircraft. Therefore, skin-friction drag and drag due to lift represent the drag sources with the greatest potential for reduction and hence fuel conservation. The other sources individually¹⁴ may not be large, but collectively can add significantly to the total drag and fuel consumption. The remainder of this review will examine methods for reducing the drag of the sources indicated on Figures 15 and 16.

5. AERODYNAMIC DRAG REDUCTION

5.1 Roughness/Excrescence Drag

Roughness or excrescence drag is an incremental pressure drag resulting from local flow separations and vortex formations produced by relatively small-scale two-dimensional or three-dimensional bumps, protrusions, and recesses on an aircraft surface. These excrescences, which may be unavoidable and caused by manufacturing techniques, include such things as surface waviness, rough surface finish, projecting or countersunk fasteners, panel joints, overlapping joints, air intake and exhaust openings, lights, antennae, probes, and gaps around doors, windows, and control surfaces. Such roughness drag sources on a subsonic transport can contribute as much as 5-10% of the total aircraft drag at climb and 3-5% at cruise. A recent report in Reference 20 shows the specific impact that such roughness drag could have on airline economy and fuel consumption. McDonnell Douglas reported that an excessive slat trailing-edge step of only 0.05 cm on a DC-9 airplane could cost an airline approximately \$1000/year in "wasted" fuel per airplane. Boeing reported that a pressurized area seal leak of 64.5 sq cm in the entry and cargo doors and windows on the 727-200 airplane could cause as much as a 23,000-gallon increase in fuel consumption per airplane per year.

Estimates of typical roughness/excrescence drag contributions for the C-5A transport at cruise conditions are shown in Figure 17 which was compiled from data presented in Reference 21. Figure 18 illustrates the percentage contribution to the total roughness drag of the four major roughness sources and shows that 30% of the roughness drag is attributable to steps, ridges, and gaps with another 25% due to mass transfer in and out of the aircraft skin. Estimates such as these are based on a number of good wind-tunnel investigations (e.g., Refs. 22-39) which have provided valuable insight into the boundary-layer/excrescence interaction; however, many questions still remain. Such questions include: the drag of three-dimensional excrescences, the drag of excrescences in three-dimensional and pressure gradient flows, the drag for arrays of excrescences, and the drag of gaps and cavities with and without mass transfer. With these questions in mind, it is obvious that all is not known regarding the interaction effects of the excrescence drag sources indicated on Figure 18. The following roughness drag discussion will not focus on the fluid dynamics of roughness drag (Refs. 22-39 do a good job of this), but rather will show how the more typical roughness/excrescences (i.e., steps, ridges, and gaps) affect the drag and how this drag might be reduced.

The effect of step-height Reynolds number and Mach number on the drag of forward and rearward-facing steps and spanwise ridges is shown in Figures 19 to 21. These figures were taken from Reference 25 which presents a very good summary of the results of an extensive roughness drag research program at RAE Bedford. The figures show that the roughness drag of steps and ridges can be much greater than the skin friction with no excrescence. It should be noted that although the results shown in these figures were for excrescence heights small relative to the boundary-layer thickness, the results of Reference 26 for a forward-facing fence with heights exceeding the boundary-layer thickness show comparable trends. A comparison of the figures shows that the drag of rearward-facing steps is approximately one-half that of forward-facing steps, whereas the drag of ridges is twice that of the forward-facing steps. For each two-dimensional excrescence, the drag for a particular Mach number increased with increasing step-height Reynolds number. However, for a given Reynolds number, the drag variation with Mach number differed for forward- and rearward-facing steps. For forward-facing steps, the drag increased with increasing Mach number up to $M = 1.4$ and appears to be independent of Mach numbers above $M = 1.4$. For rearward-facing steps, the drag increased to a maximum at or near a Mach number of 1.4 and then decreased with additional increases in Mach number. The drag of the spanwise ridges is comparable to the sum of the drag for the forward- and rearward-facing steps. At low speeds, interference between the faces of the ridge produces a drag parameter approximately 50% greater than the sum of the drag for the two faces. As the Mach number approaches supersonic speeds, and in particular $M = 2.8$, the interference effect diminishes and becomes negligible. Doubling the streamwise thickness of the ridge produces either a decrease or an increase in the drag for a given Mach number, depending on the excrescence Reynolds number.

Several approaches are applicable for reducing the drag of steps and ridges. The most obvious of these is to eliminate the excrescence or reduce its height. The surface would be considered hydraulically smooth and have low roughness drag if the excrescence height is less than the boundary-layer sublayer thickness,

$\frac{u_{\tau} h}{\nu} < 5$ (see Ref. 24). One effective method of doing this is to bond a plastic film over the roughened aircraft skin. Figure 22, which presents unpublished data obtained in the NASA Langley Low Turbulence Pressure Tunnel by W. D. Beasley, shows that covering a T-33 aircraft wing with a 5-mil Kapton plastic film reduced the drag of the wing from 12-40% over the range of test Reynolds numbers. Calculations indicate that, by bonding a plastic film over only 50% of the surface area of a typical medium range subsonic transport wing, the total drag could be reduced by 0.7%. The wing considered in these calculations is shown in Figure 23 with unpublished estimates of excrescence drag obtained from The Boeing Airplane Company. Figure 24 shows schematically how the plastic film could be applied over the aircraft skin.

Other approaches to reducing the drag of steps and ridges involve actually modifying the geometry of the excrescence. For example, References 25 and 32 show that rounding the upstream corners of forward-facing steps and ridges can produce excrescence drag reductions of approximately 50% at subsonic speeds; rounding the step corners at supersonic speeds, although beneficial, produces much less drag reduction. Another method is that of chamfering — a ramp fairing either ahead of or downstream of a forward- or rearward-facing step. Chamfering has been shown to be an effective method for reducing the excrescence drag of both forward- and rearward-facing steps in subsonic and supersonic flows, provided the ramp angle is judiciously chosen and not too large.

Gaps, cavities, and recesses are often unavoidable in the construction of an aircraft (e.g., gaps between the wing and control surface, Fig. 23). Although the drag associated with such excrescences is generally small when compared to that of steps, it can still be significant and must be considered. Unfortunately, the available data are often contradictory for gap and cavity drag since this type of excrescence drag is dependent on a number of important parameters (e.g., Mach number, Reynolds number, cavity planform and shape, cavity depth, cavity width, cavity lip geometry, and mass transfer through the cavity or gap). The results presented in References 25 and 27 for rectangular cavities illustrates such a contradiction. Figure 25 (from Ref. 25) indicates that the drag of a rectangular cavity increases with increasing Mach number; Reference 37 shows that the drag of rectangular cavities decreases with increasing Mach number. Although this discrepancy has not been resolved and needs clarification, it should be pointed out that the work of Reference 37 was focused on another potentially serious problem associated with cavities or gaps — the effect of strong acoustical radiation coupled with internal cavity pressure oscillations. This effect, acoustic resonance, was shown to be responsible for cavity drag increases of up to 250% in the work of Reference 37.

Although the effect of all parameters influencing cavity or gap drag have not been resolved, particularly the effect of mass transfer into and out of the cavity, References 23, 25, 28, 31, and 35-39 provide useful information for configuring the gaps to reduce drag. General guidelines include maintaining gaps as narrow as practical with the downstream lip of the cavity rounded (rounding the upstream cavity lip increases drag by forcing additional flow into the cavity). Other improvements to reduce gap drag indicate that gap drag reduction is more of an art than a science. For example, Figure 26 (from Ref. 23) indicates a unique way of reducing the control gap drag of a particular airfoil. The figure shows that by reducing the airfoil thickness by 15% just ahead of the control surface, the gap drag was reduced by 76%. The reason for this drag reduction was attributed to a reduction in flow separation over the gap resulting from the flow being accelerated as it is directed against the face of the control surface. Other rather unique methods of reducing central gap drag are discussed for three spanwise gap configurations in Reference 31.

Although other sources of roughness/excrescence drag such as lights, antennae, probes, and flap tracks have not been discussed here, they are also important and add to the overall drag of the aircraft configuration (see Fig. 17). Generally, the drag associated with these excrescences can only be reduced through the appropriate fairings and shaping. The reader who is interested in these techniques is directed toward such works as References 23, 25, 34, and 40.

5.2 Wave Drag

5.2.1 Transonic Speeds

As the speed approaches sonic velocity, the pressure drag increases substantially and this drag increase is referred to as wave drag or compressibility drag (see Ref. 41 for a good introductory discussion of wave drag). Transonic wave drag is produced by the unstable formation of shocks and shock-induced boundary-layer separation on the aircraft surfaces. As the speed increases and becomes supersonic, the shock formations stabilize, the regions of flow separation are reduced, and the drag coefficient decreases. Figure 27 illustrates the typical flow field over an airfoil at transonic speeds. Also shown on Figure 27 is a typical variation in wing drag coefficient with increasing Mach number. The free-stream Mach number where the drag coefficient increases rather abruptly is defined as the drag-divergence Mach number and large increases in propulsive force are required to propel the aircraft to speeds beyond this Mach number.

The question of how to reduce transonic wave drag is actually a question of how to increase the drag-divergence Mach number to a value closer to 1.0. A number of effective methods are available for accomplishing this; however, these methods often have serious disadvantages. The methods include: the use of thin airfoils, wing sweep, low-aspect-ratio wings, boundary-layer control, supercritical wing technology, area ruling, and oblique wings. The following discussion will focus briefly on each of these methods showing how they can reduce wave drag at zero lift conditions and what their disadvantages are. Wave drag at lifting conditions will be discussed in the drag-due-to-lift section of this paper.

Thin Airfoils. The wave drag associated with transonic flow is approximately proportional to the square of the thickness-to-chord ratio.⁴¹ By decreasing the thickness of an airfoil section, the flow speed around the airfoil is decreased and, hence, the aircraft can fly at a higher free-stream Mach number before the local flow becomes sonic (i.e., critical Mach number) or before the drag-divergence Mach number is reached. Figure 28 (from Ref. 41) shows that decreasing the wing thickness-to-chord ratio by 67% increased the drag-divergence Mach number from 0.7 to 0.85 or 21%. The major disadvantages of using thin wings are (1) they are less effective in generating lift at subsonic speeds and (2) they cannot accommodate as much structural load as a thicker airfoil (resulting in lower aspect ratio, greater drag due to lift).

Wing Sweep. Sweeping the wing will delay the formation of shock waves in transonic flow to higher Mach numbers; the Mach number normal to the wing leading edge is reduced and therefore the local Mach numbers on the wing are reduced. Figure 29 (obtained from Ref. 41) shows the variation in the drag-divergence Mach number with increasing wing sweep angle; the drag-divergence Mach number is increased with an accompanying decrease in the drag coefficient. Both forward and rearward sweep will produce these desired results, however, forward sweep can produce stability and handling difficulties at low speeds. The major disadvantage of swept wings is that they produce a spanwise flow along the wing which thickens the boundary layer near the wing tips. This results in a loss of aileron roll-control effectiveness because of premature

Analytical tools for optimizing the aerodynamic shape of supersonic configurations have been based on linearized theory, whereas for hypersonic configurations Newtonian theory has been used.^{45-47,52-55} Results, typical of such theories for various minimum drag bodies, are shown in Figures 35-37. Two-dimensional wings of minimum total drag (wave drag and skin friction) are presented in Figure 35 (obtained from Ref. 53) for an unspecified (free) thickness, given enclosed area, given contour moment of inertia, and given area moment of inertia. The thickness distribution of the wing was substantially affected by the choice of constraints. Also, the minimum skin friction was found for the wing without a specified thickness. Figures 36 and 37 (both from Ref. 54) illustrate the coordinates and drag coefficients for the minimum-drag axisymmetric body optimized for a given length and volume (i.e., the Sears-Haack body). The importance of this axisymmetric body shape is that it provides the lowest total drag coefficient at zero lift for the Mach number range from 2 to 12⁵⁴ and is used as the reference shape in applying the area rule to supersonic aircraft configurations. Figure 37 (from Ref. 54) shows the importance of closing the aft end of the axisymmetric body shape. For cutoffs greater than $k = 0.1$, the drag of the Sears-Haack bodies increased appreciably, especially for Mach numbers less than approximately 5-6.

The results presented in Figure 38 (from Ref. 54) aid in showing the validity of the analytical theories for minimum drag bodies. The data were obtained experimentally at a Mach number of 10 for power-law bodies with fixed volumes and lengths and show that the minimum drag axisymmetric power-law body has a value of $n \approx 0.66$. This result agrees precisely with the theoretically determined value for an optimum profile when the analysis was restricted to power-law bodies.⁵⁶

Another, less obvious, method for optimizing the shape of a supersonic configuration for minimum wave drag is nose blunting.^{57,58} Results for constant fineness-ratio cones with varying degrees of nose bluntness are shown in Figure 39 compiled from the data of Reference 58. Note that there exists an optimum bluntness for each fineness ratio and at this bluntness value the drag is minimized and the volume has increased. In fact, the results show that a blunt cone with greater volume can have identically the same drag coefficient as a sharp cone. Two aerodynamic effects combine to produce the reduced wave drag with increased nose or forebody bluntness. First, the overexpansion downstream of the blunt nose/cone junction produces a lower pressure on the conical portion of the blunt body when compared to that of a sharp cone. Figure 40, which presents results obtained in Reference 59, shows the pressure distribution ratioed to sharp cone values for various bluntnesses and cone angles at a Mach number of 8 and indicates this phenomenon. Secondly, the bluntness reduces the semiape angle of the conical portion of the body and this produces a further reduction in the surface pressure. Together, these effects can more than offset the drag increases caused by the high pressures acting only over a small area on the blunt nose.

Before discussing interference drag in the next section of this paper, a few additional comments regarding wing sweep are in order. As has been pointed out in the preceding discussion, wing sweep is primarily used to reduce the wave drag at transonic and supersonic speeds and has many disadvantages at low or subsonic speeds (e.g., high induced drag, and loss in lift). Therefore, for an aircraft with multimission role, such as near transonic cruise and supersonic cruise, variable sweep or a swing-wing concept is an attractive idea.⁶⁰ Thus, at low speeds, the aircraft can take advantage of a straight wing, while at transonic and supersonic speeds the wing can be swept to minimize wave drag. Although this concept may not be the optimum for each speed range, over the total flight profile the aircraft performance would be enhanced. The major disadvantage of this concept is weight and complexity of the variable wing sweep mechanisms.

5.3 Interference Drag

Interference drag is caused by the complex flow-field interactions between adjacent aircraft components. Typical interference regions include the fuselage wing, fuselage empennage, horizontal-vertical tail, fuselage nacelle, wing nacelle, and wing tail. Although considerable research has been directed toward understanding and predicting interference effects between such components,⁶¹⁻⁷³ additional research is still needed. Present estimates of interference drag must depend heavily on ad-hoc wind-tunnel testing at relatively low Reynolds numbers supplemented by potential flow analyses and empirical "engineering" techniques. Even though viscous effects strongly affect the flow behavior in the junctions between adjacent aircraft components, no methods are currently available for satisfactorily predicting three-dimensional interference in viscous flows.

The potential for minimizing interference drag is represented by Figure 41 (from Ref. 65) for a supersonic transport configuration. The envelope of the interference effects corresponds to 25% of the sum of the isolated components; however, properly designing the configuration to eliminate, reduce, or take advantage of the interference effects is indicated to have the potential for reducing the total aircraft drag to values less than that for the sum of the isolated components. Thus, interference drag can be favorable as well as detrimental. This is shown in Figure 42 (from Ref. 69) where favorable interference between a particular wing nacelle was obtained for subsonic Mach numbers less than approximately 0.66.

Techniques for controlling the effects of component interference include: shaping/contouring to avoid excessive superelevations and adverse pressure gradients, area ruling to provide smooth area distributions, component filleting, and component positioning. Of these techniques, shaping, contouring, and area ruling probably depend most on the available analytical methods for minimizing interference effects. Wing-fuselage, wing-nacelle, and fuselage-nacelle interactions represent the areas where shaping, contouring, and area ruling have been applied very successfully. Figures 43 to 46 illustrate specific examples of body shaping for controlling interference. Streamline contouring (i.e., fuselage shaping to account for the lateral streamline pattern existing over an infinitely swept wing), area ruling and a combination of the two are shown in Figure 43 (from Ref. 61) to substantially reduce the interference drag of a wing-body configuration at transonic and supersonic velocities. The influence of area ruling on the pressure distribution over a Sears-Haack body and wing combination is presented in Figure 44 (from Ref. 65); the interference pressure distributions from the body on the wing and the wing on the body are plotted in their respective locations. Area ruling reduced the drag of the configuration by 25% based on the sum of the drag for the isolated wing and body. Favorable interference through nacelle contouring is shown in Figure 45 (from Ref. 72). Properly contouring the nacelle weakened and displaced the wing shock formation. Wing leading-edge contouring and pylon trailing-edge contouring are shown to have either favorable or adverse effects on the nacelle-wing interference drag in Figure 46 (from Ref. 69), depending on the free-stream Mach number.

With the development of the high bypass ratio engine, engine sizes have become very large. Therefore, one of the most challenging interference problems facing the aerodynamicist is that of engine nacelle installation. The choice of where to locate the engines on an airplane cannot be made a priori and must depend upon the mission of the aircraft, the aircraft size, engine size, and the specific aerodynamic performance objectives. Studies such as Reference 72 point out the advantages and disadvantages of locating engine nacelles under the wing, over the wing, and on the fuselage. However, regardless of where the nacelle is located, the flow field about it will be extremely complex (e.g., see Fig. 47 obtained from Ref. 71 for an underwing nacelle arrangement) and will be influenced by parameters such as the nacelle distance from the adjacent body, longitudinal position of nacelle relative to the adjacent body, the configuration lift coefficient and the free-stream Mach number. The representative effects of nacelle location on interference drag are shown in Figures 48 (from Ref. 73) and 49 (from Ref. 62) for subsonic flows and in Figure 50 (from Ref. 63) for supersonic flows. Although these figures show useful trends for positioning nacelles for relatively low drag, it should be emphasized that the selection of a good nacelle location does not depend totally on minimized interference drag; the effect of the nacelle location on the lift coefficient and the transonic drag rise are additional aerodynamic factors that must be considered.

5.4 Base and Separated Flow Drag

Base drag occurs because of the presence of a viscosity-induced low-speed layer of fluid near the wall or surface of an aircraft body or wing. In ideal inviscid (potential) low-speed flow, the pressure drag of a body is zero. However, the flow in the viscous boundary layer cannot negotiate the adverse pressure gradients which occur as the flow approaches the rearward potential flow stagnation point on the airfoil or fuselage and the flow separates. The resultant drag is a pressure or form drag since the separated or base flow has a lower pressure than in the absence of a boundary layer, that is, the recompression process is arrested once separation occurs. This type of drag is of particular concern on nacelles, fuselage closures, and wing/empennage trailing edges. Flow separation and the resultant drag is not unique to base flows, but also occurs whenever adverse pressure gradients are large (including shock/boundary-layer interaction regions), in the presence of large surface mass injection (leaks, etc.) and surface discontinuities.

The basic philosophy for drag reduction in base/separated flows is obvious; since the low momentum boundary-layer flow is responsible, thin the low momentum region to the maximum possible extent or introduce other flow structures, such as longitudinal vortices, which not only pump high energy air into the low momentum region but also may be more resistant to adverse pressure gradient influences. The usual methods used to provide a thinner low momentum region include: (a) suction, (b) wall jets (tangential injection with $u_1 > u_\infty$), (c) wall cooling, and (d) vortex generators (vanes or discrete air jets). The fuller velocity profile and larger cross-stream momentum transport which occurs in turbulent boundary layers makes them much less susceptible to separation. Additional methods utilized specifically to reduce base drag include (1) boattailing (reduces the adverse pressure gradient approaching the base region), (2) concave surface curvature (generates longitudinal vortices and is currently used on the lower surface of transonic supercritical wing sections), (3) splitter plates (reduces occurrence of Karman vortex street by interrupting top-to-bottom "cross-talk" in the base flow), (4) combustion/base bleed (increases base pressure directly and energizes shear layer), (5) recessed base geometry (may act like splitter plates), and (6) serrated trailing edges (introduces longitudinal vortices?).

For specific details of the base drag problem, the recent review by Tanner⁷⁴ is particularly useful, as are the companion volumes by Chang.^{75,76} See also the paper by Sedney,⁷⁷ the book edited by Lachmann,⁷⁸ the book edited by Murthy,⁷⁹ and the literature summaries of References 80 and 81. According to Tanner⁷⁴ for two-dimensional low-speed flows, where much of the base drag problem involves vortex shedding, the most effective base drag reduction approaches are splitter plate, boattailing, serrated trailing edges, and base bleed. For the three-dimensional case (axisymmetric), base bleed seems to give the best performance. Base drag reductions of the order of 50% are possible with such devices.

An interesting example of a base drag reduction experiment is shown in Figure 51 (from Refs. 82 and 83). Base drag was measured on an unswept fin attached to the undersurface of an F-104 fighter aircraft. Two base modifications were used: a splitter plate and a "vented cavity" (actually a serrated trailing edge). The flight results, shown on Figure 52, indicate base drag reductions of 30-40% with the splitter plate giving better results at the lower Mach number.

The percent base drag reductions obtainable at supersonic speeds, where Karman vortices do not occur, are less than at subsonic speeds as indicated in Figures 53 (from Ref. 84) and 54 (from Ref. 85). Obviously, the boattail approach need not involve straight-line segments, but ideally should be tailored for reduction of large local adverse pressure gradients. An example of the use of various afterbody closures is shown on Figures 55 and 56 (from Ref. 86). As expected, Figure 56 shows that the steeper boattail angles (larger adverse pressure gradient) are less effective in reducing base drag.

Base bleed is shown to be an effective base drag reduction approach in Figure 57 (from Ref. 87). For relatively large mass flow rates, the results for base bleed are very similar to those for splitter plates. Results for combinations of boattail angle, mass injection, and nozzle center body are shown in Figure 58 (from Ref. 88).

In the area of separation control or boundary-layer control (BLC) for wings, as opposed to base flows, several drag reduction approaches using wall suction are possible. The most obvious approach is to use a thicker wing (subsonic aircraft only) and maintain attached flow on the upper wing surface with BLC which allows greater structural efficiency and a higher aspect ratio (lower drag due to lift) wing. This was used in the early development of natural laminar flow airfoils⁸⁹ since the thicker airfoil sections provided large regions of favorable (disturbance stabilizing) pressure gradients. An alternate use of BLC for transonic wings is the reduction of flow separation caused by shock-boundary-layer interactions (increasing the drag-divergence Mach number). A third approach, again for low speeds, is the reduction of the lee surface separation thus delaying wing stall to higher angles of attack and thus increasing lift coefficient. Although this permits a more highly loaded wing with reduced chord and lower skin friction, the wing drag due to lift would be increased (higher angle of attack).

5.5 Drag Due to Lift

Drag due to lift refers to those drag components that are directly and necessarily associated with the generation of lift. At subsonic speeds, drag due to lift is primarily induced drag, but also includes some incremental drag increase in the form of skin friction and pressure drag. At transonic and supersonic speeds, drag due to lift also includes wave drag due to lift. The induced drag or vortex drag is caused by the shedding of vorticity along the wing span and, in particular, the wing tip. This drag appears as a momentum deficiency in the wake of the wing. The wave drag due to lift is an additional wave drag (other than that at zero lift which is discussed in Section 5.2) associated with the wing and body configuration being at lifting conditions and appears as a momentum deficiency in the surrounding flow field. A more complete discussion of drag due to lift is presented for those desiring greater details in References 23 and 41.

Subsonic drag due to lift depends primarily on the wing aspect ratio and the spanwise lift distribution over the wing. Increasing the aspect ratio and/or obtaining a nearly elliptical spanwise lift distribution will significantly reduce the induced drag. However, structural considerations become a dominant factor influencing the length of a large-aspect-ratio wing and a design compromise must be achieved. Current design approaches for reducing the subsonic drag due to lift (induced drag) are discussed in detail in Reference 90.

Supersonic drag due to lift is, of course, very similar to subsonic drag due to lift with the exception of the additional supersonic wave drag due to lift. To minimize supersonic drag due to lift, the wings should have large spans, long lengths, and elliptical spanwise load distributions (uniform downwash) for all area-ruled azimuthal angles (see Refs. 91-94 for a discussion of supersonic area ruling and equivalent body analysis for minimum wave drag). However, large skin-friction penalties result with large span and large length wings; also, as for subsonic speeds, the structural weight of such wings is large. Two solutions to this large skin-friction problem are the arrow-wing and the asymmetric or oblique-wing concepts. The oblique wing concept for transonic or low supersonic speeds was discussed in Section 5.2. The arrow-wing concept utilizes leading-edge sweep behind the Mach line (limited to the lifting line) to avoid large wave drag penalties and a rear notch to eliminate the inefficient lifting area over the aft part of the wing. Unfortunately, structural considerations drive the planform of the arrow wing toward that of a delta wing. Figure 59 (obtained from H. W. Carlson of NASA Langley) shows the reduced drag associated with arrow wings. Figure 60 (from Ref. 92) shows the effect of the arrow wing on the wave drag due to lift at supersonic speeds.

Wing twist and camber are another means by which supersonic drag due to lift is reduced. Since flat wing leading edges do not achieve suction at supersonic speeds, the flat wing drag is relatively large. By twisting and cambering the wing leading edge, lift is generated on the forward-facing wing slopes thus creating an upwash at the wing leading edge and thrust, not drag. Figure 61 (from Ref. 95) illustrates the influence of wing warp (twist and camber) on the supersonic drag due to lift. Note that although the flat wing has the lowest drag at zero lift, the warped wing has significantly less drag at the lifting conditions. The value $C_{L,deg}$ is an index of the camber surface severity and is the lift coefficient for which the warped wing surface is designed to produce a minimum drag. The term $C_{L,opt}$ is the lift coefficient yielding the maximum lift-drag ratio for a theoretically optimum surface. Linearized theory⁹⁵⁻⁹⁸ is used as the basis for designing optimum twisted and cambered wings. Figure 62 (from Ref. 99) shows how the elements of a wing can be represented in the analysis of lifting surfaces. Details of this theoretical/numerical analysis are provided in References 95, 97, and 99.

Designing a supersonic configuration to have low drag due to lift requires paying close attention to details and, in many cases, is somewhat an art rather than a science. Fuselage integration is one such example as shown in Figure 63 (from Ref. 95). Note that with the fuselage aligned to give equal areas above and below the wing surface, the most significant improvements in aerodynamic performance are obtained. Another example of attention to details is shown in Figure 64 (from Ref. 95) for nacelle alignment. Note that aligning the pylon or nacelle at a cant angle one-half of the local flow angle minimized drag contribution of the nacelle. Figure 65 (from Ref. 95) shows a configuration employing optimized lift design features such as these two examples. The configuration employs twisted and cambered wings, nacelle and fin alignment, and wing reflexing in the nacelle region, is self-trimmed at cruise speeds, and has an $L/D \approx 9-10$ at cruise lift coefficient and Reynolds number.

5.6 Viscous Drag Reduction

As discussed in the Introduction Section, skin friction comprises 40-50% of the drag on current CTOL aircraft. Since transition Reynolds numbers are generally the order of 4×10^6 or less, and the aircraft Reynolds number is the $O(100-400 \times 10^6)$, the usual state of the boundary layer is turbulent. The prime subject of the present discussion is the reduction of this turbulent skin-friction drag.

The most obvious drag reduction scheme, and the one technically most advanced, is that of laminar flow control (LFC), that is, delaying the transition process. Using a particular LFC approach (e.g., suction through closely spaced transverse slots), wing flows have been laminarized up to chord Reynolds numbers of approximately 60×10^6 . However, several maintenance and economic problems must be studied before aircraft application is practical. Also, an LFC system requires surface smoothness and cleanliness criteria considerably more stringent than that dictated by current practice on conventional aircraft.

Because of this possible operational "sensitivity" of LFC systems (and the requirements for high-altitude, low Reynolds number, long stage length), there exists considerable interest in an alternate drag reduction philosophy; reduce the turbulent shear but let the flow stay turbulent. The possible payoff in this approach is generally less than half as large as for LFC, but the system should be more stable to operational perturbations. This section of overview discusses both LFC methods and possibilities for altering the developed turbulent structure of the boundary layer. In general, the theory for the various LFC approaches and several of the turbulent alterations is well founded, but the detailed mechanisms responsible for the more spectacular effects in turbulent flows, such as those due to polymers, particles, and compliant walls, are not yet identified.

Although the emphasis is upon aircraft application, for completeness and as an aid in identification of common mechanisms, the review includes most of the skin-friction drag reduction approaches currently available; some are applicable only to liquids, or require additives or equipment which are obviously out of the question for aircraft.

5.6.1 Laminar Flow Control

On smooth surfaces and in the absence of large background disturbances (usual flight case), the process of transition from laminar to turbulent flow includes a linear regime where disturbances are growing, but have not yet reached a large, or nonlinear, level (\leq order of 1-3% disturbance level). A well-developed theory ("Stability Theory," i.e., Ref. 24) exists for this flow region, and can be used to determine possible methods for increasing the stability (and subsequently the transition Reynolds number) of the flow.

The usual LFC methods rely on a combination of two effects (1) thinning the boundary layer (lower the effective Reynolds number) and (2) altering the mean profile to a more stable shape. The LFC approaches which have received most attention for gases include (a) suction, (b) favorable pressure gradient, and (c) wall cooling. Other possibilities are use of MHD forces and compliant walls.

Figure 66 gives an example of the possible payoff from the use of LFC on the wings of CTOL aircraft. The laminarization method assumes suction through small, closely spaced transverse slots. Even with suction power considered in the overall system penalty, a fuel saving of from 25-40% is possible, depending upon the stage length.

Actual local drag reductions obtained using the slot suction LFC approach are shown on Figure 67 for the subsonic case and on Figure 68 for supersonic flow (both Figs. from Ref. 100). In both cases substantial reductions occur, even up to quite high Reynolds numbers. It should be noted that the optimum LFC suction system would involve continuous area suction. However, the practical aspects of suction duct/surface design dictate some sort of discrete suction. Dr. Pfenniger developed the present "best bet" approach consisting of closely spaced small transverse slots. The penalty for this discrete suction system versus area penalty is not known, but is probably not large.

A problem in the development and use of LFC systems is the sensitivity of boundary-layer transition to free-stream disturbances and roughness, particularly if these are near the critical Tollmien-Schlichting frequency/scale. Figure 69 (obtained from Dr. W. Pfenniger of NASA Langley Research Center) gives an indication of the free-stream disturbance effect upon transition Reynolds number with suction. The facility disturbance level shown on the abscissa is the usual wide-band rms average, and in the case of a sound disturbance the u' level is taken as the sound induced particle speed. The practical free-flight situation corresponds to the lower fluctuating velocity (u') levels (higher Reynolds numbers). The disturbances in flight which limit the LFC operating envelope are typically either roughness, surface vibration, and/or noise from adjacent viscous flows. Separate studies of the permissible surface roughness for optimal performance yield results such as shown on Figure 70. Three dimensionality of the roughness particle decreases the permissible roughness height.

At the present time, there are no known "barrier problems" to the application of LFC to the wings of CTOL aircraft. The remaining tasks involve optimization of an already good concept and, mainly, determining technical and economical problems involved with operation and maintenance of LFC surfaces/systems.

An earlier and still useful approach to LFC (can be combined with suction) involves application of favorable pressure gradients. Figure 71 (from Ref. 24) indicates the influence of pressure gradient upon the conventional neutral stability curves. A favorable pressure gradient both increases the lower critical Reynolds number and decreases the amplification rates. This approach was utilized on low-speed, unswept airfoils to produce the so-called "naturally laminar" wings.⁸⁹ The stabilizing effects of favorable pressure gradients are compromised in the swept wing case due to crossflow instabilities induced by three-dimensional flow within the boundary layer.

Another LFC approach, but one which is probably impractical for aircraft, is the use of MHD body forces to produce a more stable boundary-layer profile. An example of the computed stabilization effect is given on Figure 72 (from Ref. 101). Yet another stabilization technique (for gases) is wall cooling. This technique may become useful if liquid hydrogen is adopted as an alternate aircraft fuel. Figure 73 (from Ref. 102) indicates an example of the stabilization obtained theoretically from wall cooling at supersonic speeds. However, Figure 74 (Ref. 103) indicates experimentally that, at higher Mach numbers, there can be little or no stabilization, depending upon Mach number (and, in all probability, details of the facility disturbance level). In all of the LFC research, one must constantly be aware of the Morkovin concept of "dominant and multiple responsibility" for transition. That is, as soon as the major disturbance level is reduced, another type of disturbance may cause transition and this "new" dominant disturbance may have different functional dependence upon independent parameters. In the case of Figure 74, there is a possibility that facility disturbances cause a "high intensity bypass" type of transition¹⁰⁴ which "swamps out" the influence of the wall to total temperature ratio (T_w/T_t).

A final LFC concept, which has seen considerable theoretical development but little experimental or practical application, is the use of compliant walls. There are basically two general types of compliant walls (1) truly compliant or flow perturbation following (small phase lag between gas and wall motion) and (2) resonant or excited eigenmode walls (random phase). The theory is well developed for the former, but for boundary-layer stabilization the resulting walls are essentially impossible to construct, particularly for air. Typical theoretical requirements include (1) wall density the order of the fluid density, (2) shear modulus the order of dynamic pressure, and (3) small damping. Typical theoretical results are shown on Figure 75 (from Ref. 105). The case of the resonant walls is opposite — almost no theory but considerable experiment, mostly Russian.¹⁰⁶ The data indicate such walls can increase, as well as decrease, the lower critical Reynolds number, depending upon the detailed wall design.

Once the boundary layer is laminarized, the question can be raised as to whether the laminar level can be further reduced. One possible approach is to reduce the tangential momentum accommodation coefficient,

that is, relax the conventional "no-slip" boundary condition at the wall. Unfortunately, the research thus far¹⁰⁷ indicates the surface must be much cleaner, and kept much cleaner, than is currently possible in aircraft operating practice. The question of satellite drag is obviously another matter. Figure 76 (from Ref. 107) gives the measured reduction in tangential momentum accommodation coefficient for various surface treatments (polished, removal of absorbent layers, etc.).

Another approach to generation of a slip boundary condition is the use of a liquid layer on the surface. However, aside from obvious problems with the stability of such thin liquid layers, simplified analysis indicates the presence of a liquid layer causes an increase in drag, except for something exotic such as liquid hydrogen, which has a lower viscosity than air.

5.6.2 Alteration of Turbulence Structure

Additives. Three types of additives have been used to reduce the level of turbulent C_f drag — particles, polymers, and bubbles. Except for particles, the approach is applicable only to liquids. An example of the results for gas-particle suspensions is shown on Figure 77 (Ref. 108). Considerable reductions are possible, but the orientation of the pipe has a first-order effect. This orientation problem may be connected with sedimentation of the particles, especially in view of recent South African research¹⁰⁹ where sound fields increased the efficiency of the particles for horizontal pipes (sound pressure forces may have kept the particles in suspension).

The major effect of the particles is to increase the sublayer thickness, as can be seen in Figure 78 (Ref. 110). The slope in the law of the wall region ("Prandtl or Karman wall constant") is essentially unchanged. This thickening of the sublayer in law of the wall coordinates is common to most of the skin-friction reduction methods which alter the turbulent structure. The point is further quantified in Figure 79 (Ref. 110) where the amount of drag reduction is shown as a function of sublayer thickness.

Although the addition of particles causes a drag reduction, the turbulence intensity level can actually increase (Fig. 80, Ref. 110). This increase may be due, at least partially, to the velocity perturbation induced by the particle wakes. The extent of drag reduction increases with increasing particle density and decreasing particle size (Fig. 81, Ref. 111).

The data therefore indicate that particles can reduce turbulent skin-friction drag by 50% or more, with small diameter, large length/diameter particles being the most effective. Considering the weight problems of carrying suitable particles on an aircraft and the various pollution laws, the application of particles for drag reduction on aircraft is obviously not currently feasible. However, if the mechanism which causes this reduction could be isolated, perhaps other boundary condition changes could be used to produce a similar effect. Unfortunately, the drag reduction mechanism has not yet been identified. There are three obvious possibilities, either (a) turbulence dissipation increases due to the particle wakes, (b) the time-varying particle velocity phase lag produces a modulation in the near wall flow which decreases burst production or, finally, (c) an anisotropic viscosity which increases the profile stability. At the present time the mechanism is not understood.

Another additive which reduces drag, at least for liquids, is long chain polymers. The molecular weights involved are the order of 10^6 and concentration on the order of a few parts per million can result in reductions greater than 50%. However, the polymer must be "fresh," that is, the polymer chains must not be broken. Some threshold level of shear is evidently necessary to stretch the chains out for optimal effect. Therefore, there exists several conditions which must be met in practice before drag reduction is achieved. As in the case of particles, the basic mechanism for drag reduction is unclear, but several points can be made, primarily from References 112 and 113; (1) the number of turbulent "bursts" is definitely reduced and therefore the polymers are probably working by alteration of the very near wall flow and (2) the intensity of the bursts which do occur seems to be reduced. Typical drag reductions for various additives are shown on Figure 82 as a function of concentration.¹¹⁴ Figure 83 (Ref. 114) indicates that, as advertised previously, the major influence is an increase in sublayer thickness, with the slope of the law of the wall or logarithmic region essentially unaltered.

A further "additive" is the generation of bubbles in liquids. Very little research is available¹¹⁵ but the effect seems to occur in both fresh and salt water. One method of producing bubbles is by electrolysis of water (H_2 gas production).¹¹⁵ Data from Reference 115 for bubble drag reduction are shown on Figure 84. The mechanism responsible is unknown, but is probably similar to that responsible for the reduction with particle additives.

Reduction of Near Wall Momentum. For this class of drag reduction methods, the reduction mechanism is known, and simple. One strives to reduce the $\bar{\rho} \bar{u}^2$ level near the wall and thus reduce the wall shear directly. Any fundamental alteration of turbulence structure is of secondary importance. No new physics or mechanisms are necessary to explain these approaches. The more usual methods of reducing near wall momentum include (1) tangential slot injection, (2) normal or porous wall injection, and (3) adverse pressure gradient. Figure 85 indicates the typical flow field and skin-friction distribution for tangential slot injection. Just downstream of the slot, the wall senses the slot flow as the effective "free stream" and the drag is quite low primarily a $f \left(\frac{u_1}{u_\infty} \right)$. Once the mixing region, which originates at the slot lip,

nears the wall the skin friction increases until, far downstream, an "undisturbed level" is again reached. Obviously, additional slots could be used downstream of the first one to keep the skin-friction level low. In general, lower u_1/u_∞ gives lower initial skin-friction levels, but also shorter low skin-friction regions (faster shear layer mixing with small u_1/u_∞). Therefore, there is an optimal u_1/u_∞ for overall drag reduction ($\int C_f dx/S$). Typical measured and predicted slot flow skin-friction distributions are shown on Figure 86 for both transonic and hypersonic Mach numbers. There does not seem to be much of a Mach number effect, although the skin-friction level without slot injection does change with Mach number. The application of slot injection as an aircraft drag reduction scheme presupposes the existence of a supply of slot air. Unfortunately, except for laminar flow suction air, which has a relatively low mass flow rate (only enough for one slot), there is no known mass flow source with a low enough inlet loss to

allow an overall system benefit (net drag reduction). A further problem with the slot scheme is the base drag of the slots, which may be considerable.

An alternate approach to mass addition is normal injection through a porous surface. The amount of skin-friction reduction possible with this approach is considerable as seen on Figure 87 (Ref. 116). However, the method can also use slot injected air, and research in Reference 117 indicates that, on a skin-friction reduction per pound of air basis, slot injection is a more effective drag reduction scheme.

The influence of adverse pressure gradient is straightforward. For quasi-parallel inviscid flow

$$\frac{\partial u}{\partial x} = - \frac{\partial p}{\partial x} \frac{1}{\rho u}$$

Therefore, for $+\frac{\partial p}{\partial x}$, $\frac{\partial u}{\partial x}$ is negative, with a larger influence near the wall due to the $\frac{1}{\rho u}$ term. For aircraft, the use of adverse pressure gradients for skin-friction reduction has seen most application on low Reynolds number airfoils. L/D values of 200 to 300 have been obtained on airfoils designed with a nearly separated or "Stratford" type boundary-layer condition over the rear portion of the airfoil.¹¹⁸

Moving Walls. Two types of wall motion have been used to reduce turbulent skin friction; uniform in-plane motion and moving surface waves. The uniform in-plane case is relatively straightforward. The production of turbulence is directly proportional to the mean shear $\frac{\partial u}{\partial y}$. The imposition of a wall velocity in the main stream direction essentially acts as a slip boundary condition and reduces $\frac{\partial u}{\partial y}$. The typical trend of skin friction with u_{wall} is indicated on Figure 88 (Ref. 119). The end point at the lower right is obvious; if $u_{\text{wall}} = u_{\infty}$, then there is no mean shear and the boundary-layer thickness is zero. The variation is approximately quadratic, which is what one would expect from a simple Gallalian transformation. The application of this approach ($u_{\text{wall}} > 0$) as a drag reduction scheme on an aircraft is probably not feasible, particularly as the wall speed would have to be some reasonable fraction of sonic for CTOL long-haul aircraft. However, the concept has received little serious consideration.

The alternate wall motion effect, moving surface waves, is not straightforward. The concept is an outgrowth of the compliant wall work for transition retardation. For low modulus, correctly designed walls, the turbulent wall pressure fluctuations, along with the self-induced "flutter forces," can excite structural eigenmodes and produce traveling surface waves. There is some evidence (see IUTAM paper by Bushnell et al. on compliant walls)¹²⁰ that the surface waves can interfere with the turbulence production processes, particularly for the high-frequency, small wave length case. An example of the more dramatic compliant (resonant) wall data for turbulent boundary layers is shown on Figure 89 (Ref. 121).

Convex Curvature. The basic mechanism is the stabilization of turbulence when $\frac{\partial(ur)}{\partial r} > 0$ where r is the local streamline curvature. This flow curvature can be forced by wall curvature and the effect is present, but generally unrecognized, in much of the airfoil data. Sizable effects are possible, a typical example is shown on Figure 90 (Ref. 122). Reference 123 comprises an excellent review of the influence of curvature, both convex and concave, upon turbulence.

5.6.3 Reduction/Alteration in Wetted Area for Drag Minimization

There exists several approaches for skin-friction drag reduction by alteration or reduction in the wetted area. The total wall friction drag force is obviously $\int C_f dA (q_{\infty})$. For a given flight altitude and velocity (q_{∞}), one can either alter the area distribution so that the skin friction is lower over a larger portion of the area, or reduce the absolute magnitude of the area. Figure 91 (Ref. 124) indicates results for what is essentially an area redistribution, increasing the sweep so that more of the area is at high Re_x (low skin friction). An example of absolute area reduction would be the use of boundary-layer control to produce high C_L on a smaller chord (less area) wing.¹²⁵ Another example is shown on Figure 92 (Ref. 126), where the use of active controls technology allows a reduction in control surface empenage area and thus a skin-friction drag reduction.

5.6.4 Alternative Approaches to Skin-Friction Drag Reduction

Corrugated Surfaces. Consider the skin-friction distribution over a stationary sine-wave shaped wall for wave amplitudes much less than the boundary-layer thickness (no wave-induced local flow separation). The wave shaped wall produces alternating regions of positive and negative axial pressure gradient. Due to the quasi-nonlinearity of the convective terms in the Navier-Stokes equations, there is more of a skin-friction decrease due to the adverse pressure gradient portion than there is increase due to the favorable pressure gradient. Representative wall shear stress distributions are shown on Figures 93 (Ref. 127) and 94 (Ref. 128). The average skin friction over a wall wave cycle is seen to be less than the flat wall level.

There is, however, a problem with this possible drag reduction approach. The presence of a mean velocity gradient in the effective "free stream" for the wall waves (amplitude $\ll \delta$) produces a phase shift in the wall pressure distribution such that a net pressure drag occurs. This pressure drag is generally greater than the reduction in average skin friction. There has evidently not yet been an effort to circumvent this problem by using asymmetric waves or other tricks to locally distort the pressure field.

Noncircular Duct Geometry. Although not directly related to the reduction in skin friction on the external skin of an aircraft, it is of interest to note the apparent lower drag which occurs in noncircular ducts, particularly ducts which have acute included angles (such as triangle channels). The work of Reference 129 indicates at least some of this is due to the co-existence of laminar and turbulent flow within the same duct (Fig. 95). Simplistically, the turbulence seems to react to a Reynolds number based upon the local distance between adjacent walls. There may be a way of utilizing this behavior for the external drag problem by employing quite small longitudinal v-grooves, but this is pure speculation.

5.6.5 Outlook for Viscous Skin-Friction Drag Reduction

Laminar flow control has the largest payoff, is best understood, and is the most advanced technically of any skin-friction reduction approach. The major problems with LFC are a lack of applicability to short (≈ 700 miles or less) stage length and questions such as maintenance cost, reliability, and cleanliness/smoothness requirements. There is a need, especially at the shorter stage lengths, for an alternate scheme which reduces the turbulent skin-friction level. For localized application, fixes such as convex walls, adverse pressure gradient, and slot injection can be used, but, especially for the fuselage, a more "global" concept is needed. Currently, the compliant (resonant) wall approach offers the most hope as a new concept, but our knowledge and understanding in the area is, to put it charitably, in an early stage.

6. REFERENCES

- ¹Nagel, A. L.; Alford, W. J., Jr.; and Dugan, J. R., Jr.: Future Long-Range Transports — Prospects for Improved Fuel Efficiency. NASA TM X-72659, February 1975.
- ²Maddalon, D. V.; and Wagner, R. D.: Energy and Economic Trade Offs for Advanced Technology Subsonic Aircraft. NASA TM X-72833, April 1976.
- ³Schairer, G. S.: Some Opportunities for Progress in Aircraft Performance. Journal of Aircraft, Vol. 1, No. 2, March-April 1964, pp. 49-70.
- ⁴Braslow, A. L.; and Whitehead, A. H., Jr.: Aeronautical Fuel Conservation Possibilities for Advanced Subsonic Transports. NASA TM X-71927, December 1973.
- ⁵Goodmanson, L. T.; and Gratzner, L. B.: Recent Advances in Aerodynamics for Transport Aircraft, Part 2. Astronautics and Aeronautics, January 1974, pp. 52-60.
- ⁶Grey, J. E.: Aircraft Fuel Conservation: An AIAA View. Proceedings of a Workshop Conference, Reston, Virginia, March 13-15, 1974.
- ⁷Maddalon, D. V.: Air Transportation: Energy Cost-Effective or Not? AIAA Sixth Aircraft, Design, Flight Test, and Operations Meetings, Los Angeles, California, Paper No. 74-959, August 12-14, 1974.
- ⁸Maddalon D. V.: Rating Aircraft on Energy. Astronautics and Aeronautics, December 1974, pp. 26-43.
- ⁹Black, R. E.; and Stern, J. A.: Advanced Subsonic Transports — A Challenge for the 1990's. AIAA 11th Annual Meeting and Technical Display, Washington, D.C., February 24-26, 1975, Paper No. 75-304.
- ¹⁰Clay, C. W.; and Sigalla, A.: The Shape of the Future Long-Haul Transport Airplane. AIAA 11th Annual Meeting and Technical Display, Washington, D.C., February 24-26, 1975, Paper No. 75-305.
- ¹¹Nicks, O. W.; Whitehead, A. H., Jr.; and Alford, W. J., Jr.: An Outlook for Cargo Aircraft of the Future. NASA TM X-72796, November 1975.
- ¹²Dornier, C., Jr.: Thoughts on the Future Tasks of the European Aviation Industry in the Realm of Civil Aviation. Foreign Technology Division, Air Force Systems Command, FTD-ID (RS) I - 2214-75, June 1975.
- ¹³Poisson-Quinton, P.: Technologies for the Air Transport of Tomorrow. ONERA, TP. No. 1975-62, 1975, pp. 81-100.
- ¹⁴Peckham, D. H.: Range Performance in Cruising Flight. RAE Technical Report 73164, October 1973.
- ¹⁵Brooks, G. W.: Some Trends in Aircraft Design-Structures. NASA University Conference on Aeronautics. NASA CR-142559, October 1974, pp. 212-270.
- ¹⁶Pride, R. A.: Materials Application to Civil Aircraft Structures in the Seventies and Beyond. Conference on Vehicle Technology for Civil Aviation — The Seventies and Beyond. Paper No. 10. NASA SP-292, November 1971.
- ¹⁷Boeing Commercial Airplane Company: Fuel Conservation Possibilities of Terminal Area Compatible Aircraft. NASA CR-132608, 1975.
- ¹⁸Corson, B. W., Jr.; and Schmeer, J. W.: Summary of Research on Jet-Exit Installations. Conference on Aircraft Aerodynamics. NASA SP-124, May 1966, Paper No. 15.
- ¹⁹Butler, S. F. J.: Aircraft Drag Prediction for Project Appraisal and Performance Estimation: Conference on Aerodynamic Drag. AGARD CP-124, April 1973, Paper No. 6.
- ²⁰Drag Reduction Seen as Source of Fuel Savings. Aviation Week and Space Technology, Vol. 105, No. 17, October 25, 1976, p. 55.
- ²¹Paterson, J. H.; MacWilkinson, D. G.; and Blackerby, W. T.: A Survey of Drag Prediction Techniques Applicable to Subsonic and Transonic Aircraft Design. Conference on Aerodynamic Drag. AGARD CP-124, April 1973, Paper No. 1.
- ²²Wieghardt, K.: Increase in Turbulent Skin Friction Caused by Surface Irregularities. Armed Services Technical Information Agency. Translation No. 103, June 1946.
- ²³Hoerner, S. F.: Fluid-Dynamic Drag. Hoerner Fluid Dynamics, Brick Town, New Jersey, 1965.
- ²⁴Schlichting, H.: Boundary Layer Theory. Fourth Edition, McGraw-Hill Book Company, New York, 1960.

- 25 Gaudet, L.; and Winter, K. G.: Measurements of the Drag of Some Characteristic Aircraft Excrescences Immersed in Turbulent Boundary Layers. Conference on Aerodynamic Drag. AGARD CP-124, April 1973, Paper No. 4.
- 26 Good, M. C.; and Joubert, P. N.: The Form Drag of Two-Dimensional Bluff-Plates Immersed in Turbulent Boundary Layers. Journal of Fluid Mechanics, Vol. 31, Part 3, 1968, pp. 547-582.
- 27 Czarnecki, K. R.; Servier, J. R.; and Carmel, M. M.: Effect of Fabrication-Type Roughness on Turbulent Skin Friction at Supersonic Speeds. NACA TN-4299, July 1958.
- 28 Tani, I.; Inchi, M.; and Komoda, H.: Experimental Investigation of Flow Separation Associated With a Step or Groove. Aero. Res. Inst., University of Tokyo Report 364, April 1961.
- 29 Czarnecki, K. R.: The Problem of Roughness Drag at Supersonic Speeds. NASA TN D-3589, October 1966.
- 30 Czarnecki, K. R.; and Monta, W. J.: Roughness Drag Due to Two-Dimensional Fabrication-Type Surface Roughness on an Ogive Cylinder From Force Tests at Transonic Speeds. NASA TN D-5004, January 1969.
- 31 Cook, T. A.: The Effects of Ridge Excrescences and Trailing-Edge Control Gaps on Two-Dimensional Aerofoil Characteristics. Ministry of Defence, RAE, R&M No. 3698, April 1971.
- 32 Pallister, K. C.: Wind Tunnel Measurements of the Transonic Drag of Excrescences Immersed in a Turbulent Boundary Layer. ARA Report No. 37, December 1974.
- 33 Kovalenko, V. M.; and Nesterovich, N. I.: The Drag Ridges of Finite Length in a Turbulent Boundary Layer. RAE Library Translation 1852, May 1975.
- 34 Coe, P. L., Jr.: Review of Drag Cleanup Tests in Langley Full-Scale Tunnel (From 1935 to 1945) Applicable to Current General Aviation Airplanes. NASA TN D-8206, June 1976.
- 35 Ellis, B. K.; and Ryan, H. S., Jr.: Drag Resulting From Separated Flow Induced by Surface Cavities at a Mach Number of 3.74. Department of the Navy, DTMB-AL-9, November 1964.
- 36 Howell, R. H.; and Korst, H. H.: Drag Associated With Separated Flow Over Two-Dimensional V-Shaped Notches Under Transonic and Supersonic Conditions. NASA CR-1132, September 1968.
- 37 McGregor, O. W.; and White, R. A.: Drag of Rectangular Cavities in Supersonic and Transonic Flow Including the Effects of Cavity Resonance. AIAA Journal, Vol. 8, No. 11, November 1970, pp. 1959-1964.
- 38 Friesing, H.: Measurement of the Drag Associated With Recessed Surfaces: Cut-Outs of Rectangular and Elliptical Planform. RAE Library Translation No. 1614, October 1971.
- 39 Nash, J. F.; and Bradshaw, P.: The Magnification of Roughness Drag by Pressure Gradients. J. R. Aeronaut. Soc., Vol. 71, January 1967, pp. 44-49.
- 40 Richards, E. J.: A Review of Aerodynamic Cleanness. Royal Aero. Soc. Journal, March 1950, pp. 137-186.
- 41 Talay, T. A.: Introduction to the Aerodynamics of Flight. NASA SP-367, 1975.
- 42 Whitcomb, R. T.; and Clark, L. R.: An Airfoil Shape for Efficient Flight at Supercritical Mach Numbers. NASA TM X-1109, July 1965.
- 43 Whitcomb, R. T.: Review of NASA Supercritical Airfoils. The Ninth Congress of the International Council of the Aeronautical Sciences, Haifa, Israel, August 1974, Paper No. 74-10.
- 44 Whitcomb, R. T.: A Study of the Zero-Lift Drag Rise Characteristics of Wing-Body Combinations Near the Speed of Sound. NACA RM L52H08, 1952.
- 45 Hayes, W. D.: Linearized Supersonic Flow. North American Aviation, Inc., Report AL-222, June 18, 1947.
- 46 Heaslet, M. A.; and Lomax, H.: Recent Developments in the Theory of Wing-Body Wave Drag. Journal Aero. Sci., Vol. 23, No. 12, December 1956, pp. 1061-1074.
- 47 Jones, R. T.: Theoretical Determination of the Minimum Drag of Airfoils at Supersonic Speeds. Journal Aero. Sci., Vol. 19, No. 12, December 1952, pp. 813-822.
- 48 Jones, R. T.: Aerodynamic Design for Supersonic Speeds. Proceedings of First International Congress in Aeronautical Sciences, Madrid, September 1958. Advances in Aeronautical Sciences, Vol. 1, pp. 34-51.
- 49 Jones, R. T.: Reduction of Wave Drag by Antisymmetric Arrangement of Wings and Bodies. AIAA Journal, Vol. 10, No. 2, February 1972, pp. 171-176.
- 50 Jones, R. T.: New Design Goals and a New Shape for the SST. Astronautics and Aeronautics, Vol. 10, No. 12, December 1972, pp. 66-70.
- 51 Graham, L. A.; Jones, R. T.; and Boltz, F. W.: An Experimental Investigation of Three Oblique-Wing and Body Combinations at Mach Numbers Between 0.60 and 1.40. NASA TM X-62256, April 1973.

- ⁵²Graham, E. W.; Lagerstrom, P. A.; Licher, R. M.; and Beane, B. J.: A Theoretical Investigation of the Drag of Generalized Aircraft Configurations in Supersonic Flow. NACA TM-1421, January 1957.
- ⁵³Theory of Optimum Aerodynamic Shapes. Edited by A. Miele, Academic Press, New York, 1965.
- ⁵⁴Stivers, L. S., Jr.; and Spencer, B., Jr.: Studies of Optimum Body Shapes at Hypersonic Speeds. NASA TN D-4171, October 1967.
- ⁵⁵Love, E. S.: Design of Bodies for Low Drag and High Performance in Practical Hypersonic Flight — Performance and Dynamics of Aerospace Vehicles. NASA SP-258, pp. 103-174.
- ⁵⁶Lusty, A. H., Jr.: Slender, Axisymmetric Power Bodies Having Minimum Zero Lift Drag in Hypersonic Flow. Boeing Scientific Research Laboratories, Flight Science Laboratory, TR No. 77, 1963.
- ⁵⁷Pugh, P. G.; Lacombe, M. J.; and Ward, L. C.: Recent NPL Research on Supersonic Aerodynamics. NPL Aero Note 1074, April 1968.
- ⁵⁸Pugh, P. G.; and Ward, L. C.: A Parametric Study of the Use of Nose Blunting to Reduce the Supersonic Wave Drag of Forebodies. ARC-CP-1271, 1974.
- ⁵⁹Roberts, J. F.; Lewis, C. H.; and Reed, M.: Ideal Gas Spherically Blunted Cone Flow Field Solutions at Hypersonic Conditions. AEDC-TR-66-121, August 1966.
- ⁶⁰Polhamus, E. C.: Subsonic and Transonic Aerodynamic Research. Vehicle Technology for Civil Aviation — The Seventies and Beyond. NASA SP-292, November 1971, Paper No. 3, pp. 27-44.
- ⁶¹Howell, R. R.; and Braslow, A. L.: An Experimental Study of a Method of Designing the Sweptback-Wing-Fuselage Junction for Reducing the Drag at Transonic Speeds. NACA L54L31a, March 1955.
- ⁶²Patterson, J. C.: Wind-Tunnel Studies of Nacelle Interference Drag at High Subsonic Speeds Including the Effect of Powered Jets. Conference on Aircraft Aerodynamics. NASA SP-124, May 1966, Paper No. 18, pp. 259-270.
- ⁶³Bagley, J. A.: Some Aerodynamic Problems of Powerplant Installation on Swept-Winged Aircraft. Royal Aeronautical Society, Proceedings of Two-Day Convention on Short-Range Transports, London, England, May 14-15, 1969.
- ⁶⁴Kuchemann, D.: Some Remarks on the Interference Between a Swept Wing and a Fuselage. Aerodynamic Interference. AGARD CP-71-71, January 1971, Paper No. 1.
- ⁶⁵Kane, E. J.; and Middleton, W. D.: Considerations of Aerodynamic Interference in Supersonic Airplane Design. Aerodynamic Interference. AGARD CP-71-71, January 1971, Paper No. 3.
- ⁶⁶Aerodynamic Components of Aircraft at High Speed. Edited by A. F. Donovan and H. R. Lawrence, Princeton University Press, Princeton, New Jersey, 1957, pp. 281-585.
- ⁶⁷Runkel, J. F.: Aerodynamic Interference Between Exhaust System and Airframe. Aerodynamic Conference. AGARD CP-71-71, January 1971, Paper No. 15.
- ⁶⁸Williams, P. R. G.; and Stewart, D. J.: The Complex Aerodynamic Interference Pattern Due to Rear Fuselage Mounted Powerplants. Aerodynamic Interference. AGARD CP-71-71, January 1971, Paper No. 22.
- ⁶⁹Aldridge, S. E.; and Nye, J. L.: Experimental Results of High Bypass Ratio Turbofan and Wing Aerodynamic Interference. Aerodynamic Interference. AGARD CP-71-71, January 1971, Paper No. 23.
- ⁷⁰Hess, J. L.; and Faulkner, S. M.: Determination of Low Speed Interference Effects by Superposition. Aerodynamic Interference. AGARD CP-71-71, January 1971, Paper No. 24.
- ⁷¹Jaarsma, F.: Engine-Airplane Interference in Transonic Tests. Engine-Airplane Interference and Wall Corrections in Transonic Wind Tunnel Tests. AGARD AR-36-71, August 1971, Part II.
- ⁷²Swan, W. C.; and Sigalla, A.: The Problem of Installing a Modern High Bypass Engine on a Twin Jet Transport Aircraft. Conference on Aerodynamic Drag. AGARD CP-124, October 1973, Paper No. 17.
- ⁷³Ewald, B.: Airframe-Engine Interaction for Engine Configurations Mounted Above the Wing. Part II: Engine Jet Simulation Problems in Wind Tunnel Tests. Conference on Airframe/Propulsion Interference. AGARD CP-150, March 1975, Paper No. 26.
- ⁷⁴Tanner, M.: Reduction of Base Drag. Progress in Aerospace Sciences, Vol. 16, No. 4, 1975, pp. 369-384.
- ⁷⁵Chang, P. K.: Separation of Flow. Pergamon Press, New York, 1970.
- ⁷⁶Chang, P. K.: Control of Flow Separation. Hemisphere Publishing Corporation, Washington, D.C., 1976.
- ⁷⁷Sedney, R.: Review of Base Drag. AGARD CP-10, 1966, pp. 211-240.
- ⁷⁸Boundary Layer and Flow Control. Edited by G. V. Lachmann, Pergamon Press, New York, 1961.
- ⁷⁹Aerodynamics of Base Combustion. Edited by S. N. B. Murthy. Progress in Astronautics and Aeronautics, Vol. 40, MIT Press, Cambridge, Massachusetts, 1976.

- 80 Anon.: Base Flow: A Bibliography (1950-1972) National Aeronautical Laboratory, Bangalore, Bibliography Series No. 46, October 1973.
- 81 Murthy, S. N. B.; Osborn, J. R.; and Bruestle, H. R.: Base Flow Data With and Without Injection: Bibliography and Semi-Rational Correlations. Thermal Sciences and Propulsion Center, Purdue University, May 1973.
- 82 Pyle, J. S.; and Saltzman, E. J.: Review of Drag Measurements From Flight Tests of Manned Aircraft With Comparisons to Wind-Tunnel Predictions. Aerodynamic Drag. AGARD CP-124, Paper No. 25, October 1973.
- 83 Saltzman, E. J.; and Hintz, J.: Flight Evaluations of Splitter-Plate Effectiveness in Reducing Base Drag at Mach Numbers From 0.65 to 0.90. NASA TM X-1376, May 1967.
- 84 Fuller, D. E.; and Wassum, D. L.: Preliminary Study of Drag Reduction for Coasting Missiles at Mach Numbers From 1.57 to 4.63. NASA TM X-1537, April 1968.
- 85 Pollock, N.: Some Effects of Base Geometry on Two-Dimensional Base Drag at Subsonic and Transonic Speeds. ARL/Aero Note 316, October 1969.
- 86 Mair, W. A.: Reduction of Base Drag by Boat-Tailed Afterbodies in Low-Speed Flow. The Aeronautical Quarterly, Vol. XX, November 1969, pp. 307-320.
- 87 Wood, C. J.: The Effect of Base Bleed on a Periodic Wake. Journal of the Royal Aeronautical Society, July 1964, pp. 477-482.
- 88 Bergman, D.: Effects of Engine Exhaust Flow on Boattail Drag. AIAA Eighth Aerospace Sciences Meeting, New York, New York, January 19-20, 1970, Paper No. 70-132.
- 89 Keeble, T. S.: Development in Australia of a Thick Suction Wing. Proceedings of the Third Anglo-American Aeronautical Conference, Brighton, September 4-7, 1971, pp. 45-76.
- 90 Whitcomb, R. T.: Methods for Reducing Subsonic Drag Due to Lift. AGARD/VKI Special Course on "Concepts for Drag Reduction." von Karman Institute for Fluid Dynamics, March 28-April 1, 1977.
- 91 Harris, R. V., Jr.: An Analysis and Correlation of Aircraft Wave Drag. NASA TM X-947, March 1964.
- 92 Harris, R. V., Jr.: A Numerical Technique for Analysis of Wave Drag at Lifting Conditions. Conference on Aircraft Aerodynamics. NASA SP-124, May 1966, Paper No. 27, pp. 399-408.
- 93 Yoshikawa, K. K.: An Improved Method of Designing and Calculating the Minimal Wave Drag Configuration by Supersonic and Moment-of-Area Rules. NAL TR-184T, October 1969.
- 94 Baals, D. D.; Robins, A. W.; and Harris, R. V., Jr.: Aerodynamic Design Integration of Supersonic Aircraft. AIAA Fifth Annual Meeting and Technical Display, Philadelphia, Pennsylvania, October 21-24, 1968, Paper No. 68-1018.
- 95 Carlson, H. W.; and McLean, F. E.: Current Methods for Prediction and Minimization of Lift-Induced Drag at Supersonic Speeds. Conference on Aircraft Aerodynamics. NASA SP-124, May 1966, Paper No. 26, pp. 383-398.
- 96 Graham, E. W.; Lagestrom, P. A.; Licher, R. M.; and Beane, B. J.: A Theoretical Investigation of the Drag of Generalized Aircraft Configurations in Supersonic Flow. NACA TM 1421, January 1957.
- 97 Carlson, H. W.; and Middleton, W. D.: A Numerical Method for the Design of Camber Surfaces of Supersonic Wings With Arbitrary Planforms. NASA TN D-2341, June 1964.
- 98 Bera, R. K.: Warping of Delta Wings for Minimum Drag. AIAA Journal of Aircraft, Vol. 11, No. 12, December 1974, pp. 777-779.
- 99 Carlson, H. W.; and Harris, R. V., Jr.: A Unified System of Supersonic Aerodynamic Analyses. Analytic Methods in Aircraft Aerodynamics. NASA SP-228, October 1969, pp. 639-658.
- 100 Antonatos, P. P.; Nenni, J. P.; and Mueller, R. X.: Summary of Laminar Flow Control Techniques for Aircraft. ASD-TDR-63-689, September 1963.
- 101 Wu, Y. K.; and Anderson, G. F.: Torpedo Drag Reduction Using Magneto-hydrodynamic Boundary-Layer Control. Southeastern Massachusetts University Technical Report. (Contract N00140-69-C-0338) January 1972.
- 102 Mack, L. M.: Boundary-Layer Stability Theory. Jet Propulsion Laboratory, California Institute of Technology (Contract No. NAS 7-100), November 1969.
- 103 Fischer, M. C.: Influence of Moderate Wall Cooling on Cone Transition at $M_e = 13.7$ in Helium. Journal of Spacecraft and Rockets, Vol. 10, No. 4, April 1973, pp. 282-283.
- 104 Morkovin, M. V.: Critical Evaluation of Transition From Laminar to Turbulent Shear Layers With Emphasis on Hypersonically Traveling Bodies. AFFDL-TR-68-149, March 1969.
- 105 Kaplan, R. E.: The Stability of Laminar Incompressible Boundary Layers in the Presence of Compliant Boundaries. MIT, Report ASRL TR 116-1, June 1964, pp. 1-179.

- 106 Babenko, V. V.; and Kozlov, L. F.: Experimental Investigation of Hydrodynamic Stability at Rigid and Elastic-Damping Surfaces. *Akademiia Nauk SSSR, Izvestiia Mekhanika Zhidkostif Gaza*, January-February 1973, pp. 122-127.
- 107 Steinheil, E.; Scherber, W.; and Seidl, M.: Reduction of Momentum Transfer From Gases Onto Solid Surfaces. Third Symposium on Gas-Surface Interaction, Meersburg, Germany, October 2, 1975.
- 108 Pfeffer, R.; and Rosetti, S. J.: Experimental Determination of Pressure Drop and Flow Characteristics of Dilute Gas-Solid Suspensions. NASA CR-1894, August 1971.
- 109 Marcus, R. D.; Dickson, A. J.; and Rallis, C. J.: Drag Reduction and Pressure Pulsations in Horizontal Dilute Phase Pneumatic Conveying. Third International Conference on the Pneumatic Transport of Solids in Pipes, Bedford, England, April 7-9, 1976.
- 110 Kane, R. S.; and Pfeffer, R.: Characteristics of Dilute Gas-Solids Suspensions in Drag Reducing Flow. NASA CR-2267, June 1973.
- 111 Boyce, M. P.: Fluid Flow Phenomena in Dusty Air. Ph. D. Dissertation, University of Oklahoma, 1969.
- 112 Donohue, G. L.; Tiederman, W. G.; and Reischman, M. M.: Flow Visualization of the Near-Wall Region in a Drag-Reducing Channel Flow. *Journal of Fluid Mechanics*, Vol. 56, Part 3, 1973, pp. 559-575.
- 113 Oldaker, D. K.; and Tiederman, W. G.: Spatial Structure of the Viscous Sublayer in Drag Reducing Channel Flows. IUTAM Symposium on Structure of Turbulence and Drag Reduction, Washington, D.C., June 7-12, 1976.
- 114 Lumley, J. L.: Drag Reduction in Turbulent Flow by Polymer Additives. *Journal of Polymer Sciences: Macromolecular Reviews*, Vol. 7, 1973, pp. 362-290.
- 115 McCormick, M. E.; and Bhattacharyya, R.: Drag Reduction of a Submersible Hull by Electrolysis. *Naval Engineers Journal*, April 1973, pp. 11-16.
- 116 Bushnell, D. M.; Cary, A. M., Jr.; and Harris, J. E.: Calculation Methods for Compressible Turbulent Boundary Layers. AGARD LS-86, March 1-5, 1976.
- 117 Schetz, J. A.; and van Overeem, J.: Skin Friction Reduction in Supersonic Flow by Injection Through Slots, Porous Sections and Combinations of the Two. NASA CR-2471, March 1975.
- 118 Carmichael, B. H.: Application of Sailplane and Low-Drag Underwater Vehicle Technology to the Long-Endurance Drone Problem. AIAA/MIT/SSA Second International Symposium on the Technology and Science of Low Speed and Motorless Flight, Cambridge, Massachusetts, September 11-13, 1974, Paper No. 74-1036.
- 119 Roper, A. T.; and Gentry, G. L., Jr.: Analysis of a Turbulent Boundary Layer Over a Moving Ground Plane. NASA TN D-6788, July 1973.
- 120 Bushnell, D. M.; Hefner, J. N.; and Ash, R. L.: Compliant Wall Drag Reduction for Turbulent Boundary Layers. IUTAM Symposium on Structure of Turbulence and Drag Reduction, Washington, D.C., June 7-12, 1976.
- 121 Fischer, M. C.; Weinstein, L. M.; Bushnell, D. M.; and Ash, R. L.: Compliant Wall Turbulent Skin Friction Reduction Research. AIAA Eighth Fluid and Plasma Dynamics Conference, Hartford, Connecticut, June 16-18, 1975, Paper No. 75-833.
- 122 So, R. M.; and Mellor, G. L.: An Experimental Investigation of Turbulent Boundary Layers Along Curved Surfaces. NASA CR-1940, April 1973.
- 123 Bradshaw, P.: Effects of Streamline Curvature on Turbulent Flow. AGARD AG-169, August 1973.
- 124 Peterson, J. B., Jr.; and Monta, W. J.: Considerations Regarding the Evaluation and Reduction of Supersonic Skin Friction. Conference on Aircraft Aerodynamics. NASA SP-124, Paper No. 30, pp. 437-454.
- 125 Kohlman, D. L.: Drag Reduction Through Higher Wing Loading. Proceedings of NASA/Industry/University General Aviation Drag Reduction Workshop. University of Kansas, July 14-16, 1976, NASA CR-145627, pp. 157-169.
- 126 Rediess, H. A.; and Azalai, K. J.: Status and Trends in Active Control Technology. NASA/University Conference on Aeronautics: The Future of Aeronautics. University of Kansas, October 23-24, 1974, NASA CR-142559, pp. 271-320.
- 127 Sigal, A.: An Experimental Investigation of the Turbulent Boundary Layer Over a Wavy Wall. Ph. D. Dissertation, California Institute of Technology, 1971.
- 128 Kendall, J. M.: The Turbulent Boundary Layer Over a Wall With Progressive Surface Waves. *Journal of Fluid Mechanics*, Vol. 41, Part 2, 1970, pp. 259-281.
- 129 Eckert, E. R. G.; and Irvine, T. F., Jr.: Flow in Corners of Passages With Noncircular Cross Sections. *Transactions of the ASME*, May 1956, pp. 709-718.

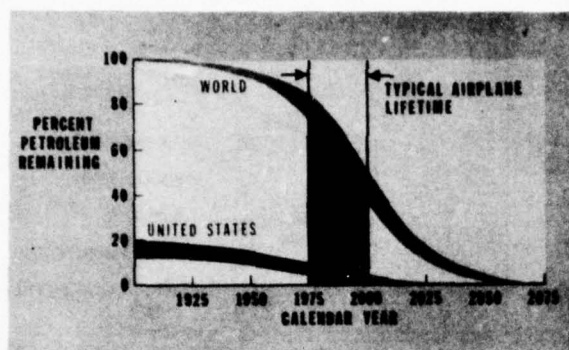


Figure 1. Natural petroleum supply.

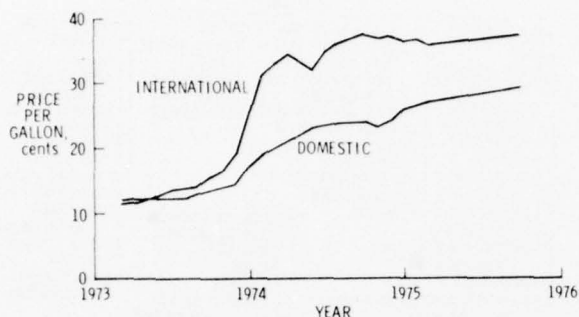


Figure 2. Average U.S. commercial jet fuel price.

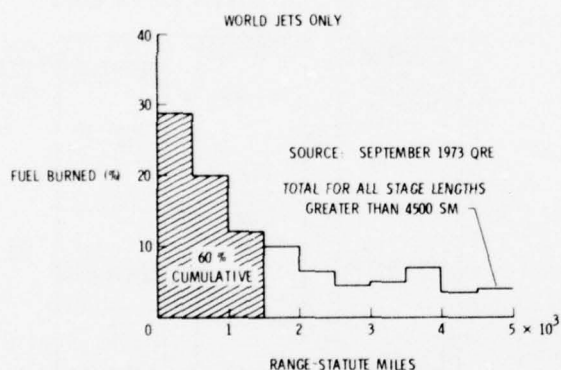


Figure 3. World jet fuel consumption versus stage length. World jets only.

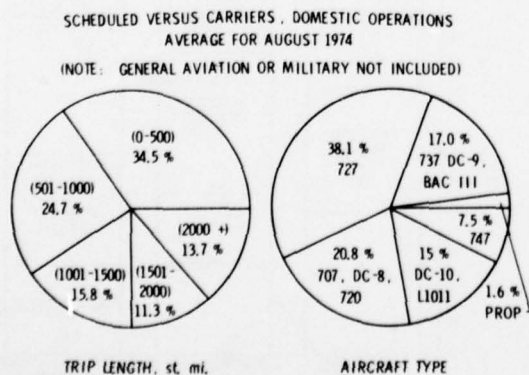


Figure 4. Representative aircraft fuel use distribution.

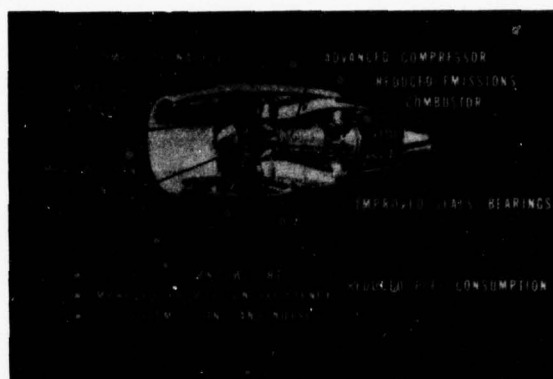
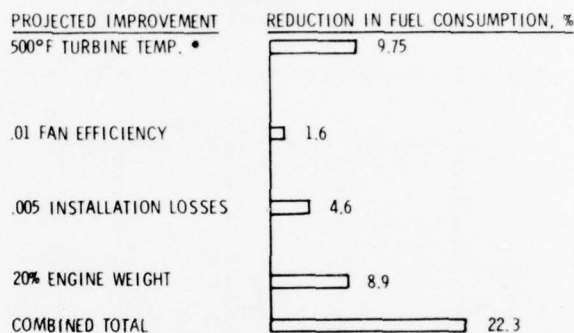


Figure 5. Advance turbofan engine.

1985 ENGINE TECHNOLOGY, MACH 0.85, 200 PASSENGERS,
3000 n. mi., FAR 36 - 10 EPNdB



* ADVANCED FULL-COVERAGE FILM COOLING ALLOWS THIS 500°F INCREASE. OPTIMUM BYPASS RATIO INCREASES FROM 6 TO 10.4 AND OVERALL PRESSURE RATIO FROM 28 TO 40.

Figure 6. Sensitivity of fuel consumption to turbofan improvements.

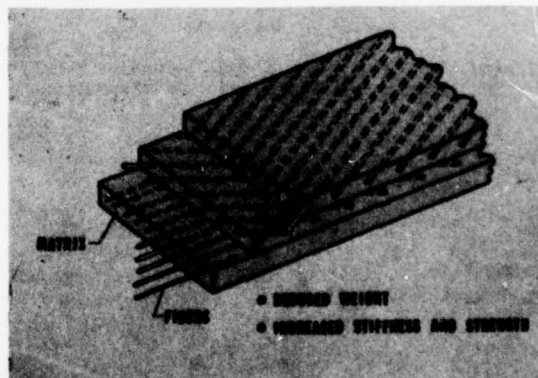


Figure 7. Composite material.

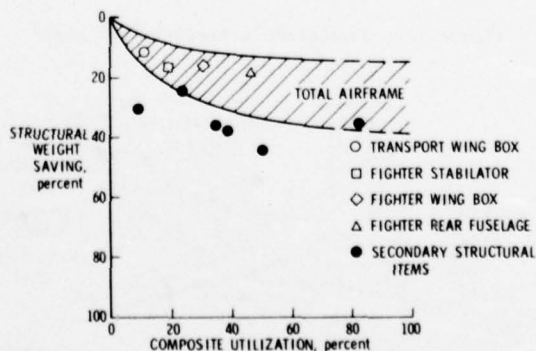


Figure 8. Potential weight savings from composites.

- PERCENT WEIGHT SAVING RELATIVE TO CONVENTIONAL ALUMINUM SKIN STRINGER CONSTRUCTION
- ▨ GRAPHITE-EPOXY HONEYCOMB
- ▤ GRAPHITE-EPOXY INTEGRATED ACOUSTICS STRUCTURE
- PRD-49 HONEYCOMB
- CONVENTIONAL DESIGN
- ▧ STIFFENED GRAPHITE-EPOXY HONEYCOMB

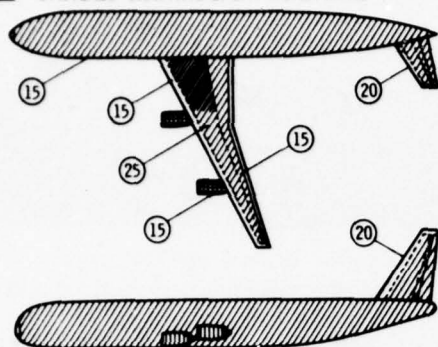


Figure 9. Composite primary aircraft structures.

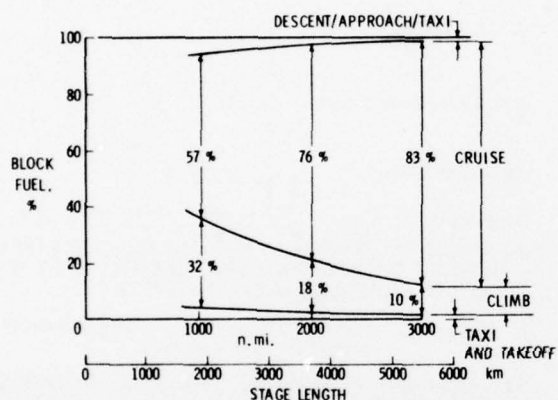


Figure 10. Percentage of fuel burned as a function of flight profile for subsonic transports.

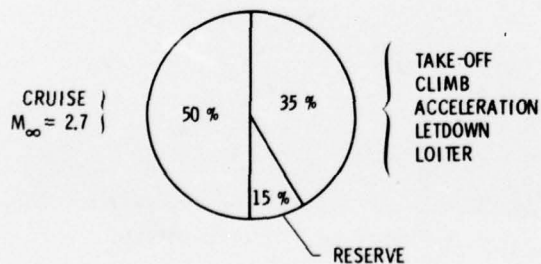


Figure 11. Supersonic transport fuel usage.

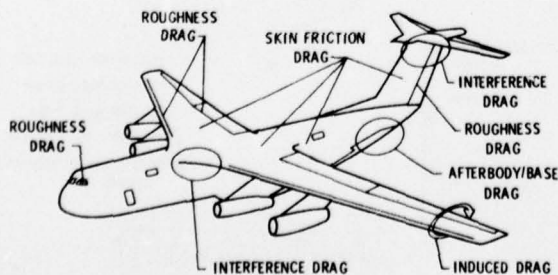


Figure 12. Aircraft drag.

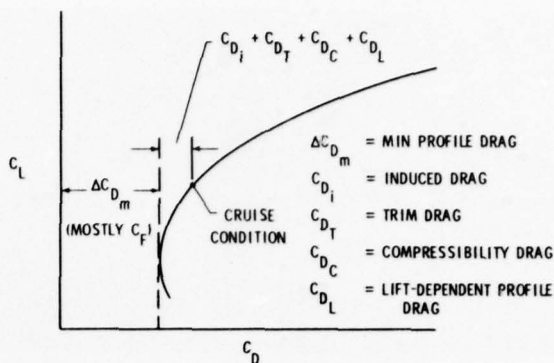


Figure 13. Total aircraft drag.



Figure 14. Conventional aircraft drag breakdown for shock-free flow outside ground effect.

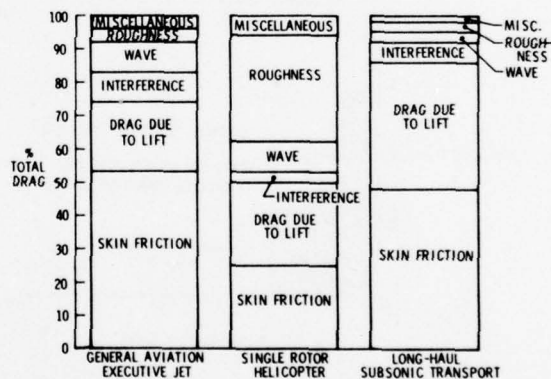


Figure 15. Drag buildup of typical subsonic aircraft configurations.

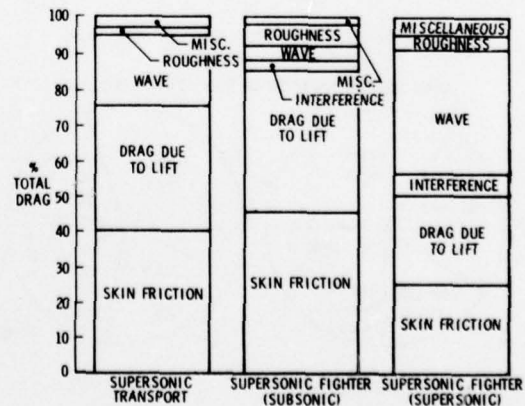


Figure 16. Drag buildup of typical supersonic aircraft configurations.

CONTRIBUTION		ΔC_D
● ANTENNAE		.53
● WINDSHIELD WIPER		.16
● ANTI-COLLISION LIGHT		.01
● JOINTS/STEPS/GAPS		2.73
● EXPOSED FLAP TRACKS		1.60
● APU EXHAUST OUTLET		.02
● BUMPS/BLISTERS/PROTRUSIONS		1.05
● DOORS		.26
● VENTS/PRESSURIZATION LEAKS/AIR COND. I/O		2.30
● WAVINESS/FAIRINGS/MISC.		.42
TOTAL		9.08 $\approx 3.5\%$ OF TOTAL DRAG

Figure 17. Estimates of typical roughness drag contributions for a long-haul cruise aircraft.

BASED ON A RELATIVELY SMOOTH LONG-HAUL TRANSPORT

	% OF TOTAL ROUGHNESS DRAG
● JOINTS/STEPS/GAPS	30
● VENTS/PRESSURE LEAKS/AIR COND. I/O	25
● EXPOSED FLAP TRACKS	17
● BUMPS/BLISTERS	12

Figure 18. Major areas for roughness drag reduction. Based on a relatively smooth long-haul transport.

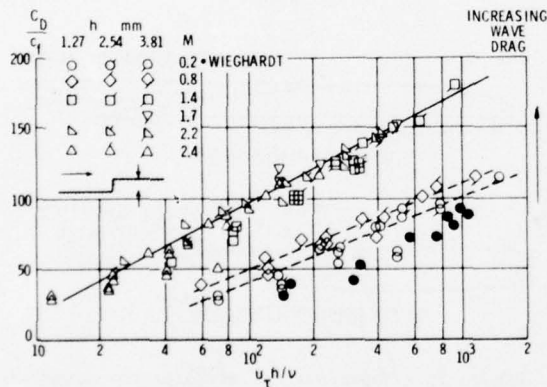


Figure 19. Drag of forward-facing steps.

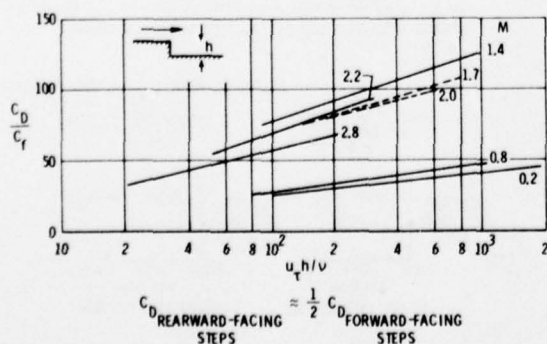


Figure 20. Drag of rearward-facing steps.

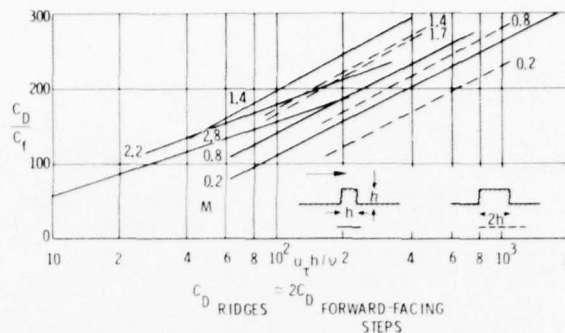


Figure 21. Drag of spanwise ridges.

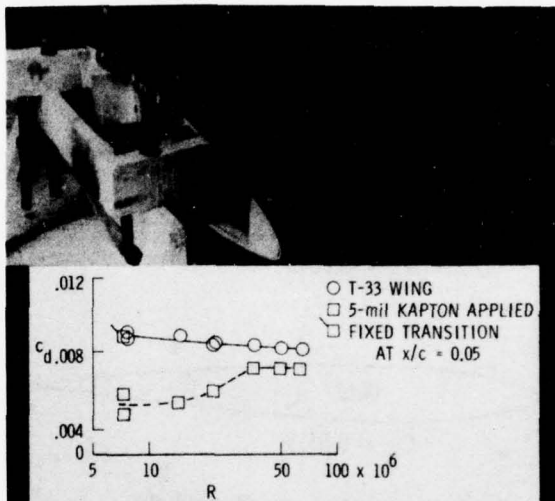


Figure 22. Drag reduction with Kapton coating.

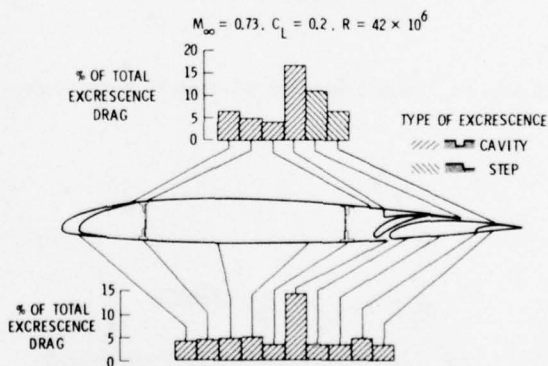


Figure 23. Roughness drag breakdown for a typical medium-range subsonic transport wing.

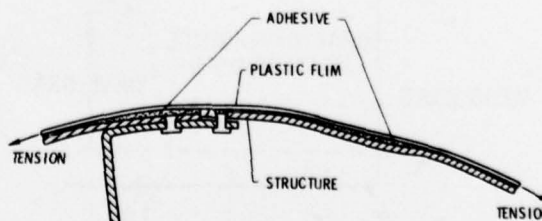


Figure 24. Application of plastic coatings to reduce roughness drag.

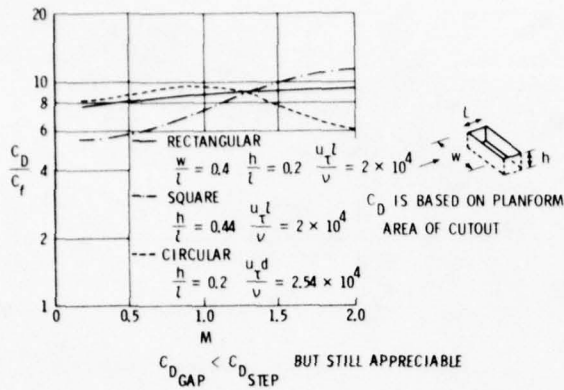


Figure 25. Drag of gaps with no mass transfer.

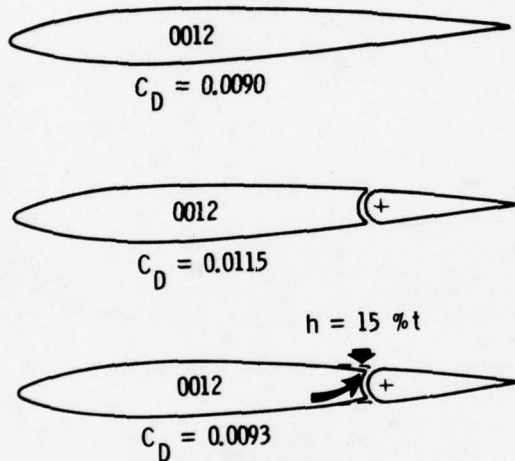


Figure 26. Drag reduction of control surface gap.

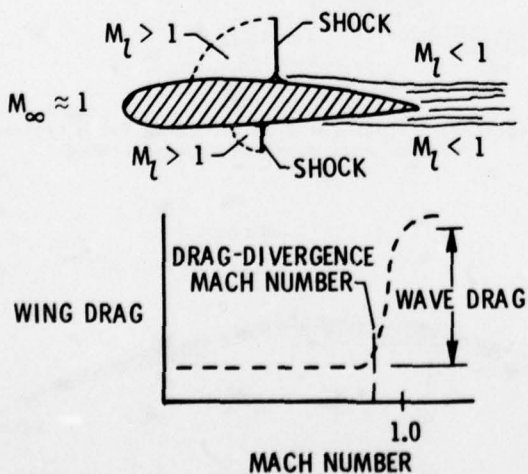
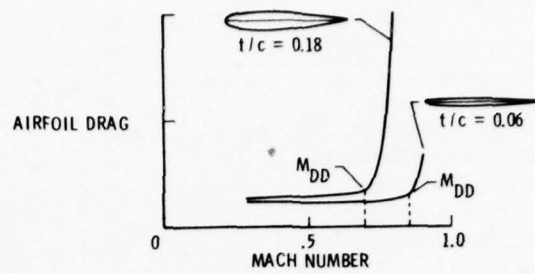


Figure 27. Transonic wave drag.



DISADVANTAGES OF THIN AIRFOILS:

- LOW SUBSONIC LIFT
- LESS STRUCTURAL STRENGTH

Figure 28. Effect of airfoil thickness on transonic wave drag.

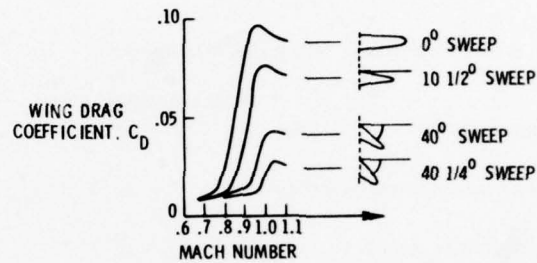


Figure 29. Effect of wing sweep on transonic wave drag.

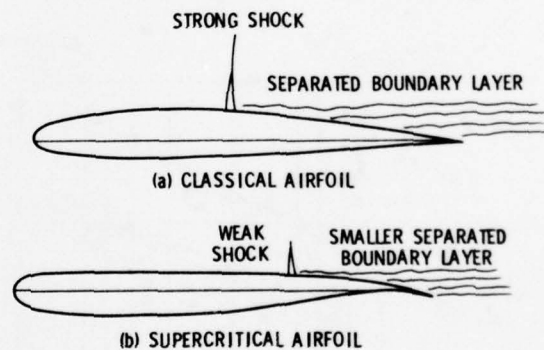


Figure 30. Supercritical airfoils for transonic wave drag reduction.

CONCEPT

- WAVE DRAG MINIMIZED WHEN CROSS-SECTIONAL AREA DISTRIBUTION OF THE AIRPLANE ALONG THE LONGITUDINAL AXIS CAN BE PROJECTED INTO A BODY OF REVOLUTION WHICH IS SMOOTH AND SHOWS NO ABRUPT CHANGES IN CROSS SECTION ALONG ITS LENGTH

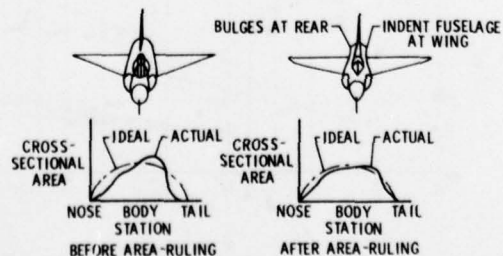


Figure 31. Area-rule concept for transonic wave drag reduction.

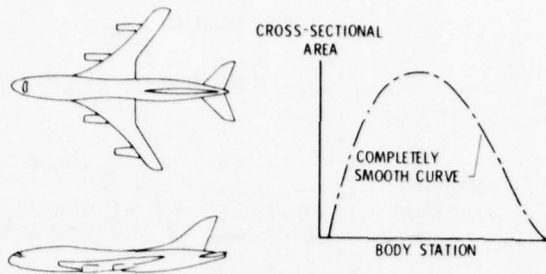


Figure 32. Area ruling for a transonic transport.

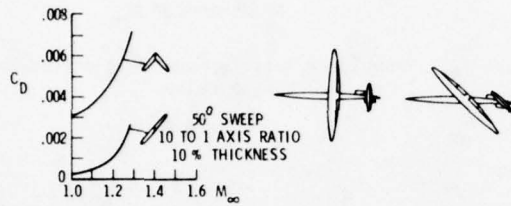


Figure 33. Oblique (antisymmetric) wings for transonic wave drag reduction.

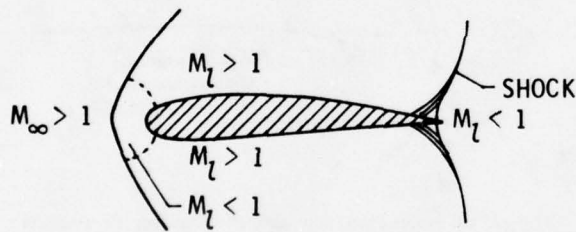


Figure 34. Supersonic/hypersonic wave drag.

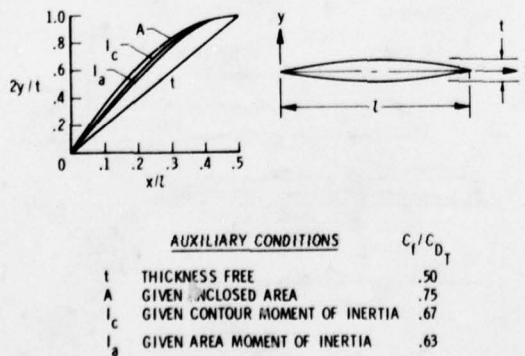


Figure 35. Two-dimensional wings of minimum total drag. Wave drag plus skin friction.

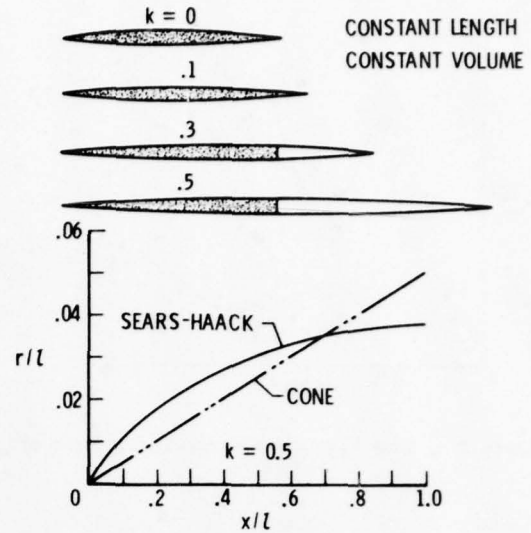


Figure 36. Axisymmetric body optimized for a given length and volume.

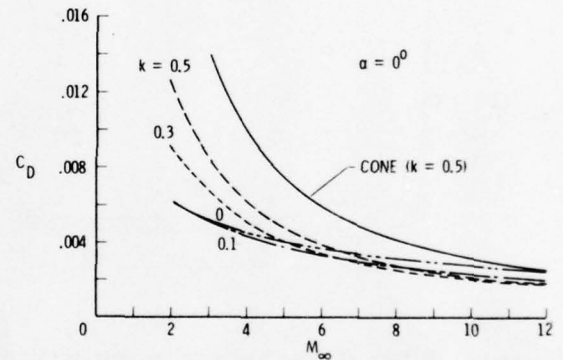


Figure 37. Drag characteristics for Sears-Haack bodies. Wave drag plus base drag plus skin friction.

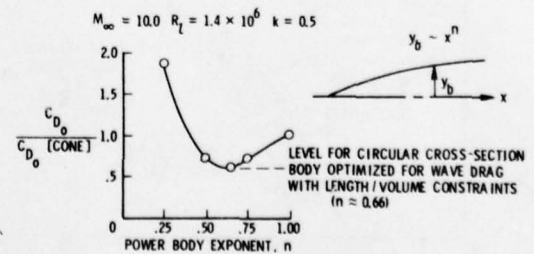


Figure 38. Experimental performance of axisymmetric bodies.

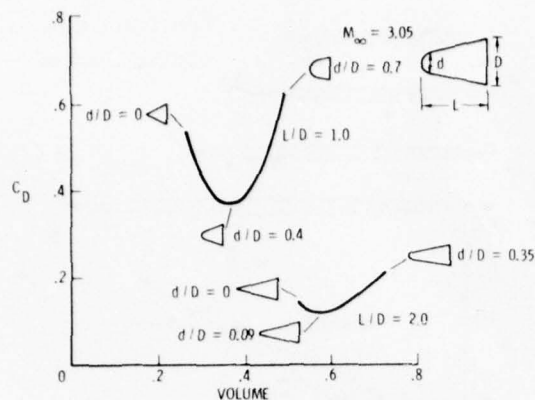


Figure 39. Nose blunting for supersonic wave drag reduction.

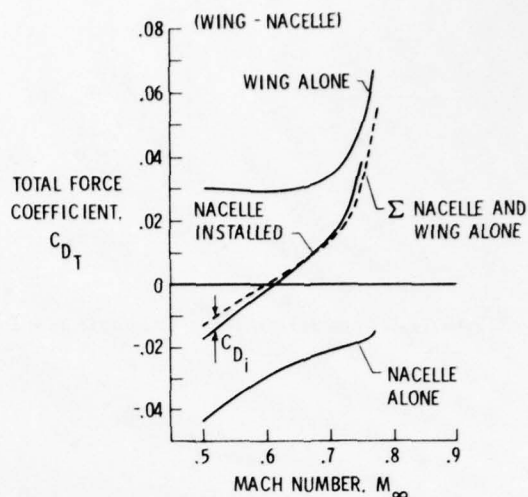


Figure 42. Example of interference drag contributions. Wing nacelle.

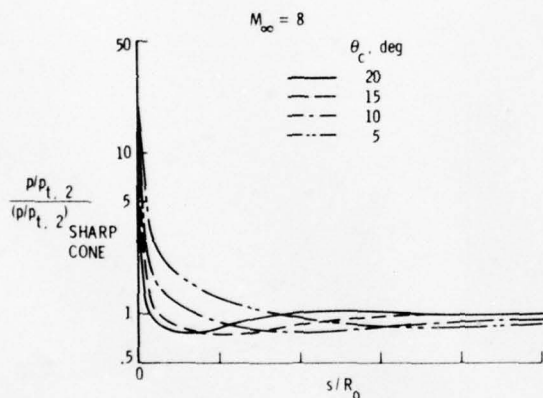


Figure 40. Effect of nose blunting on cone surface pressure distribution. $M_\infty \approx 8$.

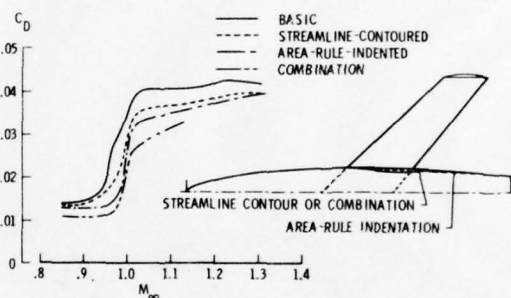


Figure 43. Area ruling and contouring to reduce interference drag.

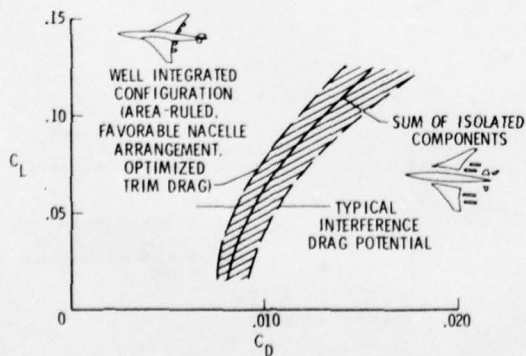


Figure 41. Potential for minimizing interference drag.

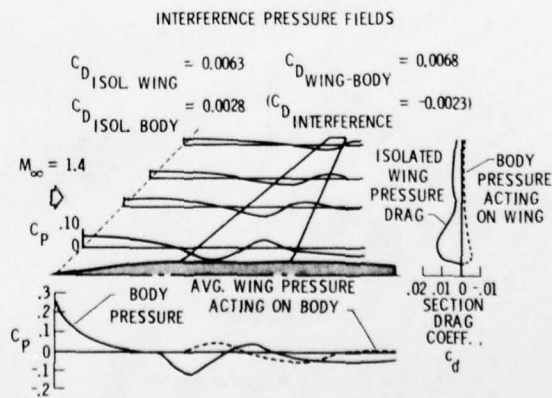


Figure 44. Area ruling to minimize wing-body interference effects. Interference pressure fields.

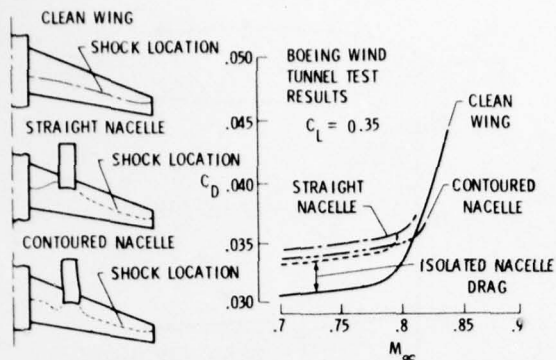


Figure 45. Nacelle contouring to reduce interference drag.

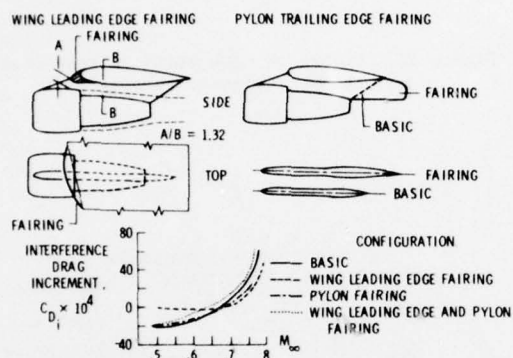


Figure 46. Effect of wing leading-edge fairing and pylon trailing-edge fairing on nacelle-wing interference drag.

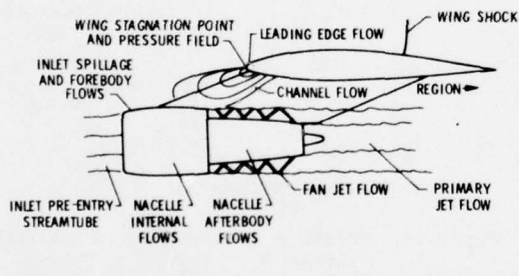


Figure 47. Wing-pylon-nacelle flow field.

CLEAN (A)	UNDER WING (B)	OVER WING (C)	ON WING (D)

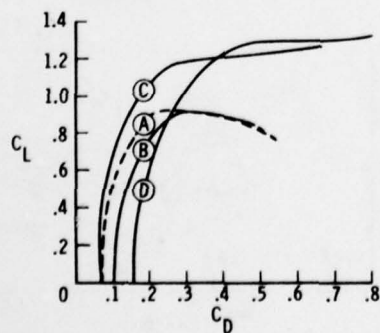


Figure 48. Effect of engine location on jet-wing interference.

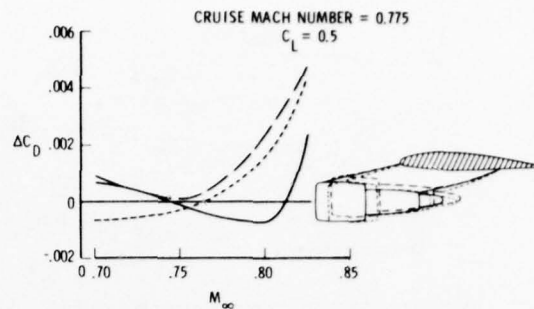


Figure 49. Effect of underwing engine positioning on interference drag.

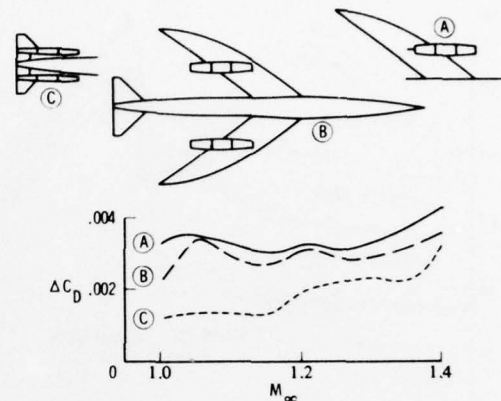


Figure 50. Effect of nacelle installation on interference drag.

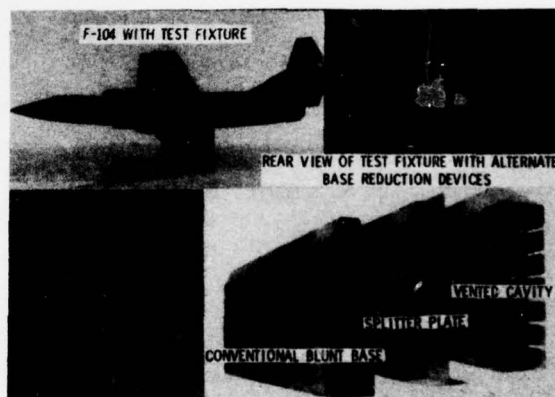


Figure 51. Flight base drag reduction experiment.

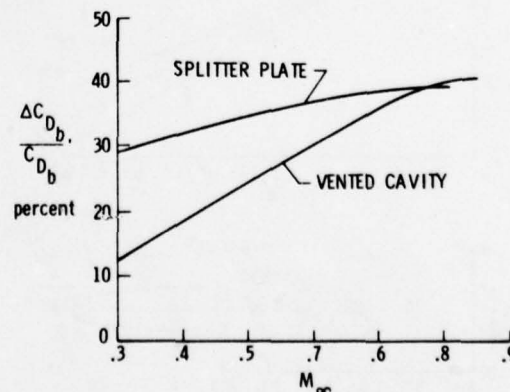


Figure 52. Results of flight experiment for splitter plate and vented cavity configurations.

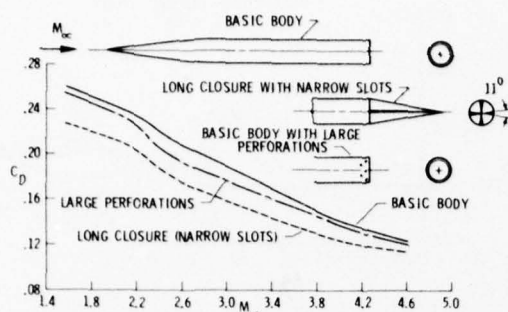


Figure 53. Effect of afterbody modifications on supersonic base drag for axisymmetric bodies.

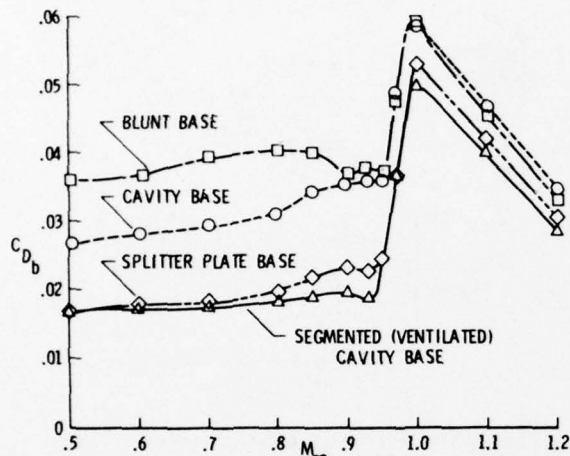


Figure 54. Effect of Mach number on two-dimensional base drag.

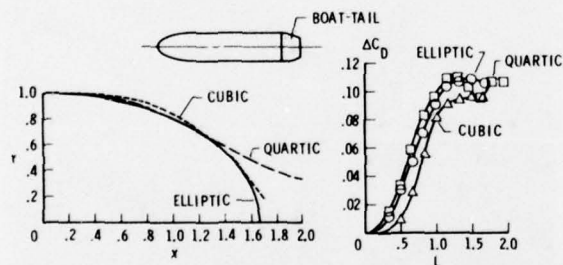


Figure 55. Effect of boattail shape on base drag. Axisymmetric bodies — subsonic speeds.

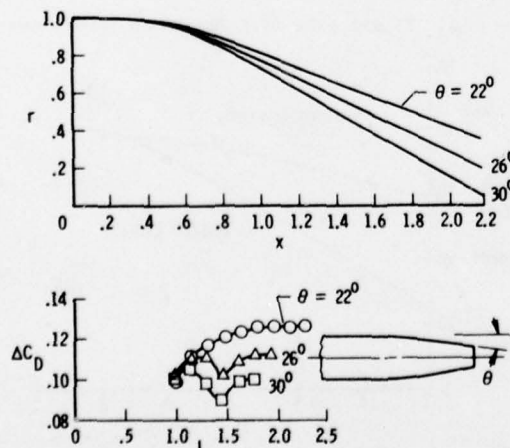


Figure 56. Effect of boattail angle on base drag. Axisymmetric bodies — subsonic speeds.

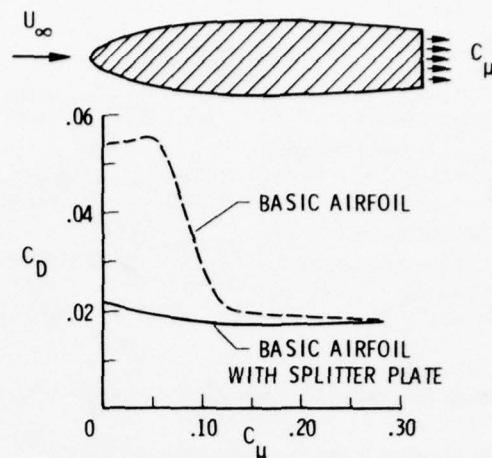


Figure 57. Effect of base bleed on base drag reduction. Subsonic speeds.

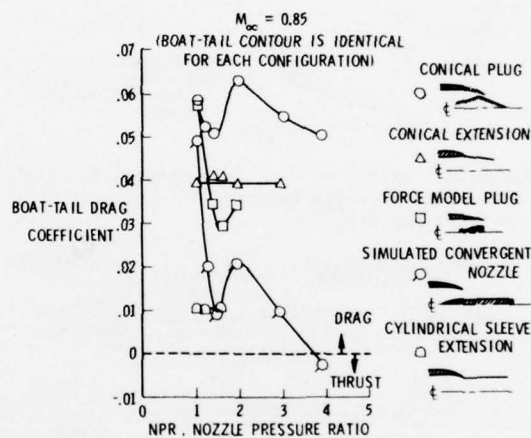


Figure 58. Effect of exhaust flow on boattail drag. $M_{\infty} = 0.85$.

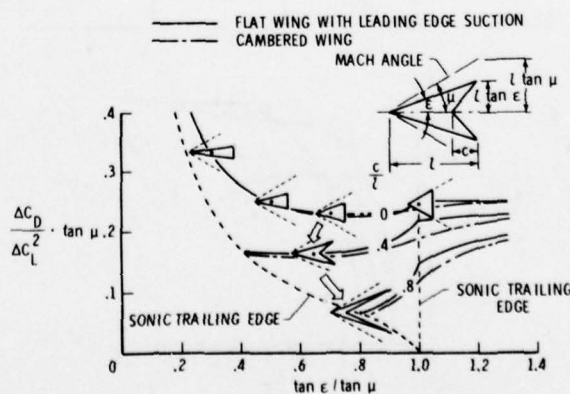


Figure 59. Theoretical drag-due-to-lift factors for supersonic arrow wings.

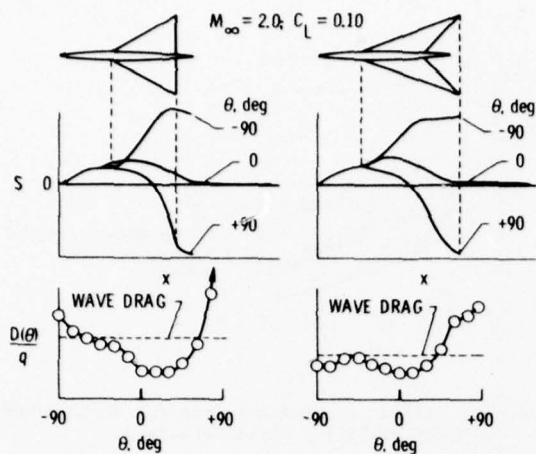


Figure 60. Effects of wing configuration on wave drag due to lift.

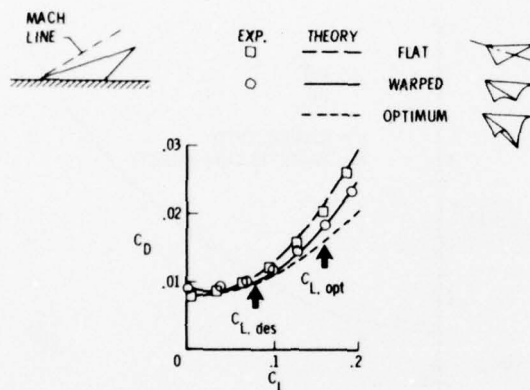


Figure 61. Wing twist and camber (warp) to reduce drag due to lift.

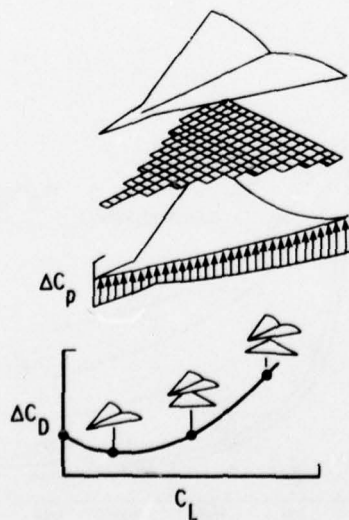


Figure 62. Elements of numerical solutions for drag due to lift.

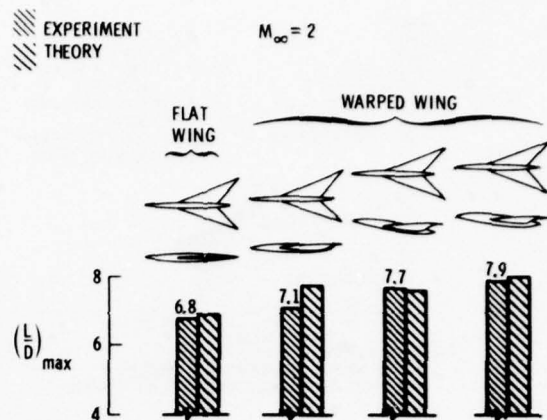


Figure 63. Effect of fuselage alignment.

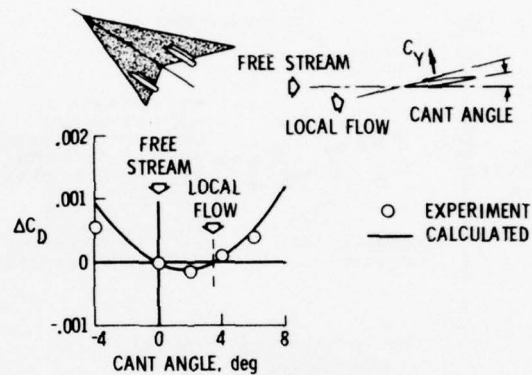


Figure 64. Effect of nacelle alignment.

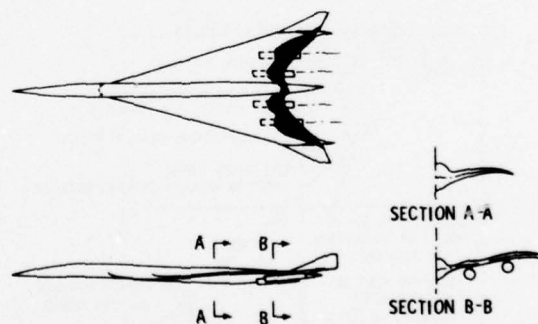


Figure 65. A configuration employing optimized lift design features.

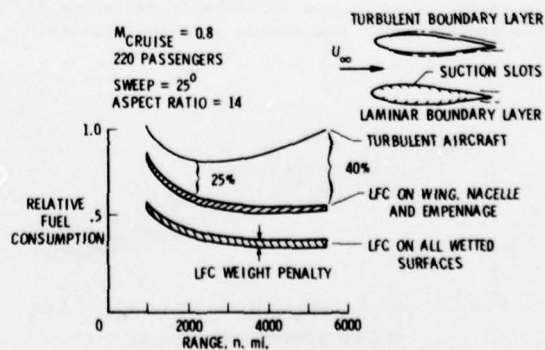


Figure 66. Laminar flow control fuel conservation potential using suction.

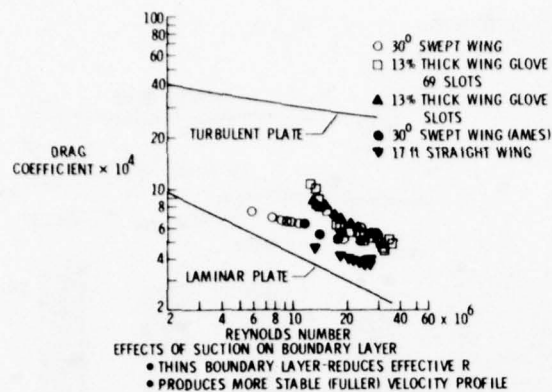


Figure 67. Summary of subsonic LFC results using surface suction.

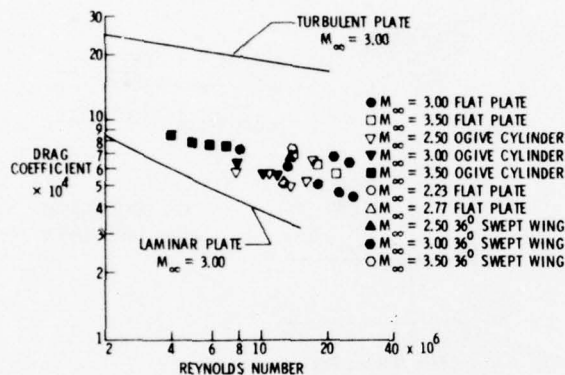


Figure 68. Summary of supersonic LFC results using surface suction.

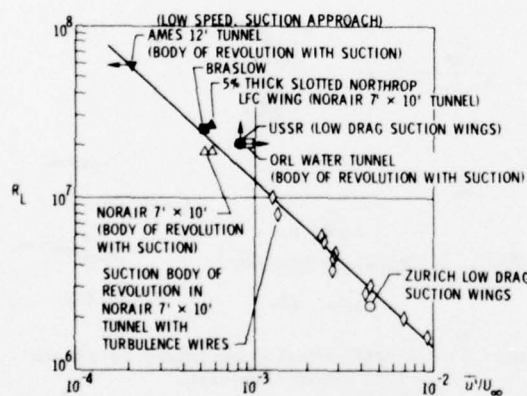


Figure 69. Free-stream disturbance influence on LFC performance. Low speed, suction approach.

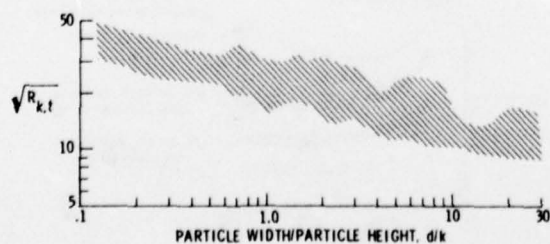


Figure 70. Permissible surface roughness for application of LFC.

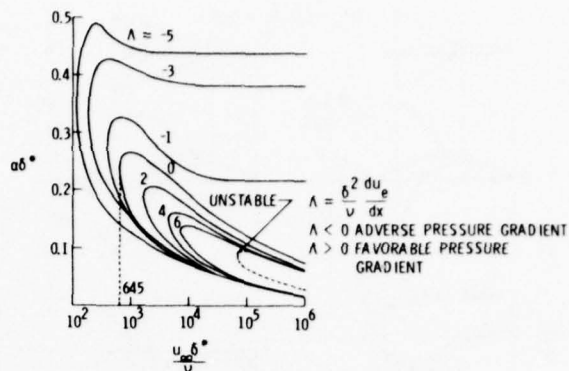


Figure 71. Effect of pressure gradient on boundary-layer stability characteristics.

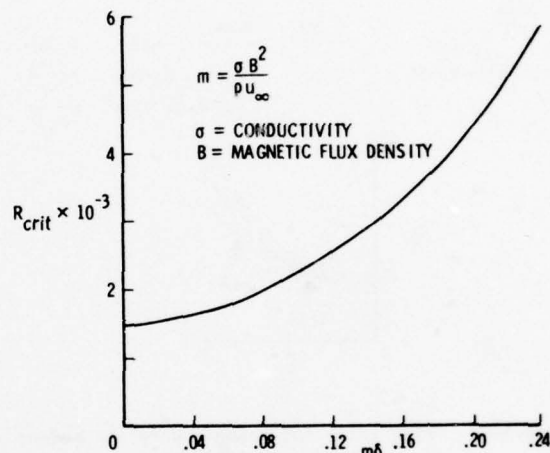


Figure 72. Influence of applied magnetic field upon critical Reynolds number.

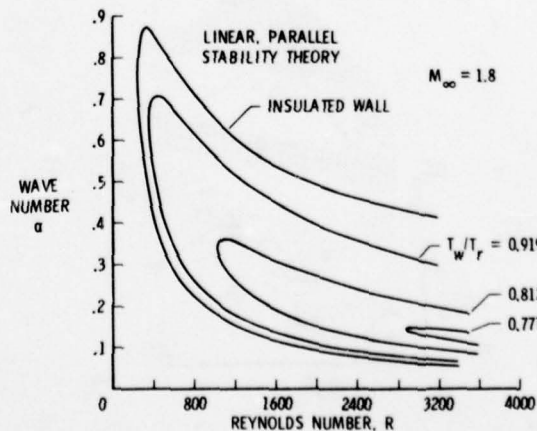


Figure 73. Effect of wall cooling on boundary-layer stability characteristics.

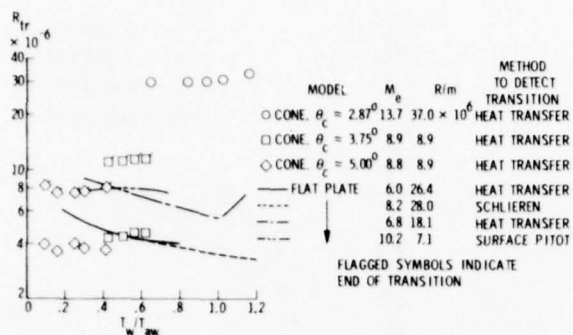


Figure 74. Effect of wall cooling on boundary-layer transition.

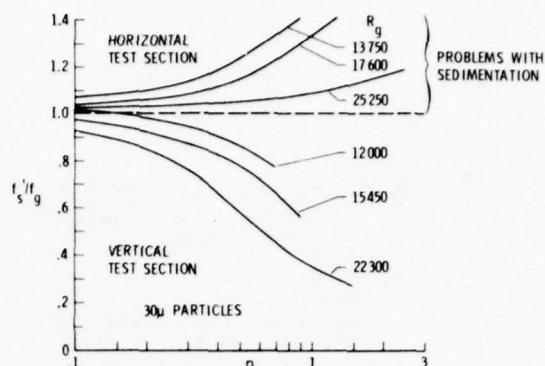


Figure 77. Particle injection for drag reduction in turbulent flows. Gas-solid suspensions in pipe flow.

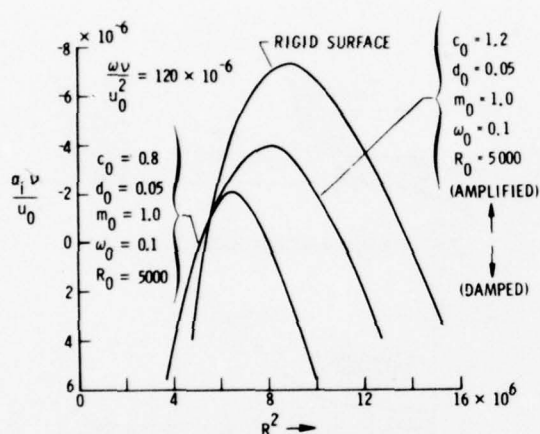


Figure 75. Effect of compliant walls on boundary-layer stability characteristics.

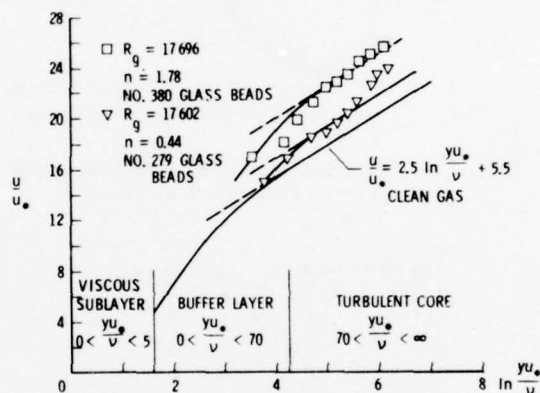


Figure 78. Influence of drag reducing particle suspension on turbulent velocity profiles. Pipe flow.

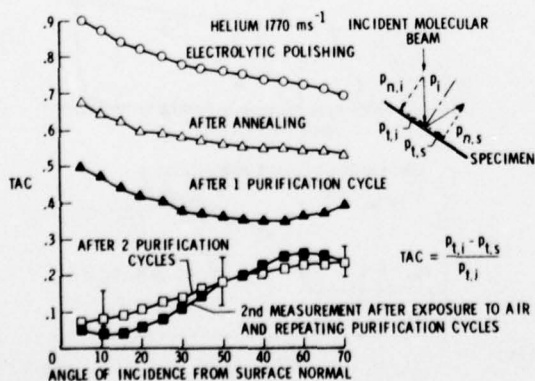


Figure 76. Effect of surface polishing on tangential accommodation coefficient.

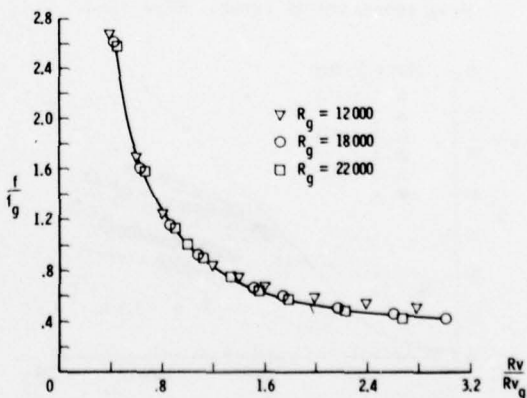


Figure 79. Correlation of particle-induced drag reduction with sublayer thickness.

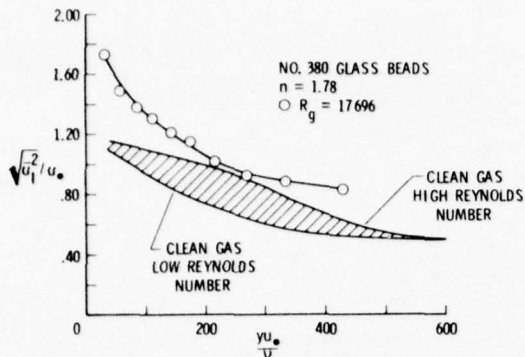


Figure 80. Influence of drag reducing suspension on turbulent energy.

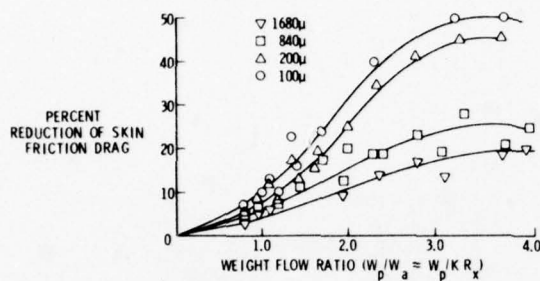


Figure 81. Skin-friction drag reduction using particles. Flat plate in air.

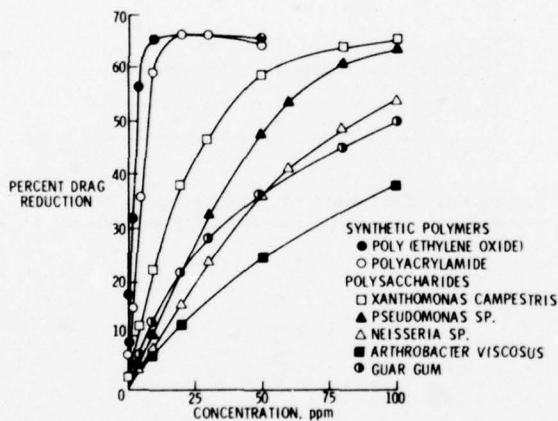


Figure 82. Effect of various polymer additives on drag reduction in water. Pipe flow.

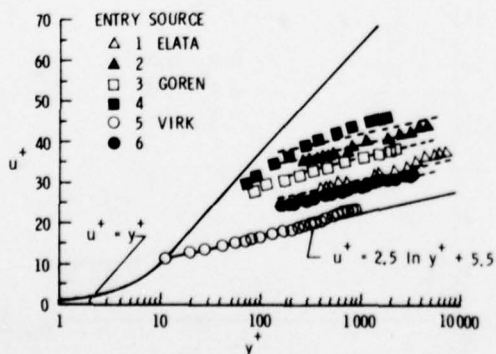


Figure 83. Velocity profiles for polymer drag reduction cases.

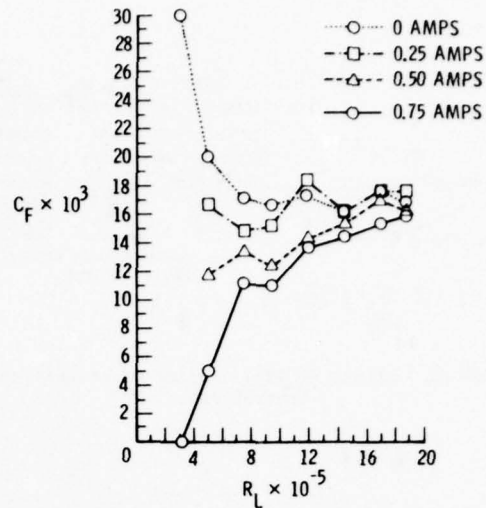


Figure 84. Effect of water electrolysis on drag.

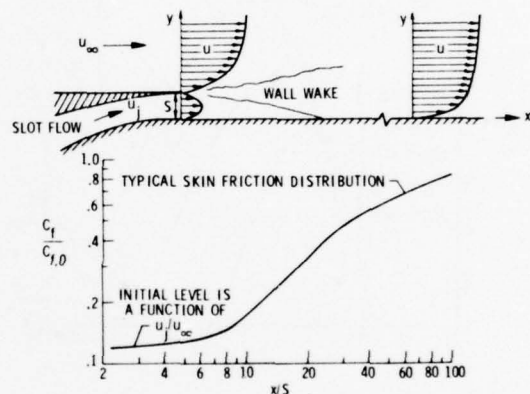


Figure 85. Skin-friction drag reduction by tangential slot injection.

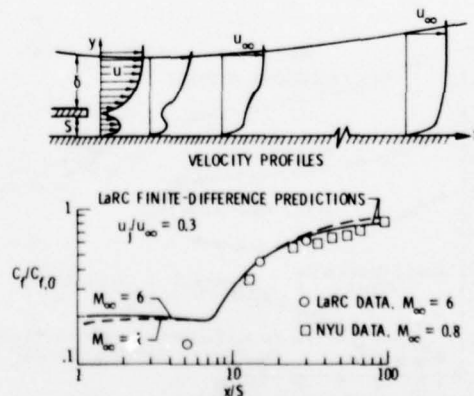


Figure 86. Comparison of skin-friction reduction downstream of slot injection into subsonic and supersonic flows.

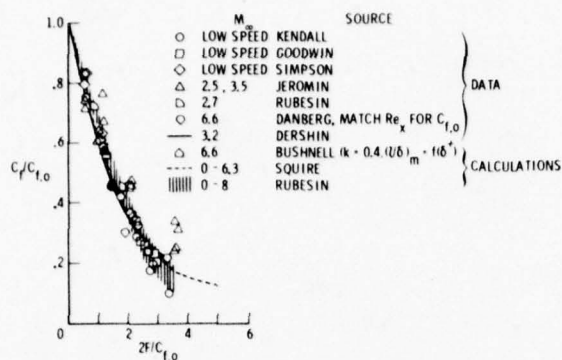


Figure 87. Influence of wall injection on turbulent skin friction.

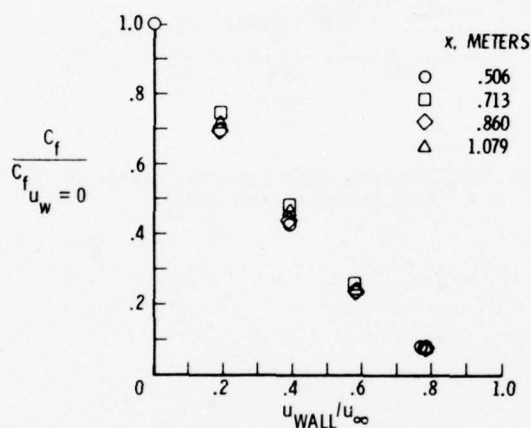


Figure 88. Skin-friction drag reduction with rectilinear wall motion.

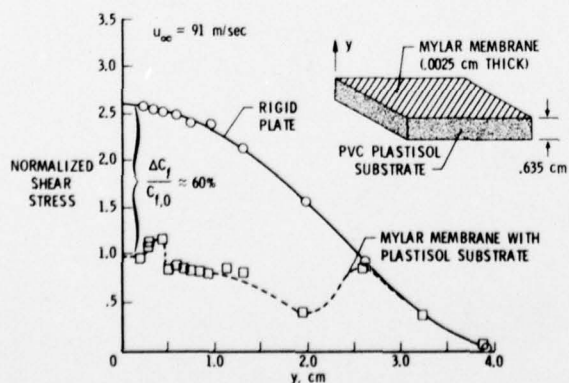


Figure 89. Effect of compliant walls on turbulent shear stress.

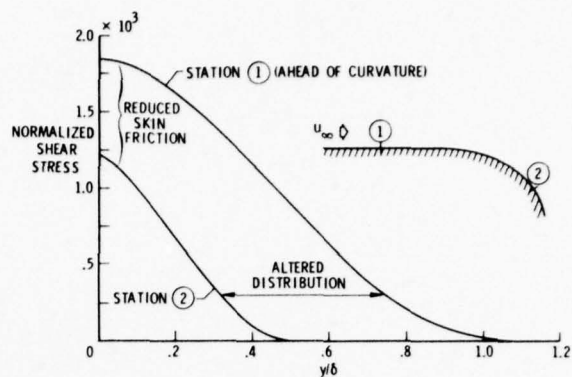


Figure 90. Influence of convex curvature on turbulent shear stress.

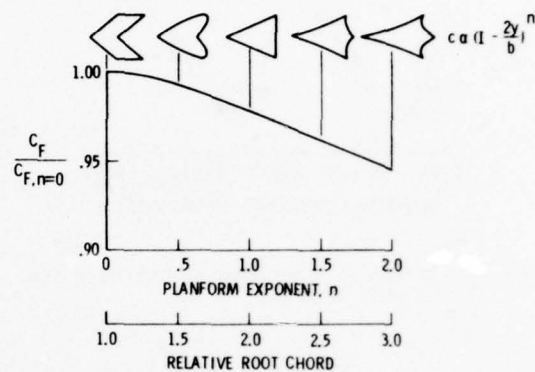
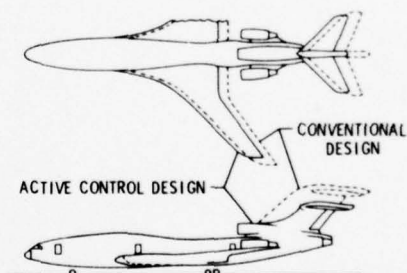


Figure 91. Effect of wing planform on skin-friction drag.



REDUCED TAIL/WING AREA RESULTS IN REDUCED SKIN FRICTION DRAG

Figure 92. Influence of active controls on size of tail control surfaces.

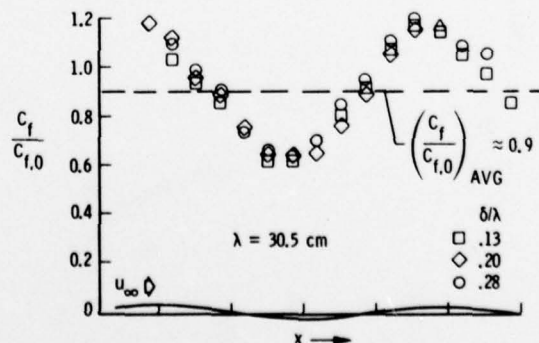


Figure 93. Effect of transverse stationary waves on skin friction. $\delta < \lambda$.

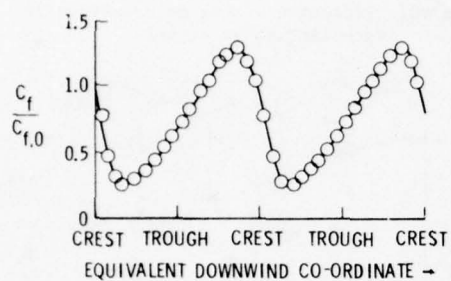


Figure 94. Effect of transverse stationary waves on skin friction. $\delta \approx \lambda$.

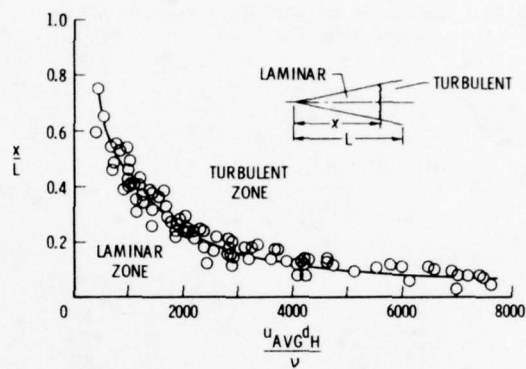


Figure 95. Possible drag reduction mechanism for flow in noncircular ducts.

METHODS FOR REDUCING SUBSONIC DRAG DUE TO LIFT

Dr. R. T. Whitcomb
 NASA Langley Research Center
 Hampton, Virginia 23665
 U.S.A.

SUMMARY

The results of recent experimental research at the NASA Langley Research Center on methods for reducing subsonic drag due to lift are discussed. First, the NASA supercritical airfoils and their application to structurally practical wings with increased aspect ratio are described. Also, a design approach and experimental results for wing-tip-mounted winglets are presented. In addition, several methods for utilizing the thrust of jet engines to provide reductions in the drag due to lift are discussed.

1. INTRODUCTION

The drag due to lift of a finite span wing is usually due primarily to the induced drag associated with the shedding of vorticity along the span and, in particular, at the tip. It is also due in part to an increase in the skin friction and form drag associated with an increase in the lift coefficient. For most airplane configurations, this drag due to lift is between 40 and 50% of the total drag at near cruise conditions. Considerable experimental research has been conducted at the NASA Langley Research Center in recent years on means for reducing drag due to lift. In this research, substantial attention has been given to practical aerodynamic and structural considerations. Among the approaches that will be discussed are practical methods for achieving increases in the aspect ratio for configurations designed for flight at high subsonic speeds through the utilization of NASA supercritical airfoils, strut brace wings, advanced composite structural materials, and active load relief. Also discussed are wing-tip-mounted winglets and the exploitation of the effects of the thrust of fan-jet engines on the induced drag. The discussion is limited to research conducted at subsonic speeds.

2. INCREASED ASPECT RATIO

It has been recognized for several generations that the induced drag can be reduced by increasing the aspect ratio, however, the aspect ratio that is utilized in actual airplane configurations is usually constrained by practical considerations, particularly those associated with the wing structural weight. When the aspect ratio is increased, the bending moments in the wing structure also increase with the resulting requirement for more structural material in the wing. Since the performance of the airplane is determined by the structural weight as well as the aerodynamic efficiency, the optimum aspect ratio for the best overall performance must be a compromise. The optimum compromise aspect ratio varies depending on the particular mission of the aircraft. For example, for the present generation of high subsonic speed jet transport wings the aspect ratios are approximately 7; for fighter aircraft the aspect ratios are roughly 4; for supersonic cruise aircraft the aspect ratio is even lower; for long-range, but not necessarily high-speed aircraft such as sea search types, the aspect ratios have been about 10; for sailplanes the aspect ratios may be as high as 25.

For cantilever wing structures, the structural material that must be incorporated in the wing to withstand the bending moments imposed on the structure is reduced by an increase of the wing depth or, in aerodynamic terms, the thickness-to-chord ratio of the airfoil sections. However, it has long been known that increasing the thickness ratio also substantially increases the transonic and supersonic drag of a wing. Thus the optimum thickness ratio for high-performance wings is a compromise between the aerodynamic and structural considerations. For progressively higher speed configurations, the optimum compromise thickness ratio and, as a result, the optimum compromise aspect ratio generally progressively decreases. If means are developed for reducing the adverse aerodynamic effects associated with an increase in thickness ratio, such as NASA supercritical airfoils, then the optimum compromise thickness ratio can be increased with a resulting increase in the optimum compromise aspect ratio. Further, if means are developed for reducing the stresses in the wing associated with the bending moment or if new structural materials with improved strength-weight ratios are made practical then the optimum compromise aspect ratios also can be increased.

When the aspect ratio is increased, the optimum lift coefficient for the wing also increases. Thus, for higher aspect-ratio wings, the airfoil must be shaped to prevent excessive form drag at the higher lift coefficients.

3. NASA SUPERCRITICAL AIRFOILS

3.1 General Characteristics

Description. The NASA supercritical airfoil shapes are characterized by substantially reduced curvature of the middle region of the upper surface with a large amount of camber near the trailing edge. Also, the leading-edge radius is larger than previously used and the trailing-edge closure angle is very small. (See Fig. 1.)

Flow Phenomena at Design Condition. A comparison of the supercritical flow phenomena for the NASA supercritical airfoil and an NACA 6-series airfoil at the cruise lift coefficient is presented in Figure 1. For the NACA 6-series airfoil, as shown at the top of the figure, the supersonic flow accelerated to the

shock wave. This wave is followed immediately by a subsonic pressure recovery to the trailing edge. The energy loss in the shock causes some drag increase. However, the dominant problem is severe boundary separation caused by the large, steep total streamwise pressure increase. This separation, of course, produces the well-known abrupt drag rise, buffeting, and stability problems.

The surface pressure distribution and flow field shown at the bottom of Figure 1 are representative of those obtained for NASA supercritical airfoils. The upper surface pressure and related velocity distributions are characterized by a shock location significantly aft of the midchord, an approximately uniform supersonic velocity from about the 5% chord station to the shock, a plateau in the pressure distribution rearward of the shock, a relatively steep subsonic pressure recovery on the extreme rearward region, and a trailing-edge pressure near ambient. The lower surface has roughly constant negative pressure coefficients corresponding to subcritical velocities over the forward region and a rapid increase in pressure rearward of the midchord to a substantially positive pressure forward of the trailing edge.

The elimination of the flow acceleration on the upper surface ahead of the shock wave, which results primarily from the reduced curvature of the midchord region, obviously provides a reduction of the Mach number ahead of the shock for a given lift coefficient with a resulting decrease of the shock strength. The strength and extent of the shock at the design condition can be reduced below that for the pressure distribution shown by shaping the airfoil to provide a gradual deceleration of the supersonic flow from near the leading edge to the shock wave.¹⁻³ However, such a shape may have an increased drag at lower Mach numbers. Extensive experiments indicate that the shape associated with the design point distribution shown provides acceptable drag values over the Mach number and lift-coefficient range.

The plateau in the pressure distribution rearward of the shock wave allows a reenergization of the boundary layer by mixing after it moves through the severe adverse pressure gradient of the shock and before it moves through the pressure gradient near the trailing edge. As a result, the boundary layer can move through a greater total pressure rise without separating. The importance of this effect is shown by the experimental data to be presented later. The near-ambient pressure at the trailing edge, which results from the small included angle of the trailing edge, reduces to a minimum the total pressure rise the upper surface boundary layer must traverse and thus minimizes the tendency toward separation.

The maintenance of subcritical flow over the forward region of the lower surface eliminates the possibility of a shock wave on that surface. The pressure rise of a possible shock wave superimposed on the pronounced pressure rise on the rear portion of this surface would greatly increase the tendency for the boundary layer to separate. The streamwise pressure increase rearward of the midchord is defined by the Stratford criteria.⁴ The substantially positive pressure on the rear part of the lower surface, associated with the surface concavity of this region, provides a substantial increase in the circulation around the airfoil with a resulting reduction in the angle of attack required to achieve the design lift coefficient. Usually, this angle is slightly negative (about -0.5°). With this negative angle of attack, the crest (the maximum vertical coordinate with respect to the free airstream) of the upper surface is near the midchord. This factor together with the reduced curvature of the midregion of the upper surface, results in favorable chordwise forces associated with the supersonic flow region, even with the rearward shock location. The significance of the distribution of the chordwise forces for supercritical flow is discussed in Reference 1.

Theory and experiments indicate that with the upper surface pressure distribution shown and at the negative angle of attack required to obtain the design lift coefficient the vertical extent of the supersonic field decreases ahead of the shock wave as shown on the left in Figure 1. This effect is similar to that for airfoils designed specifically to minimize the extent of the shock at the design point¹⁻³ although, in this case, the effect is somewhat smaller. The flow-field calculations of Reference 3 illustrate the origin of this effect.

The relatively large leading-edge radii of the NASA supercritical airfoils allow simultaneous reductions of the curvatures of the midchord regions of both the upper and lower surfaces with resulting reductions of the induced velocities.

Experimental Results. A comparison of the drag variation with Mach number at a normal-force coefficient of 0.7 for a 10% thick conventional airfoil (NACA 64A-410) and two 10% thick versions of the NASA supercritical airfoils is shown in Figure 2. The early supercritical airfoil for which results are shown is similar to that used for all applications from 1967 to 1973. The abrupt drag rise for this airfoil is more than 0.1 Mach number later than that for the 6-series airfoil. This early supercritical airfoil experienced a drag creep at Mach numbers below the abrupt drag rise. This drag is associated with relatively weak shock waves above the upper surface at these speeds.

Much of the recent work at Langley has been devoted to the elimination of this undesirable drag creep, and the solid curve of Figure 2 shows an example of the results of these efforts. Refinements to the airfoil were involved primarily with changes which resulted in a more favorable flow over the forward region of the upper surface and the elimination of the region of flow overexpansion near the three-quarter chord location on the upper surface. A slight loss in force-break or drag-divergence Mach number is noted (about 0.015) as a result of slight increased wave losses at the higher Mach numbers, but this compromise is felt to be of little consequence relative to the gains achieved in eliminating drag creep. It should be noted that, unlike the early work, the shaping changes used in the design of the recent airfoils were guided in part by the use of the recently developed analytical program of Reference 5 to achieve desired pressure distributions for the various cases.

Recent airplane designs incorporate airfoils with somewhat higher drag rise Mach numbers than for the NACA 6-series shown here. However, it has been difficult to acquire two-dimensional data for such airfoils. Results obtained with a C-5A airplane model in the Langley Research Center 8-foot tunnel indicate that one of these new shapes, the Pearcey "peaky" airfoil, delays the drag-rise Mach number 0.02 or 0.03 compared with the NACA 6-series airfoils but at a loss in the maximum lift.

Flow Phenomena at Off-Design, Subcritical, and High-Lift Conditions. At a Mach number slightly above the design value (Fig. 3) the shock wave location is rearward of that for the design condition with a small

acceleration ahead of the wave. This change causes a slight increase in the shock losses but does not result in boundary-layer separation. Separation occurs when the shock wave moves farther rearward and the pressure plateau described earlier is eliminated.

At a Mach number just below the design value (Fig. 4) the shock location is significantly farther forward than for the design condition and the flow experiences a reacceleration rearward of the shock with a supercritical peak velocity near the 75% chord station. This reacceleration causes a substantially greater and steeper pressure increase to the trailing edge as compared with the design condition. This steeper recovery results in a small adverse effect on the trailing-edge pressure recovery and drag. For unslopped airfoils designed to achieve a shockless design condition³, the reacceleration velocity can be sufficiently great to cause a second rearward shock wave.⁶ The total pressure rise of this second shock and the immediately following subsonic pressure recovery may cause significant boundary-layer separation near the trailing edge.

At subcritical Mach numbers (Fig. 5) the pressure distribution has a significant peak near the leading edge. The presence of this peak results in a small drag increment for subcritical and slightly supercritical conditions. If an airfoil is shaped to provide a decelerating supersonic velocity distribution on the upper surface at the design condition as discussed earlier, this subcritical peak is substantially greater than that shown with a resulting increase in the drag for the subcritical and slightly supercritical conditions.

Theoretical Analyses. Considerable progress has been made during the last 3 years in providing theoretical methods for the design and analysis of two-dimensional airfoils at supercritical Mach numbers. No attempt will be made to cover all this work, instead, the method being used at Langley in a continuing effort on supercritical airfoils will be described.

The initial comparisons of theoretically derived pressure distributions on NASA supercritical airfoils with experimental results indicate very poor agreement. The differences are associated with the development of the boundary layers on these airfoils, illustrated in Figure 6. The steep pressure rise near the trailing edge of the upper surface causes the boundary layer to thicken significantly. On the lower surface the pressure rise from about the 0.5 to the 0.9 chord results in a substantial thickening of the boundary layer in the cusp while the rapid pressure decrease near the trailing edge causes a pronounced thinning of the boundary layer. Each of these effects contributes to a substantial reduction of the effective aft camber of the airfoil. It was concluded that for NASA supercritical airfoils any analytic method must include the effect of the boundary layer.

Recently, an analytic method which includes the effect of the boundary layer has been developed.⁵ This iterative procedure is based on the method of Korn and Garabedian⁷ for analyzing the external supercritical field, which implements a mixed finite-difference scheme related to that of Murman and Cole.⁸ A similar method was also developed by Jameson.⁹ The coordinate system shown in Figure 7 was suggested by Sells¹⁰ and consists of mapping the interior of the unit circle conformally onto the exterior of the airfoil with the point at infinity corresponding to the origin. These flow-field computations are made for airfoil shapes modified by the calculated displacement thicknesses of the upper and lower surface boundary layers. Since the boundary-layer calculations are not applicable near the trailing edge, an empirical correction is applied for this region.

The effect of including the boundary layer on analytical predicted pressure distributions for a NASA supercritical airfoil is illustrated in Figure 8. These comparisons are for lift coefficients substantially greater than the design value. At a subcritical Mach number, including the effect of the boundary layer causes a moderate change in the predicted lift. However, at a supercritical Mach number including the effect of the boundary layer results in substantial changes of the position of the shock wave and the lift. Comparisons of theoretical pressure distributions obtained by this method with experimental distributions for a NASA supercritical airfoil at a subcritical and a supercritical condition are presented in Figures 9 and 10, respectively. Again, these comparisons are for lift coefficients substantially greater than the design value. In both cases, the agreement is quite good. The difference in pressures just rearward of the shock wave for the supercritical condition (Fig. 10) is due to the fact that the field calculation underpredicts the pressure jump through the shock. Recently, Jameson has solved this problem and the method is now being modified to incorporate his solution. It should be noted that the airfoil shapes shown at the bottom of these figures include the displacement thicknesses of the upper and lower surface boundary layers.

3.2 Flight Demonstration Program

Because of the drastically different nature of the flow over the NASA supercritical airfoil, there was considerable concern as to how the new shape would operate in actual flight. Therefore, the several United States government agencies responsible for aircraft, that is, NASA, the Air Force, and the Navy, undertook a coordinated, three-part flight demonstration program. The program was to evaluate the application of the new airfoil to a swept, long-range transport wing configuration, a thick wing, and a variable-sweep fighter wing. In each case, existing military aircraft were used as test beds. However, in none of the cases was it intended the test wing would be applied to production versions of these aircraft. The transport supercritical wing configuration was flown on a Navy F-8 fighter (Fig. 11). The wing configuration for this program was designed for increased speed ($M = 0.98$) rather than improved aerodynamic efficiency. Wind-tunnel and flight results obtained during this program are presented in Reference 11. The other two flight demonstration programs will be described later.

3.3 Increased Thickness-to-Chord Ratio

As indicated earlier, increasing the thickness-to-chord ratio leads to increased drag at transonic and supersonic speeds. The onset of the drag rise as discussed in the previous section also occurs earlier. This is illustrated in Figure 12. If the thickness ratio for a wing intended for flight near the drag rise is increased to allow a higher aspect ratio, the speed of the aircraft must be reduced or the wing sweep must be increased. Increasing the wing sweep leads to added structural weight for a given aspect ratio and a loss of lift for landing and take-off. As indicated in the previous section, the NASA supercritical

airfoil provides a higher drag rise Mach number for a given thickness ratio. It also allows an increase in thickness ratio for a given drag rise Mach number as illustrated in Figure 12. Therefore, for a given airplane speed, the use of such an airfoil allows a higher optimum compromise aspect ratio.

A 17% thick supercritical airfoil designed by Palmer of the Rockwell International Columbus Division in 1969 is shown in Figure 13. Wind-tunnel results obtained for a model of a T-2C Navy trainer incorporating this airfoil are shown in Figure 14. The data are compared with that for the original T-2C configuration which had a 12% thick NACA 6-series airfoil. The drag rise for the 17% supercritical airfoil is approximately the same as that for the original 12% thick airfoil. This thicker supercritical airfoil was flight tested on the T-2C. A comparison of the flight vehicle incorporating the thicker supercritical airfoil with an original airplane configuration is shown in Figure 15. The results of the flight program verified the wind-tunnel data. A summary of the flight results for this configuration is presented in Reference 11.

Since the airfoil shown in Figure 13 was designed, considerably improved thick supercritical airfoils have been design and investigated at the Langley Research Center. In particular, the drag creep indicated in Figure 15 has been eliminated.

3.4 Increased Design Lift Coefficient

As indicated earlier, if the aspect ratio is increased the design lift coefficient for a wing must also be increased. Also, for fighter aircraft which are intended to maneuver at very high lift coefficients the airfoil shape must be designed to achieve the lowest possible form drag at these high lift coefficients. The supercritical airfoil not only allows a greater thickness-to-chord ratio for a given drag rise Mach number but it also can be used to reduce drag at substantially increased lift coefficients.

The advantage of the supercritical airfoil at higher lift coefficients is illustrated in Figure 16. The onset of drag rise versus lift coefficient for the supercritical airfoil described in the previous section is compared with that of a comparable NACA 6-series airfoil. These results indicate that not only does the supercritical airfoil delay the drag rise at the usual cruise design lift coefficients of approximately 0.6 but it also delays the drag rise at much higher lift coefficients. Further, it increases the maximum lift coefficients available at the knee of the drag rise curve.

The phenomena associated with the increased maximum lift coefficient provided by the supercritical airfoil are illustrated in Figure 17. The pressure distribution shown is that measured at the high lift corner of the variation of normal force for separation onset with Mach number for an 11% thick early supercritical airfoil. The shock wave, associated with a local upstream Mach number of 1.4, causes a very large adverse pressure gradient. However, the trailing-edge pressure recovery and a surface oil-flow study indicate that the boundary layer does not completely separate. The bulge in the pressure distribution aft of the shock wave and the surface oil study indicate a very large separation bubble under the shock which reattaches near the 0.75-chord station. For previous airfoil shapes, such as the NACA 6-series, the presence of a shock wave associated with an upstream Mach number of 1.4 causes very severe boundary-layer separation.¹² The key to the greater stability of the boundary layer for the supercritical airfoil is the plateau in the pressure distribution aft of the shock wave described earlier. For previous airfoils, the subsonic pressure recovery downstream of the shock wave opposes boundary-layer reattachment. With the plateau on the supercritical airfoil, this adverse effect is eliminated. It is of interest that boundary-layer surveys indicate that the boundary-layer separation development under the shock for supercritical airfoils is quite similar to that on a flat plate.^{11,13}

The marked improvement in not only the drag rise at high lift but also the increase in maximum lift provided by the supercritical airfoil can be exploited to substantially improve the high-lift maneuver capability of fighter aircraft. Extensive wind-tunnel experiments have been made of various supercritical wing configurations on the F-111 fighter bomber. One of the sets of data is presented in Figure 18. The variations of drag with lift at a Mach number of 0.90 for a supercritical wing at various angles of sweepback are compared with those for the original wing on the F-111 which had an NACA 64-series airfoil shape. For 26° of sweep and a lift coefficient of about 0.9 at which this aircraft maneuvers, the drag due to lift is reduced by approximately 40% through the use of the supercritical wing. Because of the marked improvement in the maneuverability that would be associated with the drag reduction shown in Figure 18, the Air Force funded the construction of a new supercritical wing for flight demonstration on the F-111. The flight configuration with the new wing is shown in Figure 19. This airplane is still being flown at the NASA Dryden Flight Research Center. The results obtained in flight have verified the wind-tunnel data.

3.5 Application to Wings With Increased Aspect Ratio

Recently, wind-tunnel experiments have been conducted on a series of high-aspect-ratio wings incorporating supercritical airfoils with increased thickness-to-chord ratios and design lift coefficients. (See Fig. 20.) The range of sweepback angles of the wings investigated is less than that for present transport aircraft. In spite of this change, the supercritical airfoil allows the same drag rise Mach number as for current aircraft. In the design of these new advanced supercritical wing configurations, the aspect ratios have been limited to those that would result in approximately the same weight as present transport wings. For wings at progressively greater thickness ratios, progressively higher aspect ratios were utilized.

Wind-tunnel results obtained for these new advanced supercritical wing configurations indicate that the drag due to lift can be reduced by approximately 30% for wings with approximately the same weight of current transport wings. This reduction in drag due to lift results in approximately an 18% increase in lift-to-drag ratio. Research on this family of advanced high-aspect-ratio supercritical wings is continuing.

4. NONAERODYNAMIC MEANS FOR INCREASING THE OPTIMUM COMPROMISE ASPECT RATIO

4.1 Strut Bracing

In the early years of aircraft development, external strut braces below monoplane wings were utilized to carry most of the tension forces associated with the bending moments in the wing. This substantially reduced the weight of the wing. It has been suggested by W. Pfenninger that a similar approach be used on long-range aircraft designed for cruise at high subsonic speeds. (See Fig. 21.) Such bracing could allow an increase in aspect ratio for a given wing weight. Thus the optimum compromise aspect ratio would be higher than for a purely cantilever wing. Several severe problems are associated with this approach. In particular, there would be large high-speed aerodynamic interferences between the flow around the lower surface of the wing and the external brace. Extensive theoretical analysis and wind-tunnel experiments would be required to eliminate these interferences. No investigations on this approach are presently planned at the NASA Langley Research Center.

4.2 Advanced Composite Materials

Extensive developmental research and flight demonstrations are being conducted in the U.S.A. and other countries on the use of carbon fiber composite structural materials for aircraft construction. Analysis indicate that the use of such material should significantly reduce the structural weight of aircraft components. With such a reduction in weight of the primary wing structure, the optimum compromise aspect ratio would be significantly increased. The exact magnitude of such an increase in aspect ratio allowed by the use of the new material has not yet been completely defined.

4.3 Active Load Relief

Extensive system studies and flight demonstrations are to be conducted in the U.S.A. on means for relieving the bending moments in a wing at critical structural design conditions through computer controlled variable aerodynamic surfaces on the wing. In such an approach, a buildup of load is sensed and the computer commands the appropriate surface deflection required to reduce the associated bending moments. A full utilization of this approach requires fail-safe electronic equipment. The development of such equipment is being actively pursued. As for the two approaches previously discussed, the use of such a system would allow an increase in the optimum compromise aspect ratio for wings.

5. WINGLETS

5.1 Introduction

It has been recognized for many years that a nonplanar lifting system should have less induced drag than a planar wing. As early as 1897 a patent was obtained by Lanchester for vertical surfaces at the wing tips. Since that time a number of theoretical analyses have indicated the significant improvements possible with nonplanar systems including vertical surfaces at the tip.¹⁴⁻¹⁶ On the basis of these encouraging theoretical studies, a number of experimental investigations of various end plates at the wing tips have been made. Usually, these surfaces have reduced the drag at very high lift coefficients but have resulted, at best, in only slight reductions in drag near cruise lift coefficients. Near cruise conditions, the viscous drag increments associated with the end plates were nearly as great as the reductions in induced drag.

An analysis of the effect of vertical surfaces at the tip on overall airplane performance must include consideration of the effect of such surfaces on the structural weight. Loads on the vertical surfaces and the increased loads on the outboard region of the wing associated with adding these surfaces increase the bending moments imposed on the wing structure. The greater bending moments, of course, require a heavier wing structure. Aircraft designers have found that for the same structural weight penalty associated with adding end plates, a significantly greater improvement in drag could be achieved by merely extending the wing tip. As a result, no aircraft designs have incorporated such surfaces for the sole purpose of reducing drag. However, vertical surfaces have been placed near the tips of some sweptback and delta wings to provide directional stability. The objective of the work described herein was to develop nearly vertical, tip-mounted surfaces which would provide, near cruise conditions, substantially greater reductions in drag coefficient than those resulting from tip extensions with the same added bending moments imposed on the wing structure.

The factor that most previous experimental investigators have overlooked is that to be fully effective the vertical surface at the tip must efficiently produce significant side forces. These side forces are required to reduce the lift-induced inflow above the wing tip or the outflow below the tip. Obviously, a low-aspect-ratio flat end plate as generally tested previously is not an efficient lifting surface. To achieve the stated objective of the present work, the nearly vertical surfaces placed at the tip for the purpose of reducing drag due to lift have been designed to produce significant side forces, even at supercritical conditions, according to the well-established principles for designing efficient wings; hence, the name winglets. Flow surveys behind the tip of a wing with and without winglets, presented in Reference 17, indicate that the basic physical effect of the winglets, which leads to drag reduction, is a vertical diffusion of the tip vortex flow at least just downstream of the tip. The large inward components of the vortex flow near the center of the vortex are substantially reduced while the small inward components in the region above the tip of the winglet are increased slightly. Thus these surfaces could be called vortex diffusers.

The initial development investigations of wing-tip mounted winglets were conducted at subsonic speeds on a representative second-generation, wide-body jet transport wing in the Langley 8-foot transonic pressure tunnel during 1974. The results of that investigation are discussed in general terms in Reference 18. Complete results for the final configuration of that investigation are presented in Reference 17. More recently, improved winglets have been investigated on a wide variety of high subsonic speed airplane configurations. In this paper the design approach for winglets is described and selected results for an application to a first-generation jet transport wing are presented.

5.2 Design Methodology

The theoretical calculations of References 16 and 19 provide an indication of the span load distributions required on the wing and vertical surfaces at the tip to obtain the optimum induced drag in subcritical flow. However, they do not describe how the configuration should be shaped to obtain these load distributions or how it should be designed to achieve the maximum improvement in overall performance. The tip-mounted winglets of the present investigation were developed with the available theoretical calculations, physical flow considerations, and extensive exploratory experiments. Consideration has been given to the effect of adding the winglets on the structural weight and the high-lift off-design performance as well as to the drag reduction at design conditions. Because of the limitations of the methods used, the winglets of this investigation are undoubtedly not optimum.

Since the development of the design approach described herein, several new theoretical lifting surface methods for analyzing and optimizing nonplanar lifting systems for subcritical flows have been developed. Among them are References 20 and 21. These methods should greatly aid in future aerodynamic designs of more nearly optimum winglets. Calculations based on the method of Reference 21 have already been used to verify a number of the assumptions made in the design procedure presented herein. They have also indicated several areas where the design might be improved. Some of the applications of this theory are described subsequently in this report.

5.3 Upper Winglet

Arrangement. The primary component of the winglet configuration (Figs. 22 and 23) is a nearly vertical surface mounted rearward above the wing tip. The upper winglet is placed rearward so that the increased velocities over the inner surface of the winglet are not superimposed on the high velocities over the forward region of the wing upper surface. Thus adverse flow interference effects at supercritical design conditions are reduced. The results of exploratory investigations suggest that to minimize adverse interference effects at supercritical conditions, the leading edge of the root of the winglet should probably not be significantly ahead of the upper-surface crest of the wing-tip section. Conversely, if the leading edge of the upper winglet is moved aft of this crest, attachment of this surface to the wing becomes a greater problem since the structural box for the winglet moves aft of the usual rear spar location for the wing. Also, analyses and exploratory experiments indicate that the shorter winglet root chord caused by moving the leading edge aft of the wing section crest results in a perceptible loss of winglet effectiveness. Therefore, the leading edge of the winglet has been placed near the crest for cruise conditions. Results of exploratory experiments also indicate that the greatest winglet effectiveness is achieved with the trailing edge of the winglet near the trailing edge of the wing.

Loads. The theories of References 16, 19, and 21 indicate that to achieve the reductions in induced drag theoretically predicted for wing-tip mounted vertical surfaces requires not only substantial inward normal loads on these surfaces but also significant increases in the upward loads on the outboard region of the wing. Exploratory experiments made both during the investigation of Reference 17 and during the present investigation indicate that the greatest measured reductions in drag due to adding the upper winglet are achieved with normal loads on the winglet, and associated added loads on the outboard region of the wing, substantially less than those indicated as optimum by the theories of References 16, 19, and 21. These differences are probably due primarily to viscous effects not included in theory. Calculations based on Reference 21 indicate that reducing these loads from the theoretical optimum values to the measured values decreases the effectiveness of the winglets only slightly (induced drag increases slightly). This effect is probably more than offset by a reduction in viscous drag for both the winglet and the wing resulting from lower induced velocities on these surfaces at the lower load condition. Further, with such reduced loads the added bending moments imposed on the wing and the resulting structural weight increase are less than those associated with the theoretically optimum loads.

The theories of References 16 and 19 indicate that the optimum span load distributions for the winglet are characterized by relatively high loads near the winglet root in comparison with the optimum elliptical load distribution for planar wings.

Height. The available theories¹⁶ indicate that the reduction in induced drag associated with tip-mounted vertical surfaces increases slightly less than linearly with increase in height. However, the theories indicate that the normal loads on such surfaces and the loads on the outboard region of the wing required for the calculated induced drag reduction also increase with an increase in winglet height. These greater loads, together with a greater moment arm of the loads on the winglet associated with increased height, of course, increase the bending moments in the wing with a resulting weight penalty. Therefore, the optimum height must be a compromise between aerodynamic and structural weight considerations.

Further, the required normal-force coefficients for the winglet increase with an increase in winglet height. For excessive winglet heights, the required normal-force coefficients would lead to substantial boundary-layer separation particularly for high-lift off-design conditions. For the most satisfactory results, the required normal-force coefficients for the winglet should probably be limited to values of the same order of magnitude as the lift coefficients of the wing.

The height of the winglet of the investigation described herein was selected arbitrarily on the basis of very limited exploratory experiments and analyses. A precise determination of the most satisfactory height must await more definite information on the structural weight penalties associated with adding winglets.

Planform. As for wings, the winglet should have the highest aerodynamic efficiency when it is tapered so that the normal-force coefficient is approximately constant along the span of the winglet. To achieve this situation for the desired span load distribution requires substantial taper. For satisfactory winglet effectiveness at supercritical design conditions, the effective sweep of these surfaces should be approximately the same as that of the wing.

Airfoil Section. The winglet airfoil should be shaped to meet two important basic requirements. First, it should efficiently provide the desired inward normal-force coefficients for the design wing lift coefficient and Mach number. For supercritical design conditions, this objective is achieved with an airfoil shaped to avoid a strong wave on the surface and to minimize the added induced velocities on the outboard region of the wing upper surface associated with the presence of the winglet. Secondly, the airfoil should be shaped so that the onset of significant boundary-layer separation on the winglet surface is delayed to the conditions for which such separation occurs on the wing. This latter objective should be achieved even for low-speed high-lift conditions with the stall control devices extended on the wing.

These objectives are probably accomplished most effectively with an airfoil similar to the NASA general-aviation airfoil described in Reference 22 with a design camber significantly greater than that for the wing. Experiments and theoretical analyses have indicated that such an airfoil provides superior low-speed high-lift characteristics and satisfactory supercritical characteristics. Also, to accomplish the high-speed objectives most effectively, the maximum ratio of airfoil thickness to chord should be as low as possible without causing a severe weight penalty or significantly degrading the low-speed stall characteristics. Preliminary structural and aerodynamic studies suggest that the most satisfactory thickness ratio may be about 8%.

Incidence and Twist. The upper winglet is generally toed out and thus has negative geometric incidence, since the effective inflow angles are greater than the winglet angles of attack required to achieve the desired normal-force coefficient for design conditions. With the large amount of camber required in the winglet, this negative incidence can be substantial. Because the available theories do not as yet incorporate effects of viscosity, thickness, and supercritical flow, the most satisfactory incidence must, at present, be determined by a systematic experimental investigation of various incidence angles.

To obtain the desired span load distribution on a swept upper winglet in an undistorted flow field would require substantial twist. However, the decrease in inflow with increase in winglet height above the wing approximately provides the desired aerodynamic twist. Thus, no geometric twist is usually required for this surface.

Cant or Dihedral. A study, based on theoretical calculations made by J. L. Lundry using the method of Reference 19, of the trade offs between induced drag reduction, skin friction, and wing bending moments indicates that the optimum practical winglet configuration should have a small amount of outward cant as shown in Figure 22. Outward cant also reduces the flow interference at the root of the upper winglet at supercritical conditions.

5.4 Lower Winglet

Rationale. Theoretically, a nearly vertical surface below the wing tip is as effective as one of the same height above the tip. However, a lower winglet usually must be shorter than the optimum height because of ground clearance problems. The theoretical calculations of Reference 16 indicate that a lower winglet of practical vertical height, in combination with larger upper winglet, produces relatively small additional reductions in induced drag. However, experiments indicate that even such a shortened surface may improve overall winglet effectiveness, particularly at both high-lift coefficients and supercritical conditions. The presence of a lower winglet lessens both the theoretically desired critical conditions. The presence of a lower winglet lessens both the theoretically desired^{16,19} and actually measured optimum induced velocities on the upper winglet, with a resulting decrease in boundary-layer separation on the winglet inner surface.

Forward placement of the lower winglet maximizes the reduction in the usual maximum induced velocity on the forward region of the inner surface of the upper winglet at high wing lift coefficients. This effect is roughly similar to that of a slat near the leading edge of a wing; in both cases, the local angle of flow at the leading edge is reduced. It is conjectured that this favorable effect is nearly optimum when the trailing edge of the root of the lower winglet coincides streamwise with the leading edge of the upper winglet.

Configuration. Because of the pronounced interactions of the high induced velocities on the forward portion of the wing with those on the lower winglet, the definition of the most satisfactory configuration of the lower winglet for the complete range of flight conditions is far from complete. However, it is known that, as for the upper winglet, the lower winglet requires substantial camber (upper surface outward) and toe-in. Preliminary analyses, substantiated by calculations based on Reference 21, also suggest that, in contrast to the upper winglet, the lower winglet should probably be twisted with washout.

An analysis based on the theoretical results of Reference 16 suggests that outward cant of the lower winglet would increase the favorable effect of this surface on the flow over the upper winglet. Therefore, substantial outward cant was incorporated in this surface for the configuration of Reference 17 and that of the present report. However, a more recent analysis, using the method of Reference 21, indicates that the most satisfactory overall performance is probably achieved with little or no cant in this surface.

5.5 Experimental Results

Model Description. The model utilized for the experiments discussed herein is shown in Figure 22. In an effort to obtain the highest possible winglet Reynolds number and sufficient winglet size to install surface-pressure measurement tubes, a semispan model was utilized. The fuselage was not attached to the balance but did rotate with the wing through the angle-of-attack range.

Lift Drag. The increase in lift coefficient for a constant drag coefficient resulting from the additional surfaces at a Mach number of 0.78 is presented in Figure 24. These changes are equivalent to changes in the lift-drag ratio. The effects presented differ from those for a complete full-scale airplane. At full-scale conditions, the skin-friction drag penalties associated with the additions would be somewhat less than those for the test Reynolds number. More importantly, the drag due to lift for the complete airplane would be greater than for the exposed panel of the wind-tunnel configuration. Therefore, the relative

increase in lift coefficient for a constant drag coefficient would be less. It has been estimated that because of these two compensating factors, the relative changes for the total full-scale airplane would be about 10% less than those shown in Figure 24.

Addition of the upper winglet only increases the lift-drag ratio of the exposed wing panel by about 9% near design conditions of $M_\infty = 0.78$ and $C_{L, \text{basic wing}} = 0.44$ (Fig. 24). At higher lift coefficients the improvement is decreased because of wave drag and boundary-layer separation associated with a strong shock wave in the region of the juncture of the winglet and wing tip. Unpublished results indicate that at lower Mach numbers the losses in winglet effectiveness at high-lift coefficients are much less severe.

An analysis of the basic results indicates that addition of the upper winglet reduces the basic induced drag by about 20% for lift coefficients up to the design value. This reduction is substantially greater than the value predicted in Reference 16 for a vertical tip-mounted surface with the same ratio of height to wing span as the winglet investigated. Calculations based on the theories of References 19 and 21 indicate that the difference is due primarily to the tilt of the winglet outward. Calculations based on Reference 21 indicate that the dihedral and bending of the wing investigated also slightly increase the effectiveness of the winglet.

Reductions in induced drag obtained in this investigation are associated with an approximately elliptical span load distribution to the basic wing (Fig. 25). Calculations based on Reference 21 indicate that the reductions would be significantly less for a wing with the center of lift located farther inboard.

Near design conditions of $M_\infty = 0.78$ and $C_{L, \text{basic wing}} = 0.44$, adding the lower winglet has little effect on the lift-drag ratio (Fig. 24). However, at high-lift coefficients, adding the lower winglet results in a significant improvement in the lift-drag ratio (Fig. 24). As indicated in the section "Lower Winglet," these favorable effects of adding the lower winglet for higher lift coefficients are associated with reductions in the relatively high induced velocities on the forward region of the inner surface of the upper winglet and near the tip region of the wing opposite the forward part of the upper winglet (Figs. 26 and 27) with consequent reduction in shock-induced boundary-layer separation.

An analysis of the effects of adding the lower winglet for all flight conditions indicates that the improvement in overall performance would be marginal.

Comparison With Tip Extension. The tip extension investigated has a span equal to 0.38 of the span of the upper winglet. The added wing area is about 90% of the exposed surface area of the upper winglet. The increase in root bending moment for the tip extension is approximately the same as the increase for the upper and lower winglets, and it is greater than the increase for the upper winglet only (Fig. 28). Near design conditions of $M_\infty = 0.78$ and $C_{L, \text{basic wing}} = 0.44$, this extension increases the lift-drag ratio by about 4% (Fig. 24) which is less than half that achieved by adding the winglets.

The bending-moment coefficients (at a constant lift coefficient) at the horizontal elastic axis of the wing-fuselage juncture resulting from the additional surfaces, presented in Figure 28, were obtained by correcting the rolling-moment increments measured by the balance for the moments determined by multiplying the side-force increments by the vertical distance from the balance center to the elastic axis of the wing root. These side-force increments, not measured by the balance, were obtained by integrating the measured pressure distributions on the wing and winglets.

Loads. As indicated earlier, the loads on the upper winglet and the added loads on the outboard region of the wing associated with adding the upper winglet, shown in Figure 25, are substantially less than the theoretical values for minimum induced drag determined by the theories of References 16, 19, and 21. For the configuration of this investigation, the measured loads on the winglet are about two-thirds of the optimum theoretical values. For other wing configurations, these ratios may be somewhat different.

Adding the lower winglet increases the loads on the outboard region of the wing (Fig. 25) with a resulting increase in the bending-moment increments at the wing-fuselage juncture (Fig. 28). Data obtained at the one row of pressure orifices on the lower winglet indicate that, as for the upper winglet, the normal-force coefficients on the lower winglet are about the same as the lift coefficients for the wing near design conditions.

At lift coefficients from the design value to the value at which the angle-of-attack and pitching-moment-coefficient curves break (approximately 0.7) the normal-force coefficient for the winglet is roughly the same as the lift coefficient (Fig. 29). The decrease in the relative magnitude of winglet normal-force coefficient at higher lift coefficients is associated with the unloading of the outboard region of the wing due to increased boundary-layer separation on the wing at these conditions.

Effect of Upper Winglet Incidence. Near design conditions of $M_\infty = 0.78$ and $C_L = 0.48$ for the configuration with winglets, increasing the incidence of the upper winglet above -4° (selected for the final configuration) increases the drag coefficient (Fig. 30). This incidence increase also significantly increases the loads on both the winglet and the outboard region of the wing (Fig. 31) with a resulting increase in bending moments imposed on the structure.

Low-Speed Results. The addition of the upper winglet substantially reduces the drag at a Mach number of 0.30 (Fig. 32).

6. EFFECTS OF THRUSTING JETS

6.1 Jet at Wing Tip

An investigation was conducted in the Langley 8-foot transonic pressure tunnel of the effect of the jet wake of a typical fan jet type engine mounted at the tip of a lifting surface on the induced drag.²³ The configuration utilized for this investigation is shown in Figure 33. A semispan model was utilized. The fuselage was not attached to the balance but would rotate with the lifting surface. The lifting surface

had a 12% thick symmetrical NACA 6-series airfoil. The use of a symmetrical surface eliminated the influence of camber on the determination of the drag due to lift. The lifting surface was untapered to concentrate the vorticity at the tip. The model engine installation was representative of a high bypass ratio fan-jet engine. As shown in Figure 34, the jet was produced by an internal fan driven by a turbine. The turbine was driven by compressed nitrogen ducted to the engine through the lifting surface. The ratio of the total pressure at the fan jet to the stream total pressure was approximately 1.5, a value representative of modern fan-jet engines. The thrust of the engine was calculated on the basis of extensive static and total pressures and temperature measurements at the exits of the engine (Fig. 34). The spanwise location of the tip of the lifting surface used as a basis of comparison was at the center line of the engine of the engine-on configuration.

The effect of the thrusting engine at the tip on the drag due to lift is shown in Figure 35. The drag due to lift for the basic lifting surface without the engine installed, indicated by the solid line, is somewhat greater than the ideal drag due to lift for a planar lifting surface, that is, $1/\pi AR$. This increased drag is due primarily to the fact that an untapered lifting surface does not produce the ideal span-load distribution. With the engine mounted at 0° with respect to the lifting surface, the drag due to lift is reduced by approximately one-third. Tests were also conducted with an engine nacelle without a thrusting jet but with a simple duct through the center which allows the same mass flow through the nacelle as for the powered engine case. This configuration produced a reduction in drag due to lift equal to approximately 40% of that achieved with the thrusting engine. Thus the favorable influence of this tip-mounted engine is due in part to the simple physical presence of the nacelle, however, it is obvious that the jet wake also contributes substantially to this gain.

When the engine incidence was changed from 0° to -4° with respect to the lifting surface, the effectiveness of the tip-mounted engine in reducing drag due to lift at lower angles of attack was essentially eliminated, however, at the highest angle of attack of the investigation the effectiveness for this negative incidence was almost as great as that for the 0 incidence condition. At the lower angles of attack with the negative incidence of the engine, the angle of the jet was substantially different from the downward angle of flow of the induced field produced by the surface. However, at the higher angles of attack, the angle of the jet approached more closely the downflow angle. It thus appears that the effectiveness of the jet wake in reducing the losses in the vortex of a lifting surface is highly dependent on the geometric relationship of the jet to the induced field of the lifting surface.

No completely satisfactory explanation for the effects shown has yet been developed. However, flow surveys made directly behind the configuration indicate that the jet wake completely destroys the concentration of the vorticity in a tip vortex that usually occurs behind a simple lifting surface.

For a tapered wing with an approximately elliptical span load distribution, the reduction in induced drag provided by a powered engine at the tip would be substantially less than that shown in Figure 35. Also, studies made of the practical problems associated with mounting an engine at the tip of a wing indicate that the yawing moment associated with the failure of a tip-mounted engine would require an increase in the vertical tail size and that the engine mass at the tip might cause flutter problems. No further research has been conducted on engines mounted at the tip of a wing. A passive winglet at the tip as described in a previous section appears to be a more practical approach to reducing the induced drag associated with the tip vorticity.

6.2 Inboard-Under-Winged Engine Installations

For wing-mounted engines, the usual procedure is to locate the engine below the wing at intermediate spanwise locations. Extensive research has been conducted in the Langley 8-foot transonic pressure tunnel on this type of engine installation utilizing semispan wings and model engines similar to that shown in Figure 34. A typical configuration is shown in Figure 36. For engine installations such as this the interference between the nacelle, the pylon, the wing, and the jet wake is extremely complex and can result in very adverse aerodynamic interference. To evaluate this complex problem, the various components must be investigated separately to determine the interference. The model setup used to investigate the characteristics of the engine alone is shown in Figure 37.

Most of the research conducted on underwing engine installations has been directed toward eliminating adverse interference, however, results obtained in the 8-foot transonic pressure tunnel indicate that with such installations favorable interference can be obtained at lifting conditions if the engine installation is properly designed. Results showing such an effect are presented in Figure 38. The configuration investigated is shown on the right. The wing was swept, tapered, and incorporated cambered airfoils. It is representative of high subsonic speed jet transport wings. The engine configuration is the same as that shown in Figure 34. At the upper left of Figure 38 the variation of the incremental interference drag coefficient with lift coefficient is shown. The interference drag is the difference between the drag for the total configuration and the sum of the drags for the components. Data are presented for a condition having a ratio of the fan exit total pressure to the stream total pressure of 1.0, which corresponds to no engine thrust, and a pressure ratio of 1.47, which is representative of the ratio for fan jet engines operating at cruise conditions.

For the configuration with a pressure ratio of 1.0, a small favorable interference was measured at the higher lift coefficient. At a pressure ratio of 1.47, this favorable interference is more than doubled. Since the favorable interference increases with an increase in lift coefficient the drag due to lift is being reduced. The reductions in drag due to lift are due to the reduction of the outward spanwise flow below the wing associated with lift. This effect is similar to the effect of a winglet at the tip.

These favorable effects are explained by surface pressure measurements made on the nacelle pylon arrangement. At the lower left part of Figure 38 the difference in pressure across the pylon for a lift coefficient of 0.4 is shown. For a pressure ratio of the fan of 1.0 shown by the solid line, an integration of these pressure differences indicate a side force on the pylon as for the wing-tip-mounted winglet. This side force reduced the outward flow below the wing. For engines with a pressure ratio of 1.47, the side force obtained by integration of these pressure differences is substantially greater than for the pressure

ratio of the 1.0 case. Therefore, it must be reducing the outward flow below the wing by a greater amount than that provided by the pressure ratio of 1.0 condition. The added effect due to engine thrust is similar to that of a tip-mounted arrangement discussed in the previous section. In this case, the jet wake is reducing the vortex development around the engine pylon arrangement. The thrust effect is essentially increasing the effective vertical height of the engine pylon arrangement. Complete results for this investigation are presented in Reference 24.

Research on this approach to reducing the drag due to lift is continuing at the Langley Research Center.

6.3 Over-the-Wing Blowing

Experimental results of Reference 25 and analytical calculations of Reference 26 have shown that it may be possible to reduce the induced drag of airplanes cruising at subsonic speeds by locating the engine nacelles such that the jet exhaust is blown over the wing. Gains in performance possible with such an engine arrangement are shown in Figure 39 from calculations made using the method of Reference 26 and the data of Reference 27. These results show reductions in induced drag of approximately 7% (about 3% of total drag) are possible for this configuration due to jet blowing at cruise conditions. Substantially larger reductions in induced drag are indicated for the climb segment. The theoretical analysis of Reference 26 indicates that this reduction in the drag due to lift is associated with the entrainment of stream energy by the jet over the upper surface. Because of this effect, the velocities of the flow over the upper surface are increased. It follows that the circulation and the lift developed for a given angle of attack are increased.

To achieve a total gain in aerodynamic efficiency, the engine nacelles must be placed high enough above the wing to prevent increased skin-friction drag due to the jet exhaust washing or scrubbing the wing upper surface. This scrubbing effect is illustrated in Figure 40. As the engine nacelle position is moved downward toward the wing upper surface the local skin-friction coefficient increases to values substantially greater than the basic skin-friction coefficients for the wing without the jet present.

The use of over-the-wing blowing also requires substantial attention to the design details of the nacelles and pylons. This need is illustrated in Figure 41. With the simple symmetric nacelles and pylons, the critical Mach number is substantially less than that for the basic wing without these additions. This reduction in the critical Mach number results in substantial interference drag increments due to the additions of these components. When the nacelles and pylons are properly contoured, the critical Mach number is increased to essentially the same value as the basic wing without the additions. As a result, the drag increments due to the additions is substantially reduced at the higher Mach numbers.

Extensive research on this approach is continuing at the Langley Research Center. The effects of engine location, engine operating pressure ratio, wing sweep, camber, thickness, and airfoil shape will be investigated.

7. REFERENCES

- ¹ Pearcy, H. H.: The Aerodynamic Design of Section Shapes for Swept Wings. *Advances in Aeronautical Sciences*, Vol. 3, p. 277, Pergamon Press, 1962.
- ² Whitcomb, R. T.; and Clark, L. R.: An Airfoil Shape for Efficient Flight at Supercritical Mach Numbers. NASA TM X-1109, 1965.
- ³ Bauer, F.; Garabedian, P. R.; and Korn, D. G.: *Supercritical Wing Sections*. Springer-Verlag, 1972.
- ⁴ Stratford, B. S.: The Prediction of Separation of the Turbulent Boundary Layer. *J. Fluid Mech.*, Vol. 5, pp. 1-16, 1959.
- ⁵ Bauer, Frances; Garabedian, Paul; Korn, David; and Jameson, Antony: *Supercritical Wing Sections II*. Springer-Verlag, 1975.
- ⁶ Kacprzynski, J. J.; Ohman, L. H.; Garabedian, P. R.; and Korn, D. G.: Analysis of the Flow Past a Shockless Lifting Airfoil in Design and Off-Design Conditions. NRC Report LR-554, 1971.
- ⁷ Garabedian, P. R.; and Korn, D. G.: Analysis of Transonic Airfoils. *Comm. on Pure and Applied Math.*, Vol. 24, pp. 841-851, 1971.
- ⁸ Murman, E. M.; and Cole, J. D.: Calculation of Plane Steady Transonic Flows. *AIAA J.*, Vol. 9, No. 1, pp. 114-131, 1971.
- ⁹ Jameson, A.: Transonic Flow Calculations for Airfoils and Bodies of Revolution. Grumman Aero. Corp. Rep. 390-71-1, 1971.
- ¹⁰ Sells, C. C. L.: Plane Subcritical Flow Past a Lifting Aerofoil. *Proc. Roy Soc. (London)*, Vol. 308A, pp. 377-401, 1968.
- ¹¹ *Supercritical Wing Technology. A Progress Report on Flight Evaluations*. NASA SP-301, February 1972.
- ¹² Daley, N.; and Dick, S.: Effect of Thickness, Camber, and Thickness Distribution on Airfoil Characteristics at Mach Numbers Up to 1.0. NACA TN 3607, 1958.
- ¹³ Seddon, J.: The Flow Produced by Interaction of a Turbulent Boundary Layer With a Normal Shock Wave of Strength Sufficient to Cause Separation. R & M No. 3502, British A.R.C., March 1960.

- 14 Nagel, F.: Wings With End Plates. Memo. Rep. 130, Eng. Div., McCook Field, Nov. 4, 1924.
- 15 Mangler, W.: The Lift Distribution of Wings With End Plates. NACA TM 856, 1938.
- 16 Weber, J.: Theoretical Load Distribution on a Wing With Vertical Plates. R & M No. 2960, British A.R.C., 1956.
- 17 Flechner, Stuart G.; Jacobs, Peter F.; and Whitcomb, Richard T.: A High Subsonic Speed Wind-Tunnel Investigation of Winglets on a Representative Second-Generation Jet Transport Wing. NASA TN D-8264, 1976.
- 18 Bower, Robert E.: Opportunities for Aerodynamic-Drag Reduction. NASA/University Conference on Aeronautics. NASA SP-372, pp. 323-352, 1975.
- 19 Lundry, J. L.: A Numerical Solution for the Minimum Induced Drag, and the Corresponding Loading, of Nonplanar Wings. NASA CR-1218, 1968.
- 20 Lamar, John E.: A Vortex-Lattice Method for the Mean Camber Shapes of Trimmed Noncoplanar Planforms With Minimum Vortex Drag. NASA TN D-8090, 1976.
- 21 Goldhammer, M. I.: A Lifting Surface Theory for the Analysis of Nonplanar Lifting Systems. AIAA Paper No. 76-16, Jan. 1976.
- 22 McGhee, Robert J.; Beasley, William D.; and Somers, Dan M.: Low-Speed Aerodynamic Characteristics of a 13-Percent-Thick Airfoil Section Designed for General Aviation Applications. NASA TM X-72697, 1975.
- 23 Patterson, James C., Jr.; and Flechner, Stuart G.: An Exploratory Wind-Tunnel Investigation of the Wake Effect of a Panel Tip-Mounted Fan-Jet Engine on the Lift-Induced Vortex. NASA TN D-5729, May 1970.
- 24 Patterson, James C., Jr.: A Wind-Tunnel Investigation of Jet-Wake Effect of a High-Bypass Engine on Wing-Nacelle Interference Drag of a Subsonic Transport. NASA TN D-4693, Aug. 1968.
- 25 Putnam, Lawrence E.: Exploratory Investigation at Mach Numbers From 0.40 to 0.95 of The Effects of Jets Blown Over a Wing. NASA TN D-7367, Nov. 1973.
- 26 Putnam, Lawrence E.: An Analytical Study of the Effects of Jets Located More Than One Jet Diameter Above a Wing at Subsonic Speeds. NASA TN D-7754, Aug. 1974.
- 27 Ewald, B.: Airframe-Engine Interaction for Engine Configurations Mounted Above the Wing. Part II: Engine Jet Simulation Problems in Wind Tunnel Tests. AGARD CP-150, pp. 26-16, 26-17, 26-18, and 26-19, 1975.

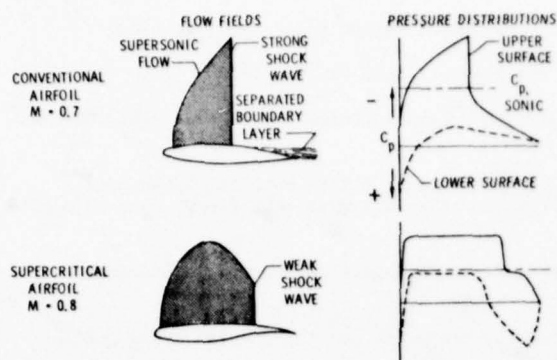


Figure 1. Supercritical phenomena.

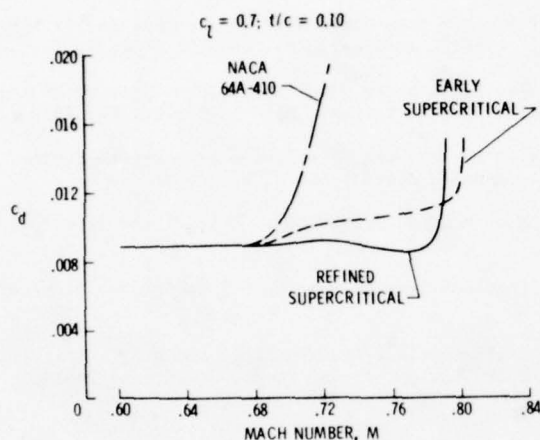
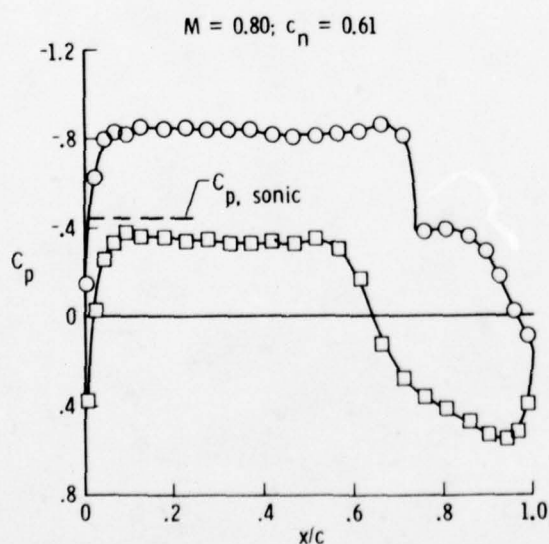
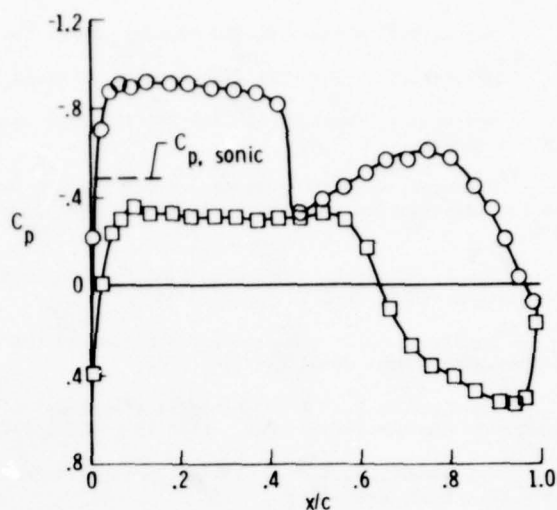
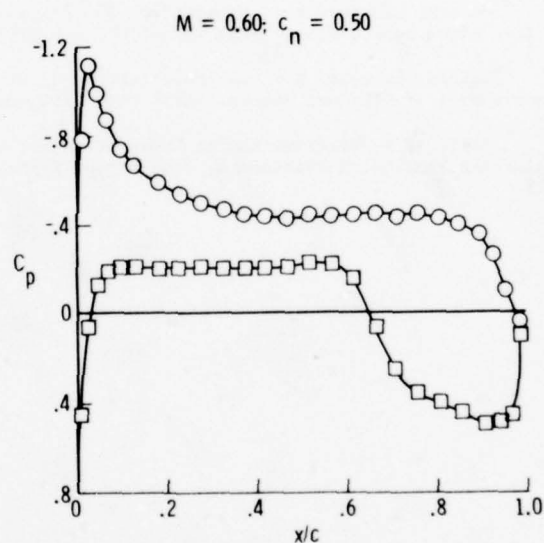
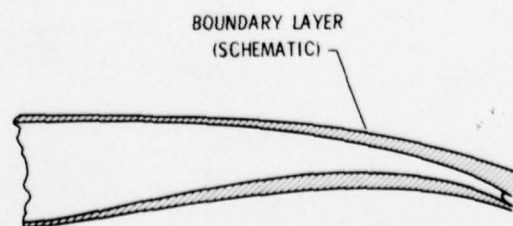
Figure 2. Drag-rise characteristics for various airfoils. $c_t = 0.7$; $t/c = 0.10$.Figure 3. Near-design pressure distribution on 11% thick NASA supercritical airfoil. $M = 0.80$; $c_n = 0.61$.Figure 4. Off-design pressure distribution on 11% thick NASA supercritical airfoil. $M = 0.78$; $c_n = 0.58$.Figure 5. Subcritical pressure distribution on 11% thick NASA supercritical airfoil. $M = 0.60$; $c_n = 0.50$.

Figure 6. Influence of boundary-layer displacement on effective camber of supercritical airfoil.

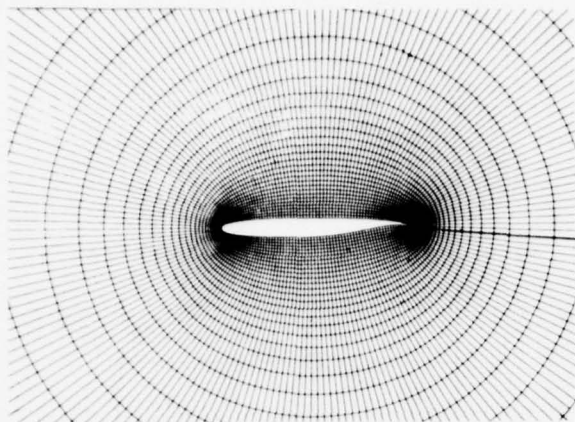


Figure 7. Conformal coordinate system for two-dimensional calculations.

NASA SUPERCRITICAL AIRFOIL

$M = 0.76$

— THEORY
• EXPERIMENT

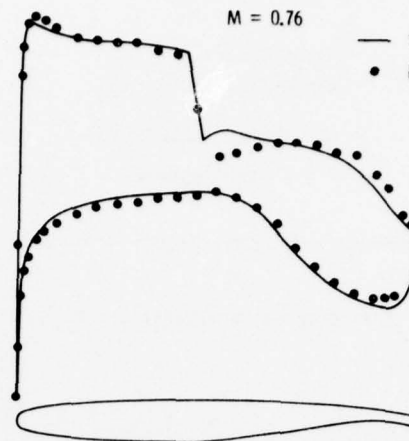


Figure 10. Comparison of experimental and theoretical pressure distributions.

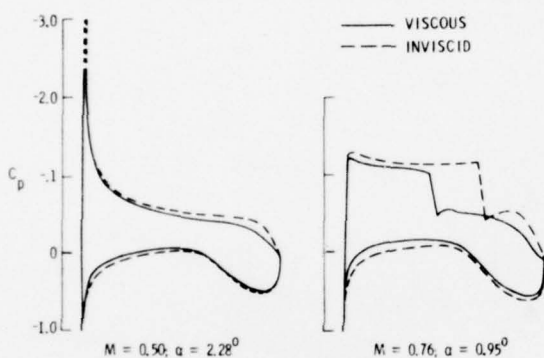


Figure 8. Viscous effects on pressure distributions for a supercritical airfoil.

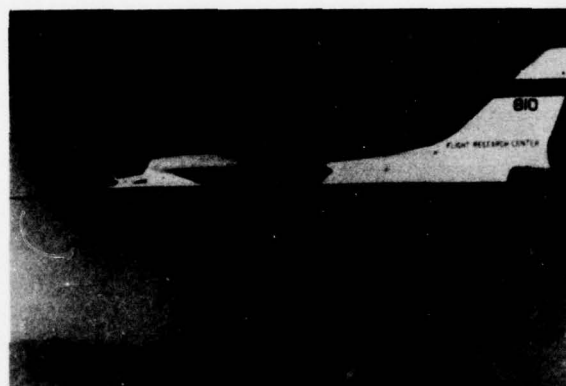


Figure 11. F-8 aircraft with transport supercritical wing.

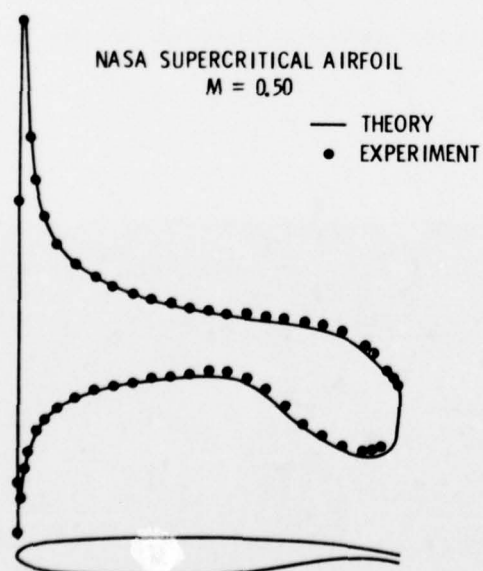


Figure 9. Comparison of experimental and theoretical pressure distributions.

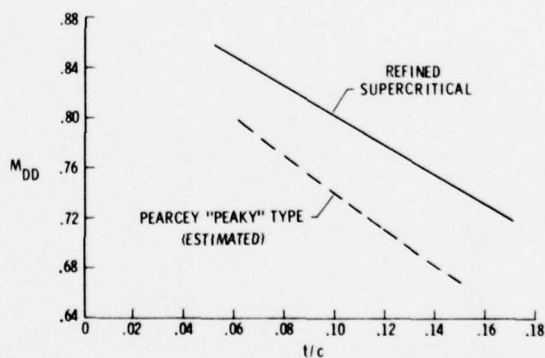


Figure 12. Airfoil drag divergence against thickness. $C_L = 0.5$.



Figure 13. Thick supercritical airfoil (Palmer of North American Rockwell, Columbus).

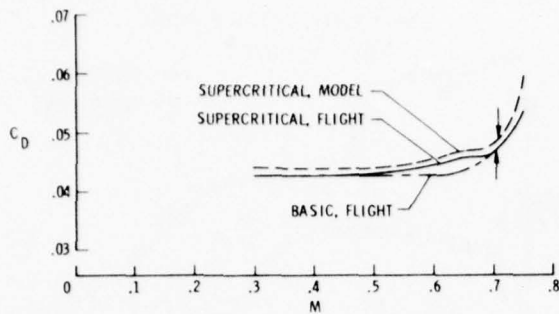


Figure 14. T-2C drag characteristics. $C_L = 0.5$.

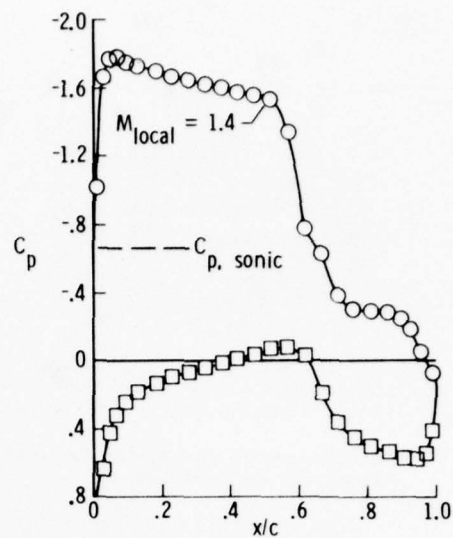


Figure 17. High-lift pressure distribution on 11% thick NASA supercritical airfoil. $M = 0.73$; $c_n = 1.32$.

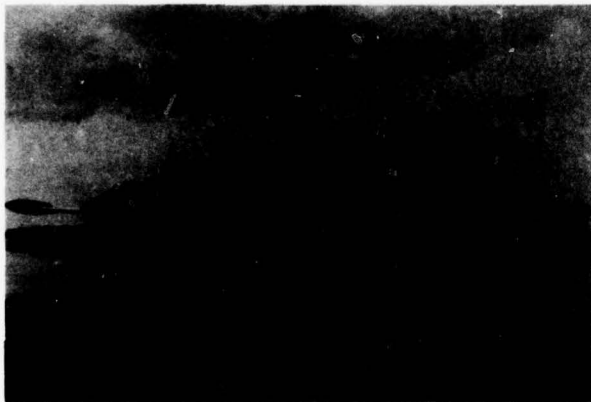


Figure 15. Aircraft with and without supercritical airfoil.

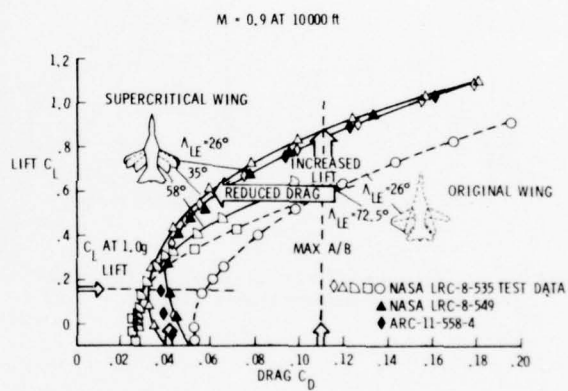


Figure 18. Maneuver aerodynamics. $M = 0.9$ at 10,000 feet.

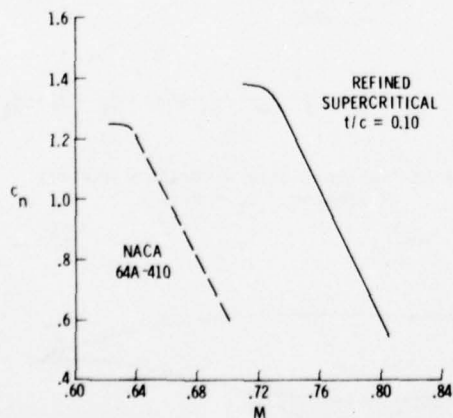


Figure 16. Onset of drag rise.

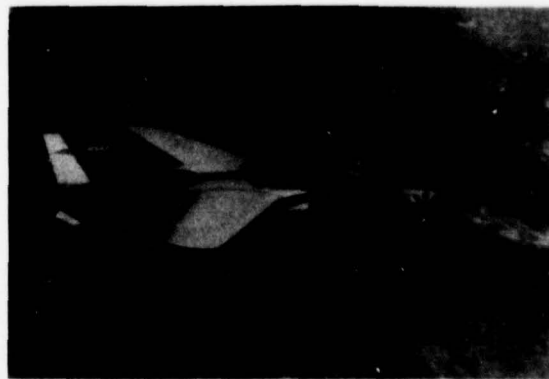


Figure 19. U.S. Air Force F-111 with supercritical wing

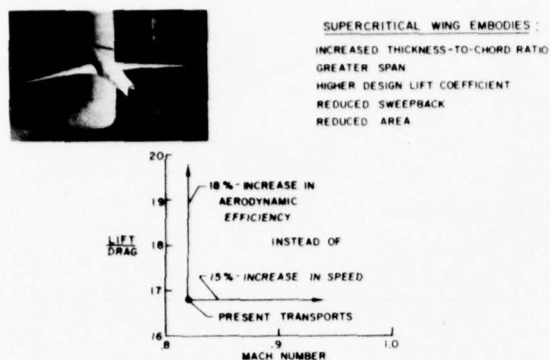


Figure 20. Supercritical wing for increased lift to drag.

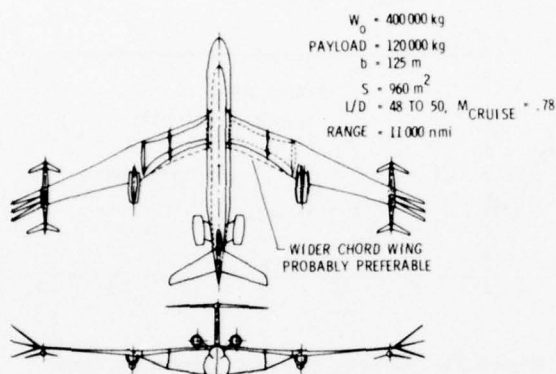


Figure 21. Turboprop powered long-range LFC transport.



Figure 22. Winglets on jet transport wing model.

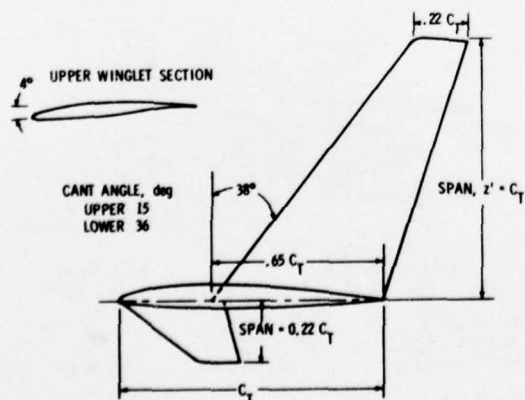


Figure 23. Basic dimensions of winglets.

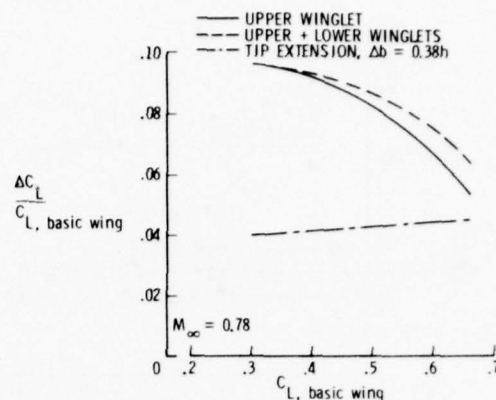


Figure 24. Tip configuration effects on lift coefficient.

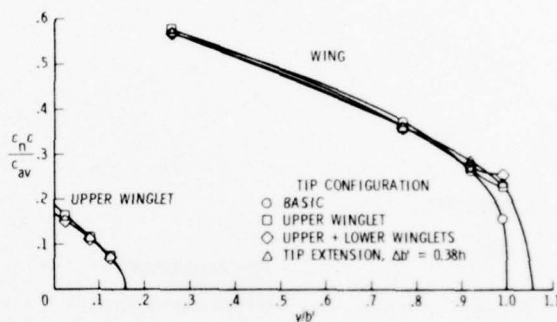


Figure 25. Spanwise distributions of load.
 M_∞ = 0.78; C_L = 0.48.

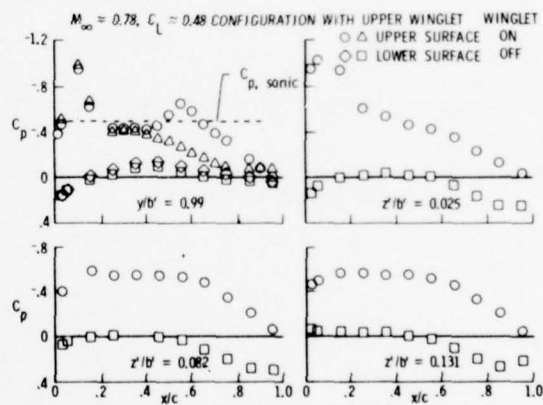


Figure 26. Chordwise pressure distributions.

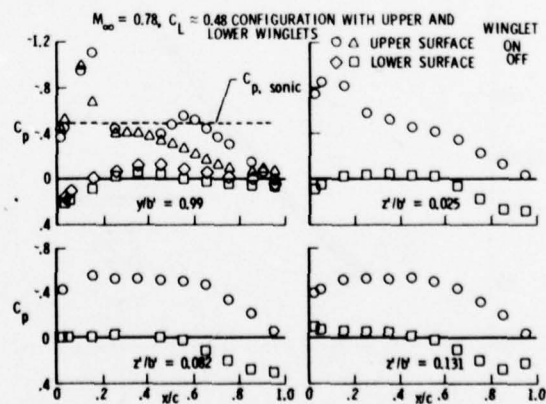


Figure 27. Chordwise pressure distributions.

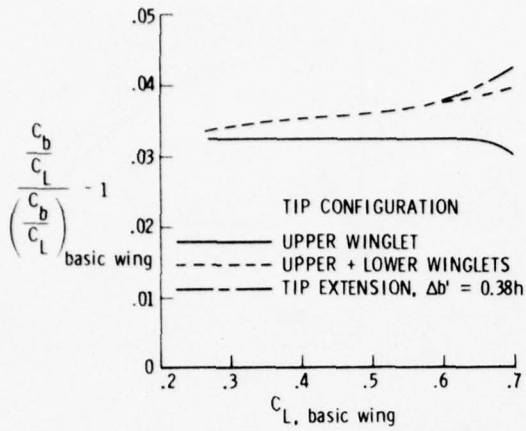


Figure 28. Tip effects on bending moments.

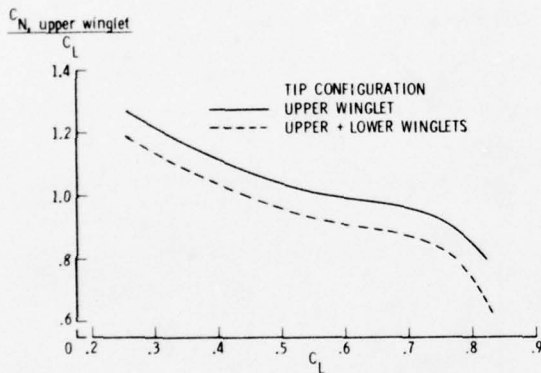


Figure 29. Comparison of normal force on upper winglet with wing lift.

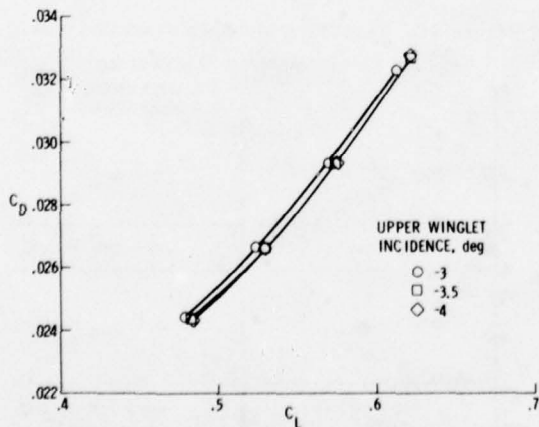


Figure 30. Effect of upper winglet incidence on configuration drag.

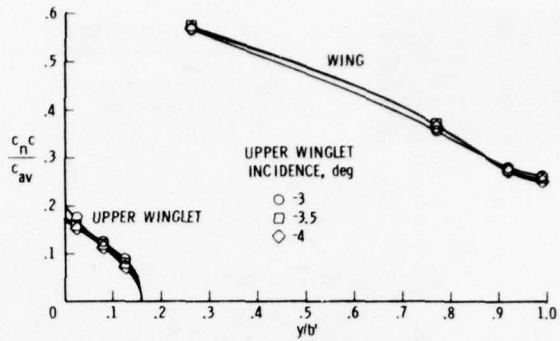


Figure 31. Effect of angle of incidence of the upper winglet on the spanwise distributions of load for the configuration with both the upper and lower winglets.

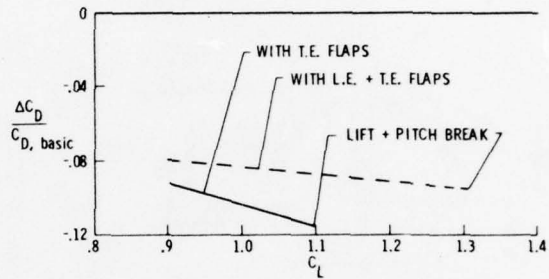
Figure 32. Effects of upper winglet on drag.
 $M = 0.30$; $R = 4.7 \times 10^6$.

Figure 33. Test setup for tip-mounted engine.

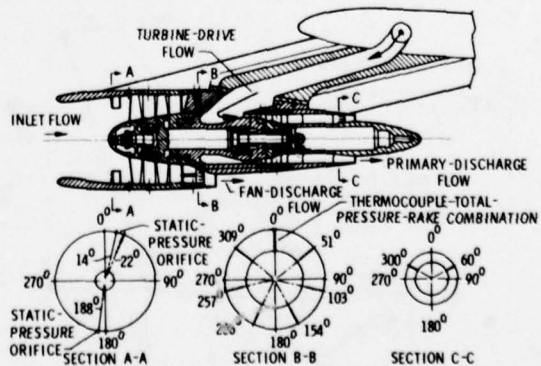


Figure 34. Cross-sectional view of the powered model fan-jet engine.

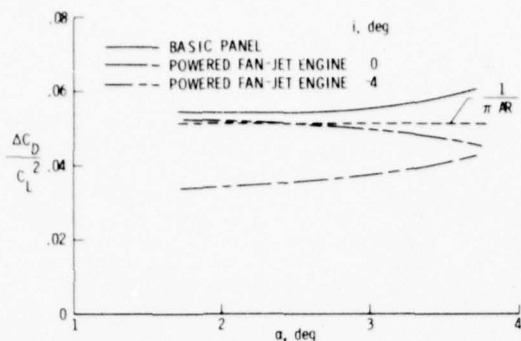


Figure 35. Effect of tip-mounted engine on drag due to lift.

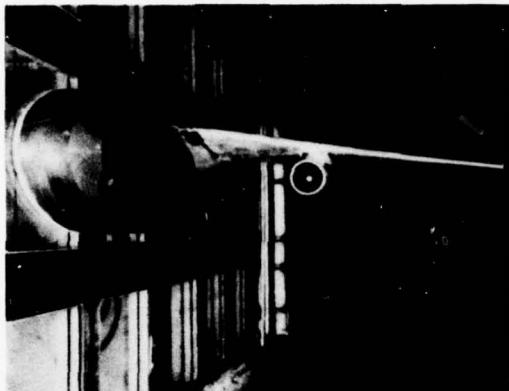


Figure 36. Test setup for wing-powered engine interference.

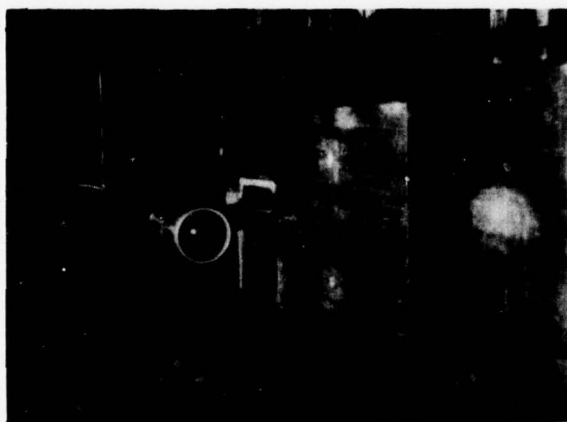


Figure 37. Test setup for engine alone.

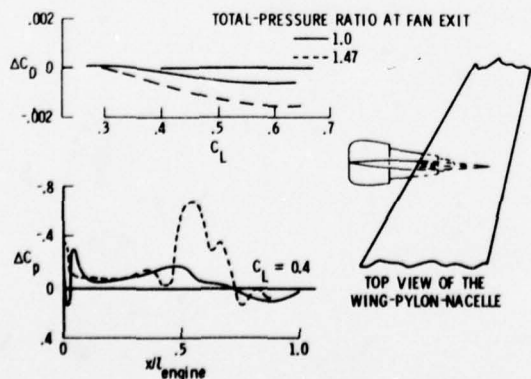


Figure 38. Power effect on drag due to lift.

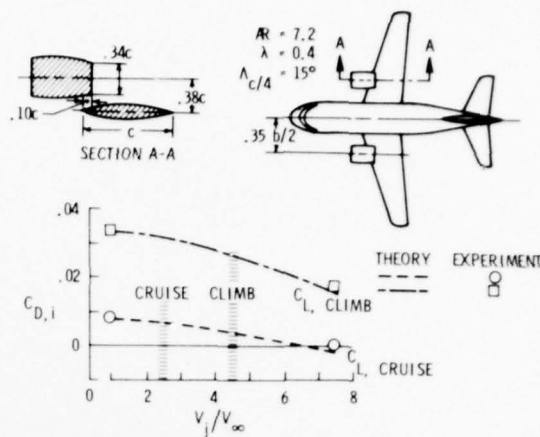


Figure 39. Induced drag reduction by over-the-wing blowing.

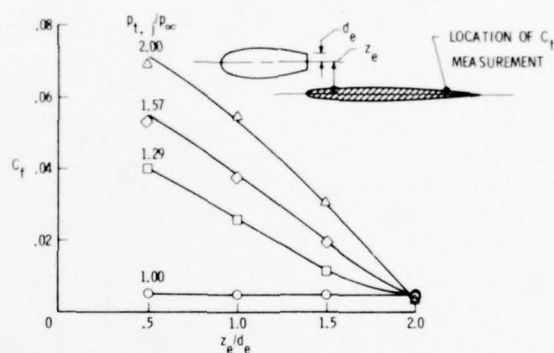


Figure 40. Effect of nacelle vertical location on scrubbing drag.

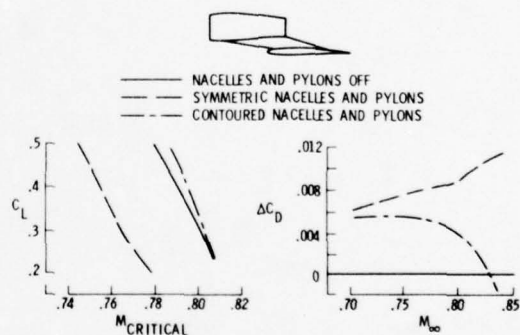


Figure 41. Effect of contouring over-the-wing nacelles.

LAMINAR FLOW CONTROL

LAMINARIZATION

by

Dr. Werner Pfenninger

Chief Scientist
Aeronautical Systems Division
Langley Research Center
National Aeronautics and Space Administration
Hampton, Virginia 23665

SUMMARY

According to theory, verified experimentally, boundary layer suction prevents laminar separation and transition in decelerated flow areas up to any pressure rise of practical interest at high Reynolds numbers, as long as external disturbances are very weak. As a result, 100 percent laminar flow was observed with $C_{D_{\min}} = C_{D_{\text{suct.}}} + C_{D_{\text{wake}}} = .0011$ (both wing sides) on a slotted 15 percent thick LFC wing in the Langley TDT tunnel at $Re_c = 16.4 \cdot 10^6$, confirming suction laminarization at substantially higher Re_c 's and correspondingly lower $C_{D_{\min}}$ when the external turbulence level is drastically reduced.

A practical aerodynamically and structurally reasonably efficient LFC suction method, removing the slowest boundary layer particles through many closely spaced fine slots, was developed and subsequently applied to a second F94 LFC wing glove in flight: 100 percent laminar flow was observed up to the F94 test limit ($Re_c = 37.5 \cdot 10^6$) within $M_{\text{local}} \leq 1.08$, with $C_{D_{\min}} = .00045$ for the upper glove surface

at $Re_c \approx 30 \cdot 10^6$. Laminar flow on LFC wings in flight is thus possible at much higher Re_c 's than even in the best low turbulence tunnels as a result of the negligible influence of the atmospheric microscale turbulence on transition. F94 LFC glove comparison experiments, with suction starting at 0.08c and 0.4c, verified the theoretically predicted boundary layer stabilization by suction starting at 0.08c, thus maintaining laminar flow at substantially higher Re_c 's, as compared to boundary layer stabilization by flow acceleration; i.e., geometry alone without suction upstream of 0.4c.

The theoretically predicted boundary layer stabilization at high Re_c 's by distributed suction, applied practically along the entire surface, was verified in the Ames 12-foot tunnel on a 8:1 fineness ratio Reichardt LFC body of revolution with 114 suction slots located between $X/L = 0.03$ and 0.99: 100 percent laminar flow and $C_{D_{\min}} = .00027$ (based on body wetted area, including $C_{D_{\text{suction}}}$) resulted

at $Re_L = 57.8 \cdot 10^6$. As in the F94 and TDT LFC experiments $C_{D_{\text{suction}}}$ was the major drag contributor, with $C_{D_{\text{wake}}} \sim 1/3$ to $1/4$ of $C_{D_{\text{total}}}$.

$Re_{L_{\text{transition}}}$ of the Reichardt body and other LFC surfaces varied as $(\frac{u'}{u_{\infty}})^{-1}$ for comparable turbulence spectra; i.e., drastically reduced initial disturbances enable substantially higher $Re_{L_{\text{lam}}}$. LFC airplane, propulsion, and suction system induced aerodynamic and acoustic disturbances, controlling transition on LFC airplanes rather than atmospheric turbulence, should therefore be minimized.

The design of swept LFC wings at high Re_c 's is usually strongly influenced by stability considerations of the boundary layer crossflow and streamwise crossflow disturbance vortices caused by crossflow pressure gradients. According to theoretical investigations of the boundary layer development and stability especially of the crossflow on swept LFC wings, boundary layer suction must be applied practically over the entire wing chord for full-chord laminarization. Particularly high local suction rates are needed in the wing leading edge region to control the local boundary layer crossflow instability induced by the strong flow acceleration in the nose region at higher Re_c 's and sweep angles. Much weaker suction is usually adequate in the extensive flat pressure region of swept LFC wings for control of boundary layer crossflow and TS-type disturbances, followed again by much stronger suction in the rear pressure rise area of the wing, with the suction rates for swept LFC wings somewhat larger than those for unswept LFC wings for control of boundary layer crossflow - rather than TS-type instability. The penalty in $C_{D_{\min}}$, resulting from the higher suction rates of swept LFC wings, is relatively modest; the major disadvantages arising from the increased suction rates of swept LFC wings are increased complexity and sensitivity of the boundary layer to surface - and possibly acoustic disturbances.

NACA Ames 12-foot tunnel experiments on a 30° swept Northrop modified NACA 66012 LFC wing with closely spaced suction slots verified these theoretical expectations: full chord laminar flow was observed at $\alpha = 0^\circ$, $\pm 1^\circ$ up to $Re_c = 29 \cdot 10^6$, with $C_{D_{\min}} = .00096$ (both sides, including $C_{D_{\text{suction}}}$).

Without strongly amplified TS-oscillations at $\alpha = 0^\circ, -1^\circ$ the minimum boundary layer crossflow stability limit $Re_{\chi_{min}}$ could, on the average, be about doubled, leading to a linearized total growth of the boundary layer crossflow disturbance vortices e^0 to e^6 in the region upstream of the rear pressure rise. However, whenever more strongly amplified oblique TS-oscillations induced for example at $\alpha \geq 1^\circ$ by free-stream disturbances as well as external or internal duct noise interacted nonlinearly with boundary layer crossflow disturbance vortices through their mutual nonlinear interaction Reynolds stresses linearized boundary layer stability theory ceased to be valid. Boundary layer crossflow disturbance vortices on swept LFC wings then became unstable at substantially lower Re_θ and grew considerably quicker, as compared to small disturbance theory, as verified on the 30° and 33° swept Northrop LFC wings in the presence of external and internal noise. Stabilization of the tangential boundary layer component against TS-disturbances through increased suction and/or flow acceleration minimized such nonlinear interaction and raised accordingly the permissible noise level on swept LFC wings substantially.

At still higher Re_θ 's spanwise turbulent contamination along the front attachment line of swept LFC wings may destroy their laminarization where $Re_\theta \geq Re_{\theta_{a.l. crit}}$. Large attachment line disturbances,

such as a large surface roughness or an initially turbulent boundary layer at the upstream end of the wing attachment line (wing-fuselage intersection) cause transition and spanwise turbulent contamination directly at $Re_\theta \geq 90$ to 100 without the intermediate mechanism of amplified boundary layer

oscillations. It can be eliminated relatively easily by local leading edge extensions, leading edge suction fences, or by removing the entire turbulent attachment line boundary layer through local suction, raising Re_θ substantially above 90 to 100. Transition at the attachment line may then

result from amplified TS-oscillations of the spanwise attachment line boundary layer; i.e., Re_θ

then becomes a function of the disturbance level of the external flow and in the initial attachment line boundary layer where laminar attachment line flow has been established, of the spanwise length

Reynolds number $\frac{W \cdot Z}{\nu}$ along the attachment, line of the suction rates $V_o^* = \frac{V_o/U_o}{\sqrt{\nu(\frac{\partial U}{\partial S})}}$ at the attachment

line, and of the wing sweep angle ϕ (since ϕ controls the lateral stretching $a.l.$ of the TS-disturbance vortices and thus their stability in the diverging attachment line flow field). As verified in the Northrop 7- by 10-foot tunnel on a 45° swept blunt-nosed wing particularly high Re_θ resulted by

starting with an undisturbed laminar initial attachment line boundary layer and stabilizing the attachment line boundary layer by suction through closely spaced vertical nose slots ($Re_\theta = 300$ to 330 at

at $\frac{W \cdot Z}{\nu} \approx 6 \cdot 10^6$). Considerably higher Re_θ (at given $\frac{W \cdot Z}{\nu}$) or $\frac{W \cdot X}{\nu}$ (at given Re_θ) can be expected at lower external disturbance levels (Ames 12-foot tunnel, flight).

On swept LFC wings, an undisturbed initial laminar attachment line boundary layer may be established by means of sufficiently strong suction in a local attachment line suction patch, suitable leading edge extensions with opposite sweep at their in-board end, laminarized leading edge suction fences, etc.

Among suction induced disturbances slot wake oscillations downstream of the slot exit in the small spanwise plenum chambers underneath the slots at slot flow Reynolds numbers $\frac{\bar{v} \cdot S}{\nu} \geq 100$ induce flow fluctuations v' at the slot inlet, which, in turn, excite amplified boundary layer oscillations on the external LFC surfaces to cause premature transition at higher Re_θ 's, as verified on the 15% thick 33° swept Northrop LFC wing of the X-21 group. Such disturbances vanish when the slot wake flow is viscous and steady at $\frac{\bar{v} S}{\nu} \leq 100$; indeed, no difficulties from such disturbances had previously been observed up to $Re_L = 58 \cdot 10^6$ when $\frac{\bar{v} S}{\nu} < 100$. With perforated LFC surfaces suction hole induced streamwise or horse-shoe vortices shed from the suction holes had often caused premature transition either directly or as a result of amplified TS-oscillations, especially when the streamwise spacing of rows of suction holes was comparable to the wavelength of amplified TS-oscillations (as verified during transition experiments at the attachment line of a 45° swept blunt-nosed wing). Perforated LFC surfaces are acceptable at high Re_θ 's when the suction hole induced 3-dimensional aerodynamic roughness and the resulting streamwise disturbance vorticity is too weak to significantly affect transition, requiring a very large number of closely spaced small suction holes. Such suction hole induced disturbance vorticity must be minimized particularly on swept LFC wings where it will superimpose with the streamwise boundary layer mean- and disturbance-vorticity induced by spanwise pressure gradients.

Permissible 2- and 3-dimensional surface disturbances for laminar flow (steps, gaps, waves, roughness) were established on straight and swept LFC wings. Properly placed weak local suction in the rear flow reattachment region downstream of rear facing 2-dimensional surface steps has doubled the permissible step height Reynolds number.

As verified by supersonic low-drag suction experiments in the Tullahoma A-tunnel on a laminar suction plate and a suction ogive of revolution with a large number of closely spaced slots full length laminarization at supersonic speeds by means of boundary layer suction was surprisingly easy in the absence of shockwaves and boundary layer crossflow up to high length Reynolds numbers ($Re_L = 51 \cdot 10^6$ at $M = 3$ on the LFC ogive of revolution) in spite of the severe acoustic disturbances radiated from the turbulent tunnel wall boundary layers. This result is explainable by the higher TS-stability limit Reynolds numbers of supersonic laminar boundary layers. At higher Re_θ 's, the minimum equivalent drag (including C_D suction) of these LFC surfaces at $M = 3$ was 3 to 4 times smaller than the corresponding turbulent skin friction drag.

In the presence of incident shock waves at supersonic speeds, carefully laid out boundary layer suction in the boundary layer-shock interaction region of a flat suction plate eliminated laminar separation and premature transition in this area to enable full length laminar plate flow up to plate length Reynolds numbers $Re_L = 26 \cdot 10^6$ at $M = 3$ and 1.6 pressure ratio across the shock.

Suction duct design investigations showed small duct total pressure losses when the sucked boundary layer was deflected into the direction of the duct flow through carefully laid out flow turning nozzles ($\Delta P_{\text{tot. duct}} / q_{\text{duct end}} = 1$ for $\ell_{\text{duct}} / D_{\text{hydr. at duct end}} = 100$ to 120, as compared to $\ell/d = 12$ when the suction medium was dumped through holes at 90° angle into the duct). In principle, suction ducts can be designed with a rising total- and static-pressure towards the downstream duct end through jet mixing, when the nozzle exit velocity of the sucked boundary layer is larger than the mean duct velocity.

Structural investigations of slotted LFC wings with many closely spaced slots were conducted, leading from structural tests on small scale panels to investigations of progressively larger structural panels, and finally to the structural investigation of an LFC wing box. Many of the results of these studies were incorporated later in the X-21 wing design. These structural investigations showed that the structural weight penalty of LFC wings can be kept small by carefully integrating the suction ducting system with the wing structural layout, using a load carrying LFC wing surface instead of a non-load carrying LFC wing glove, a careful structural overall- and detail-design, and using the fact that a substantially steeper rear pressure rise is possible on the upper wing surface by means of suction in this area to allow accordingly (under otherwise the same conditions) thicker and thus structurally lighter wings.

USAF AND NAVY SPONSORED NORTHROP
LFC RESEARCH BETWEEN 1949 AND 1967

1. LOW DRAG SUCTION INVESTIGATIONS ON UNSWEPT LFC WINGS AT HIGH REYNOLDS NUMBERS AND LOW TURBULENCE.

1.1 Free Stream Turbulence Effects in LFC Experiments

The author's 1975 Zurich experiments on a 17% thick LFC wing with discrete slots, connected to individual suction chambers (figure 1), had shown full chord laminar flow up to wing chord Reynolds numbers $Re_c = 2.3 \cdot 10^6$ with $C_{D_{min}} = C_{D_{suction}} + C_{D_{wake}} = 0.0023$ (ref. 1). At higher Reynolds No.,

however, full chord laminar flow was lost as a result of the relatively high turbulence level $u'/U = 0.4\%$ of the Zurich 2.1m by 3 m wind tunnel. In view of the large dimensions of the atmospheric boundary and shear layers and the correspondingly large size of the atmospheric boundary and shear layers and the correspondingly large size of the atmospheric eddies (see for example ref. 2 and fig. 2) the microscale turbulence of the atmosphere, primarily responsible for transition, is extremely weak and thus is not expected to cause premature transition in flight up to high Reynolds numbers, as confirmed by the British flight transition experiments on the smooth NACA 66-216 wing of a "King Cobra" fighter airplane (ref. 3). Therefore, the question arose concerning the maximum laminar flow Re_c -values on LFC wings at such low turbulence levels. To answer this question, low drag suction experiments were conducted in the Langley TDT-tunnel ($u/U = .03\%$ to $.07\%$) 1951 on a 15 percent thick slotted Northrop LFC wing of modified NACA 66-1.815 section (fig. 3, ref. 4) followed by flight experiments on a slotted LFC wing glove mounted on the upper surface of an F94-A airplane (refs. 5-10). On the Langley TDT-model, suction had been applied through discrete slots connected to individual suction chambers and located primarily in the rear pressure rise area between 0.61 c and 0.97 c. To further stabilize the boundary layer in the upstream flat pressure region of the wing, additional suction slots were installed between 0.4 c and 0.61 c. No slots had been installed upstream of 0.4 c, hoping that the flow acceleration in this region would adequately stabilize the boundary layer in this region to prevent premature transition at higher Re_c 's, at least at the design angle of attack, $\alpha = 0.5^\circ$. This expectation did not fully materialize. In spite of this fact, the 8 to 10 times lower turbulence level of the TDT-tunnel, as compared to the Zurich tunnel, enabled laminar flow on the 15 percent thick slotted Northrop model at $\alpha = 0.5^\circ$ up to $Re_c = 16 \cdot 10^6$ to $17 \cdot 10^6$, with $C_{D_{min}} = 0.0011$ at $Re_c = 16.3 \cdot 10^6$ (fig. 4). At $Re_c > 17 \cdot 10^6$ full chord laminar flow was lost as a result of tunnel turbulence. With the slots sealed between 0.4 c to 0.61 c and suction applied only in the rear pressure rise area, full chord laminar flow at $\alpha = 0.5^\circ$ was maintained only up to $Re_c = 11 \cdot 10^6$ and lost at $Re_c > 11 \cdot 10^6$; i.e., weak suction in the flat pressure area between 0.4 c and 0.61 c apparently stabilized the boundary layer sufficiently to raise Re_c with full chord laminar flow from $11 \cdot 10^6$ to $16 \cdot 10^6$. Substantially higher laminar flow Re_c -values than $16 \cdot 10^6$ should probably have been possible by extending suction further upstream towards the wing leading edge.

With increasing angle of attack and correspondingly weaker flow acceleration in the upstream non-suction region of the upper wing surface, full chord laminar flow was lost at progressively lower Re_c 's. The TDT experiments on the 15 percent slotted Northrop LFC wing model as well as Braslow's LFC experiments on a NACA 64A010 area suction LFC wing model (ref. 11) had thus verified full chord laminar flow and very low equivalent profile drags at low turbulence levels up to high Reynolds numbers.

1.2 Development of Practical LFC Suction Method

The question now arose concerning the development of a reasonably practical LFC suction method which approached the aerodynamically ideal area suction more closely than the previously used widely spaced discrete slots, connected to individual chambers, without the structural, weight and fatigue life disadvantages of porous LFC skins available at the time. Relatively few discrete slots operating at rather high slot flow Reynolds numbers require extremely close manufacturing tolerances and present difficulties in providing a closed structural wing torsion box; furthermore, with such relatively widely spaced slots, the boundary layer downstream of a slot returns rather rapidly to a substantially less stable non-suction boundary layer. Thus, low drag suction through such widely spaced individual slots did not appear sufficiently promising for a practical suction laminarization, especially at high length Reynolds numbers. For these reasons attempts were started in 1952 to develop more practical and at the same time aerodynamically and structurally more efficient LFC suction methods which approached area suction more closely. Low drag suction through perforated as well as slotted LFC surfaces with a large number of closely spaced fine slots was subsequently investigated between 1952-1954 (refs. 12-21).^{*} Low drag suction through perforated surfaces generates 3-dimensional streamwise and horse-shoe type disturbance vortices in a similar manner as an inverted 3-dimensional surface roughness (refs. 15-26). Premature transition may then result (fig. 5), especially when these disturbance vortices superimpose with boundary layer crossflow due to spanwise pressure gradients on swept LFC wings, unless an extremely large number of very closely spaced small suction holes is used (refs. 26, 27). Since perforated LFC surfaces of this type at the time did not appear feasible at reasonable costs and efforts, it was decided instead to continuously remove the slowest innermost boundary layer particles in the vicinity of the surface through a large number of closely spaced continuous 2-dimensional narrow slots. With the resulting low slot flow velocities, little is gained by trying to recover the kinetic energy of the suction air in slot diffusers. The slots can then be formed in a relatively simple manner, for example, by simple sawcuts; sharp slot leading- and trailing-edges are well acceptable in view of the

^{*}The idea to approach distributed suction by using closely spaced spanwise slots has been suggested by Ackeret (J. Ackeret, M. Ras, W. Pfenniger; Verhinderung des Turbulentwerdens einer Grenzschicht durch Absaugung; Die Naturwissenschaften, Heft 41, 29. Jahrgang, p. 622 (1941); at Ackeret's suggestion it was further investigated by Ras (Contributions à l'étude de la couche limite aspirée; These Paris, Zurich, 1945).

dominating influence of the viscous slot flow forces at the low slot flow Reynolds numbers involved. The suction air then passes through closely spaced slots, cut in a thin outer sheet, into small spanwise plenum chambers underneath the slots and through holes, drilled in a thicker continuous structural inner skin which is bonded to the thin outer skin, and flow turning nozzles (refs. 28, 29) into the suction ducts (refs. 13, 29, fig. 6). Such an LFC surface with closely spaced 2-dimensional slots approaches distributed suction aerodynamically reasonably closely, it minimizes or avoids streamwise disturbance vortices; such a surface can be made structurally highly efficient for wing bending strength and stiffness and reasonably efficient for wing torsional stiffness. Such slotted LFC surfaces did not prove unduly difficult to manufacture with the close surface tolerances required for laminar flow.

Streamwise disturbance vortices caused by spanwise variations of the local suction rates between adjacent suction holes, drilled in the inner skin, should be minimized to prevent premature transition. Figure 7 shows for various suction surface geometries the measured spanwise variation of the suction rates between adjacent suction holes (refs. 30-33). For most LFC experiments with closely spaced slots, the spanwise suction rate variation between adjacent suction holes was usually kept below ± 1 percent of the mean suction flow rate. Figure 8 shows structural variations of LFC suction surfaces with closely spaced fine slots, using solid as well as different types of sandwich LFC skins (ref. 34).

The aerodynamic performance of LFC suction surfaces with closely spaced fine slots in regions of strongly decelerated external flows at low turbulence levels and high length Reynolds numbers was first investigated in 1952/53 in the inlet length of a laminar flow tube, consisting of a 26-foot (or 29 ft.) long 2-inch inside diameter nonsuction tube with accelerated flow, followed by a 60-inch long suction tube with decelerated flow and low drag suction applied through 80 slots (0.75" spacing), (fig. 9, ref. 12-14). At $Re_x \approx 17.5 \cdot 10^6$ full length laminar flow was maintained through substantial rear pressure rises by means of suction through 80 slots with small suction flow rates (fig. 10), with transition (index T) occurring at some distance downstream of the suction tube. With further increased suction rates laminar pressure rises of 0.8 to 0.9 $\times q_{\max}$ (max. dynamic pressure) and in extreme cases as high as 0.99 $\times q_{\max}$ had been observed in similar experiments at higher Re_x ; i.e., any laminar pressure rise of practical interest appears basically feasible by means of boundary layer suction.

Similar results had previously been obtained with the same experimental setup with suction applied through discrete slots connected to individual suction chambers (fig. 11, refs. 13, 35). The suction flow rates required to maintain laminar flow through the same pressure rise, though, were about 30% larger than with 80 slots (fig. 12, ref. 13).

1.3 Performance Evaluation of a Fictitious LFC Wing from Tube Test LFC Experiments

The tube test results may be used to evaluate the equivalent profile drag of a fictitious 8.5-percent thick symmetrical LFC wing with the same chordwise pressure distribution as in the tube, giving $C_{D_{\infty}} = C_{D_{\text{suct.}}} + C_{D_{\text{wake}}} = .00063$ for both wing surfaces at $Re_c = 18 \cdot 10^6$, close to the laminar flat-plate skin friction drag (fig. 13). This low corresponding equivalent profile drag is explainable largely by the extremely low laminar skin friction drag; in addition the otherwise lost kinetic energy of the boundary layer wake can be largely recovered through boundary layer suction and reacceleration of the suction air to undisturbed velocity to further reduce the propulsive power and equivalent profile drag of an LFC wing. In fact, Ackeret (ref. 36) has pointed out that the thermodynamically minimum propulsion power for a flat plate is

$$L_{\min} = D_{\text{friction}} \cdot U_{\infty} - \text{Kin. Energy}_{\text{wake}}.$$

This ideal propulsion method is closely approached with low drag suction. For the case of a laminar flat nonsuction plate the kinetic energy of the boundary layer at the end of the plate is 0.214 ($D_{\text{frict.}} \cdot U_{\infty}$); i.e., the propulsion power and thus the equivalent drag of the plate might be reduced by 21.4 percent by reaccelerating the boundary layer at the end of the plate individually and without losses to the flight speed U_{∞} (ref. 37). For an infinitely long flat plate with distributed suction the minimum propulsion power would be 0.5 ($D_{\text{frict.}} \cdot U_{\infty}$) by reaccelerating the suction air to U_{∞} (ref. 37).

1.4 Flight Experiments on F94 LFC Wing Glove with Closely Spaced Slots

The next question arose concerning the performance of a slotted LFC wing with a large number of closely spaced slots under actual flight conditions. For this purpose an LFC wing glove (fig. 14) of modified NACA 65213 section with 69 suction slots, located on the glove surface between 0.4c and 0.96c, was mounted on the upper wing side of a straight wing F94A airplane (fig. 15, refs. 7, 10). The suction system (see experimental setup fig. 16) was operated by a radial flow suction compressor, driven by a radial flow air turbine, which was fed by main engine bleed air (ref. 38). The suction rates of the individual suction chambers and the total suction flow rate could be controlled by adjustable needle valves and varying the amount of air bleed from the lower wing surface into the common suction box.

Full chord laminar flow was maintained up to $Re_c \approx 37 \cdot 10^6$ with $C_{D_{\infty}} = C_{D_{\text{suct.}}} + C_{D_{\text{wake}}} = .00045$ and the corresponding optimum suction weight flow coefficient $C_{w_{\text{opt}}} = 0.000275$ to 0.0003 for the F94 LFC glove upper surface (fig. 17). As shown by plots $C_{D_{\text{suction}}}$, $C_{D_{\text{wake}}}$, and $C_{D_{\infty}}$ versus C_w for different Re_c 's (fig. 18) the wake drag is extremely small ($C_{D_{\text{wake}}} \approx .0001$) and represents about 1/4 of the total equivalent profile drag, while the equivalent suction drag contributes the remaining 75 percent of the total equivalent profile drag $C_{D_{\infty}}$.

The F94 LFC wing glove experiments thus verified full chord laminar flow under actual flight conditions at twice the wing chord Reynolds numbers of the Northrop TDT-model, confirming the King Cobra results (ref. 3) that the microscale atmospheric turbulence, primarily responsible for transition, is far too weak to significantly influence transition on LFC wings in flight. Transition on LFC surfaces in flight is then rather controlled by disturbances originating from the airplane and its propulsion and suction drive system; i.e., if such disturbances in the frequency range of amplified boundary layer oscillations were minimized or preferably eliminated through a particularly careful aerodynamic and acoustic design extensive or full length laminar flow would be feasible at further increased length Reynolds numbers.

In order to minimize or preferably avoid suction in the region of the main load carrying box of the wing and thus simplify the main wing structure, the flow acceleration in the front part of the wing was relied upon to adequately stabilize the boundary layer for prevention of premature transition. In contrast to the King Cobra results (ref. 3), however, an unexpectedly strong flow acceleration was needed on the F94 LFC glove in the nonsuction region upstream of 0.4c to maintain full chord laminar flow (fig. 19). Engine noise in the critical Tollmien-Schlichting (TS) frequency range may have excited amplified TS-boundary layer oscillations on the F94 LFC glove to require a surprisingly strong stabilizing flow acceleration in the front part of the glove, as compared to the smooth NACA 66216 King Cobra wing where propeller and engine noise frequency was far below the frequency range of amplified TS-boundary layer oscillations on the test surface.

In order to better stabilize the boundary layer of the F94 LFC glove up to substantially higher C_L 's and α 's, suction was subsequently extended upstream to 0.08c (refs. 9, 10). Full chord laminar flow was then observed with low suction rates at much higher C_L 's even with slightly decelerated flow between 0.08c and 0.5c (fig. 20, refs. 9, 10). Relatively weak suction thus appears surprisingly effective in stabilizing a laminar boundary layer, as compared to laminar boundary layer control through geometry (i.e., flow acceleration) alone. The same experience had previously been made by A. Braslow in the TDT-tunnel (ref. 11) on a 3-foot chord NACA 64A010 LFC wing model with a rather dense sintered bronze LFC suction surface with suction applied from 0.05c to the wing trailing edge. Full chord laminar flow had been maintained on this model up to $Re_c = 20 \cdot 10^6$ and $24 \cdot 10^6$.

At higher airplane speeds full chord laminar flow was maintained on the F94 wing glove up to a local Mach number $M_{local} = 1.08$ to 1.10 without shock waves (or perhaps very weak multiple shocks) and a gradual isentropic pressure recovery from supersonic to subsonic flow (fig. 21, refs. 6, 7, 10). At higher Mach numbers shock waves developed, and full chord laminar was then lost. This result should not necessarily be interpreted that laminar flow is lost as soon as shocks develop; tailoring the suction distribution according to the pressure distribution with shocks might avoid laminar separation and premature transition as in the case of boundary layer shock interaction with suction at supersonic speeds (refs. 39-41).

2. LFC INVESTIGATION AT VERY HIGH LENGTH REYNOLDS NUMBERS ON A SUBSONIC BODY OF REVOLUTION AND THE EFFECTS OF FREE-STREAM TURBULENCE.

With the application of LFC to large airplanes and possibly to fuselages the question arises concerning the suction laminarization at increasingly higher length Reynolds numbers Re_L . According to theory (refs. 42, 43), stable laminar boundary layers should be possible through area suction up to very high boundary layer - and length Reynolds numbers Re_θ and Re_L to enable full length laminar flow at extreme Re 's. These theoretical expectations were largely confirmed by transition experiments on a laminar flow Reichardt LFC body of revolution of fineness ratio 8 (figs. 22-34, refs. 44-46). Fig. 22 shows the body contour, suction slots and chambers with the boundary layer measuring rake at the rear end of the body. Area suction was approached by means of suction through 114 closely spaced 0.003" wide slots (body length 12 ft), with a particularly close slot spacing in the rear pressure rise area of the body where the body diameter decreases. Fig. 23 shows the potential flow velocity distribution, indicating a very flat pressure distribution over 80 percent of the body length, followed by a steep rear pressure rise over the rear 20 percent of the body. The figs. 24-26 present examples of the variation of the body wake drag $C_{D_{Wake}}$, equivalent suction drag $C_{D_{suction}}$ and total equivalent

drag $C_{D_{total}} = C_{D_{Suction}} + C_{D_{Wake}}$ versus the total suction flow coefficient $C_{Q_{total}}$ for a body length Reynolds number $Re_L = 37.8 \cdot 10^6$, $55.7 \cdot 10^6$ and $56.74 \cdot 10^6$, as measured in the Ames 12 ft pressure tunnel at five atmosphere tunnel pressure. (C_D and C_Q are based on body wetted area.) Full length laminar flow was observed up to $Re_L = 57.8 \cdot 10^6$ (*), with minimum equivalent drag values $C_{D_{total}}^{min} = 0.00027$ at optimum suction flow coefficients $C_{Q_{opt}} = .00017$. Fig. 27 presents $C_{D_{tot min}}$ and the corresponding $C_{Q_{opt}}$ versus Re_L . Up to $Re_L = 55 \cdot 10^6$ $C_{D_{tot min}}$ was only about 20 percent to 40 percent larger than the laminar flat plate skin friction drag and at higher Re_L 's about eight times smaller than the corresponding turbulent flat plate skin friction drag (!). $C_{D_{suction}}$ was again the main drag contributor, with $C_{D_{Wake}}$ contributing only about 1/3 to 1/4 to the total

(*) Laminar flow was lost at $Re_L > 58 \cdot 10^6$ as a result of contamination by a roughness particle in the tunnel, which at the time had been rather dirty from welding repair work done in the tunnel immediately prior to testing. Lack of testing time prevented cleaning of the model and a rerun at higher Re_L 's. $Re_L = 58 \cdot 10^6$ therefore does not necessarily indicate the upper length Reynolds number limit on this model in the Ames 12 ft. tunnel.

body drag at $Re_L \sim 50 \cdot 10^6$ (fig. 26). At lower Re_L 's ($37.8 \cdot 10^6$, fig. 25) laminarization seemed to be surprisingly insensitive to oversuction; even with nearly twice the optimum suction flow rates the total body drag increased only about by 35 percent.

Fig. 27 shows for comparison the drag results of the same body, as measured in the Northrop 7×10 ft low turbulence tunnel. Full length laminar flow was maintained up to $Re_L \sim 18 \cdot 10^6$ to $19 \cdot 10^6$ and lost at higher Re_L 's as a result of the higher tunnel turbulence, as compared to the extremely low turbulence level of the Ames 12 ft pressure tunnel at five atmospheres tunnel pressure.

Fig. 28 shows a correlation of the maximum laminar flow length Reynolds number Re_L on this Reichardt LFC body versus the external turbulence level u'/U_∞ for similar types of turbulence spectra, including results with turbulence wires mounted upstream of the body (ref. 47). For comparison, results are included from Braslow's porous bronze NACA A4 A010 LFC model (ref. 11) and USSR results on LFC wings at Tsagi (ref. 48). According to fig. 28 $Re_{L, \text{laminar}}$ of LFC surfaces, with area suction reasonably closely approached, varies approximately inversely proportional to the turbulence level u'/U_∞ . Thus, if it should prove possible to minimize or preferably avoid LFC airplane - or - propulsion induced disturbances in the frequency range of amplified boundary layer oscillations through an aerodynamically highly efficiency design and since the atmosphere can be considered as turbulence-free for transition it follows that substantially higher laminar flow length Reynolds numbers appear basically feasible on carefully laid out high performance LFC airplanes, as compared to the Ames 12 ft tunnel results.

Fig. 29 shows the equivalent area suction distribution along the body length at various Re_L 's (ref. 44), confirming Pretsch's theoretical result that for most effective boundary layer stabilization at high Re_L 's the highest suction rates should be applied rather far upstream where the boundary layer is least stable. After rapidly stabilizing the boundary layer in the front part of the body through stronger suction the suction rates can be progressively reduced in downstream direction, until higher suction velocities are required further downstream in the region of decreasing body radius and rear pressure rise.

The measured boundary layer profiles at the rear end of the body have been compared in fig. 30 with theoretical values, indicating a reasonably close agreement. Fig. 31 shows measured boundary layer profiles at the rear end of the body for different suction rates, showing the gradual loss of laminar flow by turbulent bursts at lower suction rates. The analysis of the boundary layer development along the body at $Re_L = 56.74 \cdot 10^6$ and $C_{q, \text{total}} = .000178$ shows laminar Re_θ - values somewhat above 3000 at the downstream end of the flat pressure region and as high as 5500 at the rear end of the body, with $H \equiv \delta^*/\theta \approx 2.3$ over a large part of the flat pressure region of the body (fig. 32). The figs. 33, 34 show the corresponding calculated boundary layer profiles at various stations along the body. Surprisingly stable and highly convex boundary layer profiles with rather low H-values were needed in the rear pressure rise area for full length laminarization, indicating that a laminar boundary layer with suction may be substantially less stable and boundary layer oscillation grow more rapidly when the external flow rapidly decelerates, just as disturbances entering a diffuser may rapidly grow, as compared to the case of constant free-stream velocity.

3. DEVELOPMENT OF SWEEP LAMINAR SUCTION WINGS.

3.1 Boundary Layer Crossflow Considerations on Swept LFC Wings.

With the higher critical Mach numbers of swept wings, the question arose in 1952 concerning the suction laminarization of swept LFC wings. In 1951 Gray (ref. 49) had discovered premature transition unexpectedly far forward on the smooth swept wing of an AW52 airplane at the R.A.E., Farnborough. China clay observations on this wing showed closely spaced streamwise striations prior to transition, indicating the development of closely spaced stationary and approximately streamwise boundary layer crossflow disturbance vortices induced by pressure gradients in crossflow direction, as interpreted by Owen and Randall (ref. 50) and independently by H. B. Squire. Figure 35 shows similar China clay pictures on a swept wing in the Ames 12-foot pressure tunnel (ref. 51), showing the formation of closely spaced streamwise striations corresponding to approximately streamwise boundary layer crossflow disturbance vortices induced by crossflow pressure gradients and apparently rotating in the same direction.

Figure 36 explains the formation of such crossflow disturbance vortices on swept LFC wings. With accelerated flow in the front wing area, followed by the rear pressure rise towards the wing trailing edge, pressure gradients develop in the direction n normal to the tangential flow direction t . Since the kinetic energy of the boundary layer especially close to the surface is smaller than that of the potential flow, the boundary layer streamline - in order for the boundary layer to be in equilibrium with the same crossflow pressure gradients as the potential flow - must be more strongly curved than the potential flow streamline (fig. 36). Inflexional-type boundary layer crossflow profiles then develop in the direction normal to the potential flow streamline. Due to the existence of inflexion points, such profiles are dynamically highly unstable at low boundary layer crossflow Reynolds numbers

$Re_n \equiv \frac{W_n \cdot \delta_{0.1}}{v}$ with high local amplification rates C_1 over a wide range of crossflow disturbance wave numbers α ; i.e., vortex spacings $\lambda = 2\pi/\alpha$.

The boundary layer stability problems of swept wings under crossflow conditions were discussed in a classical publication by Stuart et. al. (ref. 52), showing that the boundary layer crossflow stability on swept wings can often be treated to a first reasonably good approximation by solving the (linearized) Orr-Sommerfeld equation (1) (assuming mean parallel flow and $V = 0$ for the mean flow) for the

disturbance flow in the direction normal to the most critical crossflow disturbance wave-or-vortex front, coupled with the disturbance equation (2) along the wave front:

$$(W - C)(v'' - \alpha^2 v) - W'' \cdot v + \frac{i}{\alpha Re} (v^{IV} - 2\alpha^2 \cdot v'' + \alpha^4 v) = 0 \quad (1)$$

$$(W - C)u + \frac{i}{\alpha Re} (u'' - \alpha^2 u) - \frac{i}{\alpha} \cdot v \cdot U' = 0 \quad (2)$$

$$i\alpha w + v' = 0 \quad (3)$$

Primes denote derivatives with respect to the distance normal to the surface; W, w = boundary layer mean- and disturbance velocity normal to the wave front; $C = C_r + iC_i$ = complex phase velocity of disturbance wave; v = disturbance velocity normal to the surface; α = wave number = $2\pi/\lambda$ (λ = vortex spacing); Re = boundary layer Reynolds number; U, u = boundary layer mean and disturbance velocities along disturbance wave front. The above equations are valid under the assumption of small disturbances, parallel mean flow, $V = 0$, and neglecting small order terms in Stuart's general disturbance equations (ref. 52) due to streamline- and surface curvature.

Since the solution of (1) critically depends on the second derivative W'' of the mean boundary layer profile in the direction normal to the most critical crossflow disturbance vortices it follows for the design of swept LFC wings that their boundary layer development and stability must be analyzed at several angles between the crossflow disturbance wave front and the potential flow direction, until the most unstable disturbance flow has been found. Transition experiments by Gregory (ref. 52) on a rotating disc in the presence of boundary layer crossflow due to centrifugal forces showed substantially higher boundary layer crossflow stability limit- and transition Reynolds numbers as in the front part of swept wings. This result can be explained by the larger negative W'' -values of the normalized mean boundary layer crossflow profile on a rotating disc in the critical inner region of the crossflow boundary layer, as compared to the corresponding crossflow boundary layer in the leading edge region of swept wings. Therefore, the tangential- and crossflow boundary layer development on swept LFC wings was analyzed in many cases, with the figures 37, 38 showing as an example the case of the Ames test run 13 on the 30-degree swept Northrop LFC wing (*) of modified NACA 66012 - section at $Re_c = 23.7 \cdot 10^6$, $\alpha = 0^\circ$, $C_q = 3.84 \cdot 10^{-4}$ (one wing side). According to fig. 38 the crossflow velocity n/Q_∞ decreases progressively from relatively high values in the leading edge region towards the start of the rear pressure rise at 0.64c. With the simultaneous chordwise increase of the boundary layer thickness in this region the crossflow Reynolds number Re_n rises rapidly in the wing leading edge region and then remains approximately constant up to 0.64c. The shape of the normalized boundary layer crossflow profile between the leading edge and 0.64c changes insignificantly towards a slightly less stable boundary layer crossflow at 0.64c. In the rear pressure rise area, however, the combination of a relatively thick boundary layer with large crossflow pressure gradients generates a severe boundary layer crossflow with high Re_n 's towards the wing trailing edge region. Fortunately, W'' of the normalized boundary layer crossflow profiles in the vicinity of the surface is substantially more negative in the rearmost part of the wing, as compared to the wing leading edge region, i.e. boundary layer crossflow in this area is expected to be considerably more stable than in the front part of swept LFC wings. Therefore, much higher Re_n 's appear generally acceptable in steep rear pressure rise areas of swept LFC wings, as compared to the leading edge - and flat pressure areas.

3.2 Results of Brown's Analysis of the Boundary Layer Crossflow Instability on Swept Wings and a Rotating Disc.

The necessary analysis of the stability of the boundary layer crossflow was carried out by W. B. Brown (ref. 54) in the period from 1953 to 1959. The now common practice of integrating the Orr-Sommerfeld equation numerically was originated by Brown and the author.

Brown's boundary layer crossflow stability calculations, solving the Orr-Sommerfeld disturbance equation (for parallel mean flow and $V = 0$) in the direction normal to the most critical crossflow disturbance wavefront by finite difference methods, indeed verified substantially higher crossflow stability limit Re_n 's $Re_n = f(\alpha)$, when the location of the maximum crossflow velocity of normalized crossflow profiles was closer to the wall and W'' was accordingly more negative in the inner region of the boundary layer (fig. 39).

The figs. 40-45 show Brown's boundary layer crossflow stability diagrams α versus Re_n for the boundary layer crossflow profiles in the leading edge region of a swept wing, on a rotating disc, and in the rear pressure rise area of a swept LFC wing, both for the pure crossflow profile as well as the "critical" profile, where $W_n = 0$ at the inflexion point and the phase velocity $C_r \approx 0$ (i.e. stationary disturbance vortices) (fig. 46, 47; ref. 54). Curves of constant amplification factor C_i and phase velocity C_r are included in the figures 40-45. Both for the crossflow profiles in the leading edge region of swept wings as well as on a rotating disc, Brown's theoretical results showed lower crossflow stability limit Reynolds numbers and larger C_i -values (i.e. stronger local amplification) for the "critical" profiles with stationary crossflow disturbance vortices than for the pure crossflow profiles, as confirmed experimentally. In contrast, the pure crossflow profile 8 with travelling crossflow disturbance vortices in the steep rearmost pressure rise area of a swept LFC wing was less stable than the corresponding "critical" profile with stationary disturbance vortices. Indeed, hot wire observations on the 30° swept Northrop 66012 wing in the Michigan 5 x 7 ft low turbulence tunnel have

*ref. 53

confirmed the existence of travelling crossflow disturbance vortices, while naphthalene sublimation pictures have sometimes also shown stationary crossflow disturbance vortices.

The figures 48, 49 present the resultant boundary layer crossflow streamlines for two different initial disturbances over a disturbance wavelength, (ref. 54) confirming Stuart's result (ref. 52) as well as China clay flow observations (refs. 49-52) that the crossflow disturbance vortices rotate in the same direction. Furthermore, the figs. 48, 49 show that the crossflow disturbance vortices will penetrate for a considerable distance into the potential flow region.

Figure 50 shows boundary layer crossflow disturbance velocities w in crossflow direction and v perpendicular to the surface for the rotating disc "critical" profile, showing W_{max} around the location of the inflexion point, while v is a maximum close to the outer edge of the boundary layer where W crosses through zero and changes sign (ref. 54).

3.3 Low Drag Suction Experiments on the Northrop 30-Degree Swept 66012 LFC Wing.

The question now arises as to how far the boundary layer crossflow stability limit Reynolds number X_{min} on swept LFC wings can be safely exceeded. Assuming for the time being that X_{min} could be exceeded by the same margin as in the AW52 transition experiments (ref. 50), full chord laminar flow appeared theoretically feasible on swept LFC wings at high Re_c 's by extending suction far upstream towards the wing leading edge, stabilizing the boundary layer crossflow generated by the flow acceleration in the leading area by locally increased suction, and raising the suction rates in the rear pressure rise area somewhat over those of an equivalent unswept LFC wing (ref. 53) at a relatively minor penalty in equivalent wing profile drag. In order to confirm these theoretical expectations, a 30-degree swept slotted Northrop LFC wing of modified NACA 66012 suction with closely spaced slots was built and tested in the Michigan 5- by 7-foot, Northrop 7- by 10-foot, and Ames 12-foot pressure tunnel.

The experimental setup is shown in figure 51. To minimize blockage and maintain undisturbed spanwise flow, all tunnel walls were shaped according to the undisturbed streamlines around an infinitely long isolated yawing wing. Figure 52 shows the cross-section of the model with details of the suction slots and chambers. To maintain undisturbed, fully developed spanwise boundary layer crossflow in the test region of the model, auxiliary suction areas and chambers were provided (fig. 51).

Figure 53 shows $C_{D_{total}} = C_{D_{Suction}} + C_{D_{Wake}}$ versus Re_c at $\alpha = 0^\circ, \pm 1^\circ$, as measured in the Ames 12-foot and Northrop and Michigan tunnels (refs. 53, 55). Full-chord laminar flow was maintained up to $Re_c = 29 \cdot 10^6$, with $C_{D_{min}} = .00048$ for one surface. Only many years later was it realized that the loss of laminar flow at $Re_c > 29 \cdot 10^6$ was probably due to spanwise turbulent contamination along the front wing attachment line, originating from the upstream intersection of the wing leading edge with the supporting endplate. Figure 54 shows the corresponding optimum suction weight flow coefficient $C_{Q_{opt}}$ versus Re_c , indicating very low suction rates.

Figure 55 shows for a few typical cases the variation of $C_{D_{Suction}}$, $C_{D_{Wake}}$ and $C_{D_{total}}$ versus C_Q , indicating again the major drag contribution of $C_{D_{Suction}}$, while $C_{D_{Wake}} \approx 1 \cdot 10^{-4}$ contributed only about 20 percent to 25 percent to the total profile drag.

Figure 56 presents $C_{D_{total}}(Re_c)$ for $\alpha = \pm 1.5^\circ$ and -2° , as measured in the Ames 12-foot tunnel.

At these larger angles of attack, full-chord laminar flow was lost at progressively lower Re_c 's, presumably due to the above mentioned spanwise turbulent contamination along the front wing attachment line (at $\alpha = \pm 1.5^\circ$ and -2° , $(\partial U / \partial S)_{a.l.}$ is smaller and $Re_{\theta a.l.}$ is accordingly larger than at $\alpha = 0^\circ, \pm 1^\circ$).

Without suction in the upstream 0.25C in the Michigan 5- by 7-foot tunnel, full-chord laminar flow could be maintained up to $Re_c = 12 \cdot 10^6$, $\alpha = 0^\circ$ and was lost at higher Re_c as a result of premature transition due to excessive crossflow in the front nonsuction region (fig. 57, ref. 55).

Figure 58 shows typical chordwise suction distributions for several cases, showing peak suction rates close to the wing leading edge for control of the local boundary layer crossflow at higher Re_c 's, followed by weak suction in the flat pressure region and much stronger suction in the rear pressure rise area.

An analysis of the boundary layer development at $\alpha = 0^\circ$ and -1° showed that the minimum boundary layer crossflow stability limit Reynolds number X_{min} could be safely about doubled (figs. 59, 60, refs. 53, 56). Corresponding linearized growth calculations of boundary layer crossflow disturbance vortices (figs. 61, 62), using Brown's theoretical results (ref. 54), gave a total integrated growth factor of the crossflow disturbance vortices on this wing $e^{\int a_{ci} dt} = e^6$ to e^8 . For comparison, transition experiments of J. Carlson on a 25 percent-thick, 33-degree swept nonsuction wing (ref. 57) gave transition values at fully developed turbulent flow $e^{\int a_{ci} dt} = e^{12}$.

In the region of the rear pressure rise of the 30-degree swept Northrop LFC wing, $\int a_{ci} dt$ was somewhat lower than in the upstream flat pressure region of the wing (fig. 63), neglecting initial upstream stationary boundary layer crossflow disturbance vortices originating from the upstream flat pressure area of the wing. Since such upstream stationary boundary layer crossflow disturbance vortices may superimpose with the mean boundary layer crossflow in the rear pressure rise area, the

resulting crossflow is accordingly more pronounced locally to lead to higher integrated growth rates $\int \alpha \, c_i \, dt$.

When weakly amplified oblique Tollmien-Schlichting oscillations may superimpose with boundary layer crossflow disturbance vortices in the flat pressure region of swept LFC wings, such as at $\alpha = 1^\circ$ angle of attack or in the presence of acoustic disturbances, the crossflow vortices will be distorted 3-dimensionally and thus stretched and convected downstream. Under the action of the resulting nonlinear interaction Reynolds stresses of the two disturbance modes involved, the boundary layer crossflow disturbance vortices may then grow substantially quicker than according to linearized disturbance theory. Indeed, an analysis of the linearized growth of boundary layer crossflow disturbance vortices on the 30-degree swept Northrop LFC wing at $\alpha = 1^\circ$ gave substantially lower growth rates $\int \alpha \, c_i \, dt$ than at $\alpha = 0^\circ$ and -1° angle (figs. 64a, b) - i.e., linearized growth calculations of crossflow disturbance vortices give unrealistic results whenever oblique TS-oscillations interact nonlinearly with them.

3.4 Investigation of Swept LFC Wings in the Presence of Acoustic Disturbances.

In a similar manner, external as well as internal acoustic disturbances, originating from the air-plane and its propulsion and suction drive system, can excite amplified TS-boundary layer oscillations especially in the flat pressure area of swept LFC wings, where relatively weak suction is adequate for control of boundary layer crossflow instability to render the streamwise boundary layer flow component accordingly more sensitive to TS-type disturbances. External acoustic disturbances become particularly critical for larger high subsonic speed LFC airplanes with wing-mounted engines, which are usually advantageous from the standpoint of wing structural weight and balance of the airplane. For this reason, the previously mentioned 30-degree swept Northrop LFC wing was tested in the Northrop 7- by 10-foot tunnel in the presence of external tone- and broad-band noise (ref. 58, fig. 65). "Longitudinal" sound wave fronts were supposed to be generated by an air-modulated transducer located upstream of the wind tunnel screens (fig. 65). "Lateral" sound waves were supposed to be generated by an air-modulated transducer as well as speakers mounted on top of the tunnel wall (fig. 65). To minimize sound reflections and standing waves in the test section, the tunnel walls in the test section and part of the wind tunnel walls were acoustically lined; furthermore, the tunnel turning vanes downstream of the first diffuser were acoustically lined to further reduce reflected sound waves. Even with all these precautions, the experimental setup was far from ideal; standing sound waves often developed in the test section especially with pure tones.

Additional transition experiments with internal tone- and broad-band noise in the suction ducts were subsequently conducted on a 33-degree swept LFC wing designed by the X-21 group (ref. 59).

Sufficiently strong external tone- and broad-band sound caused premature transition on the 30-degree swept LFC wing in the region of the flat pressure distribution, where the streamwise boundary layer flow component was least stable with respect to amplified TS-oscillations. External sound usually did not cause premature transition in the rear pressure rise area, where the streamwise boundary layer profiles on swept LFC wings were highly stable with respect to TS-disturbances. External as well as internal sound, especially pure tones, were particularly critical in the frequency range of amplified TS-oscillations in the flat pressure region of swept LFC wings (fig. 66, refs. 33, 58, 59). Outside of this frequency range, the permissible sound pressure (or sound particle velocity ratio t'/Q_∞ , evaluated under the assumption of 2-dimensional sound waves) rose rapidly (fig. 66), especially in the presence of internal-duct tone noise. The maximum internal duct sound pressure increased rapidly by stabilizing the boundary layer in the area of the particular duct where sound was applied by raising its suction rate or the flow acceleration at smaller angles of attack (fig. 66). Evidently, in the presence of internal duct noise, increased local flow acceleration or suction stabilizes the streamwise boundary layer flow component such as to minimize amplified TS-oscillations in this region, which otherwise would interact nonlinearly with boundary layer crossflow disturbance vortices through their mutual nonlinear Reynolds interaction stresses to lead to a particular rapid resonance-like growth of boundary layer disturbances.

Figure 67 shows the variation of the permissible sound particle velocity ratio t'/Q_∞ , assuming 2-dimensional sound waves, versus Re_c for the 30-degree swept Northrop LFC wing in the presence of external sound in the most critical frequency range. With normal or slightly increased suction, Re_c with full-chord laminar flow varies approximately inversely proportional to t'/Q_∞ and is of similar magnitude as with external turbulence, i.e. $(t'/Q_\infty)_{crit} \sim (u'turb/Q_\infty)_{crit}$ (fig. 28). X-21 data, as measured on the upper wing surface at substantially higher Re_c 's, are included for comparison in figure 67. With substantially increased suction rates in the flat pressure region of the wing and especially in the wing leading edge area, considerably higher sound pressures were acceptable (fig. 67). In addition, figure 67 shows the sensitivity of the 30-degree swept LFC wing to even very weak acoustic disturbances especially at higher Re_c 's, when they caused a periodic in- and outflow out of small surface cavities such as pin holes, static pressure orifices, open nonsucking slots or slots with very small suction flow rates and correspondingly small pressure drops, etc., even though such surface cavities were airtight at their inside end. In other words, open surface cavities, even though sealed inside, as well as other surface roughness can become substantially more critical on LFC wings when strong external and internal acoustic disturbances - especially in the frequency range of amplified TS-boundary layer oscillations are present, as compared to the case when such acoustic disturbances are absent.

The critical sound pressure was generally appreciably lower with marginal suction rates and correspondingly small pressure differences Δp_{skin} between the external surfaces and the suction ducts especially in the upstream flat pressure region of swept LFC wings - particularly with internal duct noise. Indeed, figure 68 shows increasingly larger velocity fluctuations v' at the slot inlet with

decreasing Δp_{skin} at a given duct sound pressure $P_D(*)$. Therefore, acoustic disturbances - especially in the suction ducts - become more critical when the pressure drop Δp_{skin} across the suction surface in the flat pressure area of swept LFC wings is reduced; i.e., when superior performance is emphasized, and vice versa.

Among internal acoustic duct disturbances, standing sound waves in the suction ducts in the presence of duct tone noise can generate particularly high local duct sound pressures to precipitate transition at the location of maximum duct sound pressure (fig. 69). Such standing sound waves in the suction ducts should, therefore, be prevented through sound absorption by acoustic linings in the duct, especially at the duct ends, possibly by suitable duct geometry and if at all possible, by avoiding or minimizing duct tone noise in the first place.

In contrast to duct tone noise standing waves in the ducts were absent with duct broadband noise even with narrow frequency bands (fig. 69).

According to the naphthalene sublimation pictures with standing sound waves in the suction ducts of the 33-degree swept LFC wing (fig. 69) as well as with external sound on the 30-degree swept LFC wing (fig. 70) transition with noise is preceded by the formation of closely spaced streamwise striations, indicating streamwise boundary layer crossflow disturbance vortices generated by the external and internal sound, being otherwise absent without such sound. Amplified oblique TS-disturbance vortices, induced by sound in the flat pressure region of swept LFC wings, may then interact with boundary layer crossflow and crossflow disturbance vortices through their mutual nonlinear interaction Reynolds stresses. Evidently, even with weakly amplified oblique TS-oscillations, the TS-disturbance velocity component in crossflow direction becomes large as compared to the usually rather small mean boundary layer crossflow velocity in the flat pressure region of swept LFC wings; i.e., the nonlinear interaction Reynolds stresses between the two disturbance modes become large. The boundary layer crossflow stability limit Reynolds number then decreases below its small disturbance value (see Stuart, ref. 60); i.e., crossflow disturbance vortices on swept LFC wings in the presence of acoustic disturbances can develop at substantially lower Re_c 's. Furthermore, as a result of the stretching and convection of the boundary layer crossflow disturbance vortices by oblique TS-oscillations, the resulting disturbance motion may eventually grow in a particularly rapid resonance-like manner to precipitate transition at substantially smaller boundary layer crossflow Reynolds numbers than in the absence of sound (refs. 60-64). To minimize or preferably avoid such nonlinear interaction between amplified TS-oscillations and crossflow disturbance vortices on the swept wings of an LFC airplane, either amplified TS-oscillations or boundary layer crossflow disturbance vortices in the flat-pressure region of swept LFC wings should be minimized or preferably avoided. This can be accomplished either by minimizing or eliminating aerodynamic and acoustic disturbances generated by the airplane and its propulsion system in the frequency range of amplified TS-oscillations, by sufficiently stabilizing the boundary layer against TS-disturbances through increased suction in the flat pressure area of swept LFC wings and/or designing swept LFC wings in such a manner that boundary layer crossflow is critical only over a relatively small percentage of the wing chord.

3.5 Investigations on the Elimination of Spanwise Turbulent Contamination Along the Front Attachment Line of Swept LFC Wings.

A necessary condition for laminar flow on swept wings at high Re_c 's is the elimination of spanwise turbulent contamination along the front wing attachment line. This phenomenon was discovered first in 1951 by Gray (ref. 49) during flight transition experiments on the AW52; it was further investigated by Gregory (ref. 66) and rediscovered by the author in connection with the X21 airplane flight tests (refs. 33, 67-71). Similarly, the British as well as the Russians originally encountered extensive loss of laminar flow on the British Lancaster 40° swept LFC fin and the 35° swept Soviet LFC wing in the Tsagi tunnel without being aware of the cause; after discussing the problem with the author and adopting partially similar methods as developed by the Northrop Boundary Layer Group and the author they were able to eliminate such spanwise turbulent contamination on their swept LFC wings as on the X-21 airplane.

Since each element of a turbulent wedge can be considered as a starting point of a new turbulent wedge it is obvious from fig. 71 that turbulent wedges, originating from a large leading edge roughness or an initial turbulent attachment line boundary layer, for example at the wing-fuselage intersection, can spread both chordwise as well as spanwise along the front attachment line of swept wings whenever the angle between the local potential flow streamline and attachment line is smaller than the half spread angle of a turbulent wedge. The question then arises concerning the condition for spanwise turbulent contamination along the front attachment line of swept wings in the presence of large leading edge disturbances. Since the condition of the attachment line boundary layer depends on the balance of the pressure - and inertia forces versus the viscous forces acting on the boundary layer it follows that the spanwise attachment line boundary layer momentum thickness Reynolds number Re_{θ} should be a useful parameter in defining the condition for spanwise turbulent contamination,

a.l.
as long as transition is caused directly by large disturbances; i.e., when the pressure and inertia forces acting on the attachment line boundary layer dominate over the corresponding viscous forces above a critical $Re_{\theta, a.l. crit}$ the attachment line boundary layer will be turbulent. Vice versa, the dominating viscous forces in the attachment layer below $Re_{\theta, a.l. crit}$ suppress the formation of turbulent eddies in the attachment line boundary layer, i.e., the attachment line flow becomes laminar when $Re_{\theta, a.l.} < Re_{\theta, a.l. crit}$ even with large leading edge disturbances or an initially

(*)See R. F. Carmichael and P. E. Finwall; Analysis of the results of the laboratory duct model test for the X21A laminar flow aircraft; Northrop Rep. NOR-65-303, 1965.

turbulent attachment line boundary layer, as verified for example during the first flight tests on the outboard X-21 wing. The enclosed table shows $Re_{\theta_{a.l. \text{ crit}}} = 90$ to 100, as evaluated from different sources, when spanwise turbulent contamination is caused directly by large disturbances.

$$\text{Since } Re_{\theta_{a.l.}} = \frac{W \cdot \theta_{a.l.}^*}{\sqrt{v \cdot (\partial u / \partial s)_{a.l.}}} \approx \frac{\theta_{a.l.}^*}{\sqrt{1 + (t/c)_{ell}}} \cdot \frac{\sin \phi}{\sqrt{\cos \phi}} \cdot \sqrt{\frac{Q_{\infty} R_{o_1}}{v}},$$

$$\text{Where } \theta_{a.l.} = \theta_{a.l.}^* \sqrt{\frac{v}{(\partial u / \partial s)_{a.l.}}} \quad \text{and } \theta_{a.l.}^* = \text{function of } v_o^* \equiv \frac{v_{o_{a.l.}}}{\sqrt{v \cdot (\partial u / \partial s)_{a.l.}}},$$

it follows that $Re_{\theta_{a.l.}}$ can be reduced to safe values by decreasing wing sweep ϕ , leading edge radius R_{o_1} , and unit length Reynolds number Q_{∞}/v . In addition, boundary layer suction at the attachment line of swept wings thins the attachment line boundary layer (fig. 72) and thus further decreases $\theta_{a.l.}$, $\theta_{a.l.}^*$ and $Re_{\theta_{a.l.}}$ (ref. 72).

Of course, as demonstrated first on swept wind-tunnel models and applied later to the X-21 wing (refs. 33, 71) spanwise turbulent contamination on swept wings can be eliminated relatively easily by locally removing the entire turbulent attachment line boundary layer, including all the turbulent boundary layer eddies which intermittently penetrate far out into the potential flow, by means of boundary layer suction (through one or many slots or rows of holes, etc.) or by means of a leading edge fence, with suction applied on its outboard side to maintain attached flow (fig. 73). After reestablishing laminar attachment line flow the previously quoted transition value $Re_{\theta_{a.l. \text{ crit}}} = 90$ to 100 for large disturbances could be appreciably exceeded, depending on the magnitude of the initial attachment line boundary layer disturbances where laminar flow had been reestablished (refs. 33, 71) (fig. 73).

In order to substantially raise $Re_{\theta_{a.l. \text{ Transition}}}$, turbulent eddies in the initial attachment line boundary layer must be completely eliminated. This can be accomplished for example by means of sufficiently strong local suction (suction patch) (refs. 33, 65), a laminar flow leading edge suction fence (refs. 33, 73), a local leading edge bump with opposite sweep on its inboard end (Gaster), a local intake at the wing leading edge, or by sweeping the wing backwards in both directions and starting with an undisturbed laminar boundary layer at the wing apex stagnation point. This latter approach was adopted during transition experiments with and without boundary layer suction at the front attachment line of a 45° swept blunt-nosed wing in the Northrop 7 x 10 ft tunnel (fig. 74) (refs. 65, 72).

On its impervious leading edge without suction turbulent bursts started at the downstream end of the attachment line at $Re_{\theta_{a.l. T}} = 243$ and a spanwise length Reynolds number $Wz/v = 5.5 \cdot 10^6$ (ref. 72) (Z = spanwise distance along attachment line). Similar $Re_{\theta_{a.l. T}}$ - values without suction had been observed on a 33° swept 15 percent thick LFC wing of the X-21 group with a laminar flow leading edge suction fence in the Ames 12 ft tunnel at $Wz/v = 17.5 \cdot 10^6$ (ref. 73). Apparently, the extremely low turbulence - and noise level of this tunnel enabled laminar attachment line flow up to substantially larger Wz/v - values than at the higher turbulence level of the Northrop-tunnel. In flight, where the atmospheric turbulence has but an insignificant influence on transition (except in ice clouds), Wz/v at a given $Re_{\theta_{a.l.}}$ might be considerably larger than even in the Ames 12 ft tunnel, provided disturbances generated by the airplane and its propulsion - and suction drive system in the frequency range of amplified attachment line boundary layer oscillations are minimized.

Although the described $Re_{\theta_{a.l. T}} = 240$ is substantially increased by eliminating large initial disturbances Re_{θ_T} is still very much smaller than for flatplate flow ($Re_{\theta_T} \approx 1100$ to 1480 at the beginning of transition) or on the King Cobra wing with a flat pressure distribution ($Re_{\theta_T} \approx 1800$). These relatively low values are explainable by the destabilizing influence of the transverse stretching of the TS-attachment line boundary layer disturbance vortices in the diverging potential flow field of swept wings (ref. 76), the long laminar run lengths along the front attachment line (expressed in multiples of the TS-wave length) and the fact that (as a result of the practically constant boundary layer along the attachment line) the local TS-growth factor C_i is essentially constant along the entire attachment line to lead to a particularly large total growth for TS-oscillations. Therefore, the (already low) attachment line boundary layer stability limit Reynolds number may not be appreciably exceeded.

Besides thinning the attachment line boundary layer, area suction changes the shape of the attachment line boundary layer profiles (fig. 72, table , ref. 72) such as to increase their stability limit Reynolds number with increasing suction. To verify the stabilizing influence of area suction on the attachment line boundary layer of swept wings and better understand the transition mechanism involved, transition experiments were conducted on the aerodynamically smooth attachment line of a 45° swept wing in the Northrop 7 x 10 ft tunnel (fig. 74, ref. 72). Area suction in the attachment line region was approached by suction through 0.002 to 0.0025 "wide and 0.232" spaced chordwise slots (fig. 75) whose slot flow Reynolds number $\bar{v} s/v \leq 100$, except in local nose suction

patches with strong local suction, where two rows of suction holes, symmetrical to the slots, had been used to minimize suction slot wake induced disturbances at higher $\bar{v} s/v$'s (refs. 74, 75).

Regular amplified TS-attachment line boundary layer oscillations had been observed on this model (fig. 76, ref. 72) leading to transition at higher $Re_{\theta a.l.}$. The frequency of these oscillations correlated with corresponding theoretical results of Brown (ref. 76, fig. 77). Fig. 78 shows $Re_{\theta a.l.}$

versus the nondimensional equivalent area suction velocity $v_{o.a.l.}^* \equiv \frac{v_{o.a.l.}}{\sqrt{\gamma \cdot (\partial u / \partial s)_{a.l.}}}$ for different

spanwise length Reynolds numbers Wz/γ along the attachment line. $Re_{\theta a.l.}$ increases substantially for higher suction rates at the attachment line and decreases with increasing Wz/v - values. As mentioned previously, substantially higher Wz/v 's at given laminar $Re_{\theta a.l.}$'s should be possible at

lower initial disturbance levels, especially in flight with drastically reduced airplane - and propulsion-induced disturbances in the amplified TS-frequency range of the attachment line boundary layer.

In case roughness, etc. should cause spanwise turbulent contamination in the form of turbulent bursts or a fully developed turbulent attachment line boundary layer at such high $Re_{\theta a.l.}$'s, local

leading edge suction patches with strong suction followed by progressively weaker suction downstream along the attachment line - with the local suction rates controlled by suitable attachment line boundary layer sensors - can reestablish undisturbed laminar attachment line flow at high $Re_{\theta a.l.}$,

as verified experimentally (ref. 65).

4. INFLUENCE OF SUCTION INDUCED - AND SURFACE DISTURBANCES ON SUCTION LAMINARIZATION.

Similar to sound, laminar boundary layer oscillations and transition can result from suction induced disturbances at high Reynolds numbers (refs. 15-26, 74, 75). For example, slot flow fluctuations can be induced by slot wake oscillations in the small plenum chambers underneath the slots at higher slot flow Reynolds numbers, which may cause premature transition. When the flow in the slots in the plenum chambers located below the slots was viscous and steady below a critical slot flow

Reynolds number $Re_{s.crit} = \frac{\bar{v} \cdot s}{\nu} = 100$ (fig. 79, 80). No suction induced disturbances had been

experienced on laminar suction surfaces with full length laminar flow beyond $50 \cdot 10^6$ length Reynolds number. Above $Re_{s.crit}$, however, according to low speed flow experiments on large scale slots in

water and air, the slot wake became unstable and started oscillating downstream of the slot exit, until transition developed further downstream. These wake flow oscillations in the plenum chambers induced flow fluctuations, v' , at the slot inlet and in the external boundary layer (refs. 74, 75), which grew rapidly when $Re_{s.crit}$ was exceeded (see for example curve for deep plenum chambers in figure 80).

Such slot wake fluctuations seem to have caused premature transition and a correspondingly higher drag on the 33-degree swept laminar suction wing in the Ames 12-foot tunnel when $Re_{s.crit}$ was appreciably

exceeded in the rear pressure rise region downstream of 0.4c at $Re_c > 25 \cdot 10^6$ to $30 \cdot 10^6$ (fig. 81), (ref. 73). The design slot flow Reynolds number in this area was 200 at $Re_c = 40 \cdot 10^6$. At $Re_c >$

$20 \cdot 10^6$, the boundary layer in the rear pressure rise area of this model became unexpectedly sensitive against oversuction. More extensive laminar flow with lower drags was usually observed with alternating high and low suction rates in adjacent suction chambers of the rear pressure rise area, as compared to a uniform suction distribution in this region (fig. 82). Presumably with the nonlinear growth of v'/\bar{v} versus Re_s , boundary layer oscillations on this suction wing grew slower in downstream direction with alternating suction rates and Re_s - values (for example, $Re_s = 100$ and 300 in adjacent suction chambers) than with uniform suction ($Re_s = 200$). Preceding transition regular high frequency boundary layer oscillations in the critical Tollmien-Schlichting frequency range, superimposed over rather regular oscillations of about 10 times lower frequency were observed at 80 percent chord at $Re_c > 30 \cdot 10^6$.

In order to minimize the number of slots on laminar suction surfaces without inducing slot wake fluctuations, the question arose as to how to raise $Re_{s.crit}$ and maintain a viscous steady flow in

the plenum chambers underneath the slots at further increased slot flow Reynolds numbers. This can be accomplished for example by using shallow plenum chambers and a corresponding larger number of suction holes located in two rows at opposite sides of the slot (fig. 80).

A single row of suction holes aligned with the slot showed a similar increase of $Re_{s.crit}$ with decreasing plenum chamber depth as two rows of holes located symmetrically with respect to the slot (fig. 80). Small displacements of such a single row of holes against the slots, however, rapidly reduced $Re_{s.crit}$ to 100. Plenum chamber flow observations explained this unexpected drop of $Re_{s.crit}$ (fig. 83) for a displaced single row of suction holes: With a single row of holes, aligned with the slot, or two rows of holes at opposite equal distances from it the slot wake was deflected 2-dimensionally (except close to the holes) about symmetrically in fore and aft direction downstream

of the stagnation region on the lower surface of the chamber towards its sides. In shallow chambers ($h \leq 2s$), three or more spanwise vortices generally developed on each side of the slot and carried the suction medium towards the holes (fig. 83). Slot flow fluctuations started when these vortices became unstable and oscillated. With deeper plenum chambers, these vortices were less pronounced. When the slot wake, after impinging on the bottom chamber surface, split into two separate and practically equal chordwise flow components whose Reynolds numbers were only half as large, as compared with a wake flow deflected entirely towards a single displaced row of holes (fig. 83), the above-mentioned chamber vortices were accordingly weaker and therefore became unstable at higher $Re_{s, crit}$.

In contrast to a single row of suction holes, the flow in relatively shallow plenum chambers changed insignificantly when two rows of suction holes were located at different distances from the slot; i.e., two rows of holes opposite to the slot are relatively insensitive to hole misalignment. Furthermore, slot flow fluctuations induced by internal duct noise as well as spanwise suction variations along the slot from one hole to the next are weaker with two rows of displaced holes, as compared to a single row of holes in line with the slot.

In conclusion, slotted laminar suction surfaces at high Reynolds numbers should preferably be laid out for viscous steady slot wakes, achieved by maintaining purely viscous slot wakes either at $Re_s \leq 100$ with unsophisticated plenum chamber designs or by using shallow plenum chambers and two rows of holes located at opposite sides of the slot, enabling considerably higher Re_s with purely viscous plenum chamber flow.

Similarly, with low drag suction applied through perforated surfaces, transition can be caused directly as a result of the breakup of streamwise and horseshoe vortices originating from the suction holes (fig. 6, refs. 15-26). Alternately, amplified TS-type boundary layer oscillations may be excited by disturbance vortices trailing downstream from suction holes to cause premature transition, especially when the boundary layer is thin and the height of the mean sucked layer per row of holes is relatively large compared to the boundary layer thickness. Such premature transition was indeed experienced during transition experiments at the front attachment line of the described 45-degree swept blunt-nosed wing when suction at the attachment line had been applied through rows of closely spaced holes, as shown in figure 84 (refs. 33, 65). Naphtalene flow sublimation photographs (fig. 85) show streamwise striations, indicating streamwise disturbance vortices, trailing downstream of each suction hole, introducing periodic disturbances into the front wing attachment line boundary layer to cause premature transition at ridiculously low mean Reynolds numbers, $\bar{u}h/\nu$ per row of holes.

\bar{u} and \bar{h} are the mean velocity and mean height of the sucked layer per row of holes, respectively.

Many other suction induced disturbances can cause transition either directly or as a result of amplified boundary layer oscillations whenever the spanwise vorticity of the boundary layer $\partial u/\partial y$ changes abruptly in spanwise direction downstream of suction discontinuities to generate accordingly streamwise disturbance vorticity, which in addition may superimpose with the mean- and disturbance streamwise vorticity already present in the crossflow boundary layers of swept LFC wings. Such suction discontinuities are encountered with slot ends, with partially or fully clogged holes or plenum chambers underneath the slots, with partially or fully clogged slots, damaged slot edges or discontinuous irregular slots, with rapid spanwise changes in the local suction rates in the area of chordwise suction duct dividers, in regions of chordwise splices or chordwise gaps between the main wing and flaps, etc., etc. Since surface disturbances critically affect laminarization, emphasis was given to establish permissible 2- and 3-dimensional surface tolerances on unswept and swept LFC wings. As an example, figure 86 shows the maximum permissible amplitude of 2-dimensional single continuous surface waves, as measured on the straight wing F94 LFC glove in flight and at considerably lower Re_c 's on the 30-degree swept Northrop LFC wing for different wave lengths. For multiple waves, the permissible wave amplitude decreases substantially (fig. 87, refs. 8, 77, 78). Taking into account that such surface waves are not necessarily continuous along the span, thus adversely affecting the local suction distribution in the region of the wave, it is recommended to provide substantial margins for the permissible surface waviness.

The influence of 3-dimensional surface roughness on unswept laminar flow wings with and without suction has been reported in detail by V. Doenhoff and A. Braslow (ref. 79). Their results have essentially been verified by F94 LFC flight experiments with 3-dimensional roughness. Figure 88 shows in particular the rapid increase in permissible roughness height with decreasing unit length Reynolds number at higher altitudes (ref. 8). See also refs. 80-83 for three-dimensional roughness influence on transition.

The figures 89, 90 show the maximum permissible height of three-dimensional roughness particles in the critical leading edge region of the 15 percent thick 33-degree swept Northrop LFC wing model (ref. 84), indicating comparable critical roughness Reynolds numbers Re_k as on unswept LFC wings, as long as the boundary layer crossflow is adequately stabilized by suction. On swept laminar flow nonsuction wings, however, when the boundary layer crossflow is not stabilized by suction, premature transition may occur at some distance downstream of the three-dimensional roughness element at considerably lower Re_k - values than on unswept laminar flow wings (fig. 90b).

Figure 91 shows the variation of the height h of back- and forward-facing 2-dimensional spanwise steps and of spanwise gaps, assuming that air leakage into the boundary layer is prevented. The critical step height Reynolds number $(\bar{u}h/\nu)_{wall, crit}$ of 2-dimensional spanwise steps varies from 800 to 1,200 for backward facing steps in the front and center to rear region of LFC wings; the corresponding values for forward facing steps vary from 2,000 to 2,700. Nonleaking 2-dimensional spanwise gaps show surprisingly large critical Reynolds numbers $(\bar{U}l/\nu)_{crit} \sim 25,000$. Weak local suction in the flow

reattachment area of backward facing steps has doubled the permissible step Reynolds number from $U_h/v = 1,100$ to $2,200$ (ref. 85).^{*} It is to be expected that suction may similarly shorten the chordwise extent of the free vortex layer in areas of forward facing spanwise steps or spanwise gaps to substantially raise the height of such forward facing steps and spanwise gaps.

5. SUPERSONIC LFC EXPERIMENTS.

5.1 Experiments on a Laminar Suction Plate and Suction Body of Revolution at Supersonic Speeds in the 40- by 40-Inch Tullahoma A Tunnel (copied from ref. 87).

These experiments were conducted at the supersonic Tunnel A of the Arnold Engineering Development Center in Tennessee. Tunnel A is a continuous closed circuit variable density wind tunnel with a 40- by 40-inch test section. The present program utilized the Mach number range between 2 and 4, predominantly at high Reynolds numbers. A maximum Reynolds number of $8 \cdot 10^6$ per foot was available at $M = 3.0$.

The flat plate suction model of 41-inch chord is shown in figure 94. The model was mounted in the tunnel walls. Suction was applied through 76 slots arranged in eight suction chambers. The first slot was located 2.0 inches from the leading edge. The average slot width was 0.005 inch, and the average slot spacing 0.5 inch. The spanwise extent of the slots decreased along the chord by allowing a wedge angle of about 8 degrees for the spread of turbulent disturbances originating at the slot ends.

In the suction area, the model was composed of two layers which were bonded together. An inner structure of 0.31-inch thickness contained small spanwise plenum chambers and rows of holes; the outer skin was 0.02 inch thick and the slots were cut into this layer at the location of these plenum chambers after bonding. The sucked air flowed through the slots and holes into collecting suction chambers inside the model. The values of slot widths and hole diameters were determined according to the expected suction requirements for the test program.

The sucked air from the chambers was ducted through the tunnel wall to individual suction boxes where the suction quantities were controlled and measured by means of calibrated nozzles. The sucked air was removed through a 12-inch diameter pipe connected to the vacuum system of the facility.

The model was equipped with pressure and temperature instrumentation for measuring the suction quantities. A movable rake of total head probes permitted the observation of the boundary layer at several chordwise stations.

The experiments were conducted in such a way that - at a given Mach and Reynolds number - laminar flow was established over the suction area by a suitable suction distribution. Then suction was varied systematically and the boundary layer profiles were recorded at the aft end of the suction area.

The wake drag coefficient, C_{DW} , was determined by the momentum loss of the boundary layer at the plate trailing edge. Since all experiments thus far were conducted in the absence of surface heating or cooling, the boundary layer velocity and density profiles were evaluated from the measured total head readings under the assumptions of constant static pressure and total temperature through the boundary layer. The equivalent suction drag coefficient, C_{DS} , was evaluated from the measured suction mass flow rates and static pressures in the individual chambers, assuming the same values for suction compressor and propulsive efficiency and acceleration of the suction air to free-stream velocity.

Since the wake drag with full laminar flow decreases and the suction drag increases with increasing total suction mass flow (see figure 95 for typical example), an optimum total suction mass flow coefficient exists at which the total drag, being equal to the sum of wake and equivalent suction drag, reaches a minimum. These minimum total drag and optimum total suction mass flow coefficients were evaluated as functions of Mach and Reynolds numbers.

The drag results for the flat plate suction model are presented in figure 96. Maximum Reynolds numbers (based on a length of 40.2 inches) with full chord laminar flow were $26 \cdot 10^6$ at $M = 3.0$ and $22 \cdot 10^6$ at $M = 3.5$. They were obtained at the highest pressures available in Tunnel A. The minimum total drag coefficients at $M = 3.0$ and 3.5 , including the equivalent suction drag, were 28 percent and 39 percent, respectively, of the skin friction coefficients of a turbulent flat plate at the same Mach and Reynolds number.

The optimum suction mass flow coefficients varied between 2 to $3 \cdot 10^{-4}$, being of the same order of magnitude as in subsonic flow. More suction was required at the higher Mach number.

Laminar flow control by means of boundary layer suction was also applied to pointed bodies of revolution at zero angle of attack. As an example, a 78-inch long suction body with a cylindrical aft body of 9.2-inch diameter (fig. 97) was tested in the Tullahoma A Tunnel to demonstrate the feasibility of laminar flow at high Reynolds numbers by means of boundary layer suction in a wind tunnel. Suction was applied through 150 slots connected to 13 suction chambers. The model was built of an inner structure with rows of holes for the passage of the suction air. Then outer rings were shrunk airtight over the inner structure, and the gaps between adjacent rings were opened with a cutting tool to the desired slot widths. The air collected in each chamber was ducted through the bulkheads of the following chambers so that the mass flow rates of the various chambers could be adjusted and measured individually.

^{*}Figures 92, 93.

Full length laminar flow was achieved over the whole body up to the maximum tunnel pressures available, resulting in length Reynolds numbers of $42 \cdot 10^6$ at Mach number 2.5 and $51.5 \cdot 10^6$ at Mach 3.0. The minimum total drag (including the equivalent suction drag) and the corresponding optimum total suction mass flow coefficients at $M = 3.0$ are plotted versus length Reynolds number in figure 98. The total drag at $50 \cdot 10^6$ Reynolds number is only 23 percent of the friction drag of a turbulent plate. The measured boundary layer profiles at this Reynolds number and with near optimum suction was about 0.070 inch thick. At the rear end of the body the boundary layer momentum thickness Reynolds number, Re_θ , with laminar flow was larger than 3,000. For comparison, the corresponding laminar Re_θ -values on the flat plate suction model at Mach 3.0 and a length Reynolds number of $25 \cdot 10^6$ stayed slightly below 3,000.

Included in figure 98 are the results of two earlier suction experiments on smaller bodies of revolution which were conducted in the 12-inch supersonic blowdown tunnel at the Arnold Center. The first experiments which were conducted at $M = 3$ in 1958 produced a maximum length Reynolds number of $7 \cdot 10^6$ with suction through relatively few slots, while the drag of the nonsuction body with slots sealed started to rise at a Reynolds number of $4 \cdot 10^6$. A second model of the same shape and an improved suction system with a considerably larger number of slots produced laminar flow at $M = 3$ to a Reynolds number of $12 \cdot 10^6$. The laminar drag coefficients of the three configurations can be connected by a single straight line in the logarithmic scale. Its slope indicates that the minimum total drag of the suction bodies is approximately proportional to the $(-1/3)^{rd}$ power of the length Reynolds number. The optimum total suction mass flow coefficients of the three models also fall on a single curve.

5.2 Interaction of Incident Shock Waves with Laminar Boundary Layers at Supersonic Speeds (refs. 39-41).

The present experiments on the laminar suction plate and body of revolution were conducted in the absence of incident shock waves which might interact with the laminar boundary layer. With the possibility of such weak incident shock waves at supersonic speeds, the question arose concerning the maintenance of extensive laminar flow at supersonic speeds across incident shock waves and the interaction of such shock waves with the boundary layer of laminar suction surfaces.

In the region of incident shock waves, the static pressure rises abruptly across the shock in the supersonic part of the boundary layer and beyond its outer edge. In the subsonic region of the laminar boundary layer, however, the disturbance induced by the incident shock is propagated upstream, and the pressure along the wall in the area of the incident shock increases then over a finite distance. Laminar separation, leading to premature transition which would normally be encountered in the presence of such a local pressure rise, can in principle be prevented by means of boundary layer suction.

The basic feasibility of laminar flow by means of boundary layer suction across incident shock waves at supersonic speeds was first verified during shock boundary layer interaction experiments at $M = 2$ on a flat plate of 8-inch span in the 8- by 8-inch supersonic tunnel of the MIT gas turbine laboratory. The plate was mounted between the walls of the tunnel (fig. 99, ref. 39). Incident shock waves of various intensities were generated by an inclined flat plate above the model, whose incident could be varied. In the boundary layer shock interaction region of the test plate 8 suction slots of 0.002-inch width and 0.2-inch spacing, connected to a single suction chamber, were installed over a chordwise extent of 1.4 inches, starting 2.2 inches from the plate leading edge. Three additional slots, connected to a separate chamber, were located further downstream. They were, however, not needed to maintain full laminar flow on the test plate.

The following three figures show typical results obtained with suction in the shock boundary layer interaction region of this model. The figure 100 shows the chordwise distribution of static pressure and wall shear stress along the plate with and without suction at $M_\infty = 2$, a free stream unit length Reynolds number of $3.24 \cdot 10^6/\text{ft.}$ and 1.5 pressure ratio across the shock interaction region. Without suction, the boundary layer separates laminar in the first weak initial pressure rise (wall shear stress decreases to zero and negative values). In the shock interaction region without boundary layer suction, the static pressure first rises relatively slowly to a plateau, followed by a rapid and much stronger pressure rise in and downstream of the transition region, accompanied by a high turbulent surface friction. When boundary layer suction (suction mass flow coefficient $c_w = 0.0012$ based on the suction area in the shock interaction region) was applied laminar separation was prevented in the shock interaction region, and the static pressure rose continuously to its final value without passing through an intermediate plateau region. The wall surface friction decreased somewhat in the shock interaction region. Laminar flow with low wall shear stresses was observed on the plate downstream of the shock interaction region (see plot of c_f versus chordwise distance), as verified by boundary layer measurements at various chordwise distances (fig. 101). Schlieren photos (fig. 102) without suction show laminar separation on the test plate upstream of its intersection with the plate.

The incident shock is followed by an expansion fan, when the flow is turned around the corner at the outer edge of the boundary layer, followed by a more gradual compression when the flow is turned back to the undisturbed flow direction. With suction ($c_w = 0.0012$) laminar separation was absent, although a slight increase in boundary layer thickness was observed in the shock interaction region. The expansion fan downstream of the shock interaction location was much weaker than without suction.

With smaller suction flow rates than $c_w = 0.0012$, laminar separation was gradually approached in the shock boundary layer interaction region, without first loosing extensive laminar flow, however. Laminar flow was lost only with much weaker suction when the Reynolds number based on the chordwise length of the separated laminar region was sufficiently large to cause premature transition as a result of the instability of the free vortex layer in the separated laminar region.

The above-described boundary layer shock interaction experiments were conducted at relatively low length Reynolds numbers $\frac{U_{\infty} \cdot \ell_{\text{plate}}}{\nu_{\infty}} \sim 10^6$ to $1.4 \cdot 10^6$, with ℓ_{plate} = distance from plate leading edge to the measuring station at the end of the plate. The question then arises as to the pressure rise in regions of incident shock waves through which a laminar boundary layer with suction can pass at high Reynolds numbers.

According to theory, as confirmed by the above experiments, the pressure rise which a laminar boundary layer with suction can sustain in a region of an incident shock wave decreases with increasing unit length and length Reynolds number, unless the thickness of the initial laminar boundary layer upstream of the boundary layer shock interaction region is reduced by means of boundary layer suction in the upstream areas. In order to verify this hypothesis the interaction experiments at supersonic speeds between incident shock waves and laminar boundary layers with suction were continued on the previously mentioned supersonic laminar suction plate in the Tullahoma A Tunnel up to plate length Reynolds numbers of $26 \cdot 10^6$ with full length laminar flow at $M_{\infty} = 2.5, 3$ and 3.5 . Incident shock waves were generated by an inclined flat plate (Fig. 103), whose angle of attack could be varied. Additional closely spaced suction slots, connected to separate suction chambers, were provided in the boundary layer shock interaction area of the plate. Full length laminar flow was observed on the plate at $M_{\infty} = 3$ and a plate length Reynolds number up to $26 \cdot 10^6$ with a pressure ratio through the shock interaction region of about 1.6 by applying relatively strong local suction in this region with somewhat increased suction rates over the remaining areas as compared with the results obtained without incident shock waves. The chordwise pressure distribution on the plate shows a strong local pressure rise in the shock interaction region, followed by a second weak pressure rise, a gradual pressure drop and a final third pressure rise in the rear part of the plate. The absence of a plateau in the first strong pressure rise indicates that relatively strong local boundary layer suction has prevented laminar separation in the shock interaction region. The second pressure rise is probably caused by the weak shock wave which originated at the plate leading edge and was reflected at the shock generator. The gradual drop further downstream on the plate was caused by the expansion fan originating from the trailing edge of the shock generator. A shock wave finally originates from the wake downstream of the shock generator, when the main flow is deflected back to the freestream direction and intersects the plate at the location of the third pressure rise. The observed boundary layer profile at the downstream end of the plate is a typical laminar profile with suction (fig. 103).

With decreasing suction rates in the main shock boundary layer interaction region, a plateau reappeared in the local pressure distribution; and transition started to move upstream towards this area. Figure 104 shows the pressure ratio across the main shock with full length laminar plate flow at various free-stream Mach and plate-length Reynolds numbers. As in the first boundary layer shock interaction experiments with suction in the MIT 8-inch tunnel, the maximum pressure ratio across the shock with full laminar plate flow decreased with increasing plate length Reynolds number.

6. BOUNDARY LAYER SUCTION DUCTING DESIGN CONSIDERATIONS (REFS. 88-97).

6.1 General Considerations of Losses in Boundary Layer Suction Ducting Systems (Ref. 90, see also Ref. 98).

6.1.1 Introduction, Statement of the Problem

To reduce the suction power needed for high subsonic speed cruise laminarization as well as high lift suction at low speeds the suction system total pressure losses ΔH between the external surfaces and the suction air exit should be minimized. Furthermore, to maintain the proper spanwise suction rate variation, the local static or total pressure difference across the suction surface, depending on how the suction air is fed into the suction ducts, should be reasonably constant along the wing span. This is easier to accomplish when large duct losses can be avoided.

Lower duct losses enable longer ducts and as a result fewer and correspondingly larger and usually more efficient suction compressors (due to higher blade chord Reynolds numbers Re_{Blade}), especially when Re_{Blade} becomes small at high design cruise altitudes.* For minimum total losses in the entire suction system (duct + suction compressor) the sum of the losses in the suction ducting system and suction compressors should then be minimized. The basic question thus arises as to how to minimize the losses in boundary layer suction ducting systems, especially for cruise laminarization. The specific question arises as to how best to mix the suction air of different total energy levels with minimum throttling and mixing losses, particularly in the rear pressure rise area of the upper surface of LFC wings where the total energy of the sucked boundary layer increases substantially from the location of minimum pressure towards the wing trailing edge.

Other secondary considerations, of course, strongly affect these optimization considerations, such as suction compressor maintenance, control of the chord- and spanwise suction distribution and of the suction system at different flight conditions, design of the suction compressor inlet especially with wing mounted suction compressors, wing fuel volume considerations, etc.

(*) At high subsonic cruise speeds the kinematic viscosity ν at the low static pressure of the suction compressor inlet is substantially larger than at the gas generator inlet of the propulsion engines, resulting in relatively low suction compressor blade chord Reynolds numbers. Therefore, blade chord Reynolds number considerations become important in the suction compressor.

Further considerations affect the LFC suction ducting design as follows: Aerodynamic and acoustic disturbances in the suction ducting system and suction compressor as well as mechanical suction duct wall vibrations can excite suction duct flow fluctuations, which in turn may induce amplified boundary layer oscillations on the external LFC surfaces to eventually cause premature transition. Such disturbances should, therefore, be minimized by establishing a uniquely defined duct flow with as uniform an inflow into the suction compressor as possible, providing sufficient structural stiffness to minimize duct wall vibrations and using if necessary acoustic duct linings to absorb internal duct noise and especially standing sound waves excited in the suction ducts by suction compressor tone noise.

6.1.2 General Basic Considerations of LFC Suction Ducting Layouts and - Losses.

The total energy losses in the suction ducting system of LFC wings between the external surface and the suction compressor consist of kinetic energy-, throttling- and mixing losses, as well as flow separation-, duct wall friction- and secondary flow losses. Which one of these losses dominates depends on the type of suction ducting design, the suction method selected and to a large extent on the aerodynamic refinements applied in the ducting design.

The aerodynamically ideal LFC area suction is assumed to be closely approached by suction either through a large number of closely spaced spanwise slots, perforated surfaces with a very large number of small holes or a porous surface. In a similar manner as the blood in the human body is carried from a large number of small capillaries to progressively larger and fewer blood vessels and finally to the heart, the suction air passes through small openings in the external LFC surfaces at low velocities and flow Reynolds numbers and is ducted to progressively larger and fewer suction ducts at increasingly higher duct flow velocities and - Reynolds numbers and finally to the suction compressors. Thus, due to the very low flow Reynolds numbers in the external suction skin viscous friction losses dominate there, while kinetic energy exit losses at the downstream side of the suction skin are usually less important in view of the low velocities involved, when area suction is closely approached. The dominating viscous forces suppress the formation of turbulent eddies at the low flow Reynolds numbers of the external suction skin to allow aerodynamically relatively crude flow passages in this skin. After passing through the suction skin the suction air is collected in small spanwise plenum chambers, located underneath the external suction skin whose main purpose is the maintenance of a uniform spanwise suction distribution. From these plenum chambers the suction air is ducted through holes, drilled in a continuous structural inner skin, into relatively small first spanwise suction ducts formed, for example, by the structural elements of a corrugated sandwich skin. To retain most of the spanwise momentum of the suction air during its passage from these holes into the first spanwise ducts and at the same time minimize duct losses, the above mentioned holes may be drilled at an oblique angle to the skin; furthermore, stress concentrations around these holes in the structurally particularly critical spanwise direction under the action of vertical bending loads would be substantially reduced to greatly improve the fatigue life of the inner skin. Low duct flow velocities in the first spanwise ducts are easily possible and enable small duct losses even with a relatively crude introduction of the suction air into these ducts through oblique holes. Since the above mentioned sandwich skin and the rear part of the wing are usually too thin to carry the suction air over long spanwise distances in such first spanwise ducts in a corrugated sandwich skin, the suction air may often have to be ducted from the first spanwise ducts to short chordwise ducts, which dump the suction air into larger main spanwise ducts to suction compressor booster stages. To minimize structural weight these chordwise ducts may be integrated with chordwise ribs especially in the area of the main load carrying box; in the rear pressure rise area they may be formed by chordwise corrugations integrated for example with a sandwich wing skin. The main spanwise ducts can be located in areas where the wing is sufficiently thick to allow long spanwise ducts of adequate cross-section and small losses, with their vertical walls (lightweight sandwich skins) carrying vertical and torsional shear, thus minimizing wing structural weight. The above mentioned suction compressor booster stages reenergize the suction air of ducts of different total energy levels to a common total pressure level, from where a common duct leads to the main suction compressor, which accelerates the suction air to flight speed (for a turboprop powered LFC airplane) or close to fan air exhaust velocity (for a turbofan powered LFC airplane). Whenever the suction air is transferred and turned into other ducts flow turning nozzles should preferably be provided to minimize local losses and flow pulsations; local flow separation should be avoided and aerodynamic losses minimized through a careful aerodynamic design, providing adequate overall flow acceleration through these turning nozzles. Furthermore, to retain the momentum of the suction air in duct flow direction and minimize at the same time duct losses the suction air should be introduced into the suction ducts through carefully laid out flow turning nozzles or vanes, preferably in such a manner that secondary flow losses and the relatively high duct friction losses associated with secondary flow in ducts (see for example G. I. Taylor or J. Ackeret) are minimized. Duct wall friction losses, of course, decrease rapidly by lowering the duct flow velocities (by increasing the duct diameters and cross-sectional areas) and the duct length to hydraulic diameter ratio l_{hyd}/d . For given duct exit conditions, and duct lengths, the duct total energy losses, resulting from the formation of duct wall boundary layers under the action of surface friction and pressure gradients, can be further reduced by strong duct flow acceleration; i.e., maintaining low duct flow velocities and adequate duct cross-sections in the upstream duct areas and locally introducing the suction air into the duct at about the same or only slightly higher velocities than the local duct velocity everywhere along the duct.

In principle at least, if it should prove feasible to strongly accelerate the duct flow minimize or preferably eliminate secondary flow in the ducts and always introduce the suction air into the ducts at the local duct flow velocity along the entire duct length, extensive or full length laminar duct flow may be feasible at least from the standpoint of amplified TS-disturbances in the duct boundary layers up to surprisingly high duct length Reynolds numbers. Of course, to avoid premature transition due to the turbulent wakes of the duct inflow turning nozzles local suction is probably required to establish thin laminar wakes downstream of the duct flow turning nozzles. Since the duct total pressure losses due to the formation of the duct wall boundary layers depend on the boundary layer displacement thickness δ^* at the duct exit transition should be enforced at this station to decrease δ^* by 40 percent to $\delta^*_{turb.}$, assuming constant boundary layer momentum thickness θ during transition.

Extremely small duct total energy losses would thus basically result with full length laminar duct flow especially at higher duct length Reynolds numbers.

6.1.3 Minimization of Suction Ducting Throttling - and Mixing Losses In the Rear Pressure Rise Area of LFC Wings

The external static pressure and as a result the total pressure of the sucked boundary layer increases substantially from the location of minimum pressure towards the trailing edge of LFC wings, where the highest suction rates are usually needed for laminarization, causing additional throttling and/or mixing losses as a result of the chordwise variation of the pressure difference Δp between the external surface and the suction duct. The question then arises concerning the minimization of the sum of these additional throttling and/or mixing losses and the duct wall friction losses.

The additional duct throttling and/or mixing losses associated with the chordwise variation of Δp in the rear pressure rise area of LFC wings can basically be minimized by closely approaching the ideal individual reenergization of each sucked boundary layer particle in a large number of separate relatively small suction ducts with individual suction compressor booster stages, at the cost of increased complexity and duct wall friction losses (due to larger total duct wetted area with more ducts). Therefore, to decrease the number of suction ducts in the rear pressure rise area of LFC wings without excessive additional losses the mixing losses of each individual duct should be minimized as follows: Instead of throttling the suction air in the outer suction skin and/or the inner structural skin (method a) in slots, holes or other throttling devices the sucked boundary layer can be injected tangentially (in duct flow direction) into the ducts through flow turning nozzles or vanes (method b).^{*} In the areas where the pressure difference between the external surface and a particular duct are especially large (i.e. towards the rear part of the wing in each duct) the pressure drop across the above mentioned flow turning nozzles is also larger to raise accordingly the corresponding nozzle exit velocity at the entrance into the duct, being usually substantially larger than the mean duct velocity. Under such conditions the duct total pressure rises substantially due to jet mixing according to conservation of mass and momentum to often more than compensate for duct wall friction losses. To maintain uniform spanwise suction in the presence of such a rising duct total pressure due to jet mixing the duct regions of lower static pressure at the beginning of the duct should preferably be connected with external suction surfaces which are located somewhat further upstream on the wing surface in a region of lower static pressure, and vice versa, thus ensuring reasonably uniform total pressure difference along the span between the duct and the external surface.

Duct mixing losses in pressure rise areas might decrease further by introducing lower total energy suction air of upstream wing areas into lower total energy areas of suction ducts (preferably short ducts), along which the duct total pressure rises as a result of jet mixing between the duct flow and the suction air entering the duct through vanes at higher than duct velocities, and vice versa (method b'), fig. 106). For a given number of suction ducts the chordwise variation of the total pressure difference of the suction air between the external surface and the suction ducts and the resulting duct mixing losses then decrease approximately by the ratio $(1 + \eta_{\text{mixing}})^{-1}$, or for the same duct mixing losses the chordwise external static pressure variation across a particular duct may be raised by the ratio $(1 + \eta_{\text{mixing}})$ to allow $(1 + \eta_{\text{mixing}})$ times fewer spanwise ducts. At the duct ends the suction air of two or more ducts with relatively small total energy differences may be mixed efficiently by booster fans, rotating preferably on the same shaft as the main suction compressor booster stages which raise the total energy of all ducts to a common level (fig. 107). Simpler but less efficient jet mixing at the duct ends may substitute for above mentioned booster fans (fig. 107) with the disadvantage of a more irregular inflow into the suction compressor booster stages to raise accordingly their noise.

Estimates of duct total energy losses $\frac{\Delta H}{q_0} = \frac{\Delta H}{\rho/2 U_0^2}$ (U_0 = flight speed) due to duct wall friction and mixing are shown in the figures 107-111 versus the ratio u_{duct}/U_0 with the methods (a), (b), (b') for different external pressure rises $\Delta p/q_0$ across individual ducts and various duct lengths. Uniform chord and spanwise suction, a linear external pressure rise, constant duct velocity u_D along the duct (*), and turbulent pipe friction losses without major secondary flow losses were assumed $\frac{\Delta p_{\text{duct}}}{q_{\text{duct end}}} = 1$ for $l_D/\text{hydr. } D = 40$). Additional duct wall friction losses due to jet mixing of the incoming suction air with the duct flow as well as total energy losses in the external suction skin and inlet flow turning nozzles or vanes were neglected in this simplified analysis.

In view of the smaller duct losses with methods (b) and (b'), as compared to throttling method (a), primary emphasis is given to the methods (b) and (b'). With increasing duct velocity u_D the duct friction losses increase approximately proportional to u_D^2 (more accurately $\sim u_D^{1.8}$ for turbulent duct flow), while the duct mixing losses with methods (b) and (b') (proportional to $u_D^2 (u_E - u_D)^2$) decrease at larger duct velocities u_D (see figs. 108-110) as a result of the smaller velocity difference $u_E - u_D$ between the suction air tangentially entering the duct at velocity u_E and the mean duct flow. Correspondingly higher jet mixing efficiencies η_{mixing} then result at higher duct velocities u_D (figures 112, 113; η_{mixing} versus u_D/u_0 for different external pressure rises $\Delta p/q_0$ across individual ducts with methods (b) and (b')). The duct total energy losses $\Delta H_{\text{friction} + \text{mixing}}$ then minimize at an optimum duct velocity $u_{D \text{ opt}}/U_0$. For smaller or larger duct velocities the respective

^{*}Figure 105

^{*}In practice, the duct velocity will usually increase from the beginning to the end of the duct.

mixing or friction losses dominate. For longer ducts, duct friction losses increase, shifting the optimum duct velocity to lower values, and vice versa. In contrast, the duct total energy losses with the throttling method (a) increase continuously with increasing duct velocity and are substantially larger than with the more efficient methods (b) and especially (b'). Furthermore, duct total energy losses due to the formation of thick duct wall boundary layers, when the suction air is introduced at a normal angle into the duct through throttling holes, are substantially larger than the conventional turbulent pressure drop in pipes, as verified experimentally. Therefore, throttling method (a) should be used only for smaller $\Delta p_{\text{surface}}/q_0$ and with low duct velocities.

With increasing external pressure rises $\Delta p_{\text{surface}}/q$ for individual ducts the duct mixing losses increase, while the duct wall friction losses, on the other hand, decrease as a result of the smaller total duct wetted area and the correspondingly increased duct hydraulic diameter with the fewer larger size ducts for larger ratios $\Delta p_{\text{surface}}/q$; the total duct losses, i.e. the sum of duct friction and mixing losses, then increase with increasing $\Delta p_{\text{surface}}/q_0$.

The duct mixing and total losses decrease further by connecting the low pressure rise areas on the external surface with the lower total pressure areas at the beginning of relatively short mixing ducts in a suitable manner, and vice versa (method (b'), fig. 106). With the resultant smaller pressure differences between the external surface and the duct (at a given $\Delta p_{\text{surface}}/q_0$ for an individual duct) the duct mixing losses are inherently smaller in addition to the correspondingly higher jet mixing efficiency (fig. 113) due to the smaller total pressure difference between the duct and the external surface with method (b'), as compared to (b). Under otherwise the same conditions the optimum duct velocity for minimum duct friction + mixing losses is lower with method (b') than with (b) (figures 108-110).

Equal duct mixing losses with methods (b) and (b') result when the pressure differences between the duct and the external surface are equal. $\Delta p_{\text{surface}}/q_0$ for a particular duct then increases by the factor $(1 + \eta_{\text{mix}})$ to decrease accordingly the duct number by the ratio $(1 + \eta_{\text{mix}})^{-1}$. With such fewer ducts turbulent duct wall friction losses (assuming the same total cross-sectional area) decrease by a factor $(1 + \eta_{\text{mix}})^{-0.6}$; i.e., for a given sum of duct friction + mixing losses (for the same duct length and - cross-sectional area) the number of suction ducts with method (b') may be 40 percent to 45 percent smaller than with method (b). This consideration can become crucially important in simplifying the LFC suction ducting design.

In many practical applications the suction ducts cannot always be designed according to loss minimization considerations. At the beginning or end of the duct the duct flow velocity will usually be smaller or larger, respectively, than the optimum duct flow velocity. However, considerable deviations from the optimum do not raise the duct losses appreciably. To reduce duct cross-sectional areas somewhat larger duct velocities than for minimum duct friction + mixing losses will usually be chosen.

Additional mixing losses must be accepted when suction ducts of different total energy levels are joined to a larger common duct prior to entering the booster suction compressors, which reenergize the suction air to a common total energy level. These additional losses can be kept relatively small by accelerating the flow of the various ducts in the mixing region to a higher velocity, being feasible as long as the suction air does not have to be decelerated into the booster suction compressors.

Assuming, for example, $U_{D_{\text{End}}} = 0.39 U_0$, $\Delta p_{\text{surface}}/q_0 = 0.1$ and mixing two adjacent ducts with a total pressure difference of $0.1 \cdot q_0$ the additional mixing losses at the end would be $\Delta H = 0.005 \cdot q_0$.

6.2 Experimental Suction Duct Investigations (Refs. 88, 89, 93-97).

In order to develop suction ducts with minimum losses, the total pressure losses in various ducts were investigated. Ducts (1), (2) are relatively simple ducts where the suction air entered the duct through a 2-dimensional slot or through holes in the direction normal to the duct flow (figs. 114, 115); no attempts had been made to retain the momentum of the suction air in duct flow direction during its entry into the duct. Figure 116 represents the measured static pressure distribution along ducts 1 and 2, indicating large duct total energy losses $\Delta H/q_{D_{\text{End}}}$ far beyond turbulent pipe

friction losses ($\Delta H/q_{D_{\text{End}}} = 2$ and 2.3 with $l_D/d_{\text{hydr. } D_{\text{End}}} = 22.5$ for ducts (1) and (2), respectively).

Evidently, with the suction air entering duct (1) through a 2-dimensional slot without flow turning vanes, a strong secondary flow with correspondingly high losses must have developed in duct (1). With the suction air entering duct (2) through holes normal to the duct flow, even higher duct losses apparently resulted from the accumulation of a very thick low-energy boundary layer on the duct wall containing the holes, with the duct flow passing at high velocity through a small effective duct area towards the opposite duct wall. These high duct losses could be greatly reduced by turning the incoming suction air tangentially into the direction of the duct flow by means of vanes or nozzles. The figures 117-119 show the geometry and cross-sectional area variation along the length of such ducts (1v), (3v) with flow inlet turning vanes and duct (2n) with flow inlet turning nozzles. The figures 120-122 show the static pressure along the duct length, from which the duct pressure variation due to duct flow acceleration and jet mixing of the incoming suction air with the mean duct flow were subtracted to obtain the duct total energy losses due to duct wall friction and secondary flow. The exit cross-section of the inlet vanes and nozzles had been constant along the duct length; thus, with suction reasonably uniform in spanwise direction, the suction air entered the duct at approximately the same tangential velocity u_p along its entire length. As a result, with the lower duct velocities u_D and the correspondingly larger velocity differences $u_E - u_D$ towards the beginning of the ducts (2n), (3v) and especially (1v), jet mixing caused a rather rapid rise of

the duct static pressure in this region, compensated further downstream in the region of higher duct velocities by increased duct friction and secondary flow losses. The duct pressure rise due to jet mixing increased with increasing suction air inlet velocity ratio $u_E/u_{D_{End}}$ from a ratio 0.88 for duct

(2n) to 1.05 for duct (3v) and 1.5 for duct (1v). The duct wall friction and secondary flow losses follow by subtracting from the measured duct static pressure the duct pressure variation due to duct flow acceleration and jet mixing (figures 120-122 for ducts (1v), (2n), (3v)). With the ducts (2n) and (3v) $\Delta H/q_{D_{End}} = 0.7$ for $\ell_D/d_{hyd_{D_{End}}} = 22.5$ and a duct length Reynolds number

$Re_\ell = \frac{u_{D_{End}} \cdot \ell_D}{\nu} = 600,000$; i.e., the duct total energy losses were about 3 times smaller as with ducts

(1), (2), when the suction air had not been turned tangentially into the direction of the mean duct flow. At $Re_\ell = 600,000$, the total energy losses of duct 1v were $\Delta H/q_{D_{End}} = 1.05$ for $\ell_D/d_{hyd_{D_{End}}} = 22.5$.

Further investigations, however, showed substantially smaller losses with duct (1v) at higher Re_ℓ 's, indicating that laminar separation on the turning vanes of duct (1v) at their low flow Reynolds numbers must have caused substantially increased local pressure drag and, as a result, duct total energy losses at lower duct length Reynolds numbers (ref. 123).

In summary, as compared to plain ducts or plenum chambers, where the tangential momentum of the suction air in duct flow direction was not retained, duct total energy losses decreased by a factor 3 to 4 when the incoming suction air was turned tangentially into duct flow direction by suitable vanes or nozzles.

Since the duct total energy losses thus evaluated still appeared relatively large as compared to theoretical values expected from turbulent-pipe friction losses, the question arose concerning the origin of such additional duct losses and the possibility for a further substantial reduction of duct losses.

The measured static duct pressure depends on the duct total energy losses, the mean duct flow acceleration, and the jet mixing of the incoming suction air with the mean duct flow. Therefore, in order to eliminate or minimize any uncertainties associated with the duct pressure rise due to jet mixing, further suction ducts (I) to (III) were investigated whose suction-air inlet velocity u_E into the duct was everywhere equal or close to the local mean duct velocity u_D . The first duct (I) thus investigated was similar to duct (3v) and had flow-turning vanes designed and located similarly as with duct (3v), except that $u_E \sim u_D$ everywhere along the duct (fig. 123). In order to separate duct total energy losses due to the formation of duct wall boundary layers from those resulting from duct secondary flow boundary layer measurements were conducted at the downstream end of the duct at different Re_ℓ 's. The duct total energy losses, subtracting the duct flow acceleration and the very minor pressure rise due to jet mixing was of the same order as with the previous ducts (1v), (2n), (3v) (fig. 124). However, the duct total energy losses due to the formation of the wall-boundary layer at the downstream end of the duct were substantially smaller and consistent with turbulent pipe-flow estimates; hence, rather strong secondary flow-duct losses must have substantially contributed to the duct losses (figure 124). Therefore, in order to minimize such secondary flow losses, suction duct (I) was modified in such a manner that secondary flow in the suction ducts induced by the incoming air should be greatly reduced (duct II, figure 125), maintaining the same duct cross-sectional areas and inlet vane geometry as with duct (I). Subtracting the duct pressure variation due to mean duct flow acceleration and the weak jet mixing from the measured duct static pressure, gave substantially smaller duct total energy losses due to duct-wall friction and secondary flow (figure 126), as compared to ducts (I), (1v), (3v), (2n), (Y). Subtracting the duct total energy losses due to the formation of wall boundary layers at the downstream duct end from the duct total energy losses showed, indeed, substantially reduced duct secondary flow losses with the more ideal duct (II) where the suction air entered the duct symmetrically without major secondary flow, as compared to duct (I) where the suction air entered the duct asymmetrically to cause a secondary flow in the duct (figs. 123, 124). The puzzling question, though, arose as to the higher duct-wall boundary layer losses of duct (II), as compared to duct (I). Apparently, the duct inflow turning vanes of duct (II) had been improperly sealed against the side walls, increasing as a result duct friction and secondary flow losses. After correcting this deficiency, the duct-wall boundary layer losses were, indeed, further reduced, while duct secondary flow losses practically vanished, at least at higher Re_ℓ 's (figs. 127, 128). Thus, extremely small duct total energy losses ($\Delta H/q_{D_{End}} = 0.125$ for $\ell_D/d_{hyd_{D_{End}}} = 20$) appear feasible

with carefully designed ducts, introducing the suction air tangentially into the suction duct by properly designed vanes at the local duct velocity in such a manner that duct secondary flow is minimized.

Boundary layer measurements at the duct end showed laminar and turbulent duct wall boundary layers, respectively, at low and higher duct length Reynolds numbers Re_ℓ , respectively (figs. 129, 130). The duct losses due to the boundary layer displacement thickness δ^* at the end of the duct with laminar duct flow at lower Re_ℓ 's might be reduced by about 40 percent by enforcing transition at the duct ends and lowering δ^* by 40 percent (assuming θ remains constant during transition).

In view of the strong flow acceleration in LFC suction ducts, one might speculate from the standpoint of amplified TS-duct wall boundary layer oscillations for laminar duct flow and, as a result, extremely low duct losses up to higher duct flow Reynolds numbers (figure 131). This may be accomplished by strongly accelerating the duct flow, minimizing duct secondary flow losses, introducing the suction air everywhere at the local duct velocity into the duct, and maintaining laminar wakes downstream of the duct inflow turning vanes through local suction close to their trailing edges.

Duct (II) is an ideal suction duct of negligibly small secondary flow losses with symmetrically located suction air inlet vanes, where the suction air enters the duct everywhere at or close to the local duct velocity. The duct total pressure decreases then essentially according to the duct wall friction losses, while the duct flow acceleration must, in addition, be taken into account to obtain the duct static pressure. In order to ensure the uniform spanwise suction variation desirable in most cases, the suction ducts should preferably be connected with the external LFC surfaces in such a manner that the difference between the external surface static pressure (being about equal to the total pressure of the sucked boundary layer when area suction is closely approached) and the duct total pressure (assuming $u_{E,local} = u_{D,local}$) is reasonably uniform along the span. In other words, the downstream duct areas at the duct end of lower total energy should preferably be connected with upstream external LFC surfaces of somewhat lower static pressure in the rear pressure-rise area of LFC wings, and vice versa.

In many cases, long suction ducts of constant total energy along their length with their slots, etc. along isobars, appear simpler in securing uniform spanwise suction, especially in the flat-pressure region of LFC wings. This can be accomplished by compensating for the duct-wall friction and secondary flow total pressure losses by a pressure rise due to jet mixing, when the suction air enters the duct at a velocity u_E somewhat larger than the mean duct flow velocity u_D . For carefully laid-out ducts with negligible secondary flow and small wall friction losses, this duct pressure rise due to jet mixing can accordingly be relatively small.

In other cases, as experienced for example sometimes in the flat-pressure region of the X-21 upper-wing surface, the static pressure on the external LFC surface may be lower at the beginning of the duct than at the duct end. To ensure adequate suction in the low-pressure region of the wing at the beginning of the duct, suction ducts with a rising total pressure along the duct are needed. This can be accomplished by further increasing the ratio $(u_E/u_D)_{local}$ and the resulting duct total pressure rise due to jet mixing to more than compensate for duct-wall friction and pressure-drag losses. In other words, the static and total pressure distribution in suction ducts can be tailored within a rather wide range by judiciously selecting u_E and u_D along the duct length. It should be cautioned, though, that the duct-wall boundary layer thickness increases more rapidly in the presence of a rising duct pressure due to jet mixing, resulting from the pressure gradient term in the momentum equation of the duct-wall boundary layer. Furthermore, with the suction air entering the ducts at velocities larger than mean duct velocity, correspondingly higher duct-wall friction losses must in addition be expected. In other words, strong jet mixing in suction ducts should preferably not be used to compensate for a sloppy design of the external LFC surfaces.

Figure 132 shows the measured static pressure distribution in duct (II) when the suction air inlets to the duct were partially taped off at the beginning of the duct and u_E of the incoming suction air was therefore larger than the local duct-flow velocity u_D to raise the static pressure over a large part of the duct length in spite of the pressure drop due to duct-flow acceleration. Theoretical estimates of K. Rogers, using conservation of momentum and mass, agree reasonably close with the measured duct static pressure distribution.

7. STRUCTURAL LFC INVESTIGATIONS.

Structural aspects of LFC wings have been studied in considerable detail by the Northrop Boundary Layer Research Group, leading essentially with relatively minor modifications to the structural development of the X-21 LFC wing. The enclosed appendix: "Structural Aspects of Low Drag Suction Airfoils," by J. Wieder and W. Pfenninger, presents a summary of some of these activities.

CONCLUDING REMARKS

1. 100% laminar flow with $C_{D_{\infty}} = .0011$ was obtained up to $Re_c = 17 \cdot 10^6$ on a 15% thick slotted Northrop LFC wing in the NACA Langley TDT-tunnel, confirming suction laminarization at much higher Re_c 's at lower turbulence levels.
2. A practical aerodynamically and structurally satisfactory LFC suction method, using closely spaced spanwise slots, was developed.
3. 100% laminar flow existed on the F94 LFC wing glove up to $Re_c = 37 \cdot 10^6$ (test limit), with $C_{D_{\infty}} = .00045$ (upper surface) at $Re_c = 30 \cdot 10^6$. Laminar flow in flight on LFC wings is thus possible at much higher Re_c 's than in low turbulence tunnels due to the vanishing influence of the atmospheric microscale turbulence on transition.
4. On a 8:1 fineness ratio Reichardt LFC body of revolution with 114 slots (between $X/L = 0.03$ and 0.99), 100% laminar flow with $C_{D_{\infty}} = .00027$ (based on wetted area) existed up to $Re_L = 57.8 \cdot 10^6$ in the Ames 12-foot tunnel. The theoretically predicted strong boundary layer stabilization by distributed suction was thus verified, being much more effective than geometry alone. For the Reichardt LFC body and other LFC surfaces $Re_{L, \text{lam.}} \sim (u'/U_{\infty})^{-1}$; i.e., drastically reduced initial disturbances enable much higher $Re_{L, \text{lam.}}$ on LFC surfaces.

5. To prevent transition and control the particularly critical boundary layer crossflow instability especially in the leading edge- and rear pressure-rise areas of swept LFC wings at higher Re_c 's, suction is needed along the entire chord with somewhat higher overall suction rates than for straight LFC wings, with particularly strong suction in the leading edge- and rear pressure rise areas (according to an analysis of the boundary layer development and stability on swept LFC wings, confirmed experimentally on 30° swept modified NACA 66012 slotted LFC wing in Ames 12-foot tunnel with full chord laminar flow up to $Re_c = 29 \cdot 10^6$, with $C_{D_{\infty \min}} = .00096$ at small α 's).
6. Without special precautions, spanwise turbulent contamination along the front attachment line of swept LFC wings usually destroy their laminarization at $Re_{\theta_{a.l.}} \geq 90$ to 100. It is delayed to higher $Re_{\theta_{a.l.}}$ by establishing a new undisturbed laminar initial attachment line boundary layer by means of a laminarized leading edge suction fence, suitable leading edge extensions, etc.
7. The influence of external and internal acoustic disturbances on LFC surfaces was studied. A better understanding of physical phenomena involved was gained. Methods were established to raise the permissible external and internal sound pressure.
8. The influence of various types of suction induced disturbances on LFC was studied, and approaches were developed to minimize or avoid such disturbances.
9. Permissible LFC surface tolerances were established for unswept and swept LFC wings. (2- and 3-dimensional surface disturbances). Properly placed local suction in areas of surface steps doubled the permissible step height.
10. Laminar flow existed on a supersonic low drag suction plate and a suction ogive of revolution up to $Re_L = 51 \cdot 10^6$ with three to four times smaller drags than for a turbulent plate. Laminar flow by means of suction was demonstrated on laminar suction plates through and downstream of relatively strong incident shocks up to $Re_L = 26 \cdot 10^6$ at $M = 3$ (1.6 shock pressure ratio).
11. Structural and suction duct design investigations verified low structural LFC weight penalties and duct losses through careful designs.

APPENDIX A

STRUCTURAL ASPECTS OF LOW DRAG SUCTION AIRFOILS

J. Wieder and W. Pfenninger
Presented at IAS-Meeting, June 1961, L.A.

1. Introduction

Extensive laminar flow on the surfaces of an airplane by means of boundary layer suction will increase its range and endurance. The airplane range depends on the airplane lift to drag ratio, the specific fuel consumption of the propulsion system and the airplane weight ratio between beginning and end of the flight, which in turn, is influenced by the airplane structural weight.

With the reduction in friction drag by means of boundary layer suction, the induced drag becomes increasingly important. In order to achieve the full advantage from the application of boundary layer suction, it is desirable to reduce the induced drag at the same time as the friction drag by increasing the wing span. With the large wing spans of an optimized laminar suction airplane, the structural designer is thus immediately faced with the problem of designing these large suction wings with minimum structural weight within the requirements of strength and stiffness, with the suction air ducting system installed, and with the close surface tolerances required for extensive laminar flow. In order to minimize the wing structural weight, the inertia weights should be distributed over the wing span, the walls of the suction air ducts should preferably be combined with the structural elements of the wing, such as wing skin, shear webs, longitudinal stiffeners, ribs, etc. Continuous suction on the wings, being optimum aerodynamically, can be closely approached by removing the slowest boundary layer air particles close to the wing surface through a large number of fine slots. The resulting low flow velocities and small Reynolds numbers for the slot flow enable the use of relatively simple suction slots, which can be cut into a thin outer wing skin, which in turn is bonded to a continuous thicker inner skin. The suction air passes through the slots, spanwise grooves and holes, drilled into the inner skin underneath the slots, into the suction ducts and to the suction compressor. With the exception of the holes in the inner skin, both wing skins are structurally efficient for wing bending strength and stiffness.

2. BLC Wing Components

Two current wing skin versions (fig. 133) type A, the solid skin, representative of inboard loading indices, and type B, the honeycomb sandwich, of outboard loading indices and trailing edge surfaces, exemplify upper and lower high subsonic wing surfaces. The range of geometries indicated is determined by the chordwise location of the slot. These are all bonded assemblies with drilled holes and the slots cut by means of a trackmounted saw with a rotating blade. The sheet with plenums in the honeycomb sandwich is chemically milled to the proportions shown.

Previously reported static tension and shear tests of perforated sheets of an aluminum alloy with comparable hole diameter to row ratios (ref. 99) indicate no measureable loss of net area efficiency. Built-up panels tested in compression similarly developed net area deformations and buckling stresses. Groups of 4" x 20" simply supported panels, representative of low loading indices and trailing edge upper skins, were compressed in the spanwise direction. Figure 134 shows the cross section of .16 overall depth, and their specific strengths. Of the three types, the chemically milled core sandwich was unreliable due to the narrow bond ledges of the core; the corrugated core type is promising when the core is fabricated with precision dies, and the honeycomb sandwich is a current design choice.

A series of 19" long 6061-T6 aluminum alloy tubes was tested in torsion (fig. 135, 136). The encircled 3 and 5 on the relative rigidity and yield stress diagram designated spacings skin to those of BLC main wing-box surfaces and indicate torsional rigidity losses of about 5%. The 25% decrease in shear yield stress is consistent for all configurations; in actual design, a replacement of local area removed will bring these values close to normal allowables. In those specimens taken to failure, there was the expected elliptical shape of the holes with a 45° major axis; the failure proceeded along the plenum chamber from the top of one ellipse to the bottom of the next following the least net section in a saw-tooth fashion. Fig. 137 shows the twist at failure relationship among the various slot locations with holes; the fail stress was 22,000 psi based on effective transverse shell thickness. Thus, the strength is a function of the least net area; the rigidity, in the elastic range, approximately of the net cross sectional area transverse to the axis, and the twist, in the plastic range, a non-linear function of the number of slots.

In the region of the main structural box of the wings of large long range or endurance airplanes, the integration of the internal suction air ducting system with the structural layout usually leads to an open double skin panel for the upper and lower wing surface. The small suction velocities on straight as well as swept wings in the area of the main box ($v_o/U_o = 1$ to 2×10^{-4})*, with a chordwise slot spacing of approximately 2% of the wing chord, generally permit suction duct arrangements on the basis of structural optimization. Over a range of 8,000 to 20,000 lbs/inch of chord, optimized open sandwiches would give clear duct depths of 1" to 2.75", which are sufficient for keeping duct losses minimal.

The family of open sandwiches is limited to continuous corrugations or a variety of discrete element geometries and cover plates. Corrugated sandwiches would be a first choice from the standpoint of chordwise stiffness, and as a torsional shear transfer medium from the partial depth intermediate ribs. However, they have the following disadvantages: 1. increased fabrication difficulties of tapering corrugations in

* v_o = suction velocity for equivalent area suction (FPS)
 U_o = free-stream velocity (FPS)

planform and elevation to maintain structural efficiency along the span, 2. in some cases the variation of the suction velocities along the chord may lead to a chordwise variation of the depth and spacing of the suction ducts, and certain duct depths may exceed those for structurally optimum corrugation thickness. With the relatively many ribs necessary in a wing with fuel, the use of extruded stiffeners with cover plates eliminates most of these objections and permits more flexibility in arrangement.

A BLC compression skin assembly for a wet wing is shown in fig. 138. The solid upper cover becomes the honeycomb type at the lower loading indices; the "I" sections, or equivalent stringer types, are extruded and machined (with controllable warpage because of their two axis symmetry); the inside face of the skin assembly is a minimum gauge aluminum honeycomb panel. In a BLC airfoil this panel partially functions as a lifting surface and as a fuel liner; it further functions to prevent rolling of the "I" at high stress levels which might wave the skin locally. This type of main box eliminates mechanical fasteners in the upper and lower surfaces of the integral fuel tanks and minimizes leaks into the ducts. All elements are bonded to provide, with the non-wrinkling structural members, smooth suction ducts and to minimize possible local depressions on the outer surface, as in the case of mechanical fasteners. As some prying action occurs, it is important that suitable taper be given the flange legs to decrease peel tendencies; a 1:3 taper ratio is satisfactory for transferring about 100 in-lbs. of moment per square inch of bonded flange surface. With this arrangement, bending material and torsional material is kept primarily in the upper skin with a minimum in the lower skin; the neutral axis is for a large part of the span considerably above the geometric center of the open sandwich. All elements are non-buckling to yield. A group of columns 20" long and a 3" stringer pitch involving equivalent cross sections with riveted Z's and bonded I-stringers gave a favorable specific strength ratio of 1.15 for the cross section of fig. 138. The instability shape of the latter was undistorted in cross section and sinusoidal; some of the former failed in a twisting and explosive tearing of the Z-flange. It is noted that the increasing thickness ratio of the inner skin to outer skin in the outboard half of the wing is a fail-safe aspect of this double skin configuration.

In relation to the wing torsional stiffness, it may be pointed out that for the inboard third of the wing, 85 percent of the skin face material is in the outer face, and for the outboard two-thirds of the wing, it may vary from 85-65 percent. A series of torsional load applications for a straight rectangular box 100" long and with cross sectional dimensions shown, (fig. 139), demonstrated that the "J" value is calculated as a three cell box or as a single cell system with the inner and outer skins assumed at the bending center of gravity of the skin system. This may be conservative as the tests were run with no direct attachment of stringers to either the loading devices or reacting column. A possible 5 percent reduction in "J" over a comparable skin stringer arrangement is estimated. It was further demonstrated that the skin system developed full rigidity regardless of the load applications being at inner and outer skins directly or at the inner skin only. It is of significance that this or equivalent systems function in this manner, as a BLC wing would have a minimum of ribs attached to the outer skin since the consequent interruption of the suction airflow in the ducts should be minimized. This, in effect, means that the intermediate ribs, attached to the inside honeycomb sandwich only, transfer airload torsion to the box. The box failed in the web of the stringers, at an applied shear of 2800#/in. on the inside surfaces (ref. 100).

In the rear part of the wing in the region of the rear pressure rise, considerably higher suction velocities are required to maintain full chord laminar flow, ($-v_o/U_o = 5$ to 8×10^{-4}), as compared with the suction rates in the region of the main structural box. As a result, in order to avoid excessive pressure losses in the suction ducts, the full wing thickness has to be used for the air flow in this part of the wing. In order to minimize the duct losses in critical areas, it may become necessary to deflect the incoming suction air into the direction of the duct flow by means of turning vanes or turning nozzles. The suction air, after passing through the skin, would first be ducted in a spanwise direction through small auxiliary spanwise ducts, formed for example, by closed longitudinal stiffeners or by spanwise corrugations in the outer skin, into turning nozzles and into the main suction ducts. In this manner secondary flow pressure losses in the suction ducts are drastically reduced (refs. 90, 95).

One version of the wing trailing edge design is a Warren truss type structure with continuous spanwise honeycomb webs forming smooth full depth duct walls (Fig. 140). The eccentric web attachment facilitates assembly; the straight web face is thicker than its opposite. Stress coating showed that a compression web of this type carried its load through the thicker skin acting on an elastic medium. A 9" x 50" simple beam of "T" flanges and eccentric sandwich web failed at 90 percent of calculated with a deep buckle at the center; there were no local separations due to the offset of load. Similarly a two cell box beam with .25 inch thick sculptured compression skins loaded in shear and bending, failed in a full panel buckle of the eccentric sandwich web (.016 faces, .156" thick 4.5# honeycomb) at 95 percent ultimate. The all sandwich trailing edge is non-wrinkling; a 24" chord deforms about .12" at the trailing edge at limit load or a nominal deflection at cruise. Another version of the non-buckling trailing edge consists of chordwise machined truss-like ribs and vertical spanwise sandwich webs, with the rib members streamlined to maintain small suction air duct losses.

With the suction ducts installed in the wing, one might superficially conclude that a laminar suction wing cannot carry as much fuel as a turbulent non-suction wing. However, since wing span and area of an optimized low drag suction airplane are considerably larger than for an optimized turbulent airplane, the wing volume remaining for fuel is generally considerably larger for the optimized low drag suction airplane, as compared with the corresponding turbulent airplane.

3. Surface Limits

Surface irregularities cause velocity fluctuations in the laminar boundary layer leading to transition. Allowable limits to roughness, steps, gaps and waviness have been established through wind tunnel models and in flight tests. Figs. 141 and 142 show these allowable and current production standards. It is observed that high subsonic transports cruising at 30,000 ft. and above fall within the surface tolerance limits with the exception of surface steps. This area requires special attention and the submerged splice is a possible solution to this problem. As the down step is more critical, design and manufacturing tolerances should accumulate as positive or up steps. The waviness allowables, in terms of a sinusoidal shape

in the chordwise direction are shown in fig. 142. The requirements depicted here are for the one G cruise condition. The limits of contemporary products presently meet a fair proportion of these requirements.

Waviness and slot deformations were frequently checked in the course of axial load $4'' \times 20''$ specimen testing at one G and two G load levels and found to be within acceptable limits. In the aforementioned torsion box test, the 6 mil slots were checked along the span with feeler gauges for all loading conditions to over 3° of box twist; no measurable variation was obtained. The waviness was within 1 mil per inch. A leading edge segment $14''$ of cantilever by $2'$ wide, representative of a BLC 6 percent wing and weighing $4\#/ft^2$, was tested under simulated air load. The maximum tip deformation was $.05''$ at 1.25 G and the load induced waviness was $.0005$ in/in.

Akin to the surface irregularity problem is the surface corrosion problem. An initial effort to evaluate environmental effects was the exposure of $3'' \times 12''$ solid and honeycomb skin panels to an industrial climate and an ocean and a jungle site. Suction efficiencies subsequent to exposure were checked with and without steam cleaning of surfaces. Results are shown in fig. 142.

Successful anodic treatment of exposed edges and holes on bonded assemblies with no loss of bond strength has been gained and is under continuing investigation (refs. 101, 102).

4. Concentration Factors

In common with most design efforts, we seek to encompass aspects of the safe-life and the fail-safe approach to fatigue problems. One trend of long range or endurance BLC operation which may relax somewhat the criteria of the first, is suggested by fig. 144. For an assumed like a BLC long range aircraft type, with an efficient laminar wing and tail, and turbulent fuselage, cruising at over 40,000 ft. has a potentially more favorable cumulative damage history than equivalent turbulent aircraft by about 43 percent in the lower wing surface root area and about 55 percent in the mid-span area. These estimates are based on an optimum aircraft usage involving 40 percent fewer ascents and descents, and cruising encounters with 5 to 10 fps gusts at $1/4$ normal frequency.

Significant design questions are concerned with the concentration factors of holes, plenum chambers and slots. Of these discontinuities, the holes are influential in all directions and their small size precludes shaping for possible stress neutralization, or effective symmetrical local reinforcing. Some cycling gains were noted in minimum tests of pre-stressed hole rims. However, the depth of the pre-stressing effect involves areas around the hole which are in multi-axial stress fields where yield increases in one direction may be offset by decreases in another, according to the Bauschinger effect. Although 75ST has been used for BLC specimens, fabrication and tests, it is believed only representative of the aluminum spectrum; for example, 7178 or the more notch accommodating 2024 could be used. To the increasing evidence of the superiority of 2024 in all facets of crack life, with the exception of reversed high stress levels, is added some evidence of a possible 35 percent gain in nominal fatigue strength over 75ST for sheet with holes such as are encountered in BLC skins (ref. 103). In a single instance of investigation of a row of .04 holes in a contour, this percentage was not borne out. However, the use of 2024 for lower main box skins is a design consideration.

The development of maximum tangential stresses in the elastic range for intermediate holes in typical BLC patterns is based on photoelastic results and summarized in Fig. 145 (ref. 104). A simple superposition of the tangential stresses at the rim of the hole due to the applied multiaxial stresses results in critical planes at 90° and 135° , to the direction of applied tension or shear. Where the shear stress to spanwise tension stress ratio exceeds 2, the shear effect dominates; below 2, the tension effect dominates, with combined load K_T 's between 2.75 and 3.5.

The plenum chamber with its full depth radii has notch effects due to loadings in planes transverse to its axis. The effect of tension stress at the base of the fillet for a representative width to depth plenum in a solid skin is shown in fig. 146. For the heavy skins with little induced bending, the ratio $\sigma_{max}/\sigma_{gross} = 3.0$; for .1 thick skins $\sigma_{max}/\sigma_{gross}$ is in the vicinity of 3.9. The problem of the thinner skins with increasing eccentricity is circumscribed by the use of the honeycomb sandwich. Results of chordwise tension-tension tests of the honeycomb sandwich type showed the significance of controlling flexibility in the notched sheet. On fig. 147 the dashed S-N curve is a run with the base of the plenum not bonded to the honeycomb and the honeycomb sandwich curve with the base bonded; the line increase is almost 10:1.

If the row of holes is assumed dominant, a K_{Tnet} spanwise = 2.65, and chordwise = 2.40. Assuming $K_f = 1 + \frac{K_T - 1}{1 + a/r^*}$ and $a = .02''$, a material constant, for 75ST sheet, then K_f at the fatigue limit = 1.82 and 1.70 respectively. The value from the S-N diagram of the spanwise and chordwise honeycomb sandwich at fatigue limit is approximately $K_{fNET} = 1.85$, indicating the prime effect of the holes.

Similarly, the solid skin spanwise is $K_{fNET} \approx 1.85$ but chordwise $K_{fNET} \approx 2.5$ where the plenum eccentricity dominates (fig. 148).

There are seemingly more favorable basic shapes for the plenum chamber itself than the one shown; for example, an arc of a circle, "U" type, or elliptical notches. In most of these the presence of the hole in the critical base area of the notch is an additive concentration factor. In the concept shown, the concentrations are adequately separated, at least on the generally verified basis of the very local deterioration of the maximum stress of steep stress gradients. As a result of these investigations, it is believed that with a judicious replacement of material removed from BLC skins, the design K_T and gross stress of comparable riveted airfoils may be used in the design approach.

It has been noted that wing span is a significant parameter in BLC airplane performance. A traditional method of obtaining additional span within the range of contemporary cantilever deformations is

* r = radius of hole, in.

with external bracing. If either a straight or swept wing is braced at $1/3$ of its semi-span with a jury strut system, a potential 15 percent increase in span results in a 12 to 15 percent increase in range (ref. 105). The brace system is composed of laminarized airfoil shapes and designated by reverse loads.

Northrop has been conducting a BLC research and development program for several years. Many aerodynamic wind tunnel and in flight models have demonstrated the effectiveness of laminar flow control. Similarly, structural and environmental components were tested in the laboratories.

To demonstrate further the practicality of this system, Northrop is presently modifying a B66 airplane by substituting an increased planform suction wing for the present wing. This flight program of a load bearing laminar flow controlled wing, comprising a wide spectrum of off design conditions, will establish limits of operational effectivity of a swept, high subsonic wing and the percent efficiency of the laminarization under a variety of uses. Significant answers to corrosion fatigue, variable amplitude cycling with combined stress, the effects of highly local skin variations under fuel pressure and curvature, and the required maintenance of a live wing will be obtained.

APPENDIX B

NORTHROP'S STRUCTURAL LFC INVESTIGATIONS OF BLC GROUP

<u>BLC Number</u>	<u>NOR Number</u>	<u>Title and Authors</u>	<u>Class.</u>
8	None	DESIGN TESTS OF Y-STIFFENED PANELS ETR 7980-1--DESIGN TEST OF "Y" STIFFENED PANELS (SPECIMENS 2 and 14), J. A. Ralls and V. L. Cole, June 1953 ETR 7980-2--DESIGN TEST OF "Y" STIFFENED PANELS (SPECIMEN 12), V. L. Cole, August 1953	U
9	None	Y-STIFFENED PANEL EVALUATION, J. E. Jean and I. R. Stoughton, August 1953	U
10	None	STABILITY OF Y-STIFFENED MULTI-WEB BEAMS, H. C. Schjelderup, August 1953	U
15	None	DEFLECTION OF AN INITIALLY CURVED PLATE CAUSED BY AXIAL FORCES, H. C. Schjelderup, November 1953	U
17	None	COMPRESSION TESTS OF ANGLE-STIFFENED PANELS WITH CORRUGATED WINGS, J. R. Clem and W. W. Dedon, February 1954	U
18	None	COMPRESSION TEST OF A 3-WEB Y-STIFFENED BONDED PANEL, J. R. Clem and W. W. Dedon, December 1953	U
19	None	COMPRESSION TESTS OF SINGLE-WEB Y-STIFFENED PANELS USING RETURN FLANGES, J. R. Clem and W. W. Dedon, December 1953	U
20	None	COMPRESSION TESTS OF SINGLE-WEB Y-STIFFENED PANELS WITH BONDED REINFORCEMENTS, J. R. Clem and W. W. Dedon, January 1954	U
26	None	SHEAR TEST OF ALUMINUM ALLOY STRIP CUT WITH HOLES, J. R. Clem and W. W. Dedon, January 1954	U
27	None	THICKNESS OF ATTACHMENT ANGLE NECESSARY FOR MULTISPAR, THICK SKIN, WING BOX CONSTRUCTION, H. C. Schjelderup, January 1954	U
32	None	BENDING TESTS OF HONEYCOMB SPARS, J. R. Clem and W. W. Dedon, March 1954	U
34	None	COMPRESSION TEST OF TWO SINGLE-WEB Y-STIFFENED PANELS WITH BONDED REINFORCEMENTS, J. R. Clem and W. W. Dedon, April 1954	U
35	None	TENSILE TEST OF SLOT CONNECTION PANEL, J. R. Clem and W. W. Dedon, April 1954	U
39	None	DEFLECTION INDUCED LOADS ACTING ON A CONTINUOUSLY HINGED UNLOADED AILERON, H. C. Schjelderup, April 1954	U
41	None	SHEAR AND COMPRESSION TESTS OF SANDWICH PANELS WITH BONDED OVERLAY STRIPS, J. R. Clem and W. W. Dedon, May 1954	U
44	None	THE STABILITY AND LINEAR DEFORMATION OF A FRAMEWORK FORMED BY A CANTILEVER, KNEE BRACE, AND JURY STRUT, H. Schjelderup, May 1954	U
55	NAI-54-490	A METHOD OF MANUFACTURE OF SUCTION SLOTS FOR A LAMINAR SUCTION AIRPLANE, R. N. Worth and W. R. Slagg, July 1954	U
60	NAI-54-643	THEORETICAL ANALYSIS AND COMPRESSION TEST OF A SLOTTED SANDWICH PLATE, H. C. Schjelderup and W. W. Dedon, August 1954	U
66	NAI-54-799	ADDITIONAL THEORETICAL STUDIES OF DEFLECTION INDUCED LOADS ACTING ON A CONTINUOUS HINGE CONTROL SURFACE, H. C. Schjelderup and W. W. Dedon, November 1954	U
81	NAI-55-945	STRUCTURAL DESIGN CONSIDERATIONS FOR LOW DRAG BOUNDARY LAYER CONTROL, W. W. Dedon, W. R. Slagg and W. Pfenninger, October 1955	U
128	59-608	EFFECT OF WEATHERING ON TYPICAL BONDED BOUNDARY LAYER CONTROL STRUCTURE, R. N. Worth, November 1959	U
133	61-211	EFFECT OF ENVIRONMENTAL EXPOSURE ON BOUNDARY LAYER CONTROL SURFACES AND OPERATIONS, R. N. Worth, September 1961	U

SUMMARY REPORT ASD-TDR-63-554 (1964: Summary of Laminar Boundary Layer Control Research:

J. Wieder and W. Pfenninger: Structural Aspects of Low Drag Suction Airfoils, pp. 794-800.

R. N. Worth: Skin Directing System Configuration for LFC Aircraft, pp. 801-808.

R. N. Worth: Effect of Weathering on Typical Bonded LFC Structure, p. 809.

STUDIES OF LFC AIRPLANE PROPULSION PROBLEMS:

Pfenninger, W.: Cycle Studies of Gas Turbines for Laminar Boundary Layer Control Aircraft. Northrop Report AM-88, 1949.

Newton, J. S. and Pfenninger, W.: Studies of Gas Turbine Power Plants Suitable for Laminar Suction Airplanes. Northrop Report BLC-49, NAI-54-485, 1954.

Connors, J. W.; Pfenninger, W.; and Smith, D. B.: Propulsion Systems for Laminar Flow Aircraft. IAS Paper 61-52, January 1961.

Pfenninger, W.: Cycle Calculations of the Propulsion System of a Subsonic Laminar Suction Airplane with Turbo Fan Gas Turbines with Suction Compressors Driven by a Bleed and Burn Cycle. BLC-110, NAI-58-489, Northrop, July 1958.

Pfenninger, W.: Propulsion Studies of Laminar Suction Airplanes of Moderate Size. Northrop Report BLC-118, NOR-59-260, April 1959.

Pfenninger, W.: Design Considerations of Propulsion Systems for Low Drag BLC Airplanes Cruising at High Subsonic Speeds. Northrop Report BLC-122, NOR-59-418, July 1959.

Pfenninger, W.: Propellers for Long Range Laminar Suction Airplanes Flying at High Subsonic Speeds. Northrop Report BLC-37, April 1954.

LFC AIRPLANE DESIGN STUDIES:

Design Considerations for Hypothetical Boundary Layer Control Airplane:

Part 1 - Pfenninger, W.: Design Considerations. May 1951

Part 2 - Bacon, J. W.: Aeroelastic Study. March 1953

Northrop Report BLC-1

Bacon, J. W., Jr.: An Aeroelastic Study of Configuration II of a Laminar Boundary Layer Control Airplane. Northrop Report BLC-2, May 1953

Bacon, J. W., Jr.: Experimental Investigation of Structural Effect of Sweepback on a Strut-Braced Wing. Northrop Report BLC-47, NAI-54-475, July 1954.

Fiul, A.: A Preliminary Report on a Comparison of Aeroelastic Effects on Cantilevered and Strut-Braced Swept Wings. Northrop Report BLC-67, NAI-54-800, November 1954.

Pfenninger, W.: Note About the Range Performance of High Altitude Long Range Photoreconnaissance Airplanes with Low Drag Boundary Layer Suction. Northrop Report BLC-85, NAI-56-264, March 1956.

Pfenninger, W.; and Bacon, John W., Jr.: General Design Investigations of Long Range Laminar Suction Airplanes. Northrop Report BLC-90, NAI-56-615, August 1956.

Pfenninger, W.: Note on Long Range Photoreconnaissance Airplane with Low Drag Cruising at Very High Altitudes. Northrop Report BLC-98, NAI-57-710, May 1957.

Bacon, John W.; Fiul, A.; and Pfenninger, W.: WADC 10-Ft Transonic Wind Tunnel Tests on Strut-braced Boundary Layer Airplane. Northrop Report BLC-99, NAI-57-826, June 1957.

Pfenninger, W.: Design Considerations of Large Subsonic Long Range Transport Airplanes with Low Drag Boundary Layer Suction. Northrop Report BLC-111, NAI-58-529, July 18, 1958, revised April 1960.

Pfenninger, W.: Preliminary Design Studies of Large Low Drag BLC Long Endurance Airplanes. Northrop Report BLC-127, 59-613, December 1959.

REFERENCES

1. Pfenninger, W. Experiments on a Laminar Suction Airfoil of 17% Thickness. IAS-Journal, vol. 16, no. 4, 1949.
2. McCready, P. Turbulence Measurements by Sailplane. Journal of Geophysical Research, vol. 67, no. 3, pps. 1041-1050, 1962.
3. Gray, W.E.,
Fullam, P. Comparison of Flight and Tunnel Measurements of Transition on a Highly Finished Wing (King Cobra). RAE TN Aero. 2383, 1950.
4. (a) Pfenninger, W. Experiments with a 15% Thick Slotted Laminar Suction Wing Model in the NACA Langley Low Turbulence TDT Tunnel. AFTR 5982, 1951.

(b) Loftin, L.,
Horton, E. Experimental Investigation of Boundary Layer Suction Through Slots to Obtain Extensive Laminar Boundary Layers on a 15% Thick Airfoil at High Reynolds Numbers. NACA Research Memorandum L52D02, NACA/TIB/3491, 1952.
5. Pfenninger, W.,
Groth, E.,
Whites, R.C.,
Carmichael, B.H. Note About Low Drag Boundary Layer Suction Experiments in Flight on a Wing Glove of an F94A Airplane. Northrop Report BLC-69, NAI-54-849, December 1954.
6. Pfenninger, W.,
Groth, E.,
Carmichael, B.H.,
Whites, R.C. Low Drag Boundary Layer Suction Experiments in Flight on the Wing Glove of an F94A Airplane, including Appendices I, II, III, Phase I: Suction Through 12 Slots. Northrop Report BLC-77, NAI-55-458, 1955.
7. Groth, E.
Carmichael, B.H.,
Whites, R.C.,
Pfenninger, W. Low Drag Boundary Layer Suction Experiments in Flight on the Wing Glove of an F94A Airplane, Phase II: Suction Through 69 Slots. Northrop Report BLC-94, NAI-57-318, 1957.
8. Carmichael, B.H.,
Whites, R.C.,
Pfenninger, W. Low Drag Boundary Layer Suction Experiments in Flight on the Wing Glove of an F94A Airplane, Phase III: Laminar Suction Airfoil Tolerances. Northrop Report BLC 101, NAI-57-1163, 1957.
9. Carmichael, B.H.,
Whites, R.C.,
Wisma, R.E. Low Drag Boundary Layer Suction Experiments in Flight on the Wing Glove of an F94A Airplane, Phase IV: Suction Through 81 Slots Between 8% and 95% Chord. Northrop Report BLC-102, NAI-57-1025, 1957.
10. Pfenninger, W.,
Groth, E. Low Drag Boundary Layer Suction Experiments in Flight on a Wing Glove of an F94A Airplane with Suction Through a Large Number of Fine Slots. Boundary Layer and Flow Control, G. V. Lachmann, Editor, vol. 2, p. 981, 1961. Pergamon Press, Inc.
11. Braslow, A.L.,
Burrows, D.L.,
Tetervin, N.,
Visconti, P. Experimental and Theoretical Studies of Area Suction for the Control of the Laminar Boundary Layer of an NACA 64A010 Airfoil. NACA TR 1025, 1951.
12. Pfenninger, W.,
Moness, E.,
Sipe, O.E. Investigation in a Tube at High Reynolds Numbers and Low Turbulence with Boundary Layer Suction Through 80 Slots. Northrop Report BLC-53, 1954.
13. Pfenninger, W. Boundary Layer Suction Experiments with Laminar Flow at High Reynolds Numbers in the Inlet Length of a Tube by Various Suction Methods. Boundary Layer and Flow Control, G. V. Lachmann, Editor, vol. 2, p. 961, 1961.
14. Meyer, W.A.,
Pfenninger, W. Preliminary Investigations of Laminar Flow in a Tube at High Reynolds Numbers and Low Turbulence with Boundary Layer Suction Through 80 Slots. Northrop Report BLC-7, August 1953.
15. Meyer, W.A.,
Goldsmith, J.,
Pfenninger, W. Note on Preliminary Laminar Suction Experiments Through Round Holes at High Reynolds Numbers and Low Turbulence. Northrop Report BLC-12, September 1953.
16. Goldsmith, J.,
Meyer, W.A. Preliminary Experiments on Laminar Boundary Layer Suction Through Circular Holes at High Reynolds Numbers and Low Turbulence. Northrop Report BLC-23, November 1953.
17. Goldsmith, J. Additional Experiments on Laminar Boundary Layer Suction Through Circular Holes at High Reynolds Numbers and Low Turbulence. Northrop Report BLC-28, February 1954.
18. Goldsmith, J. Experiments with Laminar Boundary Layer Suction Through Rows of Closely Spaced Circular Holes at High Reynolds Number and Low Turbulence. Northrop Report BLC-36, March 1954.
19. Meyer, W.A. Preliminary Report on the Flow Field Due to Low Drag Suction Through Holes. Northrop Report BLC-75, NAI-55-457, April 1955.

20. Goldsmith, J. Investigation of the Flow in a Tube with Laminar Suction Through 80 Rows of Closely-Spaced Holes. Northrop Report BLC-86, NAI-56-293, March 1956.
21. Goldsmith, J. Critical Laminar Suction Parameters for Suction Into an Isolated Hole or a Single Row of Holes. Northrop Report BLC-95, NAI-57-529, February 1957.
22. Raspet, A. Boundary Layer Studies on a Sailplane. Aeron. Eng. Review, vol. 11, no. 6, 1952.
23. Carmichael, B.H. Flight Observations of Suction Stabilized Boundary Layers. Aeron. Eng. Review, vol. 13, no. 2, pp. 36-41, 1954.
24. Wortmann, F.X., Feifel, W. Low Drag Suction Experiments in the Stuttgart Low Turbulence Tunnel on a 19-Percent Thick Highly Cambered Low Drag Suction Airfoil With Suction Through Spanwise Rows of Suction Holes. Institute for Aerodynamics report, TH, Stuttgart.
25. Gregory, N., Walker, W.S. Experiments on the Use of Suction Through Perforated Strips for Maintaining Laminar Flow: Transition and Drag Measurements. A.R.C., R. and M. 3083, 1955.
26. Head, M.R. Flight Experiments on Maintaining Laminar Flow With Suction Applied Through Perforations. Boundary Layer and Flow Control, G. V. Lachmann, Editor, p. 943, p. 950, 1961.
27. - Low Drag Suction Experiments on a Two-Meter Long Ellipsoid of Revolution by Dr. Novikov in the ITAM Novosibirsk 1 x 1 Meter Low-Turbulence Tunnel With Suction Through 0.07-Millimeter Diameter Holes of 0.5 Millimeter Spacing. (Verbal communication of Dr. Novikov to the author, March 1974.)
28. Pfenninger, W. Some General Considerations of Losses in Boundary Layer Suction Ducting Systems. Northrop Report BLC-29, 1954.
29. Pfenninger, W., Dedon, W., Slagg, W. Design of the Suction Ducting System for a Hypothetical Laminar Suction Airplane. Northrop Report BLC-40, 1954.
30. Reilly, R. Influence of Internal Flow Passages on the Spanwise Suction Distribution in a slot. Northrop Report BLC-54, NAI-54-489, 1954.
31. Reilly, R. Influence of Chordwise Separation Between a Slot and Its Suction Holes on the Spanwise Suction Distribution in a Slot. Northrop Report BLC-59, NAI-54-567, 1954.
32. Reilly, R. The Influence of Slot Width on the Spanwise Suction Distribution in a Slot. Northrop Report BLC-62, NAI-54-717, 1954.
33. Pfenninger, W. Flow Problems of Swept Low Drag Suction Wings of Practical Construction at High Reynolds Numbers. Annals New York Academy of Sciences, vol. 154, art. 2, 1968.
34. Wieder, J., Pfenninger, W. Structural Aspects of Low Drag Suction Airfoils. IAS Paper No. 61-150-1844, presented at IAS meeting June 1961, Los Angeles, California.
35. Pfenninger, W. Experiments with Laminar Flow in the Inlet Length of a Tube at High Reynolds Numbers with and Without Boundary Layer Suction. Northrop Report, May 1952.
36. Ackeret, J. Probleme des Flugzeugantriebs in Gegenwart u. Zukunft. Schweiz, Bauzeitg, Bd. 111, p. 237, 1938.
37. Pfenninger, W. Untersuchungen ueber Reibungs-Verminderungen an Tragfluegeln Insbesondere mit Hilfe von Grenzschichtabsaugung. Mitt. 13 IFA, Zurich, 1946. English translation NACA TM 1181, 1947.
38. Groth, E. The Turbine-Compressor System for the F94 Flight Tests. Northrop Report BLC-51, NAI-54-487, 1954.
39. Greber, I. Interaction of Oblique Shock Waves with Laminar Boundary Layer. Fluid Dynamics Research Group, MIT Technical Report 59-2, 1959. Conducted jointly with the Northrop Boundary Layer Research Group.
40. Groth, E.E. Investigation of a Laminar Flat Plate With and Without Weak Incident Shock Waves. ASD-TDR-63-554, vol. II, Summary of Laminar Boundary Layer Control Research, vol. II, 1964.
41. Groth, E.E. Effect of Laminar Flow Control on the Interaction of an Impinging Shock Wave with a Laminar Boundary Layer at $M = 2.5$ to 3.5 and Reynolds Numbers Between $10 \cdot 10^6$ and $26 \cdot 10^6$ AFFDL-TR-66-94, 1966.
42. Schlichting, H. Lecture Series "Boundary Layer Theory." Part I - Laminar Flows. NACA TM 1217, 1949. Part II - Turbulent Flows. NACA TM 1218, 1949.

43. Ulrich, A. Theoretische Untersuchungen Ueber Die Widerstandersparnis Durch Laminarhaltung Mit Absaugung. Schriften Der Dt. Akad. D. Luftfahrt-Forschung, 8B, no. 2, 1944. NACA TM 1121, 1947.
44. Gross, L.W., Pfenninger, W. Experimental and Theoretical Investigation of a Reichardt Body of Revolution With Low Drag Suction in the NASA Ames 12-Foot Pressure Wind Tunnel. Northrop Report NOR 63-46, BLC-148, 1963.
45. Gross, L.W. Investigation of a Reichardt Body of Revolution With Low Drag Suction in the Norair 7 x 10 Foot Wind Tunnel. Northrop Report BLC-143, NOR 62-126, 1962.
46. Gross, L.W. Investigation of a Laminar Suction Reichardt Body of Revolution in the Ordnance Research Laboratory 4-Foot Water Tunnel. Northrop Report BLC-167, NOR 65-311, 1965.
47. Gross, L.W. Influence of Turbulent Wakes on a Suction Body. Northrop Report NCL-68-46R, 1968.
48. - Verbal Communication of V. V. Struminskü to the author.
49. Gray, W. E. The Effect of Wing Sweep on Laminar Flow. RAE TM Aero. 255, 1952.
50. Owen, P.R., Randall, D.J. Boundary Layer Transition on the Sweptback Wing. RAE TM Aero 277, 1952.
51. Boltz, F.W., Kenyon, G.C., Allen, C.Q. Effects of Sweep Angle on the Boundary Layer Stability Characteristics of an Untapered Wing at Low Speeds. NASA TN D-338, 1960.
52. Gregory, N., Stuart, J.T., Walker, W.S. On the Stability of 3-Dimensional Boundary Layers with Application to the Flow Due to a Rotating Disc. Phil. Trans. Roy. Soc. London, Series A, no. 943, vol. 248, pp. 155-199, 1955.
53. Pfenninger, W., Bacon, J.W. About the Development of Swept Laminar Suction Wings With Full Chord Laminar Flow. Northrop Report BLC-130, NOR 60-299, 1960. See also Boundary Layer and Flow Control, G. V. Lachmann, Editor, vol. 2, pp. 1007-1032, Pergamon Press, Inc., 1961.
54. Brown, W.B. A Stability Criterion for Three-Dimensional Laminar Boundary Layers. Boundary Layer and Flow Control, G. V. Lachmann, Editor, vol. 2, Pergamon Press, Inc., 1961. See also: Brown, W.B.: Numerical Calculation of the Stability of Crossflow Profiles in Laminar Boundary Layers on a Rotating Disk and a Sweptback Wing. Northrop Report BLC-117, NAI-59-5, 1959.
55. Pfenninger, W., Experiments on a 30° Swept 12% Thick Symmetrical Laminar Suction Wing in the 5 x 7 Foot Michigan Tunnel; including Appendix by G. S. Raetz: Evaluation of the Profile Drag Coefficient of an Untapered Swept Suction Wing. Northrop Report BLC-93, NAI-57-317, 1957.
56. Gross, L.W. An Analysis of the Boundary Layer Development on a 30° Swept Laminar Suction Wing. Northrop Report BLC-134, NAI-61-244, 1962.
57. Carlson, J.C. Results of a Low Speed Wind-Tunnel Test to Investigate the Influence of Leading Edge Radius and Angle of Attack on the Spanwise Spread of Turbulence Along the Leading Edge of a Sweptback Wing. Northrop Report NOR-64-30, 1964.
58. Bacon, J.W., Pfenninger, W., Moore, C.R. Investigations of a 30-Degree Swept and a 17-Foot Chord Straight Suction Wing in the Presence of Internal Sound, External Sound, and Mechanical Vibrations. Summary of Laminar Boundary Layer Control Research, vol. 1, ASD-TDR-63-554, 1964.
59. Carlson, J.C., Bacon, J.W. Influence of Acoustical Disturbances in the Suction Ducting System on the Laminar Flow Control Characteristics of a 33° Swept Suction Wing. Northrop Report NOR-65-232, 1965.
60. Stuart, J.T. Nonlinear Effects in Hydrodynamic Stability. Proceedings of the Xth International Congress for Theor. and Applied Mechanics, Stresa, 1960. Applied Mechanics, Elsevier Publishing Company, 1962, p. 63-97.
61. Raetz, G.S. A New Theory of the Cause of Transition in Fluid Flows. Northrop Report BLC-121, NOR 59-383, June 1959.
62. Raetz, G.S. Calculation of Precise Proper Solutions for the Resonance Theory of Transition. Air Force Report AFFDL-TRO-64-185, October 1964.
63. Raetz, G.S. Current Status of Resonance Theory of Transition. Air Force Report ASD-TDR-63-554, March 1964.
64. Raetz, G.S. A Further Development of the Resonance Theory of Transition Including a Correlation with an Experiment. Air Force Report AFFDL-TR-66-192, November 1966.

65. Bacon, J.W.,
Pfenninger, W. Transition Experiments at the Front Attachment Line of a 45-Degree Swept Wing with a Blunt Leading Edge. TR AFFDL-TR-67-33, Wright Field, 1967.
66. Gregory, N. Transition and the Spread of Turbulence on a 60-Degree Sweptback Wing. Journal Royal Aero Society, 1960.
67. Pfenninger, W. X-21 Flight Observations and Flight Test Program for the Next Few Flights. Northrop Memo., 3850-63-352, June 10, 1963.
68. Pfenninger, W. Status of the X-21 Flights. Northrop Memo. 3850-63-356, June 24, 1963.
69. Pfenninger, W. Note About the Spanwise Turbulent Contamination of Swept Low Drag Suction Wings. Northrop Norair Internal Note, July 1963.
70. Pfenninger, W. Preliminary Note About an Experimental Verification of the Turbulent Spanwise Contamination on a Swept Wing in the Northrop 8 x 11 Foot Wind Tunnel. Memo. 3850-362, July 17, 1963.
71. Pfenninger, W. Some Results From the X-21 Program. Part I, Flow Phenomena at the Leading Edge of Swept Wings. Agardograph 97, Part IV, May 1965.
72. Pfenninger, W,
Bacon, J. Amplified Laminar Boundary Layer Oscillations and Transition at the Front Attachment Line of a 45-Degree Swept Flat-Nosed Wing With and Without Boundary Layer Suction. Viscous Drag Reduction, C. S. Wells, Editor, Plenum Press, pp. 85-105, 1969.
73. Carlson, J. Investigation of the Laminar Flow Control Characteristics of a 33-Degree Swept Suction Wing at High Reynolds Numbers in the NASA Ames 12-Foot Pressure Wind Tunnel. Northrop Report NOR-66-58, January 1966.
74. Pfenninger, W.,
Bacon, J.,
Goldsmith, J. Flow Disturbances Induced by Low-Drag Boundary Layer Suction Through Slots. Phys. of Fluids Supplement, p. S112, 1967.
75. Bacon, J.W. Study of Slot Flow Induced Disturbances. Northrop Report NCL-68-46R, 1968.
76. Brown, W.B. Stability of the Laminar Boundary Layer at the Attachment Line of a 33° Swept Wing. Northrop Report NCL-68-48R, 1968.
77. Carmichael, B.H. Surface Waviness Criteria for Swept and Unswept Laminar Suction Wings. Northrop Report BLC-123, NOR-59-438, 1959.
78. Carmichael, B.H. Surface Imperfection Experiments on a Swept Laminar Suction Wing. Northrop Report BLC-124, NOR-59-454, 1959.
79. von Doenhoff, A.E.,
Braslow, A.L. The Effect of Distributed Surface Roughness on Laminar Flow. Boundary Layer and Flow Control, G. V. Lachmann, Editor, vol. II, p. 657, 1961.
80. Tani, Itiro Effect of Two-Dimensional and Isolated Roughness on Laminar Flow. Boundary Layer and Flow Control, G. V. Lachmann, Editor, vol. 2, pp. 637-656, 1951.
81. Carmichael, B.H. Prediction of Critical Roughness Reynolds Numbers for Three-Dimensional Roughness Elements. Northrop Report BLC-109, NAI-58-412, 1958.
82. Carmichael, B.H. Critical Roughness Reynolds Numbers for Multiple Three-Dimensional Roughness Elements. Northrop Report BLC-112, NAI-58-589, 1958.
83. Gregory, N.,
Walker, W.S. The Effect on Transition of Isolated Surface Excrescences in the Boundary Layer. A.R.C. 13436, 1950.
84. Carlson, J.C. Low Drag Boundary Layer Suction Experiments Using a 33° Swept 15 Percent Thick Laminar Suction Wing With Suction Slots Normal to the Leading Edge. Northrop Report NOR-64-281, 1964.
85. Hahn, M.,
Pfenninger, W. Prevention of Transition Over a Backward Step by Suction. Journal Aircraft, vol. 10, no. 10, pp. 618-622, October 1973.
86. Groth, E. Low Drag Boundary Layer Suction Experiments on a Flatplate at $M = 3$ and 3.5. Northrop Report BLC-135, NOR-61-251, 1961.
87. Groth, E.,
Pate, S.R.,
Nenni, J. Recent Developments in Boundary Layer Research; Laminar Flow Control at Supersonic Speeds. Agardograph 97, Part IV, 1965.
88. Rogers, Kenneth H. Preliminary Investigation of the Pressure Drop in Suction Ducts. Northrop Report BLC-13, September 1953.
89. Rogers, K.H. Investigation of the Pressure Distribution in Suction Ducts. Northrop Report BLC-22, November 1953.
90. Pfenninger, W. Some General Considerations of Losses in Boundary Layer Suction Ducting Systems. Northrop Report BLC-29, February 1954.

91. Rogers, K.H. A Method of Calculating the Pressure Distribution in Suction Ducts. Northrop Report BLC-30, February 1954.
92. Pfenninger, W.,
Dedon, W.W.,
Slagg, W.R. Design of the Suction Ducting System for a Hypothetical Laminar Suction Airplane. Northrop Report BLC-40, May 1954.
93. Rogers, K.H. Investigation of the Pressure Distribution and Boundary Layer in a Suction Duct with Zero-Decelerated Duct Inlet. Northrop Report BLC-50, NAI-54-486, July 1954.
94. Rogers, K.H. Investigation of the Pressure Distribution and Boundary Layer in a Suction Duct with Smooth-Transition Duct Inlet. Northrop Report BLC-64, NAI-54-716, October 1954.
95. Pfenninger, W.,
Rogers, K.H. Further Investigations on an Improved Suction Duct. Northrop Report BLC-70, NAI-55-547, May 1955.
96. Rogers, K.H. Investigation of the Pressure Distribution Along a Constant Area Suction Duct with 90-Degree Drilled-Hole Inlet. Northrop Report BLC-71, NAI-55-286, March 1955.
97. Rogers, K.H. Experimental and Analytical Investigation of a Vee Inlet Suction Duct. Northrop Report BLC-89, NAI-56-614, July 1956.
98. Kosin, R.E. Design of Boundary Layer Control Suction and Blowing Ducts with Arbitrary Flow Distributions. WADC TR 52-196, 1952.
99. Cliett, C.B. Structural Comparison of Perforated Skin Surfaces with Other Means of Effecting Boundary Layer Control by Suction. Aeronautical Engineering Review, September 1953.
100. Wieder, J. BLC Untapered Rectangular Box Torsion Test. Norair Report in Preparation.
101. Worth, R. Effect of Weathering on Typical Bonded Boundary Layer Control Structure. Norair Division, Northrop Corporation, Report No. Nor-509-608, BLC-128, January 1960.
102. Hill, W.L. Preliminary Investigation on the Effect of Weathering and Sulfuric Acid Anodizing on Selected Metal-To-Metal Adhesive Systems. Norair Division, Northrop Corporation, Report No. Nor-61-35, March 1961.
103. WADC TR 59-507 Proceedings of the Symposium on Fatigue of Aircraft Structures. Wright Air Development Center, USAF, Wright-Patterson Air Force Base, Ohio, August 1959, p. 290.
104. Dally, J.W.,
Durelli, A.J. Stresses in Perforated Panels. Product Engineering, March 1956, pp. 188ff.
105. Pfenninger, W. Design Considerations of Large Subsonic Long Range Transport Airplanes with Low Drag Boundary Layer Suction. Norair Division, Northrop Corporation, Report No. NAI-58-529, BLC-111, October 1959.

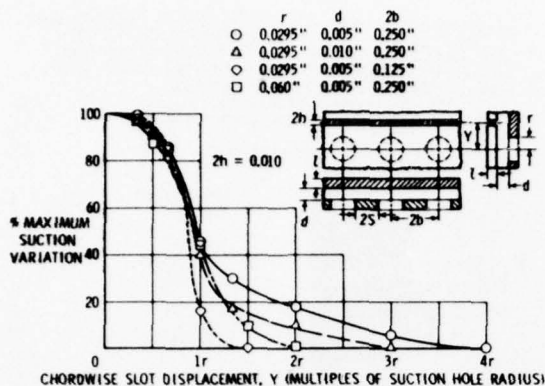


Figure 7(b).— Spanwise suction variation between adjacent suction holes.

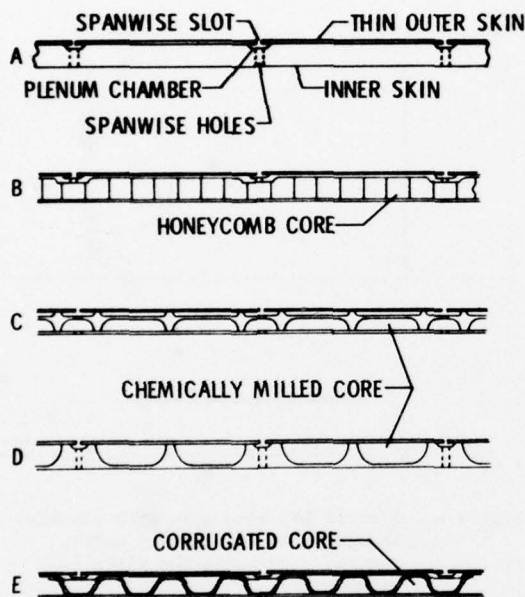


Figure 8.— Structural variations of LFC wing skins with closely spaced slots.

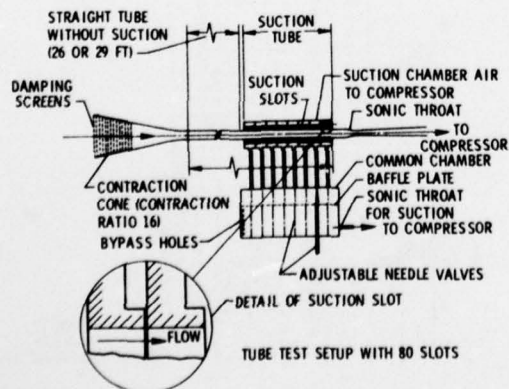


Figure 9.— Low drag suction test setup with 80 slots in the inlet length of a laminar flow low turbulence tube at high Reynolds number.

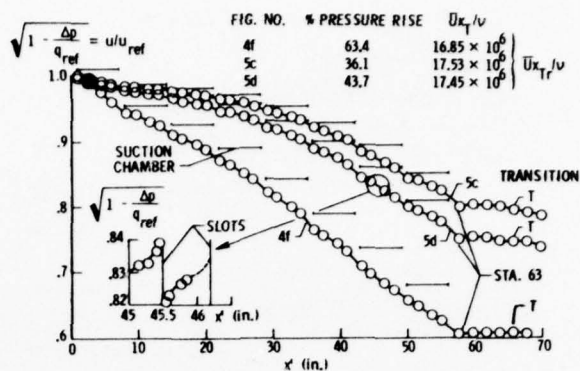


Figure 10.— Pressure distribution in suction region of the inlet length of a laminar flow tube with 80 slots, located upstream of a 26 ft. long 2" i.d. tube without suction.

$$\frac{u}{u_{ref}} = \sqrt{1 - \frac{\Delta p}{q_{ref}}}$$

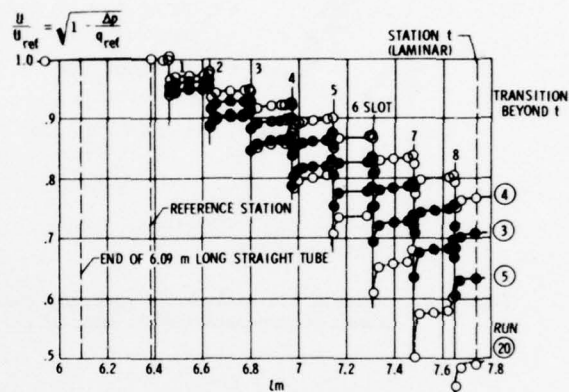


Figure 11.— U/U_{ref} with laminar flow in rear pressure rise area of a laminar flow tube with suction through 8 slots,

$$\left(\frac{\bar{u}}{v}\right)_{Tr} = 12.8 \cdot 10^6.$$

$$U/U_{ref} = \sqrt{1 - \Delta p/q_{ref}}$$

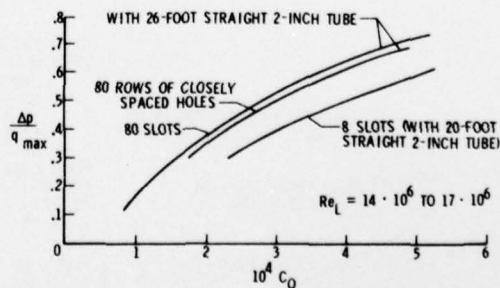


Figure 12.— LFC experiments in the inlet length of a laminar flow low turbulence tube, suction quantity

$$\text{coefficient } C_Q = \frac{Qa}{\bar{u} \cdot S} = F \left(\frac{\Delta p_{laminar}}{q_{max}} \right) \text{ with}$$

suction through 8 and 80 slots and 80 rows of very closely spaced holes.

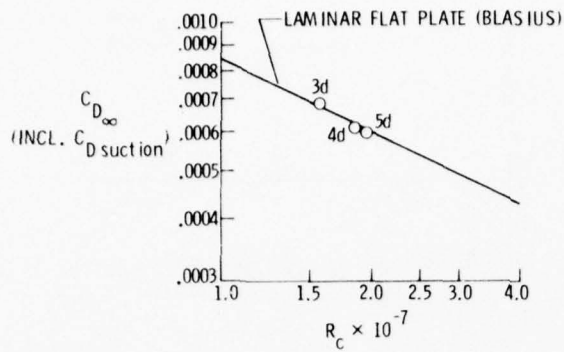


Figure 13(a).- LFC experiments in the inlet length of a laminar flow tube with suction through 80 slots; evaluation of wing profile drag of 8.5% thick equivalent LFC airfoil.

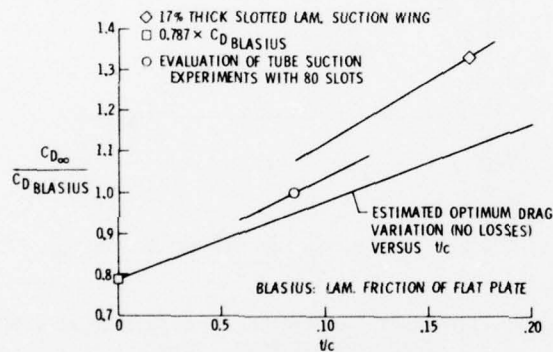


Figure 13(b).- Ratio of profile drag due to drag of laminar flat plate versus thickness ratio.

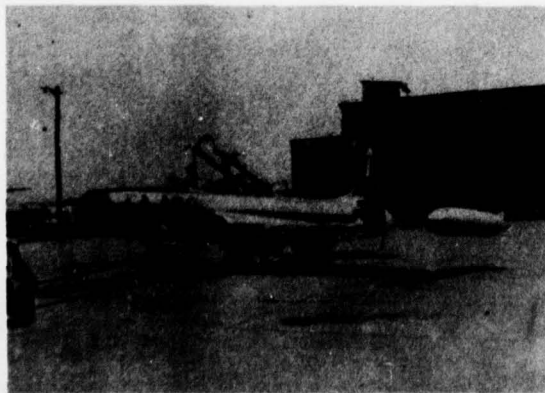


Figure 14. F94A test airplane with LFC wing glove.



Figure 15. F94A LFC wing glove.

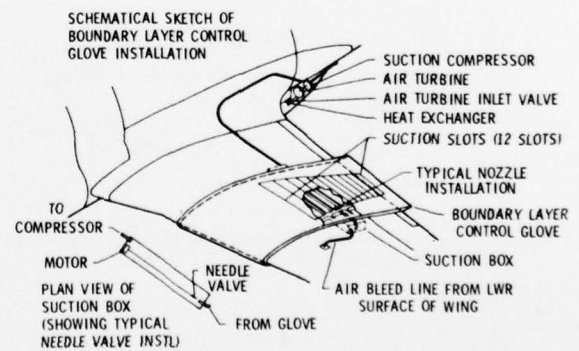


Figure 16.- Experimental setup of F94A LFC wing glove.

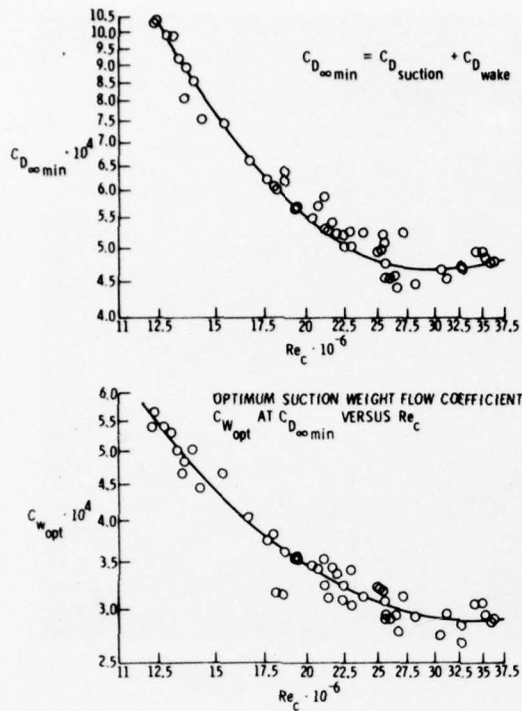


Figure 17.- F94 LFC wing glove with 69 slots located from 0.41c to 0.97c.

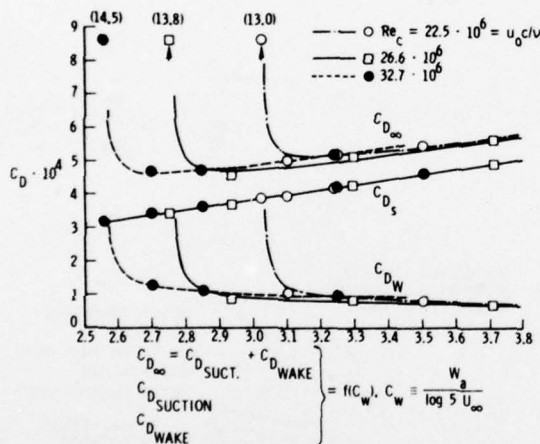


Figure 18.- F94 LFC wing glove (upper surface) with 69 slots from 0.41c to 0.97c.

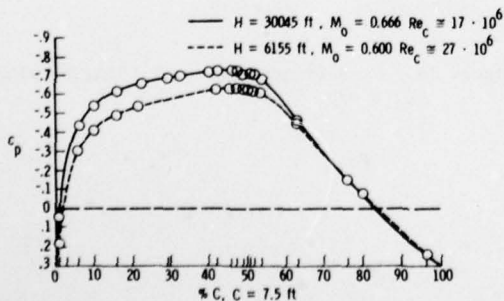


Figure 19.- F94 LFC wing glove with 69 slots from 0.41c to 0.97c. Upper surface. Full chord laminar flow. Pressure distribution $C_p(\frac{x}{c})$ with minimum flow acceleration in front part of wing.

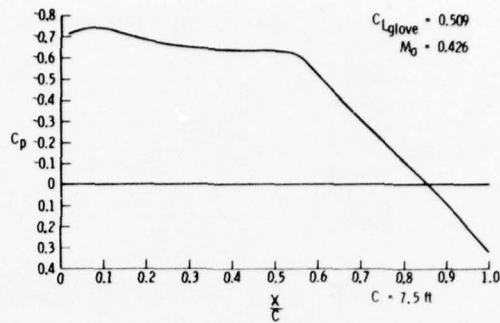


Figure 20.- F94 LFC wing glove (upper surface) with suction through 81 slots from 0.08c to 0.96c full chord laminar flow.

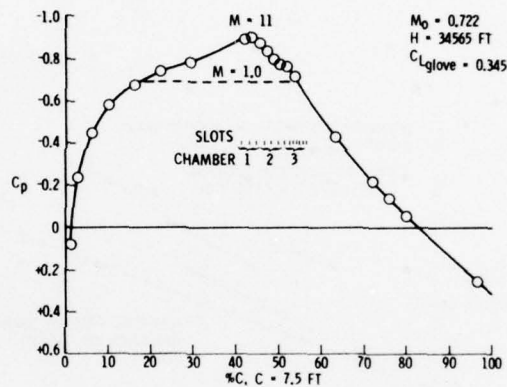


Figure 21.- Chordwise pressure distribution with full chord laminar flow, M_{crit} ($M_{local max} = 1.08$ to 1.10).

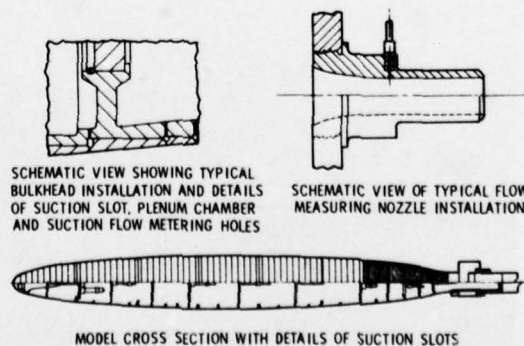


Figure 22.- Reichardt LFC body of revolution with 114 0.003" wide slots ($L = 12$ feet, $L/D = 8.0$).

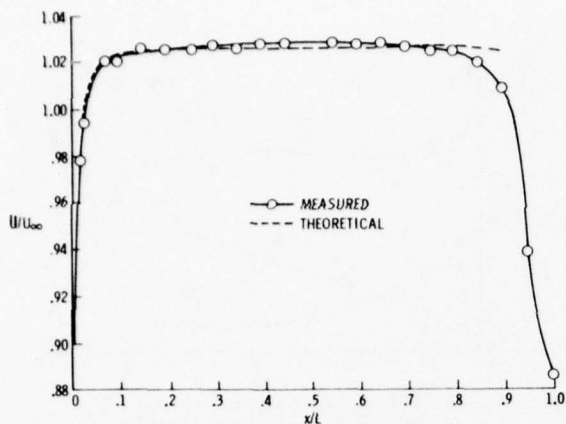


Figure 23.- Comparison of measured and theoretical velocity distributions for Reichardt LFC body ($L/D = 8$).

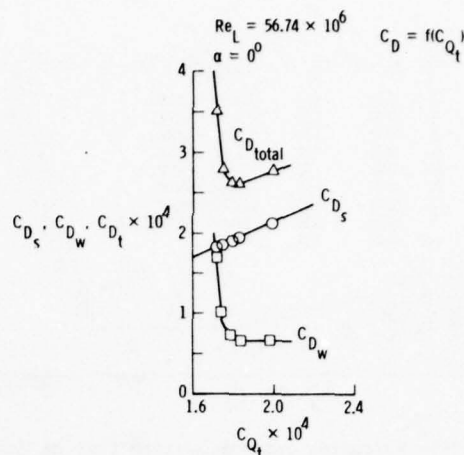


Figure 26.- Reichardt LFC body ($L/D = 8$). C_{D_s} , C_{D_w} , $C_{D_{tot}} = f(C_{Q_t})$.

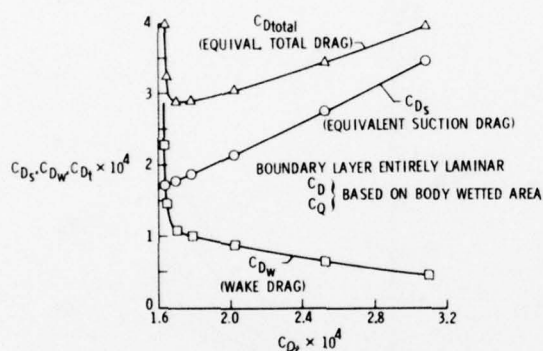


Figure 24.- Drag C_D versus suction quantity C_{Q_t} for various Reynolds numbers Re_L and angles of attack for Reichardt LFC body ($L/D = 8$). $Re_L = 37.18 \times 10^6$ and $\alpha = 0^\circ$.

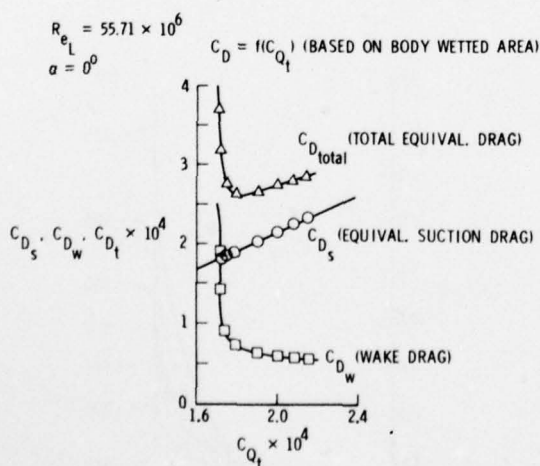


Figure 25.- Reichardt LFC body ($L/D = 8$) with suction through 114 slots. Drag coefficient $C_D = f(C_{Q_t})$ for $\alpha = 0^\circ$ angle of attack. Flow entirely laminar.

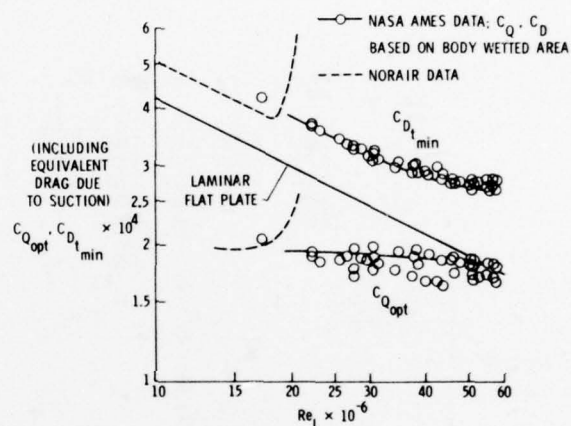


Figure 27.- Reichardt suction body of revolution, variation of minimum total drag $C_{D_{t_{min}}}$ and suction coefficient at minimum total drag $C_{Q_{opt}}$ with length Reynolds number Re_L , $\alpha = 0^\circ$; fineness ratio 8:1.

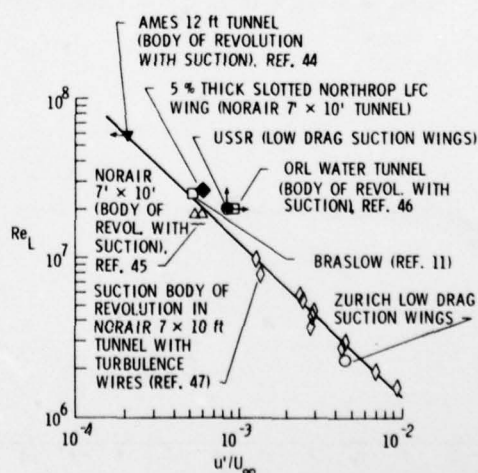


Figure 28.- Maximum length Reynolds number, Re_L , with full laminar flow versus u'/U_∞ for low drag suction wings and bodies of revolution.

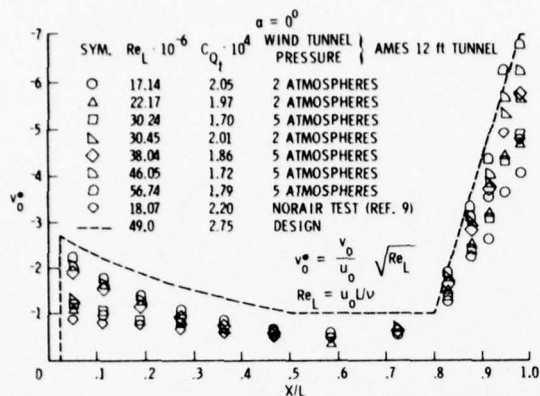


Figure 29.- Reichardt laminar suction body of revolution ($L/D = 8$). Lengthwise distribution of equivalent distributed suction velocity v_o^* for several Reynolds numbers Re_L .

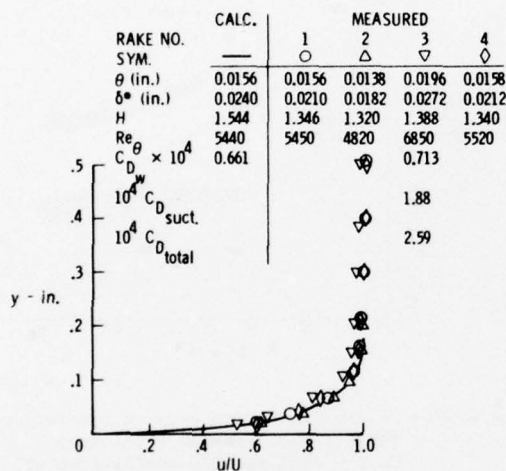


Figure 30.- Reichardt LFC body ($L/D = 8$). Comparison of calculated and measured boundary layer velocity profiles at rear end of body for the conditions of test point no. 287. $Re_L = 56.74 \times 10^6$; $C_{Qt} = 1.789 \times 10^{-4}$; $\alpha = 0^\circ$.

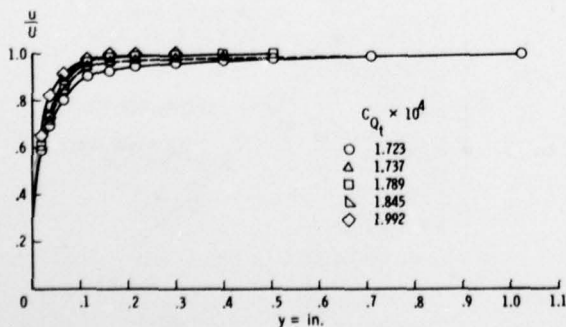


Figure 31.- Reichardt LFC body ($L/D = 8$). Variation of aft end boundary layer velocity profile with suction coefficient C_{Qt} . $Re_L = 56.740 \times 10^6$, $\alpha = 0^\circ$.

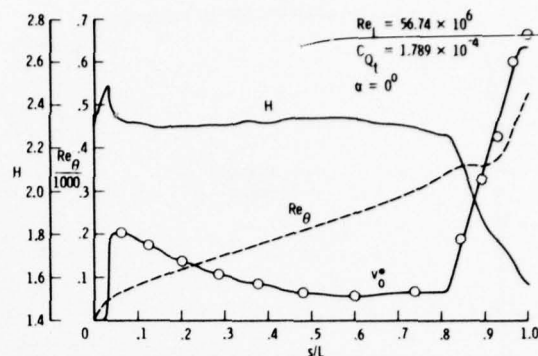


Figure 32.- Reichardt LFC body ($L/D = 8$). Non-dimensional equivalent distributed suction velocity distribution and boundary layer development for test point no. 287. $Re_L = 56.74 \times 10^6$, $C_{Qt} = 1.789 \times 10^{-4}$, $\alpha = 0^\circ$.

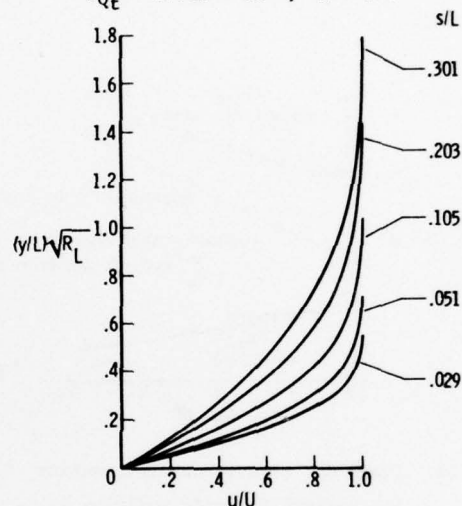


Figure 33.- Reichardt LFC body ($L/D = 8$). Calculated boundary layer profiles at various lengthwise positions s/L for the conditions of test point no. 287. $Re_L = 56.74 \times 10^6$, $C_{Qt} = 1.789 \times 10^{-4}$, $\alpha = 0^\circ$.

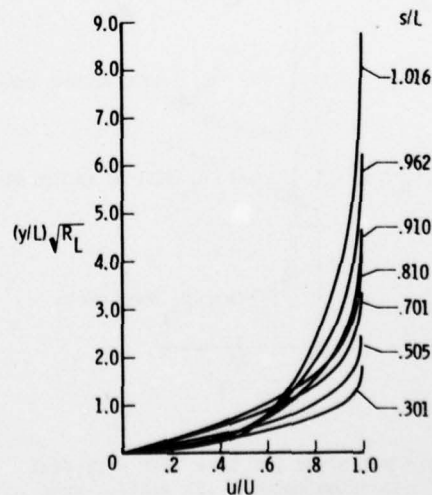


Figure 34.- Reichardt LFC body ($L/D = 8$). Calculated boundary layer profiles at various lengthwise positions s/L for the conditions of test point No. 287. $Re_L = 56.74 \times 10^6$, $C_{Qt} = 1.789 \times 10^{-4}$, $\alpha = 0^\circ$.



Figure 35. China-Clay flow observations in leading edge region swept wing (NASA Ames 12 ft tunnel experiments).

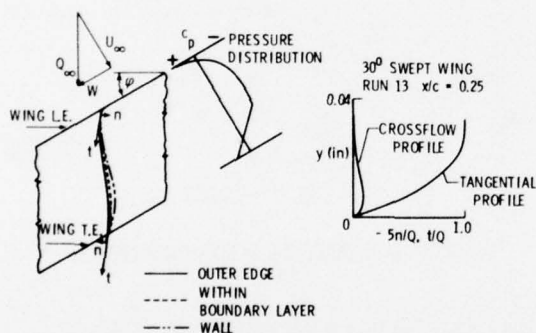


Figure 36.- Yawing LFC wing; chordwise pressure distribution, potential flow and boundary layer streamlines, tangential - and crossflow boundary layer profiles.

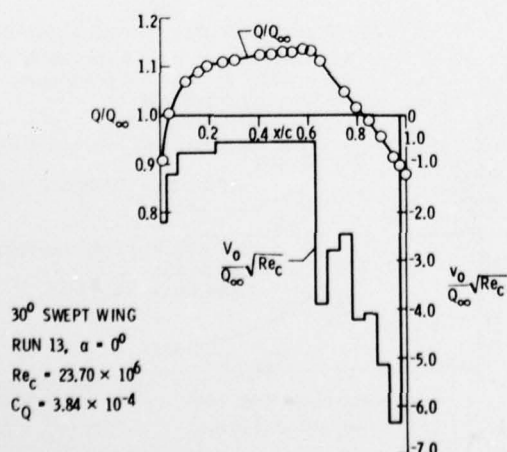


Figure 37.- Chordwise potential flow and suction distribution.

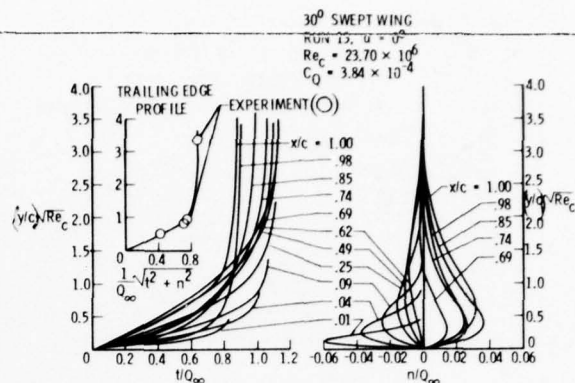


Figure 38.- Tangential and crossflow boundary layer profiles at different chordwise stations.

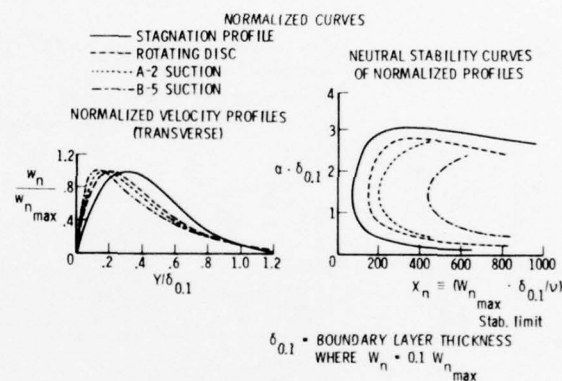


Figure 39.- Brown's boundary layer crossflow stability limit Reynolds number curves χ (based on maximum velocity W_n and boundary layer-thickness where $W = -0.1 W_{max}$ versus crossflow disturbance vortex wave number $\alpha = 2\pi/\lambda$ (λ = vortex spacing) for various normalized boundary layer crossflow profiles.

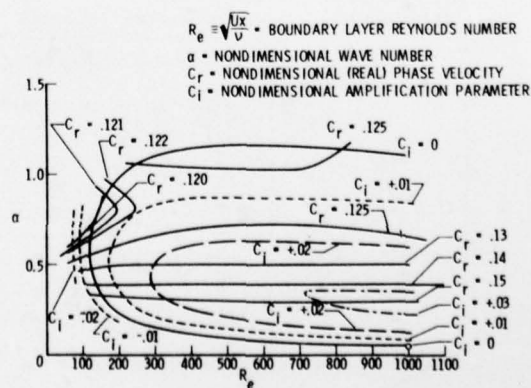


Figure 40.- Constant amplification and phase velocity curves. Swept wing stagnation line transverse profile (pure crossflow profile).

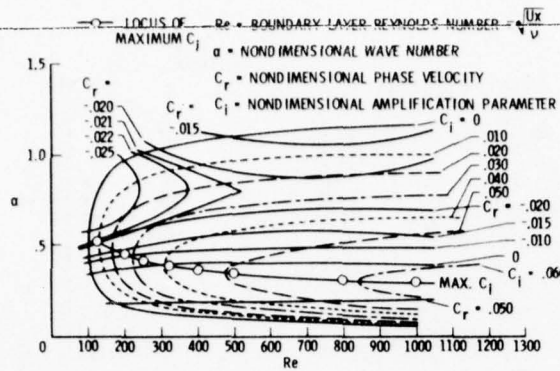


Figure 41.- Constant amplification and phase velocity curves critical profile, stagnation line ($w_n = 0$ at inflexion point), (swept wing).

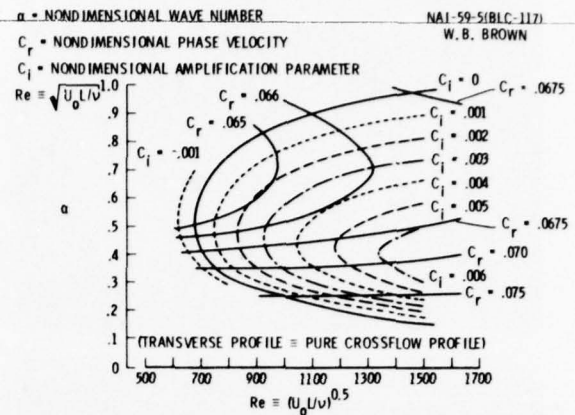


Figure 44.- Pure crossflow profile 8 in rear pressure rise area towards the trailing edge of swept LFC wing. Constant amplification and phase velocity curves.

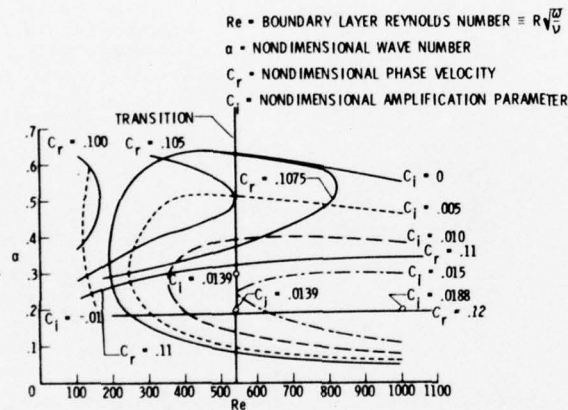


Figure 42.- Curves of constant amplification and wave velocity. Rotating disc radial (pure crossflow profile).

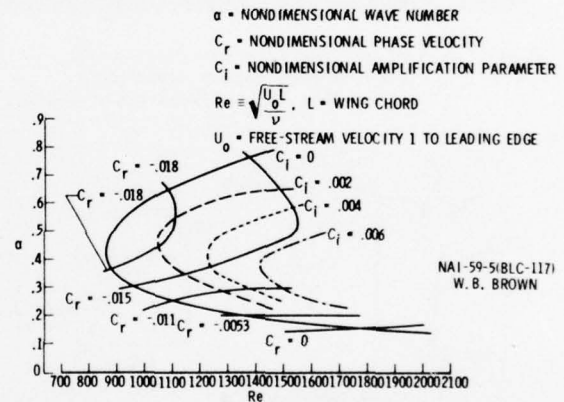


Figure 45.- "Critical" profile 9 ($w_n = 0$ at inflexion point) in rear pressure rise area towards the trailing edge of a swept LFC wing. Constant amplification and phase velocity curves.

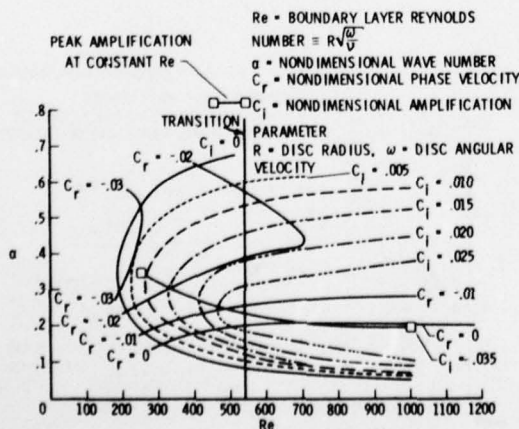


Figure 43.- Curves of constant amplification and wave velocity. Rotating disc critical. ($w_n = 0$ at inflexion point)

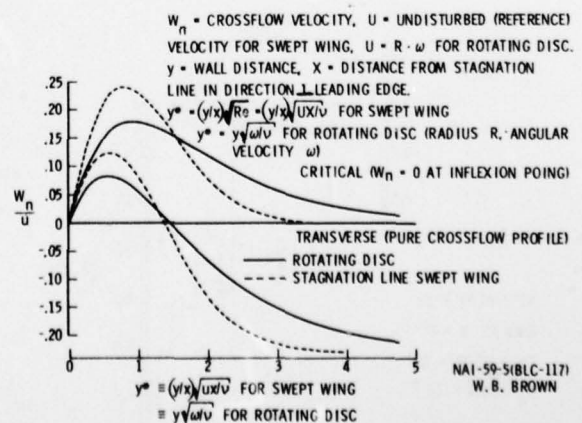


Figure 46.- Three-dimensional transverse and critical profiles.

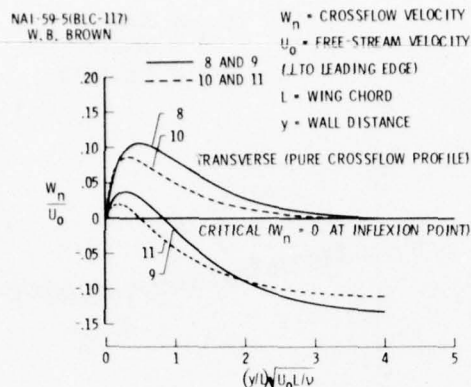


Figure 47.- Pure crossflow and "critical" profiles 8 and 9 in rear pressure rise area towards the trailing edge of a swept LFC wing.

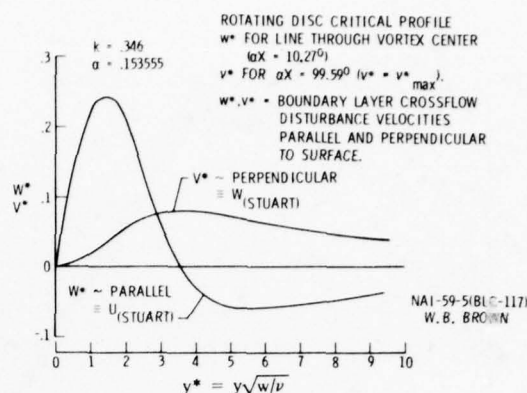


Figure 50.- Disturbance velocities parallel and perpendicular to the surface of the rotating disc. Rotating disc critical profile.

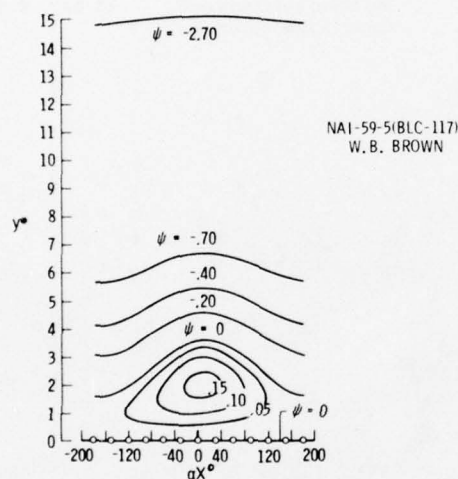


Figure 48.- Streamlines in the crossflow boundary layer with crossflow disturbance vortices for relatively weak initial disturbances. Rotating disc flow field. $C_r = C_l = 0$, $\alpha = .15356$, $R = 294.79$, $K = +1.1$.

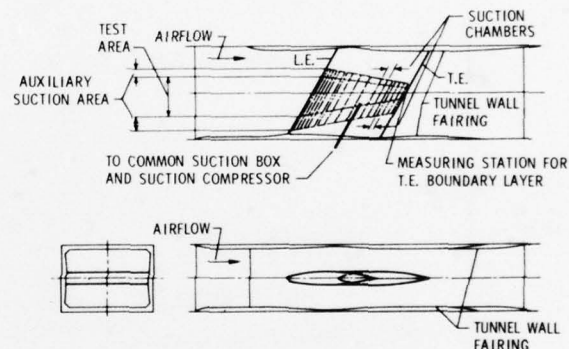


Figure 51.- 30° swept laminar suction wing model. Modified 66-012 airfoil section. Test setup in University of Michigan 5×7 ft. wind tunnel.

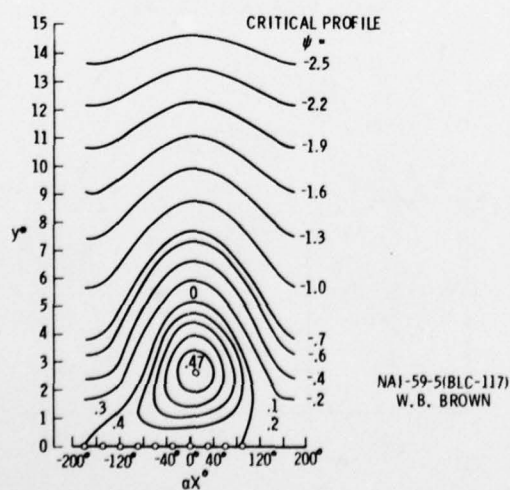


Figure 49.- Streamlines in the crossflow boundary layer with crossflow disturbance vortices for strong initial disturbances. Rotating disc flow field. $C_r = C_l = 0$, $\alpha = .15356$, $R = 294.79$, $K = .346$.

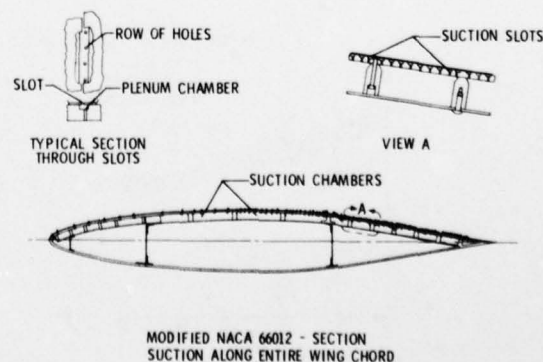


Figure 52(a).- 30° swept laminar suction wing model. Wing cross section with detail of suction chambers and suction slots.

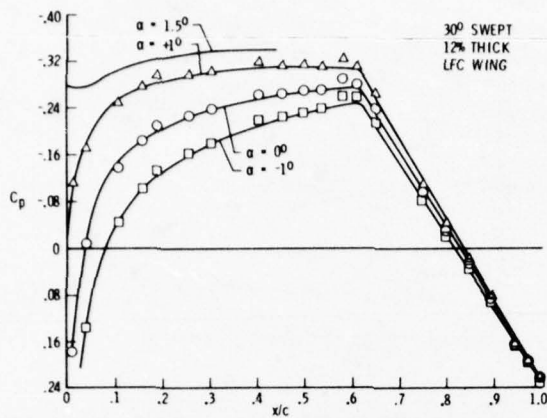


Figure 52(b).-- Comparison between measured velocity distribution and approximate velocity distribution used for calculations of boundary layer development

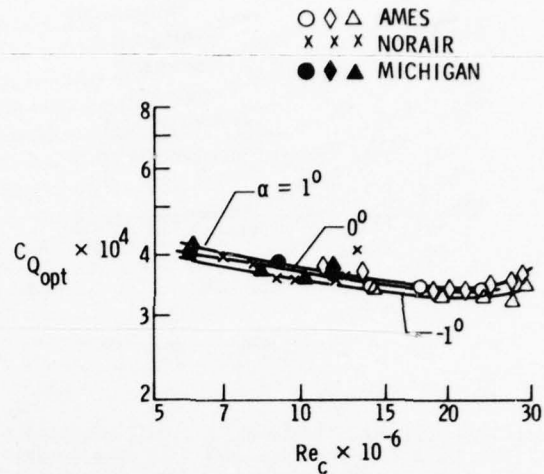


Figure 54.-- 30° swept laminar suction wing - optimum suction quantity, $C_{Q_{opt}}$ vs Re_c for upper wing surface.

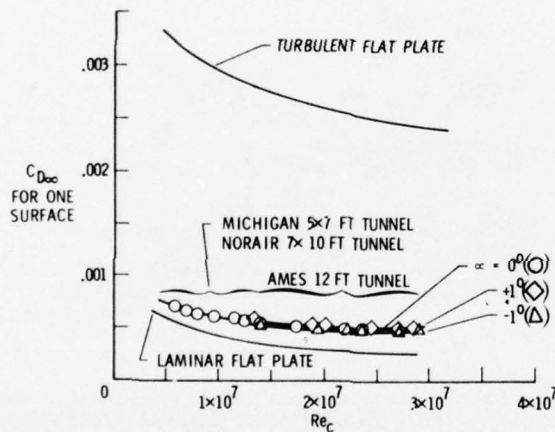


Figure 53(a).-- Wing profile drag $C_{D_{\infty}}$ of upper wing surface of 30° swept, 12% thick symmetrical laminar suction wing (incl. equivalent suction drag).

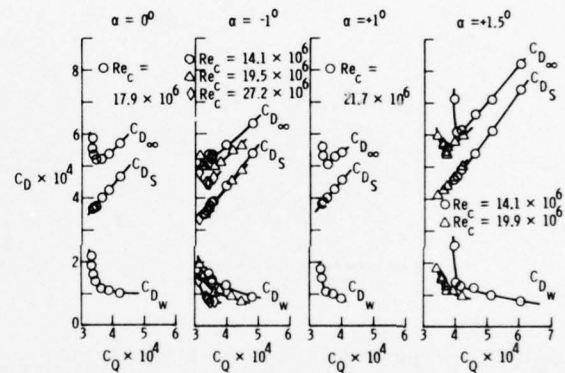


Figure 55(a).-- 30° swept laminar suction wing - measured drag coefficients (C_{DS} , C_{DW} , $C_{D_{\infty}}$) versus suction coefficient (C_Q) at various α and RN Re_c .

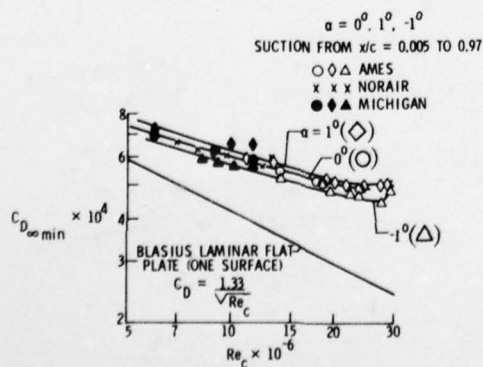


Figure 53(b).-- 30° swept laminar suction wing - minimum wing profile drag (including suction drag) vs Re_c for upper wing surface.

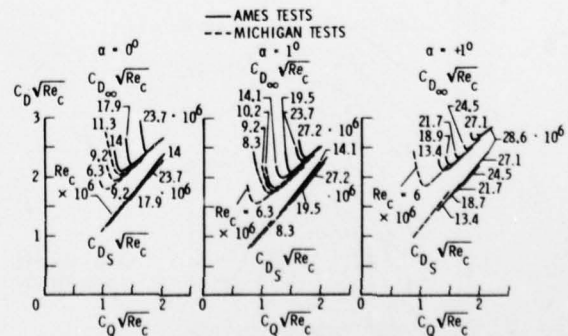


Figure 55(b).-- 30° swept laminar suction wing - measured drag coefficients ($C_{DS}\sqrt{Re_c}$, $C_{D_{\infty}}\sqrt{Re_c}$) versus suction coefficient ($C_Q\sqrt{Re_c}$) at various α and RN.

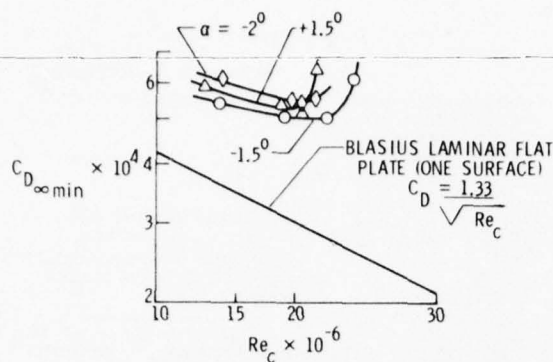


Figure 56.- 30° swept laminar suction wing - minimum wing profile drag (including suction drag) vs Re_c for upper wing surface.

Ames 12 ft tunnel tests, @ $\alpha = 1.5^\circ$, -1.5° , -2.0°

(Loss of laminar flow at higher Re_c due to spanwise turbulent contamination along front wing attachment line, starting from the upstream surbulent intersection between the wing and endplate.)

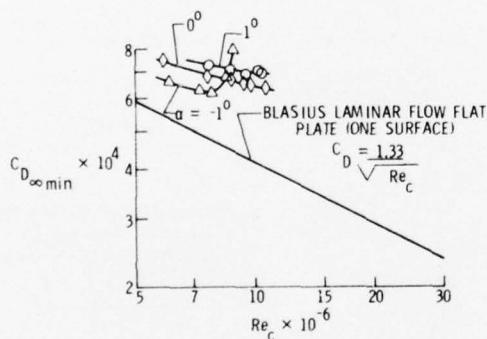


Figure 57.- 30° swept laminar suction wing - minimum wing profile drag (including suction drag) vs Re_c for upper wing surface, $\alpha = 0^\circ$, 1° , -1° , suction from $x/c = .25$ to $.97$. (Experiments in Michigan 5×7 ft tunnel.)

Note earlier loss of laminar flow at $\alpha = -1^\circ$ due to stronger crossflow as compared to case at $\alpha = 0^\circ$ and $\alpha = +1^\circ$.

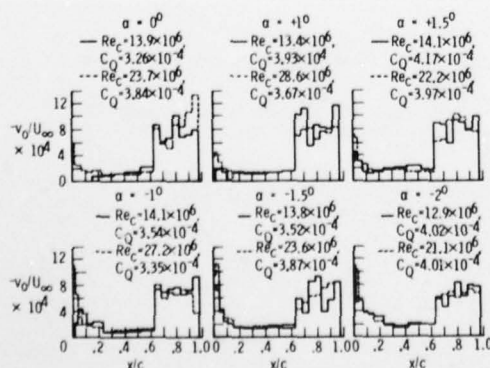


Figure 58(a).- Chordwise plots of nondimensional equivalent area suction velocity for different cases (one surface, Ames 12-foot tunnel).

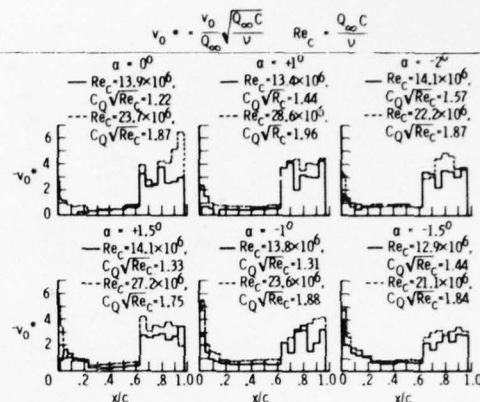


Figure 58(b).- Chordwise plots of nondimensional equivalent area suction velocity for different cases (one surface, Ames 12 ft tunnel).

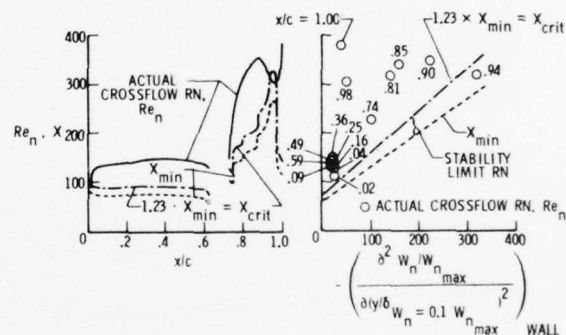


Figure 59.- Analysis of the crossflow boundary layer development for run 13 ($\alpha = 0^\circ$, $Re_c = 23.7 \cdot 10^6$, $C_Q = 3.84 \cdot 10^{-4}$) Ames 12 ft. tunnel.

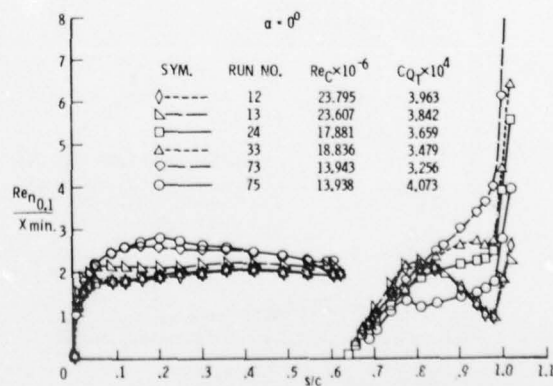


Figure 60(a).- Comparison of crossflow Reynolds number with stability limit. Reynolds number at several length Reynolds numbers, suction coefficients and angles of attack on 30° swept LFC wing.

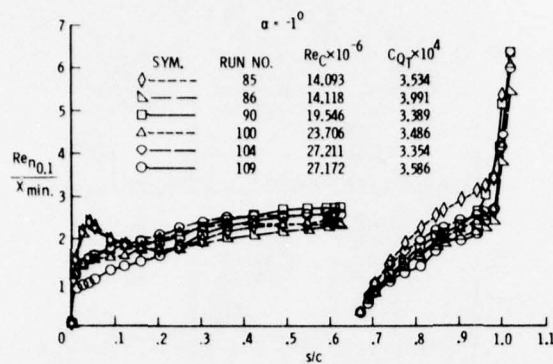


Figure 60(b).- Comparison of crossflow Reynolds number with stability limit. Reynolds number at several length Reynolds numbers, suction coefficients and angles of attack on 30° swept LFC wing.

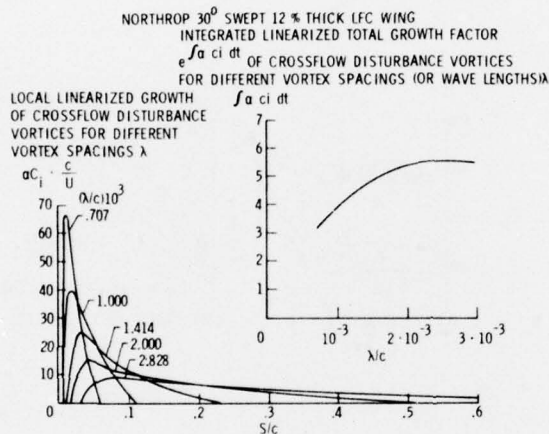


Figure 61(a).- Growth of stationary boundary layer crossflow disturbance vortices from leading edge to $s/c = 0.60$ for different vortex spacings λ for Run = 73, $Re_c = 13.94 \cdot 10^6$, $\alpha = 0^\circ$, and $C_Q = 3.206 \cdot 10^{-4}$.

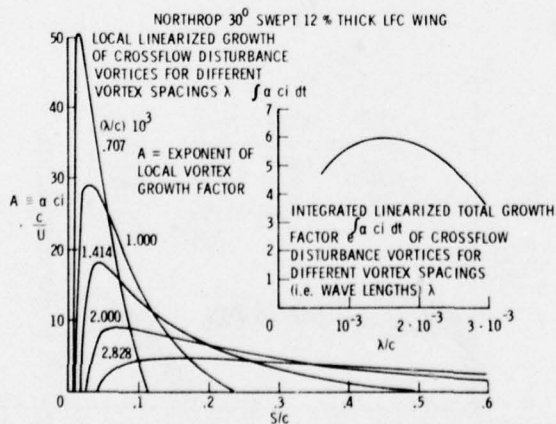


Figure 61(b).- Growth of stationary boundary layer crossflow disturbance vortices from leading edge to $s/c = 0.60$ for different vortex spacings λ for run 13, $Re_c = 23.61 \cdot 10^6$, $\alpha = 0^\circ$, and $C_Q = 3.84 \cdot 10^{-4}$.

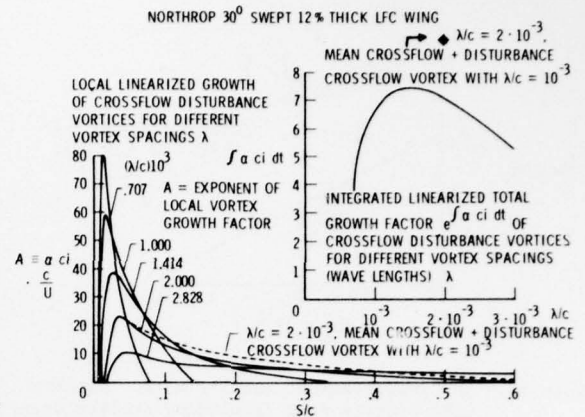


Figure 62(a).- Growth of stationary boundary layer crossflow disturbance vortices from leading edge to $s/c = 0.60$ for different vortex spacings λ for run 85, $Re_c = 14.1 \cdot 10^6$, $\alpha = -1^\circ$, $C_Q = 3.534 \cdot 10^{-4}$.

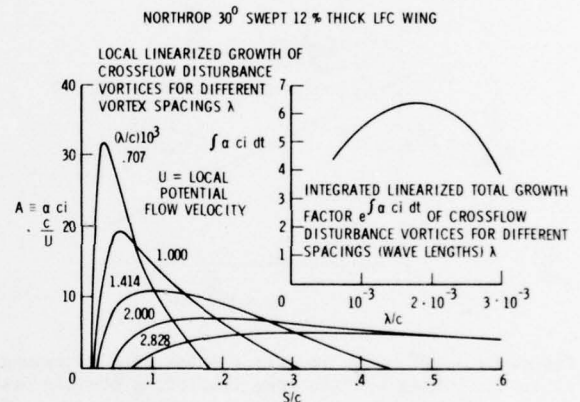


Figure 62(b).- Growth of stationary boundary layer crossflow disturbance vortices from leading edge to $s/c = 0.60$ for different vortex spacings λ for run 104, $Re_c = 27.21 \cdot 10^6$, $\alpha = -1^\circ$, and $C_Q = 3.354 \cdot 10^{-4}$.

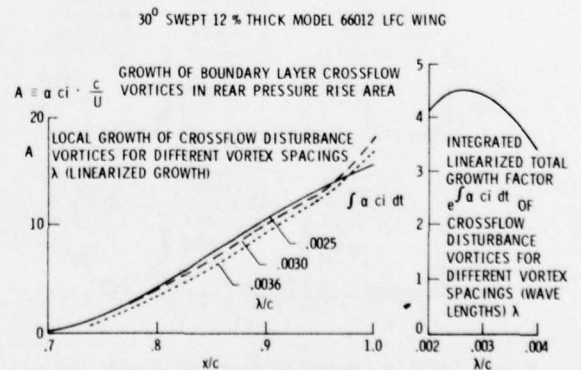


Figure 63.- Growth of boundary layer crossflow vortices in rear pressure rise area for run 33, $Re_c = 18.84 \cdot 10^6$, and $C_Q = 3.48 \cdot 10^{-4}$.

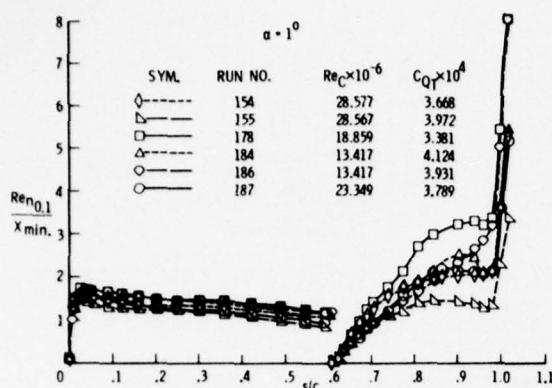


Figure 64(a).- Comparison of crossflow Reynolds number with stability limit Reynolds number at several length Reynolds numbers, suction coefficients and angles of attack on 30° swept LFC wing.

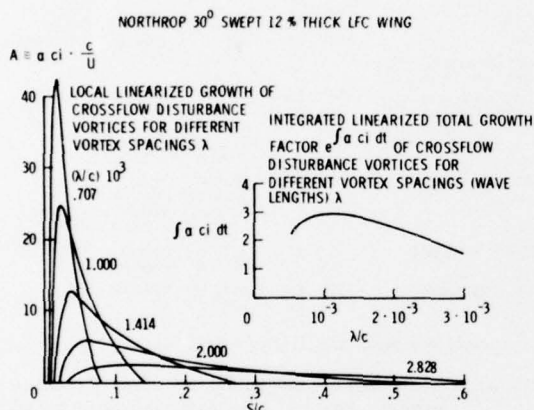


Figure 64(b).- Growth of stationary boundary layer crossflow disturbance vortices from leading edge to $s/c = 0.60$ for different vortex spacings λ for run 178, $\alpha = 1^\circ$, $Re_c = 18.86 \cdot 10^6$, $C_Q = 3.381 \cdot 10^{-4}$.

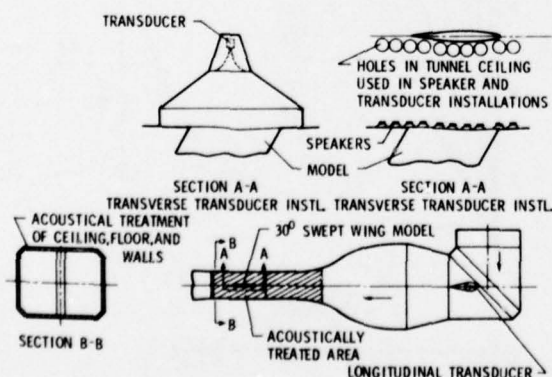


Figure 65.- 30° swept Northrop LFC wing. Experimental setup in Northrop 7 x 10 foot tunnel in the presence of acoustic disturbances.

33° SWEEP SUCTION WING INTERNAL NOISE IN DUCT 5 (~20% CHORD)

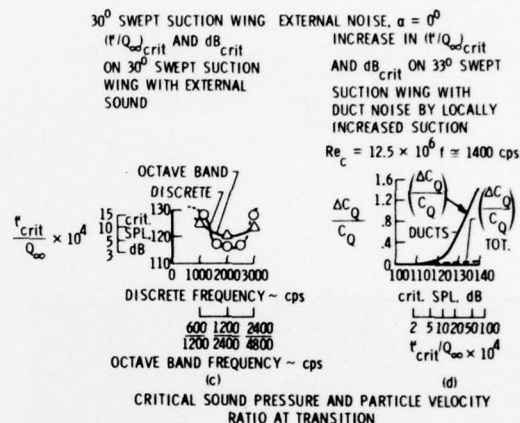
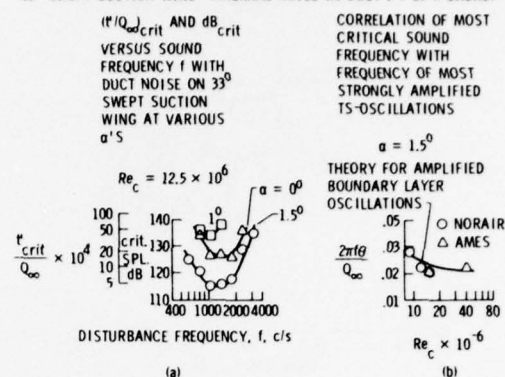


Figure 66.- Critical sound pressure and particle velocity ratio t'/Q_∞ on 30° swept Northrop LFC 66012 wing in the presence of external sound and on 33° swept 15% thick Northrop LFC wing with internal duct noise.

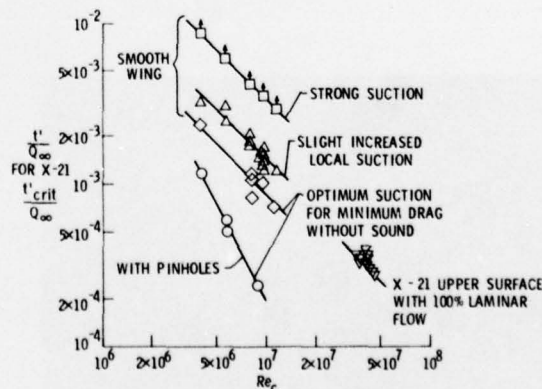


Figure 67.- 30° swept suction wing, $\alpha = 0^\circ$, t'_crit/Q_∞ (Re_c) with external sound under various conditions.

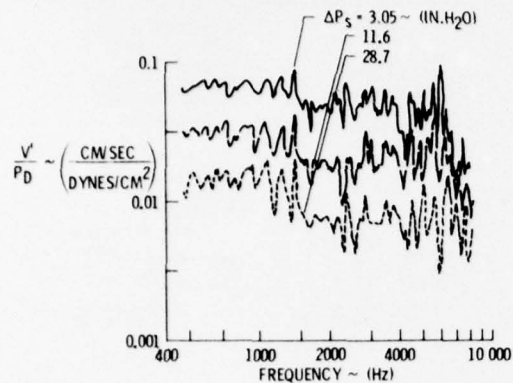


Figure 68.- Velocity fluctuation V' at slot inlet with duct noise P_D . Δp_s = pressure drop through suction skin.

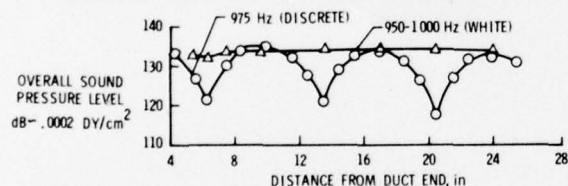


Figure 69. 33° swept suction wing, $\alpha = 1.5^\circ$. Standing sound waves in duct 5 and transition pattern.



Figure 70. 30° swept suction wing; naphtalene sublimation transition pattern in the presence of external sound.

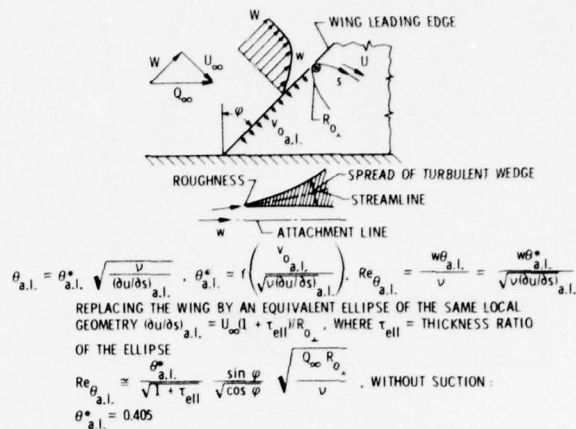


Figure 71.- Spanwise turbulent contamination on swept wing.

CASE AND REFERENCE	φ°	$R_{0,l}$	$Re_{\theta_{a.l.}^*}$	FLOW CONDITIONS AT ATTACHMENT LINE
AW52	34°	2.5	105	TURBULENT
METEOR FIN	25°	0.6	57	LAMINAR
CAR MODEL	60°	2.5	134	TURBULENT
30° SWEEP LOW DRAG SUCTION WING AT $R_c = 29 \cdot 10^6$ WITH FULL CHORD LAMINAR FLOW IN AMES 12 ft TUNNEL AT $\alpha = +1^\circ$	30°	0.59	93	UNKNOWN
X-21 AT $R_c = 16 \cdot 10^6$ IN OUTER WING				< 95 TO 100 LAMINAR > 95 TO 100 TURBULENT
45° SWEEP WING (NORAI)	45°	1.9		< 90 TO 95 LAMINAR > 104 TO 110 TURBULENT 95 TO 105 INTERMITTENT BURSTS
60° AND 67.5° SWEEP WING (NPL)	60° 67.5°	0.83		< 89 TO 94 LAMINAR > 95 TO 98 TURBULENT
33° SWEEP WING (NORAI)	33°	4.65 3.25 1.20		> 96 TO 105 TURBULENT $\alpha = 0^\circ$ TO 2°

* LOCATED IN REGION OF FULLY DEVELOPED SPANWISE FLOW

Figure 71(a).- Attachment line boundary layer Reynolds number $Re_{\theta_{a.l.}^*}$ on various swept wings in the presence of large initial disturbances.

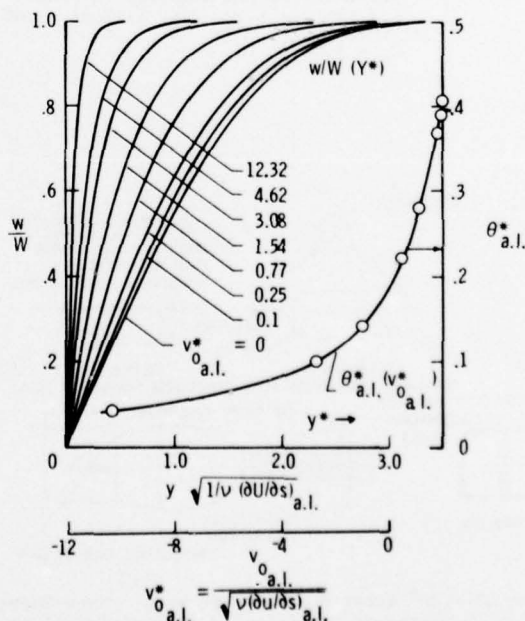


Figure 72.- Attachment line boundary layer profiles with area suction.

$$v_{o,a.l.}^* = \frac{y \sqrt{\frac{\partial U}{\partial S}}}{\sqrt{\frac{\partial U}{\partial S}}_{a.l.}}$$

w/w	0	-0.77	-1.54	-3.08	-4.62	-12.32	-0.1	-0.25
0.9975	3.5424	2.8165	2.2700	1.5636	1.1607	0.4812	3.444	3.290
0.9900	3.0571	2.3618	1.8578	1.2395	0.9054	0.3682	2.961	2.813
0.9775	2.7422	2.0715	1.6003	1.0445	0.7551	0.3036	2.649	2.504
0.9600	2.4962	1.8484	1.4058	0.9014	0.6466	0.2579	2.405	2.264
0.9375	2.2882	1.6625	1.2467	0.7872	0.5611	0.2224	2.198	2.062
0.9100	2.1039	1.5005	1.1103	0.6917	0.4903	0.1933	2.016	1.884
0.8775	1.9354	1.3590	0.9900	0.6091	0.4298	0.1687	1.850	1.722
0.8400	1.7781	1.2216	0.8816	0.5363	0.3768	0.1474	1.695	1.572
0.7975	1.6286	1.0974	0.7824	0.4709	0.3297	0.1285	1.549	1.492
0.7500	1.4843	0.9803	0.6906	0.4116	0.2872	0.1116	1.407	1.293
0.6975	1.3435	0.8688	0.6049	0.3571	0.2485	0.0963	1.270	1.161
0.6400	1.2045	0.7618	0.5243	0.3068	0.2129	0.0823	1.135	1.033
0.5775	1.0660	0.6586	0.4481	0.2600	0.1800	0.0694	1.000	0.905
0.5100	0.9265	0.5584	0.3756	0.2163	0.1493	0.0575	0.866	0.779
0.4375	0.7850	0.4607	0.3064	0.1752	0.1207	0.0464	0.730	0.653
0.3600	0.6400	0.3651	0.2402	0.1364	0.0938	0.0360	0.592	0.506
0.2775	0.4903	0.2714	0.1767	0.0997	0.0684	0.0262	0.451	0.398
0.1900	0.3345	0.1794	0.1156	0.0648	0.0444	0.0170	0.306	0.267
0.0975	0.1714	0.0889	0.0567	0.0316	0.0217	0.0083	0.156	0.135
0	0	0	0	0	0	0	0	0
$\theta_{a.l.}^*$	0.4045	0.2971	0.2231	0.1412	0.1008	0.0400	0.3899	0.3669

Figure 72(a).- (Table I) Asymptotic spanwise attachment line boundary layer profiles

$$w/w = f\left(y \sqrt{\frac{\partial U}{\partial S}}\right)_{a.l.} \quad \text{with area}$$

$$\text{suction } v_{o,a.l.}^* = \frac{v_{o,a.l.}}{\sqrt{(\partial U / \partial S)_{a.l.}}}$$

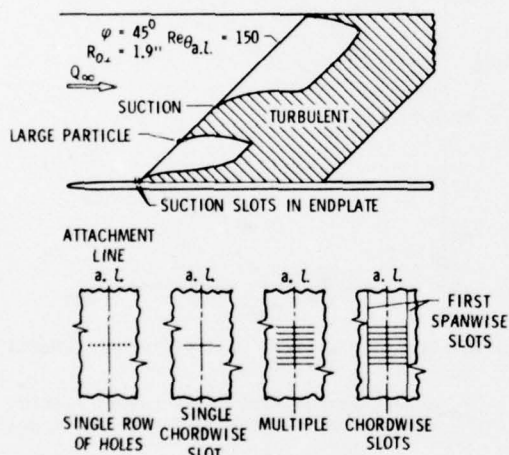


Figure 73.- Reestablishment of laminar attachment line flow on swept wings.

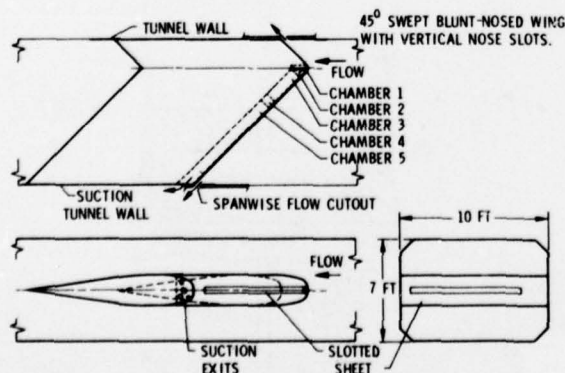


Figure 74(a).- 45° swept blunt-nosed wing with vertical nose slots. Three-view drawing of experimental setup in Northrop 7 × 10 ft tunnel.

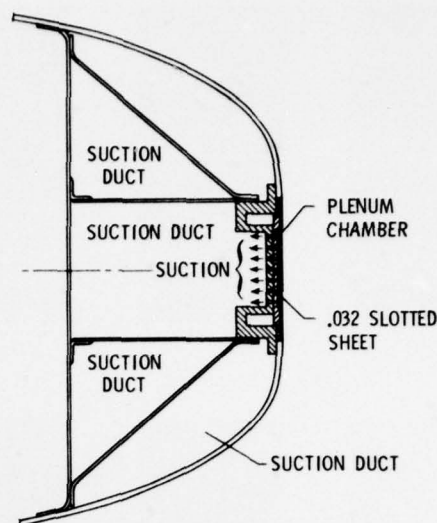


Figure 74(b).- 45° swept blunt-nosed wing with vertical nose slots. Leading edge cross-section of wing.

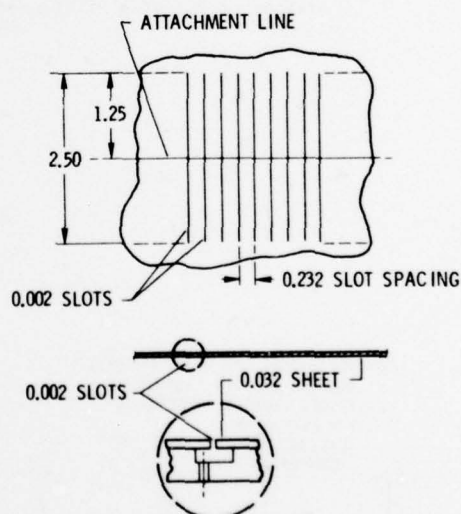


Figure 75.- 45° swept blunt-nosed wing with vertical nose slots, slotted sheet detail.

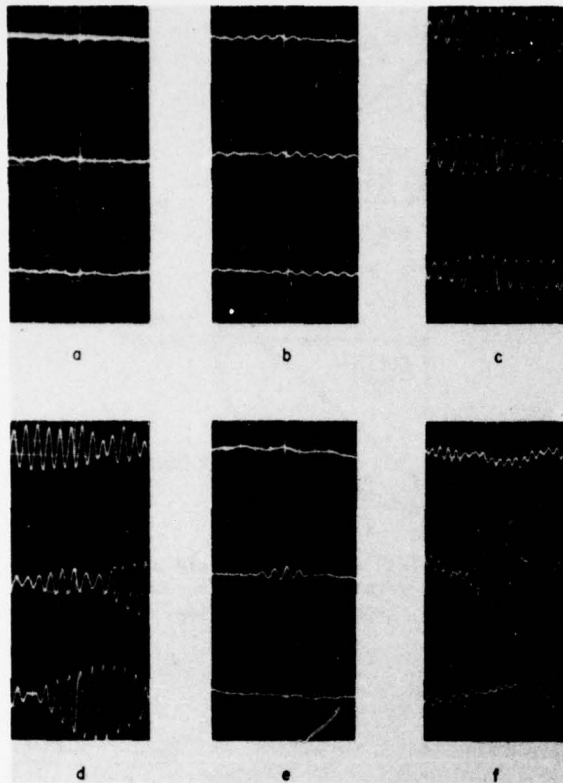


Figure 76(a). Hot wire oscillations in laminar attachment line boundary layer of 45° swept blunt-nosed wing with and without suction at the 47-inch station of the wing of figure 74.

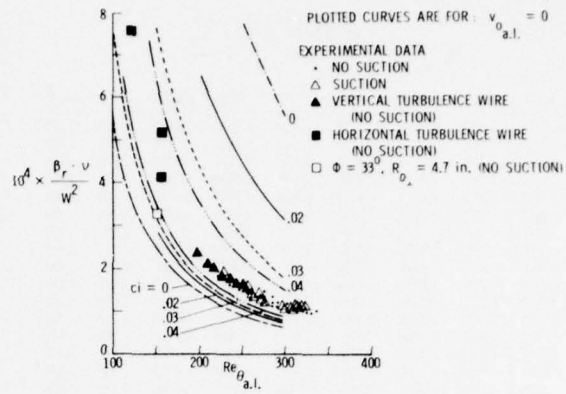


Figure 77.- Correlation of experimental boundary layer oscillation frequency at attachment line of 45° swept blunt-nosed wing with Brown's theoretical stability results. β_r = angular frequency of attachment line boundary layer oscillations.

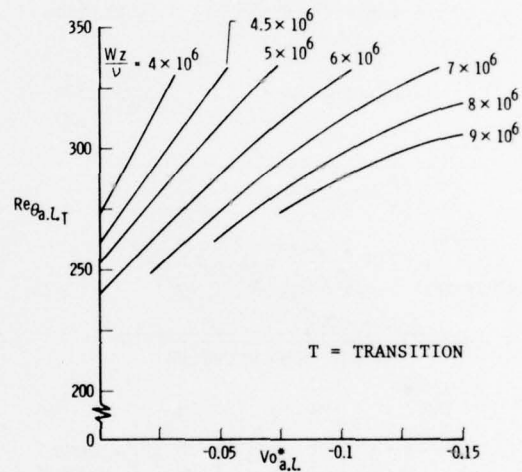


Figure 78.- $Re_{\theta_{a.l.T}} = f(v_0^*)$ for different (Wz/ν) 's at attachment line of 45° swept blunt-nosed wing in Northrop 7 x 10 ft tunnel.

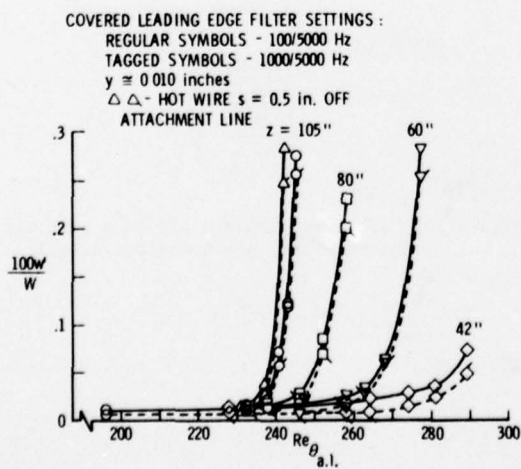


Figure 76(b).- Velocity fluctuations versus attachment line Reynolds number on 45° swept blunt-nosed wing.

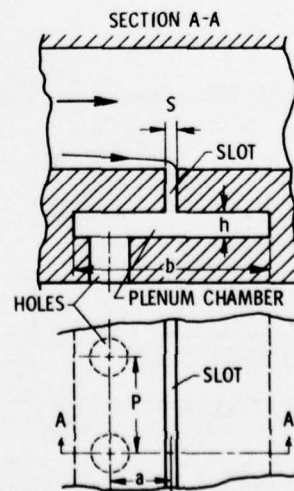


Figure 79.- Experimental setup of water channel with slot and plenum chamber.

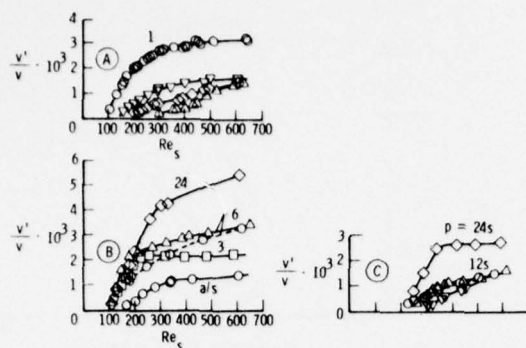


Figure 80.- Disturbance velocity ratio $v'/\bar{v} = f(Re_s)$ at slot inlet; (A) Single row of holes: Circles- $h = 19s$, $a = p = 30s$;

Δ - $h = 3s$
 \diamond - $h = 1.5s$
 \triangle - $h = s$

(B) Displaced row of holes, $h = 3s$;
 (circles, squares, triangles, diamonds)
 $p = 24s$, $a = 0$ to $24s$; (black circle)
 $p = 12s$, $a = 6s$. (C) Two rows of holes
 opposite slot; $a = \pm 5s$; (solid line)
 holes staggered; (diamonds and triangles)
 $h = 1.5s$; (deltas) $h = s$; (dashed line
 with circles) $h = 1.5s$, holes
 nonstaggered.

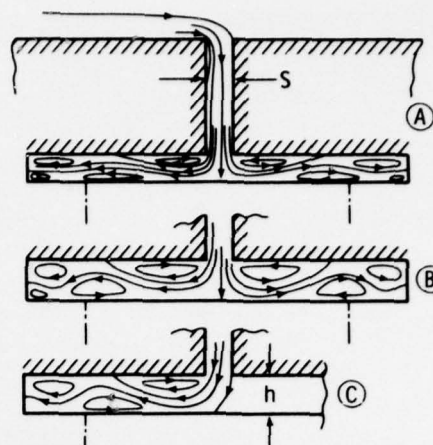


Figure 83.- Flow in plenum chamber slightly above Re_{crit} ;

(A) $h = s$ two rows of holes (dot-dashed) on opposite sides
 (B) $h = 1.6s$ of slot
 (C) Displaced single row of holes, $h = 1.5s$.

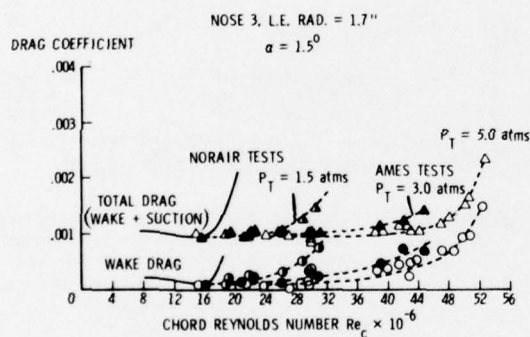


Figure 81.- 33° swept 15% thick Northrop LFC wing of the X-21 group. Variation of $C_{D_{min}}$ (Re_c) for one surface in Ames 12 ft tunnel at various tunnel pressures.

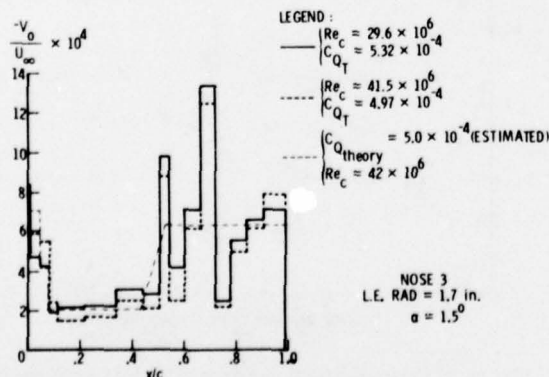


Figure 82.- Chordwise equivalent area suction distribution on 33° swept 15% thick Northrop LFC wing.

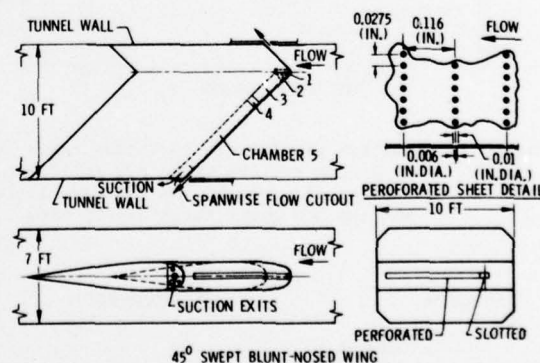


Figure 84.- 45° swept blunt-nosed wing with boundary layer suction at the front wing attachment line through rows of closely spaced holes.

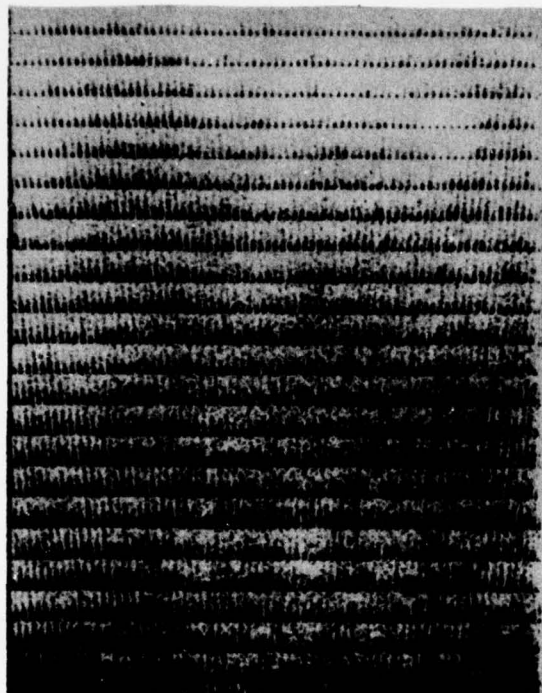


Figure 85. Naphtalene sublimation pictures in the front attachment line region of 45° swept blunt-nosed wing with suction through a perforated attachment line suction strip.

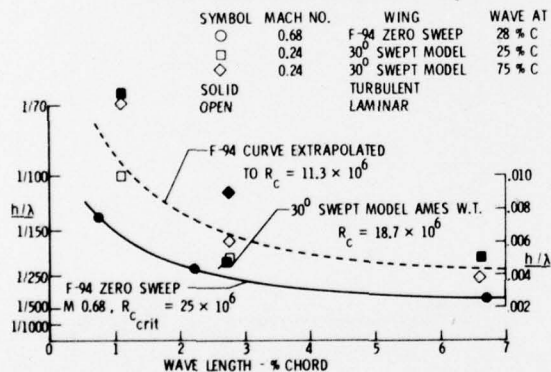


Figure 86.- Maximum permissible amplitude ratio h/λ of single surface waves for full chord laminar flow on the F94 LFC wing glove and the 30° swept Northrop LFC wing.

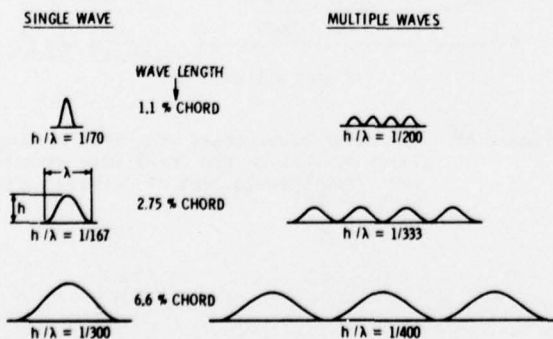


Figure 87.- Maximum permissible surface waviness on 30° swept LFC wing at $\alpha = 0^\circ$ and $Re_c = 11.3 \cdot 10^6$ for waves at 0.25c and 0.75c.

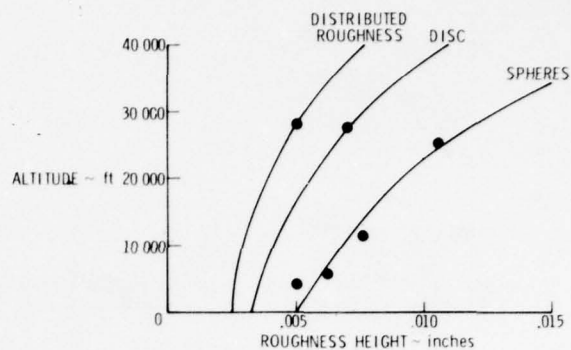


Figure 88.- Maximum permissible 3-dimensional surface roughness on F94 LFC wing glove at 0.28c, $M_\infty = 0.6$ to 0.7. Suction from 0.41c to 0.96c.

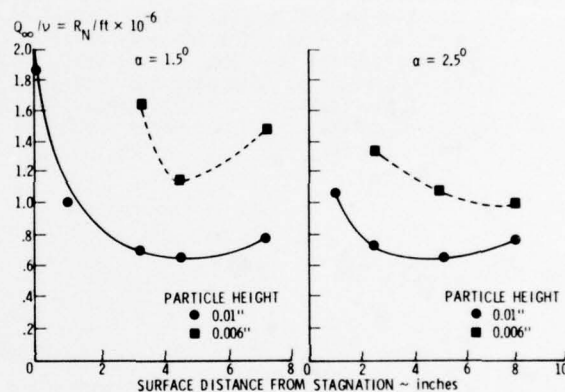


Figure 89(a).- Maximum permissible 3-dimensional surface roughness in leading edge region of 33° swept 15 percent thick 10 ft chord Northrop LFC wing with chordwise nose slots.

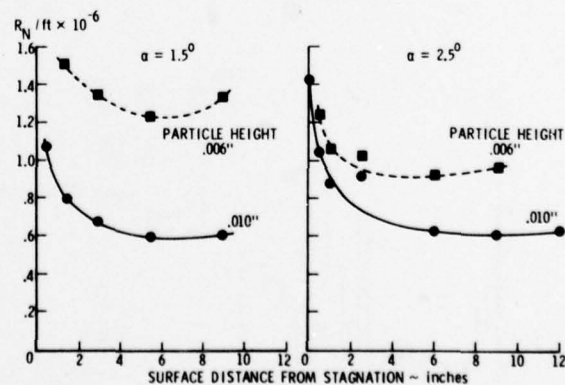


Figure 89(b).- Maximum permissible 3-dimensional surface roughness in leading edge region of 33° swept 15 percent thick 10 ft chord Northrop LFC wing without chordwise nose slots (only spanwise slots).

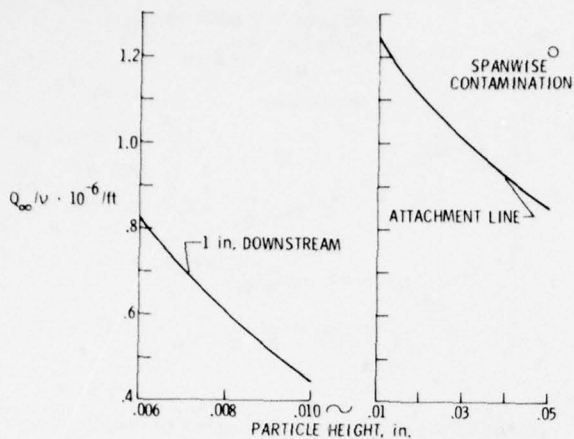


Figure 90.- Maximum permissible 3-dimensional surface roughness (0.05 inch diameter discs) in leading edge region of 45° swept Northrop nonsuction wing of 4 ft chord.

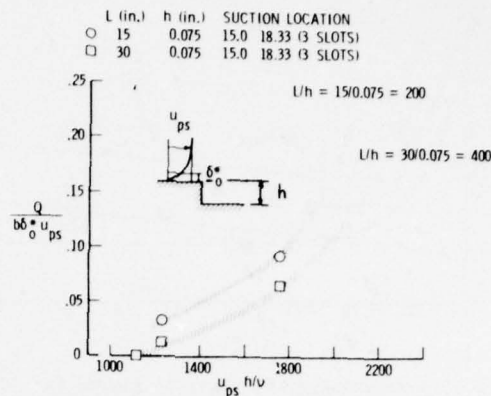


Figure 92(b).- Backward facing step with suction. Minimum suction rate required to maintain laminar flow at $x/h = 133.3$.

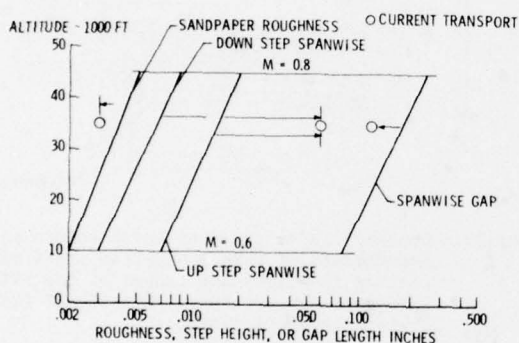


Figure 91.- Variation of the permissible height of forward and backward facing 2-dimensional surface steps and width of 2-dimensional spanwise surface gaps for laminar flow at various flight altitudes.

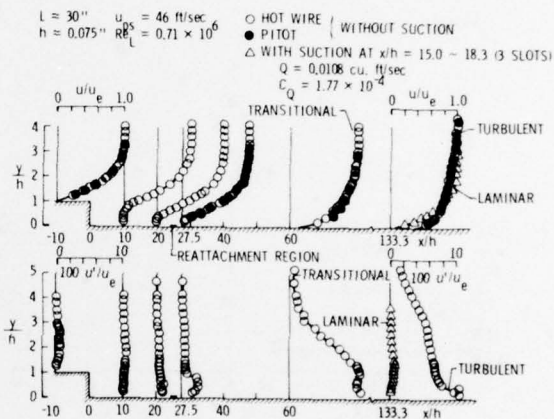


Figure 93.- Backward facing step with suction velocity and turbulence intensity profiles in boundary layer.

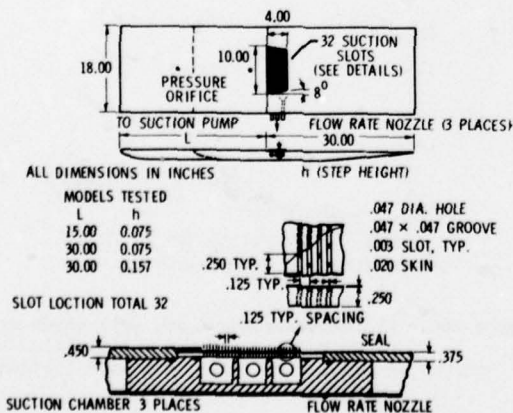


Figure 92(a).- Backward facing step with suction, test setup. Dimensions in inches

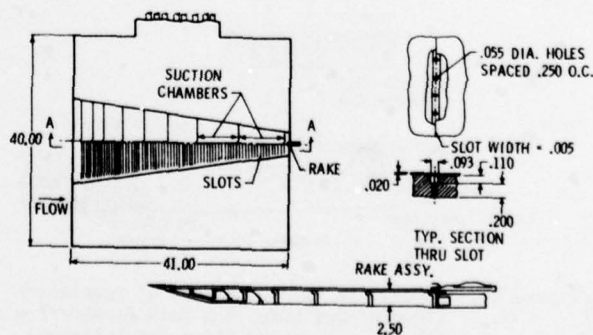


Figure 94.- Supersonic laminar suction plate with closely spaced slots for Tullahoma A-tunnel experiments. Dimensions in inches

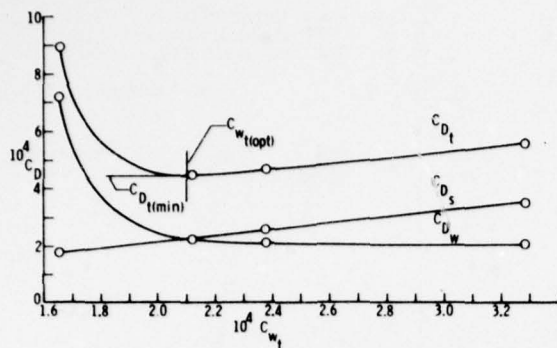


Figure 95.- Supersonic LFC plate of figure 94; $C_{D\text{Suction}}$, $C_{D\text{Wake}}$, $C_{D\text{Total}}$, versus suction weight flow coefficient C_{Wt} at $M = 3$, $Re_c = 25.7 \cdot 10^6$.

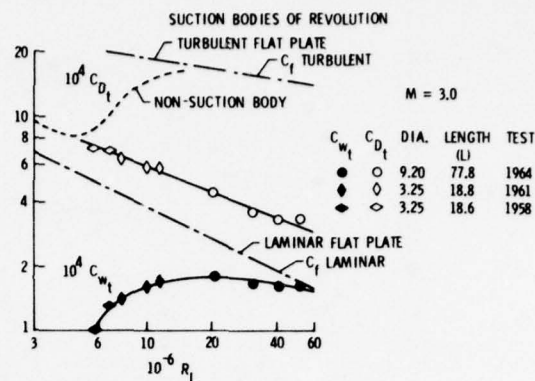


Figure 98.- Supersonic LFC ogive of revolution; $C_{D\text{tot. min.}}$ versus Re_L .

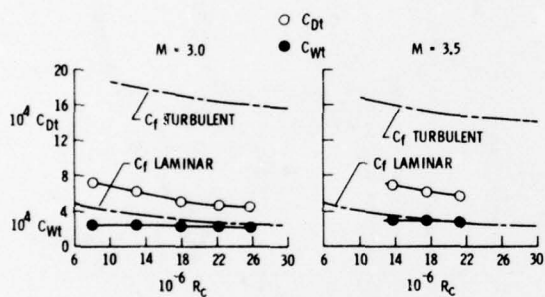


Figure 96.- Supersonic LFC plate of figure 94; minimum total drag $C_{D\text{tot. min.}}$ and optimum total suction weight flows $c_{Wt} = f(Re_c)$ at $M = 3$ and 3.5 ($c = 40.2$ in.).

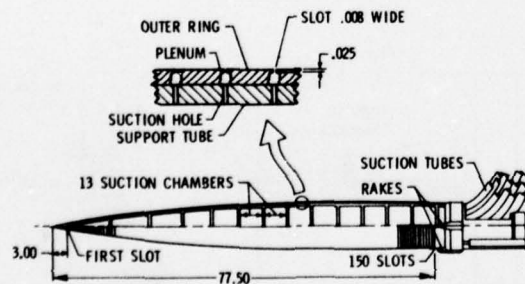


Figure 97.- Supersonic ogive LFC body of revolution (77.5 inches long, 9.2 inch diameter) with 150 closely spaced slots for Tullahoma A-tunnel experiments.

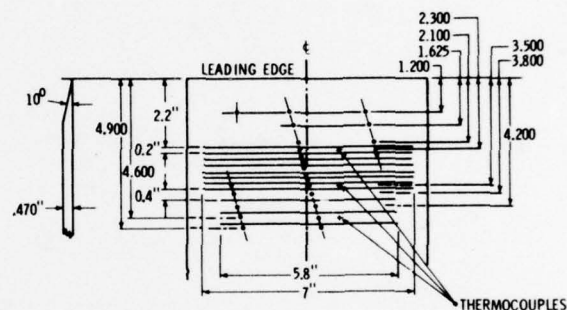


Figure 99.- Boundary layer-incident shock interaction experiments on supersonic flat plate with suction in supersonic tunnel of the MIT Gasdynamics Laboratory. Details of flat plate with suction slots.

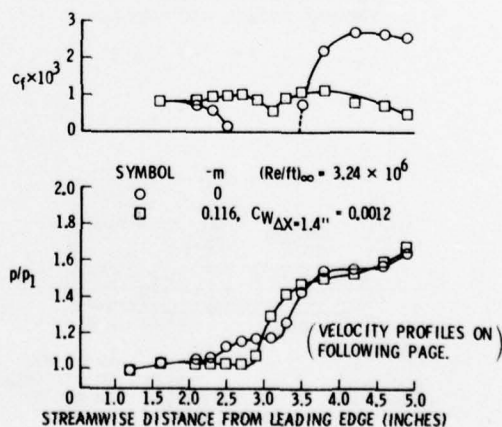


Figure 100.- Chordwise pressure and wall shear stress distribution with and without slot suction on flat plate (fig. 99) with incident shocks.

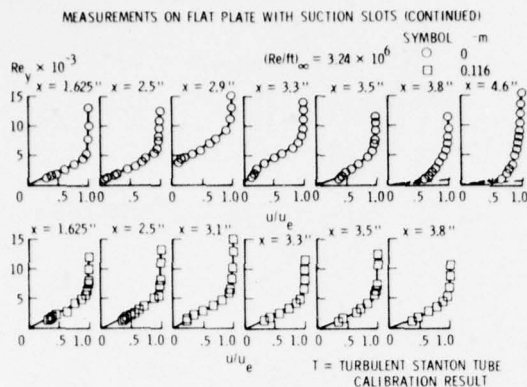


Figure 101.- Boundary layer profiles at various chordwise stations of flat plate with incident shock with and without suction.

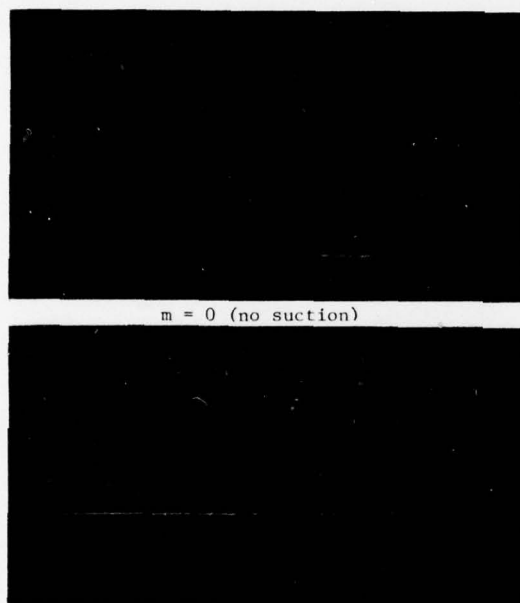


Figure 102.- Schlieren pictures in the plate-shock interaction region of flat plate with and without suction.

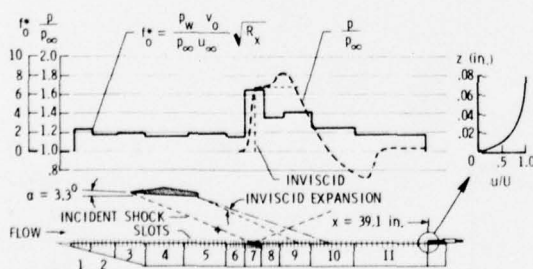


Figure 103.- Boundary layer-incident shock interaction experiments on supersonic flat LFC suction plate in Tullahoma A-tunnel. Pressure and suction distribution and boundary layer velocity profile at $X = 39.1$ inches, inclined shock generator, $M = 3.0$, $R_x = 25.9 \times 10^6$, $\alpha = 3.3^\circ$, $c_{wL} = 4.3 \times 10^{-4}$.

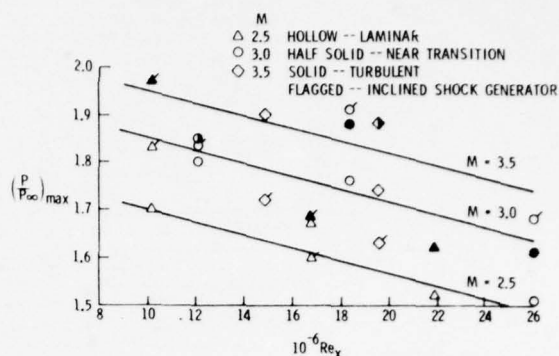


Figure 104.- Maximum pressure rise across the shock on supersonic flat LFC plate of figure 103 for different conditions at $X = 39.1$ inches for different length Reynolds numbers Re_x .

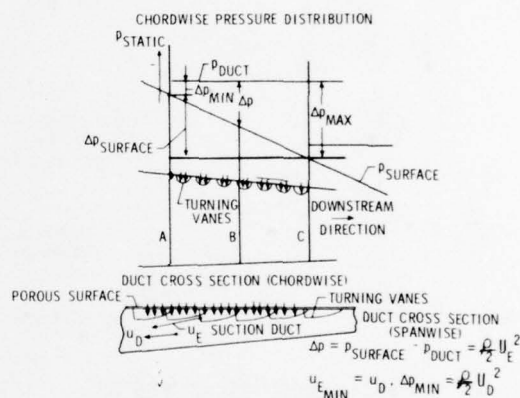


Figure 105.- Suction air mixing method (b) in rear pressure rise area of LFC wings.

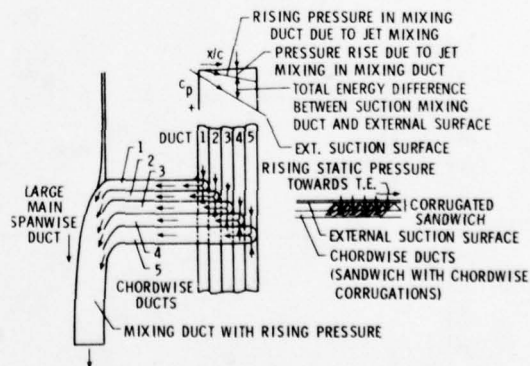


Figure 106.- Schematic suction ducting system in rear pressure rise area of LFC wing with duct mixing method (b').

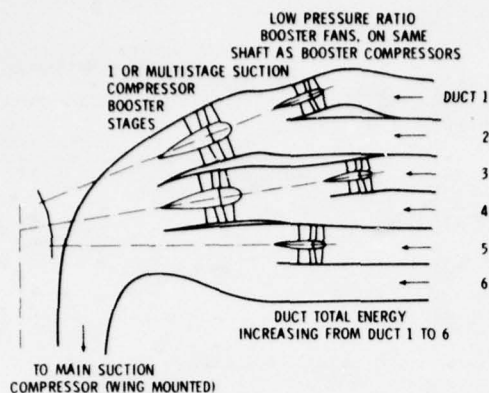


Figure 107.- Mixing of suction air of different total energy levels at duct end.

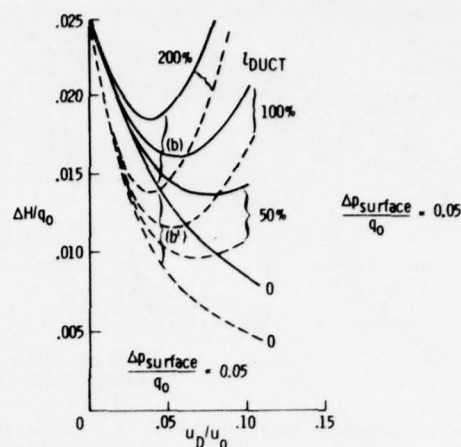


Figure 110.- Losses in suction ducting systems with methods (b) and (b').

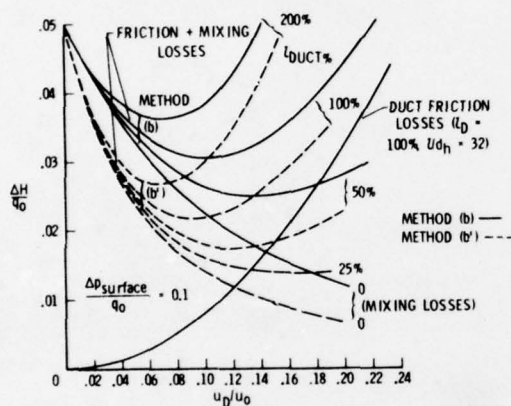


Figure 108.- Losses in suction ducting systems with method (b) and (b'). $\Delta p_{surface}/q_0 = 0.1$

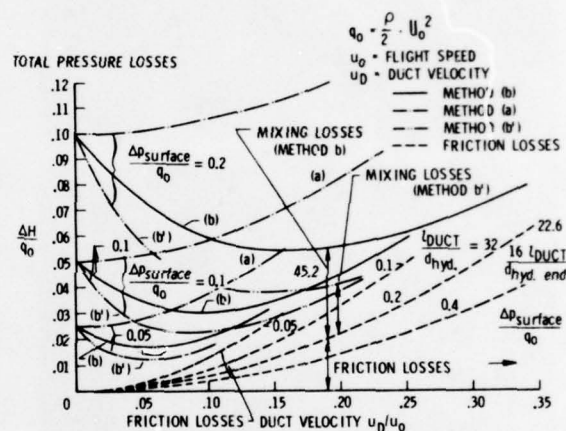


Figure 111.- Losses in suction ducting systems with method (a) and (b) and (b'), $l_{DUCT} = 100\%$.

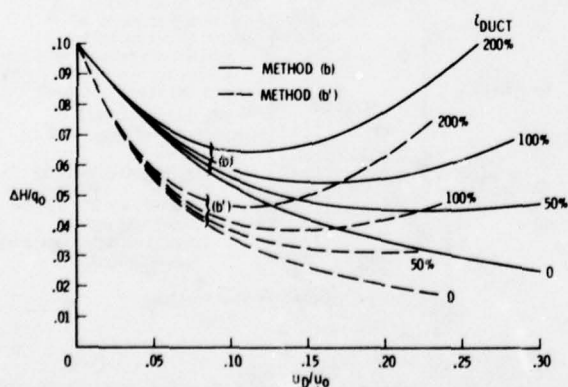


Figure 109.- Losses in suction ducting systems, methods (b) and (b'). $\Delta p_{surface}/q_0 = 0.2$.

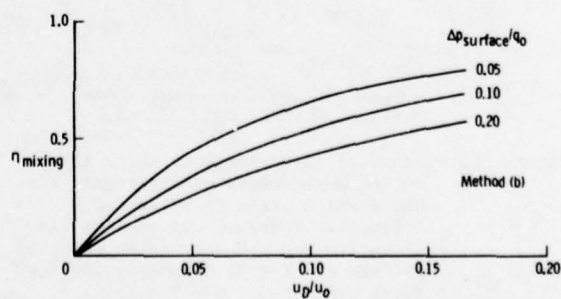


Figure 112.- Losses in suction ducting systems with method (b). Jet mixing efficiency η_{mixing} for different $\Delta p_{surface}/q_0$.

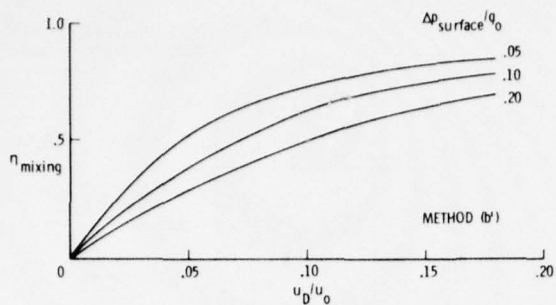


Figure 113.- Losses in suction ducting systems with method (b'). Jet mixing efficiency η_{mixing} for different $\Delta p_{\text{surface}}/q_0$.

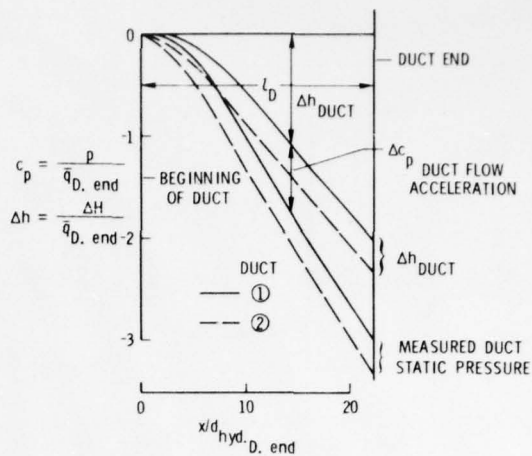


Figure 116.- Static pressure c_p and total energy losses Δh in ducts ① and ② without duct inlet turning vanes.
 $\frac{u_{D, \text{end}} \cdot l_D}{\nu} \approx 600,000$.
 Ref.: Northrop Rep. BLC-22 (1953).
 S_D as with duct ① v.

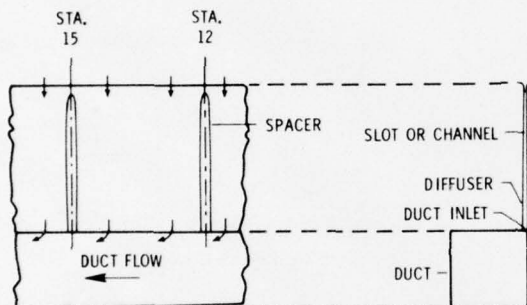


Figure 114.- Duct No. 1 - typical sections.

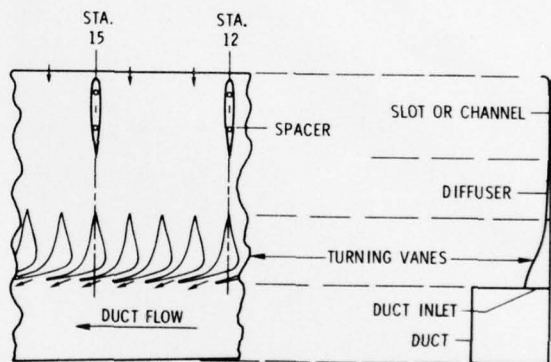


Figure 117.- Duct No. ① v with suction air inlet turning vanes.

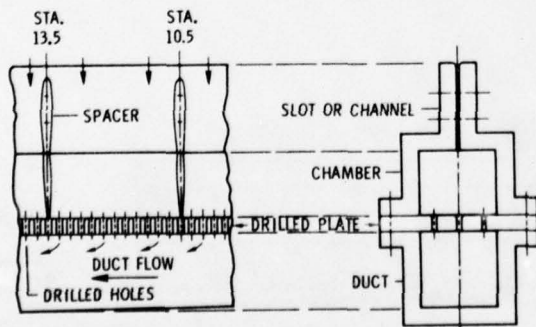


Figure 115.- Duct No. 2 - typical sections.

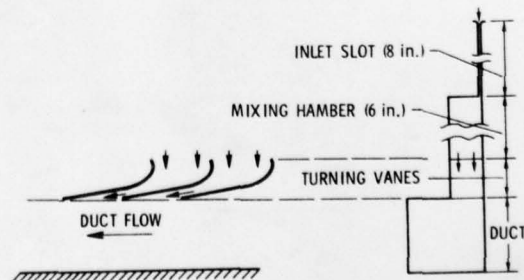


Figure 118.- Duct No. ③ v with suction air inlet turning vanes.

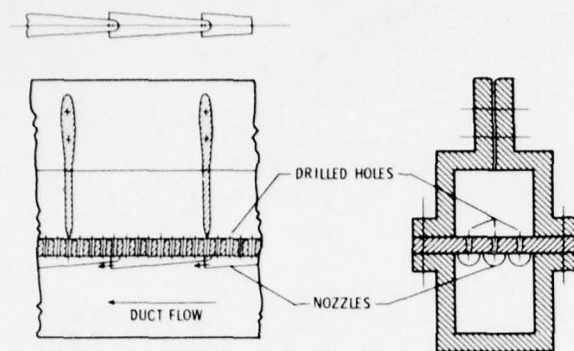


Figure 119a.- Duct no. 2n - typical sections (same duct as duct no. 2, except for addition of nozzles).

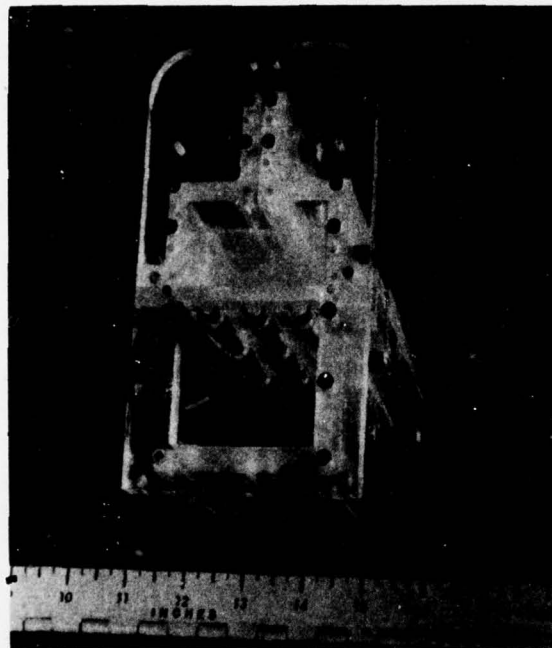


Figure 119b. Suction duct 2n with suction air inlet turning nozzles.

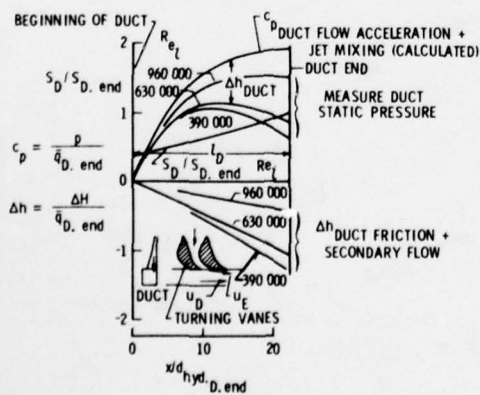


Figure 120.- Static pressure c_p and total energy losses Δh in duct (1v), $\frac{u_E}{u_{D, End}} = 1.5$. Ref: Northrop Rep. BLC-22 (1953).

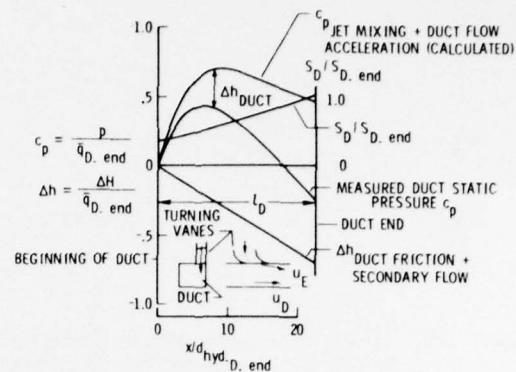


Figure 121.- Static pressure c_p and total energy losses in duct (3v), $\frac{u_E}{u_{D, End}} = 1.05$,

$$Re_t = \frac{\bar{u}_{D, End} \cdot l_D}{\nu} = 580\,000.$$

Ref.: Northrop Rep. BLC-22 (1953).

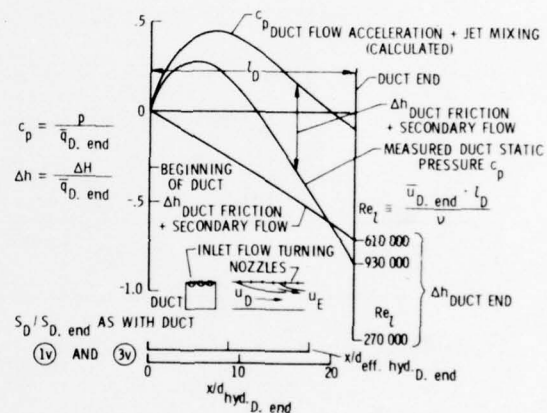


Figure 122.- Static pressure c_p and total energy losses Δh in duct (2n)

$$\frac{u_E}{u_{D, End}} = 0.88, \quad Re_t = \frac{u_{D, End} \cdot l_D}{\nu} =$$

$$610,000. \quad \frac{S_D}{S_{D, End}} \text{ as with duct (1v)}$$

and (3v). Ref.: Northrop Rep. BLC-22 (1953).

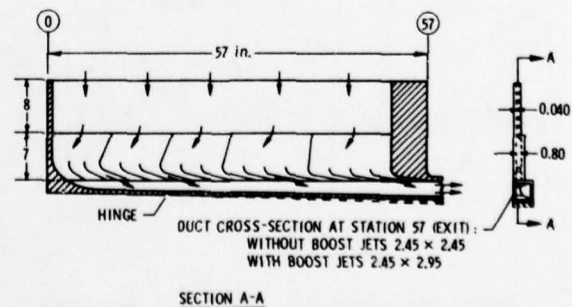


Figure 123.- Suction duct with zero-deceleration inlet.

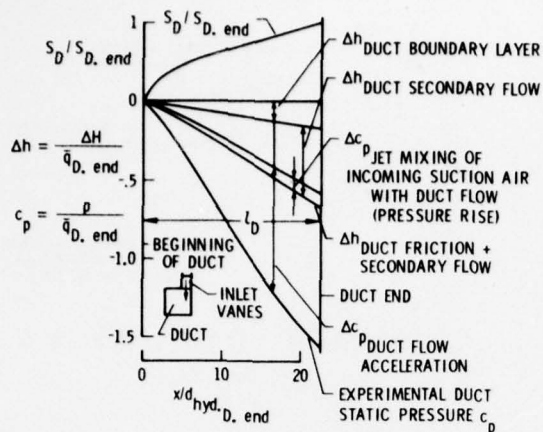


Figure 124.- Static pressure c_p and total energy losses Δh in duct I, $u_E/u_D \sim 1$ to 1.08 of along duct, $\frac{\bar{u}_{D, End} \cdot l_D}{\nu} = 580,000$. Ref.: Northrop Rep. NAI-54-486, BLC-50 (1954).

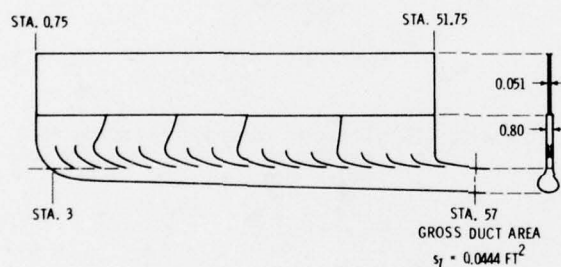


Figure 125a.- Improved suction duct (II and III).

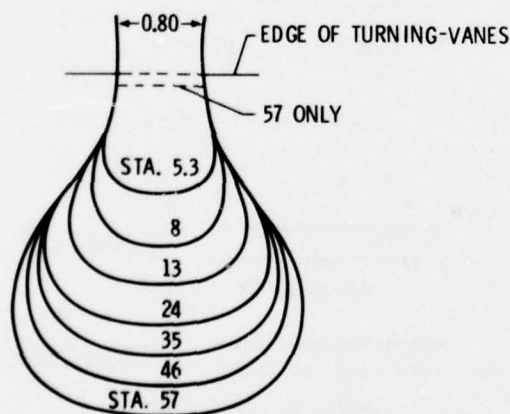


Figure 125b.- Typical cross-sections - improved suction duct (II and III).

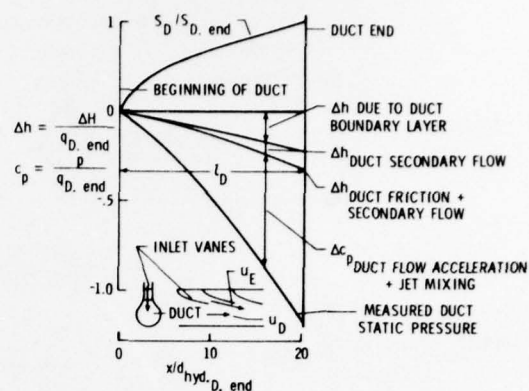


Figure 126.- Static pressure c_p and total energy losses Δh in ideal suction duct II, $u_E/u_D \sim 1.0$ to 1.08 of along duct, $\frac{\bar{u}_{D, End} \cdot l_D}{\nu} = 630,000$. Duct turning vanes improperly sealed. Ref.: Northrop Rep. NAI-54-716, BLC-64.

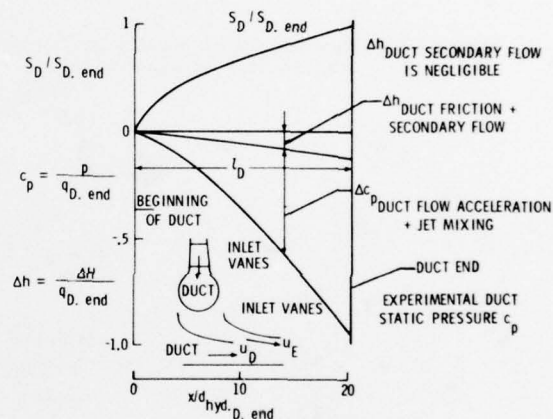


Figure 127.- Static pressure c_p and total energy losses Δh in ideal suction duct III, $u_E/u_D \sim 1$ to 1.08 along duct, $\frac{\bar{u}_{D, End} \cdot l_D}{\nu} = 1.3 \cdot 10^6$. Duct turning vanes properly sealed (improved suction duct). Ref.: Northrop Rep. NAI-55-547, BLC-70 (1955).

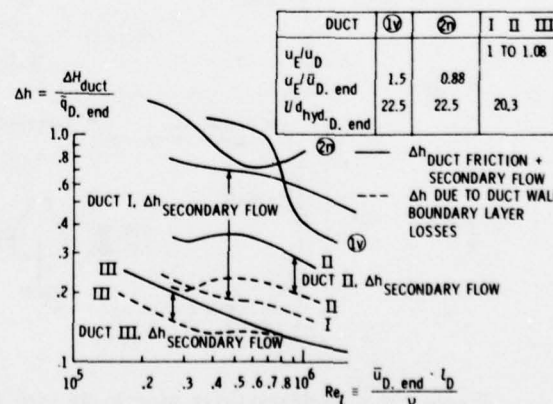


Figure 128.- Total energy losses Δh of various ducts versus duct length Reynolds number Re_L .

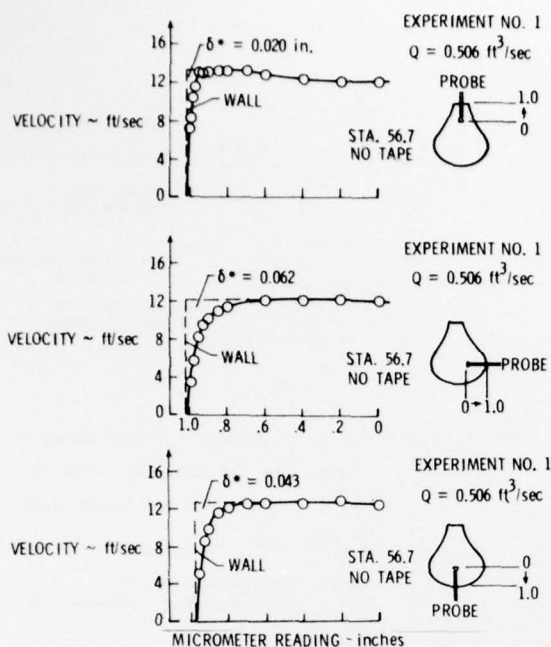


Figure 129.- Boundary layer profile at low velocity - station 56.7 opposed to inlet.

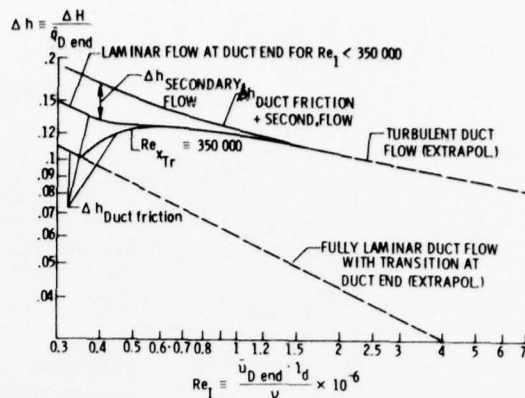


Figure 131.- Total energy losses of Duct III, $l_d/d \text{ hyd. D. End} = 20$.

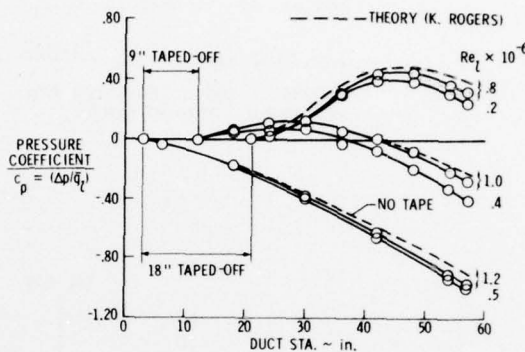


Figure 132.- Pressure distribution along duct showing effect of taping-off part of inlet slot.

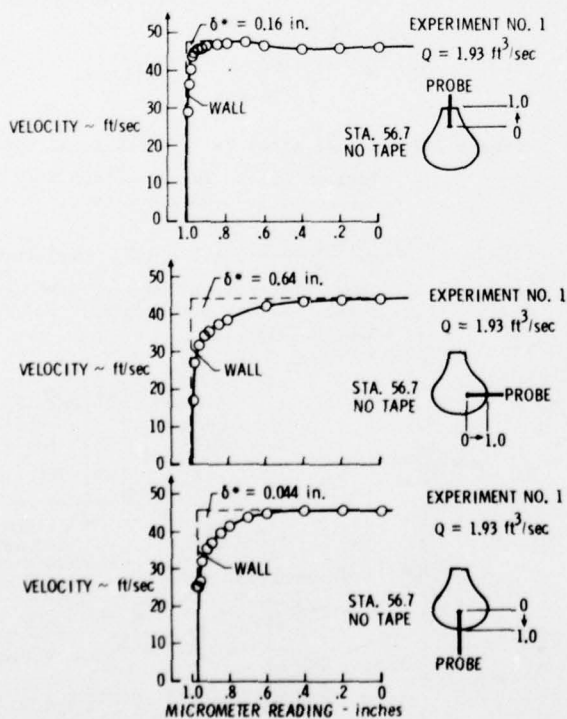


Figure 130.- Boundary layer profile at high velocity - station 56.7 side position.

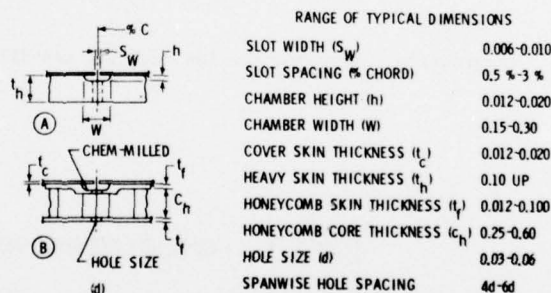


Figure 133.- BLC wing skins.

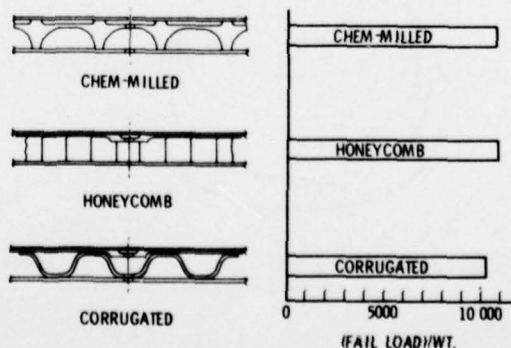


Figure 134.- Outboard and trailing edge skins.

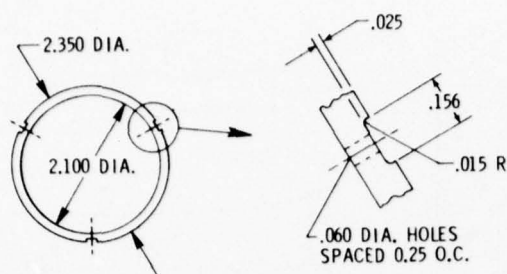


Figure 135.- 20-inch torsion tubes.

- | | |
|------------------------------|------------------------|
| ○ RIGIDITY-GROOVES | ① 3 GROOVES |
| □ RIGIDITY-GROOVES AND HOLES | ② 6 GROOVES |
| △ YIELD-GROOVES | ③ 3 GROOVES AND HOLES |
| ▽ YIELD-GROOVES AND HOLES | ④ 12 GROOVES |
| | ⑤ 6 GROOVES AND HOLES |
| | ⑥ 12 GROOVES AND HOLES |

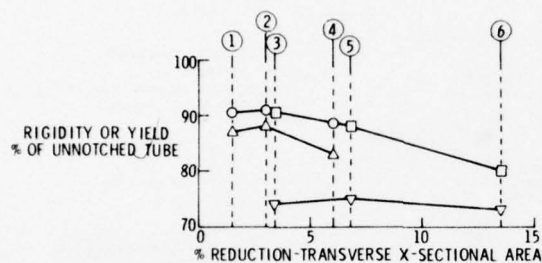


Figure 136.- Relative rigidity and yield stress.

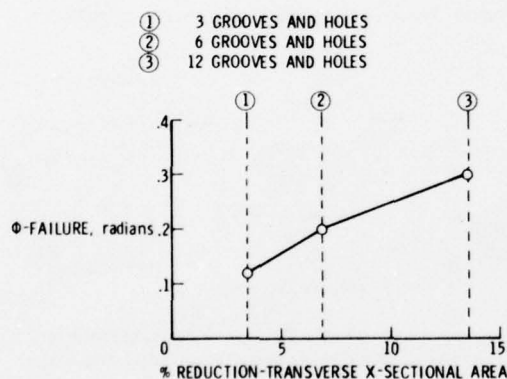


Figure 137.- Twist at failure.

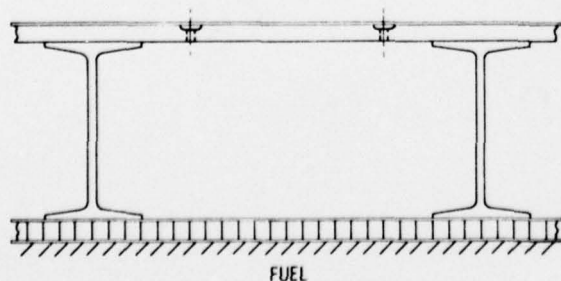


Figure 138.- All bonded upper and lower skin assembly.

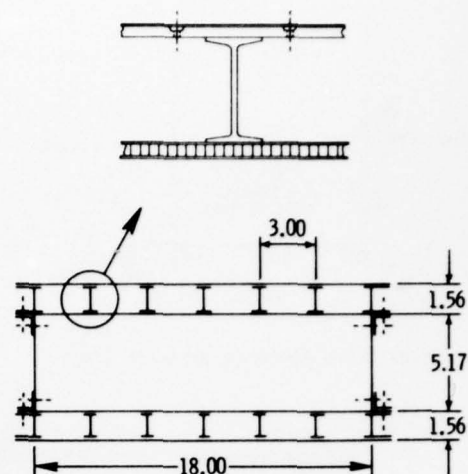


Figure 139.- Untapered torsion box.

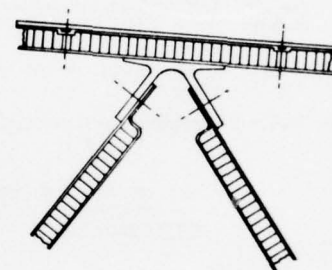


Figure 140.- Continuous truss type trailing edge.

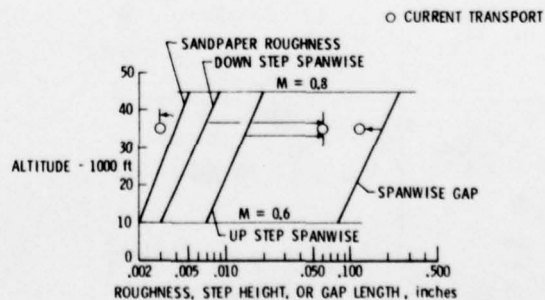
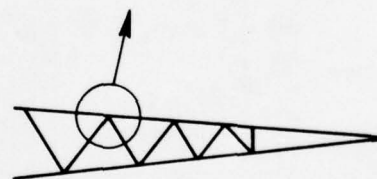


Figure 141.- Altitude-local disturbances.

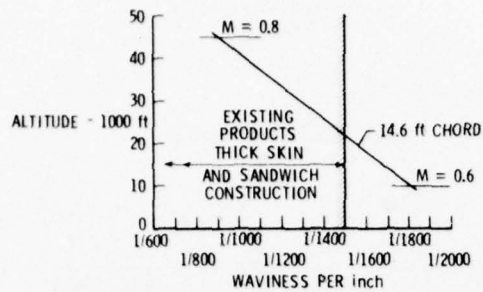


Figure 142.- Altitude-waviness chart.

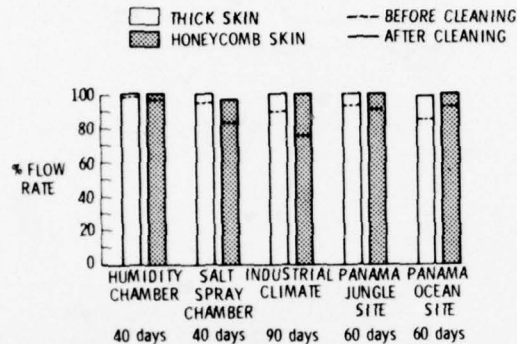


Figure 143.- Corrosion test results.

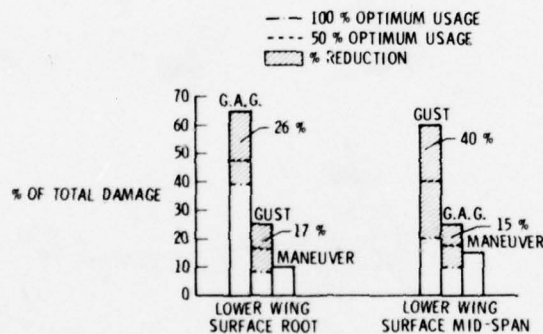


Figure 144.- Potential cumulative damage reduction for BLC aircraft.

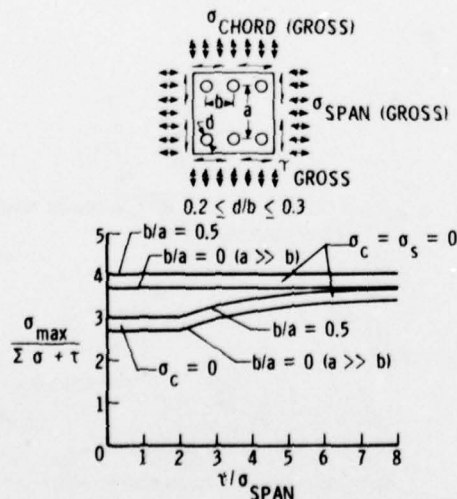


Figure 145.- Envelope of maximum stresses interior holes.

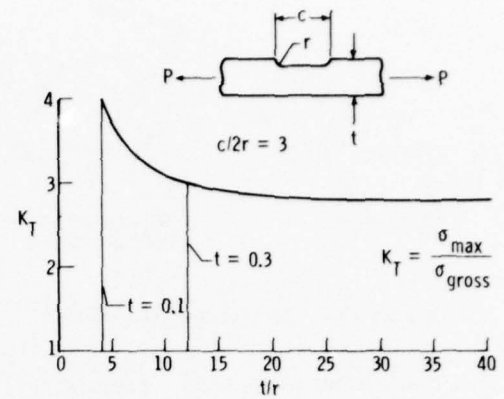


Figure 146.- Solid skin plenums chordwise tension.

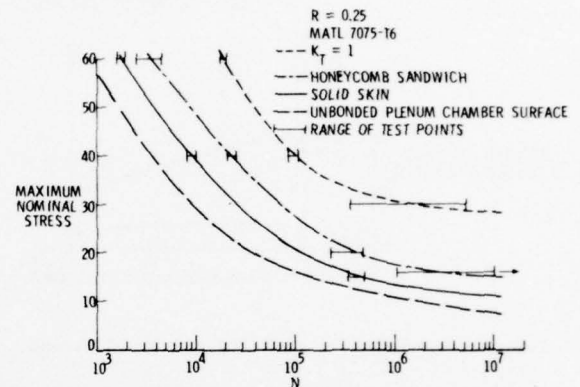


Figure 147.- S-N curve - chordwise specimens.

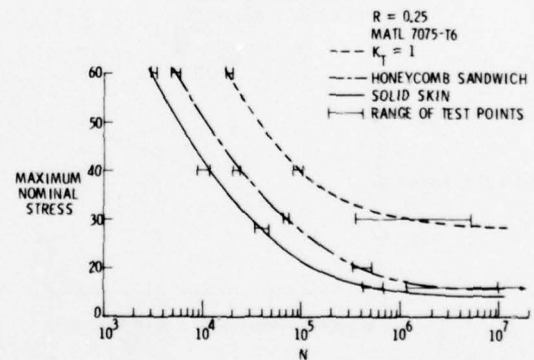


Figure 148.- S-N curve - spanwise specimens.

DESIGN CONSIDERATIONS OF LARGE GLOBAL RANGE HIGH

SUBSONIC SPEED LFC TRANSPORT AIRPLANES*

The low laminar friction drag with LFC increases substantially the cruise lift to drag ratio L/D and range of LFC airplanes to stimulate long-range transportation of heavy loads at high subsonic speeds without refueling. The question then arises concerning the design problems of such high performance LFC transports.

1. Aerodynamic Considerations.

According to the drag polar (fig. 1) of a large high subsonic speed LFC transport with an all-laminar cantilever wing of 10.4 aspect ratio and split tips (effective aspect ratio 12), the induced drag D_{ind} dominates down to relatively low lift coefficients C_L , followed by the parasite drag of the turbulent surfaces, while the suction laminarized surfaces contribute but a small percentage to the total airplane drag at optimum cruise. Therefore, to optimize the performance of long range LFC transports, the ratio $\frac{D_{ind}}{L} = \frac{L = W}{\pi q b^2}$ airplane should be reduced simultaneously with D_{∞} . Following nature's example of large

land soaring birds like the Condor (fig. 2) with split wing tips, the induced drag may thus be reduced by 12 percent to 15 percent (fig. 3). In addition, active control on split wing tips** for maneuvering, load alleviation, etc., following again nature with the Condor, appears particularly attractive due to the short response time and reduced power needed for active control as a result of the small chords of the split tips; furthermore, undesirable wing torsional moments and deformations associated with lift changes on split wing tips for active control are considerably smaller than with wing trailing edge flaps.

At a given cruise dynamic pressure q and airplane cruise weight, the ratio D_{ind}/L decreases by lowering the span loading W/b^2 ; i.e., raising the wing span b .

This aerodynamic advantage of a large span LFC wing of low induced and friction drag, though, is bought at the price of an increased wing structural weight, unless overall and detail design philosophies are applied which enable reasonably low structural weights for such large span wings. Thus, the key problem in designing wings of low span loading for large long-range LFC transport airplanes becomes immediately a problem of wing structural weight minimization. This may be accomplished by limiting the flight load envelope by designing the airplane for relatively high cruise lift coefficients and thus smaller cruise dynamic pressures, combined with gust-, maneuver-, dynamic-, and fatigue-load alleviation through active control and fly-by-wire techniques, as well as the choice of advanced structural materials of high strength and stiffness (advanced composites) and possibly a suitable distribution of the payload in the wing along the wing span. The latter approach may not always be feasible, especially for high subsonic speed transport airplanes with relatively thin wings carrying very bulky loads to require in many cases a large central fuselage for the payload; furthermore, the large moments of inertia around the longitudinal axis of airplane configurations with distributed payloads along the span limit airplane roll acceleration at low speeds. In addition, the wide landing gear treads required to avoid excessive ground-air-ground loads with distributed loads lead to wider runways and are another, though not necessarily decisive, disadvantage. To further reduce the structural weight of large span LFC wings, without resorting to distributed payloads along the span, unconventional design approaches may have to be accepted and design philosophies possibly adopted which had been used in the past when the airplane designers had to build relatively thin large span wings of sufficiently low induced drag. Just as the externally braced thin biplane wings of the WW-I fighters proved superior in combat during circling flight at high C_L 's, where induced drag dominated, it should not be surprising if large LFC transport airplanes with large span wings of low span loading, braced externally with carefully designed suction laminarized struts in composite structure, may show superior performance over equivalent transport airplanes with cantilever LFC wings of comparable structural weight and correspondingly smaller span and aspect ratio (refs. 1-10). The lower induced drag of the long strut-braced LFC wing then more than compensates for the small parasite drag of the suction laminarized struts to increase L/D and range of large LFC transport airplanes by about 20 percent or more, depending on the sophistication of the strut system. Such strut-braced designs might even prove superior for nonsuction airplanes, as verified experimentally in the Wright Field transonic tunnel on a complete airplane model with a 35-degree swept strut-braced wing designed by the Northrop Boundary Layer Research Group (ref. 10). On this model, a maximum $L/D = 20.3$ was achieved at $Re = 1.2 \cdot 10^6$ and $M_{\infty} = .89$ for the complete airplane configuration (including tail surfaces and simulated engine nacelles). Taking into account the smaller chord and higher optimum $C_{L_{cruise}}$ and cruise altitude of large span high aspect ratio strut-braced LFC wings, their maximum wing chord Reynolds number $Re_{c_{max}}$ (based on maximum wing chord C_{max}) is about 40 to 45 percent lower than for equivalent cantilever LFC wings of smaller span with the same structural weight, reducing $Re_{c_{max}}$ from about 80 to $90 \cdot 10^6$ for cantilever wing LFC transports of 400,000 kg TOWG to $45 \cdot 10^6$ with strut-braced LFC transports. The latter values correspond to maximum values observed locally on the 30-degree swept in-board X-21 wing with full chord laminar flow. In contrast, laminar Re_c - values on swept LFC wings of $80 \cdot 10^6$ to $90 \cdot 10^6$ are far beyond presently achieved experimental values.

According to table 1 the average cruise unit length Reynolds numbers U_{∞}/ν decrease from $4.8 \cdot 10^9/m$ at $H = 40,600$ ft. for the optimum $M = 0.78$ cantilever LFC wing of aspect ratio 10.4 with split tips to $3.66 \cdot 10^9/m$ at $H = 46,200$ ft. for the optimum $M = 0.78$ single strut-braced 16.4 aspect ratio LFC wing to allow 30 percent larger surface roughness tolerances. The reduced difficulties with loss of LFC due to ice cloud particles and turbulence at these higher cruise altitudes are further advantages of such large span strut-braced LFC airplanes.

* Summarized from report by W. Pfenniger, "Some Thoughts on the Design of Large Global Range LFC Transport Airplanes," January 1976.

** Using for example, small chord trailing edge flaps.

After selecting wing span the choice of wing chord or aspect ratio depends on secondary considerations such as high lift characteristics, gust loads and their possible alleviation through active control, type of wing structural layout and especially of sandwich wing skins which minimize the structural weight of larger chord wings with thin skins, critical Mach number considerations, fuel load distribution along the span, etc.

2. Preliminary Design and Structural Considerations.

Preliminary designs of hypothetical LFC transport airplanes carrying 250,000 lbs. (113,500 kg) payload at high subsonic speeds over global ranges were laid out (figs. 4 and 5). In view of their superior performance and easier laminarization externally braced LFC transport designs were emphasized. Every effort was made to take maximum advantage of the strut-braced design by assuming wide-chord suction laminarized graphite struts of low parasite drag, taking out wing bending as well as torsional moments at the wing strut intersection and minimizing the bending moments in the in-board strut-braced region of the wing. Of course, the aerodynamic interference at high subsonic speeds between the struts and the lower wing surface must be minimized or eliminated by suitable area cutouts on the lower wing surface (fig. 6), as demonstrated successfully by the strut-braced airplane model of the Northrop LFC research group in the Wright Field transonic tunnel (ref. 10). Furthermore, local suction is required to maintain laminar flow in the juncture region of the strut with an LFC wing (ref. 11).

A relatively bulky payload similar to that of the C-5 airplane was assumed, requiring a rather large central fuselage to carry the payload. In principle, at least part of the less bulky payload, such as containers, might be carried in smaller payload nacelles relatively far outboard on the wing, strongly alleviating the wing bending moments in flight (fig. 7) and thus further raising wing span and lowering induced drag without a wing structural weight penalty. The length Reynolds numbers of such nacelles can be sufficiently low during cruise to allow very extensive suction laminarization with the present state of knowledge; i.e., the parasite drag of such payload nacelles might thus be drastically reduced. Of course, with the particularly large wing span of such a design, wing torsional deflections become critical; this problem may be solved by actively controlling the wing torsional deformation by means of suitable horizontal active control surfaces on these payload nacelles. Landing gears in these nacelles (in addition to the main central landing gear) minimize negative ground-air-ground loads during taxiing, ground roll, and touchdown resulting from their weight, requiring rather wide run- and taxiways. Even though such a design approach could provide substantial performance improvements with further increased payloads (~ 400,000 lbs.) at global ranges with reasonable takeoff gross and fuel weights, this approach was finally abandoned because of the wide runways needed for the wide landing gear tread of such designs. The situation in this respect, though, might change in the future; after all, adding concrete on the sides of runways is relatively inexpensive as compared to all the other costs involved.

For the same reason, large span configurations with twin fuselages spaced relatively far apart to minimize wing bending moments in flight, carrying in each fuselage possibly 150,000 lbs. payload or so, were not further considered in spite of their possibly superior performance; again, the large landing gear tread would require rather wide runways and might therefore be presently unacceptable. Similarly, "span-loaders," with the payload located in the wing along its span, were ruled out for the time being; the bulky C-5 type payload would have required an excessively thick wing in addition to a wide landing gear tread. Therefore, designs with a large central fuselage, carrying the entire payload, were chosen, using a central landing gear in the fuselage and if necessary carrying a small percentage of the ground loads by smaller gears supported from the wing strut system or the engine nacelles.

Within this design constraint, every effort was made to minimize wing structural weight and design as large a span wing of low span loading, W/b^2 , and small induced drag with reasonably low structural weight of the lift-carrying system. In general, the wing span was chosen so as to keep the weight of the lift-carrying system at about 12 to 14 percent of the take-off gross weight, W_0 , assuming titanium for the wings and graphite for the struts and split wingtips.* To keep the maximum gust load factors below 2 to 2.5 g and minimize dynamic loads in gusts due to wing overshoot in bending (by raising the aerodynamic damping in wing bending), active control was assumed deflecting a small chord trailing edge cruise flap in the outer wing. Active horizontal control surfaces mounted on suction-laminarized external wing fuel nacelles of extremely low parasite drag (probably usually needed only in rear part of these nacelles), located in the outer wing similar to the B-52, control wing torsional deflections and thus largely compensate for the torsional wing deformation resulting from deflecting the previously mentioned trailing edge flaps for gust load alleviation through active control. A small chord trailing edge cruise flap can thus be far more effective in alleviating gust loads through active control, especially on swept LFC wings. The same horizontal surfaces on the external fuel nacelles increase the damping in pitch to raise accordingly the wing flutter speed - provided their support structure with the wing is sufficiently stiff in vertical bending requiring possibly graphite), as verified by flutter calculations of A. C. Kyser.

The previously mentioned external wing fuel nacelles, containing primarily reserve fuel, alleviate the wing bending moments to reduce accordingly wing structural weight. Outrigger landing gears, of course, appear desirable to minimize negative ground-air-ground loads induced by these fuel nacelles. Alternatively, a large percentage of their fuel might be stored further inboard when high negative loads may be encountered during taxiing, ground roll, and touchdown; after liftoff, this fuel could then be transferred to the external fuel nacelles. Since the maximum load factors at high C_L 's shortly after liftoff are limited by wing stall and the aerodynamic lift with deflected flaps at takeoff and the initial climb is, in addition, concentrated further inboard such a procedure may be permissible from the standpoint of allowable wing bending moments. In this manner, excessive negative ground-air-ground loads during taxiing, takeoff ground roll, and touchdown would be avoided while still maintaining the favorable wing bending relief by these external nacelles at higher flight speeds.

* Lower wing structural weights would result with an all composite or hybrid-composite titanium wing.

The relatively high optimum cruise lift coefficients of large span high aspect ratio strut-braced LFC wings limit the maximum cruise load factor before the wing stalls; thus, a spanwise lift distribution for low induced drag can easily be chosen at cruise to optimize the airplane cruise lift-to-drag ratio. At C_L 's $< C_{L_{cruise}}$ and correspondingly higher flight dynamic pressures, the outer wing may be unloaded by deflecting up the trailing edge flaps on the outboard wing and split wing tips (through active control) to raise the permissible gust load factors over those at cruise. The same method reduces wing bending under maneuver loads as well as during the last flight phase when the fuel of the external fuel nacelles, most of which is reserve fuel anyhow, has been consumed.

Wing bending moment calculations were conducted at 2.5 g limit load factor for a strut-braced LFC wing with a simple single as well as a longer kinked single strut, supported at the kink location by a jury strut (fig. 8). The bending moments in the strut-braced inboard wing area are drastically reduced to minimize accordingly wing structural weight in this region. The inboard wing bending moments are particularly small with a kinked strut and a jury strut located at the kink location. The jury strut kink load induced by the kinked main strut substantially reduces the bending moments in the inboard wing (refs. 2-7). At the same time, the strut kink increases the angle between wing and strut to alleviate accordingly the aerodynamic wing-strut intersection problem.

Of course, the strut is structurally far more effective if it takes out wing torsional moments at the wing strut intersection besides wing bending moments, accomplished with wide chord and/or V-type struts. With the parasite drag of suction laminarized struts being inherently very small and increasing only approximately proportional to $\sqrt{C_{strut}}$ in the range of the strut Reynolds numbers rather wide chord struts appear acceptable at the wing-strut intersection.

To increase the wing chord and thickness in the structurally critical wing-strut intersection region, with the purpose in mind of minimizing wing structural weight, relatively low C_L 's are chosen in this area, while C_L increases continuously towards the wingtip where percentage-wise thinner wing sections are structurally acceptable. The smaller local C_L - values in the wing-strut intersection region allow correspondingly larger local wing thickness ratios (t/c); locally further increased (t/c)'s are, in addition, possible due to the fact that the local super velocities due to wing thickness, tapering spanwise both towards the fuselage and the wing tip, are considerably smaller than on a yawing wing of constant chord and thickness, especially at high subsonic speeds. A still thicker wing in the wing-strut intersection region appears feasible by placing the main propulsion fan engine nacelles as well as the suction drive nacelles in the form of "Whitcomb bumps" up- and/or downstream of the wing trailing edge in the wing-strut intersection region to reduce accordingly the local super velocities on the wing in this region. In view of the torsionally very stiff inboard wing-graphite strut system, engines at the wing-strut intersection location may be placed to the rear of the wing (fig. 5) without major structural and flutter problems; this may be impossible on a cantilever wing. Still further increased wing thickness in the wing-strut intersection area may be permitted by locally increasing the isobar sweep angle on the upper wing surface. The combination of all these methods is a substantially increased wing thickness in the wing-strut intersection region, where wing bending moments are a maximum, to minimize wing bending structural weight.

Compression and buckling loads in the inboard wing region, combined with bending loads, must be carefully considered at higher positive load factors. To minimize or preferably eliminate eccentricity of the inboard wing at high loads, adversely affecting its buckling load, and avoid additional bending moments in the deflected inboard wing at high positive loads by strut-induced compression loads, the inboard wing might preferably be built precurved such that it becomes more or less straight at high positive load factors.

From the standpoint of compression and buckling loads, high strength graphite appears as a particularly promising structural material for the inboard strut-braced portion of the wing, for it could then be of surprisingly low weight.* The outer wing might be an all-graphite or graphite-titanium design.

Strut buckling load calculations under negative ground-air-ground loads and negative gust loads show that strut buckling can easily be handled with relatively low strut weights so long as graphite or other high modulus materials are used for the struts. With the struts representing rather slender columns operating at relatively low stress levels, high modulus graphite ($E \sim 3.10^6 \text{ kg/cm}^2$, $\sigma_{ult} \sim 6000 \text{ kg/cm}^2$) often appears superior over high strength graphite ($E \sim 1.6 \cdot 10^6 \text{ kg/cm}^2$, $\sigma_{ult} \sim 12,500 \text{ kg/cm}^2$). To minimize eccentricity under high negative loads, the struts might be precurved such that they become straight at high negative loads (this may not always be feasible, and graphite of higher strength and lower E might then be preferable). With the small inboard wing deflections under load, fixed joints appear feasible at the inboard strut-fuselage intersection to decrease accordingly the buckling length of the inboard struts. The jury strut supports the main strut at the kink location from the wing. Similarly, since the tension load in the main strut at high positive loads is approximately equal to the corresponding compression load in the inboard wing, the jury strut (supported from the main strut) effectively stabilizes the inboard wing against buckling; the buckling length of the inboard wing, especially with a fixed wing-fuselage joint, is thus drastically reduced.

In summary, bracing an LFC wing with wide chord suction laminarized graphite struts is equivalent to adding a very rigid inboard wing to a much more flexible cantilever outer wing to substantially increase wing span and aspect ratio without raising the structural weight of the lift carrying system, thereby reducing induced drag at a very minor penalty in strut parasite drag to increase the range by 20 percent at 40 percent lower maximum wing chord Reynolds numbers.

* Truss-type structures like wing-strut systems, loaded axially in tension and compression, lend themselves inherently better to unidirectional advanced composites as compared to cantilever wings, which need longitudinal plies for bending strength and additional diagonal plies for torsional stiffness. In other words, the reduction of wing structural weight through advanced composites can be substantially larger for strut-braced than for cantilever wings to favor strut-braced wings in advanced composite structure.

To achieve $M_{cruise} = 0.78$, 20° to 24° swept conservatively laid out transonic LFC wings, were assumed for the time being. With gust loads limited by active control and extensive use of sandwich structures in the LFC wings relatively low wing loadings W/S will optimize performance (fig. 9), especially taking into account the fact that increasingly extensive and eventually full chord laminar flow becomes easier feasible with the simpler high lift flaps and the lower cruise unit length Reynolds numbers which are possible at lower wing loadings. Furthermore, the ratio of skin thickness to wing chord is inherently larger for optimized large span high aspect ratio strut-braced LFC wings of smaller chord than for optimized cantilever LFC wings of small span and larger chord. Therefore, it appears easier to design strut-braced LFC wings of lower wing loading especially for local buckling, while maintaining high stress levels and low wing weights. From a structural standpoint large span strut braced wings may then optimize at somewhat lower wing loadings than cantilever LFC wings, provided gust loads can be limited through active control.

Large span high aspect ratio strut-braced wings with very thin inboard wings, with the thickest portion of the wing located in the wing-strut intersection region at a considerable distance from the fuselage, lend themselves inherently well to minimize the aerodynamic interference between wing and fuselage at high subsonic speeds. In many cases a favorable "high subsonic speed equivalent area distribution" appears possible with essentially a cylindrical unwaisted fuselage desirable from many aspects, even at cruise Mach numbers up to $M_\infty = .9$. With the gradual upstream fall-off of the cross-sectional area of the thin strut-braced inboard wing, leading edge strakes and similar devices are then unnecessary to achieve a smooth equivalent high subsonic speed area distribution.

After gaining design experience with various large strut-braced LFC transports, preliminary design type studies on such airplanes were continued with more elaborate double-strut-braced LFC wings of further increased wing span and aspect ratio (fig. 10). Their lower induced drag by far compensates the increased parasite drag of the more elaborate suction laminarized strut system to substantially improve the airplane range/payload performance, at least in principle. At the same time, with the smaller wing chord and higher optimum $C_{Lcruise}$ and H_{cruise} of such designs, their wing chord Reynolds numbers are substantially smaller than for the simpler strut-braced wing designs to alleviate accordingly the suction laminarization problems of large LFC wings, associated especially with boundary layer crossflow due to sweep. Structural load- and buckling-calculations of the various strut components and inboard as well as outboard wing indicate that the double-braced wing-strut system can be designed structurally highly efficiently with respect to bending and torsional loads and deformations at surprisingly low structural weights, especially if high strength or high modulus graphite material is used judiciously for the various strut members and the inboard wing, depending on the effective column buckling length-to-thickness ratio. LFC transports with such double strut-braced wings of further increased span pose more severe handling problems; furthermore, their larger wing aspect ratios and reduced wing volumes complicate the LFC suction ducting design in the wing, though not necessarily in a decisive manner.

For turbulent airplanes such double strut-braced wing designs of very high aspect ratio may become questionable in view of their very high optimum cruise lift coefficients, resulting from the rather high wing aspect ratios, adversely affecting M_{crit} of the wing as well as the rear pressure recovery on the upper wing surface at such high $C_{Lcruise}$. Therefore, the performance of such large-span, high aspect ratio, double-braced turbulent comparison airplanes was not further studied. With the small friction and parasite drag of LFC airplanes, $C_{Lcruiseopt}$ is substantially lower than for comparison turbulent airplanes; hence, M_{crit} of double-braced LFC airplanes is not yet as severely compromised by the higher $C_{Lcruise}$ of double strut-braced configurations, especially if the fuselage drag could be minimized through LFC.

3. Performance Improvements Through Fuselage Drag Reduction.

After lowering induced drag by means of a large wing span and minimizing wing and empennage profile drag through suction laminarization, the fuselage parasite drag becomes important and should preferably be further reduced. This may be possible by thickening the laminar sublayer of the turbulent fuselage boundary layer and lowering accordingly turbulent fuselage skin friction drag, accomplished for example with flexible surfaces, as demonstrated by Blick (ref. 18) as well as Bushnell (ref. 19), or perhaps by the somewhat controversial method, suggested first by Betz, of injecting low energy boundary layer air, removed by suction from the rear pressure rise area of the fuselage, into the turbulent boundary layer in the flat pressure- and accelerated-front region of the fuselage. The practical feasibility and weight penalties of such flexible fuselage surfaces and of injection of low energy air into the fuselage boundary layer must be further studied.

Pressure drag in the rear pressure rise area of the fuselage can be minimized by thinning the fuselage boundary layer in this region by means of suction (ref. 12); reacceleration of the suction air to flight speed or somewhat higher speeds recovers, in addition, a large percentage of the kinetic wake energy of the sucked fuselage boundary layer (ref. 13). Estimates of the minimum propulsive power for a turbulent fuselage with carefully laid out suction in the rear pressure rise area indicate a saving of 15 percent in propulsion power for the fuselage, as compared to the product fuselage drag times flight speed (ref. 12, fig. 11). The reduction of the fuselage pressure drag by means of suction in the rear part of the fuselage becomes essential when the turbulent fuselage boundary layer in the upstream flat pressure area has been thickened artificially by low energy blowing of decelerated fuselage boundary layer removed from the rear end of the fuselage.

On upswept rear fuselages, boundary layer thinning through suction enables a closer approach towards potential flow, especially when local boundary layer crossflow in this region can be compensated, if necessary, by a counter-secondary flow generated by suitable guide vanes (ref. 14). The fuselage drag may then closely approach the drag of aerodynamically more ideal symmetrical fuselages with suction in their rear pressure rise areas.

Of course, fuselage drag could basically be much further reduced by extensive suction laminarization. Indeed, experiments in the Ames 12-foot tunnel on a Reichardt low drag suction body of revolution of the Northrop LFC Research Group verified extremely low equivalent body drags ($C_D \sim 2.7 \times 10^{-4}$, based on body wetted area, including the equivalent suction drag) up to $Re_L \sim 60 \times 10^6$ with very small suction mass flow rates (ref. 15); i.e., the laminar fuselage drag at high Re_L with full length laminar flow might, in principle at least, be reduced by a factor of 8 to 10. The question, of course, arises concerning the maximum laminar flow length Reynolds number on such suction laminarized bodies. With atmospheric small scale turbulence too weak to influence transition in flight, as compared to the destabilizing influence of the microscale turbulence of even the best low turbulence tunnels, one might expect $Re_{x_{Transition}} \sim 1.2 \times 10^8$ on a suction body under otherwise the same conditions as on the Reichardt body. With a more sophisticated approach towards the aerodynamically ideal area suction and with disturbances from the air-plane and its propulsion and suction drive system minimized, still higher transition length Reynolds numbers than 1.2×10^8 appear basically feasible on LFC bodies, as expressed in reference 16. This theoretical expectation, though, must be verified experimentally.

4. LFC Airplane Performance.

The performance of various large $M = 0.78$ LFC transports, carrying 113,500 kg payload over global ranges without refuelling, was studied. For most of the performance calculations, a fully turbulent fuselage with suction in its rear pressure rise area (to minimize fuselage pressure drag and recover part of the kinetic energy of the sucked fuselage boundary layer) was assumed. Reduction of turbulent fuselage skin friction by flexible surfaces or injection of low energy boundary layer air was not considered in the present studies. The influence of partial suction laminarization of the fuselage on airplane performance was studied for several cases, tentatively assuming $Re_{x_{Transition}} = 120 \times 10^6$.

The figures 1, 12, and 13 show the drag polars $C_L(C_D)$ for turbofan-powered cantilever and various strut-braced $M = .78$ LFC transports with split wing-tips of $W_0 = 400,000$ kg and 113,500 kg payload with the drag contributions of the different airplane components. It is immediately evident that the drag contributions of the suction-laminarized airplane surfaces is relatively insignificant as compared to the airplane-induced drag and the turbulent fuselage friction drag. The small parasite drag contribution of the suction-laminarized wing struts is evident, even with more sophisticated double strut-braced systems of further increased wing aspect ratios. The drag polars show the very substantial reduction of the induced drag from the aspect ratio 10.4 cantilever LFC wing to the single strut-braced wing of aspect ratio 16.4 and the double strut-braced wing of aspect ratio 24.4 of the same wing structural weights. The airplane cruise lift-to-drag ratio L/D thus increases progressively from about 40 for the cantilever $M = 0.78$ LFC airplane without split tips to 42.4 with split tips and 50 for the single strut-braced LFC airplane of 16.4 aspect ratio and 57 for the double strut-braced wing of 24.4 aspect ratio (all with fully turbulent fuselage), see figure 14. Similar plots for L/D versus C_L are given in the figures 14, and 15 for cantilever and various strut-braced LFC transport configurations with a partially laminar fuselage as well as for configurations with counterrotating pusher propellers mounted downstream of the wing trailing edge.

The comparison drag polar of turbofan-powered strut-braced turbulent nonsuction airplanes (fig. 16) shows the dominating influence of the wing profile- and induced drag, with the fuselage parasite drag being relatively less important - with figure 17 showing $L/D(C_L)$ for various nonsuction turbulent airplanes.

Assuming gust load limitation by active control and laminarization of the entire wing, empennage, struts and a fully turbulent fuselage on a turbofan powered $M_{cr} = .78$ strut-braced LFC transport of aspect ratio 16.4 with split wing-tips, $W_0 = 400,000$ kg and 113,500 kg payload, the airplane range optimizes at relatively low takeoff wing loadings $W_0/S \approx 450$ kg/m², $\bar{C}_{L_{cruise}} \approx 0.55$, $\bar{H}_{cruise} \approx 45,000$ feet, $(L/D)_{cruise} \approx 48$ (fig. 9). Evidently, the parasite drag of the turbulent fuselage is comparatively so large and dominant as to optimize L/D and range at relatively low wing loadings and much higher C_L 's and altitude.

For comparison, a large LFC transport with cantilever wings of the same structural weight with 10.4 aspect ratio would optimize at slightly higher wing loadings, $\bar{C}_L \sim 0.4$ and $\bar{H} \sim 40,000$ feet.

Assuming a partially laminar flow fuselage for the above-mentioned strut-braced LFC transport of $W_0 = 400,000$ kg TOGW under otherwise the same conditions, assuming tentatively $Re_{x_{Transition}} = 120 \cdot 10^6$ on the fuselage, the range optimizes at a somewhat lower wing loading $W_0/S = 425$ kg/m², $L/D \sim 55$, $\bar{C}_L \sim 0.55$, $\bar{H} \sim 46,000$ feet (fig. 18). Evidently, as the fuselage length Reynolds number decreases at larger C_L transition on the fuselage moves downstream to decrease fuselage drag (see drag polar (fig. 12). Under such conditions L/D optimizes at surprisingly high C_L - values, with $C_{D_{ind}}$ being substantially larger than $C_{D_{\infty + par}}$.

As shown by the summary Table 1, double strut-braced LFC airplanes of further increased wing span and aspect ratio (both with fully turbulent as well as partially laminar flow fuselage) optimize at still higher cruise \bar{C}_L 's (~ 0.65) and \bar{H} ($\sim 50,000$ ft.) and surprisingly low unit length Reynolds numbers ($\bar{U}_{\infty}/\gamma \sim 3.10^6/m$). Table 1 presents results for turbofan powered LFC transports carrying 250,000 lbs payload over 14,000 nautical miles still air range without refueling.

For comparison, figure 19 shows the corresponding results of optimization studies for turbofan powered strut-braced turbulent $M_{cr} = .78$ transport airplanes of 16.4 aspect ratio, 400,000 kg TOGW and 113,500 kg payload. Extensive natural laminar flow on the struts, gust load limitation by means of active control and split wing tips were assumed. The range optimizes at $W_0/S \sim 550$ to 600 kg/m², $\bar{H} \sim 45,000$ feet,

$C_L \sim 0.75$, $L/D \sim 28.5$. For comparison, the range of turbofan powered turbulent $M_{cr} = .78$ transports of 400,000 kg TOGW and 113,500 kg payload with cantilever wings of 10.4 aspect ratio with and without split wing tips, optimizes at $W_0/S \approx 600 \text{ kg/m}^2$, $L/D \approx 24$ and 22.5, respectively, $C_L \approx 0.6$ to 0.65, $H \approx 40,000$ feet.

Figure 20 shows the variation of airplane range with W_0 for reasonably well optimized turbofan-powered cantilever and strut-braced $M_{cruise} = 0.78$ LFC airplanes, carrying 113,500 kg payload, and corresponding comparison turbulent nonsuction airplanes, assuming graphite composite material for the struts and split wing-tips and metal (preferably titanium) for wing, fuselage and empennage. The range, of course, increases with W_0 ; it increases progressively from cantilever LFC configurations with ordinary wingtips to ones with split tips, to single strut-braced LFC configurations and double strut-braced LFC airplanes. A similar trend is observed with the turbulent nonsuction comparison airplanes, except that the range at the same TOGW is about 1.65 or 1.75 times smaller than corresponding LFC airplanes with fully turbulent or partially laminar flow fuselages, respectively.

Figure 21 shows under otherwise the same conditions, plots of the range versus W_0 of strut-braced $M = 0.78$ LFC airplanes in all graphite construction as well as with only the inboard wing in graphite, indicating a substantial range increase by the use of graphite composites as structural material. Figure 21, furthermore, shows the theoretically possible range of turboprop-powered $M = 0.78$ LFC transports, indicating a surprisingly large range improvement over corresponding turbofan-powered LFC transports.

Figure 22, finally, shows the variation of the mean wing chord Reynolds number $Re_{\bar{c}}$ during average cruise for various $M_{cruise} = 0.78$ LFC transports carrying 113,500 kg payload. Under otherwise the same conditions $Re_c \sim \sqrt{W_0}$; it decreases very substantially from the high values of the cantilever wing configuration ($b^2/S = 10.4$) to the single strut-braced wing designs ($b^2/S = 24.4$) to alleviate accordingly the wing laminarization problems, especially under crossflow conditions due to wing sweep.

5. Reduction of Induced Drag and Range Improvements of LFC Airplanes by Formation Flight.

Substantial reductions in induced drag and corresponding improvements in $(L/D)_{cruise}$ and airplane range could, in principle, be possible by distributing part of the payload along the span (for example, in suction-laminarized payload nacelles and increasing the wing span accordingly). In the present study, such an approach - though highly attractive from the standpoint of performance as well as alleviation of the LFC problems (lower length and unit length Reynolds numbers as a result of the large span, high aspect ratio wings) - was finally abandoned in view of the wide landing gear trends of such designs. The same goal, though, may be accomplished by distributing the payload in several airplanes flying in formation and linked together electronically by active control using laser or other advanced electronic methods to align the individual airplanes in such a manner as to minimize the induced drag at cruise. As with birds flying in formation, the wings can be staggered in flight direction as the induced losses (neglecting dissipation) are, according to Munk's theorem, not affected by such stagger. The induced drag of such a formation of wings is then essentially a function of the span of the entire lifting system of wings, with the downwash in the Trefftz-plane far behind the wings constant for minimum induced drag. The minimum-induced drag of a combination of wings in formation flight was analyzed in reference 17 by means of measurements in an electrolytic tank using the electrolytic analogy (results, see figs. 23-26).

For minimum-induced drag in formation flight with a combination of several wings, the individual wings should be aligned such that the vertical displacement "s" of the induced trailing vortex sheets of the individual wings at cruise are minimized or preferably reduced to zero. This may be closely approached with modern laser- or electronics methods and active control. To minimize D_{ind} the circulation $\Gamma_{1,2}$ of two adjacent wings in their tip region should vary such that the downwash of the wing combination in the Trefftz-plane is approximately constant; i.e., the resultant circulation of both wings $\Gamma_{res} = \Gamma_1 + \Gamma_2$ should be reasonably continuous in the tip region of adjacent wings for small vertical displacements "s" of the individual induced vortex sheets (fig. 23). With the tips of downstream wings trailing directly downstream of preceding upstream wingtips, rectangular Γ -distributions would be needed, which are practically impossible to realize. It appears far easier to achieve a continuous resultant Γ -distribution in the wingtip region by overlapping the wingtips in spanwise direction by a distance "a" (fig. 23) and letting the circulation of each individual wing decrease approximately linearly from its maximum value Γ_0 to zero at the tip over the distance "a" (for small "s" values). Indeed, as observed by the author, pelicans seem to fly in this manner in formation (ref. 17). Furthermore, with the induced secondary flow through the "frozen" vortex sheets increasingly restricted with larger overlap distances "a", the induced drag factor $\kappa = \frac{D_{ind, formation}}{D_{ind, indiv. wings}}$ increases at a substantially slower rate when the vertical displacement "s" of the induced vortex sheets increases. κ is then a minimum for relatively large overlap ratios a/b for 3, 5, and infinitely many wings (figs. 23-25), with b = individual wing span. For $s/b = 0$, $\Gamma_{1,2}$ of each individual wing decreases linearly from Γ_0 to zero; with increasing s/b - ratios, $\Gamma(y)$ gradually approach elliptic distribution and κ asymptotically approaches one at large s/b - ratios (fig. 26).

Assuming, as an example, 3 and 5 wings flying in formation with $s/b = 0.02$, the minimum induced drag ratio is $\kappa = 0.5$ and 0.36 (figs. 24 and 25), increasing $(L/D)_{cruise}$ and range by about 40 percent and 60 percent, respectively, assuming equal $C_{D_{00}}$ - values and percentage laminar areas. Of course, with the higher $C_{L_{cruise}}$ and the correspondingly lower length and unit length Reynolds numbers Re_x and U_{∞}/v in formation flight, $C_{D_{00}}$ will be somewhat larger, compensated partially by the fact that more extensive laminar flow may be possible at these lower Re_x and U_{∞}/v 's in formation flight.

The concept of induced drag reduction in formation flight may be applicable particularly to cases where the induced flow angles of the upstream wings are not unduly large, as is the case with large span high aspect ratio strut-braced LFC wings cruising at relatively modest C_L 's (as a result of their low wing profile and parasite drag). If necessary, it may be desirable to align the downstream wings according to the local effective angle of attack in the wingtip region by twisting the wingtip by means of suitable control surfaces located on the external fuel pods, etc. With the much larger zero-lift drag of conventional turbulent nonsuction airplanes, the resulting high $C_{L_{opt}}$ and the correspondingly lower critical Mach number as well as the steep rear pressure rise on the upper wing surface and the large induced flow angles induced by the upstream wings on the downstream ones, associated with such high $C_{L_{opt}}$ - values, may render formation flight less attractive with turbulent airplanes.

REFERENCES

1. Pfenninger, W. Design Consideration of Large Subsonic Long Range Transport Airplanes with Low Drag Boundary Layer Suction. Northrop Report BLC-111, NAI-58-529, 1960.
2. Pfenninger, W. Ueber die Aerodynamische Durchbildung von Fluegelstrebenanschlussen. Flugwehr-u.-Technik, no. 9, Sept. 1942. Further Refined Wing-Strut Studies by Pfenninger at Northrop, 1954.
3. Pfenninger, W., Bacon, J. Design Considerations for Hypothetical Boundary Layer Control Airplane. Northrop Report BLC1, 1951 and 1953.
4. Bacon, J.W. An Aeroelastic Study of Configuration II of a Laminar Boundary Layer Control Airplane. Northrop Report BLC2, 1953.
5. Schjelderup, H. The Stability and Linear Deformation of a Framework Formed by a Cantilever, Knee Brace, and Jury Strut. Northrop BLC Report 44, 1954.
6. Bacon, J.W. Experimental Investigation of Structural Effect of Sweepback on a Strut-Braced Wing. Northrop Report BLC-47, NAI-54-475, 1954.
7. Schjelderup, H. An Analysis of a Swept Wing-Strut Configuration. Northrop Report BLC-57, NAI-54-557, 1954.
8. Fiul, A. A Preliminary Report on a Comparison of Aeroelastic Effects on Cantilever and Strut-Braced Swept Wings. Northrop Report BLC-67, NAI-54-800, 1954.
9. Pfenninger, W., Sipe, O.E. Note on the Reduction of Wing-Strut Interference. Northrop Report BLC-74, NAI-55-289, 1955.
10. Bacon, J.W., Fiul, A., Pfenninger, W. WADC 10-Foot Transonic Wind Tunnel Tests on Strut-Braced Boundary Layer Airplane. Northrop Report BLC-99, NAI-57-826, 1957.
11. Goldsmith, J. Laminar Flow at the Juncture of Two Aeroplane Components. Boundary Layer and Flow Control. Vol. II, G. V. Lachmann, editor, 1961.
12. Pfenninger, W. The Reduction of Losses in Strongly Decelerated Flow Regions of Diffusers, Etc. by Means of Suction. Boeing Doc. App. A, 1970.
13. Ackeret, J. Probleme des Flugzeugantriebs in Gegenwart u. Zukunft. Schweiz. Bauzeitg. Bd. 111, p. 237, 1938.
14. Sprenger, H. Experimentelle Untersuchungen an Geraden u. Gekruemmten Diffusoren. IFA Zuerich, Mittg. 27, 1959.
15. Gross, L.W., Pfenninger, W. Experimental and Theoretical Investigation of a Reichardt Body of Revolution With Low Drag Suction in the NASA Ames 12-Foot Pressure Wind Tunnel. Northrop Rep. NOR 63-46, BLC-148, 1963.
16. Pfenninger, W. Studies to Verify Laminar Flow at Very High Length Reynolds Numbers by Means of Distributed Suction in the Presence of Minimum Disturbances. Boeing Doc. D6-40281, 1972.
17. Sipe, O.E., Pfenninger, W. The Minimum Induced Drag in Formation Flight. Northrop Report BLC-31, 1954.
18. Blick, E.F. Skin Friction Drag Reduction by Compliant Coatings. International Conference on Drag Reduction, September 4-6, 1974.
19. Bushnell, D.M., Hefner, J.N., Ash, R.L. Compliant Wall Drag Reduction for Turbulent Boundary Layers. IUTAM Symposium on Structure of Turbulence and Drag Reduction, Washington, DC, June 7-12, 1976.

n	S _{wing} m ²	W ₀ kg	b ² /S m	C _L CRUISE	W ₀ n	U _∞ m/s	(L/D) CRUISE	Re _s x 10 ⁶	C _D max	Re _C max x 10 ⁶	USEFUL FUEL WEIGHT kg	C _D (L/D) OPT
116.4	1302	54250	10.4	0.39	39000	5.14	41.9	57.4	1.7	97.6	177950	0.34
113.4	1236	51640	10.4	0.42	40600	4.79	44.1	52.2	1.7	88.7	161950	0.37
128.9	1115	46440	14.9	0.52	45000	3.90	50.3	33.3	1.62	54.0	130880	0.47
133.1	1081	45030	14.4	0.55	46200	3.66	51.0	29.7	1.58	46.9	125485	0.50
152.5	951	38720	20.4	0.675	50000	2.98	57.1	19.6	1.43	28.0	100510	0.635

TURBOFAN POWERED LFC AIRPLANES WITH 18 000 n. MILES STILL AIR RANGE AND 250 000 lb. PAYLOAD
WING, EMPENNAGE AND WING STRUTS LAMINAR WITH LAMINARIZED WING FUEL NACELLES
 $W_0/S = 417 \text{ kg/m}^2$

Table 1.- Summary of Cruise Characteristics of
Various LFC Transports Payload = 113 500 kg,
 $M_{\text{cruise}} = 0.78$.

NOTE:

TURBOFAN POWERED LFC TRANSPORT
AIRPLANE, WITH CANTILEVER WINGS,
 $W_0 = 400\,000 \text{ kg}$,
 $W_0/S = 417 \text{ kg/m}^2$,
 $M_{\text{cruise}} = 0.78$

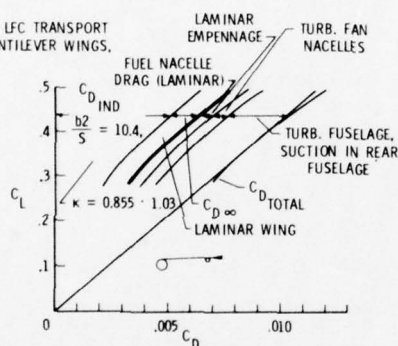


Figure 1.- Drag polar of LFC transport.



Figure 2(a). Black-footed Albatross and
California Condor (photographs
courtesy J. R. Pemberton).

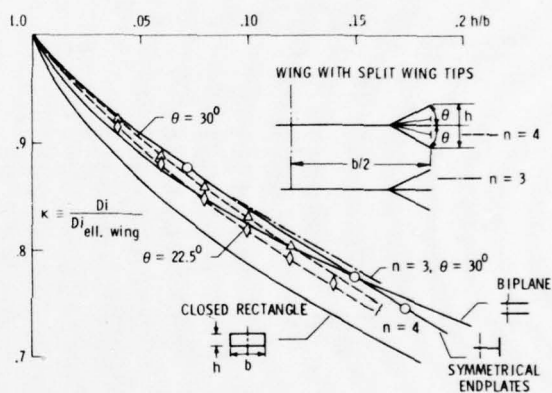


Figure 3.- Induced drag factor κ of wing with split
wing tips, comparison with closed rectangle,
biplane of equal spans, and wing with
symmetrical endplates (calculations by
D. Miller).

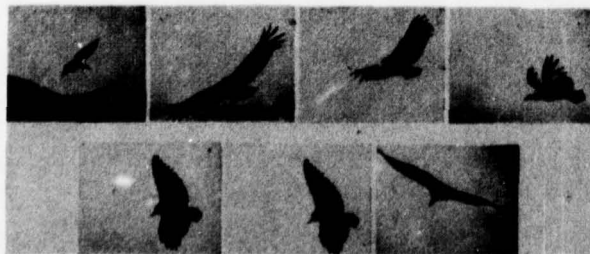


Figure 2. California Condor. (Photograph
courtesy J. R. Pemberton).

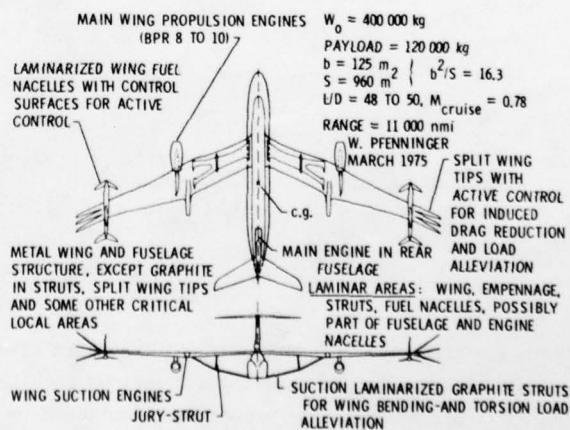


Figure 4.- Turbofan powered long range LFC transport.

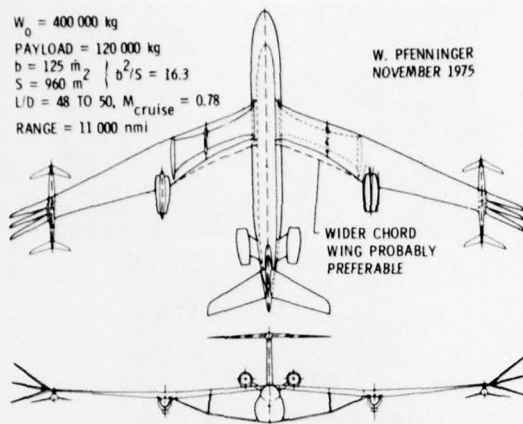


Figure 5.- Turbopowered long range LFC transport. Figure 8.- Strut-braced LFC long range transport with external fuel nacelles. Spanwise bending moment distribution at limit load ($n = 2.5g$) at full load; $W_0 = 454\,000\text{ kg}$.

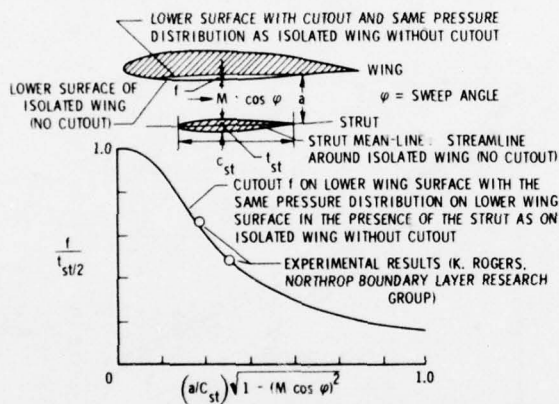


Figure 6.- Area cutouts of lower wing surface in the presence of wing struts.

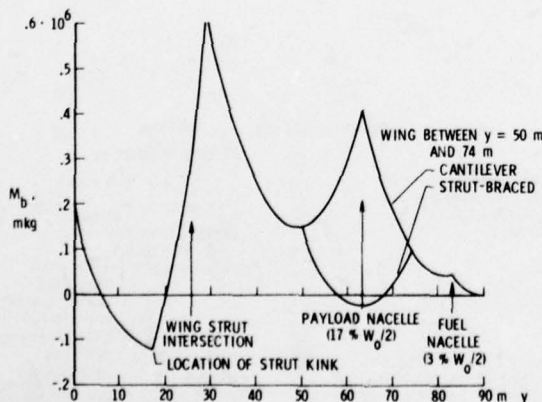


Figure 7.- Strut-braced LFC long range transport with external fuel nacelles and payload nacelles. Spanwise bending moment distribution at limit load ($n = 2.5g$) at full load; $W_0 = 400\,000\text{ kg}$.

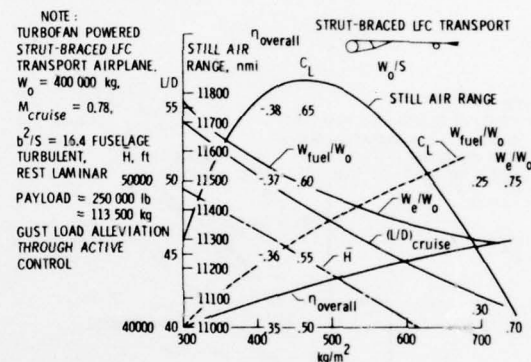
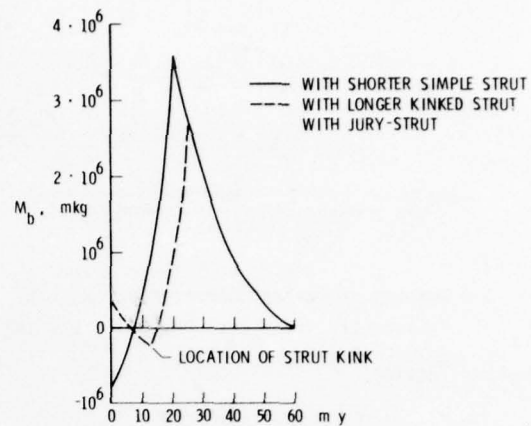


Figure 9.- $(L/D)_{\text{cruise}}$, η_{overall} , W_{end}/W_0 , W_{fuel}/W_0 , C_L , H , and range of LFC transports versus W_0/S .

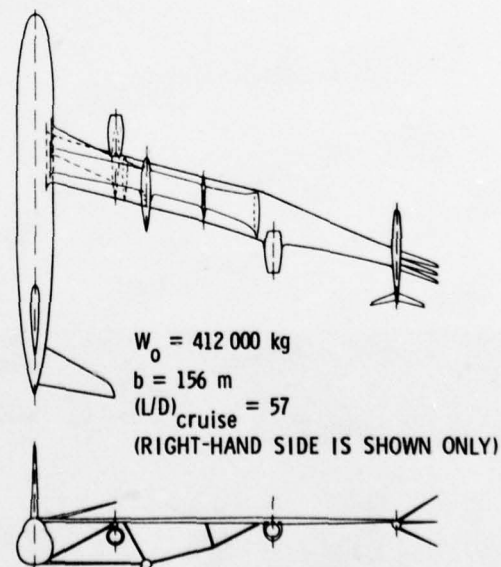


Figure 10.- Turbopowered double-braced $M = 0.78$ LFC transport, wing, empennage, struts, fuel nacelles laminar. Fuselage turbulent.

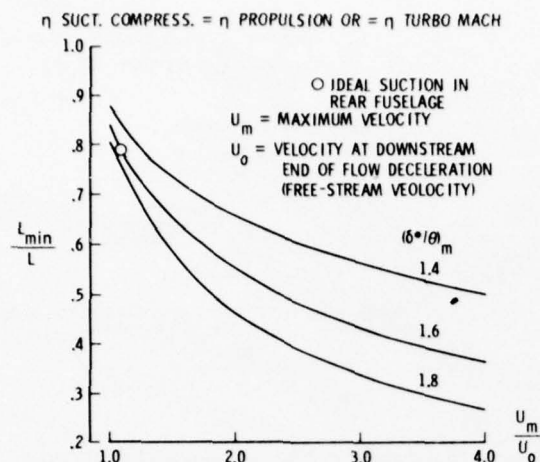


Figure 11.- Thermodynamically minimum propulsion power L_{min} in decelerated flow.

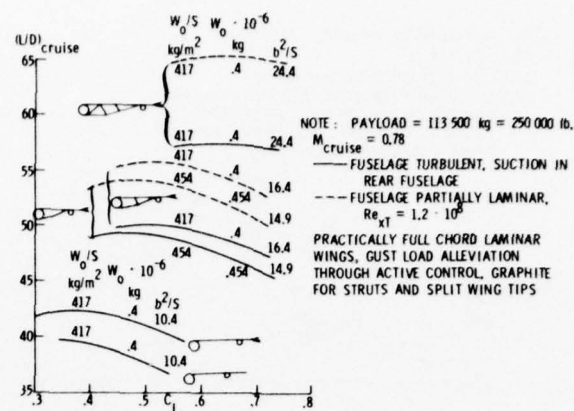


Figure 14.- $(L/D)_{cruise} = f(C_L)$ of turbofan powered LFC airplanes.

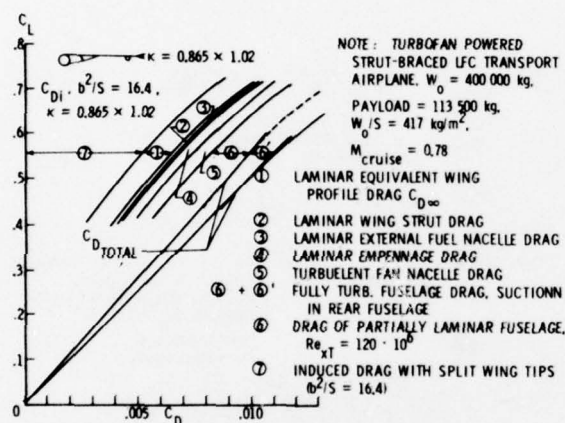


Figure 12.- Drag polar of LFC transport.

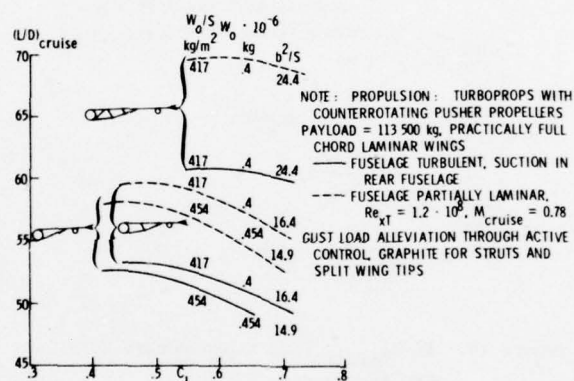


Figure 15.- $(L/D) = f(C_L)$ of turboprop powered LFC airplanes.

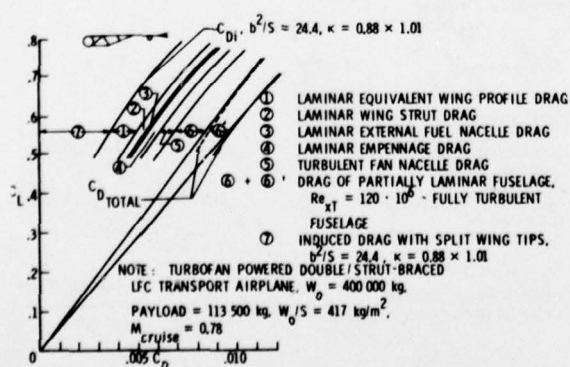


Figure 13.- Drag polar of LFC transport.

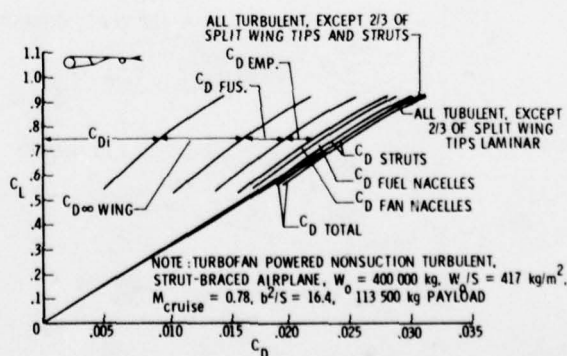


Figure 16.- Drag polar of nonsuction turbulent transport.

NOTE: $W_0 = 400\,000$ kg, PAYLOAD = 113 500 kg,
 $M_{cruise} = 0.78$

GUST LOAD ALLEVIATION THROUGH ACTIVE
 CONTROL, GRAPHITE FOR STRUTS AND SPLIT WING TIPS
 --- WING STRUTS AND SPLIT TIPS 2/3 LAMINAR
 --- SPLIT TIPS 2/3 LAMINAR, WING STRUTS AND
 REST OF AIRPLANE TURBULENT W_0/S

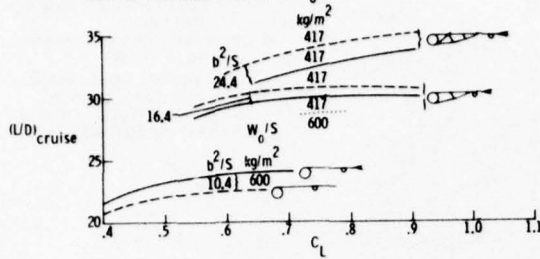


Figure 17.- $(L/D)_{cruise}$ of turbopfan powered turbulent nonsuction transport airplanes.

NOTE: $M_{cruise} = 0.78$, PAYLOAD = 113 500 kg

GRAPHITE ONLY FOR STRUTS AND SPLIT WING TIPS

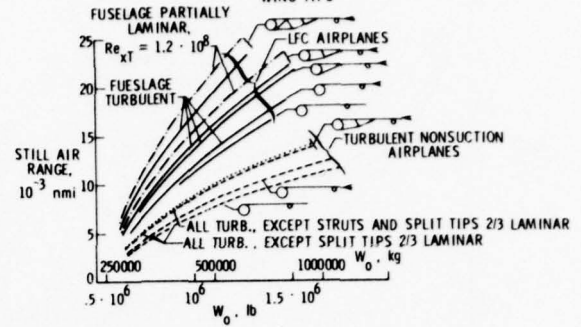


Figure 20.- Range of LFC and nonsuction turbulent transports versus W_0 .

NOTE: TURBOFAN POWERED STRUT-BRACED LFC TRANSPORT AIRPLANE, WING, EMPENNAGE, STRUTS AND EXTERNAL FUEL NACELLES LAMINAR. GUST LOAD ALLEVIATION THROUGH ACTIVE CONTROL GRAPHITE FOR STRUTS AND SPLIT WING TIPS. FUSELAGE PARTIALLY LAMINAR, $Re_{xT} = 120 \cdot 10^6$

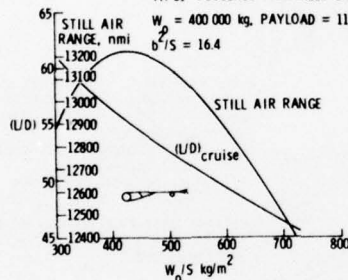


Figure 18.- $(L/D)_{cruise}$ and range versus W_0/S for LFC transports.

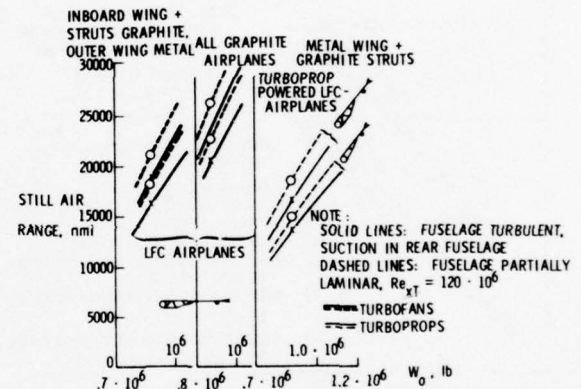


Figure 21.- Range versus W_0 of turbopfan and turbo-prop powered transports.

NOTE: TURBOFAN POWERED STRUT-BRACED TURBULENT TRANSPORT AIRPLANE, $W_0 = 400\,000$ kg, PAYLOAD = 113 500 kg, $M_{cruise} = 0.78$, $b^2/S = 16.4$ GUST LOAD ALLEVIATION THROUGH ACTIVE CONTROL GRAPHITE ONLY FOR STRUTS AND SPLIT WING TIPS

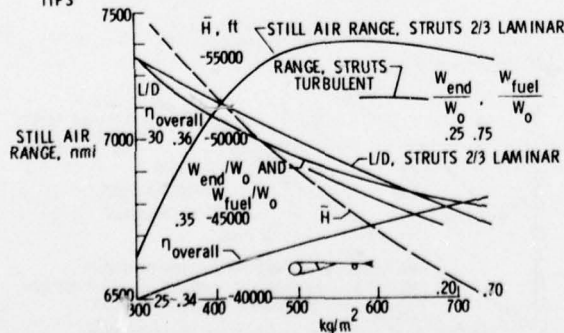


Figure 19.- $(L/D)_{cruise}$, $\eta_{overall}$, W_{end}/W_0 , W_{fuel} , range, H versus W_0/S for turbulent transports.

PAYLOAD = 250 000 lb
 113 500 kg
 $M_{cruise} = 0.78$
 $W_0/S = 417$ kg/m²

NOTE:

WING, EMPENNAGE, STRUTS AND EXTERNAL WING FUEL NACELLES SUCTION LAMINARIZED, SUCTION IN REAR FUSELAGE (TURB. FUSELAGE), HIGH BYPASS RATIO TURBOFANS

Re_c = AVERAGE CRUISE WING CHORD REYNOLDS NUMBER BASED ON MEAN CHORD \bar{c}

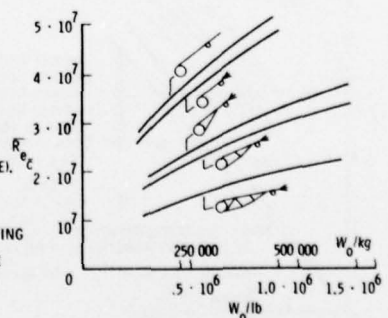


Figure 22.- Re_c versus W_0 for LFC transports.

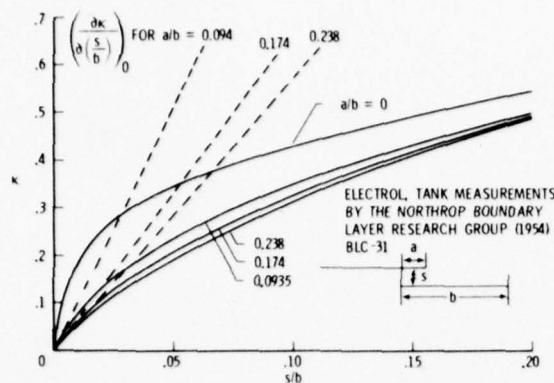


Figure 23.- Variation of induced drag for an infinite number of wings with variable overlap and fixed gap.

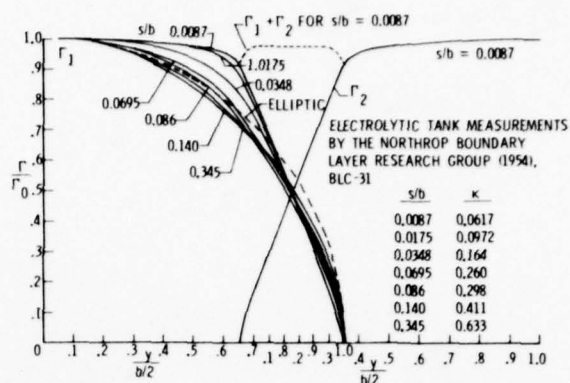


Figure 26.- Comparison of an elliptic circulation distribution with the experimental circulation distribution of an infinite number of wings with an overlap of .174b and variable gap s.

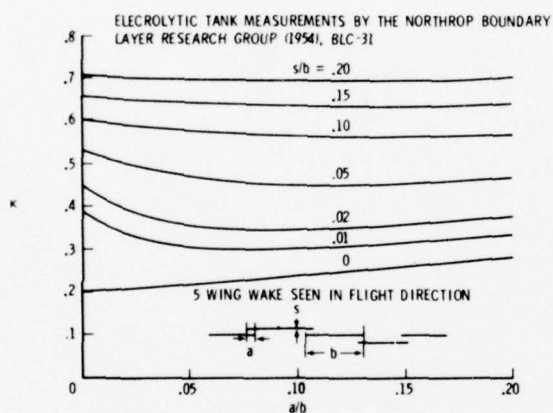


Figure 24.- Variation of induced drag for 5 wings in formation flight.

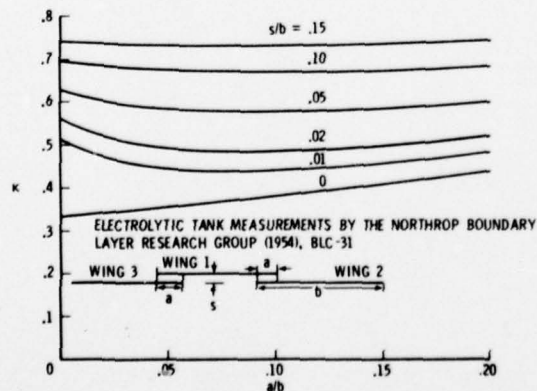


Figure 25.- Variation of induced drag for 3 wings with overlap a and vertical gap s.

LAMINAR FLOW CONTROL - CONCEPTS, EXPERIENCES, SPECULATIONS

by

Brian Edwards*

Aerodynamics Department, Royal Aircraft Establishment
Farnborough, Hampshire, GU14 6TD, England

SUMMARY

The paper describes the twin concepts of laminar flow control by suction, and of propulsion by restoring the momentum of the sucked mass flow. It goes on to discuss briefly how these concepts could be applied to reduce the fuel consumption, and perhaps also the operating costs, of transport aircraft. An account is given of the progress of some work relating to laminar flow control. This work took place during the 1950s and early 1960s and the author was involved in much of it. The position reached at the end of this work is reviewed. Doubts about the practical application of laminar flow control are aired and the reasons why the work was not continued are briefly discussed. The view is expressed that, despite the recent rapid rise in the price of fuel, future prospects for the application of laminar flow control are still uncertain.

1. CONCEPTS

1.1 The concept of laminar flow control

When air flows along a solid surface, vorticity is generated in the flow adjacent to the surface so that there is no relative velocity between the surface and the air in contact with it. This vorticity, being in the flow, is convected at a mean velocity, and in addition it is diffused into the flow in consequence of the momentum diffusivity (or kinematic viscosity) of the air (see Fig. 1). Momentum diffusivity is associated with the random motions of the individual gas molecules but diffusion can also occur through random motions of "lumps" of vorticity and this is called turbulent diffusion². The region into which vorticity is carried by the combined effects of convection and diffusion (including turbulent diffusion when it occurs) is known as the boundary layer or the wake depending on whether it borders the surface or lies further downstream. Boundary layers in which turbulent diffusion does not occur are called laminar boundary layers. Boundary layers in which turbulent diffusion does occur are called turbulent boundary layers.

A boundary layer can change from laminar to turbulent or from turbulent to laminar, but the way in which it changes from laminar to turbulent is of greatest interest in the present context since that is what laminar flow control is intended to prevent. The change from laminar to turbulent flow takes place through a transition region in which the boundary layer alternates between the laminar and turbulent states. The fraction of the time for which the flow is turbulent is called the intermittency factor. The onset of intermittent turbulent flow is preceded by a region in which the boundary layer is unsteady although it is laminar all the time (see Fig. 2). This unsteadiness results from the amplification within the laminar boundary layer itself of extraneous disturbances.

There are a number of processes (or mechanisms) through which amplification of various kinds of disturbance can occur. However, small disturbances cannot be amplified unless certain boundary layer stability criteria are exceeded. These criteria are related to the velocity profile of the laminar boundary layer and this, in turn, is characterised by its shape and its thickness. For any laminar boundary layer velocity profile shape there is a critical thickness Reynolds number below which all small disturbances will decay but above which some small disturbances are amplified. Under smooth conditions, that is to say with a relatively disturbance-free exterior flow and with low surface roughness, vibration, etc., considerable amplification may be necessary before turbulence appears.

In cases where the boundary layer velocity profile is only changing shape slowly, and its thickness is only increasing slowly, the rate of amplification of disturbances will remain low after the boundary layer has become unstable, and so the strength of any disturbance will only increase slowly. Thus they will have been convected a long way downstream before the disturbances have been amplified enough for turbulence to appear. In this way the onset of intermittent turbulence can be far downstream of the position where instability first develops. On the other hand, the distance to the onset of turbulence can be quite short. This would be the case if the boundary layer were to thicken rapidly whilst its velocity profile shape changed so that the thickness for neutral stability decreased rapidly. Then again, a boundary layer which is just stable to

*This paper expresses the opinions of the author and does not necessarily represent the official view of the Royal Aircraft Establishment. It is mainly concerned with work which took place in the 1950s and 1960s during which time the author was employed by Handley Page Ltd.

small disturbances can be unstable to large disturbances, and, allowing for some amplification, the onset of turbulence may be close to the position where the boundary layer would have first become unstable to small disturbances.

By applying suction at the surface, that is to say by the continuous removal of part of the boundary layer through the surface on which it is developing, the thickness of a boundary layer may be controlled and the shape of its velocity profile improved so that the thickness Reynolds number for neutral stability to small disturbances is increased. By this means, and by avoiding large disturbances, the development of turbulence can be prevented. This method of laminar flow control was first proposed by Griffith and Meredith³ in 1936, and is the subject of these notes.

As an example the case of a thin flat plate tangential to an airstream or moving in its own plane will be considered. The plate can only experience drag through skin friction. The drag of the plate must be balanced by a rate of change of momentum in the flow, and this change occurs in the boundary layer where elements of the flow acquire a different speed than that which they would have had if the flow had been inviscid (see Fig. 3). In the boundary layer the elements of the flow with the greatest momentum change are those closest to the surface since their speed has been changed to that of the plate itself. When the boundary layer is being sucked, all the air drawn through the surface comes from that part of the boundary layer, so it too has acquired the same speed as the plate. Thus although the momentum change takes place in the boundary layer, it is manifested in the sucked mass flow and the wake as well as in the boundary layer (see Fig. 4). Indeed, the greater part of the flux of momentum change may be in the suction flow.

The drag of a part of the plate extending from its leading-edge to any fraction of its chord is balanced by the total flux of momentum change for that part of the plate, that is to say the flux of momentum change in any flow removed by boundary layer suction on the whole of that part of the plate added to the flux of momentum change in the boundary layer leaving it. It follows from this that without boundary layer suction a thick boundary layer (and hence ultimately a thick wake) is indicative of high drag and conversely a thin boundary layer and wake indicates a low drag. However, the same inference cannot be validly drawn when the boundary layer is sucked.

The rate of change along the plate of the total flux of momentum change, as defined above, depends on the local intensity of skin friction. This in turn depends on the local rate of shear at the surface and for a given shape of velocity profile the rate of shear is inversely proportional to the boundary layer thickness. One effect of suction is to change the shape of the boundary layer velocity profile so that for the same boundary layer thickness the rate of shear at the surface is greater than it would be with the shape that the velocity profile would have without suction. However this is more than offset by the increased thickness that can be accepted on account of the very much improved stability of the velocity profile with suction. Even so, at flight Reynolds numbers, a stable sucked laminar boundary layer is thinner than an unsucked one would be (supposing turbulence did not develop), and so the drag with a controlled laminar boundary layer is greater than it would be with a natural laminar boundary layer (see Fig. 5). For example the skin friction coefficient of a flat plate with chord Reynolds number of 50×10^6 would be only 0.0002 with a hypothetical natural laminar boundary layer, but with boundary layer suction it would be 0.0010 assuming uniform inflow and a suction coefficient $C_Q = 0.0005^*$.

At the same chord Reynolds number the skin friction coefficient would be 0.0023 with a turbulent boundary layer assuming transition near the leading edge (see Fig. 6). So laminar flow control by suction could reduce the drag coefficient by 0.0013 which is about 60% of the reduction that natural laminar flow would confer. Thus from the point of view of low drag, the boundary layer should not be thinned more than is necessary to keep it laminar. Thinning the boundary layer still more increases skin friction, and consequently the drag penalty of the increased suction flow, with its attendant flux of momentum change, more than outweighs the reduced wake. The emphasis should therefore be on maintaining laminar flow and not on reducing the size of the wake.

So far these notes have been concerned with drag and how, in principle at least, it can be reduced by laminar flow control. The drag reduction offered by laminar flow control can best be exploited to reduce aircraft fuel consumption, thus enabling greater distances to be flown by an aircraft capable of lifting a given fuel load, or reducing the fuel used by an aircraft flying a given stage. The reduction of fuel consumption has, of course, always been sought by designers of aircraft and engines, and the long term trend has been always towards reduced fuel consumption. It is true that from time to time an increase in fuel consumption has been accepted (to enable the attainment of greater speed) but then the struggle to reduce fuel consumption has recommenced with intensified efforts.

The main incentive to reduce aircraft fuel consumption is the increased payload that may be carried by an aircraft of given size over a stipulated stage length. The

*The suction coefficient C_Q is defined in Fig. 4. It would not need to be as high as this to stabilise the laminar boundary layer on a flat plate, but a swept wing at full scale Reynolds number would require an overall suction coefficient approaching 0.0005.

greater the stage length the stronger this incentive becomes because the weight of fuel that has to be lifted at the commencement of flight increases and so the payload fraction gets smaller. The payload fraction has a powerful effect on the economics of an aircraft, and so apart from making longer range flight possible, reduced aircraft fuel consumption can greatly improve operating economics by increasing the payload fraction. Certainly part, and possibly all, of the reduction of operating cost would be due to the lower cost of the fuel consumed (the magnitude of this effect depends on the price of fuel and clearly rising fuel prices in the last few years must have increased the benefit of laminar flow control). But for long and very long stage lengths a laminar flow aircraft could have a lower basic operating weight (see Fig. 7) and a lower first cost.

The desirability of attaining low operating costs provides a good reason for the pursuit of low aircraft fuel consumption. This is not to argue that the lowest possible fuel consumption should be sought since attaining the lowest fuel consumption could increase operating costs in other ways. But concern about the availability of fuel and the need to conserve fuel resources provides an additional incentive to reduce fuel consumption.

1.2 The concept of momentum restoration

As well as depending on its drag an aircraft's fuel consumption depends on the thermal efficiency of its power plant and on the effectiveness with which the power developed is used to overcome its drag. Laminar flow control makes it possible to improve this effectiveness and thereby enables a greater reduction in fuel consumption than would be inferred from the reduction in drag that has already been touched on. The circumstance that makes this possible is the existence of the sucked mass flow. With laminar flow control most of the friction drag is balanced by the flux of momentum change in the sucked mass flow. It follows that the thrust that could be developed by restoring the sucked mass flow to its original momentum would very nearly counteract the whole of the friction drag. It can be shown that the power required to do this is only half the power that would be required to generate the same thrust in the most efficient conventional propulsive system, that is to say, one half the power required by a system with Froude efficiency of 100%.

The principle involved can be demonstrated very simply as follows. Consider a propulsion system with air entering at the undisturbed pressure of the stream and speed U_1 and leaving at the same pressure and speed U_2 . Consideration of momentum leads to the equation

$$\text{Thrust per unit mass flow} = U_2 - U_1$$

In an ideal system the power required would be equal to the rate at which kinetic energy is added, so

$$\begin{aligned} \text{Power required per unit mass flow} &= \frac{1}{2} U_2^2 - \frac{1}{2} U_1^2 \\ &= (U_2 - U_1)(U_2 + U_1)/2 \end{aligned}$$

$$\text{Hence} \quad \text{Power required per unit thrust} = (U_2 + U_1)/2$$

The last two equations are the key since they show that the power required is equal to the product of the thrust developed and the average speed of the propulsion system mass flow relative to the plate. Thus the lower the average speed of the flow through the propulsion system, the less power is required per unit thrust.

The thrust equation shows that U_2 must be greater than U_1 for positive thrust to be generated but the value of U_2 can be allowed to approach U_1 . As it does so the mass flow of the propulsion system must increase tending to infinity in the limit. Thus the limiting case is not a practical one but it shows that the

$$\text{Least power per unit thrust} = \frac{1}{2} (U_1 + U_1) = U_1$$

In the conventional situation the initial speed U_1 of the air approaching the propulsion system is the stream speed U_0 so for this case the

$$\text{Least power per unit thrust} = U_0$$

The expression for propulsive efficiency attributed to Froude was derived for this case and is generally defined as

$$\text{Froude efficiency} = \frac{\text{Thrust} \times U_0}{\text{Power}} \times 100\% = \frac{2 U_0}{U_0 + U_2} \times 100\%$$

So the least power found above corresponds to a Froude efficiency of 100%.

In the laminar flow control case postulated above, where the suction mass flow is restored to its original momentum, the initial speed U_1 is zero and the final speed U_2 is equal to the speed U_0 of the undisturbed stream (see Fig. 8). Thus the

$$\text{Power required per unit thrust} = \frac{1}{2} (0 + U_0) = \frac{1}{2} U_0$$

So the power required is halved, and moreover this is achieved with the finite mass flow of the suction system instead of with an infinite mass flow.

Of course, the principle responsible for the power saving does not only apply in the case of laminar flow control. In any situation where drag is experienced as a result of viscous interaction, savings would be effected in the power required for pro-

pulsion if each element of the flow were to be restored to its original momentum. But the saving would not be proportionately as great. For example, if the wake from a turbulent boundary layer* were to have its momentum restored in this way before any viscous interaction could occur in the wake, the power required would only be reduced to 9/10 instead of to 1/2 as found above for the restoration of the momentum of a sucked mass flow. And apart from the theoretical savings being smaller, great practical difficulties would beset any attempt to restore the momentum of a boundary layer wake. The only possible exception would be in the case of a body such as a fuselage at zero incidence. But it is clearly very much simpler to act on a sucked mass flow which can be ducted with very low losses to one or more powered fans.

If suction were to be applied, not to keep the boundary layer laminar, but merely to thin a turbulent boundary layer so as to leave only a thin wake, the surface friction would be very high (i.e. very much higher than for an unsucked turbulent boundary layer). Consequently the flux of momentum change in the sucked mass flow would be very large (i.e. the sucked mass flow itself would be much larger than in the case of laminar flow control). As a result, the power required for propulsion would be very large even though halved by restoring the momentum of the sucked mass flow. Thus it is important to maintain laminar flow as well as to restore the momentum of the sucked mass flow.

Before leaving the propulsion aspect of laminar flow control it is perhaps worthwhile to attempt a physical explanation for the power saving that has been shown to be possible by the restoration of momentum. To avoid complication the flat plate will again be considered and first it will be studied from a stationary viewpoint so that the air is seen to be at rest everywhere except where it has been disturbed by the passage of the moving plate. Suppose that the plate is propelled by a force F . The speed V of the plate will tend to that value at which the drag due to skin friction balances the propulsive force. At that speed the entire propulsive force is transmitted by skin friction to the air in contact with the plate and from there its influence spreads through the boundary layer, tending to draw the air in it along with the plate. At any instant, every element in the boundary layer is having momentum imparted to it at a rate equal to the net force acting on it, and the sum of the net forces acting on all the elements of the boundary layer is, of course, equal to the propulsive force F .

Consider one such element. Let its mass be Δm and suppose that at a particular instant it is moving in the same direction as the plate with speed v and being acted on by a net force ΔF (see Fig. 9). The instantaneous rate at which the element of propulsive force ΔF is doing work on the plate is $\Delta F V$ and all the work it does must appear as energy added to the air through which it is moving since the plate itself is moving at a steady speed. The rate at which the momentum of the element is being increased is given by

$$\Delta F = \frac{d}{dt} (\Delta m v) = \Delta m \frac{dv}{dt}$$

and the rate at which its kinetic energy is being increased is therefore

$$\frac{d}{dt} \left(\frac{1}{2} \Delta m v^2 \right) = \Delta m v \frac{dv}{dt} = \Delta F v$$

So the rate at which kinetic energy is being added is only a fraction v/V of the rate at which energy is being added by the force ΔF to the flow as a whole. The rest is dissipated by friction and appears as heat.

This dissipation of energy occurs because the force ΔF is transmitted from the surface of the plate to the element on which it acts (i.e. as a net force) by shearing stresses in intervening elements of the boundary layer. The rate at which heat is generated by this shearing action, being the difference between the rate at which the element of propulsive force ΔF does work on the plate and the rate at which it adds kinetic energy to the boundary layer, is equal to $\Delta F(V - v)$. This shows that most of the work done by the net force which acts on an element of flow near the outer edge of the boundary layer is dissipated by friction, but that hardly any of the work done by the net force which acts on an element of the flow much closer to the surface is dissipated by friction.

The ratio v/V is the instantaneous efficiency with which the thrust work being done by the net force acting on an element with speed v is being converted into kinetic energy. It can be shown that between the time an element of flow enters the boundary layer and the time it reaches speed v , the overall efficiency with which the work done by the net force that has acted on it is converted into kinetic energy is equal to $v/2V$.

The steady rate at which kinetic energy and heat energy are added to the whole boundary layer may be found by summing the instantaneous rates at which they are being added by the net forces associated with all the elements in the boundary layer, or alternatively by integrating the kinetic energy and heat energy through the mass flux leaving the boundary layer both at the trailing edge of the plate and through its surface. In the case of laminar flow control at flight Reynolds numbers and with near full chord laminar flow, practically half of the thrust work appears as kinetic energy because most of the flow is sucked mass flow which has all come from the part of the boundary layer adjacent to the surface. In the case of a turbulent boundary layer with a 1/7 power law velocity profile the proportion of thrust work that appears as kinetic

*A 1/7 power law velocity profile has been assumed.

energy is only 1/10, and 9/10 of the energy appears in the boundary layer as heat energy.

Whilst still retaining the stationary viewpoint adopted above, consider the power that would be required and the propulsion force that could be developed by restoring elements of mass to their original momentum. Consider an element of mass Δm leaving the boundary layer with speed v_1 . A constant propulsive force ΔF_1 could be developed for a time $\Delta t = \Delta m v_1 / \Delta F_1$. During the time Δt the plate would travel a distance $V \Delta t$ and the mass element would travel $v_1 \Delta t / 2$ in the same direction. Hence the distance through which the force ΔF_1 acting between the mass element and the plate would have to extend is $(V - v_1/2) \Delta t$ and the energy that would have to be supplied would be $\Delta F_1 (V - v_1/2) \Delta t$ which could also be written $\Delta F_1 V - \Delta m v_1^2 / 2$. Clearly the first term represents the thrust work done by the force ΔF_1 on the plate, and the second term represents kinetic energy recovered from the mass element when it is returned to its initial state of rest.

To maintain the propulsive force ΔF_1 indefinitely instead of for time Δt the propulsion system would require a succession of mass elements with initial speed v_1 at time intervals Δt . Alternatively a steady mass flux $\Delta \dot{m}$ with initial speed v_1 would produce a steady thrust $\Delta F_1 = \Delta \dot{m} v_1$ and require power input $\Delta P = \Delta F_1 (V - v_1/2) = \Delta \dot{m} V - \Delta \dot{m} v_1^2 / 2$. Summing for all the elements of mass flux restored to their original momentum shows that the resulting total thrust F_1 is equal to $\sum \Delta \dot{m} v_1$ and that the power input required is $P = F_1 V - \Delta \dot{m} v_1^2 / 2$. If all the flow with momentum affected by the passage of the plate were to be restored to its original state of rest, the thrust developed F_1 would be equal to the thrust required to propel the plate F , and the term $\sum \Delta \dot{m} v_1^2 / 2$ would be the total flux of kinetic energy developed in the boundary layer. Thus all the kinetic energy developed in the boundary layer at the expense of part of the thrust work required to propel the plate would be recovered. The flow discharged by the propulsion system would only contain the heat energy generated in the boundary layer and would not contain any kinetic energy. By this means the power required for propulsion would be minimised since the power input would only have to make good the energy dissipated in the boundary layer.

It is interesting to contrast the foregoing observations with what would be seen by an observer at a viewpoint moving with the plate. This is the more familiar viewpoint of an observer in a wind tunnel or in an aircraft, and it is also the viewpoint which is often most convenient for theoretical analyses of flow. If both observers are facing in the same direction, and if the stationary observer sees the plate moving from right to left, it will appear to the moving observer that the plate is standing still in a current of air moving from left to right. The speed U of the airstream seen by the moving observer is equal to the speed V of the plate as seen by the stationary observer, though of course it is directed in the opposite direction. The rate of change of momentum of elements of air in the boundary layer does not depend on the viewpoint of the observer and so where the stationary observer sees a mass element in the boundary layer acquiring speed v , the moving observer sees the same mass element losing speed, i.e. its speed decreases from U to u where $u = U - v$. Thus instead of the change of momentum being associated with an increase of kinetic energy equal to $\Delta m v^2 / 2$ as seen by the stationary observer, the moving observer associates it with a loss of kinetic energy equal to $\Delta m (U^2 - u^2) / 2$ (see Fig. 10).

Another striking difference is that whereas the stationary observer sees the thrust F doing work on the plate, and hence also on the boundary layer, at the rate FV to the moving observer it does no work on the plate at all because it is not moving, and hence it does no work on the boundary layer either. To the moving observer the heat generated in the boundary layer is balanced by the loss of kinetic energy in the boundary layer so that the total energy in the boundary layer remains constant, and this is consistent with the thrust force not doing any work on the boundary layer. As seen by the moving observer the power required by the propulsion system to restore all the mass elements to their original momentum is the power required to make good the loss of kinetic energy they have suffered, and it is therefore equal to the rate at which heat is generated in the boundary layer. This is what the stationary observer also found.

Thus the power required for propulsion, and the rate at which heat is generated in the boundary layer do not change with the viewpoint of the observer. But if the two observers were to draw up balance sheets to show the power inputs and outputs of the processes taking place in the boundary layer and the propulsion system they would differ about all the other items, and they would differ notably about thrust work. This difference in their assessment of thrust work demonstrates that the concept of thrust work as being the useful output of a propulsion system is dubious and suggests that it is not a satisfactory basis for defining propulsive efficiency. This was already apparent from the discovery that the power required for propulsion by the restoration of momentum was less than the power required for a propulsion system with a Froude propulsive efficiency of 100%, and that with laminar flow control it could be as little as half as much.

In the case of systems, such as propulsion systems, where all the energy is dissipated and there is no useful output, it would be better to define efficiency in terms of the minimum power input of an ideal propulsion system thus

$$\text{Efficiency} = (\text{ideal minimum power input}) / (\text{actual power input}) \times 100\%$$

The ideal system could then be specified. For an aircraft with air breathing engines

and without boundary layer propulsion (momentum restoration) it would be reasonable to adopt the Froude ideal in which only undisturbed air is regarded as being available for propulsion. But with boundary layer control the ideal should take into account the momentum of any boundary layer air considered to be available for propulsion.

For an aircraft with laminar flow control the benefit of restoring the momentum of the sucked mass flow would be so great, and in practice it would be so easy to achieve, that it is virtually certain momentum restoration would be exploited. The precise magnitude of the benefit depends on details of the aircraft and power plant, but, in the light of the foregoing discussion, it is clear that the power required to overcome the drag of surfaces on which laminar flow control is exercised could be halved, or better than halved, and so it is reasonable to suppose that the fuel consumption also could be halved. Indeed from the point of view of fuel consumption, it would be as if the drag of any laminarised surfaces were to be halved. This suggests that a convenient way of expressing the combined benefits of laminar flow control and suction mass flow momentum restoration would be by defining an equivalent drag which would reflect the propulsion power requirement.

If this is done for the flat plate considered earlier, and assuming that momentum restoration only halves the power requirement, the following comparison is obtained.

With chord Reynolds number = 50×10^6 ,

skin friction coefficient with turbulent boundary layer	= 0.0023
skin friction coefficient with laminar flow control	= 0.0010
effective skin friction coefficient with laminar flow control and momentum restoration	= 0.0005
skin friction coefficient with a hypothetical natural laminar boundary layer	= 0.0002

Thus in this example, with momentum restoration as well as laminar flow control the effective drag would be less than 22% of the drag with a turbulent boundary layer, the effective reduction of drag being 85% of the difference between the drag with a turbulent boundary layer and the drag with a natural laminar boundary layer. Fig. 11 shows how the relative importance of momentum restoration increases as chord Reynolds number is increased. The prospect of such a large reduction of drag certainly warrants some consideration being given to what would be involved in the exploitation of laminar flow control and momentum restoration principles.

1.3 The concept of transport aircraft with laminar flow control and momentum restoration

The maintenance of laminar flow on a transport aircraft fuselage would be made difficult by the presence of such features as nosewheel doors, pilot's windscreen, passenger doors and windows, doors for baggage and freight, the wing roots, etc. Moreover, the shape of a fuselage, being long in relation to its perimeter, is such that even a single turbulent wake starting from a point far forward would affect a significant fraction of its total surface area. The wings and possibly also the tail surfaces appear more amenable to treatment, and as they account for half, or more than half, of the total wetted area of a transport aircraft, a drag reduction of at least 40% might be anticipated (see Fig. 12). This would involve some increase of span to keep the induced drag in a reasonable relation to the friction and form drag. It is likely that a laminar flow control aircraft would have a somewhat lower loading per unit wing area than a conventional aircraft because with their lower effective drag there is less incentive to reduce the size of the wings. Moreover the provision of high lift devices on a laminar flow wing poses special problems and a lower wing loading would help by rendering powerful leading edge devices unnecessary as well as by permitting smaller rear flaps to be used. With the reduced wing loading as well as increased span, the aspect ratio will be higher, though perhaps not very much higher, than for a conventional transport aircraft.

The main elements of a laminar flow system would be special suction surfaces, ducting, pumping installations and discharge nozzles, controls, and instrumentation (see Fig. 13). The suction surfaces would embody means for the withdrawal of air from the boundary layer on their outer sides and for its collection in shallow compartments on their inner sides. The ducts would convey the sucked air from these compartments to the suction pumps. To enable restoration of the momentum of the sucked mass flow the suction pumps would have a higher pressure ratio than would be necessary for laminar flow control alone. The discharge nozzles would convert the extra pressure into velocity (i.e. relative to the aircraft) so that the sucked air could be discharged rearwards at a relative speed probably somewhat in excess of the forward speed of the aircraft.

The function of the controls would be to regulate the distribution of inflow as well as to adjust the overall suction mass flow rate to suit the flight conditions. The controls would have to be designed to cope with situations that could arise following a failure, for example failure of a suction pump. In such an eventuality it might be necessary to isolate the failed pump and prevent reverse flow through it. The controls might be designed to enable the suction flow to be redistributed to the remaining pumps and to operate them at higher speeds and perhaps with their discharge nozzles opened to reduce the back pressure and so enable increased flow. If the increased flow that could be attained were to be insufficient, the system might be designed to enable

suction to be shut off completely from some parts of the suction surfaces so as to enable an effective rate of suction to be maintained on the remainder. In these circumstances the areas shut down should be chosen so as to minimise the adverse effects, i.e. recognising that the payoff for suction will not be so high in some areas as in others. It is not the intention to suggest that the control system would inevitably exhibit all these features, but they are mentioned to illustrate the kinds of considerations that could arise. In any case, it must be apparent that instrumentation would be required to monitor the working of what would inevitably be a complex system.

Clearly a laminar flow control system would be an extensive system affecting many aspects of design. The interaction with the choice of high lift system has been touched upon. The attainment of an acceptable standard of surface finish too is not merely a matter of the design of the suction surfaces. The waviness of the surface of a completed wing depends also on the design of the whole wing structure and on the method of manufacture of the components and their assembly. Laminar flow control would also pose serious problems in relation to access and force the designer into difficult compromises. The provision of such a system, with all that it implies, would clearly involve a mass penalty to be set against the reduced mass of fuel. It would also add to the cost of design, development, and manufacture, and hence to the first cost of an aircraft with laminar flow control, and would involve additional maintenance costs. All these additional costs would have to be set against the reductions in the cost of the fuel consumed.

However, except for short design stage lengths, the reduced rate of fuel consumption associated with the reduced effective drag would enable a reduction in the mass of fuel required for the design mission which would more than compensate for the mass of the laminar flow control system, and therefore the take-off mass for the design mission would be reduced. For longer design stage lengths savings could be made in the structure mass, a smaller and hence lighter power plant would suffice, the wing could be reduced in size, the laminar flow control system would get lighter, the drag less, and so on. Taking all these effects and their interactions into account, an aircraft with reduced basic operating weight would be found as shown in Fig. 7. Its reduced size would lead to reductions in the cost of structure, powerplant, etc., and these reductions would help to offset the cost of the laminar flow system which could itself be reduced by the scaling process, and there would also be savings in the cost of maintenance. In addition, the scaling down process would enhance the reduction of fuel consumed and hence increase the saving in the cost of fuel. The scaling down process therefore has a favourable effect on the net benefit.

It can be seen that the savings in fuel consumption and the reduction of operating costs made possible by laminar flow control are dependant on the design stage length. It would be equally correct to state that they depend on the fuel fraction of a conventional aircraft for the same design stage length, since the benefits all stem in the first place from reductions in the fuel that has to be carried. Thus other advances in technology that would reduce the fuel fraction of a conventional aircraft lessen the benefits made possible by laminar flow control. Advances which could lead to reductions in engine fuel consumption should therefore be taken into account in any appraisal of the future of laminar flow control.

Before turning from these general aspects of laminar flow transport aircraft it seems worthwhile to draw attention to a significant difference between the range-payload characteristics of conventional and laminar flow aircraft. At ranges exceeding the maximum range with full payload, the payload that can be carried is reduced by an amount equal to the additional fuel required to fly the extra distance. This reduction in payload causes the direct operating cost per unit of payload to increase. The additional fuel required by an aircraft with laminar flow control would clearly be less than the additional fuel required by a conventional aircraft, and so the payload it could carry would not be reduced as much as that of a conventional aircraft (see Fig. 14). Consequently, the relative increase in the direct operating cost would be less for the laminar flow aircraft than for the conventional aircraft (see Fig. 15) and so the benefit of laminar flow increases at ranges greater than the maximum range with full payload. The same would only be true for ranges less than the maximum range with full payload in instances where the design stage length is very long. In such cases the laminar flow aircraft would have a lower basic operating weight than the conventional aircraft and could cost less and have lower annual and maintenance costs as well as lower fuel costs. It follows that it would have lower operating costs than the corresponding conventional aircraft at ranges shorter than the maximum range with full payload, and hence at all ranges. This may not be true of comparisons between laminar and conventional aircraft designed for shorter stage lengths since if the design stage length is short enough the laminar flow aircraft could have a higher first cost than the conventional aircraft and bigger annual and maintenance costs. In this case its operating cost could only be less on account of lower fuel costs and this advantage would decrease if the aircraft were to be operated at ranges less than the maximum range with full payload.

2. EXPERIENCES

2.1 Suction surfaces

Having briefly discussed laminar flow control by suction, its close connection with propulsion by momentum restoration, and the possible application of these two principles in conjunction to transport aircraft, it is time to consider in somewhat greater detail what is involved in laminar flow control and to relate this to some actual experiences. For the most part the experiences will be ones with which the author was closely concerned, though other work will be referred to where it is particularly

relevant or for the sake of continuity. It is hoped by this approach to convey some feeling for the subject and the sort of problems it throws up. Difficulties that were encountered will not be minimised. It is stressed that the following account should not be construed as a balanced review of British work on laminar flow control. The author disclaims any intention of reviewing British work as a whole and the American work is only mentioned by the way.

It is appropriate to begin by considering suction surfaces. With distributed suction the inflow velocities required for laminar flow control are very small, only a few thousandths of the speed of the aircraft, and clearly such small inflow velocities have no direct effect on the external pressure distribution. This is practically true of any of the suction surfaces to be discussed. Satisfactory suction surfaces have been devised which, whilst they do not, strictly speaking, provide distributed suction, nevertheless produce some approximation to distributed suction. Although it is not essential that the suction should be continuously distributed it is essential that the air is withdrawn through the surface in such a way that unacceptably large disturbances are not introduced into the boundary layer. The suction surface must be smooth. The thinned laminar boundary layer is not less susceptible to roughness effects and in fact its high rate of shear at the surface can make it more susceptible to roughness. The surface should be relatively wave-free.

The inflow distribution must approximate closely to an ideal distribution. Excessive inflow in any region will thin the boundary layer more than necessary and as well as being uneconomical it also increases sensitivity to roughness. Too little inflow in any region could result in turbulence developing. The turbulence will persist aft of the under-sucked region as well as spreading laterally to a greater or lesser extent. Inflow velocities intended to control the laminar boundary layer have relatively little effect on a boundary layer that has become turbulent and so suction applied in regions into which turbulence has spread will be ineffectual and wasted.* The very low inflow velocities required make it difficult to avoid irregularities in the inflow distribution. On the inside of the suction surface there would be a number of compartments in which flow velocities are kept small so that the variation in pressure within any one compartment is rather small. Nevertheless there would be some variation of pressure within a typical compartment and some variation of external pressure over it even though its boundaries would be defined with due regard for the external pressure distribution (its greatest dimension would be chosen to be more or less parallel with the general direction of the pressure isobars on the exterior surface).

If the pressure loss through the surface is not great enough gross distortions will occur in the inflow distribution of the area overlying one compartment even to the extent that there could be local outflow in some places when the total inflow has the desired value. Porous sintered metal surfaces could have had a high enough loss coefficient but were much too heavy except for experimental purposes. Porous sintered plastics were considered but suffered from low resistance to abrasion and also deteriorated in sunlight (they were affected by ultra violet radiation). There were also problems in obtaining porous metal or plastic with sufficiently uniform flow resistance or in large enough sizes.

An alternative which was used experimentally was a woven material. The pressure drop through a woven material is not sufficient to ensure a reasonable inflow distribution over the area overlying each compartment and it was necessary to evolve a method for increasing the loss coefficient of the surface. The method adopted in a number of early experiments made use of a system of cells immediately under a woven surface. The suction flow having passed through the woven surface into the cells next passed through small throttling holes (one to each cell) to reach the compartment underneath the suction surface (see Fig. 16). Most of the pressure drop occurred in the throttling holes and the pressure drop through the woven material had only to be sufficient to spread the inflow over the area of one cell. The cells in the surface over which the woven material was stretched were formed by a system of raised lands and, to provide additional support for the woven material, some additional lands might project like fingers into the cells.

2.2 Experiments with unswept wings

In flight experiments conducted by M.R. Head at Farnborough in 1953 rolled Monel cloth was used for the exterior covering but it was found that this surface picked up and held roughness and it was found to be necessary to cover the rolled Monel cloth with nylon. Successful results were obtained in flight with this surface, full chord laminar flow being achieved at chord Reynold's numbers approaching 30×10^6 and up to Mach numbers close to the critical Mach number of the section? The surface was not a practical one and the Monel cloth was heavy, but the tests were the first demonstration in flight of the feasibility of maintaining full chord laminar flow in full scale conditions. These tests were completed in 1954.

An attempt was then made to develop a more practical surface. The possibility of using a perforated metal sheet was explored and tests were carried out to determine the largest size and spacing of perforations. Holes with 0.18 mm (0.007 in.) diameter,

*It is possible to re-establish laminar flow behind a region of turbulence but the suction rates required are high and may not be feasible with some of the surfaces considered.

spaced 2.5 mm (0.1 in.) apart in both spanwise and chordwise direction, were found to work as well as the porous surface but satisfactory results were not obtained using 0.51 mm (0.020 in.) diameter holes. The latter was the smallest size of hole that could be made by normal perforating methods and it appeared necessary to drill the large number of holes. A surface was manufactured with holes of 0.23 mm (0.009 in.) diameter drilled every 2.5 mm (0.1 in.) i.e. about 160,000 holes per square metre (100 per in²) of surface area. The open area ratio with this surface was about 0.6%. Despite the promising results obtained in exploratory tests with a hand-made surface the machine-made surface did not work well when it was first fitted.

Before discussing the reasons for this failure another type of surface evolved from the porous ideal will be discussed. This surface was developed at the same time as the surfaces already described. In 1949 Dr. G.V. Lachmann of Handley Page Ltd. suggested a form of suction surface embodying spanwise strips of porous material let into an otherwise impervious surface (see Fig. 17). A surface was constructed having porous strips of sintered metal. The porous strips were relatively thick and the pressure drop through them was sufficient to achieve a good inflow distribution. As well as thinning the boundary layer the relatively concentrated inflow through the strips produced a very stable boundary layer profile. Before reaching the next strip downstream, the boundary layer thickened and its velocity profile deteriorated but even if its stability was allowed to become marginal, there was insufficient time for disturbances to grow before the next strip was reached.

A model wing with a chord of nearly 2.5 m (actually 8 ft.) was constructed.⁶ It had 14 porous strips. The strips were not equally spaced, but were closer together near the trailing edge where they were about 10 cm (4 in.) apart. The model was tested at the National Physical Laboratory (NPL) early in 1951. Laminar flow to 95% chord was achieved at a chord Reynolds number of 9×10^6 in the first few tests and subsequently the Reynolds number was improved to 15×10^6 (235 ft/sec tunnel speed). Based on this successful experiment Lachmann proceeded to what was intended to be a flight demonstration.

For the flight tests a suction surface embodying the same features as in the successful wind tunnel model was built on to a section of the wing of a de Havilland "Vampire" jet aircraft (the two-seater trainer version). Tests with this surface were very disappointing for a number of reasons, some of which were not understood for a considerable time. The first problem stemmed from practical causes. It was soon realised that the maintenance of smooth joints at the edges of the Porosint strips presented greater problems on an aircraft wing which deformed under load in flight than was the case with a wind tunnel model. This problem was sufficiently serious for an alternative construction to be sought, eliminating the need for so many joints.

The possibility of employing bands of holes in place of porous strips was explored in tunnel tests at the NPL and at the Royal Aircraft Establishment (RAE). In the earlier tests at the NPL, single, double and multiple rows of holes were tested with various pitch to diameter ratios, and staggered multiple rows of holes were found to be the best. The original wind tunnel model was refurbished for test at the RAE. In these tests the perforated strips were backed with felt to achieve a reasonably uniform inflow. The felt backing was not considered to be a practical proposition and so some tests were also done with a small individual throttling hole in the bottom of each large hole. Although this was successful, it was felt that it invited clogging and was not adopted.

A composite surface embodying a cell system was adopted for the surface with which the flight tests were resumed (see Fig. 18). Each suction strip in the new surface had three rows of cells which were staggered, and each row of cells had three rows of holes in a staggered pattern. Twenty-one holes fed into each cell and the suction flow then passed to the interior ducts through a single throttling hole. The size of the holes in this surface was about 0.8 mm (0.03 in.) diameter and they were spaced at a pitch diameter ratio of about $2\frac{1}{2}$. The throttling holes were about the same diameter as the holes in the surface. The overall width of the band of perforations was about 20 mm (0.75 in.) so the open area ratio of the exterior surface within the band was about 11.8%. The bands of perforations were more closely spaced than the porous strips had been. On the reconstructed surface for the flight test there were thirty-nine strips of perforations. Over the rear half of the surface the gaps between the strips of perforations was about 30 mm (1.25 in.), so that in that region the overall open area ratio for the surface was about 4.4%. Thus compared to Dr. Head's drilled surface with an open area ratio of 0.6% the velocity of the air into the surface was much lower.

With this surface better results were obtained, laminar flow being achieved with full repeatability up to more than 80% chord at unit Reynolds numbers up to nearly 6.5×10^6 per m (2×10^6 per ft.) which corresponded to a chord Reynolds number of about 15×10^6 . In relation to roughness the unit Reynolds number is more significant than chord Reynolds number, and the unit Reynolds number achieved in these tests was close to that which would be encountered by a transport aircraft at cruise conditions, being, in fact, the unit Reynolds number at the tropopause at a speed of $M = 0.864$ in standard conditions (see Fig. 19). Both Head's and Lachmann's experiments were conducted on wings of near zero sweep though, on account of taper, the leading edge was swept back and the trailing edge swept forward. So in the flight tests the flow was far from two dimensional and it was to this cause that the difficulties still experienced in Lachmann's flight work, even after the new perforated surface was fitted, were eventually attributed. But the surface developed was a big step towards a practical form of suction surface.

This work brought home to us the difference between tunnel and flight conditions and the importance of devising a surface which would be free from deterioration when subjected to repeated flight loads. Another lesson that was learnt was the need for adequate instrumentation. In Lachmann's earliest tests in the NPL tunnel, in which success was so easily achieved, the possibility to vary wing incidence and speed independently of one another made things much simpler than in flight where speed and incidence were related through the aircraft lift coefficient. If the flight speed was too low the aerofoil pressure distribution exhibited a suction peak near the leading edge which led to turbulence ahead of the first strip of perforations, while if the speed was too high the increased suction requirement exceeded the capacity of the suction pump. In the tunnel, sublimation methods could easily be used to reveal regions of laminar flow and regions of turbulence. Although a sublimation method could also be used in flight, and was used on a number of occasions, the technique was difficult and therefore not so useful.

In retrospect it became clear that insufficient thought had been put into the provision of instrumentation and it is probable that the rapidity with which success came in the first tunnel tests at NPL led to overconfidence when the flight tests were first planned. It is true also that the level of expenditure, and consequently also the level of effort available, was at a relatively low level in all of this work. At any rate progress was made rather slowly and painfully and only as instrumentation and techniques which could be used in flight were devised and brought into use. A pitot comb which could be traversed fore and aft on the centre line of the test panel was eventually developed (see Fig. 20) and became a source of much useful data for analysis and comparison with calculation, and here it is perhaps worth stressing the importance of theoretical calculations for comparison with flight measurements if a proper understanding is to be achieved. However, a stethoscope mounted on the same traversing carriage was of greater use to the flight observer in making adjustments to the suction distribution since by means of it he could hear whether the boundary layer was laminar or turbulent and also detect the beginning of any breakdown.

With the development of the fore and aft traversing gear there was a tendency to rely on it exclusively and in one instance this led to a series of tests during which progress was temporarily halted due to an unsuspected phenomenon. The cause of the trouble would have been discovered very quickly had there been gear to enable instrumentation to be traversed across the panel from side to side. In later work on a different wing such instrumentation was developed and proved of great use. In this instance however, the problem was tracked down by a sublimation test which showed that the boundary layer on the outboard half of the panel was turbulent right from the leading edge, although the transition front was well aft on the inboard half of the panel. The fore and aft traversing instrumentation was just inside the turbulent half of the panel.

The cause of this phenomenon was an external fuel tank mounted under the wing a short distance outboard of the outboard end of the test panel. This had been fitted to increase the duration of flight which was rather short, some of the internal fuel tanks having been removed to make space for the suction plant. Clearly the interference effect of this external fuel tank affected the pressure distribution in the vicinity of the leading edge to a sufficient extent to cause premature transition on rather more than the outer half of the test panel. This was another reminder that the flow in the flight tests was not as close to two-dimensional flow as that in the tunnel experiments, and that three-dimensional effects should not be overlooked.

2.3 Three-dimensional effects

The importance of three-dimensional effect had already been demonstrated in some work which was not concerned with laminar flow control by suction but rather with the attainment of the maximum extent of laminar flow purely by geometry, that is to say, by means of a low drag aerofoil having a favourable pressure gradient extending well aft. An aeroplane having such low drag aerofoil sections was the subject of flight experiment at the Royal Aircraft Establishment in 1951. This was the Armstrong Whitworth AW52, a jet-engined tail-less aircraft. The centre section of its wing had an unswept leading edge but the leading edge of the outer wing panels was swept back at a moderate angle. Even with the surface of the wing filled so that it was smooth and substantially wave-free, it was found to be impossible on the outer wings to achieve the extent of laminar flow for which the section was designed. But behind the unswept leading edge of the centre section of the wing, transition could be far back. This was reported by W.E. Gray late in 1951⁴.

Using sublimation techniques Gray was able to obtain pictures showing the jump in transition position at the spanwise station where the leading edge sweep changed. Gray went on to carry out a remarkable series of flight tests in which he obtained visual records of transition on the swept back surfaces of a variety of high speed aircraft. These records showed that for sufficiently large angles of sweep, transition occurred very close to the leading edge. The work was reported by Gray in February, 1952. Gray was subsequently able to obtain records showing closely spaced striations and these suggested that streamwise vortices were present in the laminar boundary layer and were the cause of the premature transition. It was in this manner that the occurrence of the laminar boundary layer instability associated with cross flow was discovered. Cross flow develops in the boundary layer in any region where the paths of streamlines projected onto the surface exhibit curvature, (see Fig 21) as is the case on swept wings or low aspect ratio wings.

The failure to achieve full chord laminar flow with Lachmann's perforated strip suction surface was attributed to flow curvature effects which had not been taken into account in its design. Although the wing as a whole was unswept, it was highly tapered and the test panel conformed to the wing taper. Consequently, the leading edge was swept back and the trailing edge was swept forward, and streamlines projected on to its surface showed significant curvature.

The direction of the flow over the surface in relation to the pattern of holes also turned out to be the cause of the failure experienced with Dr. Head's drilled panel. It was found that this type of surface exhibited a marked sensitivity to the direction of the flow over it. The inflow velocity into the very small holes was large enough to create a local disturbance which trailed downstream. If the flow direction was such that the disturbance was carried over a second hole before it had decayed sufficiently, the disturbance caused by the second hole could interact with the residue of the disturbance from the upstream hole. Even if the streamlines projected on to the surface had been straight and parallel, a large number of possibilities would have existed, the worst of which would have been if holes in successive rows had been in line, the second worst if holes in alternate rows had been in line, and so on.

It transpired that Head's drilled panel had been fitted at an angle differing from that of the earlier handmade surface by a small amount. The resulting small change in orientation of the pattern of holes was responsible for the disappointing results. The very regularity of the hole pattern on the machine drilled panel may have contributed to this dramatic change in behaviour, the earlier handmade panel having some small random variations in the positions of the holes. A second panel was drilled and fitted at a carefully chosen angle, and with this surface full-chord laminar flow was obtained, the repeatability being entirely satisfactory. The surface did, however, still show a degree of sensitivity to over suction, and with the total inflow quantity 50% greater than the minimum required for full chord laminar flow, transition moved forward to about 90% of the chord. The composite surfaces evolved by both Head and Lachmann were robust and demonstrated the possibility of practical construction.

Gray's discovery raised the question whether laminar flow control would be feasible on swept wings. In fact Gray very quickly demonstrated that a laminar boundary layer could be established by means of a large forward facing slot close to the leading edge which ingested the whole of the thin but already turbulent boundary layer. Theoretical studies by Owen and Randall at the RAE¹⁰ supported by wind tunnel observations as well as Gray's flight results led to a limited understanding of the problem, and it was predicted that suction close to the leading edge should be capable of preventing transition by keeping the boundary layer thin enough to suppress the instability.

It was clear that if laminar flow control were to be attempted on swept wings two penalties must be faced. One was the need to carry the suction surface forward virtually to the leading edge and the second was the greater suction flow that would be required. The first could be assessed as a weight penalty for the more extensive suction surface, though in addition to this quantifiable aspect there were other practical aspects to be considered, for example de-icing the leading edge would be more difficult. The second penalty in terms of additional weight and increased fuel consumption on account of the increased power required to operate the suction system, could only be assessed if the increase in suction quantity were known. Owen and Randall predicted the suction intensity necessary to control crossflow instability in the leading edge region. It turned out to be quite high but the additional suction quantity was not too large because only a small area was affected. However, they pointed out that there would be a tendency for crossflow to develop in the more extensive region where the pressure rises as the trailing edge is approached, and although they did not undertake a quantitative prediction of the level of increased inflow required they did suggest that the increase in the rate of inflow would be several times as great as that required at the leading edge. In view of the extent of the region affected this would have been a very severe penalty and it appeared that laminar flow control on swept wings, though in all probability possible, would not be attractive.

As it happened, Owen and Randall's qualitative assessment of the additional inflow that would be required in the region of pressure rise was unduly pessimistic. There were two reasons for this. First the inflow required to control the already recognised forms of boundary layer instability in this region contributed to the control of the cross flow instability. Second, the inflow modified the cross flow velocity profile in such a way that the neutral stability Reynolds number was increased. The credit for deducing and demonstrating that the additional suction quantity required to control cross flow instability in the rear region was quite moderate is due entirely to Dr. Pfenninger and his co-workers in the United States.

For a time after Owen and Randall's predictions our work at Handley Page was confined to studies of laminar flow control on aircraft with unswept wings. Such aircraft, because of their limited speed, were of no interest for military purposes and it slowly became clear that they could not command any real interest in the civil field either. The incentive to tackle the problems of laminar flow control on swept wings was therefore very great, and for this reason, and encouraged by the doubts being expressed by Pfenninger about Owen and Randall's unduly pessimistic prediction, we were stimulated to turn our attention to the problems and possibilities of swept wings.

In view of the sensitivity that Head's drilled surface had exhibited to the direction of the flow over it, we had to consider the possibility that our surface, with its

bands of relatively large closely spaced perforations might have similar characteristics. It was important to know whether this was the case before it could be considered a suitable candidate for the suction surface of a swept wing where the flow direction would vary with incidence as well as varying from one position to another. Head tested a sample of our surface in the apparatus he had developed and found some, but very little, variability in the level of disturbance downstream of it as the flow direction was varied whilst fairly intense suction was applied. This was reassuring, but we decided to consider a slitted surface of the type adopted by Pfenniger. We eventually adopted the slitted surface (see Fig. 22) partly because of lingering doubts about the possibility of problems with the perforated surface but mainly because the slitted surface appeared more attractive from a production viewpoint. The manufacture of a surface with a multiplicity of drilled holes was slow, and therefore expensive, and it was thought that slitting, being a continuous process, would prove to be faster and cheaper in the long run.

2.4 Initial tests with a swept wing

It was decided to build a swept wing¹² with slitted suction surface and to test this in flight mounted vertically on top of the fuselage of a Lancaster (ex-RAF bomber) aircraft being operated by the College of Aeronautics at Cranfield (now the Cranfield Institute of Technology). With this arrangement it was possible to vary the incidence independently of the speed - (in fact changing the aircraft speed changed the sweep). Means were provided inside the 'wing' for varying the inflow distribution as well as for varying the overall inflow, and likewise internal instrumentation was provided to measure the distribution of inflow. Each surface of the wing was divided into an inner zone, a mid semispan zone and an outer zone, and the leading edge constituted a separate zone (see Fig 23). The original plan was to fit a porous leading edge for the first series of tests. Unfortunately it was not possible to obtain a large enough piece of porous metal sheet with sufficiently uniform porosity, and so the tests were undertaken from the outset with a slitted suction surface throughout.

Gear was provided for traversing instrumentation during flight in a fore and aft (i.e. line of flight) direction and the instrumentation could be rigged at any spanwise position except the extreme root and tip (see Fig 24). A pitot comb carried on this instrument traversing gear could be used to measure boundary layer velocity profiles at positions between 15% chord and about 75% chord. It had ten pitot tubes logarithmically spaced between 0.2 mm (0.008 in.) and 50 mm (2 in.) from the surface. When the comb was being traversed towards the leading edge it was lifted off the surface to avoid any possibility of the lowest tube digging into a slit.

In the earlier flight experiments using the Vampire, each flight was of short duration and all the analysis of results was done on the ground. Each boundary layer velocity profile was plotted and its momentum thickness was computed. Then non-dimensional profiles of velocity divided by maximum velocity versus height from surface divided by momentum thickness were plotted for comparison with standard velocity profiles. The experimental flights with the Lancaster were generally of about one and a half hours duration and on this account it was very desirable that the main indications from the measurements should be available during flight in order to influence the course of the test. A new method of plotting the results was devised¹³ in order to improve and accelerate the process of being able to recognise whether a boundary layer profile measurement suggested laminar or turbulent conditions. The velocity ratios (which could be quickly determined) were plotted directly against tube height, but with a logarithmic scale for tube height. With this procedure it was often only necessary to plot two or three points to establish the type of profile (see Fig. 25). However, even this method was found to be slower than was desirable and it was difficult to be sure of the condition of the boundary layer if it was very thin.

For these reasons an additional type of instrumentation was developed in the form of "hot film" instruments. These worked on the same principle as hot wire anemometers used in wind tunnels, but were much more robust. The sensitive element was a thin film of platinum fired on to the leading edge of a glass wedge tapering at 15° to 0.38 mm (0.015 in.) thickness at its forward extremity. The corners were rounded and the platinum film carried round and along either side so that the electrical leads could be soldered on directly. Provision was made to process the outputs from up to 50 hot film instruments in such a way that they could be displayed on a bank of 'intermittency meters' on which a zero reading indicated the complete absence of turbulence. The outputs could also be displayed one at a time on a cathode ray oscilloscope.

The hot film instruments proved to be very practical and, although there was a steady wastage rate, they proved to be so robust that they could be pulled off the wing and allowed to trail behind with a fair prospect that they would prove serviceable for use again on a subsequent flight. Thus it was possible to fix hot films to the wing surface in forward positions and once an indication of laminar flow had been obtained they could be shed so as to get rid of their wakes on the surface further aft. It also proved possible to draw a hot film across the surface in a spanwise direction (at approximately constant chord). This was not envisaged at the outset but was evolved during the test programme. When combined with the facility provided by the chord-wise instrument traversing gear, this made it possible to locate the edges of turbulent wakes so that their sources could be determined even if they were ahead of the region in which the hot film could be traversed.

The wing had suction surfaces on both sides extending from a root fence to a

position close to the tip. On account of the rail and mechanism of the instrument traversing gear it was not worth extending the suction surface to the extreme tip. The spanwise extent of the suction surface was 2.54 m (100 in.) and the chord at its inboard and outboard ends was 2.54 m (100 in.) and 1.73 m (68 in.). The leading edge sweep was $42\frac{1}{2}$ degrees. The wing had a symmetrical section, actually an RAE 103 section scales to $12\frac{1}{2}\%$ thickness. This gave a rather large leading edge radius which together with the large angle of sweep was intended to present a severe cross flow problem. The suction surfaces on the two sides were not identical, that on the port side having only approximately three-quarters as many slits as that on the starboard side.

The earliest tests¹⁴ were disappointing, transition moving forward rapidly as Reynolds number increased. Suction was more effective on the side with the closer slit spacing, but even so transition moved forward rapidly as flight speed increased until at 140 knots EAS at 10,000 ft. altitude transition was somewhere ahead of 10% chord on both surfaces. At 135 knots transition was ahead of 10% chord on the surface with fewest slits but on the other surface it was at about 50% chord at the mid semispan station and further outboard.

It took some time to achieve an understanding of this behaviour of the transition pattern. It was investigated in a series of flights at altitudes varying between 3500 ft. and 22000 ft. and speeds between 100 knots EAS and 170 knots EAS. This gave a two to one range of unit Reynolds numbers, actually from about 3×10^6 per m (0.9×10^6 per ft.) to 6×10^6 per m (1.8×10^6 per ft.). In successive flights hot film instruments were fixed at positions closer and closer to the leading edge. Eventually flights were conducted with the hot films at the very leading edge. After observations had been made with the hot film nearest to the root it was pulled off so that observations could be made with the next one further outboard. Then this was pulled off in its turn and so on. Analysis of the results (see Fig. 26) obtained revealed the nature of the problem.

2.5 Spanwise contamination on swept wings

A swept wing does not have true stagnation at its leading edge. Instead, its attachment line, where the flow divides to pass on either side, is a quasi-stagnation line, there being a component of the stream velocity along it. In the case of a swept back wing this velocity component is directed towards the tip. Accordingly when the hot film instruments were positioned at the leading edge, they were aligned facing the wing root. The spanwise flow along the attachment line results in the formation of a boundary layer. The hot film readings showed that this attachment-line boundary layer was turbulent in certain conditions. When this was the case it contaminated the boundary layer on both surfaces of the wing and, the boundary layer being already turbulent before the first slit was reached, suction was ineffective.

Propagation of turbulence with the attachment-line boundary layer was not unknown, having been observed by W.E. Gray in 1952 during the flight tests in which cross flow instability was first discovered. Gray also reported that on a Meteor fin with 25° leading edge sweep a trip wire round the nose caused transition but that laminar flow re-established itself a short distance further along the attachment line. Also in 1952 Gregory and Walker reported having observed the spanwise spread of turbulence from a large excrescence placed on the attachment line of a swept model wing at tunnel speeds exceeding a critical value. Further observation on the spread of turbulence on a swept wing model were reported by Gregory in 1960. In these later tests unlimited spanwise contamination was only observed once, and then only with a very large excrescence carefully positioned to produce the phenomenon. The tunnel floor boundary layer at the model wing root was undoubtedly turbulent in these tests and yet did not contaminate the wing. Pfenninger and Bacon reported on wind tunnel tests conducted in 1957 to 1959 on a 30° swept wing model at chord Reynolds numbers up to 30×10^6 , and the non-appearance of spanwise contamination in these tests together with the extreme difficulty which Gregory had experienced in his efforts to provoke the phenomenon led to the probability of its occurring in the British flight experiments being underestimated.

The acceleration of the flow away from the attachment line over both surfaces of a swept wing exerts a controlling influence over the growth of the attachment-line boundary layer. Whilst skin friction tends to increase its thickness, the boundary layer is leaking away to either side of the attachment line and so it is not difficult to envisage that there will be an equilibrium thickness*. This equilibrium thickness is inversely proportional to the square root of the velocity gradient. A leading edge with a large radius of curvature has a relatively small velocity gradient at its attachment line and therefore develops a thicker attachment-line boundary layer than a leading edge with a smaller radius of curvature. This means that on a tapered wing, such as the experimental wing, the equilibrium thickness decreases from root to tip.

In the British flight tests it was found that turbulence was spreading from the large root fence on to the most inboard part of the swept back leading edge, causing the attachment-line boundary layer near the root to be turbulent. The turbulent attachment-line boundary layer spread along the leading edge until it reached a position where the notional momentum thickness Reynolds number of an equilibrium thickness attachment-

*Whereas in the case of laminar flow control by suction at the surface, flow is only "drained" away from the boundary layer at the lower extremity, in the present case it is removed to either side throughout the whole depth of the boundary layer.

line laminar boundary layer would be about 88. Beyond this position the turbulence was apparently unable to propagate and the attachment-line boundary layer became laminar all the way to the tip. The equilibrium momentum thickness Reynolds number of a laminar boundary layer on the attachment line depends on the flight unit Reynolds number as well as on the sweep and section geometry of the wing. Consequently the position of the critical point, beyond which turbulence was unable to spread along the attachment line, depended on the flight unit Reynolds number.

At low EAS and high altitude (low unit Reynolds number) turbulence was unable to travel far along the leading edge, but at high EAS and low altitude (high unit Reynolds number) turbulence was able to travel along the leading edge the whole of the way to the tip. In fact, with the geometry of the test wing turbulence spread halfway along the leading edge when the flight unit Reynolds number was about 3.9×10^6 per m (1.2×10^6 per ft.) and all the way to the tip when the flight unit Reynolds number was 4.9×10^6 per m (1.5×10^6 per ft.). The suction surfaces of the wing were designed to prevent turbulence developing in a laminar boundary layer but not to suppress turbulence that had already developed. Consequently it was not possible to manipulate the inflow distribution to recover laminar flow on any part of the wing surface lying downstream of a turbulent attachment-line boundary layer. Thus the failure of the early flight experiments was fully accounted for. The phenomenon also occurred on the Northrop X21A where it was diagnosed and explained at about the same time as its discovery in the British experiments (i.e. in late 1963).

The criterion established at this stage of the flight experiments, namely the momentum thickness Reynolds number of a notional equilibrium-thickness attachment-line laminar boundary layer being greater or less than about 88, makes it possible to distinguish between cases in which turbulence, once it is present, will or will not propagate along the attachment line (see Fig. 27)¹⁸. There is also a higher Reynolds number above which a laminar attachment-line boundary layer becomes unstable even to small disturbances and in cases where this is exceeded there is a probability that a laminar attachment-line boundary layer will degenerate into a turbulent one. This higher critical Reynolds number was well above the maximum that could be reached in the flight experiments. It is about $2\frac{1}{2}$ times the critical momentum thickness Reynolds number for the propagation of turbulence and since the laminar boundary layer Reynolds number is proportional to the square root of the flight unit Reynolds number, it would occur at a flight unit Reynolds number seven or eight times greater than the critical value for propagation of turbulence.

Consequently all that was necessary to enable the tests to proceed as originally planned was a device which would arrest the propagation of turbulence and which could be fitted close to the wing root. If such a device could be developed, the attachment-line boundary layer would remain laminar unless excessive roughness outboard of the device were to trip the boundary layer and give rise to turbulence again. Such roughness would have to be accidentally acquired and for the purposes of test flying the risk seemed small enough. A number of simple geometric modifications were tried and it was found that a laminar attachment-line boundary layer could be established by means of a small local extension of the leading edge enabling increased curvature for a short distance.

2.6 Fulfilment of the swept wing experiments

The method adopted and retained for the whole of the ensuing programme was devised by M. Gaster¹⁹. It consisted of a bump astride the leading edge attachment line, about 12.5 cm (5 in.) long and standing about 1.25 cm (0.5 in.) high at the end nearest to the wing root. At this end it rose abruptly from the basic leading edge of the wing but beyond its crest it was faired back into the wing leading edge very gradually (see Fig. 28). It was developed by cut and try methods and was found to be effective throughout the full range of test Reynolds numbers and to be tolerant to variations of wing incidence through $\pm 2\frac{1}{2}^\circ$.

This method of preventing turbulence spreading from the wing root was not envisaged by us as being suitable for application on laminar flow aircraft in normal operations. For such cases it would be desirable, and perhaps necessary, to make provision to arrest the spanwise spread of turbulence at several positions along the leading edge, so that if turbulence were to be accidentally triggered anywhere on the attachment line its spread would be confined to an acceptable proportion of the whole wing. Pfenniger investigated the effectiveness of groups of slits cut at right angles to the attachment line and ending at the first spanwise slit so that their ends did not create an unacceptable disturbance and it seems probable that some such active means of control would be most suitable for an operational aircraft.

However, Gaster's bump proved adequate for experimental purposes and it enabled the flight tests to be satisfactorily concluded²⁰. The measured results obtained in the final test flights at the end of 1965 showed very good agreement with theoretical predictions (see Fig. 29)²¹ and vindicated the aerodynamic design of the wing and its suction system some five and a half years after it had been finalised.

For some years the Handley Page company had been the principal champion of laminar flow control in Britain, though its researches had been aided by Government contracts. But it was now no longer considered justifiable to continue to support the work from public funds, and by the beginning of 1966 the Handley Page company was so beset with problems relating to its survival that it was unable to sustain further work entirely

from its own resources. So at the very time when success seemed nearer than it had ever done, the work came to an end. This is perhaps, to some extent anyway, an oversimplification of the situation. The work had been going on for a number of years and it seemed that a stage had been reached when a much higher level of expenditure would be required if it was to continue. The time was therefore ripe for a re-appraisal of the prospects of laminar flow control, taking into account changes in the general situation as well as the progress made in laminar flow control technology.

Before turning to that re-appraisal it is worth pausing to consider what broad conclusions could be drawn from the work which had been done. A succession of aerodynamic problems had been encountered and in every case a solution had been found, once the nature of the problem had been recognised. This success in surmounting aerodynamic problems could be considered a good augury. In addition, advances had been made in theoretical methods for calculating pressure distributions on wings and for calculating the development of three-dimensional laminar boundary layers with suction. Progress in the development of these methods had, of course, been greatly assisted by the rapid advances being made in computer technology, a trend which could be expected to continue. Theoretical predictions made with these methods had shown good agreement with measurements made in experiments and so the methods would clearly be of great value in future design. Experimental techniques had been advanced and special instrumentation had been evolved. Above all, laminar flow control had been shown to be possible on wings with sweep-back, with inflow rates that were economical.

But many of the difficulties experienced with the test wings demonstrated that satisfactory solutions to design problems and satisfactory methods of manufacture had not yet been evolved. This is not in any way a criticism of the designers or craftsmen involved. Apart from the fact that some lessons can be learned only by experience, the designers were severely constrained by limits on expenditure and by limitations in the manufacturing facilities available. That success was achieved at all was due to the wholehearted efforts of the craftsmen who had to make good every shortcoming by their skill and unstinting efforts. The fact remains that the hardware produced was not good enough. This was not for lack of trying. From the outset, the emphasis in all the Handley Page work had been on developing a practical method of wing construction, but in the end the results achieved fell short of what was needed.

3. SPECULATIONS

Two consequences followed from the failure to produce a trouble-free wing. The first was that it was still not possible to produce reliable estimates of the cost of constructing an aircraft with laminar flow control. The second was that it would not have been possible to embark on the design and construction of a demonstrator aircraft that would enable satisfactory trials and a valid assessment of the problems that could arise in the operation of laminar flow transport aircraft.

Until such an assessment could be performed the cost of maintaining and operating a laminar flow aircraft could not be determined, and the answers to many important questions would remain matters for conjecture. For example, would an operator require special facilities, and if so, what facilities? Would a laminar flow aeroplane be able to stand out in rain, snow, or freezing conditions? If so, would special maintenance operations be required before flight? Would there be problems in maintaining the surfaces in a smooth and wave-free condition throughout the life of the aircraft (i.e. would there be any serious tendency to deteriorate)? Would the suction system require any special maintenance other than normal maintenance of the suction pumps, controls, and instrumentation? Would there be any significant occurrences of clogging of the suction surface or any of the small passages communicating with the ducting system? Would the special measures required to provide access to the systems inside the wing prove inconvenient? Would there be inspection problems? Would corrosion problems arise in the interior of the wing? Protection of the edges of the slits themselves could also be a problem. And what about repair schemes for rectifying accidental damage? These problems may not all be real, some of them may turn out to be unimportant. There is little or no doubt that solutions could be found for the ones that proved to be real; but at what price? Would the annual utilisation be adversely affected?

And then, of course, there were worries about insect contamination or the fly problem as it was generally known. Somebody was sure to raise this topic at any discussion on laminar flow control. It attracted so much attention that other possible problems may have received less consideration than they deserved. But who was to say that the fly problem was not really a problem at all. Certainly we could not afford to ignore it. We protected the leading edges of our test wings with strips of tracing linen and, later on, with a plastic material known as Melanex. The latter was a polyester film manufactured by Imperial Chemical Industries. The Melanex film used was about 0.05 mm thick, and a type with a metalised surface was found to avoid electrostatic problems. Various methods of attaching and shedding these protective covers were investigated. Problems could arise when taxiing downwind. Alternatives which were discussed included low adhesion coatings which could be sprayed on and subsequently peeled off, and brittle lacquers and resins which could also be sprayed on but which would disintegrate at low temperatures.

A survey showed that the leading edges of small private aircraft and club aircraft that spent most of their time flying at low altitudes became liberally plastered with insect remains in warm weather. On the other hand it was rare to find any recognisable insect remains on the leading edges of commercial transport aircraft that flew faster and at higher altitudes. This was not only true of aircraft examined at Heathrow but

at Malta, Rome, Tripoli, Benghazi, Athens, Cyprus and Beirut. There was therefore a suspicion that insect remains were eroded at high altitudes and high true air speeds. Our test flights were mostly at low altitude and comparatively low true airspeed. The erosion of insect remains was investigated by impinging flies on to a specially prepared panel on the leading edge of a Victor bomber, flies being bred specially for the purpose. The impinged flies were marked so that they could be identified when the panel was examined after the aircraft had landed. This was necessary to avoid confusion being caused in the event of a fly or flies being picked up accidentally during flight and especially during landing. It was observed that the wings, legs, and other protuberances blew away quite quickly and that the remains then eroded away to a degree which depended on their location. Close to the attachment line the eroded remains could be as high as 0.25 mm (0.01 in.) but this height decreased to zero over a short distance.

These results were not quite good enough to allow the problem to be dismissed. It was noted that if the aircraft flew through even a small cloud the panel was cleaned completely, and this led to the speculation that it might be possible to devise a system to wash the leading edge in flight. Tests were therefore performed in a wind tunnel using a wing fitted with small flush nozzles (see Fig. 30). These could be used to project jets of water upstream into the airflow. The jets of water were broken up into a fine spray by the airflow, and this spray was then blown back on to the wing leading edge. The tunnel was run for various lengths of time before the water jets were operated. This was done to investigate the effect of allowing the fly remains to dry and harden. Tests were conducted to establish the minimum amount of water required and to ascertain the effects of various additives. A two shot action was found to be most economical. It was found that the weight of water required would only be a small fraction of the weight of fuel saved. The possibility of using special materials for the wing surface in the region of fly impingement was considered and some tests were done using a PTFE plastic marketed as Fluon. It appeared that the fly remains adhered much less firmly to this material.

This kind of work was undertaken to explore what possibilities there might be and to some extent as an insurance. The cost, of course, was quite low. Another problem which received some attention was that of de-icing, for which an electrical system was favoured. It was thought that 'run back' might be a source of trouble, and arrangements were in hand for wind tunnel tests in a low temperature facility at the time that our activities were brought to a stop. Thus there were many questions to which a categorical answer could not be given, and although a measure of confidence could be achieved by the kind of work touched on above, conclusive findings depended on the availability of a demonstrator aircraft. Moreover, a demonstrator aircraft was required that would be free from problems induced by shortcomings in its design and manufacture, so that it could be operated without hindrance from difficulties other than operating ones.

Because of these unresolved questions, predictions of the direct operating cost savings made possible by laminar flow control depended on judgements which involved an element of conjecture. In 1959 a joint exercise was undertaken by Handley Page with government scientists and representatives of the British operators, in an attempt to arrive at as soundly based a prediction of the benefit to be gained as was possible. It was also hoped that the prediction would find some measure of acceptance by the²² other parties. A comparison was made between a conventional and a laminar flow aircraft with transatlantic range. When all the assumptions had been discussed and agreement reached, it appeared that it should be possible to reduce the direct operating cost by about 16%. This would have been a very large saving indeed, and, despite the significant level of uncertainty, it was sufficiently promising to gain a measure of Government funding and sustain interest in the laminar flow work.

By 1966, the situation had changed. The price of fuel in real terms had been falling for many years at a rate of 6% per annum, and it seemed likely to continue falling. In addition, considerable progress had been made and could be foreseen in the technology of gas turbine propulsion systems which were therefore becoming more efficient and less thirsty for fuel. On account of this the reduction in fuel consumption that laminar flow control would make possible was getting smaller, and, of course, all the benefits of laminar flow control stem in the first instance from this reduction. In fact, for a design stage length of about 5700 km (3000 nautical miles) the Handley Page project study already referred to, showed that reductions of structure weight, power plant weight, etc. would not much more than balance the added weight of the suction system, and aircraft basic operating weight would only be slightly reduced. The take-off weight, of course, would be greatly reduced on account of the lessened fuel weight.

For longer design stage lengths the reduction of basic operating weight would have been more significant, but, at the time, operators did not evince much interest in longer ranges. This being the case most of the reduction in aircraft operating cost resulted from savings in the cost of the fuel used. With the advent of more efficient power plant lessening the fuel mass from which to make savings, and with the price of turbine engine fuel continuing to fall, it seemed inevitable that the potential benefits of laminar flow control would be continuously eroded in the years to come. And, of course, there was no concern about dwindling fuel reserves at that time. Updating Handley Page's 1959 study to take account of the power plant available in 1972 and also the fuel price prevailing in 1972, it appears that the originally predicted 16% reduction of direct operating cost would almost have disappeared. By 1972 a design stage length of 8000 km was of interest to operators and for that stage length the predicted reduction of direct operating cost would have been around 8%.

The abrupt rise of fuel prices that commenced in the following year has, of course, transformed these findings. But looking further ahead to, say, the last decade of this century it is necessary to allow for further reduction of engine fuel consumption and so the economic argument for laminar flow control will be dependent on the extent to which fuel prices continue to increase in real terms. The future prospects for laminar flow control therefore remain tantalisingly obscure.

REFERENCES

1. J.B. Edwards Boundary layer and flow control.
AGARD - VKI, Lecture Series, Course Note 62 (1967)
2. M.J. Lighthill Introduction: Boundary Layer Theory
In Laminar boundary layers, edited by L. Rosenhead pp 82-102
Great Britain, Oxford University Press (1963)
3. A.A. Griffith
F.W. Meredith The possible improvement in aircraft performance due to the
use of boundary layer suction.
Unpublished RAE report (1936)
4. J.B. Edwards Fundamental aspects of propulsion for laminar flow aircraft.
In Boundary layer and flow control, edited by G.V. Lachmann,
Vol. 2, pp 1077-1122
Great Britain, Pergamon Press (1961)
5. M.E. Head
D. Johnson
M. Coxon Flight experiments on boundary layer control for low drag.
ARC R & M 3025 (1955)
6. G.V. Lachmann
N. Gregory
W.S. Walker Handley Page laminar flow wing with porous strips. Details
of model and wind tunnel tests at NPL.
ARC 14,794 (unpublished) (1952)
7. N. Gregory Research on suction surfaces for laminar flow
In Boundary layer and flow control edited by G.V. Lachmann,
Vol. 2, pp 924-260
Great Britain, Pergamon Press (1961)
8. W.E. Gray The effect of wing sweep on laminar flow.
Unpublished RAE Technical Memorandum Aero 255 (1952)
9. W.E. Gray The nature of the boundary layer flow at the nose of a swept
wing.
ARC 15,021 (unpublished) (1952)
10. P.R. Owen
D.G. Randall The use of distributed suction to delay boundary layer
transition on swept-back wings.
ARC 15,798 (unpublished) (1953)
11. W.B. Brown Numerical calculation of the stability of crossflow profiled
in laminar boundary layers on a rotating disc and on a swept
back wing, and an exact calculation of the stability of the
Blasius velocity profile.
Northrop Corporation, Norair Division Report NAI-59-5
(BLC-117). (1959)
12. Laminar report - Handley Page progress in the field of
boundary layer control.
Flight-International 12th July 1962
13. J.B. Edwards Identification of boundary layer profiles
Handley Page Ltd., Research Department Technical Note 20 (1963)
14. R.R. Landeryou
R.S. Trayford Flight tests of a laminar flow swept wing with boundary layer
control by suction.
College of Aeronautics, Cranfield. Report Aero No. 174. (1964)
15. N. Gregory
W.S. Walker Brief wind tunnel tests on the effect of sweep on laminar flow
ARC 14,928 & 15,126 (unpublished) (1952)
16. N. Gregory Transition and the spread of turbulence on a 60 swept-back
wing.
Journal of the Royal Aeronautical Society, Vol. 64
pp 562-564 (1960)
17. W. Pfenninger
J.W. Bacon Jr. About the development of swept laminar suction wings with full
chord laminar flow
In Boundary layer and flow control, edited by G.V. Lachmann,
Vol. 2 pp 1007-1032

18. J.B. Edwards Leading edge problems on swept laminar flow wings - some observations on recent developments.
Handley Page Ltd. Unpublished report (1963)
19. M. Gaster A simple device for preventing turbulent contamination on swept leading edges.
Journal of the Royal Aeronautical Society, Vol. 69 p 788 (1965)
20. R.R. Landeryou Further tests of a laminar flow swept wing with boundary
P.G. Porter layer control by suction.
College of Aeronautics, Cranfield. Report Aero No. 192 (1966)
21. M.P. Carr The calculation of laminar boundary layers on wings.
Handley Page Ltd. Research Report 81 (1966)
22. J.B. Edwards A carefully considered assessment of the reduction of direct operating costs made possible by laminar flow.
ARC 20,967 (unpublished) (1959)

ACKNOWLEDGEMENT

Acknowledgement is made to the Cranfield Institute of Technology for permission to reproduce Fig. 26. This figure originally appeared in College of Aeronautics Report No. 174.

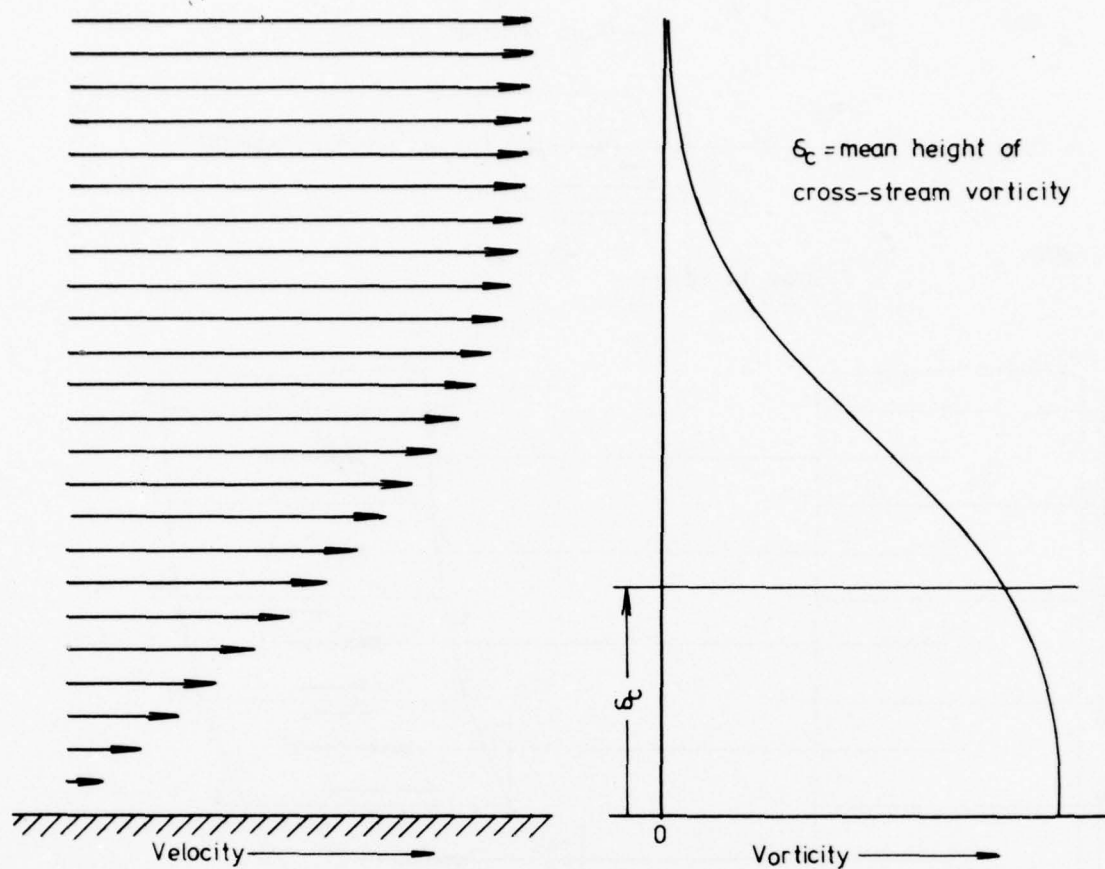


Fig. 1 Boundary layer velocity profile and vorticity distribution (Blasius).

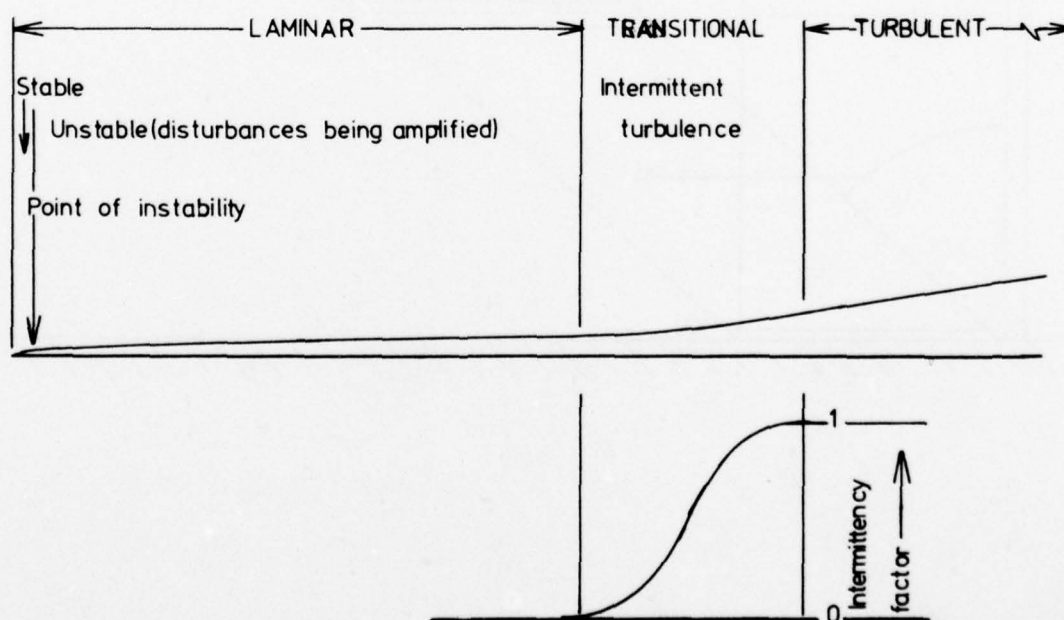


Fig. 2 Boundary layer development with transition to turbulence.

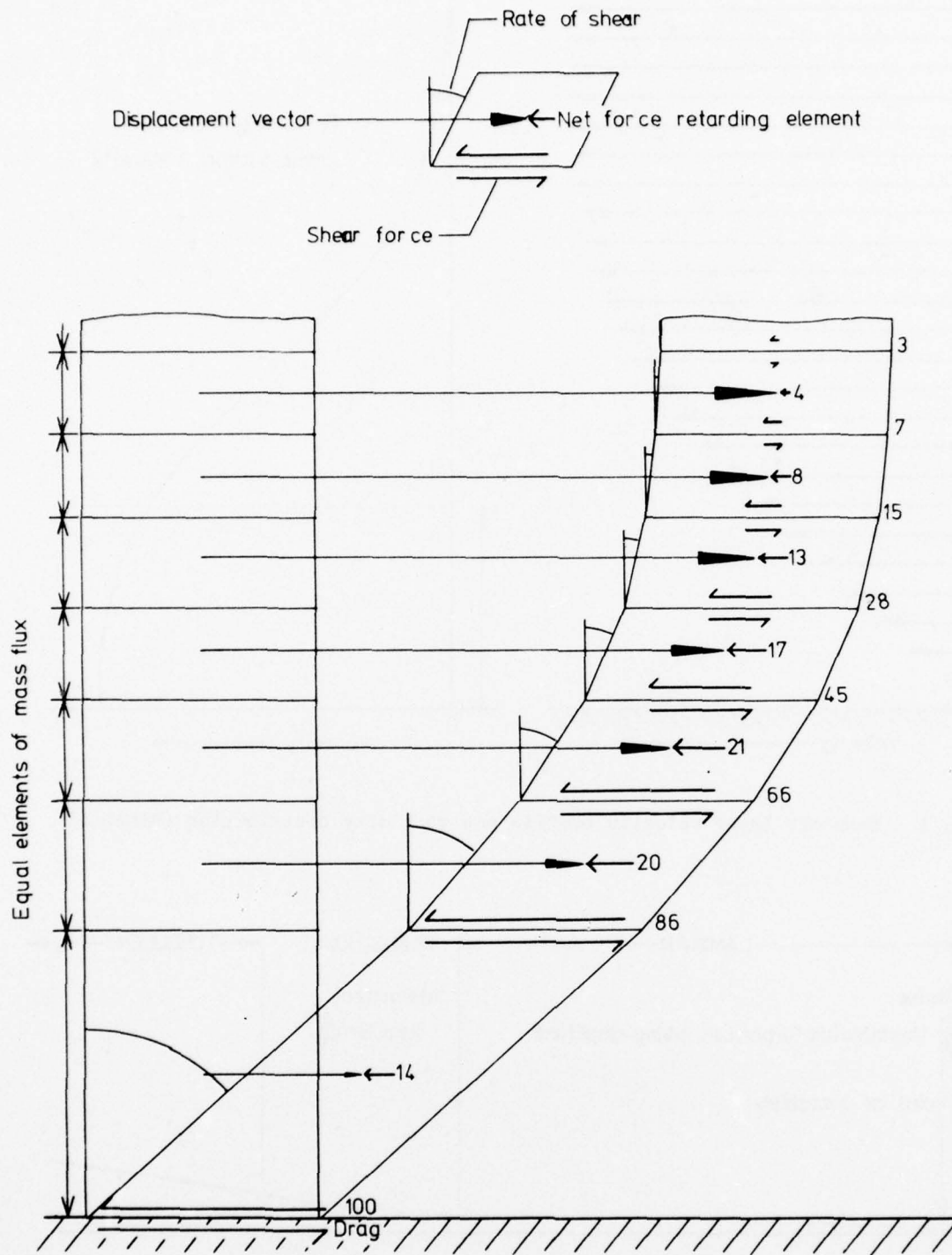


Fig. 3 Balance between the forces in a boundary layer and the drag of the surface.

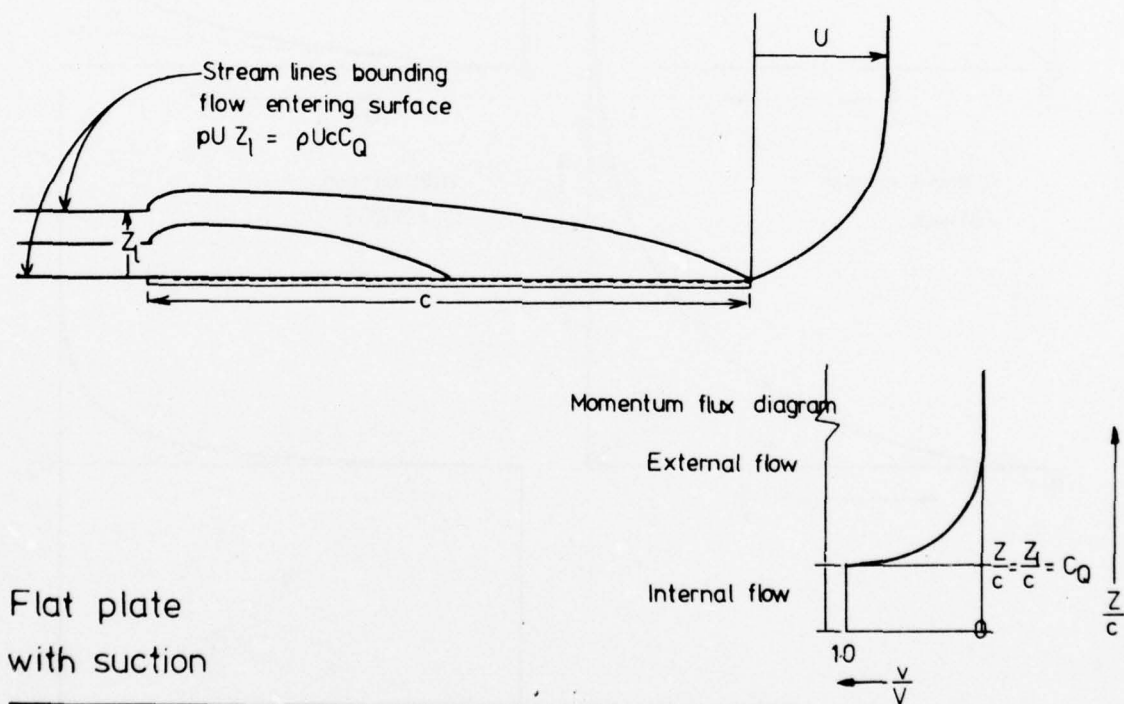
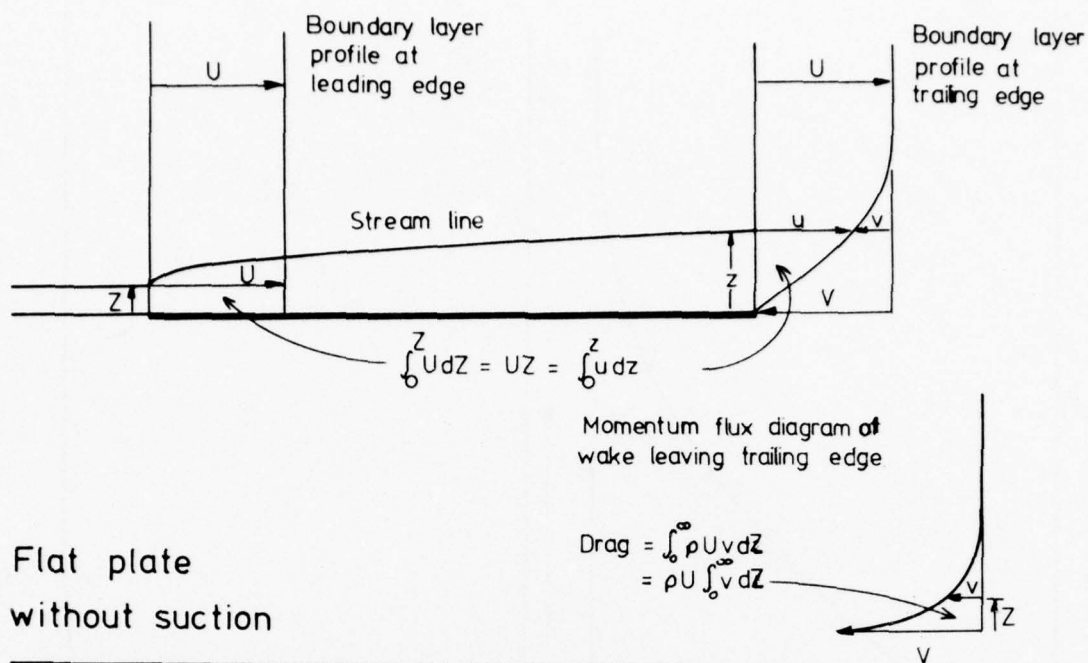


Fig. 4 Momentum flux diagrams.

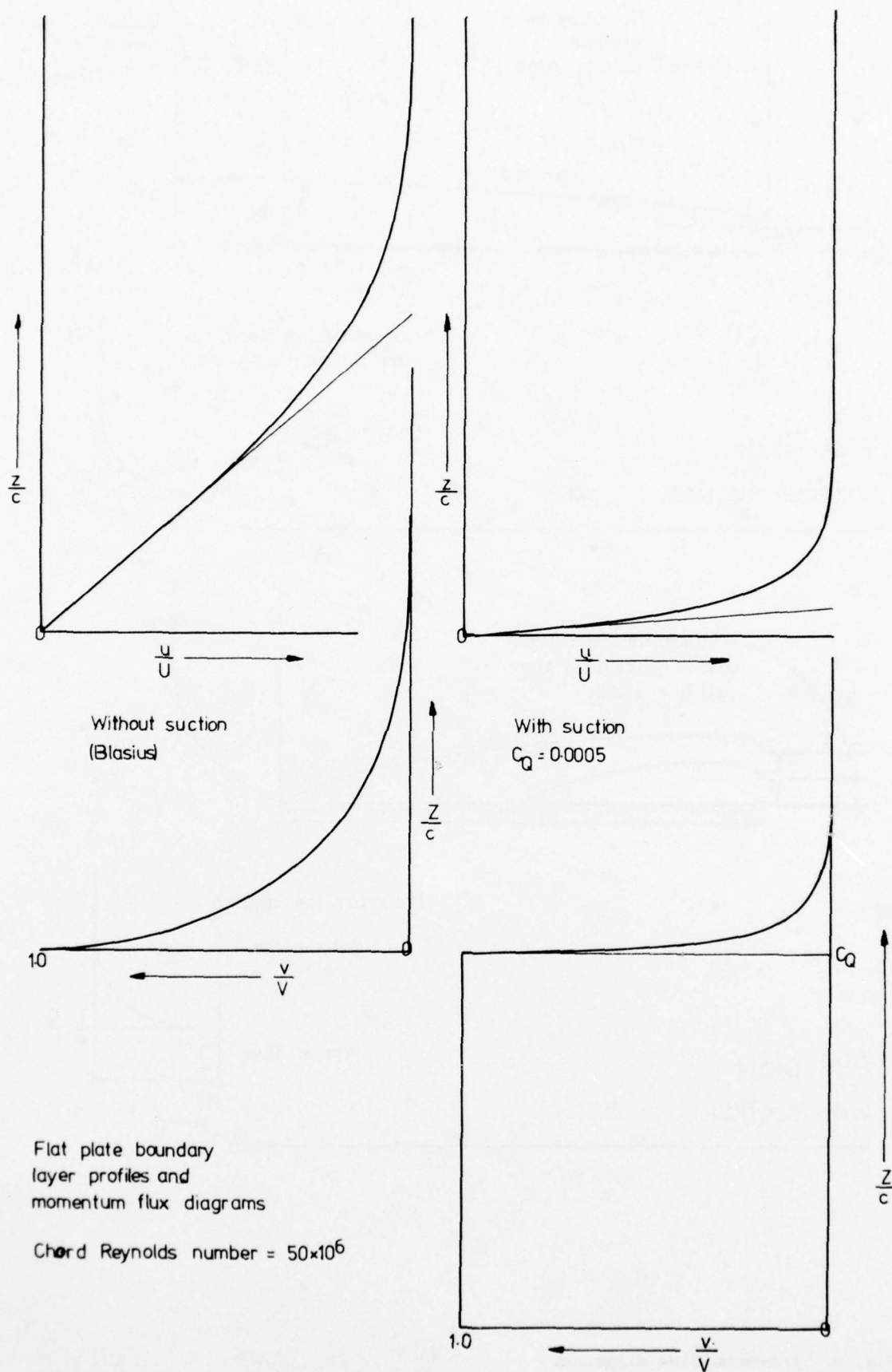


Fig. 5 Comparison of sucked and unsucked laminar boundary layers.

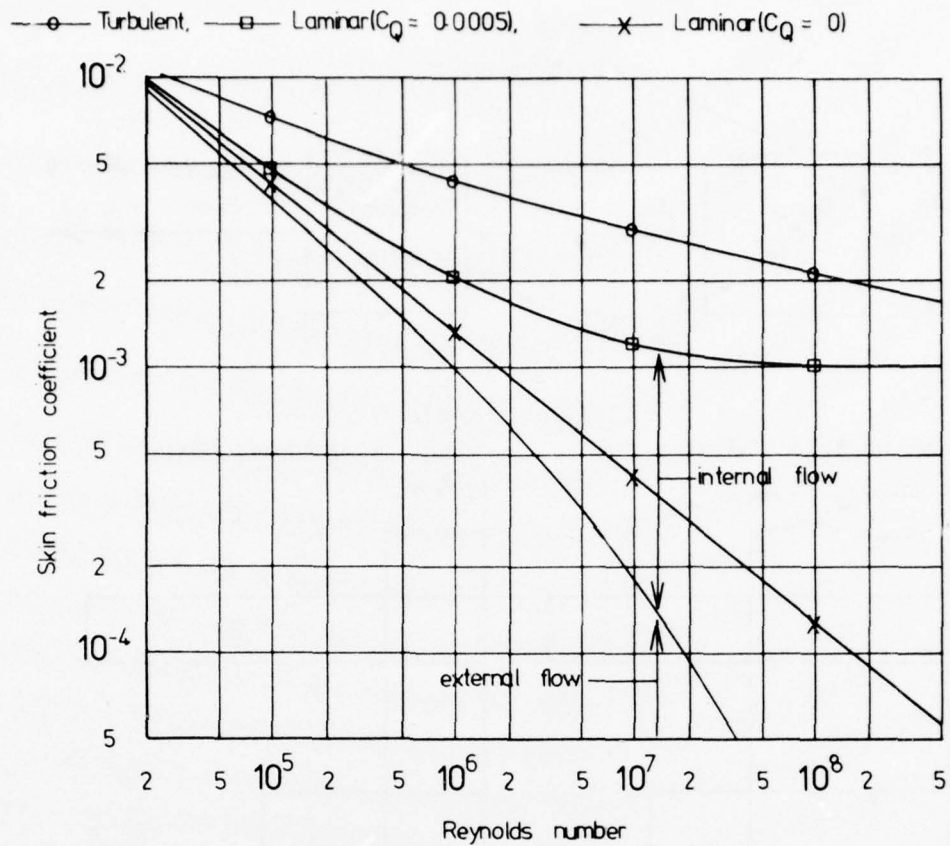


Fig. 6 Comparison of flat-plate skin friction coefficients.

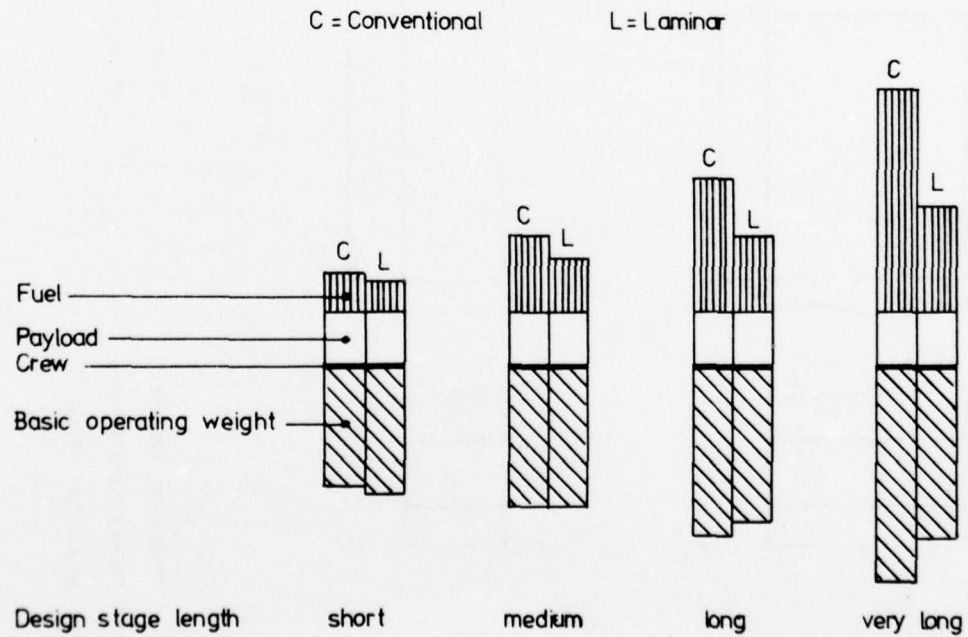


Fig. 7 Weight break-down comparisons.

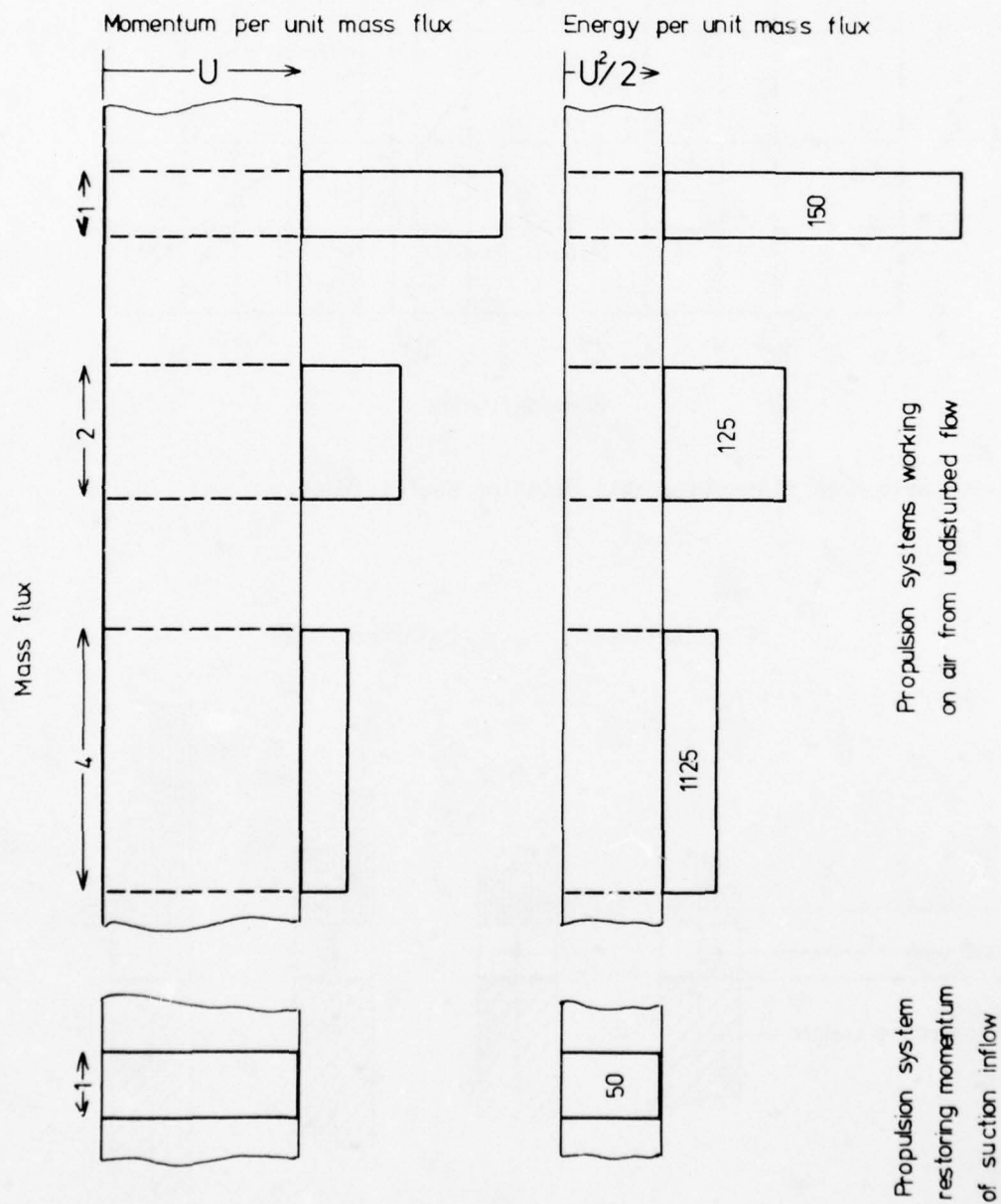
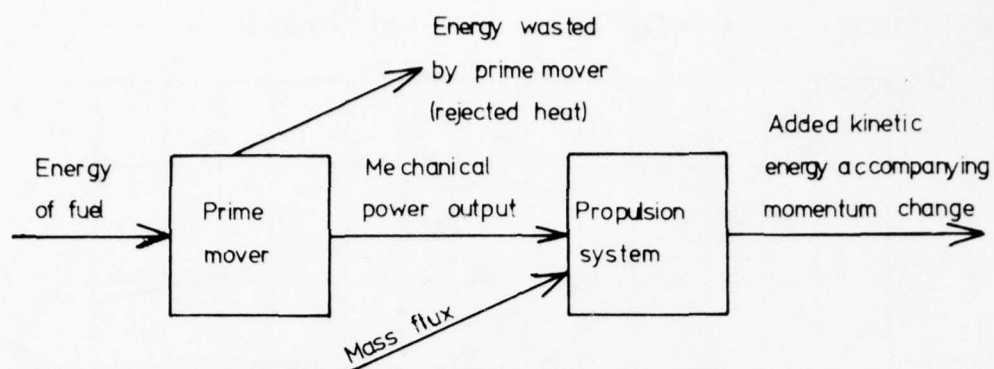


Fig. 8 Propulsion system momentum and energy diagrams.

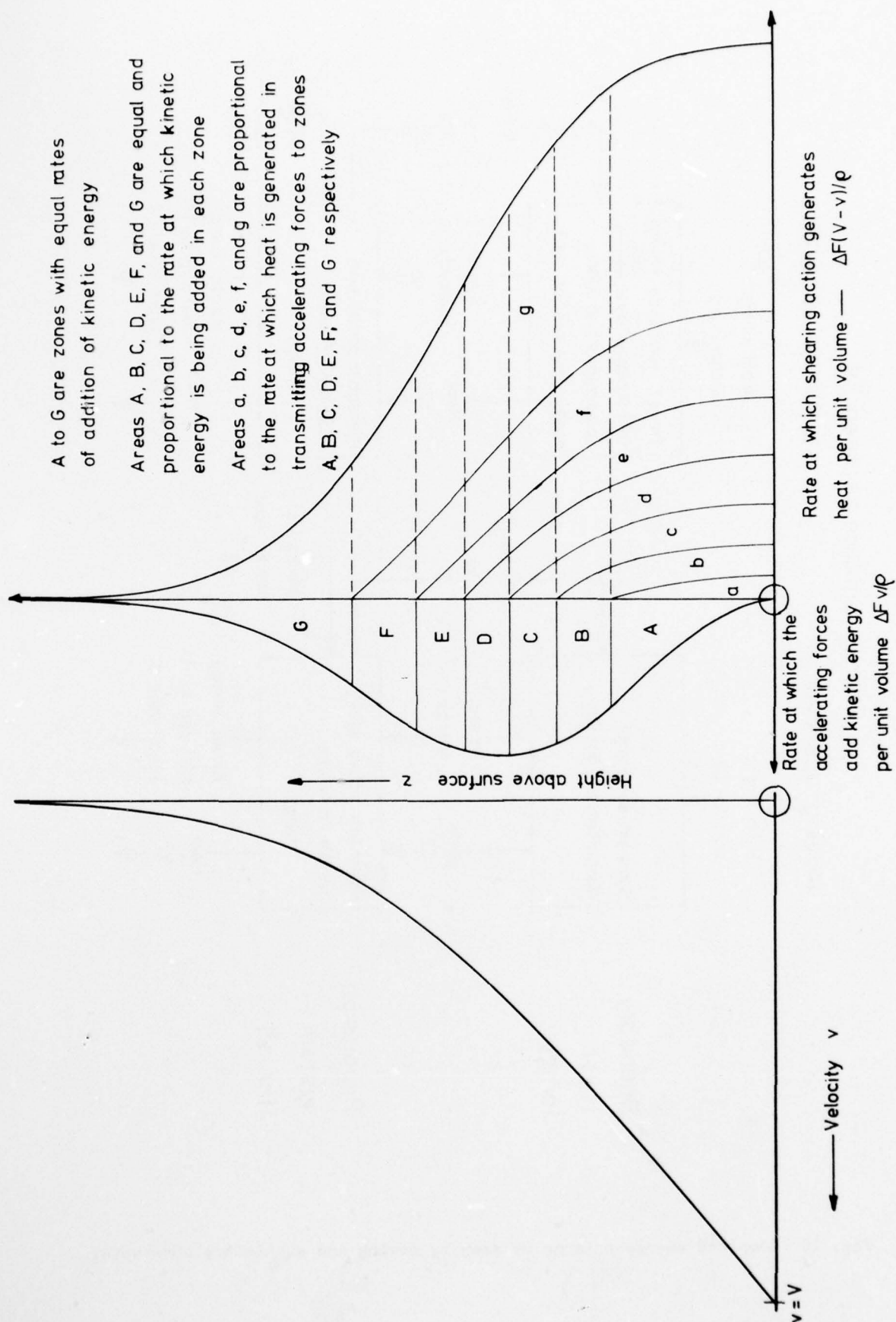


Fig. 9 Work processes in boundary layer as seen by a stationary observer.

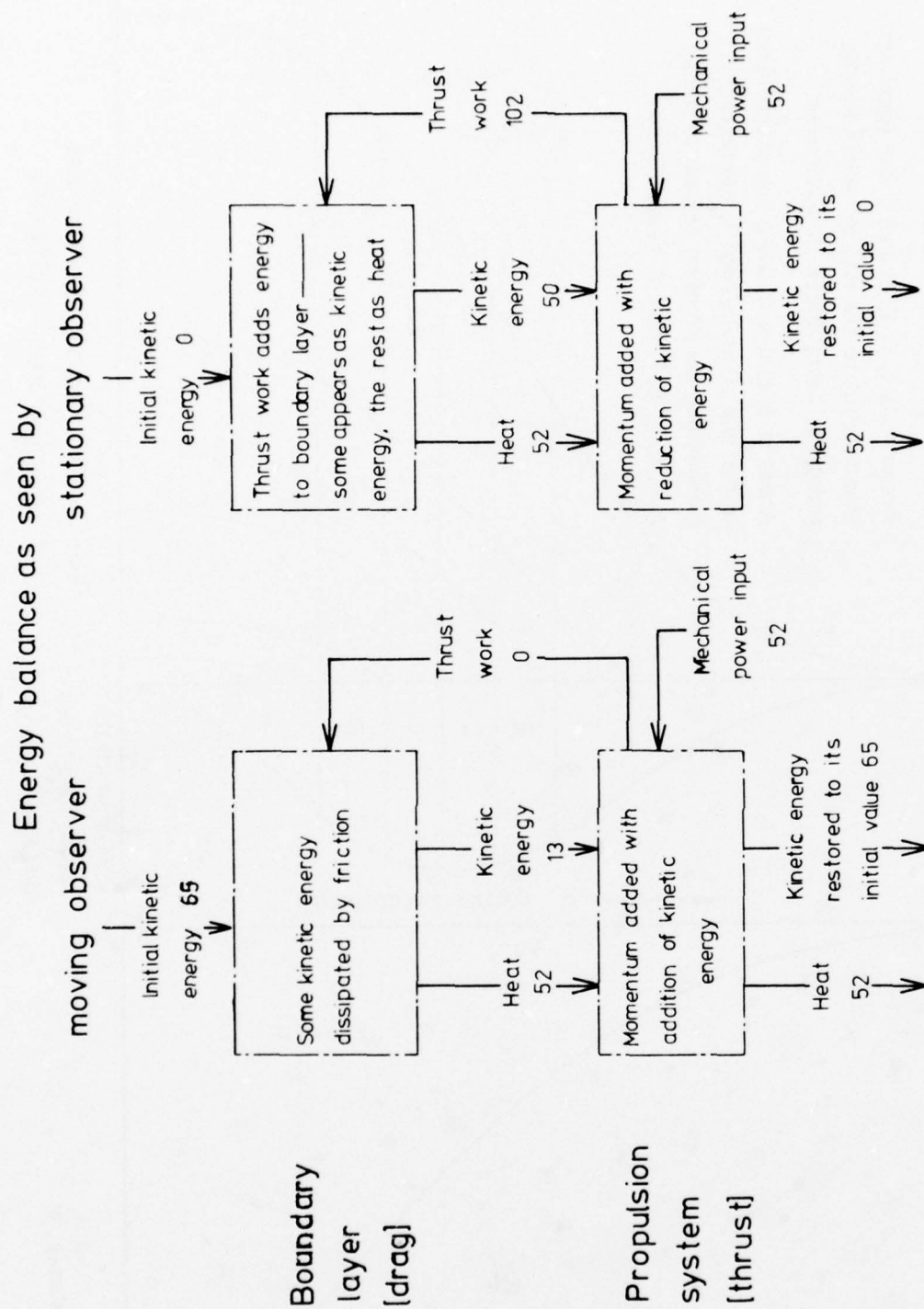


Fig. 10 Complete energy balance as seen by moving and stationary observers.

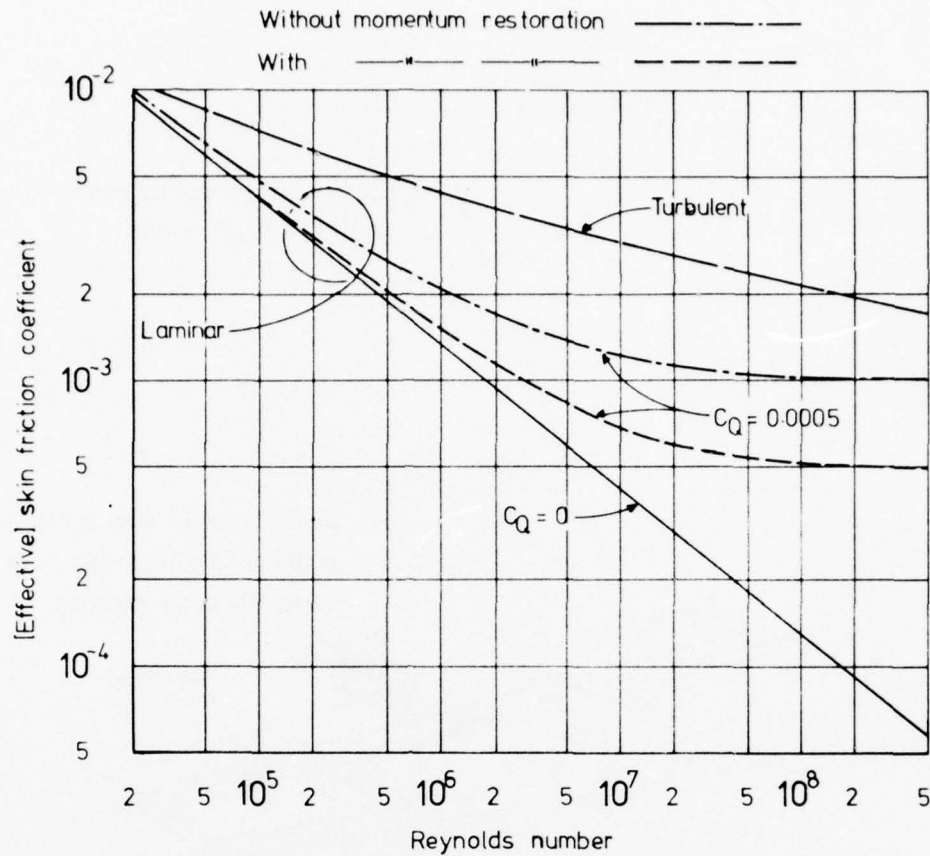


Fig. 11 Comparison of effective skin friction coefficients showing the benefit of momentum restoration.

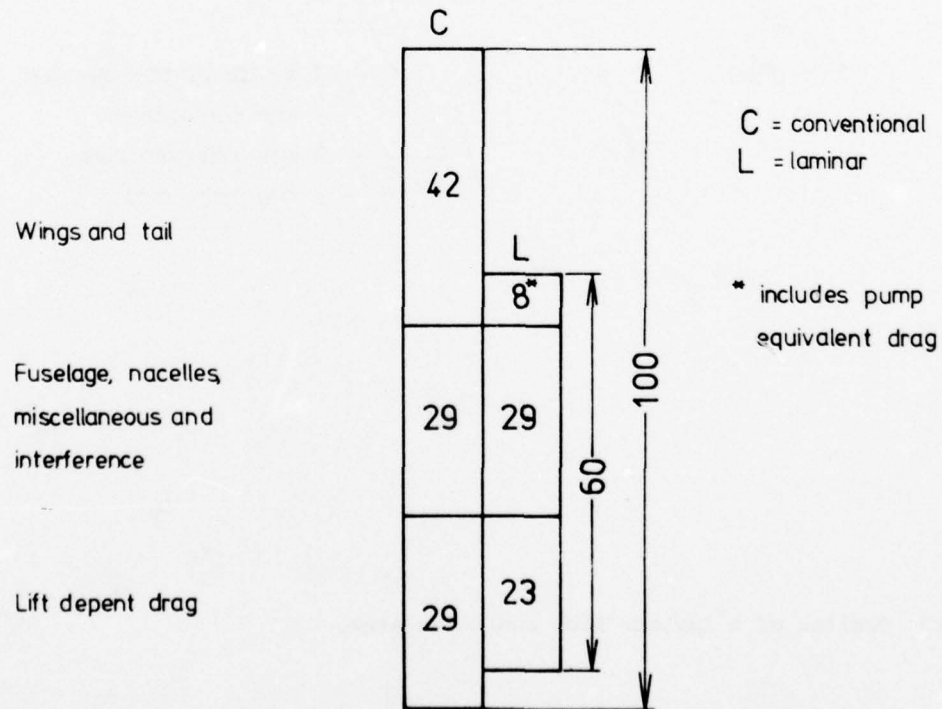


Fig. 12 Comparison of possible laminar and conventional aircraft drag break-downs.

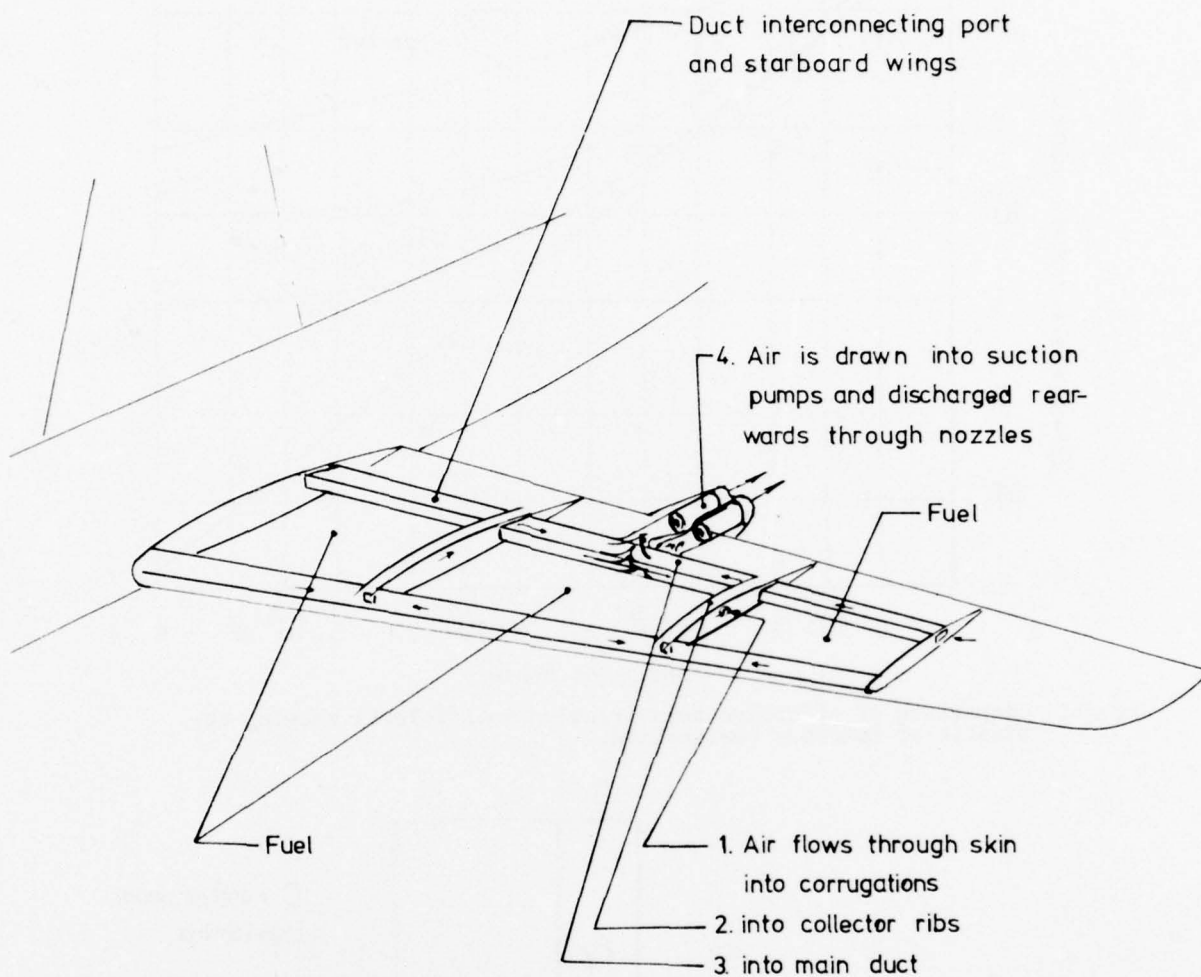


Fig. 13 Outline of a laminar flow control system.

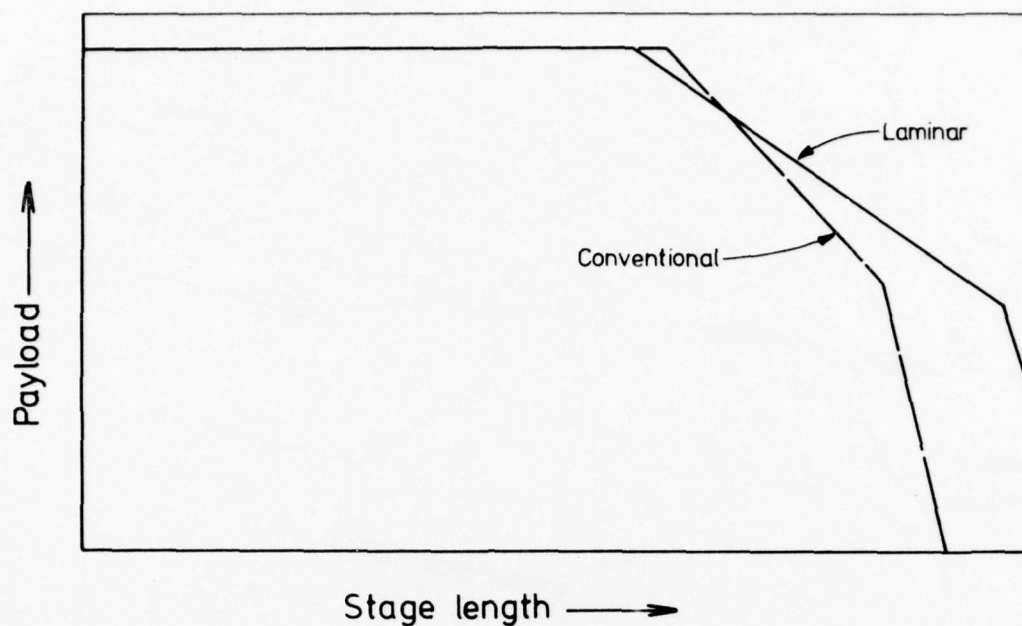


Fig. 14 Comparison of range payload characteristics.

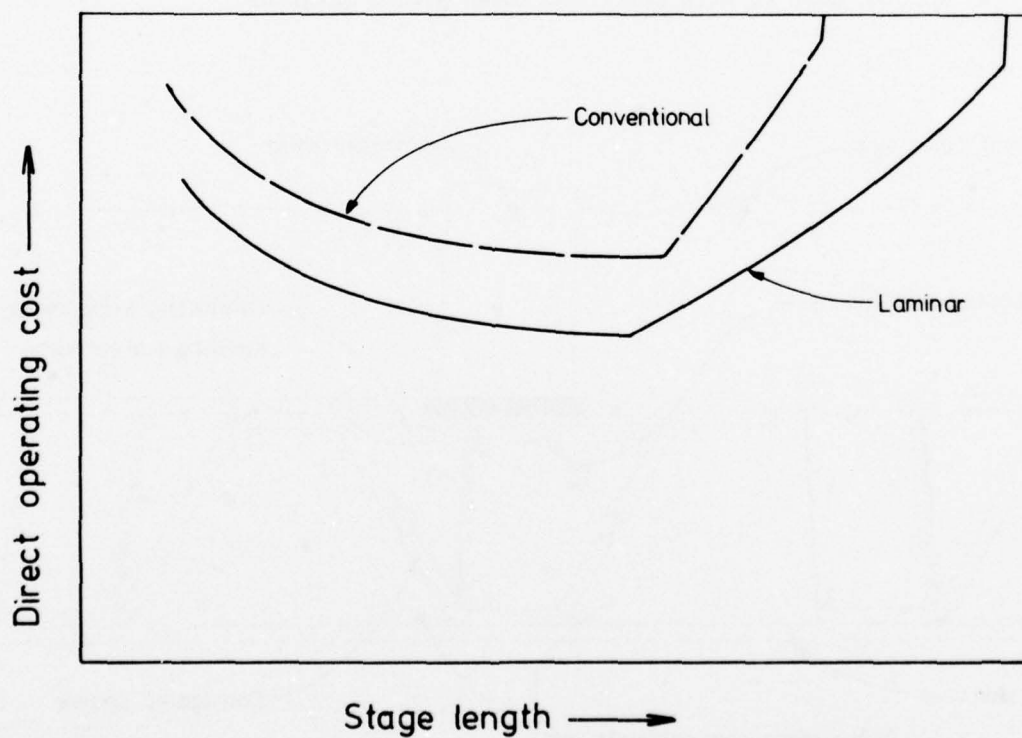


Fig. 15 Comparison of direct operating cost characteristics.

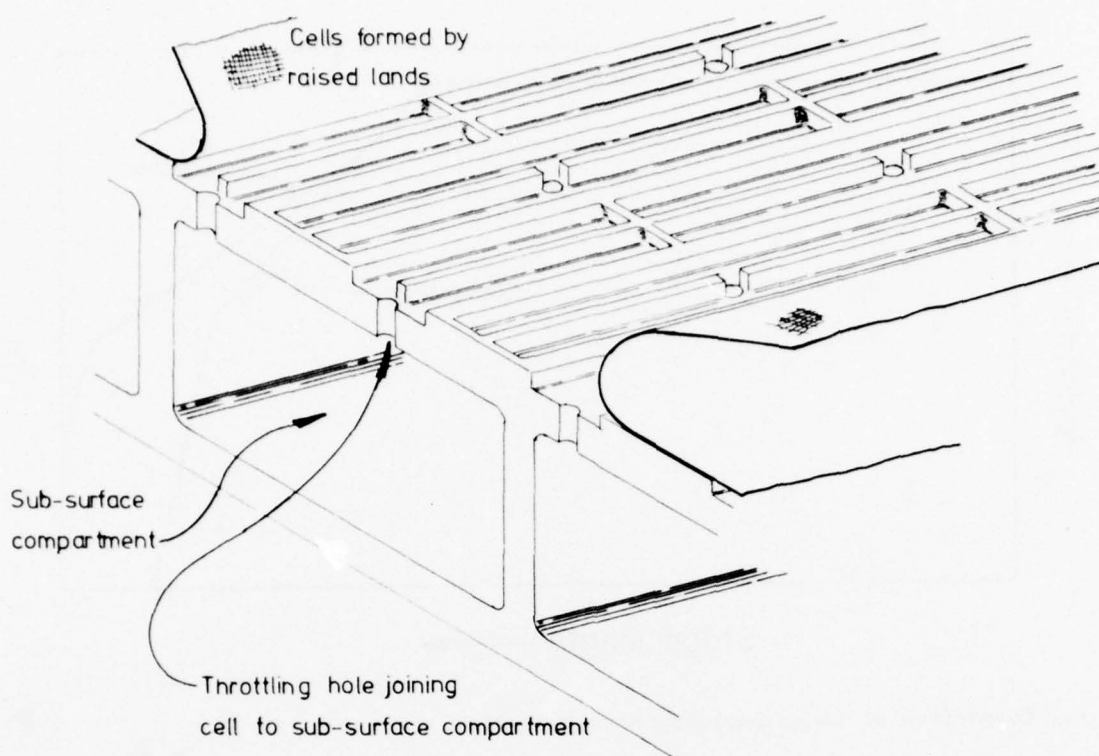


Fig. 16 Suction surface with cells and woven porous material.

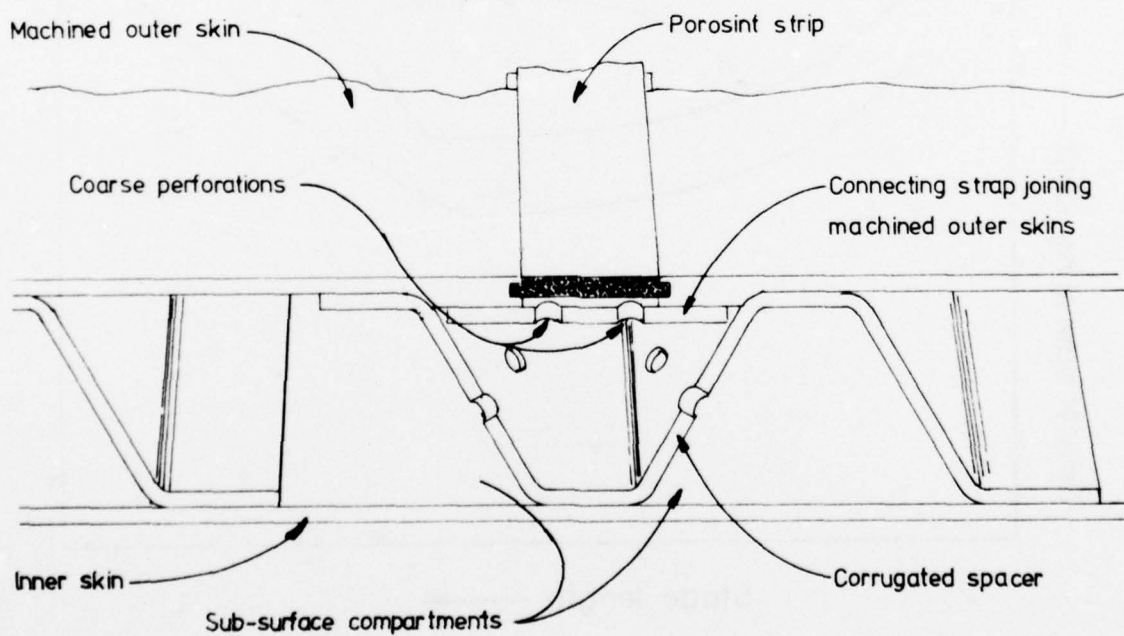


Fig. 17 Handley Page suction surface with porous strip inserts.

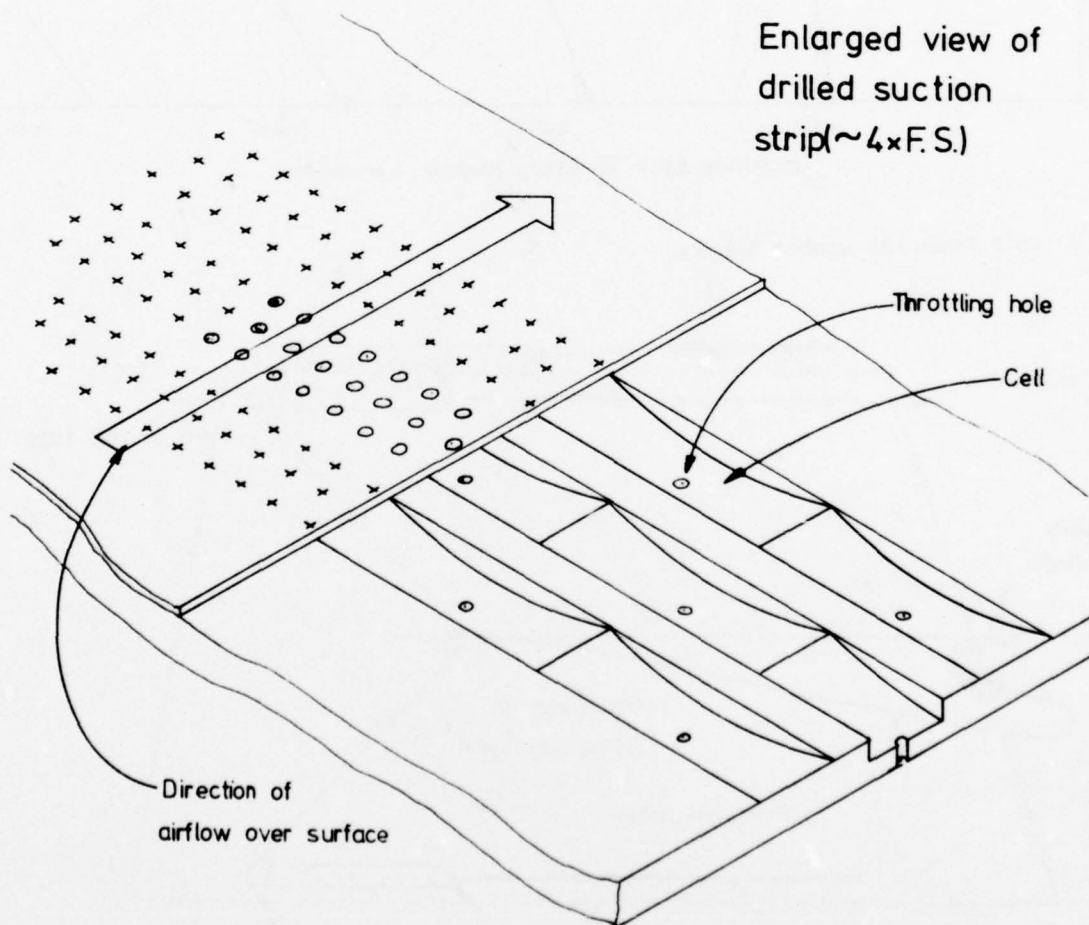
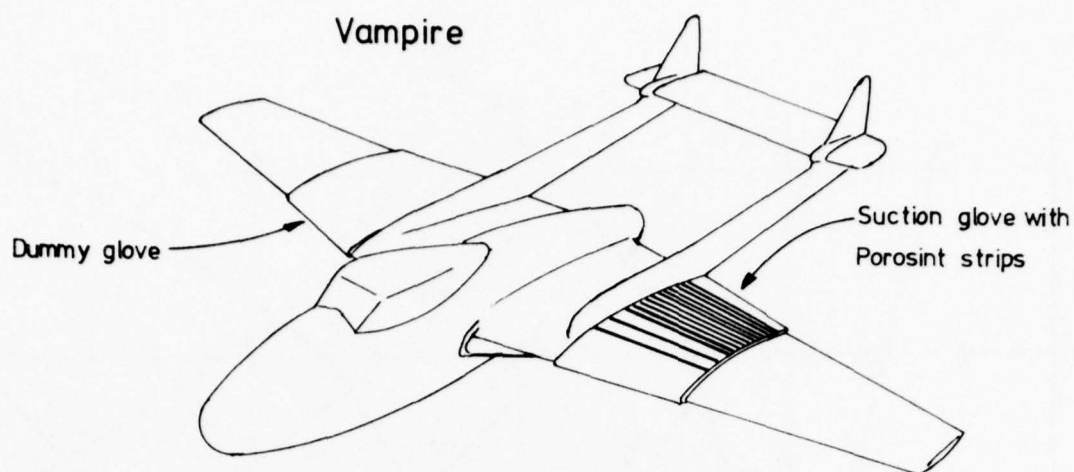


Fig. 18 Vampire with original Handley Page test surface and enlarged view of later drilled strip suction surface.

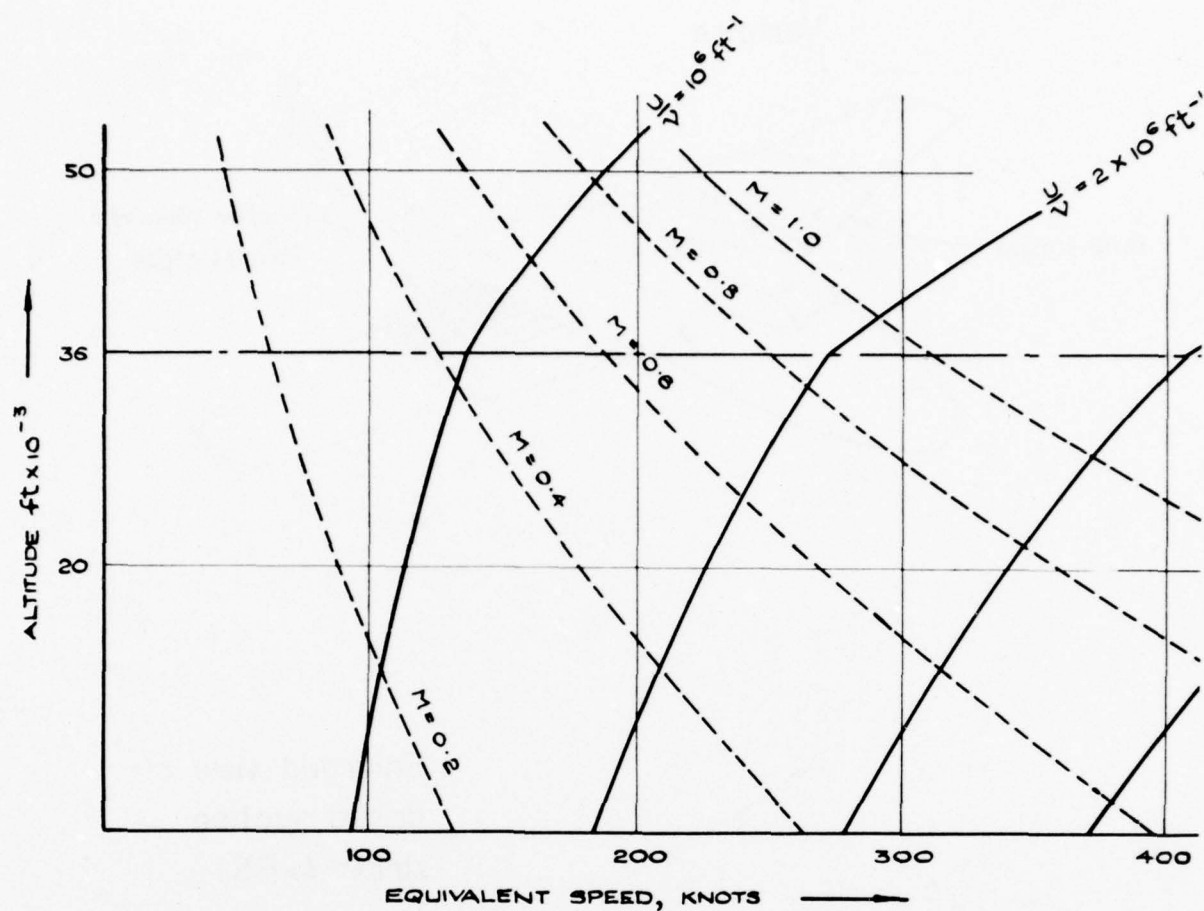


Fig. 19 Unit Reynolds number chart.

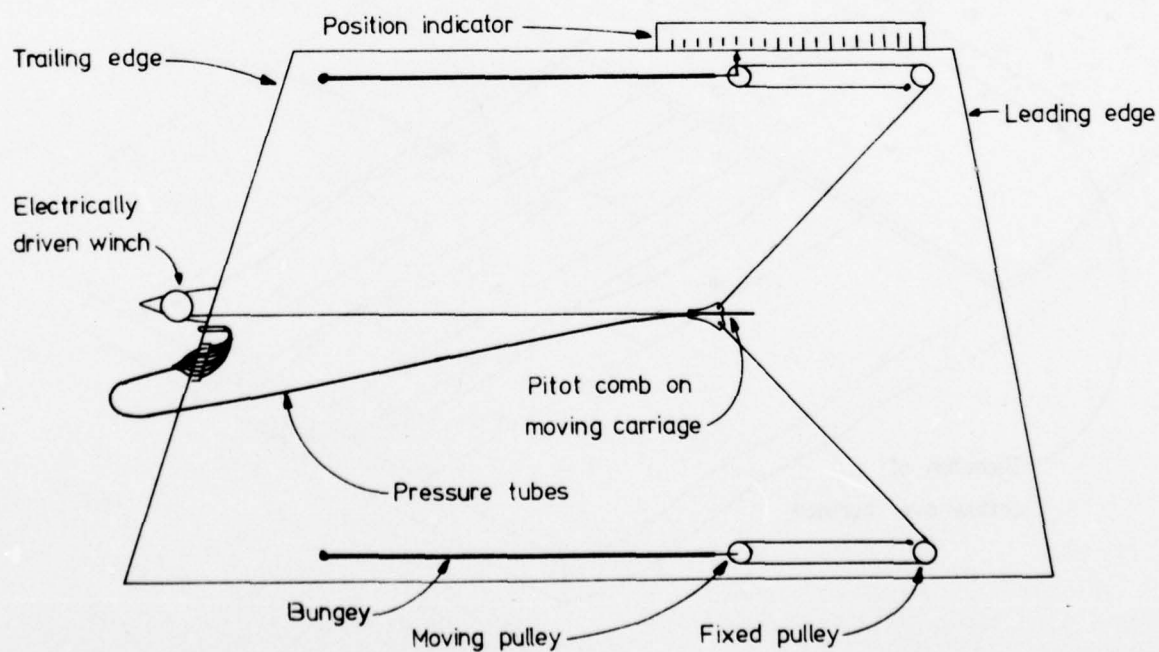


Fig. 20 Arrangement of traversing pitot comb on Vampire test surface.

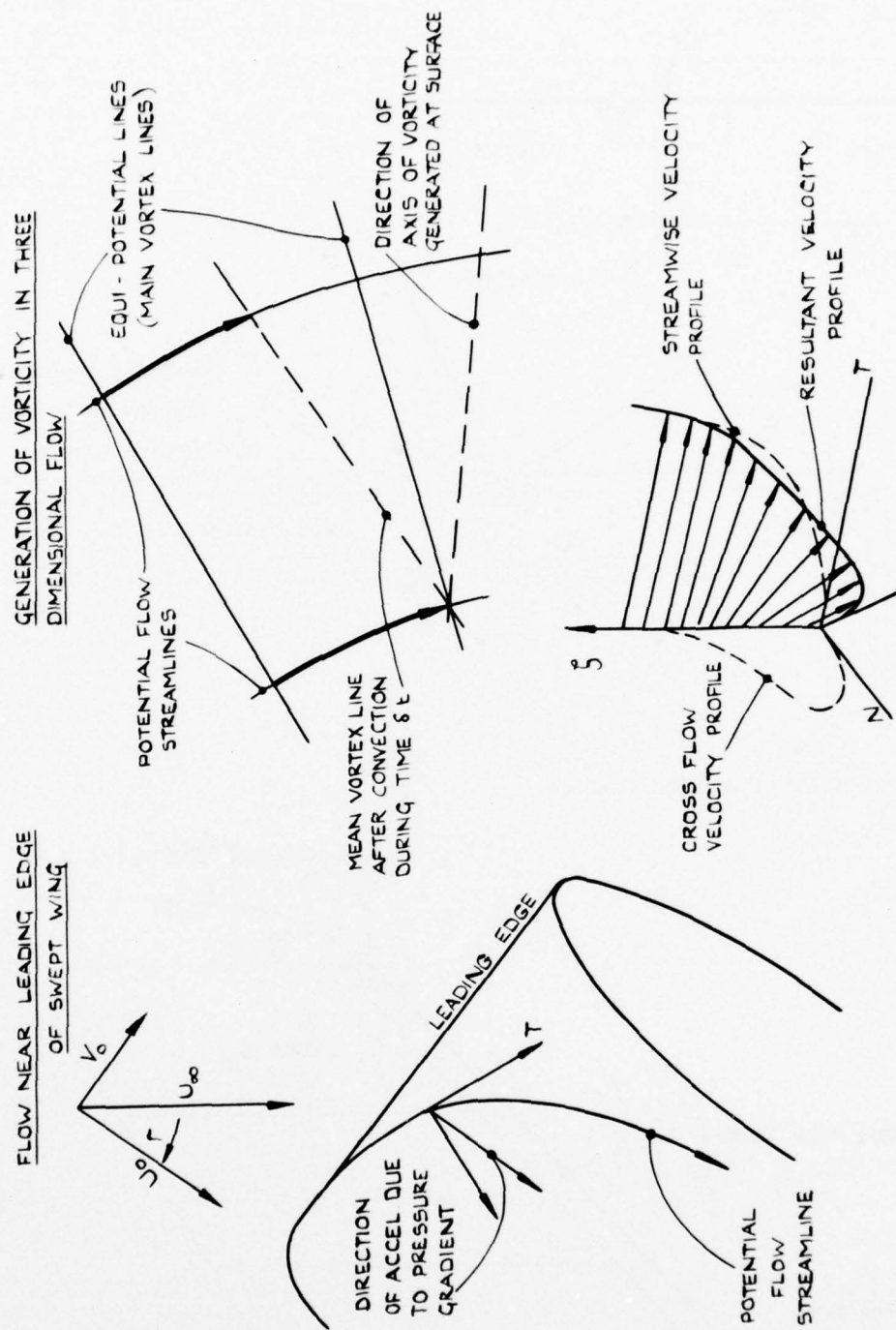


Fig. 21 The development of cross-flow.

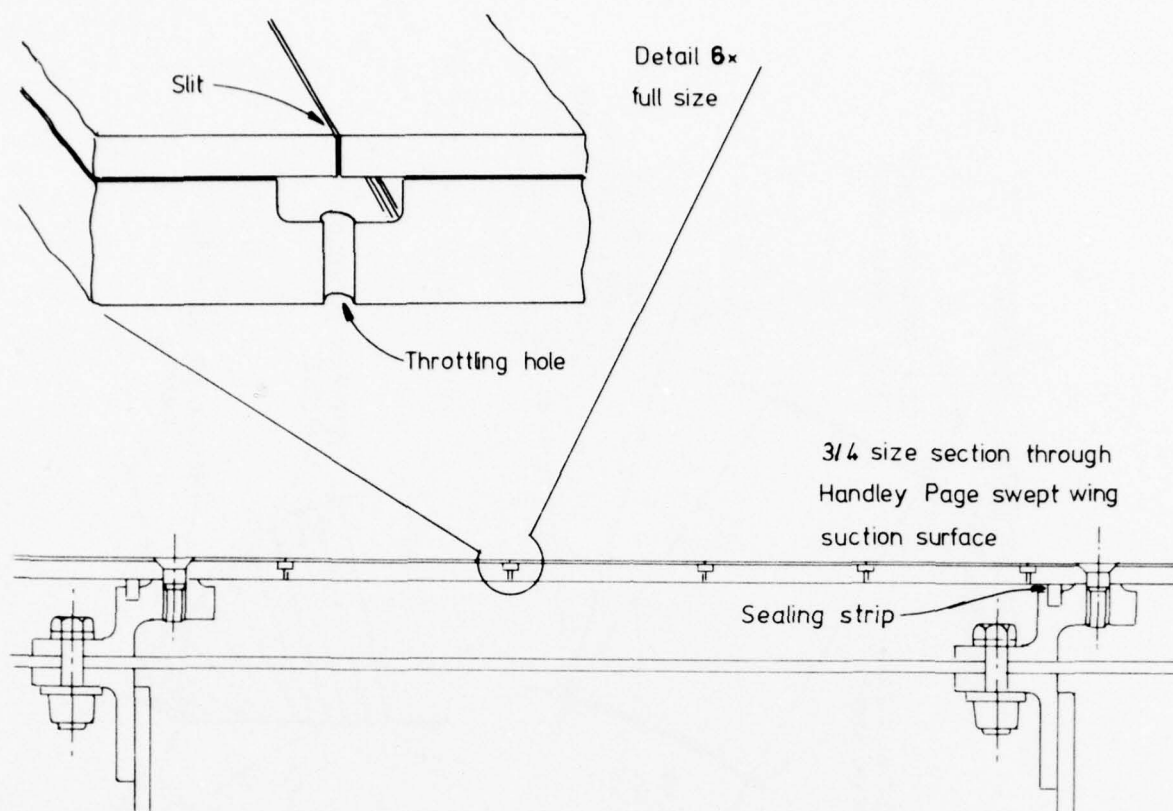


Fig. 22 Slitted suction surface.

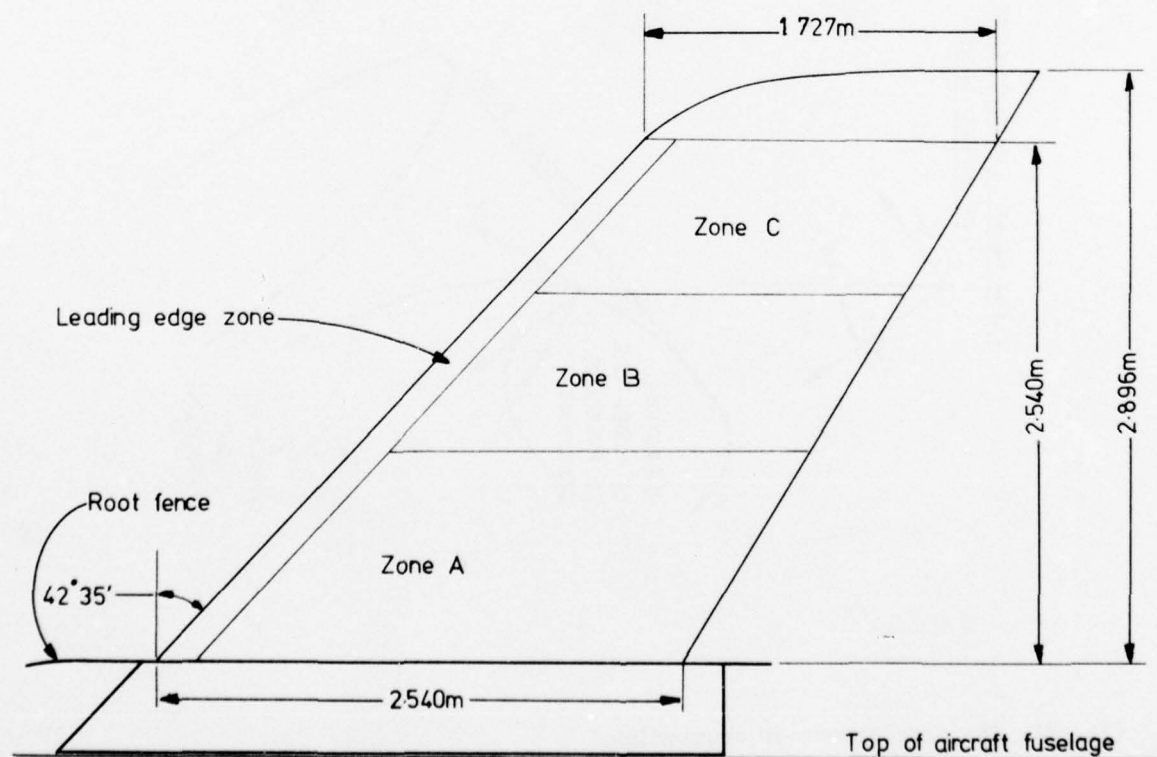


Fig. 23 Dimensions and zoning of Handley Page experimental swept-back wing.

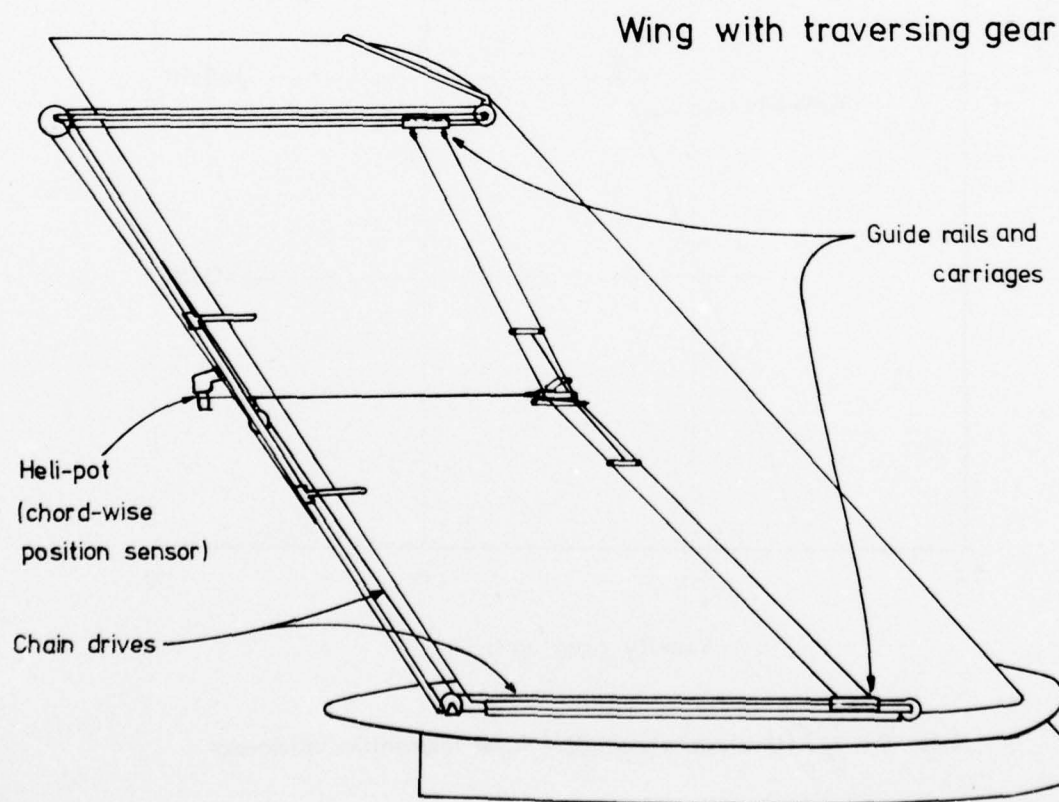
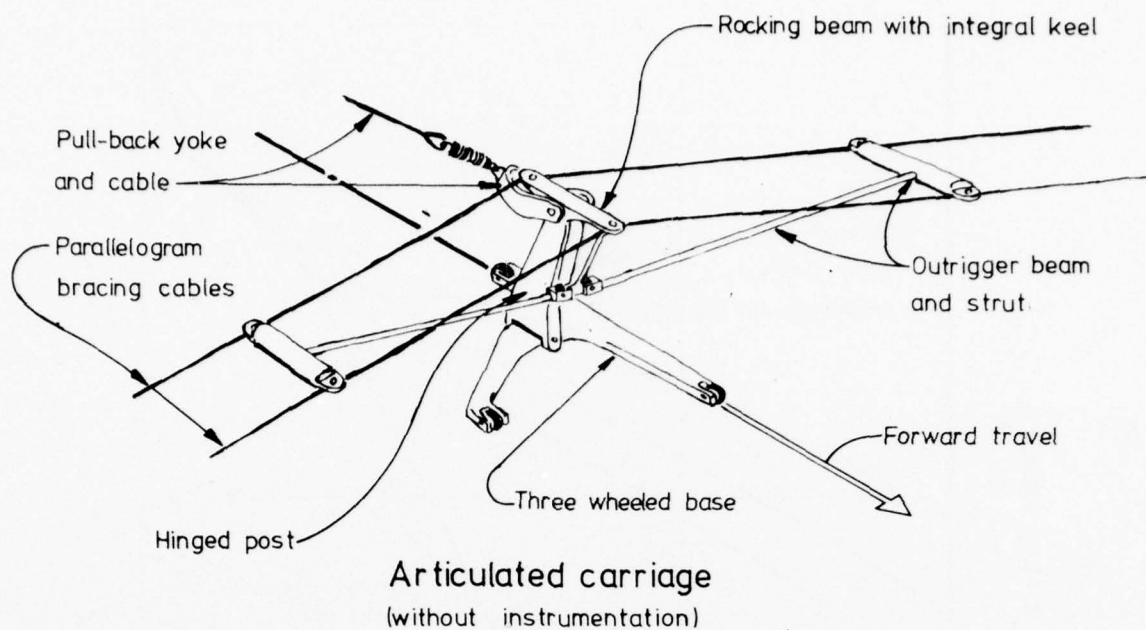
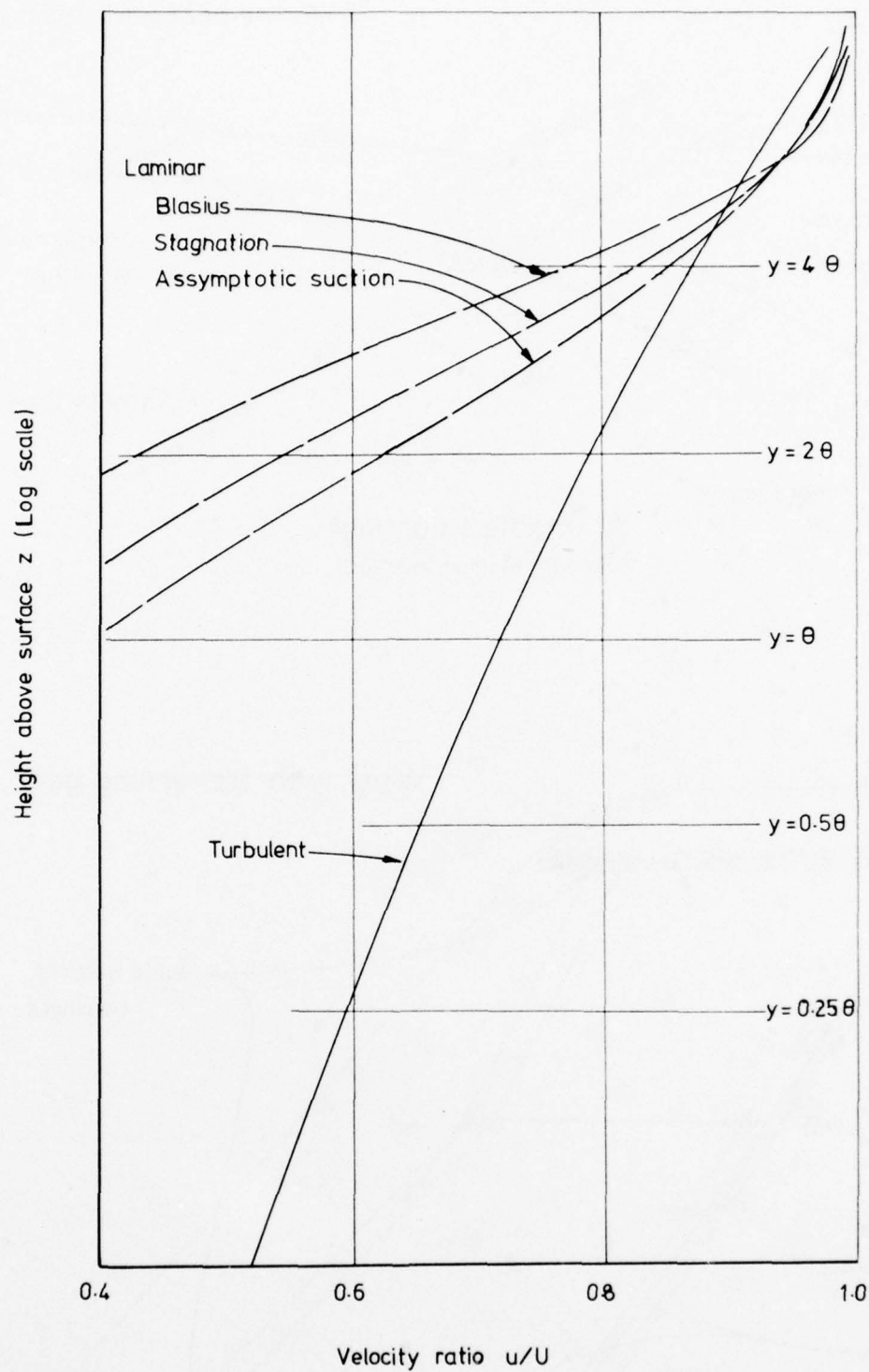


Fig. 24 Instrument traversing gear on Handley Page experimental swept-back wing.



Note: $\theta = \frac{1}{U} \int_0^{\infty} (U-u) u dz$ = Boundary layer momentum thickness

Fig. 25 Boundary layer velocity profiles plotted on log height basis.

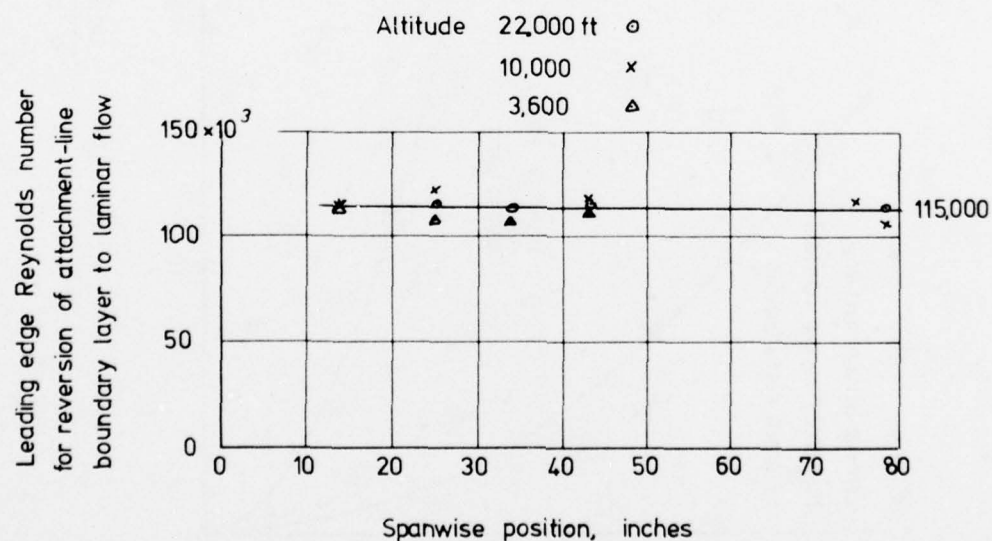
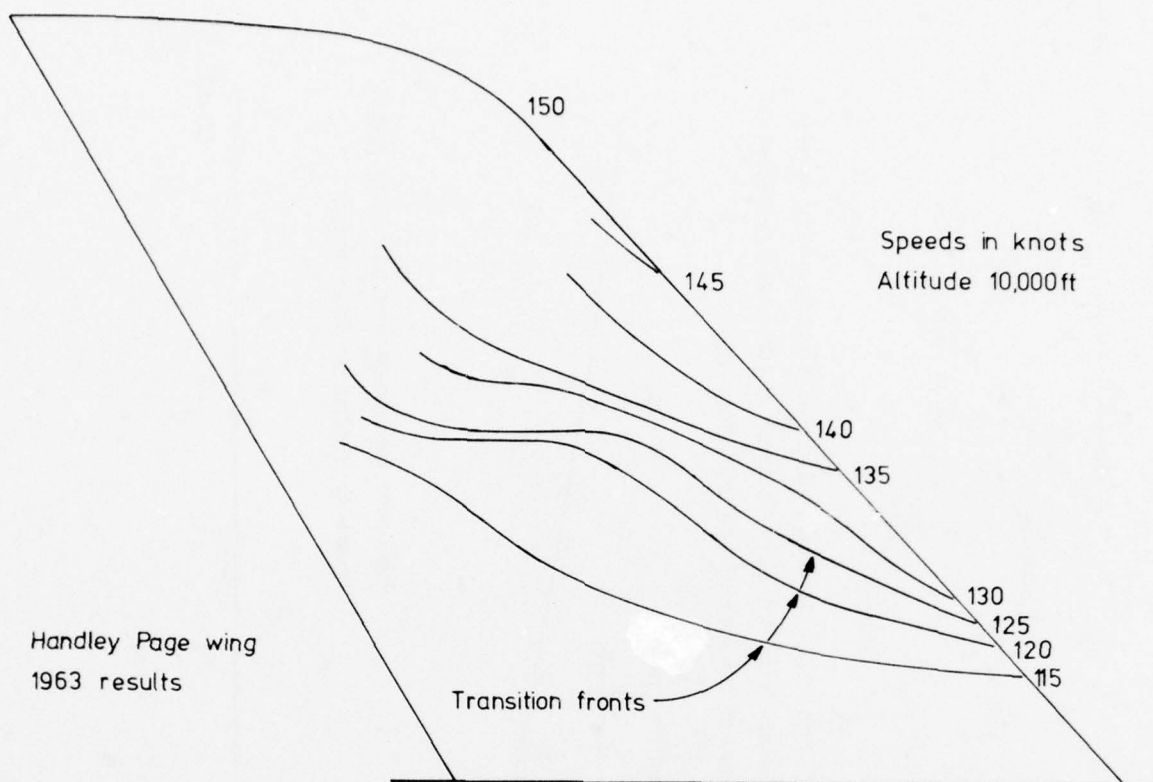


Fig. 26 Transition fronts on Handley Page experimental swept-back wing showing the effect of spanwise contamination.

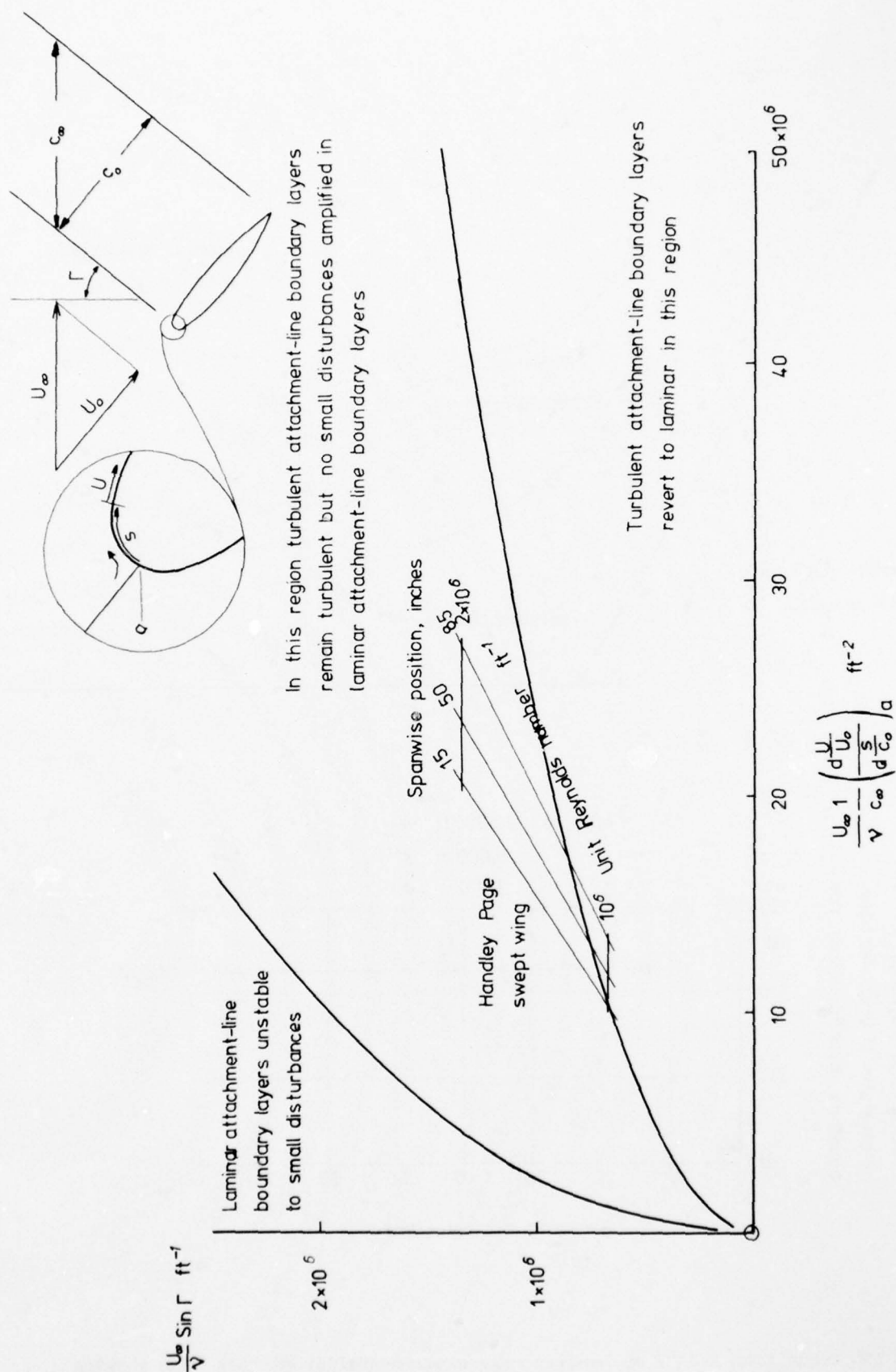


Fig. 27 Diagram showing categories of attachment-line boundary layer characteristics

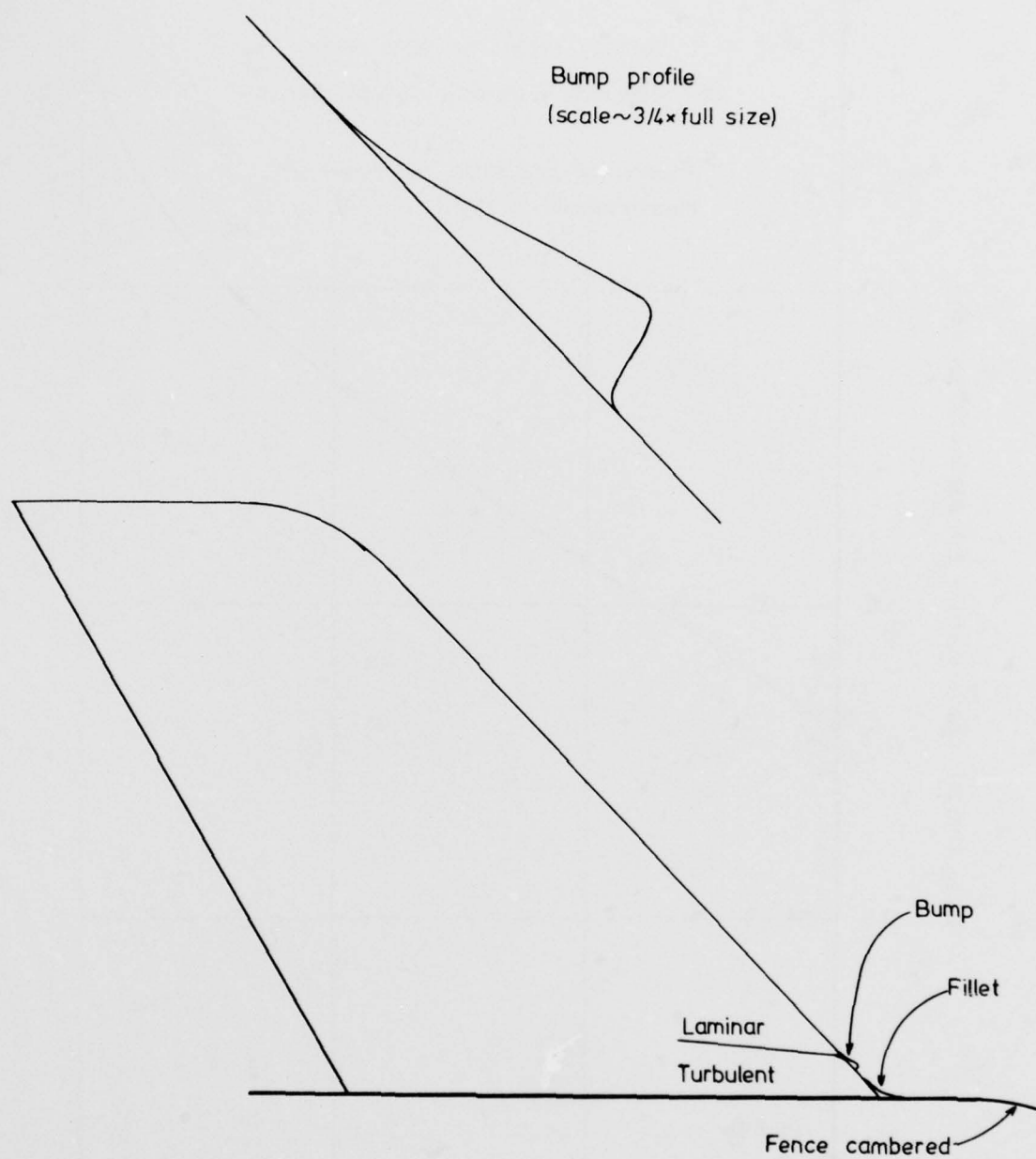


Fig. 28 The Gaster bump.

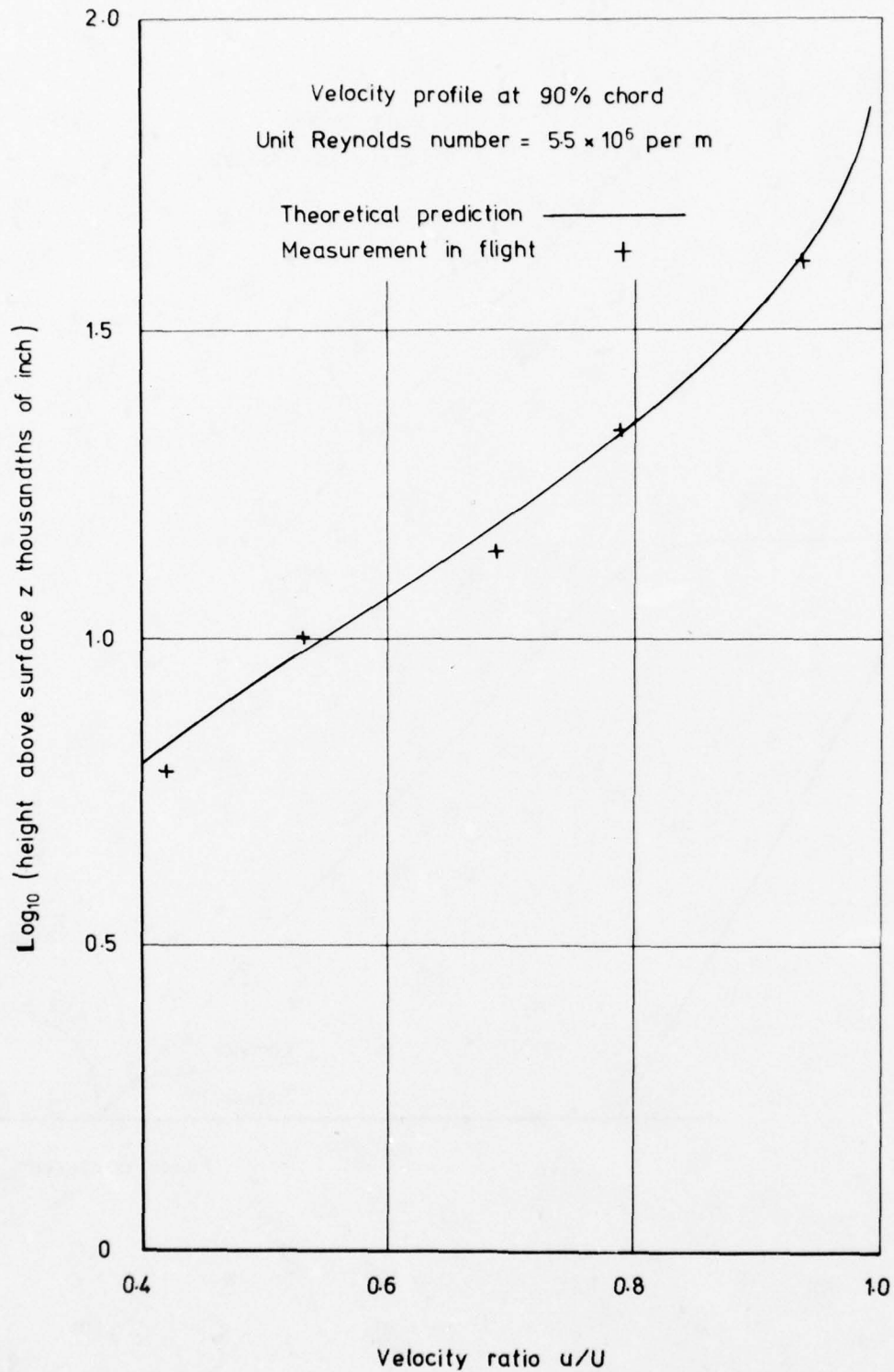


Fig. 29 Comparison of measured and calculated boundary layer velocity profiles on the Handley Page experimental swept-back wing.

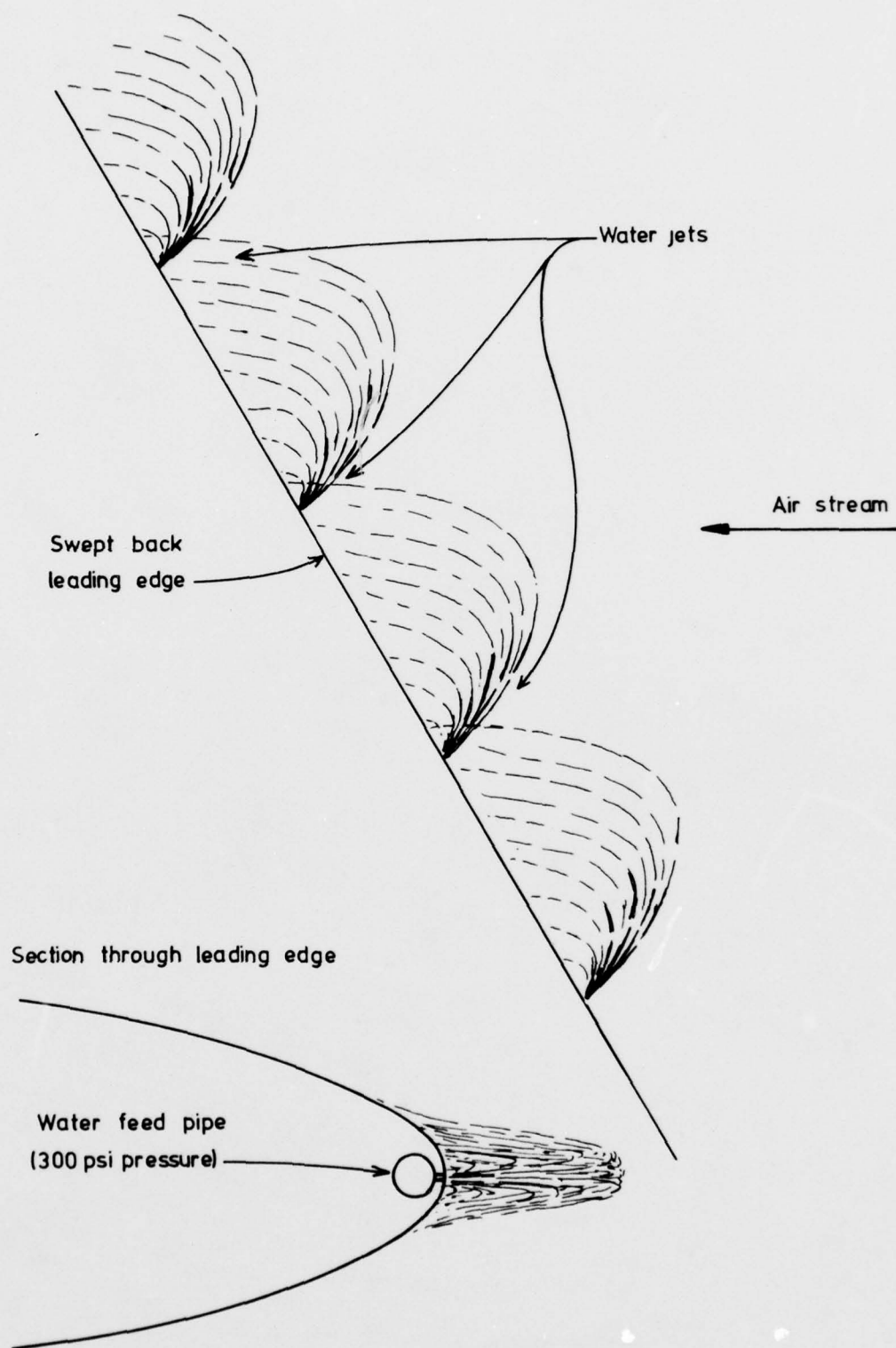


Fig. 30 Handley Page water-spray system for removing insect remains from wing leading edges.

SLOT INJECTION FOR SKIN-FRICTION DRAG REDUCTION

A. M. Cary, Jr., D. M. Bushnell, and J. N. Hefner
 NASA Langley Research Center
 Hampton, Virginia 23665
 U.S.A.

NOMENCLATURE			
		u	Velocity
A	Area	x	Coordinate along the wall (downstream of slot)
C_w	Wall concentration	y	Coordinate normal to the wall
C_f	Skin-friction coefficient	δ	Boundary-layer thickness
C_F	Total skin-friction drag, $\frac{1}{x} \int_0^x C_f dx$	λ	Mass flow ratio, $\rho_j u_j / \rho_\infty u_\infty$
C_{PB}	Base pressure coefficient	ρ	Density
D	Drag	<u>Subscripts</u>	
l	Length	EQ	Equilibrium value
M	Mach number	e, ∞	Free-stream conditions
N	Number of slots	j	Slot flow conditions
p	Pressure	o	No-slot or no-injection value
$P_{r,t}$	Turbulent Prandtl number	T	Total or stagnation
S	Slot height	w	Wall value
T	Temperature		

1. INTRODUCTION

Slot injection defined in the conventional manner describes the process of injecting a gas from a slot such that the injected gas lowers the downstream equilibrium surface temperature and, if of sufficiently low momentum, reduces downstream skin-friction drag. Most available experimental information on slot injection describes the effects of injection on downstream cooling effectiveness with only limited data available on the effects of injection on skin-friction drag reduction. It is the drag reduction aspects of slot injection that form the main theme of this paper.

The most common configuration for slot injection found in the literature is for tangential injection of air along a two-dimensional surface with air as the mainstream flow (illustrated for subsonic flow in Fig. 1). For low slot flow momentum relative to the mainstream (wall wake flow), skin-friction drag is reduced downstream of the slot; as the slot and mainstream flow mix downstream, the skin friction slowly approaches the no-slot values. Many geometric variations from this two-dimensional geometry have been investigated (including injection angle and three dimensionality with discrete holes or slots) with particular application to cooling turbine blades and engine components, see Goldstein;¹ however, most available experimental information on skin-friction reduction by slot injection is for conventional two-dimensional or axisymmetric geometries.

Direct (balance) measurements of skin-friction reductions resulting from air-air tangential injection were reported in References 2 and 3 for subsonic flow and in References 4 through 9 for supersonic/hypersonic flow. Indirect measurements of skin-friction reductions using either Clauser plots, force balances, Reynolds analogy, or Preston tubes were reported in References 10 and 11 for subsonic flow and in References 12, 13, and 14 for supersonic flow. Direct measurements of surface shear using balances are the most reliable data and will be emphasized herein. Although there is a significant body of data available describing cooling effectiveness downstream of slot injection, it is of limited use in defining the drag reduction capability of slots. The amount of experimental information available on slot injection drag reduction is insufficient to allow accurate empirical correlations to be formulated, and thus the data which are available will be used to determine the efficacy of numerical prediction methods. These numerical codes can then be used to generate necessary input for systems analyses of slot injection as a drag reduction system.

The contents of this paper includes a description and analysis of slot injection in low-speed flow, slot injection in high-speed flow, a discussion of aircraft applications, and possibilities for future improvements of slot drag reduction capability.

2. SLOT INJECTION IN LOW-SPEED FLOW

2.1 Flow-Field Characteristics

A schematic of the flow field for slot injection in subsonic flow is shown in the upper part of Figure 1. For a local skin-friction reduction, the slot velocity (u_j) must be less than the mainstream velocity (u_∞). The local skin friction is lowest near the slot and increases downstream, approaching the

no-slot values. The rate of mixing between the slot and boundary-layer flow determines the exact distribution of skin friction. The principal variables which affect the amount of skin-friction reduction are listed in Figure 1 and are sufficiently numerous so that empirical correlations become extremely difficult. In fact, the effects of most of these parameters on skin-friction reduction have never been experimentally determined. Thus, with the present state of the art, a detailed prediction method is necessary for any sensible systems analysis to be made.

2.2 Prediction Method

Several prediction methods are currently available for solving numerically the equations governing the flow development downstream of slot injection.¹⁵⁻¹⁷ Each of the prediction methods has advantages, depending on the particular equations solved and the turbulence modeling used. The method of Reference 17 will be used herein because the predictions are valid in the near slot region ($x/S < 10$) as well as far downstream, and the turbulence modeling is easy to modify. In this method, the partial-differential equations for the mean motion of a two-dimensional, compressible turbulent boundary layer with tangential injection are solved by an implicit finite-difference procedure. Reynolds stresses are modeled using conventional algebraic length scale/eddy viscosity concepts. Current restrictions on the calculation method are: (1) air-to-air injection, (2) constant normal pressure ($dp/dy = 0$ everywhere, no shocks), and (3) thin slot lip (no extensive separation/recirculation).

Typical examples of predicted velocity, concentration, and mixing-length profiles for a slot-injection flow are shown in Figure 2. The equation set includes a concentration equation in which the injected air is treated as a separate species in order to delineate the mixing region between the slot flow and the external boundary-layer flow. A representative dimension of the mixing region is then used to determine the algebraic length scale in the mixing regions. Details of the turbulence modeling are available in Reference 17. This numerical method was shown to give good predictions of surface shear, heating, and equilibrium temperature in References 4, 7, 17, and 18; however, subsequent comparisons with experimental velocity profiles (Ref. 7 and in the present lecture series) indicated poor agreement between predictions and velocity data. The turbulence modeling was therefore modified by the present authors to better represent the physical flow for the entire speed range from subsonic to hypersonic. The modifications allowed the basic philosophy for turbulence modeling of slot flows as presented in Reference 17 to remain unchanged, but the magnitude and distribution of the algebraic length scale was altered in Zones I, II, and III (see Fig. 2). The resulting predictions of velocity profile data over the speed range were quite satisfactory and examples will be presented in a later section. Initial comparisons of skin-friction data with predictions using the new turbulence modeling were not as good as expected; the wall shear was underpredicted in the region of highest mixing. Recent experimental evidence presented in References 3 and 19 indicates that the turbulence level in the near-wall region increases sharply where the mixing zone nears the wall and then relaxes downstream. It is reasonable to assume that this virulent turbulence would thin the viscous sublayer and result in increases in local shear stress. The near-wall turbulence model was therefore modified to account, at least to first order, for sublayer thinning (using the rate of change of the "wall concentration" as a measure of the mixing layer influence on the near-wall flow). This modification did not appreciably affect predictions of velocity profiles but provided excellent predictions of skin friction and equilibrium surface temperature data.

2.3 Comparison Between Prediction and Experiment

Several comparisons of predictions using the method of Reference 17 (modified as previously discussed) with subsonic experimental data are shown in Figures 3 through 6. Experimental skin-friction data with tangential slot injection at Mach 0.8 (from Ref. 3) are compared with prediction in Figure 3. Predictions with and without the near-wall modification for increased turbulence intensity are shown for comparison. Initial profiles at the slot exit as well as pressure gradients are necessary inputs; in addition, various turbulence modeling parameters such as the initial slot mixing-length coefficient, the mixing-length coefficient for the mixing region, the mixing-length coefficient for the outer portion of the turbulent boundary layer, and the Prandtl constant must be input (see Ref. for further explanation). The prediction method, as modified, used the same set of turbulence modeling parameters over the entire speed range, and in the nomenclature of Reference 17 are: $a_j = 0.14$, $a_m = 0.12$, $f_f = 0.1$, and $K = 0.4$. In Figure 3, it is clear that the near-wall modification provides a better prediction of wall shear stress than the conventional prediction. Note that the prediction is good even in the near-slot region. A prediction of equilibrium surface-temperature for Mach 0.12 flow is compared with experimental data from Reference 10 in Figure 4 ($P_{r,t} = 0.85$). The prediction using the near-wall modification again agrees well with experiment over the entire slot flow region. The extent of the region near the slot where the wall shear is lowest and the surface equilibrium temperature equals the slot flow temperature is also well predicted by the numerical method as shown in Figure 5 (experimental data from Refs. 20 through 24). This parameter is of interest when multiple slot configurations are under consideration.

Examples of velocity profile predictions for subsonic flow are shown in Figure 6. The experimental data shown in Figure 6 are from Reference 10 and cover a range of x/S from 15 to 75. Here, predictions are shown using both the original turbulence modeling of Reference 17 as well as the modified modeling. For low-speed cases, the turbulence modeling modification had little effect, and both models provide a creditable prediction of velocity profiles; larger differences will appear in later predictions for high-speed flow experiments. There is a tendency toward underprediction of the velocity profiles far downstream of the slot in Figure 6. This was even more prevalent in comparisons, not shown herein, between prediction from the present method and velocity profiles from Reference 25. Since the present numerical prediction procedure is expected to be most accurate far downstream of the slot where the mixed boundary layer is approaching "equilibrium," the underprediction cannot easily be attributed to a turbulence modeling error. The more likely explanation for the disagreement is the presence of some new physics, a possibility being that the slot lip is shedding Kármán vortices which develop downstream and increase entrainment; thus, the resulting experimental velocity profiles would be more full than the prediction. Some justification for this explanation is presented in Reference 26 where, for a subsonic mixing flow, it was shown that for u_j/u_∞ near one, Kármán vortices were shed from the splitter plate; however, as u_j/u_∞ was reduced by reducing the "slot" velocity, the vortices did not form. This is consistent with the present results where some disagreement was noted for $u_j/u_\infty = 0.63$ (Fig. 6), and considerably more disagreement for the data of

Reference 25 for which $u_j/u_\infty = 0.83$. A much more sophisticated prediction method than the present one would be necessary to include such phenomena as vortex formation effects on downstream flow characteristics. It appears, however, that the present prediction method is an adequate tool for providing input to systems analyses if the slot-to-free-stream velocity ratio is not too near one.

2.4 Parametric Calculations

Because insufficient data are available, it is necessary to use a prediction method to delineate the effects of some parameters which significantly impact the efficacy of slots as drag reduction devices. A force balance relative to slot injection is shown in Figure 7. In order for a net drag reduction to result from slot injection, the skin-friction reduction with slot injection plus the slot thrust must be greater than the losses associated with collecting, ducting, and distributing the slot air plus slot base drag.

The amount of skin-friction reduction with slot injection can be calculated using a prediction method. An example of such a calculation (using the method of Ref. 17) is shown in Figure 8 where skin-friction distributions for subsonic flow downstream of tangential slot injection are shown for several slot-to-free-stream velocity ratios (for low-speed flows, the rate of mixing between two flows is controlled to first order by the velocity and not the mass flow ratio between the streams).²⁷ If these skin-friction distributions in Figure 8 are integrated with x/S , the resulting drag reductions for each slot velocity ratio are obtained. Results from such an integration for a distance of 60 slot heights downstream are shown in Figure 9. It appears that for this case an optimum slot-to-free-stream velocity ratio for maximum drag reduction lies between 0.3 and 0.4. There are other factors such as listed on Figure 1 which impact the amount of drag reduction obtainable with any slot configuration (see Fig. 1), and most of these can be accounted for with the prediction method.

Slot base drag is extremely difficult to obtain analytically, and experiment must provide guidelines. A brief literature survey of base drag with injection resulted in the experimental information shown in Figure 10 (experimental data from Refs. 3 and 28 through 31). Here, the base pressure coefficient with injection, C_{PB} , ratioed to base pressure coefficient with no injection, $C_{PB,0}$, is shown against slot-to-free-stream velocity ratio. These meager data indicate that base drag decreases sharply with increasing injection velocity ratio, a favorable effect for drag reduction.

If the results from Figures 9 and 10 are combined, the result shown in Figure 11 is an example of drag reduction expected from slot injection including base drag for subsonic flow. The insert on Figure 11 shows three distributions of C_{PB} used in the calculations to show the sensitivity of the drag budget to base drag. Slot thrust and collecting/ducting losses are not included here. It is obvious from Figure 11 that slot base drag is extremely important and must be known accurately to evaluate slot injection as a drag reduction system since margins for error are not large. Additional results from system analyses including slot thrust and collecting/ducting losses will be presented in a later applications section.

An example calculation of the local skin-friction reduction downstream of multiple slot injection for a typical CTOL configuration at cruise flight conditions is shown in Figure 12 taken from Reference 32. These predictions were obtained by modifying the method of Reference 17 to include multiple slot injection. The modification was straightforward and consisted of using normal procedures to calculate the first slot flow field downstream to the prescribed location of the second slot; here, the calculated profiles at the second slot location along with input profiles for the slot flow of the second slot are used as inputs, and the calculation then continues downstream of the second slot. This procedure is repeated for as many slots and slot spacings as desired. The results shown in Figure 12 indicate that the absolute value of C_f decreases from slot to slot (at equivalent distances) with each slot producing lower drag than the preceding one. The favorable drag reduction for multiple slots must be weighed against the cost in drag for acquiring slot injection air, a subject addressed in a later section. Analytical predictions must provide the data necessary to evaluate multiple slot injection since almost no experimental data are available even to evaluate the prediction method (Ref. 3 presents some limited data for two slots).

3. SLOT INJECTION IN HIGH-SPEED FLOW

3.1 Additional Flow-Field Physics

When the external flow is supersonic or hypersonic, additional parameters must be considered in analyzing slot injection flows. In particular, the ratio of slot static pressure (p_j) to free-stream static pressure (p_∞) becomes important just as for supersonic nozzle flows. Schematic drawings of an overexpanded and an underexpanded slot flow for a supersonic external stream are shown in Figure 13. The presence of shock waves, expansion regions, and recompression regions greatly complicates the physical flow field. The prediction method used herein is uniformly valid only for p_j/p_∞ ratios near one, and it is in this region that the discussion will center. Examples of the effect of p_j/p_∞ being greater than or less than one on downstream surface shear are given in References 4 and 8.

It is generally difficult to obtain the ratio p_j/p_∞ exactly one. Figure 14 (from Ref. 7) shows that for Mach 6 as the mass flow rate, $\lambda = \frac{\rho_j u_j}{\rho_\infty u_\infty}$, is increased from the no-injection case, the wall static pressure at the slot exit increases until the slot flow becomes sonic; at this point, the slot pressure is slightly less than the stream static pressure $p_{w,0}$ due to the expansion of the free-stream flow over the slot lip. Further increase of the slot mass flow rate first reduces the near-slot pressure and then increases it. The subsequent increase in the near-slot pressure is caused by the slot flow fully expanding with the Mach number in the near-slot region remaining constant. The discussion in this section will be concerned with the case of the sonic slot corresponding to the first peak in the pressure distribution shown in Figure 14 ("matched" pressure condition of Refs. 4 and 7). For this condition, there are only weak shocks in the flow field and mild pressure gradients.

3.2 Comparison Between Prediction and Experiment

Examples of predictions of supersonic (Mach 3) velocity profiles with slot injection compared with experimental data (from Ref. 9, slight injection angle) are presented in Figure 15. The predictions presented in this section were calculated using the modified turbulence modeling with the method of Reference 17. The turbulence modeling constants were the same as for low-speed flow cases already discussed. The agreement between prediction and data in Figure 15 is reasonably good with some deviation obvious near the slot; this deviation probably results from the slight injection angle (15° to mainstream flow) which was not accounted for in the prediction method. Agreement far downstream of the slot would be expected for this supersonic flow since Kármán vortices are not present.

Experimental skin-friction measurements downstream of tangential slot injection at Mach 6 are compared with the prediction method in Figure 16. The prediction using the near-wall turbulence model modification to account for sublayer thinning caused by high local turbulence (same modification as for low-speed flow as discussed earlier) agrees much better with the experimental data than the prediction using conventional near-wall modeling. It thus appears that this near-wall modeling modification is a necessary ingredient for predicting skin-friction drag downstream of slot injection for high-speed flows as well as for low-speed flows. Corresponding comparisons of predictions and experiment for the equilibrium wall temperature ($P_{r,t} = 0.85$) for the same flow as in Figure 16 are shown in Figure 17. The agreement is again good except in the near-slot region where heat conduction into the slot injection manifold reduces TEQ slightly.⁴

Velocity profiles obtained for the same conditions as the data on Figures 16 and 17 are presented in Figure 18 and clearly show the necessity for the modified turbulence modeling used herein with the method of Reference 17. The modified modeling provides a vastly improved prediction of the velocity profiles downstream of the slot. Both the modified and original turbulence models will obviously give the same prediction far downstream of the slot.

The consistently good agreement between experimental surface and flow-field data and the modified prediction method of Reference 17 for both low- and high-speed flows provides an acceptable confidence level for using analytical data in systems evaluation of slot injection flows for drag reduction on practical aircraft. This approach is necessary since available experimental information on the drag reduction aspects of slot injection is scarce.

4. AIRCRAFT APPLICATIONS

Tangential slot injection is one of the few approaches which consistently reduces turbulent skin-friction drag. The amount of drag reduction is predictable and significant. As pointed out in Figure 7, the slot skin-friction drag reduction plus the thrust generated by the injected flow are the positive aspects of slot injection; on the negative side are base drag penalties (discussed earlier) and losses associated with collecting and distributing slot air. Of these, the cost of collecting slot air is the most severe penalty and has, in fact, been the main reason that slot injection is not now considered an attractive drag reduction system.

For applying slot injection to conventional transport aircraft there are several possible sources for the slot air which include: (1) accepting full ram drag penalty charged to the slot injection system for taking on outboard air, (2) air bleed from conventional engines, (3) laminar flow control suction air, (4) air from base suction on a truncated fuselage, and (5) fuselage boundary-layer air ingested into an engine. Each of these proposed air sources will be discussed in light of their potential for providing a total aircraft drag reduction. It should be pointed out here that to date no comprehensive systems analysis of slot injection as a drag reduction system for any aircraft has been attempted. In References 33 and 34, cursory analyses were made but were general and did not address system optimization.

The simplest analysis will show that if the slot injection system must use slot air obtained by decelerating free-stream air (accepting total ram drag penalty) then a total aircraft drag increase will result. The key problem is then to find a source of slot air for which the drag penalties are significantly less than the ram drag penalty. Using air bleed from conventional engines to supply slot air is unattractive from a propulsion efficiency standpoint and is not further pursued.

4.1 Laminar Flow Control Suction Air

Suction air resulting from LFC suction surfaces proposed for the wings of future conventional aircraft represents a source of slot air for which drag penalties may be relatively low. This air must be pumped through the propulsion system or dumped overboard at some penalty to the LFC system and may possibly be used to better advantage through slot injection along the fuselage. Both References 33 and 34 addressed this possibility but with nonoptimized systems. As indicated in Figure 19 from Reference 34, slot injection of LFC air on the forward portion of the fuselage resulted in a net increase of 1.2% in total fuel consumption. This slot was added as an afterthought in this study, and large penalties were charged to ducting air from the wing to the slot. If the slot had been placed in the immediate vicinity of the LFC wing, thus eliminating much of the ducting penalty, the results would probably have been more favorable. The brief analysis of Reference 33, in fact, indicates a favorable effect of the suction/slot injection combination.

Recent analyses conducted by E. Boxer of NASA Langley Research Center suggest that a 2-3% reduction in overall aircraft drag may be possible by injecting LFC air through a single fuselage slot at a velocity much less than that of the free stream rather than accelerating and discharging the LFC air at free-stream velocities. Although these analyses did not consider the additional airplane weight or length to provide ducting and machinery for pumping the LFC air to the slot exit pressure, they do indicate that a gain in total drag reduction may be possible depending on the specific design of an airplane using LFC and slot injection.

4.2 Base Suction Air

The scheme of using base suction on a truncated base of a conventional aircraft (Fig. 20) to provide slot air has not been critically analyzed. The suggestion is that sucking on a truncated base will keep the base flow attached and thus reduce base drag. In addition, the structural weight of the relatively long boattail found on most conventional aircraft will be eliminated. On the negative side, large penalties will be incurred because of the necessary pumping and relative long ducting associated with this system. There is no systems analysis of such systems as yet.

4.3 Fuselage Boundary-Layer Air

Antonio Ferri suggested a scheme³³ by which fuselage boundary-layer air (of lower momentum than free-stream air) is ingested into a turbine/compressor arrangement located peripherally around the fuselage, Figure 21. The turbine processes the slot air, and the compressor by using the turbine power accelerates a portion of the boundary-layer air and thus energizes the aircraft wake. Results from this analysis indicated that after considering the ram drag penalties and ducting losses, only a marginal total drag reduction was available. Since slot base drag was not included in this analysis, even this small drag reduction would probably evaporate.

The surface has probably not been scratched as far as the application of clever schemes to reduce ram drag for slot air. These few examples cited herein are only those for which some cursory investigation and evaluation has been done. Clearly, further research is needed before definitive decisions can be made as to the applicability of slot injection system for reducing aircraft drag.

5. POSSIBILITIES FOR IMPROVING SLOT EFFECTIVENESS

There are numerous modifications to the slot injection configuration discussed herein which may improve the net viscous drag reduction possible with such systems. To reduce the base drag penalty of the slot, a device to increase mixing in the vicinity of the slot is necessary. However, to improve the length of the low drag region downstream of the slot, it is necessary to retard mixing between the slot flow and the external boundary-layer flow. These two approaches are obviously in opposition to each other.

Very little has been done experimentally to investigate ways of increasing slot efficiency for drag reduction with the exception of studies of effects of slot geometry modifications.³⁵ Examples of ways that slot base drag can be reduced are by serrating the slot lip³⁶ or by rotating the trailing edge of the slot lip. Besides decreasing base drag, these would obviously increase downstream mixing and degrade the viscous drag reduction. There are many suggestions from the literature as to how to retard mixing downstream of the slot lip and thus increase the region of lower skin-friction drag. Some slot geometry parameters are important such as small injection angles and thin slot lips. The introduction of narrow-band, relatively high-frequency sound will retard mixing of jet flows³⁷ and may well prove useful for slot flows. Tailoring the slot velocity profile by screens or other devices or keeping the slot profile laminar (low turbulence levels) can reduce both the near-slot shear stress and retard downstream mixing. Externally applied factors such as adverse pressure gradients and thickening the external boundary layer can also lower surface shear downstream of the slot. Using multiple slots has been suggested as a method of increasing the efficiency of each succeeding slot. As shown analytically in Figure 12 for subsonic flow, each slot produces lower drag than the preceding one. A similar effect for hypersonic flow is indicated by the experimental data shown in Figure 22 for the flush slot configuration of Reference 38. If unlimited slot injection air were available at low drag penalty, multiple slots would obviously promise substantial drag reduction; however, the penalties for acquiring slot air are (as previously discussed) severe and will probably be prohibitive if large amounts of injection air are required. The analytical results from Figure 12 were integrated so that the skin-friction drag reduction as a function of the number of slots (N) could be determined. The results are shown in Figure 23. Since the drag reduction increment decreases for increasing numbers of slots, each downstream slot is actually providing less drag reduction per unit air injection than the preceding slot. With injection air at a premium, this is undesirable and suggests single slots spaced far apart are more efficient drag reducers. This discussion assumed that the injection rates from all slots were identical; tailoring the slot injection rates may improve multiple slot drag reducing efficiency on an injection mass flow basis.

6. CONCLUDING REMARKS

In summary, slot injection can consistently provide large local skin-friction reductions which are predictable with present-day numerical technology. Only crude systems studies have as yet been accomplished, and detailed, definitive, and innovative studies are required before the verdict as to the efficacy of slot injection systems to reduce aerodynamic drag can be determined. In addition, much experimental research is needed to determine methods to reduce slot base drag, decrease downstream mixing, and reduce collection and ducting losses for slot air on conventional aircraft.

7. REFERENCES

- ¹Goldstein, Richard J.: Film Cooling. Advances in Heat Transfer, Vol. 7, Academic Press, New York-London, 1971, pp. 321-379.
- ²Spangler, Jack G.: Effects of Periodic Blowing Through Flush Transverse Slots on Turbulent Boundary-Layer Skin Friction. NASA CR-634, October 1966.
- ³Zakkay, Victor; and Wang, Chi R.: Skin Friction Reduction by Slot Injection at Mach 0.8. NASA CR-2694, July 1976.
- ⁴Cary, Aubrey M., Jr.; and Hefner, Jerry N.: Film-Cooling Effectiveness and Skin Friction in Hypersonic Turbulent Flow. AIAA Journal, Vol. 10, No. 9, September 1972, pp. 1188-1193.
- ⁵McRee, Donald I.; Peterson, John B., Jr.; and Braslow, Albert L.: Effect of Air Injection Through a Porous Surface and Through Slots on Turbulent Skin Friction at Mach 3. NASA TN D-2427, August 1964.

- ⁶Kenworthy, Michael; and Schetz, Joseph A.: An Experimental Study of Slot Injection Into a Supersonic Stream. NASA CR-2128, January 1973.
- ⁷Hefner, Jerry N.; Cary, Aubrey M., Jr.; and Bushnell, Dennis M.: Investigation of the Three-Dimensional Turbulent Flow Downstream of Swept Slot Injection in Hypersonic Flow. AIAA Paper No. 76-679, ASME Paper No. 74-HT-13, Presented at AIAA/ASME 1974 Thermophysics and Heat Transfer Conference, Boston, Massachusetts, July 15-17, 1974.
- ⁸Schetz, Joseph A.; and van Overeem, Johannes: Skin Friction Reduction in Supersonic Flow by Injection Through Slots, Porous Sections, and Combinations of the Two. NASA CR-2491, March 1975.
- ⁹Peterson, John B., Jr.; McRee, Donald I.; Adcock, Jerry B.; and Braslow, Albert L.: Further Investigation of Effect of Air Injection Through Slots and Porous Surfaces on Flat-Plate Turbulent Skin Friction at Mach 3. NASA TN D-3311, March 1966.
- ¹⁰Brown, Gary L.: Gas Film Cooling Past a Non-Adiabatic Flat Plate. Ph. D. Dissertation, University of Idaho, April 1969.
- ¹¹Kacker, S. C.; and Whitelaw, J. H.: Some Properties of the Two-Dimensional, Turbulent Wall Jet in a Moving Stream. Journal of Applied Mechanics, December 1968, pp. 641-651.
- ¹²Sorrells, Russell B., III; Czarnecki, K. R.; and Satchell, Lorraine F.: Drag Reduction Due to Gas Injection Through Various Discrete Slots on a Three-Dimensional Wing at Mach 2.01. NASA TN D-5307, July 1969.
- ¹³Parthasarathy, K.; and Zakkay, V.: An Experimental Investigation of Turbulent Slot Injection at Mach 6. AIAA Journal, Vol. 8, No. 7, July 1970, pp. 1302-1307.
- ¹⁴Zakkay, Victor; and Wang, Chi R.: Effect of Adverse Pressure Gradient on Film Cooling Effectiveness. AIAA Paper No. 73-697, Presented at AIAA Sixth Fluid and Plasma Dynamics Conference, Palm Springs, California, July 16-18, 1973.
- ¹⁵Kacker, S. C.; and Whitelaw, J. H.: Prediction of Wall-Jet and Wall-Wake Flows. Journal of Mechanical Engineering Science, Vol. 12, No. 6, 1970, pp. 404-420.
- ¹⁶Kurkov, Anatole P.: Mixing of Supersonic Jets Including the Effects of Transverse Pressure Gradient Using Difference Methods. NASA TN D-6592, December 1971.
- ¹⁷Beckwith, Ivan E.; and Bushnell, Dennis M.: Calculation by a Finite-Difference Method of Supersonic Turbulent Boundary Layers With Tangential Slot Injection. NASA TN D-6221, April 1971.
- ¹⁸Miner, E. W.; and Lewis, C. H.: A Finite-Difference Method for Predicting Supersonic Turbulent Boundary-Layer Flows With Tangential Slot Injection. NASA CR-2124, October 1972.
- ¹⁹LaRue, John C.; and Libby, Paul A.: Measurements in the Turbulent Boundary Layer With Slot Injection of Helium. Accepted for publication in Physics of Fluids, 1977.
- ²⁰Chin, J. H.; Skirvin, S. C.; Hayes, L. E.; and Silver, A. H.: Adiabatic Wall Temperature Downstream of a Single, Tangential Injection Slot. Paper 58-A-107, Presented at the ASME Annual Meeting, New York, November 30-December 5, 1958.
- ²¹Nicoll, W. B.; and Whitelaw, J. H.: The Effectiveness of the Uniform Density, Two-Dimensional Wall Jet. Int. J. Heat Mass Transfer, Vol. 10, 1966, pp. 623-639.
- ²²Pai, B. R.; and Whitelaw, J. H.: The Influence of Density Gradients on the Effectiveness of Film Cooling. Aeronautical Research Council C.P. No. 1013, 1968.
- ²³Shvets, I. T.; and Repukhov, V. M.: Approximate Determination of the Effectiveness of Film Cooling With Injection Ratios Less Than Unity. Heat Transfer-Soviet Research, Vol. 3, No. 2, March-April 1971, pp. 67-75.
- ²⁴Seban, R. A.: Heat Transfer and Effectiveness for a Turbulent Boundary Layer With Tangential Fluid Injection. Journal of Heat Transfer, Vol. 82, Series C, No. 4, November 1960, pp. 303-312.
- ²⁵Samuel, A. E.; and Joubert, P. N.: Film Cooling of an Adiabatic Flat Plate in Zero Pressure Gradient in the Presence of a Hot Mainstream and Cold Tangential Secondary Injection. Journal of Heat Transfer, August 1965, pp. 409-418.
- ²⁶Boldman, D. R.; Brinich, P. F.; and Goldstein, M. E.: Vortex Shedding From a Blunt Trailing Edge With Equal and Unequal External Mean Velocities. Journal of Fluid Mechanics, Vol. 75, June 1976, pp. 721-735.
- ²⁷Brown, Garry; and Roshko, Anatol: The Effect of Density Difference on the Turbulent Mixing Layer. AGARD Conference Proceedings No. 93 on Turbulent Shear Flows Presented at the Fluid Dynamics Panel Specialists' Meeting held in London, U.K., September 13-15, 1971.
- ²⁸Valerino, Alfred S.; and Shinn, Arthur M., Jr.: Effects of Base Bleed Flow on Base Region Temperatures and Pressures of Several Simulated Missile Afterbody Configurations — Mach Number Range of 0.8 to 2.0. NASA TM X-153, April 1960.
- ²⁹Bearman, P. W.: The Effect of Base Bleed on the Flow Behind a Two-Dimensional Model With a Blunt Trailing Edge. The Aeronautical Quarterly, August 1967, pp. 207-224.

- ³⁰Leal, L. G.; and Acrivos, A.: The Effect of Base Bleed on the Steady Separated Flow Past Bluff Objects. *Journal of Fluid Mechanics*, Vol. 39, Part 4, 1969, pp. 735-752.
- ³¹Wood, C. J.: Visualization of an Incompressible Wake With Base Bleed. *Journal of Fluid Mechanics*, Vol. 29, Part 2, 1967, pp. 259-272.
- ³²Howard, F. G.; Hefner, J. N.; and Srokowski, A. J.: Multiple Slot Skin Friction Reduction. *Journal of Aircraft*, Vol. 12, No. 9, September 1975, pp. 753-754.
- ³³Marino, A.; Economos, C.; and Howard, F. G.: Evaluation of Viscous Drag Reduction Schemes for Subsonic Transports. NASA CR-132718, June 1975.
- ³⁴Sturgeon, R. F.; Bennett, J. A.; Etchberger, F. R.; Ferrill, R. S.; and Meade, L. E.: Study of the Application of Advanced Technologies to Laminar-Flow Control Systems for Subsonic Transports. NASA CR-144949, May 1976.
- ³⁵Hefner, Jerry N.: Effect of Geometry Modifications on Effectiveness of Slot Injection in Hypersonic Flow. *AIAA Journal*, Vol. 14, No. 6, June 1976, pp. 817-818.
- ³⁶Tanner, M.: Reduction of Base Drag. *Prog. Aerospace Sci.*, Vol. 16, No. 4, 1975, pp. 369-384.
- ³⁷Vlasov, Ye. V.; and Genevskiy, A. S.: Bilateral Character of Acoustic Action on Free Turbulent Jets. NASA TT F-16658, November 1975.
- ³⁸Srokowski, A. J.; Howard, F. G.; and Feller, W. V.: Direct Measurements at Mach 6 of Turbulent Skin-Friction Reduction by Injection From Single and Multiple Flush Slots. AIAA Paper No. 76-178, Presented at the AIAA 14th Aerospace Sciences Meeting, Washington, D.C., January 26-28, 1976.

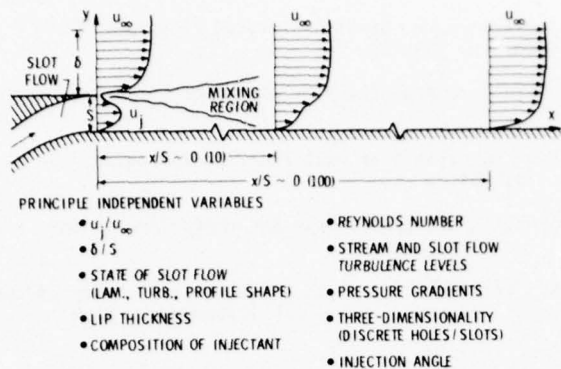


Figure 1. Flow-field characteristics of slot injection into low-speed flows.

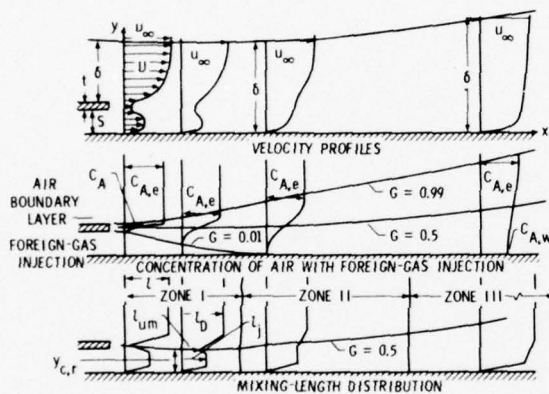


Figure 2. Schematic sketch of velocity, concentration, and mixing-length profiles for hypothetical slot-injection flow. See Reference 17 for nomenclature.

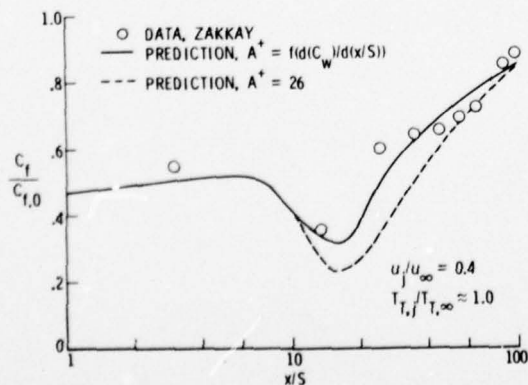


Figure 3. Comparison of prediction method with data. Subsonic skin friction.

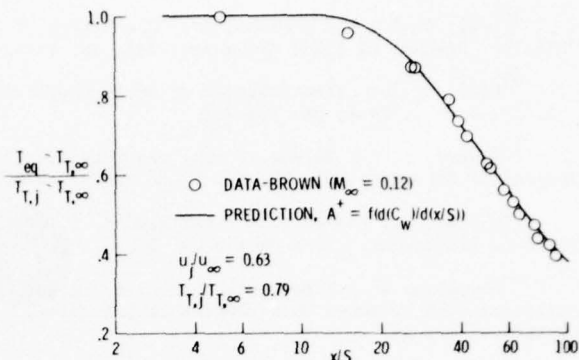


Figure 4. Comparison of prediction method with data. Low-speed effectiveness.

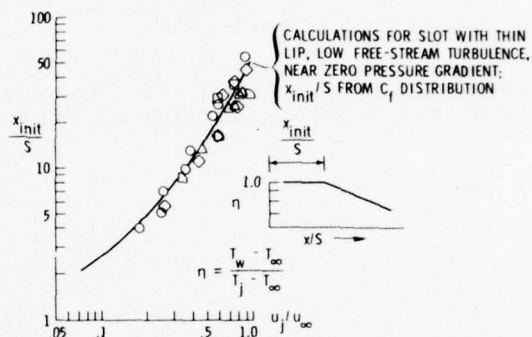


Figure 5. Extent of initial low skin-friction region downstream of slot injection in low-speed flow.

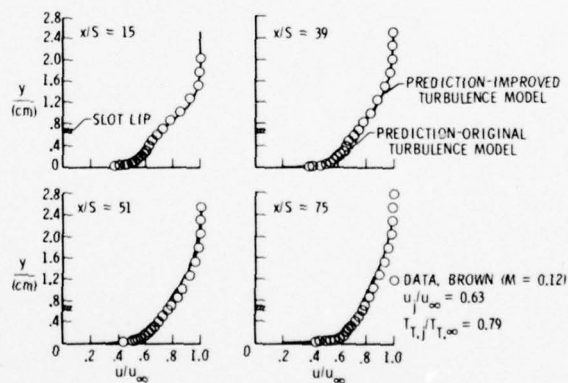


Figure 6. Comparison of prediction method with data. Low-speed velocity profiles.

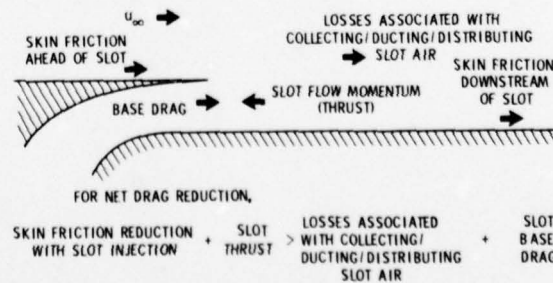


Figure 7. Force balance associated with slot injection.

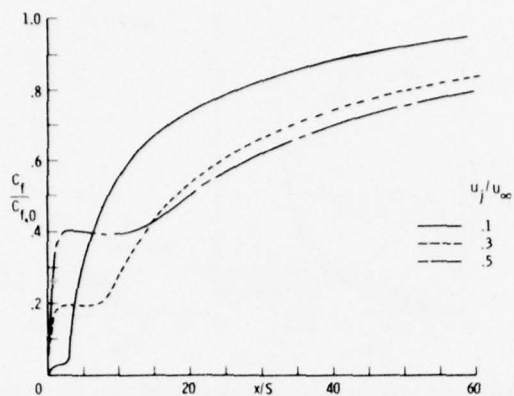


Figure 8. Predicted effect of slot velocity ratio on local skin friction at subsonic velocities.

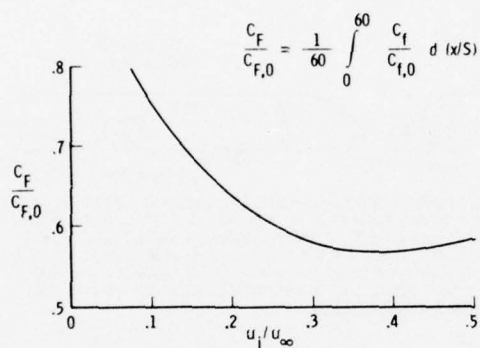


Figure 9. Influence of slot velocity on integrated skin-friction drag downstream of slot.

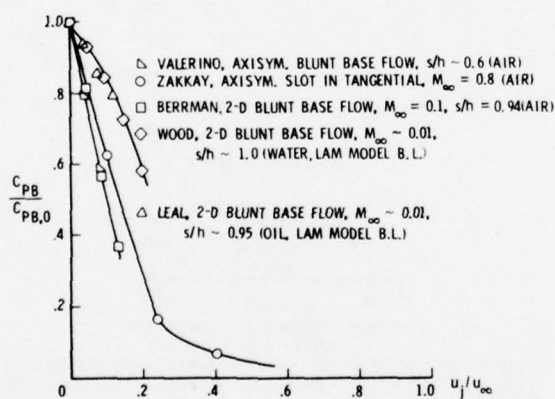


Figure 10. Effect of injection on base pressure.

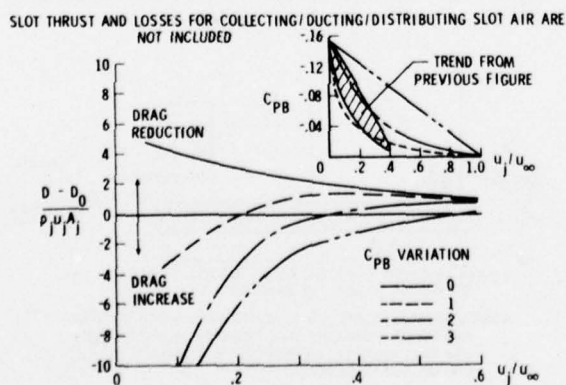


Figure 11. Integrated viscous drag reduction with slot injection including effects of base drag.

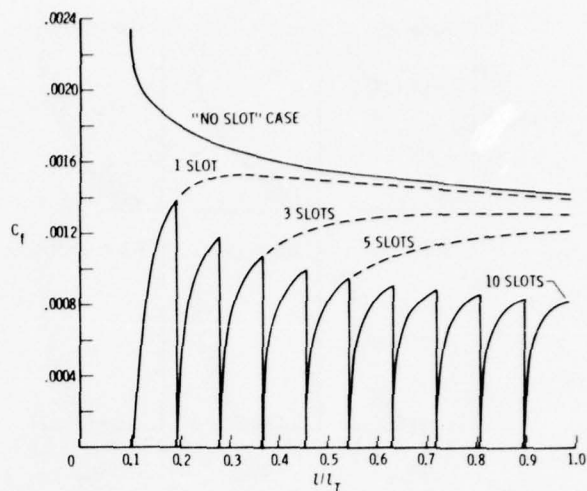


Figure 12. Example of multiple slot calculations for Mach 0.82 with $u_j/u_\infty = 0.34$ for all slots.

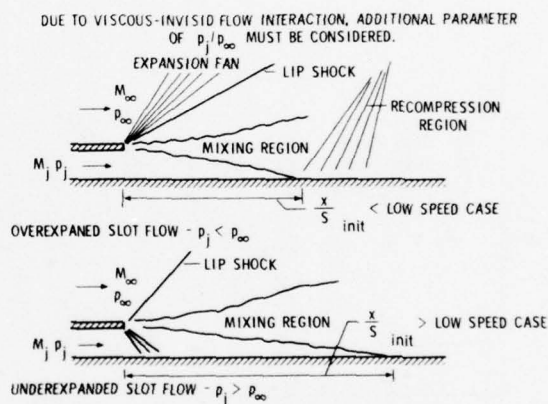


Figure 13. Slot injection into high-speed flow.

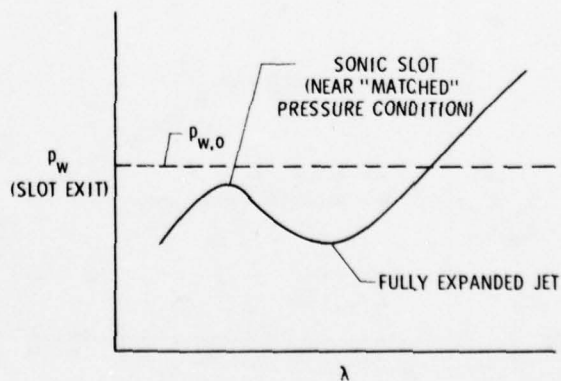


Figure 14. Effect of slot mass flow rate on surface static pressure near slot for supersonic flows.

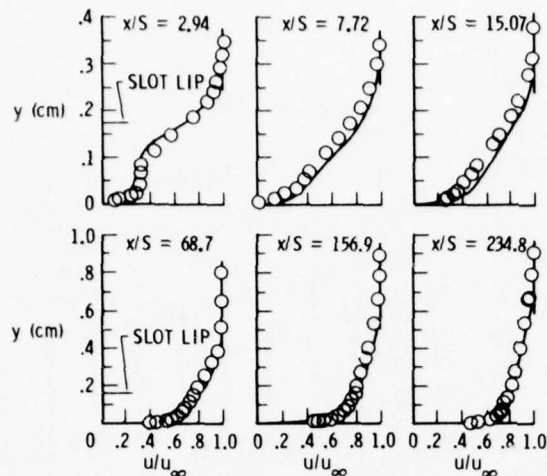


Figure 15. Comparison of calculated results with high-speed data. Part 1 - Velocity profiles at Mach 3 (Peterson's data).

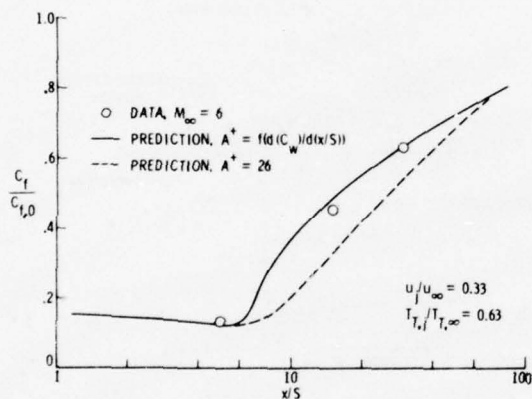


Figure 16. Comparison of calculated results with high-speed data. Part 2 - Skin friction at Mach 6.

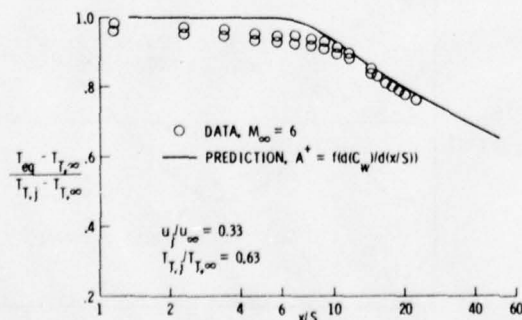


Figure 17. Comparison of calculated results with high-speed data. Part 3 - Effectiveness at Mach 6.

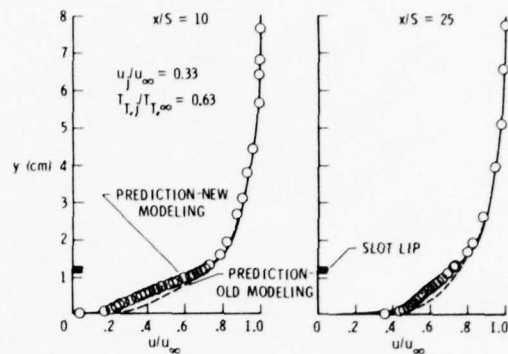
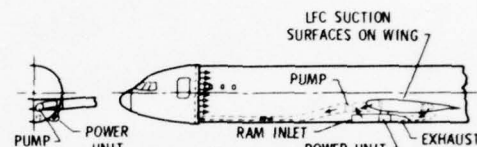


Figure 18. Comparison of calculated results with high-speed data. Part 4 - Velocity profiles at Mach 6.



FOR PARTICULAR CONFIGURATION, SLOT INJECTION REDUCED LFC ENGINE FUEL CONSUMPTION BY 28 %. HOWEVER, AS A RESULT OF THE VOLUME REQUIRED FOR FUSELAGE LFC ENGINES AND COMPRESSORS, DUCTING, AND BELLY CARGO, THE FUSELAGE HAD TO BE INCREASED IN LENGTH BY 1.82 m WHICH RESULTED IN AN INCREASE IN PRIMARY ENGINE FUEL CONSUMPTION OF 3 %. THE NET EFFECT WAS A 1.2 % INCREASE IN TOTAL FUEL CONSUMPTION.

Figure 19. Lockheed evaluation of slot injection for conventional transport aircraft using LFC suction air.



TRUNCATED BASE WITH SUCTON - KEEPS BASE FLOW ATTACHED, REDUCES BASE DRAG; STRUCTURAL WEIGHT IS REDUCED DUE TO ABSENCE OF RELATIVELY LONG BOATTAIL.

Figure 20. Slot injection with base suction on a truncated fuselage.

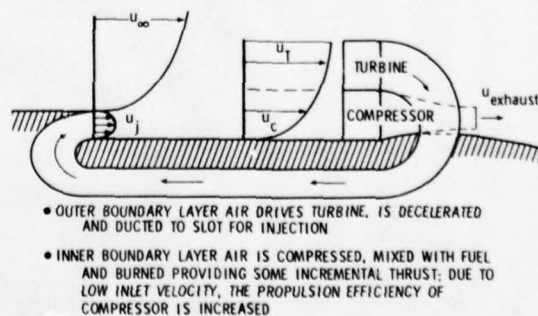


Figure 21. Slot injection combined with boundary-layer air ingestion. Ferri concept.

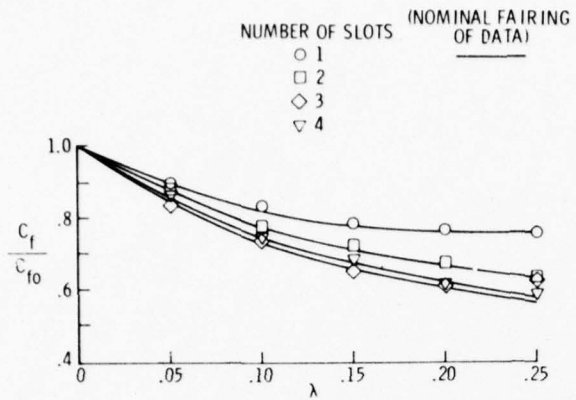


Figure 22. Effect of multiple slot injection on skin friction. $M_\infty = 6.0$, $x/S = 47$, flush slots.

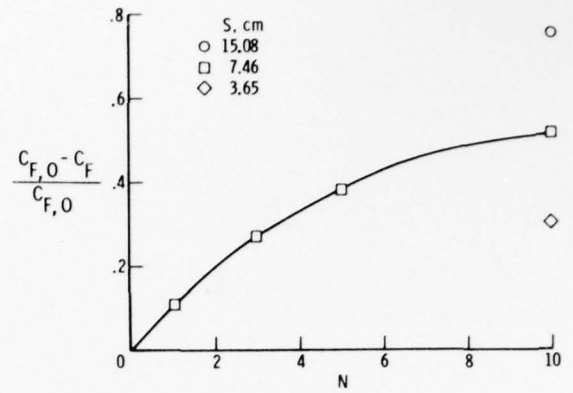


Figure 23. Skin-friction drag reduction as a function of number of slots — from integration of results shown in Figure 12.

DIFFUSERS AND THEIR PERFORMANCE IMPROVEMENT BY MEANS OF BOUNDARY LAYER CONTROL

by

R.C. Adkins
Senior Research Officer
School of Mechanical Engineering
Cranfield Institute of Technology
Cranfield, Bedford, England

1. NOMENCLATURE

A	cross-sectional area
a	aspect ratio, S/W ; depth of groove in ribbed diffuser
AR	area ratio, A_1/A_2
B	blockage factor, $1 - \bar{V}/\hat{V}$
B	proportion of mainstream removed by suction
b	height of vortex generator; width of groove in ribbed diffuser
C_p	coefficient of static pressure recovery $\frac{p_2 - p_1}{p_1 - p_i}$
C_p^*	maximum value of C_p obtainable in a given length
c	chord length of vortex generator
D	diameter
D_h	hydraulic diameter ($4 \times \text{area}/\text{wetted perimeter}$)
G	gradient parameter at diffuser inlet
G_x	gradient parameter at distance 'x' down diffuser
H	shape factor, δ^*/θ
h	height
K	vortex strength
k	constant
L	length
m	mass flow ratio
N	non dimensional distance, x/D_h
n	number of elements
P	stagnation pressure
p	static pressure
q	dynamic pressure, $(P - p)$
R	radius
R_d	Reynolds number based on hydraulic diameter
r	radial distance; hub to tip ratio
S	width of diverging wall
s	space between vortex generators
t	thickness
u	velocity
v	velocity
W	distance between diverging walls
x	distance down diffuser, parallel to axis
y	distance perpendicular to wall
z	distance between divergent pair of vortex generator vanes
α	kinetic energy coefficient
β	angle between vortex generator and local flow stream
γ	shape parameter

δ	finite increment
δ	boundary layer thickness
δ^*	boundary layer displacement thickness
η	diffuser effectiveness (actual static pressure rise/ideal static pressure rise)
θ	boundary layer momentum thickness
ρ	density
τ	shear stress
ϕ	angle between diffuser wall and major axis
ψ	angle between diffuser wall and major axis

SUFFICES

d	diameter
e	effective; element
i	inner
n	the nth element
o	outer
w	wall
x	with respect to x
1	diffuser inlet plane
2	diffuser exit plane
j	jet
I	Ideal
-	mean value
^	maximum value

2. INTRODUCTION

Diffusers have probably been used since early Roman times when they would almost certainly have featured in the complex network of drainage systems and domestic plumbing. In more recent times, due to the advent of the aeroplane, a significant amount of effort has gone into diffuser research in order to make them an efficient means of converting kinetic energy into static pressure. In spite of this the diffuser that is completely satisfactory in performance, size, and simplicity of construction has so far eluded us.

The physical nature of the problem is simple. Consider the diffuser as a divergent duct, the angle of divergence must be kept small otherwise the flow will separate from its controlling boundary and efficient diffusion will cease. Equally if the angle of divergence is too small, then considerable skin friction losses occur which will detract from the overall performance.

The art of diffuser design is clearly to make the best compromise between the two sources of loss. This point is exemplified in figure 1.

The optimum diffuser is often too long to fit within realistic constraints. This is particularly so in Aeronautical Engineering where bulk and weight carry severe penalties in terms of range and payload. For these reasons the designer has been constrained to use divergence angles significantly greater than the optimum, which has added to the difficulties of the Development Engineers. Situations have arisen when an inefficient engine intake diffuser has not only impaired engine performance, but has also reduced engine life because of the inlet flow distortion and instability which it produces (see ref.1).

Further penalties also arise from the malfunctioning of the pre-combustor diffuser inside Gas-Turbine Engines.

Several remedial devices have been investigated with varying measures of success, and it is the aim of this paper to review these devices and to present a guide as to their usage. A further objective is to review recent research programs directed at producing short but efficient diffusers.

Diffuser improvement will be considered in a later section of the paper. The following section, on simple diffusers, is intended to highlight their short-comings in order that the mechanisms for improvement can be more readily appreciated.

2.1 Simple Diffusers

In essence these exploit natural turbulent mixing to overcome deficiencies in boundary flow which are caused both by skin friction and an opposing pressure gradient. The rate of diffusion is controlled by the rate of mixing, which is unfortunately low. In order to simplify manufacture, such diffusers usually have straight walls when viewed in the plane of divergence. Performance of such ducts is reasonably well documented and a comprehensive review is summarised in the design curves made available by the Engineering Sciences Data Unit (ref. 2 to 5).

The design curves are presented in a typical fashion, using a "log, log carpet plateau" of Area ratio versus non-dimensionalised diffuser length, with curves of constant divergence angle traced across it. Diffuser performance is depicted as curves of constant static pressure coefficient, C_p . These curves are largely derived from experimental data together with some areas of inspired speculation.

A typical characteristic, taken from ref.5, is given as fig.2 which relates to conical diffusers with fully developed flow at their inlet.

The most common design problem is to choose the area ratio that will achieve the maximum pressure recovery within the confines of a given length. This may be solved directly by using the curve denoted by C_p^* . It is of interest to note that this curve cuts across the curves of constant divergence angle in such a way that diffusers of small area ratio will have a much greater optimum divergence angle than those of larger area ratio. The significance of this phenomenon will be discussed at a later stage.

A key fact apparent from ref.5, is that more data is still required to cover the wide range of variations in annular diffusers. They can be sub-divided into five types depending on the relative wall angles (see figure 3). Although the need for this design data is immediate, to obtain it by experimental means would take many years, and purely analytical techniques are still in their infancy. In order to meet present day requirements attempts are made to apply the data already available from conical diffuser research, to the case of annular diffusers. A popular method is to assume that the annular diffuser will have the same performance as an equivalent conical diffuser having identical areas at inlet and exit and which differs over the same length. Another method is to design the annular diffuser to have the same non-dimensionalised pressure gradients as would be experienced in an optimised conical diffuser, as discussed in the next section.

2.2 A Prediction Technique For Determining The Area Ratio That Will Produce The Optimum Value of C_p For A Given Length Of Annular Diffuser, (taken from Ref.6).

Argument 1 By using the Bernoulli equation and the equation for conservation of mass flow we can derive an expression for the ideal coefficient of static pressure rise, viz:

$$C_{p_I} = \left[1 - \frac{1}{(AR)^2} \right] \quad \dots \quad (1)$$

This relationship is plotted in figure 4, the most striking feature of which is the proportion of pressure recovery that is achieved at the small values of area ratio near diffuser inlet. In reality this is even more pronounced because performance further down the diffuser is marred either by the rapid growth of boundary layer or by flow separation. Thus we can reasonably conclude that the overall performance of the diffuser is closely linked to the performance near its inlet where the pressure gradient is at its steepest.

Argument 2 Consider two diffusers, A and B, geometrically similar, but of a significantly different scale. Suppose they are both subjected to the same conditions at inlet, namely dynamic pressure, Reynolds and Mach numbers, then experience dictates that the static pressure coefficient will be identical in both cases. The smaller of the two diffusers will therefore have experienced a higher static pressure gradient than the larger one by a factor equal to the inverse of the scale, thus

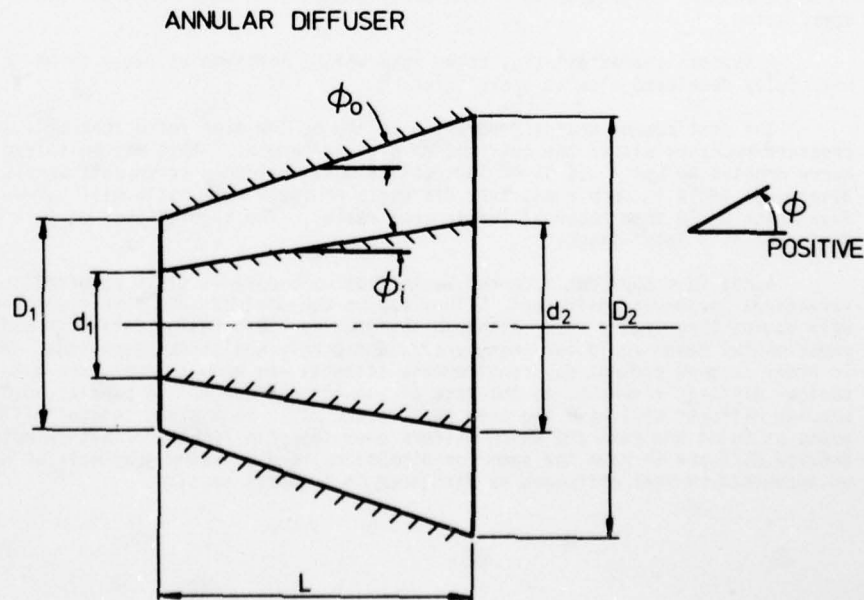
$$L_A \frac{d(C_{p_A})}{dL_A} = L_B \frac{d(C_{p_B})}{dL_B} \quad \dots \quad (2)$$

Argument 3 For the case of annular diffusers we will adopt the use of the equivalent hydraulic diameter at diffuser inlet, D_{h_1} as the characteristic dimension to be used in equation 2. This conforms to standard practice and is convenient since it reduces to the inlet diameter of a conical diffuser when the central core of the annulus is removed.

Defining the equivalent hydraulic diameter as four times the flow cross sectional area divided by the wetted perimeter we have

$$D_{h_1} = D_1 - d_1 \quad \dots \quad (3)$$

These arguments may now be applied to the generalised annular diffuser shown below:



The area ratio for this diffuser is

$$\begin{aligned}
 AR &= \frac{D_2^2 - d_2^2}{D_1^2 - d_1^2} \\
 &= \frac{(D_1 + 2L \tan \phi_0)^2 - (d_1 + 2L \tan \phi_i)^2}{D_1^2 - d_1^2} \\
 &= 1 + \frac{4L (D_1 \tan \phi_0 - d_1 \tan \phi_i) + 4L^2 (\tan^2 \phi_0 - \tan^2 \phi_i)}{D_h (D_1 + d_1)} \quad \dots (4)
 \end{aligned}$$

differentiating (4) with respect to L and then evaluating at $L = 0$ gives

$$\left[\frac{d(AR)}{dL} \right]_{L=0} = \frac{4 (D_1 \tan \phi_0 - d_1 \tan \phi_i)}{D_h (D_1 + d_1)}$$

Expressing this in the form of equation (2) and writing the inlet hub to tip ratio, d_1/D_1 as r gives

$$D_h \left[\frac{d(AR)}{dL} \right]_{L=0} = \frac{4 (\tan \phi_0 - r \tan \phi_i)}{1 + r} \quad \dots (5)$$

Differentiating equation (1) gives

$$\frac{d(Cp)}{d(AR)} = \frac{2}{(AR)^3} \quad \dots (6)$$

It is obvious from equation (4) that $AR = 1$ as L tends to zero, hence (6) may be evaluated at diffuser inlet as

$$\left[\frac{d(Cp)}{d(AR)} \right]_{L=0} = 2 \quad \dots (7)$$

The required non dimensional pressure gradient, G , can now be determined where

$$\begin{aligned}
 G &= D_h \left[\frac{d(Cp)}{dL} \right]_{L=0} = D_h \left[\frac{d(Cp)}{d(AR)} \right]_{L=0} \left[\frac{d(AR)}{dL} \right]_{L=0} \\
 \text{giving } G &= \frac{8 (\tan \phi_0 - r \tan \phi_i)}{1 + r} \quad \dots (8)
 \end{aligned}$$

Note Equation (8) is applicable to all annular diffusers since ϕ_0 and ϕ_i can be either positive, negative, or zero.

The next step is to adapt equation (8) to conical diffusers by setting $r = 0$, then

$$G = 8 \tan \phi_0 \quad \dots (9)$$

Values of ϕ_0 were then taken from the Cp^* line of figure 2 and are given in table 1 together with the corresponding values of AR and G . This information was used to plot the curve in figure 5 using the 'crossed' points and an empirical equation was developed to fit the curve, viz:

$$G = [(AR)^{1.26} - 1]^{-0.5} \quad \dots (10)$$

Points from this equation were then plotted as circles on figure 5 in order to give a measure of its accuracy. This appears to be well within usual experimental tolerances.

Assuming that fully developed flow at the inlet to conical diffusers will have similar characteristics to fully developed flow in an annulus we can now combine equations (8) and (10) to give:

$$\left[(AR)^{1.26} - 1 \right]^{-0.5} = \frac{8(\tan \phi_0 - r \tan \phi_i)}{1 + r} \quad \dots (11)$$

rearranging gives

$$AR_{OPT} = \left\{ \left[\frac{1 + r}{8(\tan \phi_0 - r \tan \phi_i)} \right]^2 + 1 \right\}^{0.7937} \quad \dots (12)$$

For most practical problems equation (12) must be solved simultaneously with equation (4).

Special cases of equation (12) are as follows:

- (i) $\phi_0 = -\phi_i$, both walls equally divergent,

$$\text{then } AR_{opt} = \left[\left(\frac{1}{8 \tan \phi} \right)^2 + 1 \right]^{0.7937} \quad \dots (13)$$

Evidence presented in reference 6 supports this equation by showing that this type of diffuser is insensitive to the hub tip ratio at inlet

- (ii) $\phi_0 = 0$, outer wall parallel (ϕ_i negative)

$$AR_{opt} = \left[\left(\frac{1 + r}{8 r \tan \phi_i} \right)^2 + 1 \right]^{0.7937} \quad \dots (14)$$

This equation is useful for designing turbine exhaust diffusers. In this case $AR = \frac{1}{1 - r^2}$ and

$$\phi_i = \tan^{-1} \left[\frac{1 + r}{8 r \sqrt{(1 - r^2)^{-1.26} - 1}} \right] \quad \dots (15)$$

(Caution: values of ϕ greater than 15° are not recommended)

- (iii) $\phi_i = 0$, inner wall parallel

$$AR_{opt} = \left[\left(\frac{1 + r}{8 \tan \phi_0} \right)^2 + 1 \right]^{0.7937} \quad \dots (16)$$

- (iv) $r = 0$, leading edge of the centre body coincides with the beginning of divergence on the outer wall

$$AR_{opt} = \left\{ \left(\frac{1}{8 \tan \phi_0} \right)^2 + 1 \right\}^{0.7937}$$

This equation is identical to (13) and suggests that performance will be the same as for a simple conical diffuser. This fact is confirmed by data presented in ref.5.

- (v) r tends to unity, this may be considered as a 2-dimensional diffuser of infinite aspect ratio. By assuming a symmetrical diffuser when $\phi_0 = -\phi_i$ then equation (12) modifies to:

$$AR_{opt} = \left\{ \left(\frac{1}{8 \tan \phi} \right)^2 + 1 \right\}^{0.7937}$$

It is again the same relationship as for a conical diffuser equation (13) but experience tells us that the optimum angle should be approximately twice that of the cone. This is the first major difference between the design technique and experimental data. The physical explanation is likely to be that a fundamental difference exists between 2-dimensional and 3-dimensional flow.

The only way to substantiate this hypothesis, and therefore vindicate what promised to be an important advance in diffuser design was to establish a relationship between G and area ratio for 2-dimensional diffusers. Fortunately this has been accomplished by using data taken from reference 4, which was collated from tests on diffusers of large aspect ratio. The new correlation is

$$G = \left[0.9 + (1 - B^3)^{-0.600} \right] (AR)^{-m} \quad \dots (17)$$

$$\text{where } m = \left[1.7 + (21.36B)^{3.314} \right] \quad \dots (17a)$$

This is significantly different to equation (10) and supports the hypothesis.

The new equation is more complex and includes a blockage factor, B , to account for the effect of boundary layer thickness at diffuser inlet, where $B = 1 - \frac{V}{V_{\max}}$. (A more detailed explanation of this term is given in reference 8).

Figure 6 shows data calculated from (17) and compares it with curves compiled from empirical data taken from reference 4.

A satisfactory degree of correlation is clearly evident but it is unlikely to hold for values of B much greater than 0.08 as will be argued in a later section. (Another limitation will be the effect of aspect ratio, $a = S/W$ for values of less than 5. This feature is discussed in

appendix 1a. From this appendix, we see that for diffusers of large aspect ratio

$$G = 8 \tan \phi \quad \dots (18)$$

which when combined with (17) gives a direct relationship with ϕ , viz:

$$\phi = \tan^{-1} \left\{ 0.125 \left[0.9 + (1 - B^3)^{-0.600} \right] (AR)^{-m} \right\} \quad \dots (19)$$

when m is obtained from equation (17a).

In order to ascertain the dependability of (19) it was used to calculate values of ϕ_{opt} for two different values of blockage factor, namely 0.05 and 0.08, over a range of area ratios. These points are plotted alongside curves taken from reference 4 and are presented as figure 7. The points calculated for using the larger blockage factor 0.08 follow the C_p^* curve remarkably closely whereas those using a blockage of 0.05 veer towards comparatively smaller angles of divergence as the area ratio is reduced below 2.0:1.

To study this phenomenon more closely, equation (17) was used to produce the curves of constant blockage factor shown in figure 8. Remembering that G is directly related to divergence angle, as stated in equation (18) we can draw the following important conclusions:

- (i) The optimum divergence angle for diffusers having an area ratio near 2:1 is sensibly independent of inlet blockage.
- (ii) Diffusers of area ratio greater than 2:1 are moderately sensitive to inlet blockage. Flow with a high degree of blockage will produce optimum pressure recovery in a diffuser having a small divergence angle.
- (iii) Diffusers of small area ratio, typically aircraft intake diffusers, will be much more sensitive to inlet blockage factors. In this case, however, as inlet blockage increases so the angle of divergence can be increased. This is fortuitous because a diffuser designed for the low blockage factor normally expected for an aircraft in level flight should not become too unstable when the blockage is increased due to changes in flight attitude. This statement will only apply so long as upstream influences do not in themselves promote flow separation at inlet.

Having established a method for obtaining the optimum divergence angle when inlet blockage is predictable we can now use published data to estimate its effect on diffuser performance. References 7 and 8 present useful design guides and Bibliography documents 1 to 6 provided useful background information. The overwhelming consensus of opinion indicates that pressure recovery will diminish as the degree of inlet distortion is increased. The reason for this will be discussed in a later section.

So far, the data discussed has related to incompressible flow and could therefore be misleading when used for applications such as intakes, where high subsonic Mach numbers are encountered.

2.3 The Effect Of Compressibility (Subsonic Flow).

A survey of the literature has shown that conflict exists as to the effect of compressibility, even when great care has been taken to produce reliable results. Numerous researchers have discovered a sudden reduction in diffuser performance as the inlet Mach number exceeds 0.8. An example of this, taken from reference 9, is given as figure 9. This shows a similar effect to occur over a range of area ratios from 2 to 10 and for cone angles (2ϕ) from 5° to 20° .

Diffusers which apparently avoided this 'choking effect' are reported in reference (10) which is the source of figures (10) and (11). The first figure shows an actual increase in performance of a 2-dimensional diffuser as the Mach number is increased to unity. This may well have been the result of advanced design but at least part of this improvement is due to the experimental technique as can be explained using figure (11). This shows a substantial drop in pressure at a short distance from the beginning of divergence, which was described as an Aerodynamic Throat. The pressure rise achieved by the diffuser was judged from this datum rather than from a point further upstream as used by the majority of researchers. In fact most diffuser performance is assessed from a datum located at least one pipe diameter upstream of divergence in order to avoid the effects of streamline curvature.

In order to clear some of the misapprehensions which have arisen over the effect of Mach number and also because of its importance to the Aeronautical Engineer this paper will once again deviate from its major objectives. Some measure of agreement on the basic effects of Mach number is necessary before we can proceed to discuss methods of improving performance.

Fundamentally, the fact that gases are compressed as they flow down a diffuser means that the effective area ratio is greater than the geometric one. This leads to an increase in the ideal pressure recovery coefficient which will therefore depend on the inlet Mach number as is shown in figure (12). The curves of constant area ratio illustrate that the effect of Mn is greatest at small area ratios. This is particularly important because we have established that the pressure gradient near diffuser inlet is a key factor in determining diffuser performance. Figure (13) was plotted in order to study the inlet pressure gradients more closely. At small area ratios, the increase in pressure coefficient near sonic velocity is around six times that of incompressible flow whereas at a Mn of 0.8 the factor is only two. If we now refer back to figure 5 we can explain the phenomenon of 'choking'.

Most diffusers tested have had an area ratio of 2:1 or greater and have been designed accordingly to incompressible flow data to give the maximum pressure recovery. A value of 'G' has therefore been chosen which is approximately half of the critical value for small area ratios. When a Mach number just greater than 0.8 is achieved then the throat pressure gradient exceeds its optimum value and large scale flow separation is quickly established.

Although there are many other factors which affect the performance of simple diffusers (e.g. turbulence, wakes etc.), these must be left to later discussions.

3. BOUNDARY LAYER CONTROL IN DIFFUSERS BY USE OF THE OPTIMUM WALL SHAPE

Design of Optimum Diffuser Walls using the G_x Technique.

In Section 1 we showed that the optimum angle of divergence for straight walled subsonic diffusers decreased as we increased the area ratio (see fig.5). As a result it would appear that for diffusers of large area ratio (1.8:1 and above) that the aerodynamic loading (in terms of pressure gradient near diffuser inlet) is well below its optimum value. It would, perhaps, seem reasonable to use larger angles of divergence near the inlet and produce a curved wall diffuser resembling the shape of a bell (see fig.14). It is clear that this will be shorter than the equivalent straight walled diffuser.

The 'G' parameter suggested in equation 8, successfully predicted the performance of straight walled diffusers, and also explained the 'choking' effect of plain walled diffusers at a Mach number of around 0.8. It seems logical to extend this technique to cover the design of curved wall diffusers. The parameter 'G' as previously explained relates only to the non-dimensionalised pressure gradient at diffuser inlet. For curved wall diffusers we require a new parameter G_x which controls the pressure gradient locally down the diffuser wall

From the definition in ref.1

$$G = D_h \cdot \left[\frac{d(Cp)_h}{dL} \right]_{L=0} \quad \dots \quad (20)$$

where Cp_i is the traditional ratio of the ideal static pressure rise divided by the dynamic pressure at diffuser inlet, q_i . Since the static pressure gradient part way down a diffuser must be generated directly from the local dynamic pressure then a local coefficient of static pressure rise gradient must be defined which is based on this local dynamic pressure q_x where

$$\left[\frac{d(Cp)}{dx} \right]_x = \frac{1}{q_x} \cdot \left[\frac{d(p)}{dx} \right]_x \quad \dots \quad (21)$$

If the cross-sectional area at plane 'x' is A_x then by using the continuity equation we can show that for incompressible flow:-

$$q_x = q_i \cdot \left(\frac{A_1}{A_x} \right)^2 = q_i \left[\frac{1}{(AR)_x} \right]^2 \quad \dots \quad (22)$$

Then from equation (21)

$$\left[\frac{d(Cp)}{dx} \right]_x = \frac{(AR)_x^2}{q_i} \cdot \left[\frac{d(p)}{dx} \right]_x$$

By definition:

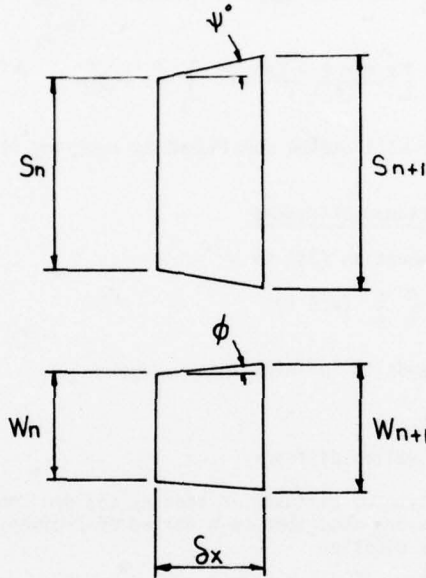
$$G_x = \left[D_h \cdot \frac{d(Cp)}{dx} \right]_x = \frac{D_{hx} \cdot (AR)_x^2}{q_1} \cdot \left(\frac{dp}{dx} \right)_x \quad \dots (23)$$

Note: D_{hx} is the local hydraulic diameter which, when necessary, can take account of change in duct shape.

In order to test the validity of equation (23) we will apply it to the design of both two-dimensional and conical diffusers and compare the results with published data.

3.1 Application of the ' G_x ' technique to Rectangular Sectioned Diffusers

Reference is made to the sketch below which shows one of numerous small elemental lengths of such a diffuser which has an arbitrary profile



$$\text{At inlet to the element, } [D_h]_n = 2 \left[\frac{s \cdot w}{s+w} \right]_n = 2 \left[\frac{W \cdot a}{a+l} \right]_n \quad \dots (24)$$

The area ratio across the element $(AR)_e$ becomes

$$(AR)_e = \frac{[W \cdot s]_{n+1}}{[W \cdot s]_n}$$

$$\text{then } (AR)_e \approx 1 + 2 \delta x \left[\frac{\tan \phi}{W} \right]_n + 2 \delta x \left[\frac{\tan \psi}{s} \right]_n \quad \dots (25)$$

The ideal pressure rise, δp_e across the element is given by

$$\delta p_e = q_n \cdot \left[1 - \frac{1}{(AR)_e^2} \right]$$

$$\therefore \delta p_e = q_n \cdot \left[1 - \left\{ 1 + 2 \delta x \left[\frac{\tan \phi}{W} + \frac{\tan \psi}{s} \right]_n \right\}^{-2} \right]$$

Expanding Binomially and neglecting terms of the 2nd order and above we obtain

$$\delta p = 4 \cdot q_n \cdot \delta x \cdot \left[\frac{\tan \phi}{W} + \frac{\tan \psi}{s} \right]_n$$

In the limit as δx tends to zero

$$\frac{dp}{dx} = 4 \cdot q_n \cdot \left[\frac{\tan \phi}{W} + \frac{\tan \psi}{s} \right]_n \quad \dots (26)$$

Then since $[G_x]_n$ may be defined as $\left[\frac{D_h}{q} \right]_n \left[\frac{dp}{dx} \right]_n$

$$[G_x]_n = 8 \left[\frac{1}{a+1} \right]_n [a \tan \phi + \tan \psi]_n \quad \dots (27)$$

Similarly at the inlet to the first element of the diffuser

$$[G_x]_1 = G = 8 \left[\frac{1}{(a+1)_1} \right]_1 [a \tan \phi + \tan \psi]_1 \quad \dots (28)$$

Dividing (27) by (28) gives

$$\frac{[G_x]_n}{[G_x]_1} = \frac{[a+1]_1}{[a+1]_n} \frac{[a \tan \phi + \tan \psi]_n}{[a \tan \phi + \tan \psi]_1} \quad \dots (29)$$

Since the objective is to keep G_x constant down the diffuser, $\frac{[G_x]_n}{[G_x]_1} = \text{unity}$, then

$$[a \tan \phi + \tan \psi]_n = \left[\frac{a \tan \phi + \tan \psi}{a+1} \right]_1 [a+1]_n \quad \dots (30)$$

The implications of this equation will now be considered by applying it to a special case.

3.1.1 2-dimensional Rectangular Sectioned Diffusers

Setting angle ψ to zero reduces equation (30) to

$$[a \tan \phi]_n = \left[\frac{a \tan \phi}{a+1} \right]_1 (a+1)_n \quad \dots (31)$$

when the aspect ratio at inlet tends to infinity then

$$[\tan \phi]_n = \tan[\phi]_1 \quad \dots (32)$$

This clearly gives us a straight walled diffuser.

Appropriate literature for this type of diffuser is sparse, the one considered to give the most relevant data is reference 12. Tests are described on a series of 2-dimensional diffuser with curved walls designed according to the equation

$$(AR)_x = 1 + (AR-1) \left(\frac{x}{L} \right)^k \left[1 + k \left(1 - \frac{x}{L} \right) \right] \quad \dots (33)$$

where k is a constant which determined the wall curvature. Positive values of k produced concave surfaces facing the fluid (bell shaped diffusers), whereas negative values produced convex surfaces facing the fluid (trumpet shaped diffusers). Clearly when k equalled zero the diverging walls were straight.

Numerous geometries, covering a range of k from -1 to +2 with two values of inlet aspect ratio, a , namely 4 and 6, were tested using area ratios of up to 4.5. A boundary layer displacement thickness, δ^* , approximating to 3% of the inlet throat height, W , was measured at the beginning of the divergent walls and the mean inlet velocity was maintained at around 50 m/s.

The authors of ref (12) concluded that 'trumpet shaped' diffusers gave inferior performance and that 'bell shaped' diffusers gave a slight improvement over the plane walled diffusers. The best improvement produced a gain in C_p of less than 3% and therefore did not justify the use of curved walls in 2-dimensional diffusers of high aspect ratio as was predicted by the G_x technique. Due to the nature of equation (33) the experimental data cannot be deemed to be absolutely conclusive since more suitable curve forms may well have produced greater benefits.

When ' a ' is finite however $\tan \phi$ will vary with distance down the diffuser. The diffuser profile can then be calculated using a 'step by step' technique employing the following equations

$$[\tan \phi]_n = \left[\frac{1+a}{a} \right]_n \left[\frac{a \tan \phi}{(a+1)} \right]_1 \quad \dots (34)$$

now at the end of the n th element:

$$a_{n+1} = \frac{a_n}{1 + 2 \frac{\delta x}{[a]_1} (a \tan \phi)_n} \quad \dots (35)$$

The local diffuser height then follows directly

$$\text{from } W_{n+1} = \frac{a_1}{a_n + 1} \quad \dots (36)$$

Equations 34 to 36 can then be solved in order by a 'step by step' method after the initial value of $\tan \phi_1$ has been determined. This is found by inserting values of blockage factor, B and overall area ratio into equations 17a and 19.

As an example two families of diffusers covering values of inlet aspect ratio, a_1 , from 0.5 to 2.0 was examined using this technique. The first employed an area ratio of 2:1 and a blockage factor, B , of 0.02 whereas the corresponding values for the second diffuser were 2.5:1 and 0.05 respectively. Further details are given in table 2 where the term $\delta x/W_i$ relates to the width of the incremental elements.

The relationships between AR and non dimensional length are shown plotted in figure 15. The most striking features of these graphs are the apparent lack of curvature and that the curves are convex facing towards the fluid (trumpet shaped). The angles and initial curvatures both increase as the aspect ratio decreases.

The physical argument for a trumpet-shaped diffuser is that as the boundary layer develops so the effective cross-sectional area is reduced. Thus in order to maintain the 'optimum' pressure gradient, ' G_x ', the divergence angle can be progressively increased. Another effect of this form of curvature is to produce a static pressure gradient over the cross-section which reduces the longitudinal pressure gradient in the boundary layer. This in turn will slow down the rate of boundary layer growth. Use of this technique was made in the "Griffiths Diffuser" which reputedly gave a good performance.

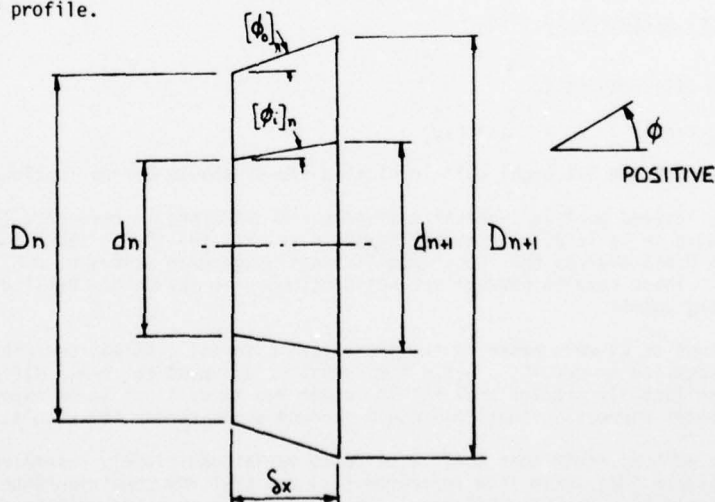
The benefit of wall curvature, with respect to overall diffuser length is illustrated graphically in figure 16). The lengths of the families of curved diffusers are compared by dividing them by the lengths of the equivalent optimum plane-walled diffuser, as determined by using the ' G ' technique. At an aspect ratio of unity ($a_1 = 1.0$), when we may expect the best performance, as argued in appendix 1(a), the curved wall diffuser of (AR) 2:1 is 81.5% of the length of its plane wall equivalent. An even greater reduction in length is achieved at (AR) 2.5:1 when the ratio is 75%.

The pressure recoveries from the curved ' G_x ' diffusers should foreseeably be greater than those for the plane wall equivalents since boundary growth is partially inhibited. This, it must be emphasized, is purely a point of conjecture as the ' G_x ' theory may need modification to cope with the effect of local aspect ratio on the optimum local pressure gradient. Research on this topic should be encouraged.

As regards the pressure loss characteristic of such a diffuser there are two opposing arguments which may conceivably cancel out each other. One is that curvature increases boundary layer velocity and thereby generates more frictional losses. The other is that losses will be reduced because the walls are shorter.

3.2 Application Of The ' G_x ' Technique to Annular Diffusers

The sketch below shows the ' n 'th element, which is situated at a distance ' x ' down an annular diffuser of arbitrary profile.



Applying equation (4) to this section we obtain an expression for the area ratio across the element

$$(AR)_e \quad \text{where } (AR)_e = 1 + \frac{4 \cdot \delta x \cdot [D \tan \phi_o - d \tan \phi_i]_n + 4 \cdot (\delta x)^2 \cdot [\tan^2 \phi_o - \tan^2 \phi_i]}{[D_h \cdot (D + d)]_n}$$

ignoring second order terms this becomes:

$$(AR)_e = 1 + \frac{4 \delta x [D \cdot \tan \phi_o - d \cdot \tan \phi_i]_n}{[D_h \cdot (D + d)]_n} \quad \dots (37)$$

then supposing the dynamic pressure at inlet to this section is q_x

$$\delta p_e \approx q_x \cdot \left\{ 1 - \left[1 + \frac{4\delta x [D \tan \phi_0 - d \tan \phi_i]_n}{[D_h (D + d)]_n} \right]^{-2} \right\}$$

Expanding Binomially and again ignoring second order terms gives

$$\delta p_e \approx q_x \cdot \left\{ \frac{8 \delta x [D \tan \phi_0 - d \tan \phi_i]_n}{[D_h (D + d)]_n} \right\}$$

in the limit as δx tends to zero

$$\frac{dp}{dx} = 8 q_x \cdot \left\{ \frac{[D \tan \phi_0 - d \tan \phi_i]_n}{[D_h (D + d)]_n} \right\} \quad \dots (38)$$

Defining ' G_x ' as $\frac{D_h}{q_x} \cdot \left(\frac{dp}{dx} \right)_x$ as previously,

$$\text{then } [G_x]_n = 8 \cdot \frac{[D \tan \phi_0 - d \tan \phi_i]_n}{[D + d]_n} \quad \dots (39)$$

and similarly at the first element along the diffuser

$$[G_x]_1 = G = 8 \cdot \frac{[D \tan \phi_0 - d \tan \phi_i]_1}{(D + d)_1} \quad \dots (40)$$

Dividing (43) by (44) gives the ratio of $\frac{[G_x]_n}{G}$ which must be kept constant, as argued previously,

$$\begin{aligned} \text{then } [D \tan \phi_0 - d \tan \phi_i]_n &= \frac{[D + d]_n}{[D + d]_1} \cdot [D \tan \phi_0 - d \tan \phi_i]_1 \\ \text{then } [D \tan \phi_0 - d \tan \phi_i]_n &= [D + d]_n \cdot \left[\frac{D \tan \phi_0 - d \tan \phi_i}{D + d} \right]_1 \quad \dots (41) \end{aligned}$$

We will now consider the application of this equation to some special cases.

3.2.1. Conical Diffusers ($d = 0$)

Equation (41) reduces to

$$[\tan \phi_0]_n = [\tan \phi_0]_1 \quad \dots (42)$$

which tells us that the 'straight wall' conical diffuser should be the 'optimum'.

Tests on 'curved profile' conical diffusers are described in reference 13 and some of the results are shown in Table 3. On averaging these results the 'Bell' shapes have a mean value of C_p equal to 0.645 whereas the 'Cone' and 'Trumpet' have mean values of 0.631 and 0.604 respectively. These results however are not conclusive in favour of 'Bell' diffusers because of the following points.

- 1) Values of C_p were based in the 'Aerodynamic throat', as was described during the discussion on ref.11. Since the curvature at inlet to 'Bell' diffusers will be significantly greater than for the other two types it is to be expected that the greater depression that this would produce would render the results optimistic.
- 2) The authors state that their area ratio variations closely resembled those of equation (33) taken from reference (12) and that the condition when k equals zero relates to a conical diffuser. This would then give the relationship

$$AR_x = 1 + x/L \cdot (AR - 1)$$

whereas in appendix 3(a) the following relationship for area variation down a conical diffuser is shown to be:

$$AR_x = \left[x/L \cdot (\sqrt{AR} - 1) + 1 \right]^2$$

There would appear to be some difference of opinion concerning diffuser profile.

3.2.2. Annular 'G_x' Diffusers Having A Parallel Core ($\phi_i = 0$)

Equation (41) reduces to:

$$[\tan \phi_o]_n = \left[\frac{D+d}{D} \right]_n \cdot \left[\frac{D \tan \phi_o}{D+d} \right]_1 \quad \dots \quad (43)$$

expressing the hub:tip ratio as $r = [d/D]$

$$\text{then } [\tan \phi_o]_n = [1+r]_n \cdot \left[\frac{\tan \phi_o}{1+r} \right]_1 \quad \dots \quad (44)$$

since $[1+r]_n$ will be less than $[1+r]_1$

these diffusers will be 'Bell' shaped.

3.2.3. Annular 'G_x' Diffusers Having A Parallel Outer Casing $\phi_o = 0$

In this instance, (41) reduces to:

$$[\tan \phi_i]_n = \frac{[1+r]_n}{[1+r]_1} \cdot \frac{[r]_1}{[r]_n} \cdot [\tan \phi_i]_1 \quad \dots \quad (45)$$

since the value of r will reduce down the diffuser

$$\text{then } \frac{[r]_1}{[r]_n} > 1$$

$$\text{and } \frac{[1+r]_n}{[1+r]_1} < 1$$

The first ratio is the 'stronger' of the two hence the diffuser will be convex facing the fluid.

The design of 'G_x' annular diffusers can be accomplished using a 'step by step' technique so long as the profile of one of the walls is known or if there is a pre-determined relationship between the local angles of the two walls.

To conclude this section, it would appear that savings in diffuser length, in the order of 20%, are feasible by careful design of curved walls. A relatively simple method which takes advantage of the abundant data available on simple conical diffusers has been suggested.

4.1 FORCED MIXING DEVICES

In the previous section it was shown that we can, in some configurations, reduce the length of the conventional diffuser by about 20%. Perhaps it is apt that in this section the devices under consideration may be applied as remedial measures if a diffuser is found to suffer flow separation.

The rate of mixing is the key factor in determining the rate of diffusion of high energy fluid into the boundary layer. Diffuser length is therefore controlled directly by this process and so it seems logical to artificially increase the mixing rate. This can be achieved by increasing the general turbulence level by using some form of grid. The difficulty is that turbulence decays relatively quickly and that a severe pressure loss penalty is incurred by the generating mechanism.

A more satisfactory approach is to encourage the local mixing of the mainstream with the boundary layer by using devices which have very little exposure to regions of high velocity fluid. In this way drag losses can be kept reasonably low so that they can be outweighed by the benefits of improved diffusion. The benefits can be achieved not only by the prevention of flow separation but also by the reduction in the rate of boundary layer growth. A thick boundary layer effectively blocks-off a significant part of the flow area near the diffuser exit, and thereby reduces the diffusing area ratio.

It was argued in reference (4) that the ideal mixing device would simply promote an exchange of fluid between the boundary layer and mainstream without consuming any of the momentum of the mean flow. This pure rearrangement implied guiding the fluid to its new position without leaving any residual circulation downstream of the mixing device. An ingenious series of tests is described where various 'plough'-like devices were installed on the floor of a purpose built pressurised wind tunnel, approximately 1830 mm wide x (350 sloping to 686 mm) deep. Adverse pressure gradients could be adjusted by rearranging gaps between a system of slats, forming part of the tunnel roof, and thereby controlling the rate of diffusion by the bleed-off of air.

Figure (17) which is taken from the reference, shows these devices (items A to F), which were designed to plough a 'furrow' in the boundary layer and then guide in mainstream air to fill it up. The intended mechanism of device G was to generate a secondary flow by turning the boundary layer in one direction, and then to cancel it out by turning it in the opposite direction. The performance of these devices was compared with two types of vortex generators (items J and K). The first was of the 'counter rotating' type which will be described more fully at a later point, and the second took the form of a shielded sink. In this last type a small quantity of flow (estimated at 5.6% of the boundary layer flow) was discharged out of an orifice situated between two parallel fences which were directed in-line with the major flow. The action of the discharge was to produce a local turning effect in the boundary layer and thereby generate trailing vortices from the fences.

It would appear that this last device is worthy of further development since its effect can be virtually switched-off when not required, by halting the flow of discharge. A comparison of size and performance of these devices is given in table (4) where $\delta(C_p)$ is the improvement in static pressure coefficient above that of the bare tunnel which had a value of C_p equal to 0.5. The drag effects of the devices are compared by use of the term $\frac{\Delta\theta}{\theta}$ where

$$\frac{\Delta\theta}{\theta} = \frac{\text{Drag Force}}{2x (\text{optimum spacing}, L) \times (\text{Local mainstream dynamic pressure})}$$

and θ was the local momentum thickness when measured in the bare tunnel.

In general, table 4 illustrates that the optimum location, x , of a device is a direct function of both its size and configuration. However, no such generalisation can be made about the optimum spanwise spacing, L . It is perhaps surprising that every device gave an increase in C_p which was attributed to their ability to delay the flow separation that otherwise would have occurred. For the purposes of diffuser improvement, device A-2 seems the most favourable since it combines a useful improvement of C_p with a low value of drag (and presumably small wakes). Device E-3 produces the most significant improvement in C_p but it would probably be unacceptable in circumstances where low total pressure loss and a uniform flow distribution are the primary objectives. Device J is a popular selection since it is simple to construct and information is available as to its optimum siting.

4.2 Vortex Generators

In spite of the measures taken to prevent trailing vortices most of the devices described in ref.(14) owe at least some of their success to residual vortices. Further studies, which were reviewed in ref.(15) showed that greater gains in performance together with smaller drag penalties could definitely be achieved from vortex generating systems. Success in inhibiting flow separation is critically dependent on the strength and placement of the individual vortices. These should be in the precise region of adverse pressure gradient.

It was also found that the scale of the generators should be related to the range of surface which needs energisation. This is so because larger vortices survive viscous dissipation for greater distances. The scale which can be used is often limited, however, because of mutual damping and interference with adjacent vortices. Although numerous types of vortex generator have been investigated those which involve simple vanes or plates mounted perpendicularly to the surface have emerged as the most popular. Two particular arrangements of these are the co-rotating and the counter rotating systems as shown in fig.18.

4.2.1. Co-Rotating Systems

The best arrangement of this system consists of identical vanes, equally spaced in line, and presumably in a region where lateral variations in velocity are minimal. The angle of inclination to the flow direction, β , is typically about 20° and the height of the vane should be about 20% greater than the local boundary layer thickness, δ , although as previously explained this may be varied according to the distance of effectiveness that is required. Aspect ratio defined as height divided by length (b/c), usually in the order of 1.0 to 1.5.

The spacing of these vanes is critical, as may be seen from fig.(19). When the spatial ratio, s/b , is less than 3.0 there is a mutual interference between adjacent vortices. In this the low energy fluid, removed from the boundary region by one vortex, is transferred to the adjacent vortex which then returns it directly to the boundary. To avoid this interference the value of spatial ratio is best set in the range from 4.0 to 8.0.

A characteristic of the vortex array is that the vortex paths have a lateral component which is dependent on the vortex strength, K . The angle, made with the local stream direction being

$$\tan^{-1} \left[\frac{K}{U_s} \cdot \coth \left(\frac{\pi b}{s} \right) \right]$$

which results in a curved trajectory but which, according to ref.(15), never exceeds a value of 15° . Most of the vortices in the array follow a path parallel to the wall, the exceptions being the two outermost. At one end the vortex is displaced towards the surface whereas at the far end the vortex is displaced away from the surface, fig.(20). This effect is amplified if side walls are in the near vicinity since one of the vortices will rapidly attach itself and lift prematurely away from the original surface. If the array is too narrow, there is a tendency for several vortices to spiral round one another. The major application for co-rotating systems appears to be when long path lengths are required and when side wall interference will not be a serious limitation. Reference (16) indicates that they are superior to counter rotating systems when used in a conical diffuser.

4.2.2. Counter Rotating Systems

In this system the vortex array is substantially different to that of the co-rotating one. Since the vanes are arranged in pairs which are divergent, so the space between the pairs is convergent and so, therefore, the flow pattern downstream of the vanes is zoned off, according to its spatial relationship with the generators. This is illustrated in fig.(21) where it can be seen that the boundary layer in the zone downstream of the divergent pairs is kept thin by the sweeping action of the vortices.

The boundary layer in the second zone has a varied history, depending on its distance downstream of the generators. Initially the vortices, which are transporting boundary layer fluid away from the first zone, are able to sweep it up into the mainstream, together with some of the low energy fluid from the second zone. However the transverse movement of the boundary layer from the first to second zone carries the vortices with it. In this manner, the width of the second zone is being diminished. At the same time, the vortices which tend to accelerate the boundary layer in the transverse direction, produce a reduction in boundary layer thickness. Because of this there is an initial tendency for the vortices to get closer to the surface.

Further downstream, as the zone width is reduced, the boundary layer being swept up by one vortex starts to get entrained into the vortex travelling away from an adjacent pair of generators. As a result of this entrainment the vortex core starts to turn away from the surface, firstly due to the increase in vortex diameter produced by entrainment, and secondly because some of the entrained low energy air is being transported back into the boundary layer, thereby causing it to thicken. This effect accelerates as the converging vortices get closer together. A point is then reached when the vertical component is sufficient to separate the vortices from the influence of the surface and they then lift off extremely rapidly.

This process therefore limits the effective range of this type of generator and will clearly depend on such factors as the distance between each set of divergent pairs, the initial strengths (K) of the vortices and the height of the generators. A reliable method for predicting the paths of the vortices was first derived in reference (17) and is also discussed in reference (15).

From the physical description given above, it is clear that counter rotating systems will be less susceptible to spanwise variations in velocity distributions and therefore are more appropriate for application to diffusers where this is likely to be a problem. Coupled with this benefit is the fact that a vortex generator can be 'paired' with a side wall and thereby avoid the problems experienced with co-rotating systems.

The problem of vortex 'lift off' can be overcome by either fitting a second row of generators or by reducing the downstream pressure gradient so that they are

To summarise this section, counter rotating vortex generators are likely to be the best mixing devices for most diffuser applications. In order to avoid heavy drag loss penalties they should be approximately 1.2 times their local boundary layer thickness, δ , and the 'pitch' between each divergent pair of vanes should be in the order of four times the distance between the leading edges of the pair. Although mixing devices are useful for preventing flow separation in relatively short areas of high pressure gradient they cannot be used for the general mixing of the complete stream, otherwise high pressure loss penalties will arise. They are therefore unlikely to be used in short diffusers when a high static pressure recovery is the primary objective.

5. SHORT DIFFUSERS

The techniques described so far lead to useful reductions in diffuser length but many applications arise where still shorter lengths are required. As a basis for discussing how to obtain a short diffuser we will consider an approximate form of the momentum-integral-equation, viz:

$$\frac{d\theta}{dx} = \frac{\theta}{q_w} \cdot \frac{dp}{dx} \cdot \left(\frac{1}{2} \cdot \frac{\delta^*}{\theta} + 1 \right) + \frac{\tau_w}{2q_w} \quad \dots (46)$$

In many instances the ratio of boundary layer displacement thickness to momentum thickness, δ^*/θ , is used as a shape parameter, H. Experimental evidence suggests that flow will tend to separate when H exceeds a value of just over 2.0. Accordingly we will rearrange equation (46) to give an expression for H, when

$$H = \frac{2}{(dp/dx)} \cdot \left\{ \frac{q_w}{\theta} \cdot \frac{d\theta}{dx} - \frac{\tau_w}{2\theta} - 1 \right\} \quad \dots (47)$$

From this equation we can list the somewhat conflicting properties needed to produce a low value of H .

- i) A high wall shear stress, τ_w . Many measures that can be taken to increase this parameter however also run the danger of increasing the momentum thickness gradient ($d\theta/dx$). Unless care is taken this latter term will increase at a greater rate than the former one.
- ii) A high adverse pressure gradient. This is obviously a direct requirement of a successful, short, diffuser. Once again, increasing this term can also lead to a larger increase in $d\theta/dx$.
- iii) A high value of boundary layer momentum thickness, θ . This term can only be beneficial when the wall shear stress is high in relation to $d\theta/dx$.
- iv) A low value of local dynamic head relative to the constraining surface, q_w .

The art of producing a short diffuser clearly depends on producing the most favourable compromise of the above factors. A number of possibilities have been investigated and we will discuss these in turn.

5.1 Diffusers With Moving Walls.

Supposing that the walls move in the same direction as the flow, then as wall velocity is increased there is initially a corresponding decrease in both the q_w and τ_w terms. This situation persists until the wall velocity equals the mainstream velocity when both terms will become equal to zero. If the wall speed is increased still further then all of the terms become negative due to the 'pumping' action of the walls. The question then arises as to whether the 'moving wall pump' should be exchanged for a more conventional one which would be more practical.

Tests on such a 2-dimensional diffuser are described in ref.18. The diffuser, as sketched in fig.22 had an inlet aspect ratio of 12 to 1 and used a boundary layer suction of 3.5 to 4% of the main flow in order to prevent separation from the sidewalls. The moving walls consisted of two rotating cylinders mounted at the ends of the approach duct, the diameter of the cylinder being equal to 3 times the approach duct height. The area ratio of this diffuser could be varied from 1.75 up to 4 by adjustment of the exit duct walls. The attainment of stable flow was a function of both area ratio and relative velocity between cylinder surface and mainstream. Stable flow was not achieved at area ratios greater than 2.125. The area ratios tested with stable flow were 1.75, 2, 2.125 and the corresponding velocity ratios needed for flow stability were 0.5, 0.875 and 2.13. In the case of the diffuser with an area ratio of 2:1 the effectiveness, η , increased from 39.6% without rotation up to 80% at the stated velocity ratio.

Applications for this type of diffuser are clearly very limited, a possible use would be in a very low speed wind tunnel.

5.2 Diffusers Using Transverse, Unbled Vortices.

Basically these vortices can be considered to replace the rotating cylinders of the previous example, but in this case the term q_w/θ can only be partially reduced since energy must be transferred from the mainstream to the vortices by some finite velocity gradient. Two types of diffuser using this principle have been reported in the literature.

5.2.1 The "Ringleb" Cusp Diffuser

The invention of this diffuser followed from observations of snow formations on the downstream side of a high mountain ridge, as illustrated in figure 23. It was postulated, by the author of reference 19, that a standing vortex was responsible for the cusp shape, and that this must have guided the flow to a clearly defined re-attachment point. He devised a theory utilising potential flow considerations and the Kutta-Joukowski condition which matched the observed formation. A diffuser, based on this idea, was constructed for a wind tunnel at Princeton University, (fig.24), in order to replace a badly separating 12° conventional diffuser. The 'cusp' diffuser greatly improved the flow condition.

Subsequent attempts to use such diffusers have met with little success, probably because there is insufficient energy interchange between the 'shielded' vortex and the mainstream flow.

An explanation for the natural snow cornice can be deduced from ref.20 where tests on cusp diffusers are described. These tests used a 'water table' for visualisation studies, during which it was observed that standing vortices were retained in the cusps during the 'starting up' phase. These were subsequently swept downstream once steady flow conditions had been achieved. In nature it may be assumed that windspeed is almost constantly changing and the large scale of the snow cornice was sufficient to retain stable recirculation of flow over long periods of time.

A later investigation into the success of the Princeton diffuser showed that stable recirculation in the cusp was linked with a secondary flow generated by a sudden bend located shortly downstream of the diffuser.

More recent studies have been conducted where rectangular sectioned 'cusps' have been used, with some success, to control the flow around 90° bends in 2-dimensional ducts. This work is reported in references 21 and 22. The technique has also been successfully employed to turn the flow into a radial diffuser as reported in reference 23.

5.2.2 Ribbed Diffusers

As previously stated, this type of diffuser also employs transverse vortices to act as 'roller bearings'. They resemble conventional diffusers apart from the fact that their angle of divergence is normally greater and that they have transverse grooves for part of the way down the wall. The name is derived from the fact that these grooves are usually machined close together and the sections of wall between them produce a 'rib-like' appearance.

The first reference to appear on this topic, ref.(24), originated from the U.S.S.R. and was quickly followed by the five other publications by the same author (four of these are listed in the Bibliography). A useful review of this work appears in ref (25) from which the following notes were extracted.

5.2.2.1 Conclusions made from U.S.S.R. research:

- i) The data was presented as a comparison of effectiveness between ribbed and otherwise identical plain conical and annular diffusers.
- ii) Ribbed diffusers are sensitive to inlet Reynolds number R_d . The ratio of effectiveness of the two diffusers rose rapidly, in favour of the ribbed type, as R_d was increased from 53,000 to 91,000. A ratio exceeding 2.0 can be reached for values of ϕ from 19° to 23° which appears to be the optimum range of wall angle.
- iii) Location of the ribs close to the diffuser inlet was necessary in order to produce good performance.
- iv) Tests were conducted on two diffusers with a scale difference of two times, no difference in performance was noted.
- v) The grooves were rectangular in section and their sides were perpendicular to the surface. The optimum ratio of groove depth to width, a/b , was found to be 2.5.
- vi) Increasing the cavity width, b , from 1 mm to 5 mm had no effect on the performance. Above this range, however, performance deteriorated. (note: This particular investigation was conducted in a 2-dimensional diffuser having a throat height of 70 mm).
- vii) Maximum effectiveness was achieved with 13 ribs when $b = 1$ mm and with 6 ribs when $b = 5$ mm.
- viii) Varying rib thickness from 1.5 mm down to a knife edge did not change the effectiveness.

Additional information was taken from ref.26 which stated the actual values of C_p obtained from a conical diffuser of area ratio 5.85 and $\phi = 20^\circ$. For the diffuser with ribs $C_p = 0.67$ which compares favourably with the value of 0.26 taken without ribs. On the other hand if an optimum conical diffuser of the same length (but a significantly smaller area ratio) was used it is likely that it would have achieved a value of C_p equal to that of the more complex ribbed diffuser. This assumption is based on figure 25 which suggests that these diffusers operated with a very thin boundary layer at inlet.

The major purpose of reference 25 was to describe a series of water table studies on ribbed diffusers. These showed that the mechanism that delayed flow separation was more likely to be due to the shedding of eddies from out of the cavities rather than any 'roller bearing' action, as had at first been postulated. The effect of these eddies was to generate mixing in the boundary layer in a similar manner to the circulations from vortex generators.

The rate and manner in which these eddies were shed was a strong function of the cavity shape. This finding was confirmed in air rig tests as described in ref.27. These air rig tests also showed that the pressure recovery can vary significantly with Mach number due to acoustic resonance. A significant reduction in C_p was obtained at a M_n of about 0.4 from the rib geometries that were used for these tests but it could be reduced by lining the bottom of the cavity with felt. A method for predicting the frequency of this self-induced resonance is given in ref.28.

Recently tests have been conducted on an annular ribbed diffuser at Cranfield. The author wishes to emphasise the high noise level which can be generated by such a diffuser when certain cavity geometries are used.

By reverting to tests using only a single cavity geometries have been produced which are insensitive to Mach number in a range of up to 0.4. These geometries are also found to be the optimum ones with regard to pressure recovery. So far no clear rule has been obtained for determining these configurations because they also appear to be a function of diffuser angle. Tests are being continued to establish this rule so that multiple cavity configurations can then be investigated using a logical rather than a statistical approach.

Although it is probable that satisfactory ribbed conical diffusers will eventually be developed it is unlikely that values of ϕ in the order of 20° will prove satisfactory. The reasoning behind this statement is that such diffusers would be only 12% of the length of conventional ones. Much of the mainstream flow would still have to depend on natural mixing to produce diffusion and there will be insufficient distance for this to be effective.

The fact that very little natural mixing can occur in a short diffuser gives some justification for the use of a simple, inviscid, finite element model. Such a model was used to predict the development of velocity profile down a short diffuser, as shown in fig.(26). It was assumed that flow had been viscous up to diffuser inlet in order that the slightly non-uniform profile could be generated. The model took no account of streamline curvature and simply assumed that static pressure was uniform across every section. The effect of pressure gradient on the boundary element 'a' is quite remarkable, particularly between the planes at area ratios 2 and 3. Clearly element 'a' is the 'weak link' in the diffusion process and it must either be removed, re-energised, or shielded from the pressure gradient.

5.3 Boundary Layer Energisation By Local Injection

By referring to equation (47) we can predict several important features of this technique.

- a) If injection makes q_w greater than the local free stream dynamic pressure, then injection will tend to increase the shape factor, H , and hence promote the likelihood of flow separation.
- b) Injection will tend to increase $d\theta/dx$, this will also raise the value of H .
- c) The shear stress at the wall, τ_w , will be increased giving a beneficial effect. (This could directly cancel 'b') above.
- d) The value of momentum thickness θ must be adjusted carefully. If θ is reduced by increasing the velocity along the wall, then this could seriously amplify the disadvantageous effects of q_w . If on the other hand the wall jet is made so strong that ' θ ' becomes negative, then the net effect will depend on the balance between q_w and τ_w . A very smooth wall would clearly be preferable at this condition. Another solution is to inject fluid in a jet with a velocity deficiency near the wall. This would reduce q_w , possibly increase θ and at the same time limit the value of $d\theta/dx$.
- e) Since any advantage will arise from a difference between the q_w and τ_w terms it will be important to use a high pressure gradient and therefore the diffusers should have a wide angle.

These predictions can be assessed by considering experimental evidence.

5.3.1 Tangential Injection

In reference (29) this technique was applied to three conical diffusers with angles ϕ of 5° , 10° and 15° , each having an area ratio of 3. Air was used as the working fluid and the test rig was designed to produce a thin boundary layer at inlet. The injected air entered through a slot of converging cross section as is shown in fig.27. The final height of this annular nozzle equalled approximately 2% of the diffuser inlet diameter, D_1 , and the point of injection was at a distance of 21% D_1 down the diffuser.

Until the mean injection velocity, u_j , exceeded 50% of the mean velocity at inlet, u_1 , there was actually a slight reduction in pressure recovery. Above this value of velocity ratio, u_j/u_1 , there was a marked improvement in performance until u_j/u_1 reached 120%, which corresponded to a mass flow ratio between jet and inlet of around 9.9%. At injection rates above these values however the pressure recovery coefficient, C_p , started to fall once again.

The best improvement in C_p was achieved in the $\phi = 15^\circ$ diffuser when the ratio of C_p with injection to C_p without injection equalled 230%. A maximum value of $C_p = 0.85$ was achieved with both the $\phi = 10^\circ$ and 15° diffusers. The benefits obtained by using injection in the diffuser of $\phi = 5^\circ$ were marginal.

A similar study but on a 2-dimensional diffuser of aspect ratio 8:1, is described in reference (30). The diffuser could be adjusted to cover a range of inlet angle, 2ϕ , from 4° to 30° . Injection slots were fitted only to the diverging walls and their heights could be adjusted from 0.33% up to 8.33% of the throat height at inlet. The exit plane of these slots was located at a distance of 88% of an inlet height from the beginning of divergence.

Performance was given both as a simple coefficient of static pressure C_p based only on main-stream pressures, and also as a corrected coefficient, C_p' , which took account of the pumping power required for injection. For this it was assumed that the pumping system had an overall efficiency of 60%.

This work, which retained an inlet boundary layer thickness of $2.6^*/W_1 = 0.02$ throughout, showed the following points.

High values of C_p could be achieved for the lowest mass flow rate when the slit was set to its narrowest. A value of C_p equal to 0.8 was achieved from all three diffusers using an injection

rate equal to 6% of the mainstream. The most significant improvement in performance was achieved by the diffuser having $2\phi = 30^\circ$.

When pumping power was taken into account, however, values of C_p' showed that the wider slits were most efficient and that this form of injection was only beneficial (energy-wise) in the diffuser having $2\phi = 30^\circ$.

Both references 29 and 30 compared their experimental data with theoretical values. In general the agreement between data was good.

The work reported in reference 31 differed from the two previous ones in that injection was parallel to the axis of a conical diffuser and that water was used as the working fluid. Injection slit heights, covering a range of 2.22% up to 6.68% of the inlet diameter were investigated and the results plotted on a basis of ratio v_j/v_1 . The optimum value of this ratio was found to be 120% over the complete range of slit heights.

The observed characteristics agree closely with those which can be deduced from equation 47. The author was unable to find reference to experiments that used thick boundary layers or distorted inflow, such data would clearly be useful.

If a cone angle, 2ϕ , of 30° is used in this type of diffuser it will be less than one third of the length of a conventional one and yet produce an improved pressure recovery. An ideal application would be when advantage could also be taken of the wall cooling effects of the injected fluid.

5.4 Boundary Layer Control by Suction

At the beginning of the previous section there was a discussion on the use of equation (47) in predicting the optimum conditions for boundary layer injection. The arguments used in that instance are equally applicable to the case of boundary layer control by the use of suction. Here we have an additional problem as to the method of removal of the boundary layer. Firstly there is a selection to be made as to whether to draw the boundary layer out through porous walls or through suction slots. This may depend entirely on such factors as the cleanliness and temperature of the fluid together with mechanical factors such as the requirement of wall strength and the space available to collect the rejected boundary layer.

5.4.1 Boundary Layer Removal Through Porous Walls

Initially this technique was limited by the choice of porous materials available, such as ceramics and sintered stainless steel. These lacked mechanical strength and the porosity was difficult to control, particularly if there was a necessity to vary the porosity factor down the length of the diffuser. Recently the advent of electron beam drilling has provided an interesting alternative since it makes possible the use of localised boundary layer control without any serious concessions to mechanical strength.

An investigation into the use of porous walls is reported in ref.(32). This describes tests on three conical diffusers, of angle 2ϕ equal to 10° , 30° and 50° , each having an area ratio of 2:1. The walls of the diffusers were constructed from sintered stainless steel, 1.6 mm thick. These walls were progressively 'sealed up' from the downstream region until a relatively narrow band of porous metal remained near the throat. Although a static pressure effectiveness, η , of near 100% could be achieved from the outset, the amount of bleed flow required to achieve it was significantly reduced as the suction zone became more localised. Eventually the bleed flow for the 30° diffuser was reduced to 3% and for the 50° diffuser it became 4%.

As may be expected from such an effective diffuser, the total pressure profile at exit was nearly uniform. These tests were conducted using a thin boundary layer and no studies were reported using a narrow porous band part way down the diffuser.

5.4.2 Boundary Layer Removal Through Slots

There has been an abundance of tests conducted on diffusers using this technique as it is simple to apply and usually produces satisfactory results. The choice of axial location and type of slot will depend on the application for which the diffuser is intended.

If minimum total pressure loss is the requirement then the best location will be just upstream of the point where flow would normally separate if boundary layer control were not applied. In this way skin friction losses will be low. Another benefit is that the air to be bled off will have gained static pressure and will have a low velocity. Both these conditions are essential if the bled air itself is not to experience significant losses in pressure during its removal.

Disadvantages of downstream slot location are as follows:-

- i) Prediction of the region where flow would normally separate can be difficult, particularly if the flow at diffuser inlet is non-uniform or if strong secondary flows are present. If either of these two factors apply then the separation point must be determined experimentally, either by using flow visualisation techniques, ref.(33), or by taking static pressure measurements down the diffuser and locating the point of discontinuity in the pressure gradient.
- ii) The region of flow separation can vary significantly with slight changes of condition at diffuser inlet or slight 'production line' variations in geometry.
- iii) If any large scale flow disturbances arise it is possible for the flow to separate upstream of the slot. Since the bleed would then originate from the separation zone it would be quite ineffective. Exceedingly large bleed flows are then required to restore effective diffusion.
- iv) Since diffusion is known to accentuate any flow non-uniformity the flow distribution in the slot region is unlikely to be uniform. If this is so, then rapid diffusion downstream of the slot will not be so effective because the mixing process in mid-stream will remain slow. A mediocre static pressure recovery will clearly be the end result.

A special type of diffuser with a suction slot part way down the wall is the Griffith diffuser (fig.28). Use is made of wall curvature to eliminate the local static pressure gradient and there is then a step increase in static pressure situated over the suction slot. A possible method of designing such a diffuser is described in reference 34.

When static pressure recovery or immunity to flow disturbance is the primary consideration then the bleed slit should be situated at diffuser inlet. The 'sink' effect of the slit has a tendency to improve the velocity distribution at inlet by increasing the boundary layer velocity. Diffusers using this technique are described in references (35) and (36). Details of the manner in which slot geometry could be varied in the 2-dimensional diffuser of reference (36) are shown in figure (29). This diffuser demonstrated that high static pressure recoveries are feasible from short diffusers when the inlet boundary layer is thin, no tests are reported in which the inlet flow is non uniform.

A possible shortcoming of this type of diffuser is that a high velocity boundary layer is produced immediately downstream of the slot and skin friction losses down the divergent wall could be high. However, so long as the angle of divergence, 2ϕ , is of the order of 30° or possibly greater then deceleration will be so rapid that this problem will not be significant.

Two types of diffuser which eliminate the need for divergent walls have been discussed in recent years. They are extremely similar in many ways and both owe their derivation to experiments on 'Cusp type' diffusers. Having discovered that a standing vortex will not normally stabilize in a cusp under steady flow conditions, attempts were made to restore the situation by use of suction directly from the vortex. In this way, it was hoped that high energy fluid would be entrained directly from the mainstream in order to replace the quantity bled-off, and thereby restore the vortex strength. The original work using this technique is reported in reference (37). A sketch of the apparatus used is shown as fig.30 where suction was applied by means of locating orifices in the side walls of a 2-dimensional diffuser. The orifices were intended to bleed off fluid directly from the vortex core. These tests were only partially successful in that pressure recoveries were modest and that relatively large quantities of suction had to be applied. It seems likely that much of the bled air originated from the boundary layer on the side walls.

The problem was overcome by the same researcher, as reported in reference (38), by using a small downstream facing slot at the top of a step in the diffuser wall, as shown in figure 31. This technique produced successful diffusers with static pressure recoveries extremely close to the ideal and which required modest bleed rates in the order of 4%. The length needed for this diffusion was remarkably short, being equal to approximately one exit pipe diameter. The boundary layer used at diffuser inlet during these tests was thin.

While unaware of these experiments, a research programme was started at C.I.T. and initial experiments were first reported in reference (39). The study was similar to that of ref.(37) apart from the fact that the bled air was taken from along the length of the vortex by removing it tangentially through a slit, as shown in fig.32. This work was hampered by flow separation from the parallel side walls.

Work at C.I.T. was continued using a pipe diffuser derivative of that shown in fig.32. and is described in ref.(40). A problem was encountered, however in that substantial quantities of bleed had to be removed before the desired vortex mechanism could be stabilised.

The problem was overcome, following a study using water flow visualisation, which showed that initially the bleed flow originated from the downstream region of the step where the fluid was virtually stagnant. In order to prevent this occurrence, a fence was fitted part way downstream of the step and the result was an immediate reduction of bleed-quantity and an almost ideal static pressure rise coefficient.

The diffuser technique has since been developed using diffusers of different configurations and varying degrees of flow distortion at inlet. Some of this work is reported in the Cranfield Theses listed in the Bibliography and summarized in reference 41. In this reference empirical equations are presented which relate the amount of bleed required to the area ratio and diffuser configuration. A method of predicting the effect of flow non-uniformity at inlet, on the overall pressure recovery, is also given. This is based on the kinetic energy coefficient, α , rather than the more usual 'blockage factor'. It is also suggested that there is a limiting area ratio that can be used, which is dependent on inlet flow conditions. If this area ratio is exceeded then there will be a reduction in static pressure recovery and flow instability will result. The remaining figures in this paper are derived from reference 41.

6. Conclusion

It has been shown that, so far, efficient short diffusers have only been produced when either boundary layer injection or suction techniques are employed. This auxiliary flow usually requires some pumping mechanism and the energy required by this must be offset against the performance of the diffuser. Unless factors such as the improvement in performance of components downstream of the diffuser together with reductions in weight are also taken into account, the benefits to be obtained from these more complex diffusers may appear to be marginal.

7. Acknowledgements

The author wishes to thank many of his colleagues at C.I.T. for their friendly assistance during the preparation of this paper.

REFERENCES

1. El-Attar, M.A.R.A.
Peacock, R.E. "An application for variable inlet guide vanes in distortion suppression". 48th P.E.P. Meeting (AGARD) Paris, 1976.
2. ESDU "Introduction to design and performance data for diffusers". Engineering Sciences Data Item 76027 (1976).
3. ESDU "Performance of conical diffusers in incompressible flow". ESDU Item 73024, (1973).
4. ESDU "Performance in incompressible flow of plane-walled diffusers with single plane expansion". ESDU Item 74015, (1974).
5. ESDU "Performance of circular annular diffusers in incompressible flow". ESDU Item 75026, (1975).
6. Adkins, R.C. "Use of the 'G' parameter in diffuser design". Cranfield Institute of Technology, S.M.E. Note No. 14, (March 1977).
7. Howard, J.H.G.
Henseler, H.J.
Thornton-Trump, A.B. "Performance and flow regimes for annular diffusers". Am. Soc. Mech. Eng. Paper 67-WA/FE-21 (1967)
8. Sovran, G.
Klomp, E.D. "Fluid Mechanics of Internal Flows". A book published by Elsevier, (1967).
9. Tyler, R.A.
Williamson, R.G. "Diffuser performance with distorted inflow". Proc. Inst. Mech. Eng. Vol. 182 (1967-68).
10. Livesey, J.L.
Odukwe, A.O. "Some effects of pipe flow generated entry conditions on the performance of straight walled conical diffusers with high subsonic entry Mach number". Israel Journal of Tech., Vol. 11, No. 4, (1973).
11. Runstadler, P.W. (Jr.)
Dean, R.C. (Jr.). "Straight Channel Diffuser Performance at high inlet Mach numbers". ASME J. of Basic Eng., Paper No. 68-WA/FE-19.
12. Carlson, J.J.
Johnston, J.P.
Sagi, C.J. "Effects of wall shape on flow regimes and performance in straight, two-dimensional diffusers". J. of Basic Eng., March 1967.
13. Dolan, F.X.
Runstadler, P.W. (Jr.) "Pressure recovery performance of conical diffusers at high subsonic Mach numbers". N.A.S.A. CR-2299 (1973).
14. Schubauer, G.B.
Spangenberg, W.G. "Forced mixing in boundary layers". J. of Fluid Mechanics, Vol. 8, (1960).
15. Pearcey, H.H. "Shock-induced separation and its prevention". Published in Vol. 2 of "Boundary Layer and Flow Control", edited by Lachman, Published by Pergamon.
16. Senoo, Y.
Nishi, M. "Improvement of the performance of conical diffusers by vortex generators". Trans ASME J. of Fluids Engineering 73-WA/FE-1.
17. Jones, J.P. "The calculation of the paths of vortices from a system of vortex generators, and a comparison with experiment". A.R.C. Technical Report C.P. No. 361 (1957).
18. Tennant, J.S. "A subsonic diffuser with moving walls for boundary-layer control". AIAA Journal Vol. 11, No. 2 (1972).
19. Ringleb, F.O. "Separation Control by standing vortices". Published in "Boundary Layer and Flow Control", edited by Lachman, Published by Pergamon.
20. Frey, K.P.H.
Vasuki, N.C. "Tests on flow development in diffusers". ASME Symposium on Fully Separated Flows (1964).
21. Eves, A. "Vortex Flow control in channel bends". Cranfield Institute of Technology Thesis (S.M.E.) 1972.
22. Krajinski, R. "The effects of optimising vortex flow control in mitred bends". Cranfield Institute of Technology thesis (S.M.E.) 1974.
23. Allen J. "A Vortex Controlled Radial Diffuser". Thesis, Cranfield Institute of Technology (SME) 1975.

24. Migay, V.K. "Diffusers with transverse fins".
Energomashinostroyeniye, No. 4, 1960.
25. Stull, F.D.
Velkoff, H.R. "Flow regimes in two-dimensional ribbed diffusers".
Trans. ASME, J. of Fluid Eng., March 1975.
26. Migay, V.K. "Study of ribbed diffusers".
Teploenergetika, No. 10/1962.
27. Stull, F.D.
Velkoff, H.R. "Effects of transverse ribs in pressure recovery in two dimensional
subsonic diffusers".
AIAA Paper No. 72-1141 (1972).
28. Stull, F.D.
Curran, E.T.
Velkoff, H.R. "Investigation of two-dimensional cavity diffusers".
AIAA 6th Fluid & Plasma Dynamics Conference, Palm Springs, July 1973.
29. Nicoll, W.B.
Ramaprian, B.R. "Performance of conical diffusers with annular injection at inlet".
Trans. ASME Journal of Basic Engineering, Dec. 1970.
30. Fielder, R.A. "Influence on Tangential Fluid Injection on the performance of two
dimensional diffusers".
Trans. ASME Journal of Basic Engineering, Sept. 1972.
31. Duggins, R.K. "Conical diffusers with annular injection".
Journal of Mechanical Engineering, April 1975.
32. Holzhauser, C.A.
Hall, L.P. "Exploratory investigation of the use of area suction to eliminate
air-flow separation in diffusers having large expansion angles".
N.A.C.A. Tech. Note 3793 (1956)
33. Slingsby B.S. "Some effects of Boundary Layer control on two-dimensional, wide-angle,
subsonic diffusers".
M.Sc. Thesis, Cranfield Institute of Technology (1967).
34. Yang, T.
El-Nashar, A.M. "Slot suction requirement for two-dimensional Griffith Diffusers".
Trans. ASME, Journal of Fluids Engineering, June 1975.
35. Furuya, Y.
Sato, T.
Kushida, T. "The loss of flow in conical diffusers with suction at the entrance".
Bulletin of J. S.M.E. Vol. 9, No. 33 (1966).
36. Furuya, Y.
Fujimoto, T.
Yamazato, E.
Tsuzuki, I.
Nishiur, I. "Performance of two dimensional diffusers with suction at the entrance".
Bulletin of J. S.M.E. Vol. 13, No. 56 (1970).
37. Heskestad, G. "Remarks on snow cornice theory and related experiments with sink flows".
Trans. ASME Journal of Basic Engineering (1966).
38. Heskestad, G. "Further experiments with suction at a sudden enlargement in a pipe".
ASME Paper No. 69-WA/FE-27. (1969).
39. Sims, M.D. "Diffuser flow control using trapped vortices".
Thesis, Cranfield Institute of Technology (1969).
40. Beatty, C.G. "Diffuser control by trapped vortices".
Thesis, Cranfield Institute of Technology (1970)
41. Adkins, R.C. "A short diffuser with low pressure loss".
Trans. ASME Journal of Fluids Engineering (Sept. 1975).

BIBLIOGRAPHY

1. Morozov, D.I. "Effect of Inlet Conditions on the Optimal Shape of a Diffuser". Energeticheskoye Mashinostroyeniye, No. 11 (1971).
2. Jones, J.R.
Douglass, W.M. "Dynamic Flow Distortion in Subsonic Air Inlets". Second Int. Symposium on Air Breathing Engines (1974).
3. MacMiller, C.J. "Investigation of Subsonic Duct Distortion". AIAA Paper 69-449 (1969).
4. Peters, A.R.
Phelps, G.A. "The Effect of Inlet Velocity Profile Shape on Flow Separation in a Confined Two-Dimensional Channel". Journal of Fluids Engineering (Sept. 1974).
5. Wolf, S.
Johnston, J.P. "Effects of Nonuniform Inlet Velocity Profiles on Flow Regimes and Performance in Two-Dimensional Diffusers". Journal of Basic Engineering (Sept. 1969).
6. Coladipietro, R.
Schneider, J.H.
Sridhov, K. "Effects of Inlet Flow Conditions on the Performance of Equiangular Annular Diffusers". ASME-CSME Fluids Engineering Conference No. 73-CSME-84 (1974).
7. Bradley, C.I.
Cockrell, D.J. "The Response of Diffusers to Flow Conditions at their Inlet". (Source Uncertain).
8. Stratford, B.S. "An experimental flow with zero skin friction throughout its region of pressure rise". Journal of Fluid Mechanics, Vol. 5 (1959).
9. Thayer, E.B. "Evaluation of curved-wall annular diffusers". ASME Paper 71-WA/FE-35.
10. Valentine, E.F.
Carroll, R.H. "Effects of Several Arrangements of Rectangular Vortex generators on the static-pressure rise through a short 2:1 diffuser". N.A.C.A. Paper KM L50L04.
11. Wood, C.C.
Higginbotham, J.T. "Effects of diffuser and center-body length on performance of annular diffusers with constant diameter outer walls and with vortex generator flow controls". N.A.C.A. Paper KM L54G21.
12. Wood, C.C. "Preliminary investigation on the effects of rectangular vortex generators on the performance of a short 1.9:1 straight wall annular diffuser". N.A.C.A. KM L51G09, October 1951.
13. Valentine, E.F.
Carroll, R.B. "Effects of some primary variables of rectangular vortex generators on the static pressure rise through a short diffuser". N.A.C.A. RM L52B13, May 1952.
14. Wood, C.C. "The Influence of vortex generators on the performance of a short 1.9:1 straight wall annular diffuser with a whirling inlet flow". N.A.C.A. RM L52L01a, February 1953.
15. Mitchell, G.A. "experimental investigation of the performance of vortex generators mounted in the supersonic portion of a mixed compression inlet". N.A.S.A. TM X2405, November 1971.
16. Martin, R.A. "Comparisons of in-flight F-111A inlet performance for on- and off-scheduled inlet geometry at Mach numbers of 0.68 to 2.18". N.A.S.A. TM D-6490, September 1971.
17. Brown, A.C.
Nawrocki, H.F.
Paley, P.N.

Metha, U.B.
Lavan, Z. "Subsonic diffusers designed integrally with Vortex generators". Journal of Aircraft Vol. 5, No. 3, May-June 1968.

"Flow in a two dimensional channel with a rectangular cavity". N.A.S.A. CR 1245, January 1969.
18. Macagno, E.O.
Hung, T.K. "Computational and experimental study of a captive annular eddy". Journal Fluid Mechanics, 1967, Vol. 28, Part 1, pp.43-64.
19. Rao, D.M. "A method of flow stabilisation with high pressure recovery in short, conical diffusers". The Aeronautical Journal of the Royal Aeronautical Society, Vol. 75, May 1971.

20. Juhasz, A.J. "Performance of a short annular dump diffuser using wall trailing-edge suction".
N.A.S.A. TM X-3093, August 1974.
21. Migay, V.K. "On improving the effectiveness of diffuser flows with separation".
Mekhanika i mashinostroyeniye, No. 4, 1960.
22. Migay, V.K. "Increase of diffuser efficiency by means of transverse fins".
Teploenergetika, No.4, 1961.
23. Migay, V.K. "The Efficiency of a cross-ribbed curvilinear diffusers".
Energomashinostroyeniye, No. 1, 1962.
24. Migay, V.K. "The Aerodynamic Effectiveness of a discontinuous surface".
Inzhenerno-Fizicheskiy Zhurnal, Vol. 5, No. 4, 1962.

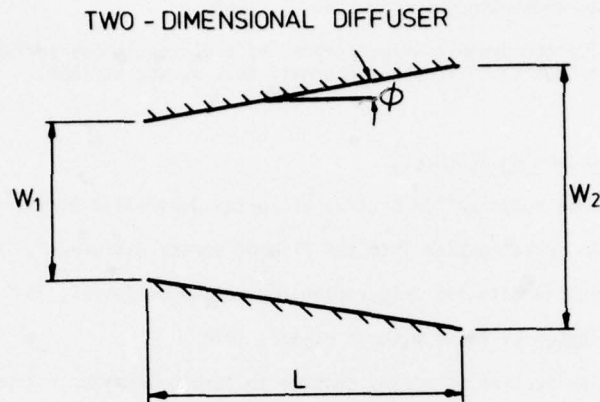
Theses of Cranfield Institute of Technology (S.M.E.)

1. Fenge B. "Some optimisation studies on Vortex Controlled Diffusers", 1971.
2. Sutherland, G.D. "An investigation into the flow of vortex diffusers", 1972.
3. Sadasivam, R. "Further studies on a vortex controlled diffuser", 1973.
4. Hallam, A. "Vortex Diffuser without bleed", 1974.
5. Mak, K.H. "Application of vortex control to turbine exhaust diffusers", 1974.
6. Allen, J.E. "A vortex controlled radial diffuser", 1975.
7. Diacakis, C. "Tail pipe diffusers", 1975.

APPENDIX 1(a)

The Effect of Aspect Ratio, a , on Two-Dimensional Diffusers.

In order to appreciate this then both geometric factors and the influence of transverse flows need to be considered.

Geometric Factors

We will assume that the diffuser width (perpendicular to the paper) is 'S'. The area ratio can be expressed as

$$AR = 1 + 2 \cdot (L/W_1) \tan \phi \quad \dots \quad (i)$$

Differentiating (i) with respect to L gives

$$\frac{d(AR)}{dL} = \frac{2}{W_1} \cdot \tan \phi \quad \dots \quad (ii)$$

As shown previously,

$$\frac{d(Cp)}{d(AR)} \Big|_{L=0} = 2$$

$$\text{Then } \left[\frac{d(Cp)}{dL} \right]_{L=0} = \left[\frac{d(Cp)}{d(AR)} \right]_{L=0} \left[\frac{d(AR)}{dL} \right]_{L=0} = \frac{4}{W_1} \tan \phi \quad \dots \quad (iii)$$

Using the previous definition for hydraulic diameter

$$D_h = \frac{2 \cdot S \cdot W}{S + W}$$

or in terms of 'aspect ratio' a ($a = S/W$)

$$D_h = \frac{2 \cdot a \cdot W}{1 + a} \quad \dots \quad (iv)$$

Then our 'G' parameter, $G = D_h \cdot \left(\frac{dCp}{dL} \right)$, can be derived directly from (iii) as

$$G = \frac{2 \cdot a \cdot W}{(1+a)} \cdot \left[\frac{d(Cp)}{d(AR)} \right]_{L=0} = 8 \left(\frac{a}{1+a} \right) \tan \phi \quad \dots \quad (v)$$

rearranging for ϕ gives

$$\phi_{opt} = \tan^{-1} \left\{ \left(\frac{1+a}{a} \right) \cdot \frac{G}{8} \right\} \quad \dots \quad (vi)$$

for diffusers of large aspect ratio where $a \rightarrow \infty$

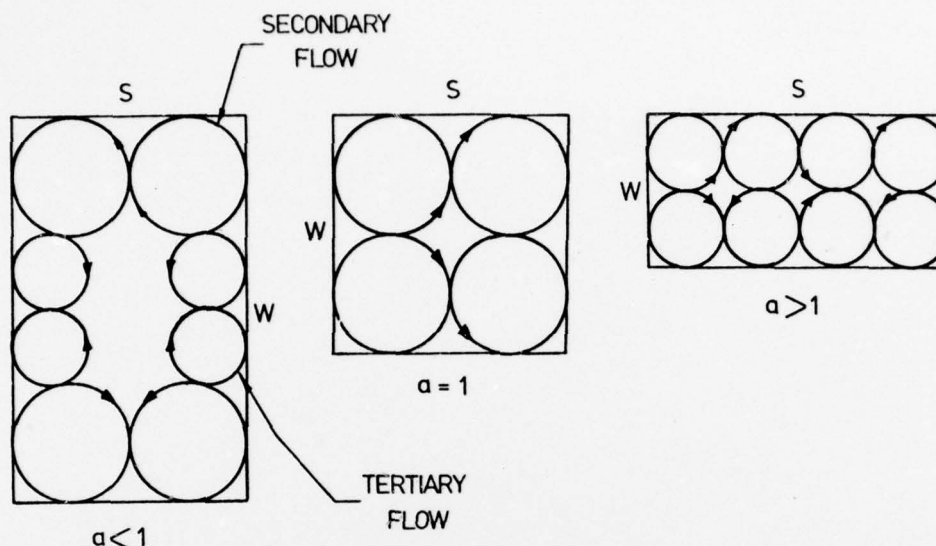
$$\text{then } \phi_{opt} \approx \tan^{-1} \left(\frac{G}{8} \right) \quad \dots \quad (vii)$$

When 'a' becomes less than about 4.0, then equation (vi) predicts that the progressive increase of ϕ_{opt} now becomes significant as 'a' is reduced.

It is likely, however, that values of G will become influenced by aspect ratio.

Flow Factors

Due to differences in boundary layer growth between the divergent walls and the side walls a secondary flow pattern develops which is perpendicular to the major axis. This has a beneficial effect because it encourages flow into the boundary layers on the divergent walls and thereby delays flow separation. The proportion of cross sectional area influenced by secondary flow will depend on the aspect ratio as is illustrated in the sketch below.

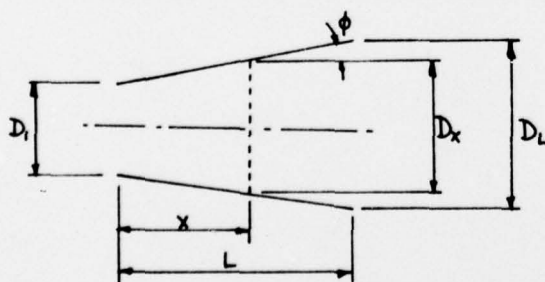


From the sketches it is apparent that the best mixing is achieved when 'a' is unity since the critical boundary layers are recharged directly from mid channel. It can be argued that the optimum aspect ratio at diffuser inlet will be marginally greater than unity so that the optimum mixing occurs just downstream of the diffuser inlet.

The influence of aspect ratio when substantially different from unity will depend on the extent to which the tertiary flows penetrate into the main stream and then convey energy into the secondary flows. Most favourable conditions are likely to arise when W is an even multiple of S but experimental confirmation is not yet available.

APPENDIX 3(a)

Area Ratio Part Way Down a Straight Conical Diffuser



$$AR_L = (1 + 2 \cdot L/D_1 \cdot \tan \phi)^2 \quad \dots (i)$$

$$AR_x = (1 + 2 \cdot x/D_1 \cdot \tan \phi)^2 \quad \dots (ii)$$

CONTINUED

Square rooting (i) and (ii) and subtracting 1 from both sides

$$\sqrt{AR_L} - 1 = 2^L/D_L \tan \phi \quad \dots (iii)$$

$$\sqrt{AR_x} - 1 = 2^X/D_L \tan \phi \quad \dots (iv)$$

Equation (iv) \div Equation (iii) gives

$$x/L = \frac{\sqrt{AR_x} - 1}{\sqrt{AR_L} - 1} \quad \dots (v)$$

where

$$AR_x = \left[x/L \cdot (\sqrt{AR_L} - 1) + 1 \right]^2 \quad \dots (vi)$$

TABLE 1

AR	ϕ	$G = 8 \tan \phi$
1.5	9	1.267
1.7	7.5	1.053
2	5.8	0.813
3	4	0.559
4	3.3	0.46
5	2.8	0.39

TABLE 2

Data used to calculate curves shown in figure 15
 ($\tan \phi_1$ was calculated using equations 17 and 32)

AR	B	a_1	$\tan \phi_1$	$\delta x / w_1$
2	0.02	0.5	0.2192	0.01
"	"	0.8	0.164	0.01
"	"	1.0	0.146	0.01
"	"	1.2	0.134	0.01
"	"	2	0.1096	0.01
2.5	0.05	0.5	0.1065	0.01
"	"	0.8	0.0798	0.01
"	"	1.0	0.0711	0.02
"	"	1.2	0.065	0.02
"	"	2.0	0.053	0.02

TABLE 3

AR	L/D	B	Cp at a Mn of 0.2 for		
			Cone	Bell	Trumpet
3.4	8	0.03	.69	.73	.65
"	"	0.06	.63	.67	.61
"	"	0.09	.58	.60	.55
"	"	0.12	.53	.55	.51
5.1	12	0.03	.73	.78	.70
"	"	0.06	.68	.67	.65
"	"	0.09	.63	.61	.60
"	"	0.12	.58	.55	.56
\bar{C}_p			0.631	0.645	0.604

where $\bar{C}_p = \frac{1}{h} \sum C_p$

TABLE 4

Comparison of Mixing Devices (Ref.14)

Device	L	x	Maximum Height	Maximum Width	$\delta(Cp)$	$\frac{\Delta\theta}{\theta}$
A-1	152	158	31.7	9.5	0.11	0.112
A-2	114	792	"	19	0.21	0.126
A-3	203	792	"	38.1	0.21	0.214
B	-	158	38.1	19	-	-
C	152	451	31.7	25.4	0.15	0.200
D	76	591	19	19	0.08	0.242
E-1	152	311	19	38.1	0.16	0.147
E-2	152	875	38.1	76.2	0.17	0.289
E-3	152	1244	76	152	0.25	0.780
F	152*	875	38.1	76.2	0.09	0.214
G-1	51	52	10.6	7.4	0.02	-
G-2	102	158	31.7	22.2	0.12	0.562
H	152	152	25.4	152	0.10	0.364
J	171	1158	44.5	186.8	0.19	0.323
K	152	814*	25.4	50.8	0.17	-0.176

Tunnel width = 1830 mm; tunnel depth 350 mm sloping to 686 mm
in a length of 6.1 metres.

* Not optimum values but relate to stated performance.

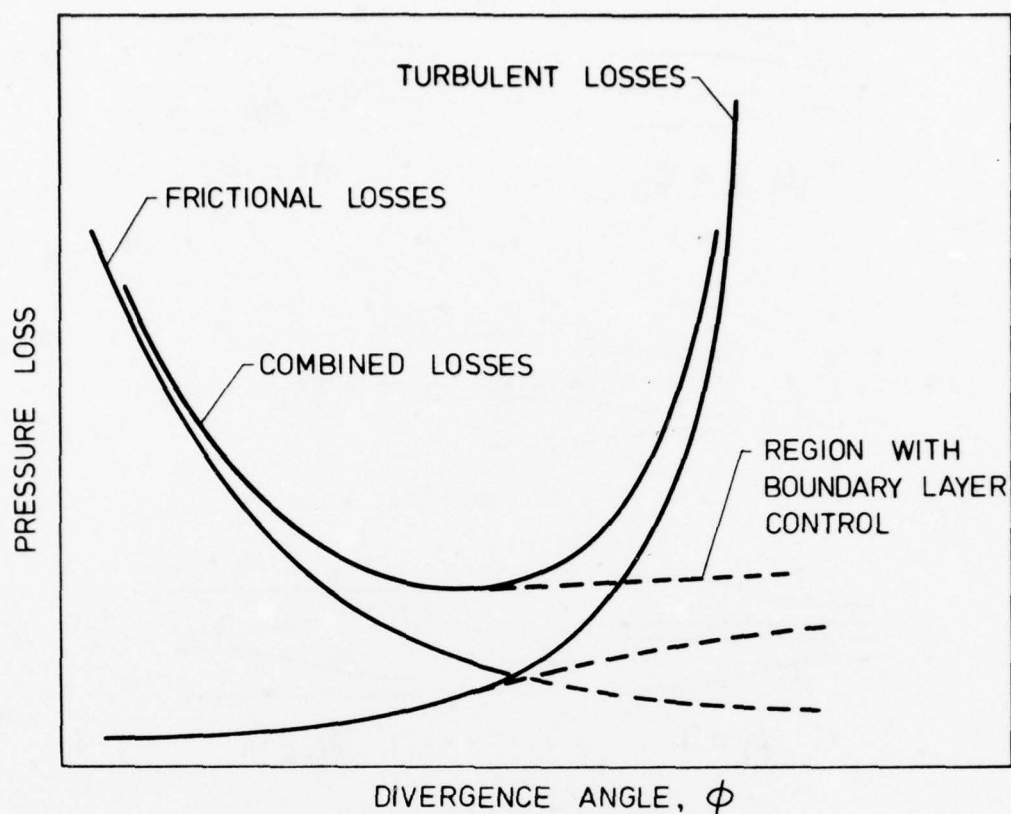


Fig.1 Diffuser pressure loss with area ratio and inlet conditions assumed constant

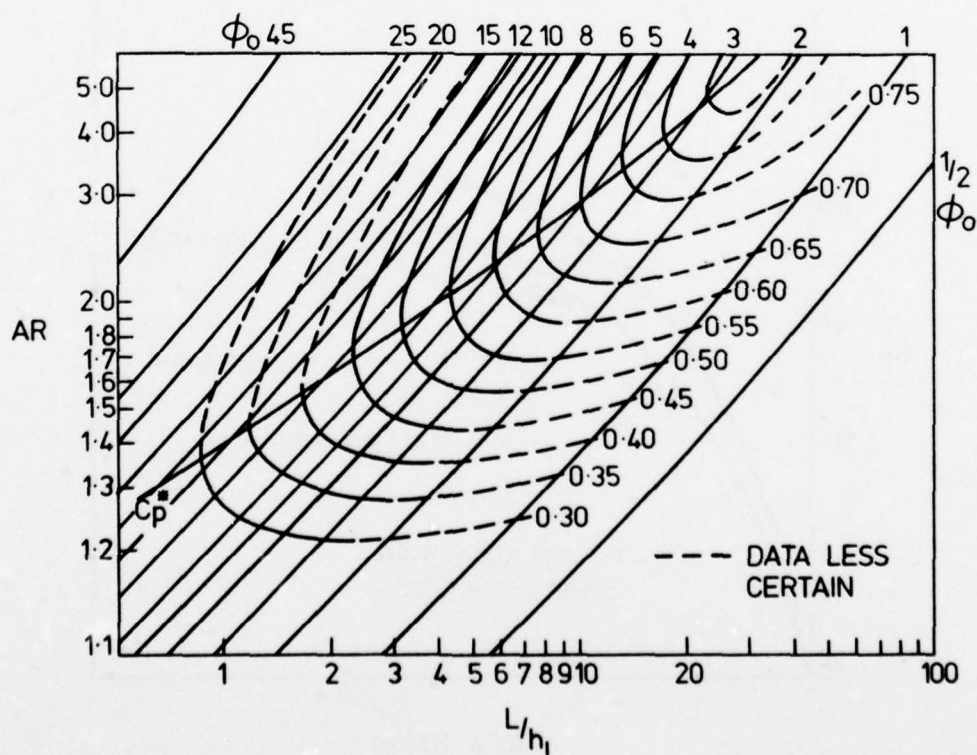


Fig.2 Static-pressure recovery coefficient, for conical diffusers without tailpipes, fully-developed entry flow. (ESDU 75026)

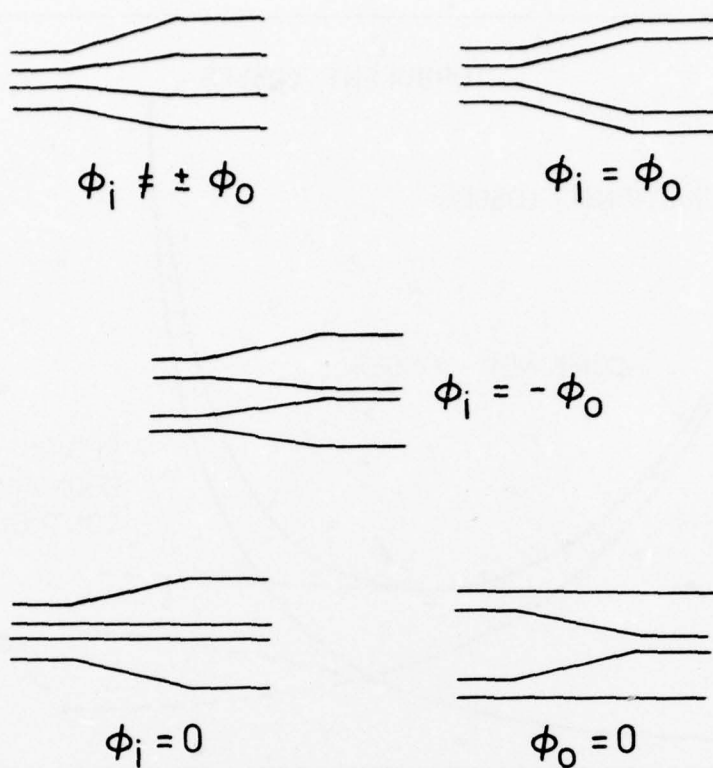


Fig. 3 Classification of annular diffusers

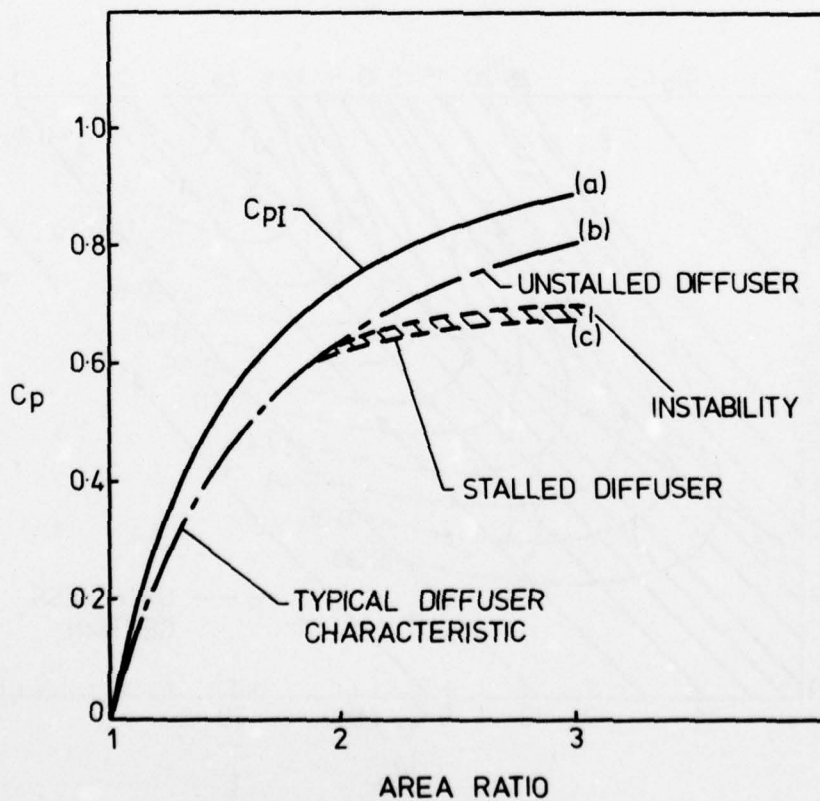


Fig. 4 Static pressure rise coefficient as a function of area ratio

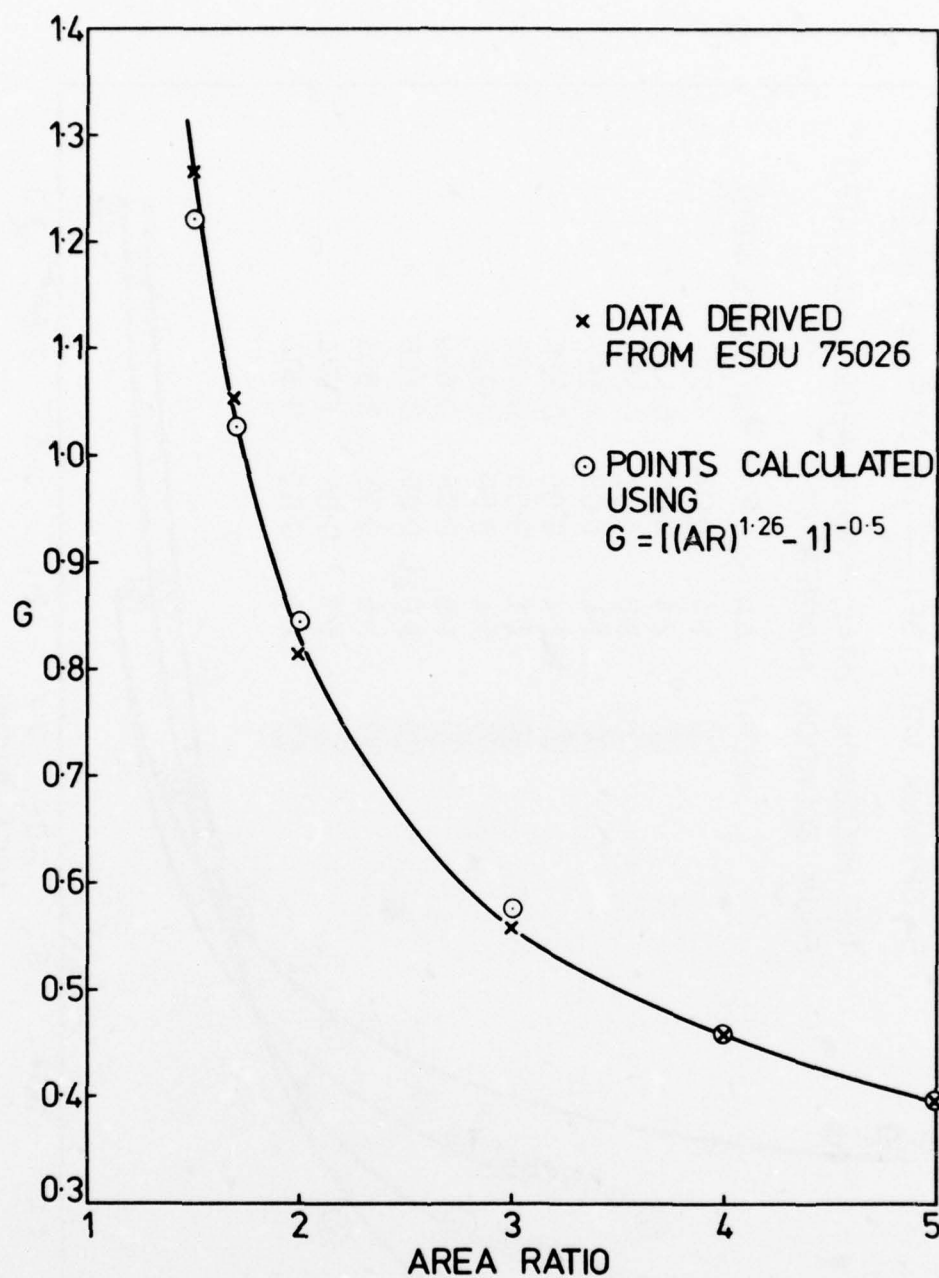


Fig.5 Data derived for conical diffuser
with fully developed flow at inlet
(ESDU 75026)

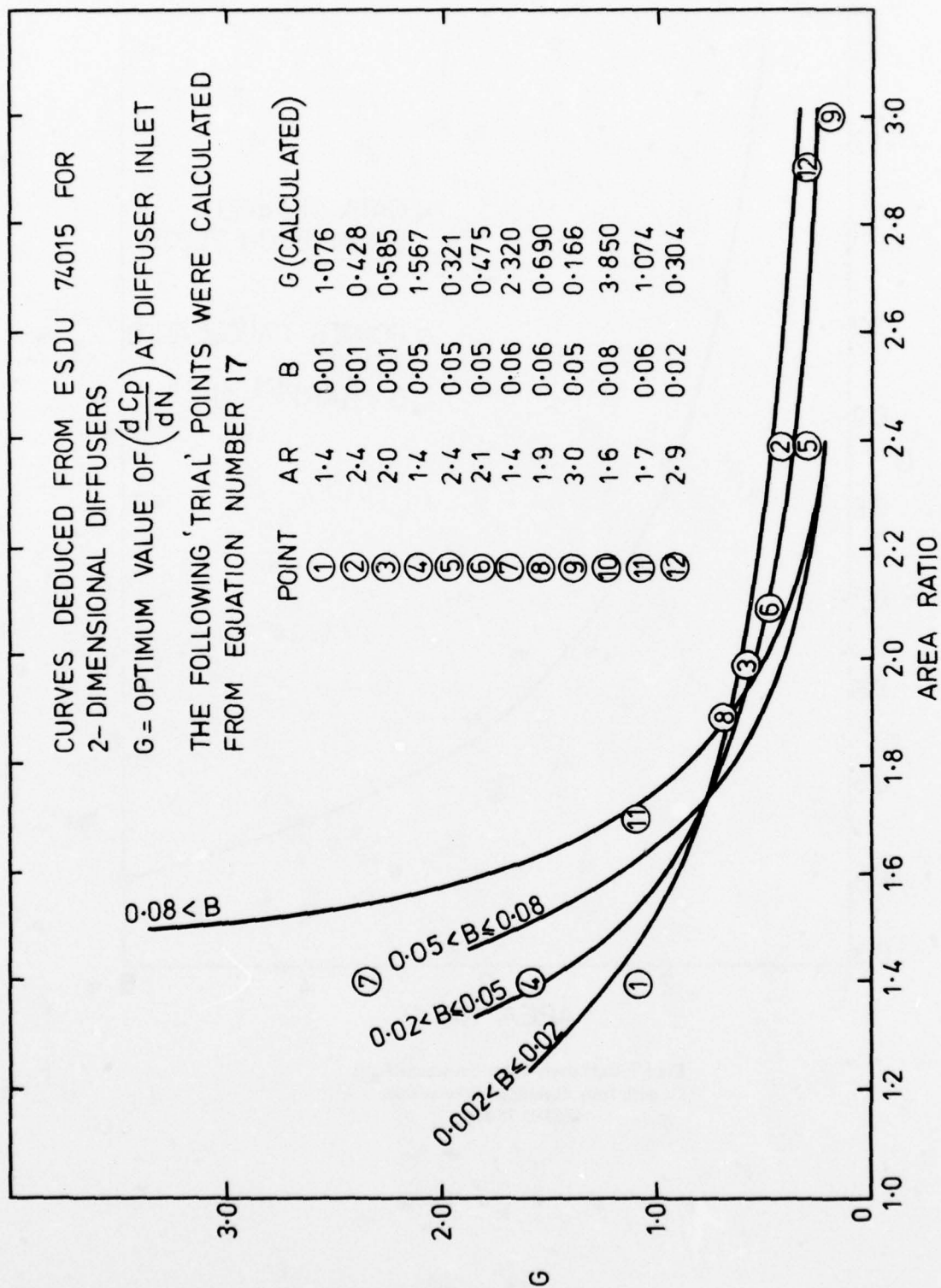


Fig.6 Comparison between correlating equation and experimentally determined curves

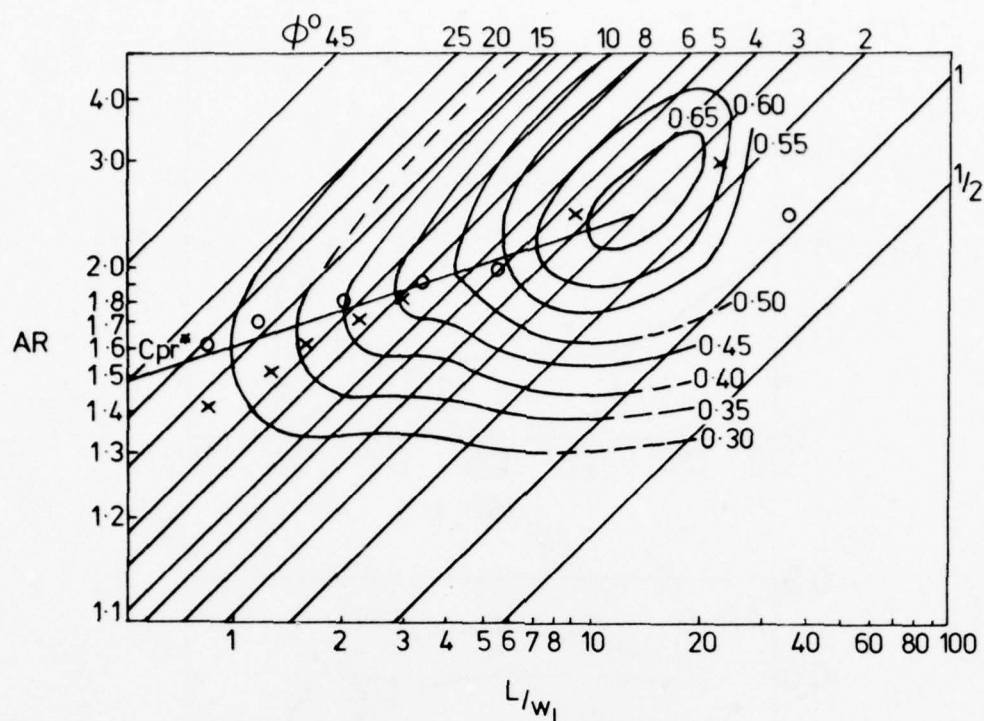


Fig.7 Pressure recovery coefficient contours for 2-dimensional diffusers without tailpipes, inlet blockage range $0.05 < B \leq 0.08$ (contours copied from ESDU 74015)
Points calculated from equation (19)
(\circ for $B = .08$; \times for $B = .05$)

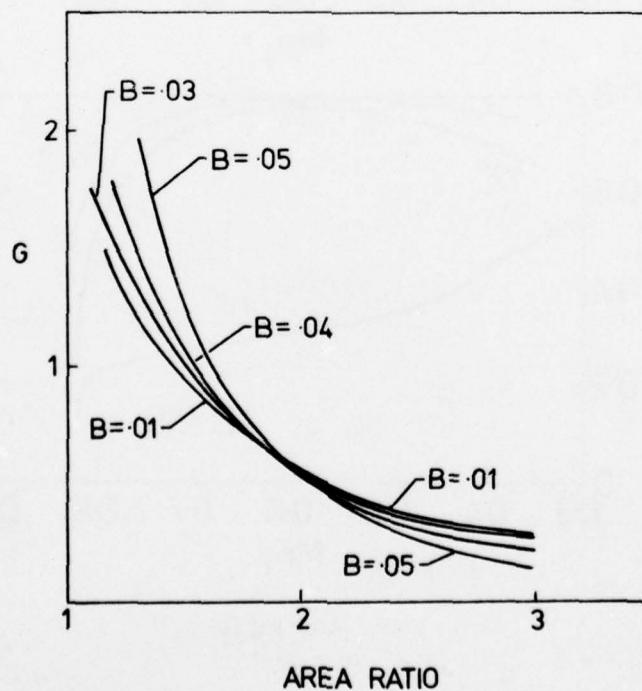


Fig.8 Curves according to Equation 17

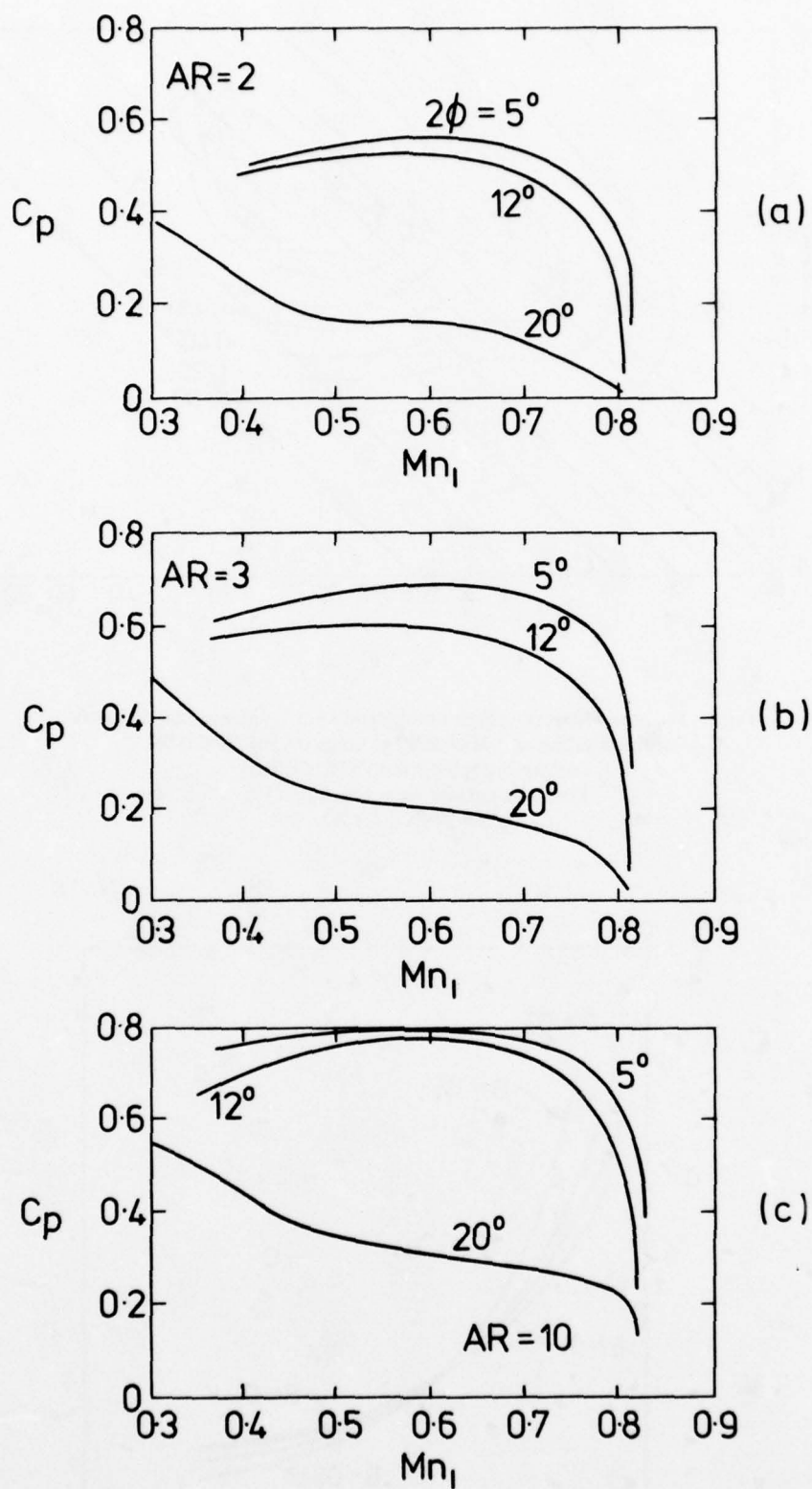


Fig.9 (After Ref.10)

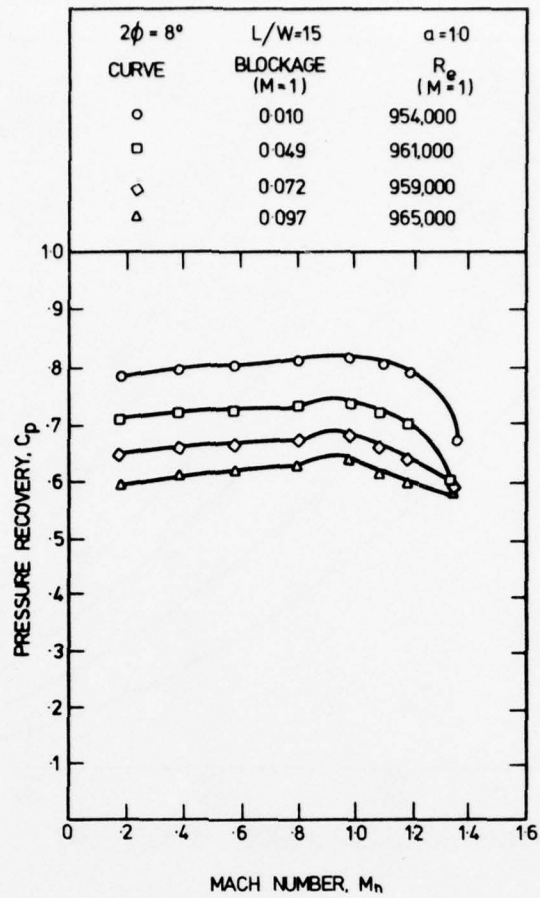


Fig.10 (After Ref.11)

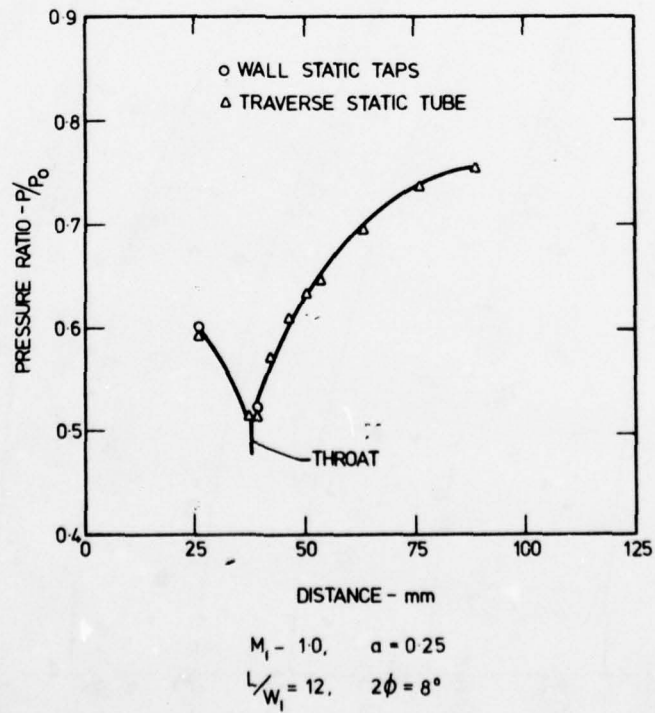


Fig.11 (After Ref.11)

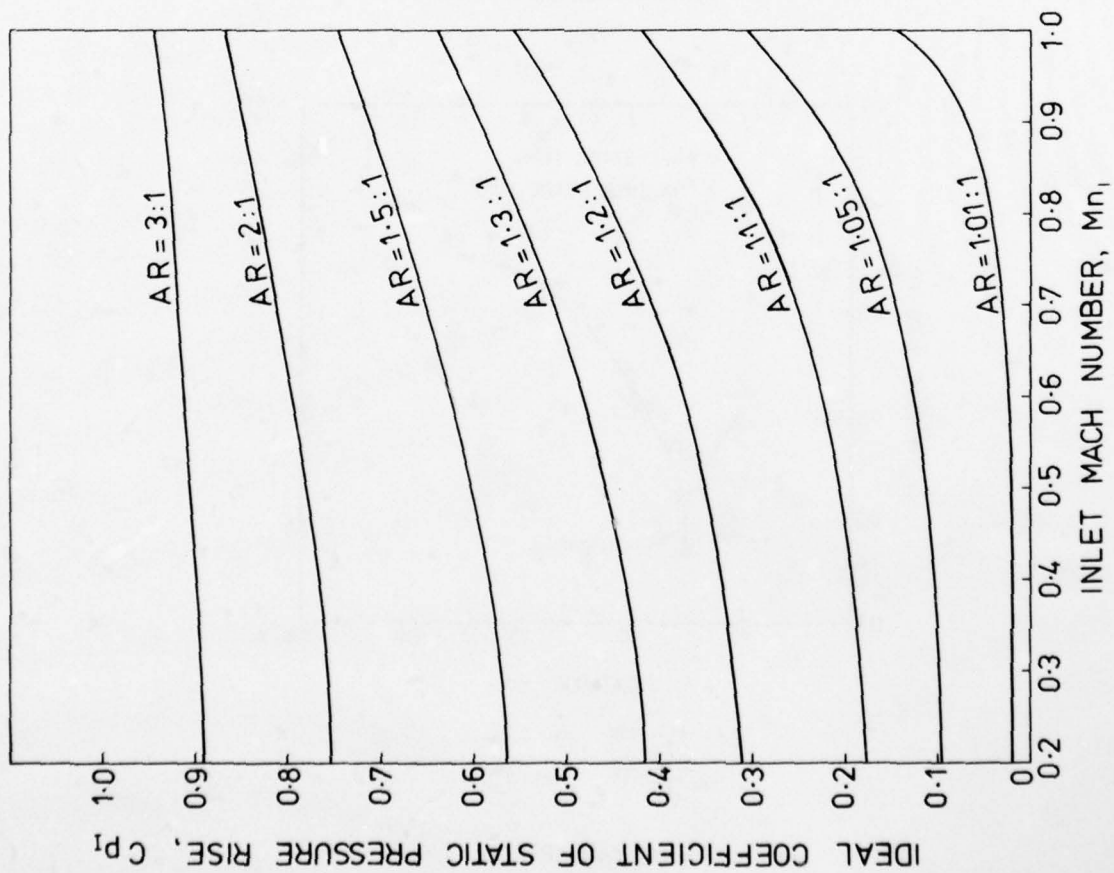


Fig.12 Relationship between C_{p1} and Mach number

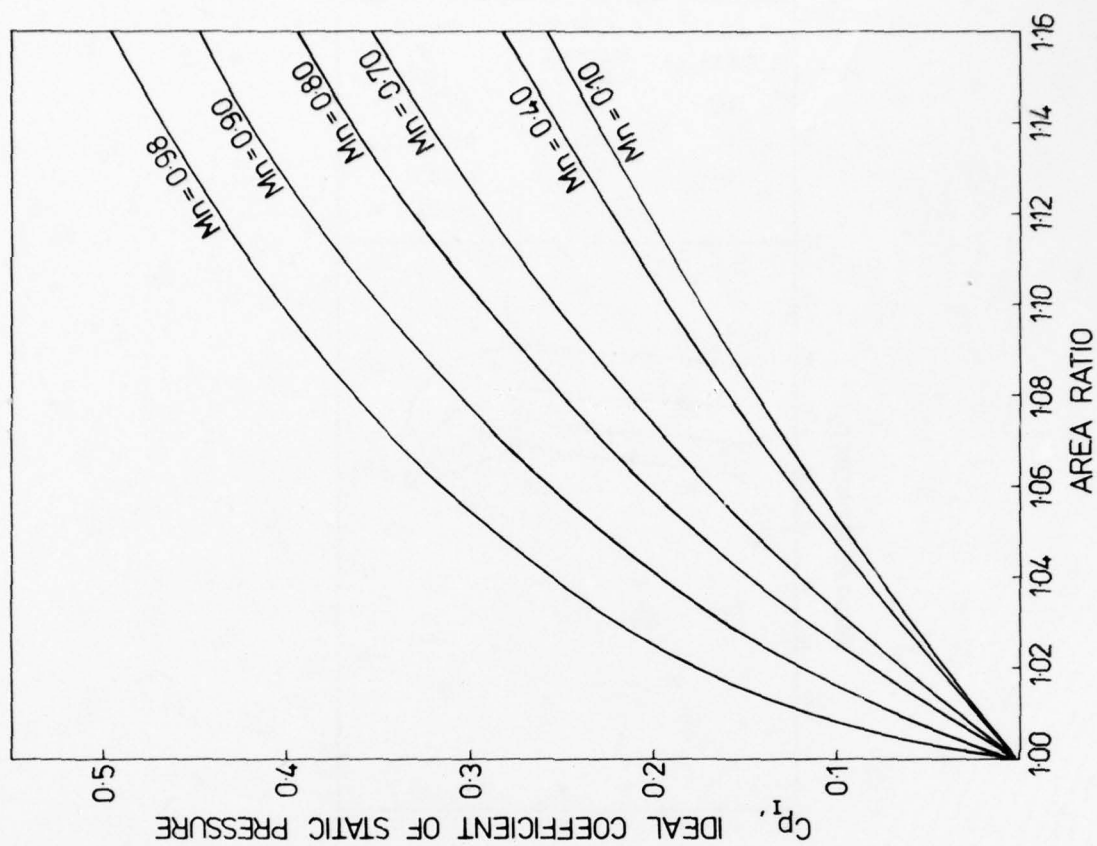


Fig.13 Variation of ideal pressure recovery near the front of a diffuser with inlet Mach number

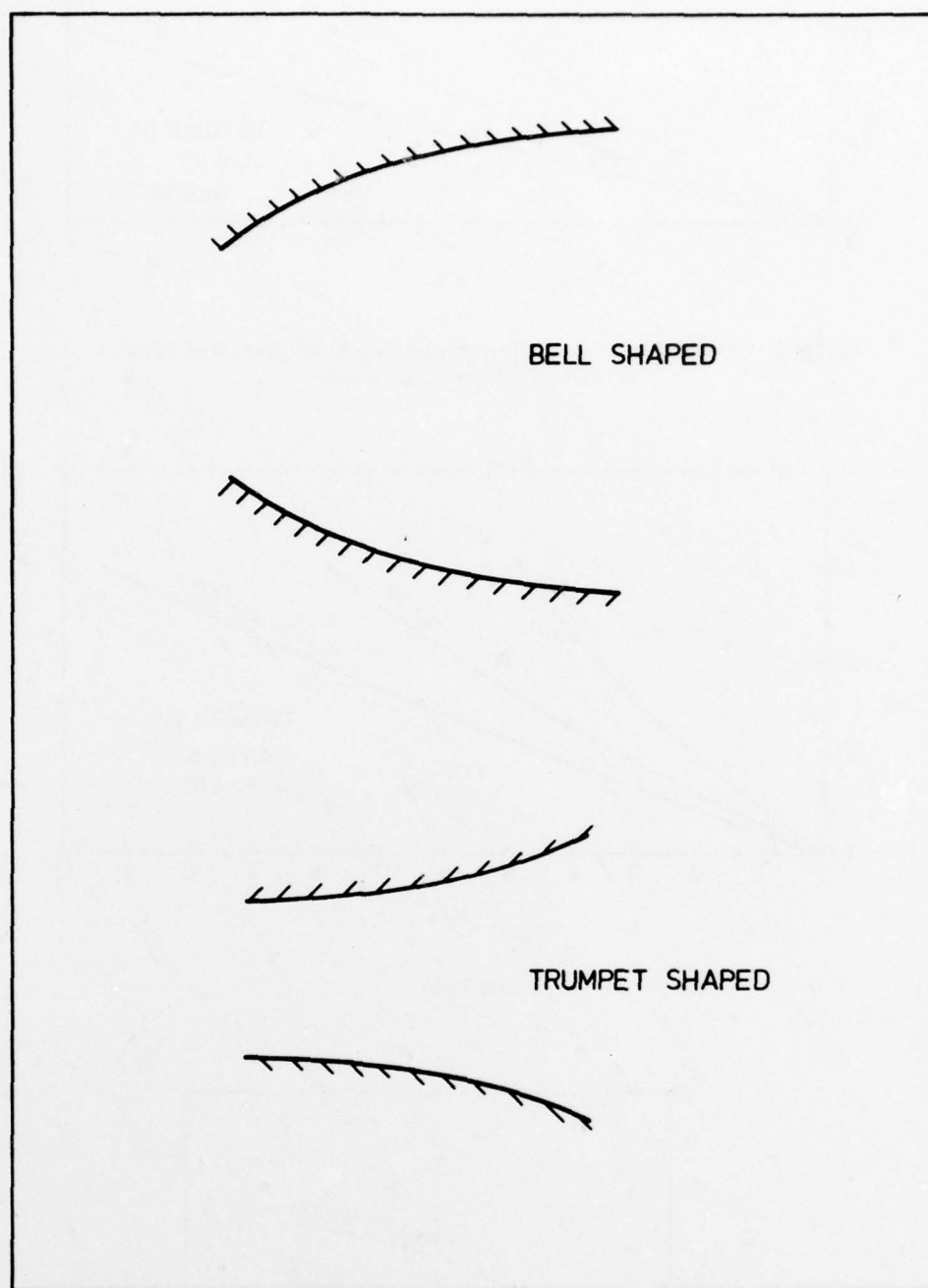


Fig.14 Curved wall diffusers

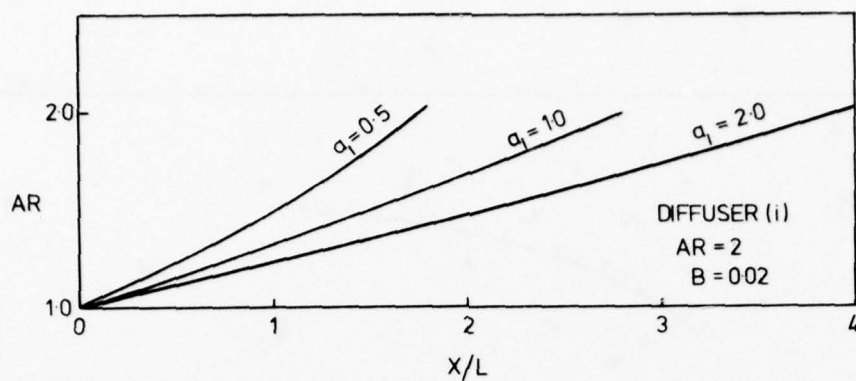


Fig. 15(a) Development of area ratio down 2-dimensional curved wall diffusers as predicted by the G_x technique

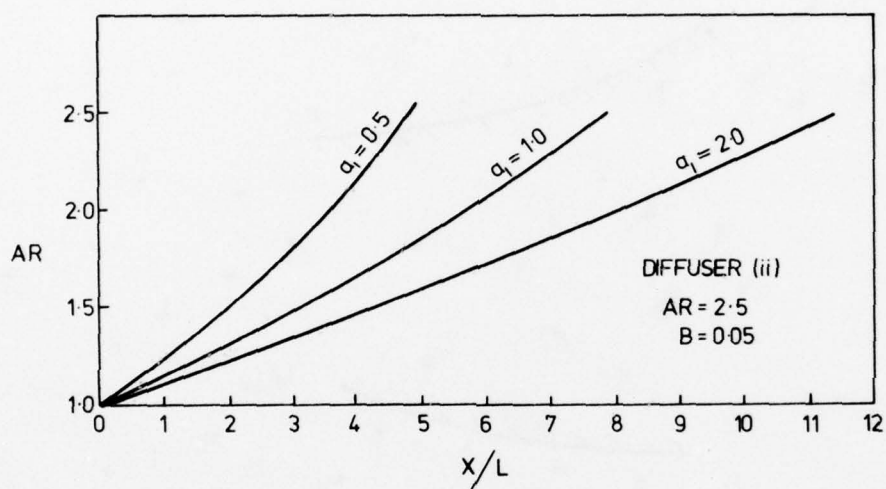


Figure 15(b)

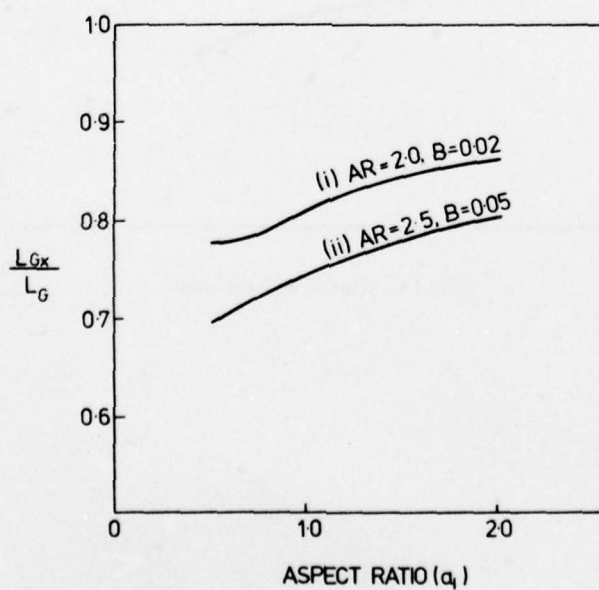
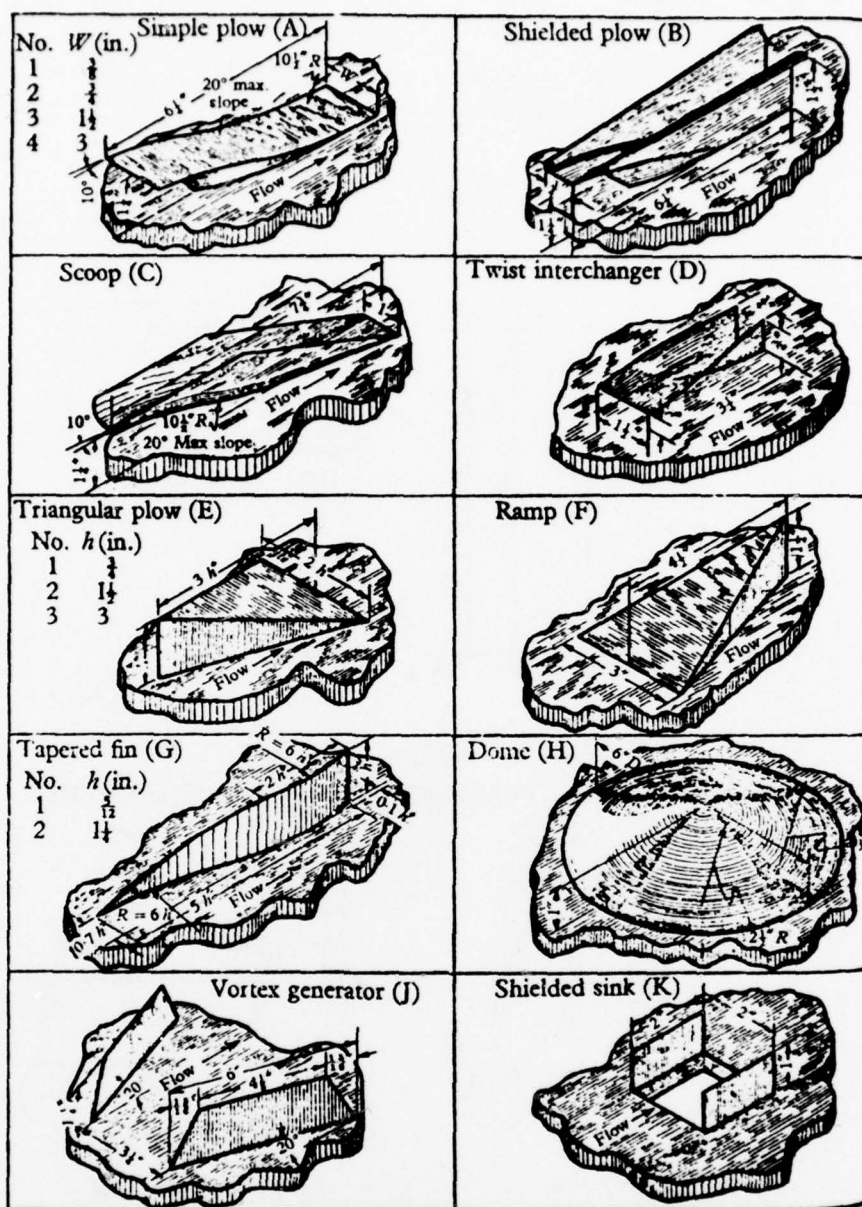


Figure 16



Mixing devices.

Fig.17 (After Ref.14)

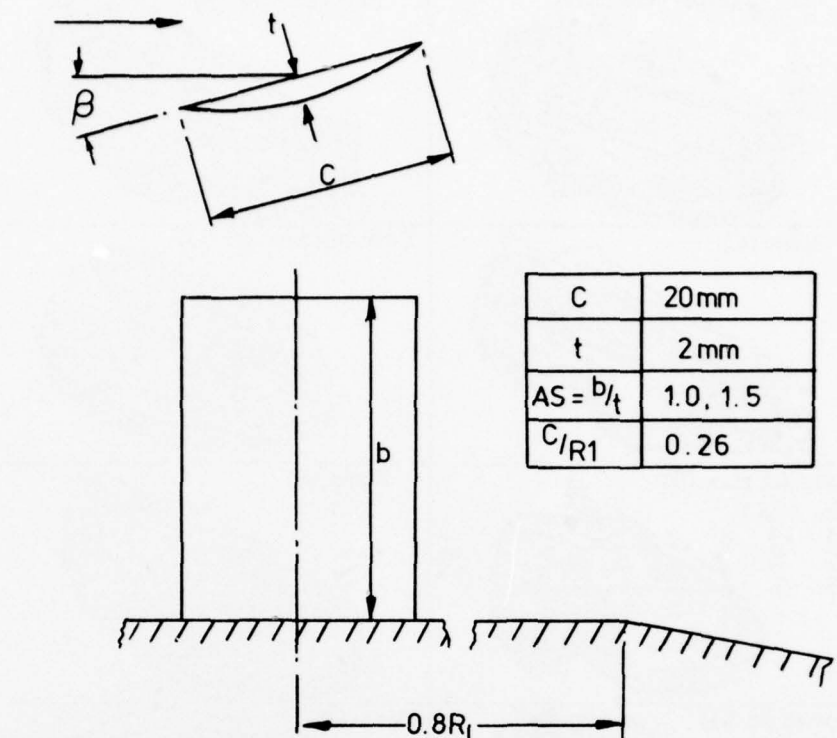


FIG. 2. GEOMETRY AND DIMENSIONS OF VORTEX GENERATORS

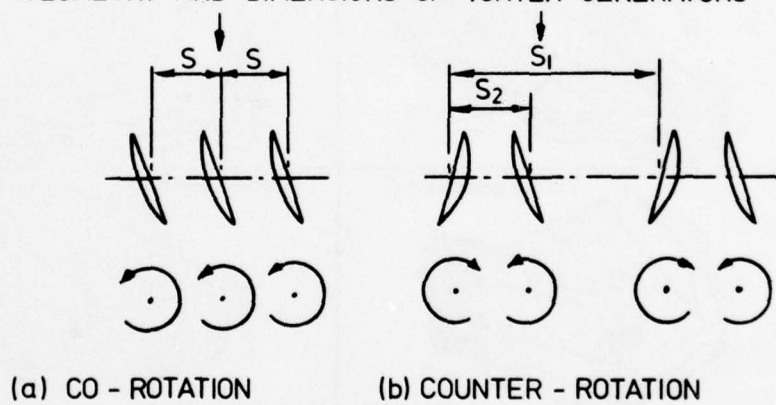


Fig.18 Arrangement of vortex generators and the trailing vortices (After Ref.16)

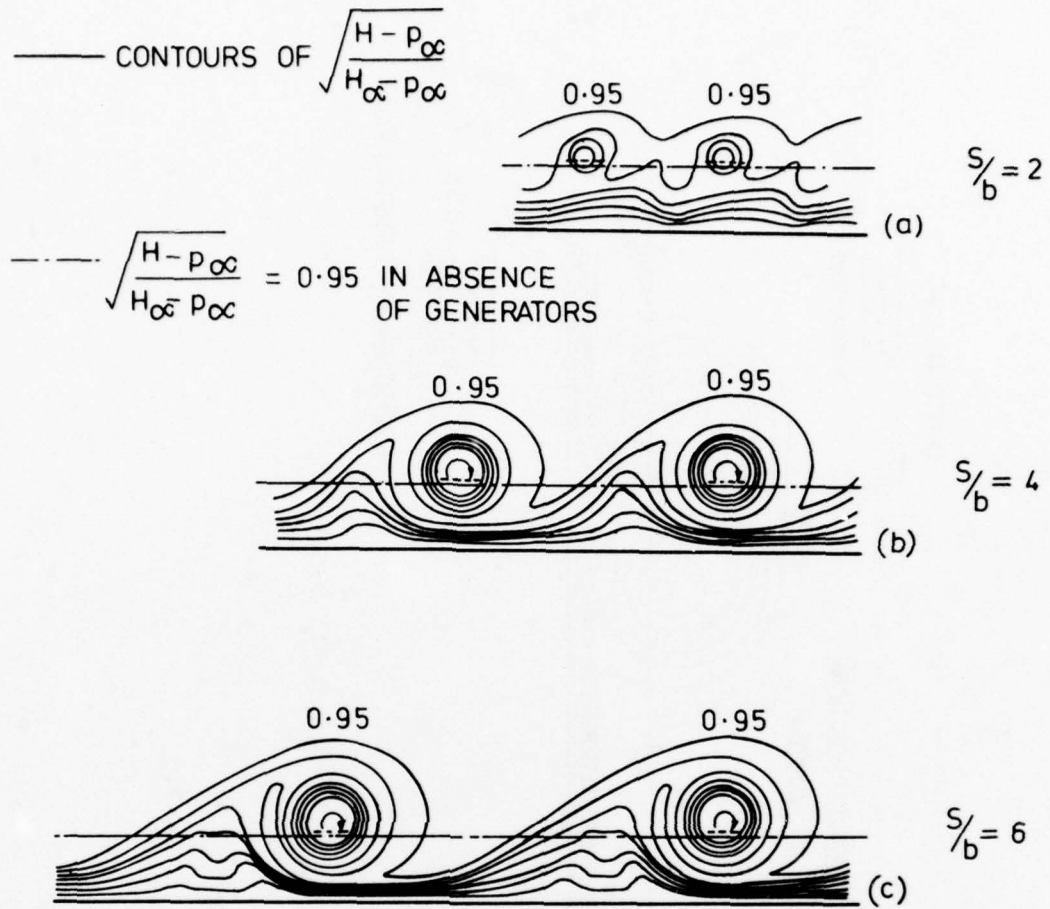


Fig.19 Contours of pitot pressure for co-rotating vortices
(at a fixed distance downstream of generators on a flat plate)
(After Ref.15)

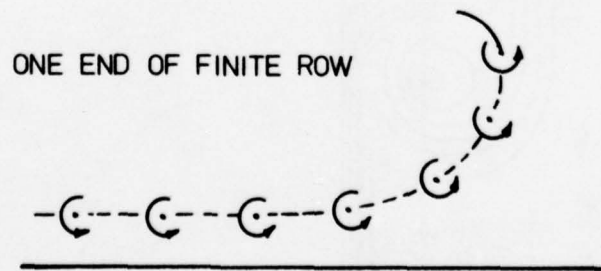


Fig.20 Co-rotating vortices

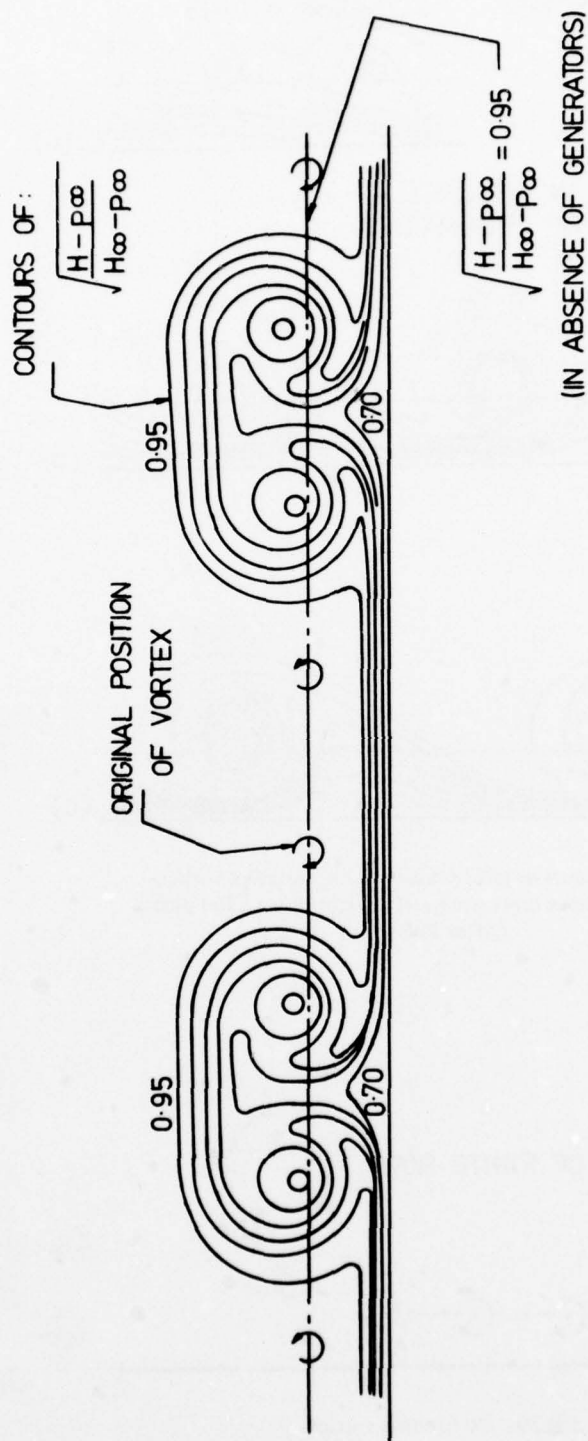


Fig.21 Counter-rotating, $\alpha = 4$, $S/b = 10$, at $x/s = 3.2$ (After Ref.15)

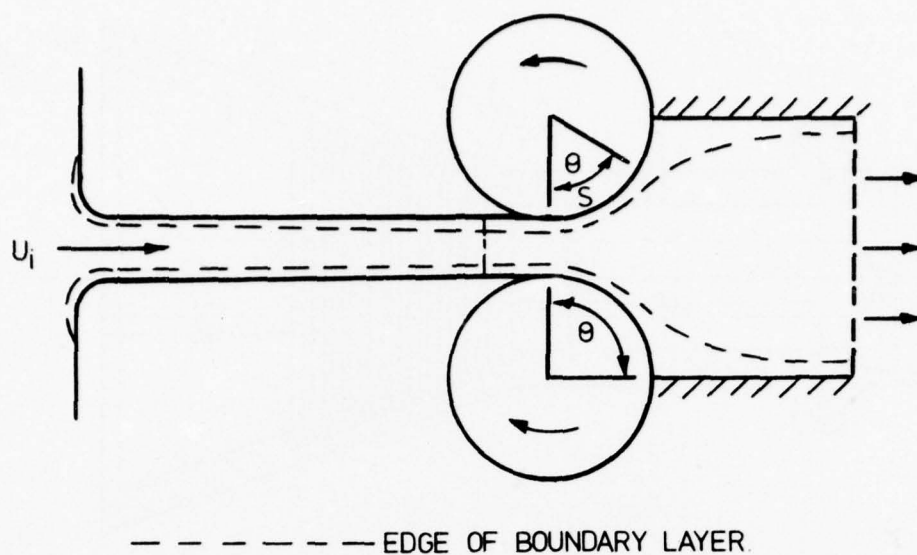


Fig.22 Moving wall diffuser (4-1 area ratio shown, area suction between dotted lines) (After Ref.18)

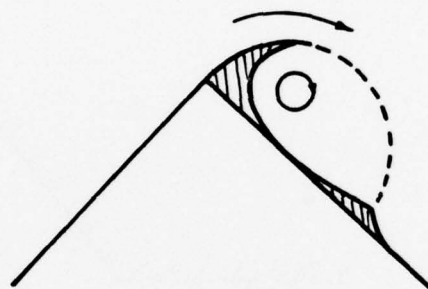


Fig.23 Scheme of flow over a snow cornice (After Ref.19)

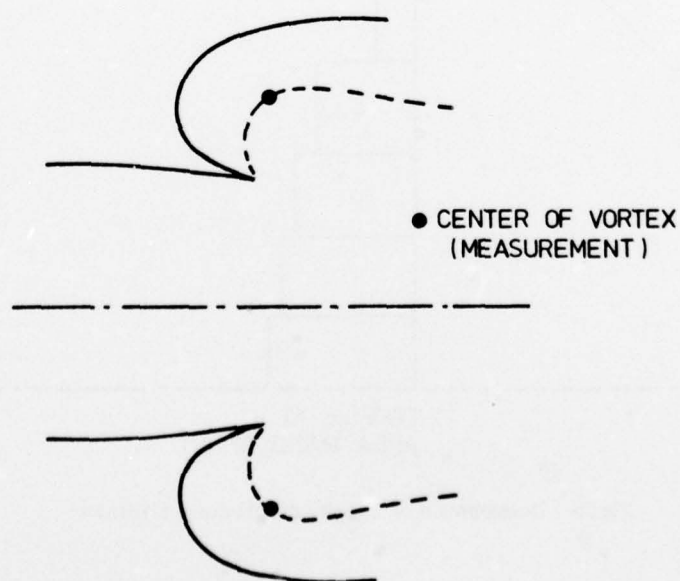


Fig.24 Cusp diffuser of the James Forrestal Research Center of Princeton University (After Ref.19)

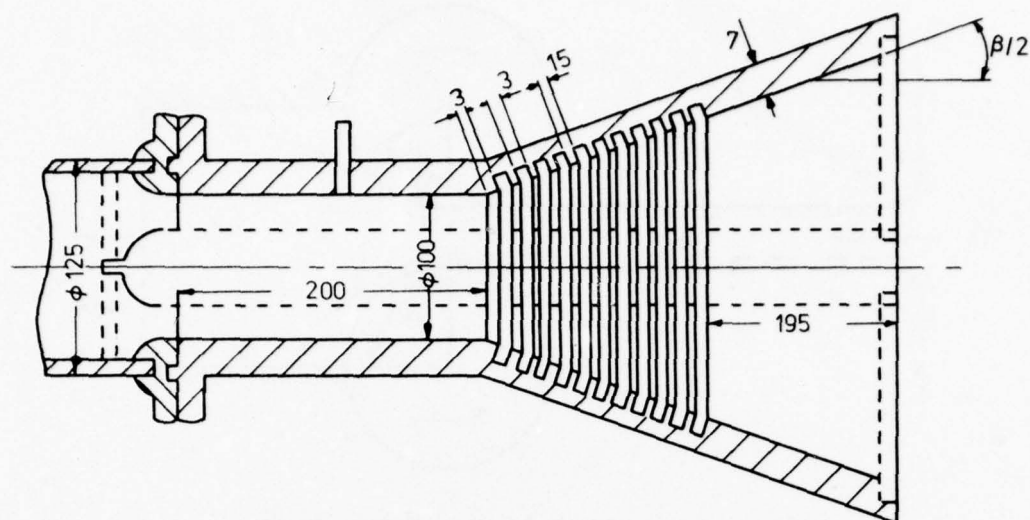


Fig. 25 Arrangement of experimental installation (After Ref.26)

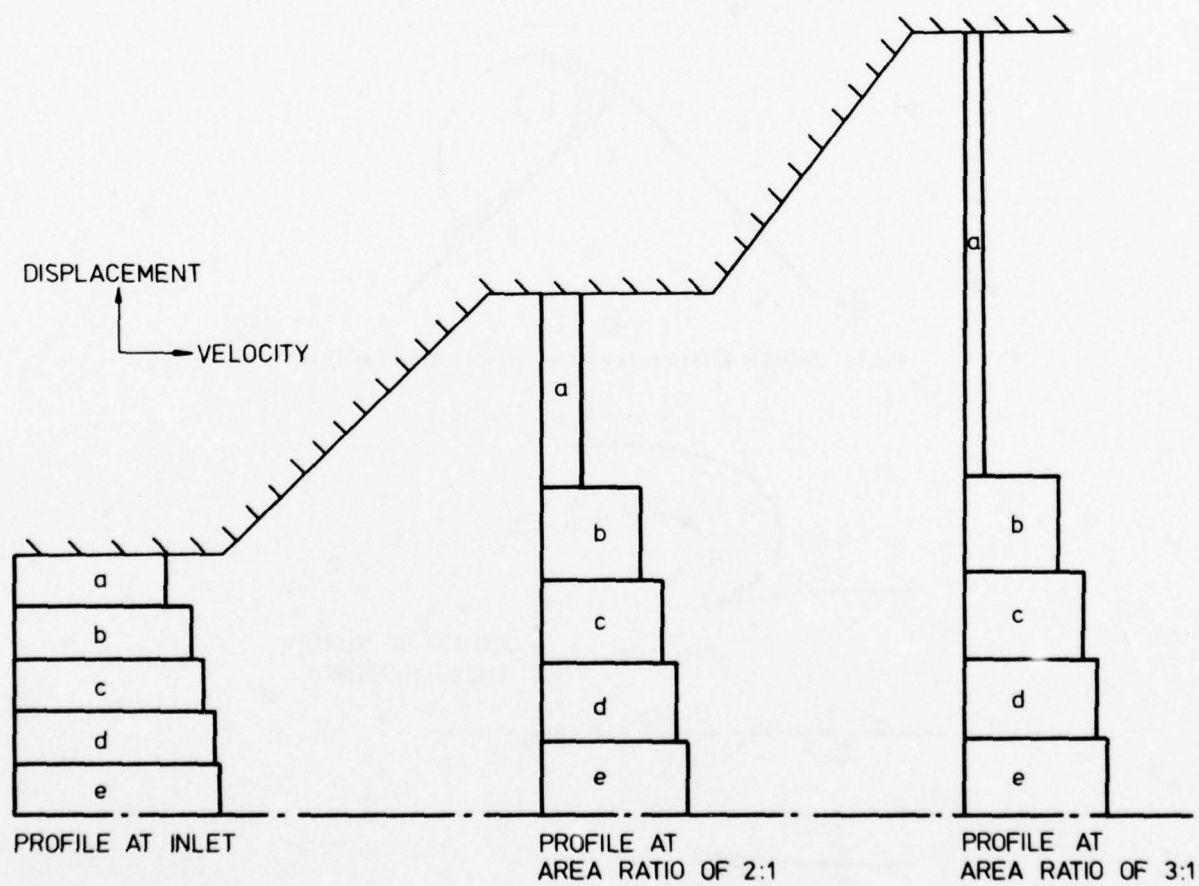


Fig. 26 Development of velocity profile down a diffuser

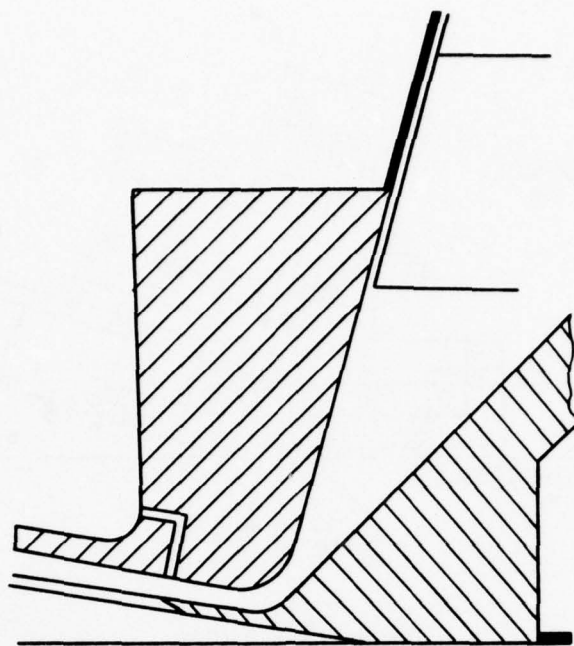


Fig.27 Tangential injection slot (After Ref.29)

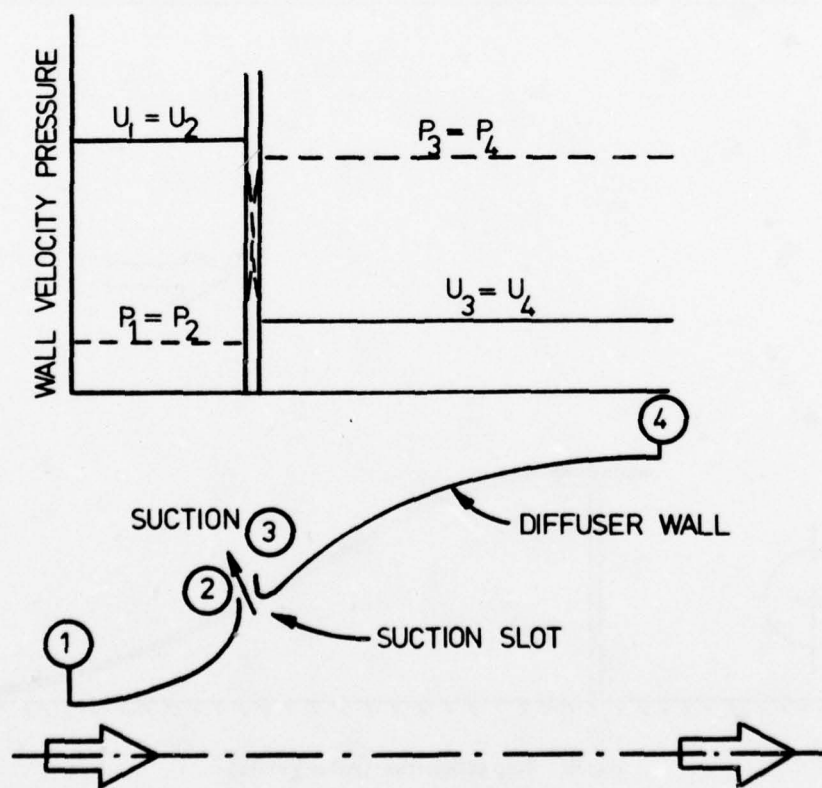


Fig.28 Velocity and pressure distribution in a Griffith-type diffuser (After Ref.31)

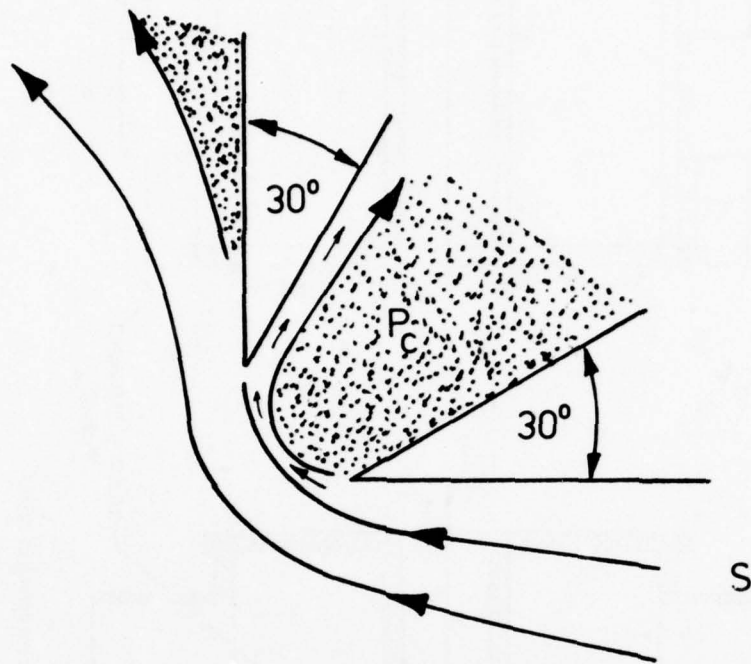


Fig.31 (c) (After Ref.35)

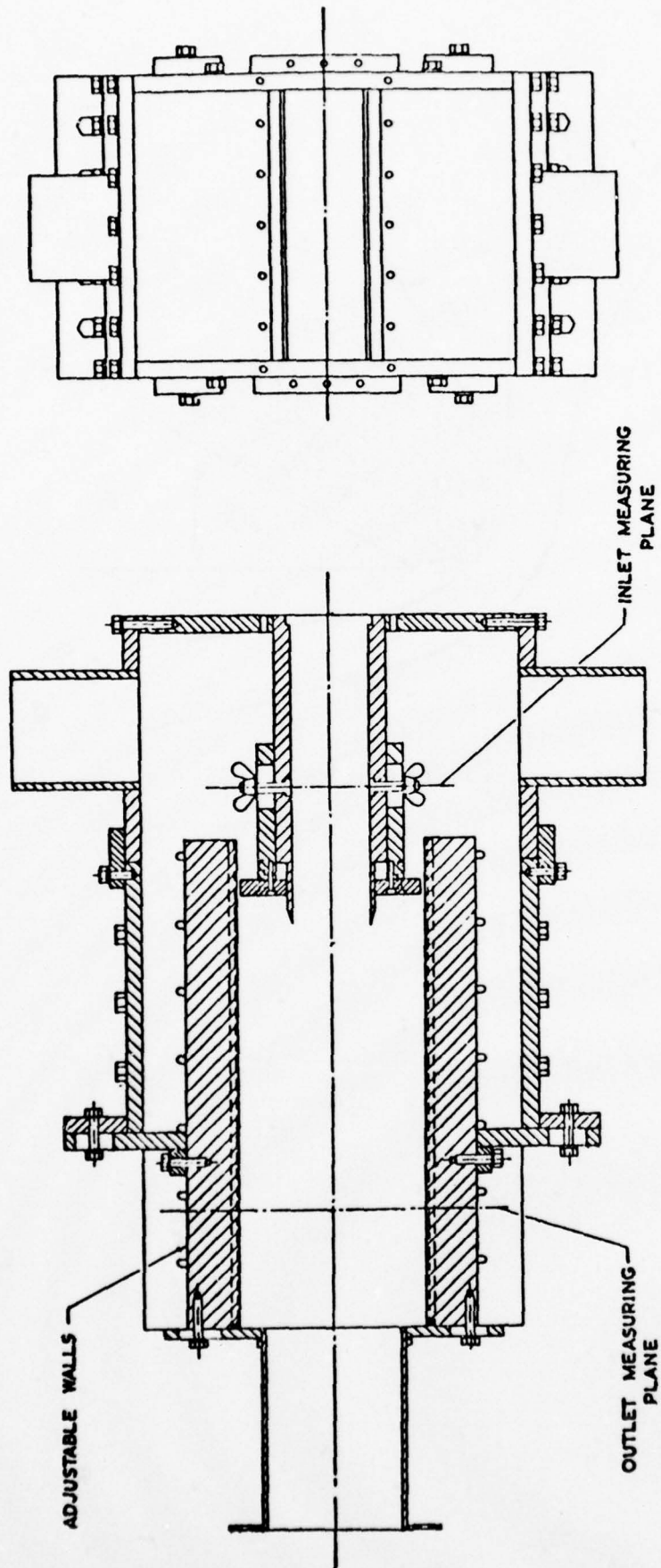


Fig.32 Generated vortex diffuser (drawn to scale)

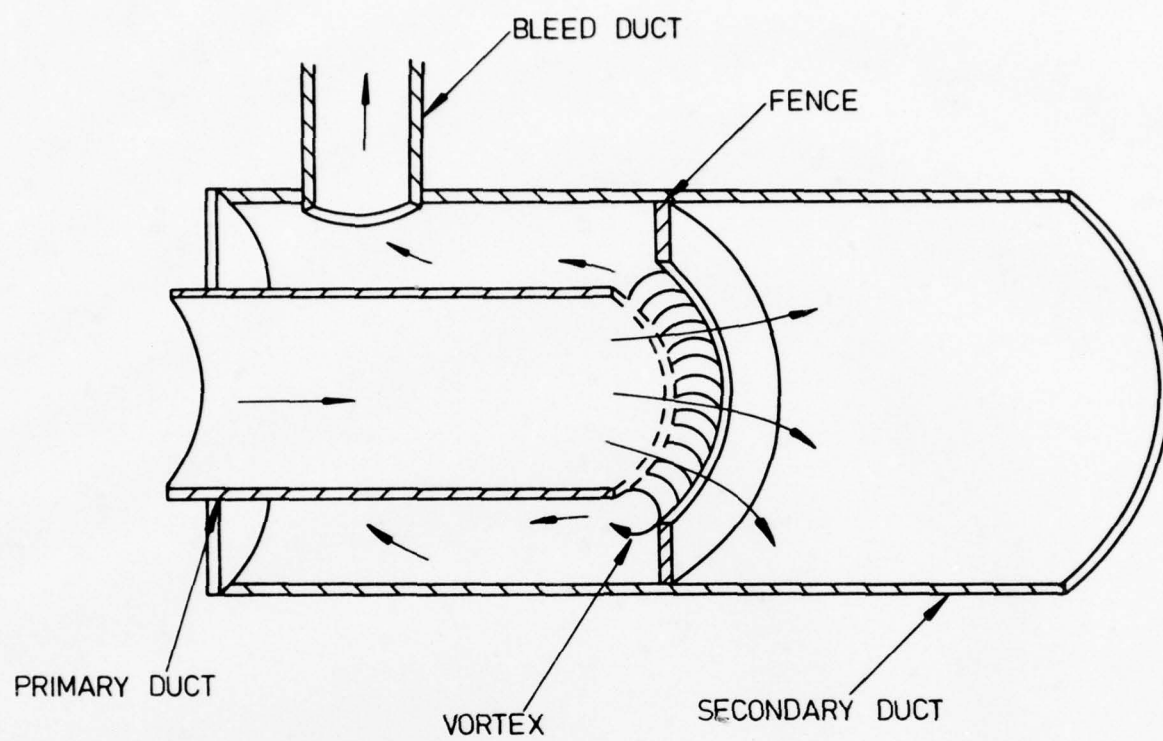


Fig.33 Diffuser with fence

DRAG REDUCTION BY COMPLIANT WALLS: THEORY

by

Priv.-Doz. Dr. G. Zimmermann
 Max-Planck-Institut für Strömungsforschung
 D 3400 Göttingen
 Germany

SUMMARY

A discussion of general properties of a compliant wall required for drag reduction is given. The difficulties of a theoretical treatment of the compliant wall problem and the simplifications and assumptions made to overcome these difficulties are discussed at two exemplary theories: one dealing with the stability of a stationary laminar boundary layer over a compliant wall, the second dealing with the turbulent boundary layer/compliant wall interaction problem. Special emphasis is given to the coupling conditions between fluid flow and compliant wall.

List of Symbols

Tensor notation: u_i (including summation convention) and symbolic notation: \underline{u} are used in parallel. Latin indices assume values 1, 2 and 3 corresponding to the x, y- and z-direction. Greek indices assume values 1 and 2 corresponding to the x- and y-direction. ∂_i and ∇ denote spatial differentiation.

A, B	constants	x, y, z	rectangular coordinates
c	velocity of Tollmien-Schlichting waves	Y, Y_m	wall admittance
c_s	velocity of free waves in the compliant wall	α	wave number of Tollmien-Schlichting waves
E, F G, H }	auxiliary functions (stability problem)	$\delta, \delta_1, \delta_0$	decay parameters
$\{u\}$	viscous solution of Orr-Sommerfeld eq.	δ_{ix}	strains
G	shear modulus	δ_s	boundary layer displacement thickness
G_i^* H_i^* }	special solution of Navier-Stokes eq.	ϵ	coupling parameter
i	imaginary unit	ν	kinematic viscosity
$\Im m$	imaginary part of	ρ_0	density of fluid
$k, k = k $	wave number	τ_{ik}	stress tensor
L	power	ψ	stream function
$\underline{n} = n^i$	normal on flow/wall interface:	$\varphi(z)$	solution of Rayleigh eq.
p	pressure		
$q = q^e$	abbreviation for linearized convection terms		
$\underline{r} = r^i$	position vector		
Re	Reynolds number		
\Re	real part of		
t	time		
$\underline{t} = t^i$	coupling force		
u_-, u_{-1} $\underline{u} = u^i$ }	velocities		
$\underline{v} = v^i$	displacement		

subscript \cdot for values at $z = 0$

superscript $^{(0)}$ and $^{(1)}$ for zero and first order in ϵ

superscript $^{\wedge}$ for Fourier transform

superscript $—$ for time mean

1. The Problem In 1957 M. O. Kramer [1] published a first report on his experiments to reduce the drag of towed underwater bodies by covering them with compliant or flexible coatings. He thus not only triggered considerable research activity in this field for the ten years following his first report, with continuing interest up to the present time; he also predetermined to some degree the idea of a flexible skin or flexible body for drag reduction purposes.

While there is just one rigid body of a given geometry there is for the same geometry an infinite variety of flexible bodies or bodies with flexible skins, differing in material composition. In his experiments Kramer in his choice of compliant coating was guided by theoretical considerations and his observation of swimming dolphins. Although Kramer may have been wrong in his initial theoretical considerations he certainly had realized the problem of selecting the proper compliant material for the purpose of drag reduction. Just picking any material at random will in almost all cases lead to negative results. One may suspect that some of the experiments following Kramer's initial tests remained unsuccessful because of this fact.

Thus while realizing that the step from the rigid body to the body with a compliant surface is the step from one single configuration to a wide variety of configurations one should also realize that the current problem should be carefully separated from related topics.

These related fields may be roughly characterised as:

- (i) animal propulsion through fluids, such as the swimming of fish;
- (ii) flutter problems, including such topics as excitation of ocean surface waves by wind;
- (iii) fatigue problems.

In case (i) above body flexibility is the means of propulsion. The body motion for propulsive purposes is large scale: amplitude and wave length are of the order of magnitude of typical body dimensions. In addition and as a separate effect there may be a favourable (in the sense of drag reduction) influence of small scale motion of the compliant body surface on the adjacent boundary layer. From a power balance: muscle power versus drag, Kramer concluded that such a drag reducing effect must be present in the dolphin's skin, which led Kramer to the design of his artificial dolphin's skin. However, as has been pointed out by J. Gray the drag of a live dolphin may be quite different from that of a 'rigid' dolphin.

In flutter problems, case (ii) above, the focus is on the structural side. Fluid dynamics plays a subsidiary role in that it supplies the aerodynamic forces, mainly pressure forces, that excite flutter motion. Back reactions of the flutter motion on the flow are of interest only insofar as they change these forces. Ships, having less of a weight problem than aircraft are simply built sufficiently strong and rigid to avoid flutter problems.

Similar remarks apply to fatigue problems, case (iii) above. Fluid dynamics only supplies the wall pressure fluctuations underneath turbulent boundary layers that excite structural vibrations, which may lead to material fatigue and thus structural failure. The vibration amplitudes are in general small even compared to the viscous sublayer of the boundary layer. Back reactions on the flow may therefore safely be ignored.

The drag that a body experiences when in motion relative to a fluid may be ascribed to three different mechanisms: (i) wave drag, due to energy radiated away from the body through excitation of waves, e. g. Mach waves (sonic boom) in supersonic flight or surface waves in surface ships; (ii) pressure drag, the component in main flow direction of the integral pressure force. No pressure drag is felt by a body moving through an ideal inviscid fluid at constant velocity (d'Alembert's paradoxon). One expects little pressure drag for a body moving through a real, viscous fluid at small constant velocities. When at higher constant relative velocities the boundary layer becomes at least partially turbulent pressure recovery at the rear part of the body will become increasingly incomplete due to higher viscous losses leading to a higher pressure drag. Eventually boundary layer separation will occur and a wake will be formed. Pressure drag then is serious; (iii) viscous drag: Due to viscosity a body moving through a fluid also experiences tangential viscous forces, directly related to the viscous dissipation in the boundary layer. When the boundary layer becomes turbulent and the viscous dissipation is increased a drastic rise in the viscous drag is felt. From the remarks on pressure drag it is clear that viscosity also has an indirect influence on pressure drag.

Compliant walls for drag reduction purposes are meant to directly interfere with the boundary layer, laminar or turbulent, thus influencing and hopefully reducing viscous drag. An indirect influence on pressure drag cannot be excluded. To this end typical wavelengths of the compliant wall surface movements will have to be of the order of the boundary layer thickness at the most. Very small wavelengths will be felt as an additional roughness, increasing viscous drag. Very large wavelengths will be felt as a change in body contour, with effects that should be discussed under the heading of aerodynamic shaping for reduced drag. Typical wave amplitudes will have to be smaller than the boundary layer thickness, of the order of the thickness of the viscous sublayer. It is also obvious from structural considerations, that wave amplitudes should be of the order of wavelengths or less.

Accordingly we will define a body with a compliant surface for drag reduction purposes as a body with a well defined undeformed shape, the surface of which, when in contact with the fluid flow around it, can exercise movements with wavelengths of the order of the boundary layer thickness and amplitudes of the order of the viscous sublayer thickness. When the body moves through the fluid at constant velocity a statistically stationary turbulent boundary layer flow/compliant wall motion will occur. This state may in some aspects differ considerably from the turbulent boundary layer flow around the corresponding rigid body, i. e. a rigid body having the shape of the compliant body in its undeformed state. The

material composition and internal structure of the compliant wall has to be determined in such a way, that the body with compliant walls experiences less drag than the corresponding rigid body. That is the problem!

It has been said that the objective of using compliant walls is drag reduction. Perhaps it would be more precise to say that the objective is power reduction or saving energy (or even cost).

Let us look at two similar bodies: a rigid body and a body with a compliant wall having in its undeformed state the same shape as the rigid body. In order to move either of these two bodies through a fluid at a constant velocity a certain propulsive power is required. In the case of the rigid body the entire power is lost to the flow, partly through viscous dissipation and partly through radiation of energy. In the case of the compliant wall the boundary layer flow may be changed in such a way that power lost to the flow is considerably decreased. If however in the case of a passive compliant wall this change is achieved through large internal damping of the wall, then the power lost in the wall may offset the power saved in the flow leading to a negative net result. In the case of an active compliant wall additional power is required for the driving mechanism of the wall. One expects that on the average power flows from the wall into the flow. This may result in additional propulsive forces or equivalently a reduction in drag. Again if the power saved in the flow in this way is offset by the power consumed by the driving mechanism of the active compliant wall the net result is negative. Following these rather general preliminary remarks a discussion of basic concepts for attacking the compliant wall problem from the theoretical side and the difficulties involved will be given.

2. Compliant Walls-Theory It is convenient to discuss the topics of this section at the example of a typical flow situation. For this example the flow of an incompressible fluid at zero pressure gradient over a semiinfinite and in its undeformed state plane plate is chosen. According to Fig. 1 a rectangular (x, y, z) -coordinate system is introduced. It is conventional otherwise to choose the distance from the wall as the y -coordinate. The present notation, however, leads to more compact formulae below.

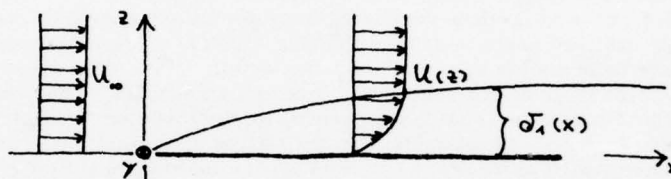


Fig. 1

All quantities are assumed to be nondimensional. A typical length is the displacement thickness $\delta_1(x)$ (for a typical downstream distance), a typical time is δ_1/U_∞ (U_∞ = upstream flow velocity), a typical velocity then is U_∞ and a typical stress or pressure is $\rho_\infty U_\infty^2$ (ρ_∞ = constant density of the fluid).

Under the ideal assumption of exactly parallel flow U_∞ upstream of the plate, theory predicts for the rigid plate the wellknown stationary, laminar and in the present case two-dimensional boundary layer with the Blasius velocity profile $U(z)$.

In a practical case, even in a carefully controlled experiment these ideal upstream conditions will never be met exactly. Rather, the flow upstream will always deviate from the exactly parallel condition by small disturbances. Due to an instability of the laminar boundary layer these disturbances will become more or less amplified in the boundary layer leading eventually to its fully developed turbulent state.

The instability of laminar boundary layers is now sufficiently well understood, as well experimentally as theoretically. Stability theory restricts attention to small disturbances. On the one hand this is in agreement with important practical and experimental situations. On the other hand this allows for considerable mathematical simplification: terms in the flow equations, consisting of products of the small disturbances, may be neglected, leading to a linear stability theory. Linear theory predicts onset of instability for critical Reynolds numbers (and beyond). With the above geometry the Reynolds number is based either on the distance x from the plate edge or the x -dependent boundary layer displacement thickness $\delta_1(x) \sim \sqrt{x}$. Thus the Reynolds number is a local Reynolds number. The critical Reynolds number then corresponds to a critical distance from the plate edge, i. e. the point of indifference. From this point downstream temporally amplified spatially harmonic disturbances occur with wave numbers from a wave number regime, that is initially small but grows downstream. These disturbances grow exponentially in time until their amplitudes have become so large, that the linear theory breaks down. Before this happens linear stability theory is able to correctly predict the point of indifference and the behaviour of the disturbances for a certain distance downstream of the point of indifference. From then onwards higher order terms in the flow equations or even the full equations have to be used. Experimentally one still observes initially spatially more or less harmonic disturbances. Then, further downstream, isolated patches of turbulence appear until the boundary layer is fully turbulent. Thus in contrast to the point of indifference there is no transition point at which the laminar boundary layer abruptly turns fully turbulent. Rather, transition occupies a whole section of the boundary layer from the point of indifference downstream to the fully turbulent part of the boundary layer.

As a first explanation for his rather successful experiments (50 % - 60 % drag reduction) Kramer suggested that his compliant wall influenced the stability of the laminar boundary layer in such a way as to shift the point of indifference downstream. This would lead to the turbulent part of the boundary layer occupying a smaller fraction of the body surface and thus to reduced drag.

Kramer's suggested explanation led theory to focus its attention at first on the influence of compliant walls on laminar boundary layer stability and transition. While a small positive influence could be established this could not explain the 50 % - 60 % drag reduction reported by Kramer. Including the compliant

wall boundary conditions into conventional rigid wall stability theory does not present severe difficulties. The restriction to small amplitude disturbances remains with the same justification as in the rigid wall case. The wall motion can then be described by a linear (elastic or visco-elastic etc.) theory, i. e. essentially by a wall admittance or wall impedance. The rigid wall boundary conditions for the flow disturbances, i. e. vanishing disturbance velocities at the wall, are then replaced by linear and homogeneous relationships between disturbance velocities and disturbance stresses at the wall. Otherwise the equations of stability theory for the rigid wall case remain valid. Especially the differential equation of conventional stability theory, i. e. the Orr-Sommerfeld equation, and its asymptotic solutions for large Reynolds numbers remain valid and can be taken over directly. These points will be discussed in a little more detail below.

When it turned out that Kramer's reported results could not be explained by an effect of the compliant wall on laminar boundary layer stability and transition the attention of theory turned to the problem of direct interaction between the compliant wall and the fully turbulent part of the boundary layer. This is a much more difficult problem than the stability problem sketched above. There exists no exact analytical representation of the turbulent boundary layer, nor even a complete statistical description. Therefore experimentally obtained knowledge on the turbulent boundary layer (for the rigid wall case) has to be introduced. This can be done by using turbulence models from the beginning or by proceeding with the calculations as far as possible introducing measured data only at intermediate or final steps. This accounts for a number of different theories that have been proposed. It turns out to be rather difficult to estimate the relative errors in the predictions of these theories or to compare results of different theories.

All these theories (at least as far as they are known to the present author) have one point in common: they fulfill the coupling conditions between flow and compliant wall at the undeformed position of the interface (i. e. at $z = 0$), while correctly these conditions should be fulfilled at the instantaneous deformed and initially unknown position of the interface. This is a tolerable approximation only if the amplitudes of the interface deformation are in some sense small. This is not always stated by the theories and mostly no justification is given for restricting to small amplitudes. The justification of linear stability theory for a similar restriction is no longer available: the turbulent boundary layer contains small and large fluctuations. A physical explanation for the wall motion amplitudes to remain small is that the wall material is relatively stiff as compared to fluid forces exerted on it by the turbulent boundary layer flow. These forces are of the order of $\rho_0 U \alpha^2$ ($\rho_0 = \text{constant density of the fluid}$). A typical elastic modulus of the wall material is the linear shear modulus G . The physical condition for small amplitude wall motion then is

$$(2.1) \quad \epsilon = \frac{\rho_0 U \alpha^2}{G} \ll 1.$$

With ϵ tending to zero the wall will tend to the rigid wall limit. For small amplitude motion ($0 < \epsilon \ll 1$) the presence of the compliant wall thus constitutes a small disturbance only of a basic state which is the turbulent boundary layer flow along the completely rigid wall ($\epsilon = 0$). There is no point in linearizing the equations governing the wall motion, while for the fluid motion the full nonlinear equations are retained. Consequently a number of theories have been put forward, which use linearized flow equations, linearized about the turbulent boundary layer flow along a rigid wall.

A proper way of doing this is by making an asymptotic expansion of the full problem with respect to the small coupling parameter ϵ .

The undisturbed state is the turbulent boundary layer flow along the rigid wall, and is assumed to be known. In practice knowledge of this undisturbed state is incomplete, only given through average velocity profiles, correlations etc. A more recent argument is that the turbulent boundary layer consists to some degree out of deterministic events, such as the sweep/burst-cycle. However these concepts do not yield easily to quantitative treatment. To repeat, approximately fulfilling the coupling conditions between fluid flow and wall motion at the undeformed interface means restricting to small amplitude wall motion which in turn implies an asymptotic expansion of the compliant wall/turbulent boundary layer interaction problem with respect to the small coupling parameter ϵ . Some of the theories using more or less explicitly such an asymptotic expansion are reviewed below in a little more detail.

It should be mentioned that the restriction to small amplitude wall motion also justifies the use of turbulence models in the compliant wall/turbulent boundary layer interaction problem. These turbulence models are in all cases derived from measurements and observation in turbulent boundary layers along rigid walls. Clearly, transfer of these models to the compliant wall turbulent boundary layer would be impossible when large scale wall motion would have led to the development of a completely different boundary layer.

One may wonder whether the explicit restriction to small amplitudes of the wall motion does not diminish the effect of this motion on the turbulent boundary layer to insignificance. However it is general experience with asymptotic expansions that they are able to correctly describe the basic physical effects and that their results are often applicable beyond the restriction $\epsilon \ll 1$.

Two basic types of theories on the problem of drag reduction by compliant walls have been recognized above: those theories which deal with the influence of compliant walls on stability and transition of laminar boundary layers (case I) and those theories dealing with the compliant wall/turbulent boundary layer interaction problem (referred to as case II below). Examples of both types of theories will be reviewed below.

However before this is done it is recognized that both types of theory have one point in common: the linearization of the coupling conditions at the interface. Difficulties connected with this linearization will be discussed in the next section.

2.1 Linearized Coupling Conditions The coupling conditions between fluid flow and compliant wall motion are twofold; they require continuity of velocities \underline{u} :

$$(2.2) \quad \langle \underline{u}^i \rangle = \sigma$$

and forces

$$(2.3) \quad \langle \tau^{ik} \rangle n_k = \sigma$$

across the interface. Here τ^{ik} is the stress tensor (in the fluid or in the wall material). n^k is the unit normal on the interface pointing, without restriction of generality, into the flow. $\langle \dots \rangle$ denotes the jump of the quantity \dots across the interface. Conditions eq. (2.2) and eq. (2.3) have to be fulfilled at the position of the deformed interface, initially unknown and only to be determined in the course of the calculation; likewise n^k is the normal on the deformed interface.

(Note: symbolic notation \underline{u} and tensor notation \underline{u}^i will be used in parallel, whichever is most convenient. Index values $i = 1, 2, 3$ refer respectively to the x, y, z -direction. Formulae, obtained below, can be written in a more compact way, when, in addition, greek indices are introduced, which are restricted to the values 1 and 2: $\epsilon = 1, 2$ etc. An additional subscript \cdot will be used to indicate values at the undeformed position of the interface, i. e. at $z = 0$. Thus, e. g., with \underline{r} or r^i indicating the position vector, \underline{r}_0 or r^i is its component in the undeformed wall plane and $\underline{r} = (\underline{r}_0, z) = (r^i, z)$.)

Above two cases had been differentiated, case I: stability of a stationary laminar boundary layer over a compliant wall, and case II: a fully turbulent boundary layer influenced by a compliant wall. In both cases linearization with respect to a small parameter ϵ about a basic state has been used. In case I ϵ is a small disturbance amplitude and the basic state is the stationary, laminar boundary layer over the compliant wall in its undeformed state. In case II ϵ is a small coupling parameter and the basic state is the fully turbulent boundary layer flow along a completely rigid wall. Although physical mechanisms are quite different expansion with respect to ϵ of the coupling conditions between fluid flow and compliant wall may be carried out for both cases in common. To this end all unknown quantities are expanded into asymptotic series with respect to ϵ , e. g. the velocities \underline{u} and the displacements \underline{v} (in the wall material):

$$(2.4) \quad \begin{aligned} \underline{u} &= \underline{u}^0 + \epsilon \underline{u}^1 + O(\epsilon^2) \\ \underline{v} &= \underline{v}^0 + \epsilon \underline{v}^1 + O(\epsilon^2), \end{aligned}$$

where the symbol $O(\epsilon^2)$ denotes terms that are of order ϵ^2 small or smaller. In the limit the compliant wall was to tend towards its undeformed state. This means $\underline{v}^0 = \sigma$. The first order displacements \underline{v}^1 have to be computed from a linear (elastic or visco-elastic etc.) theory. It is characteristic of such theories, that they render the displacements of a material point as a function of the undeformed position of that point. Accordingly, if \underline{r}_0 is the position of a material point of the interface in its undeformed state (at $z = 0$) then

$$(2.5) \quad \underline{r} = \underline{r}_0 + \epsilon \underline{v}^1(\underline{r}_0, t) + O(\epsilon^2)$$

is the position of the same material point on the deformed interface. \underline{r}_0 here plays the role of a material coordinate. Hence, the interface velocity is determined by taking the derivative of eq. (2.5) with respect to time, keeping \underline{r}_0 constant:

$$(2.6) \quad \epsilon \frac{\partial \underline{v}^1}{\partial t}(\underline{r}_0, t) + O(\epsilon^2).$$

Eq. (2.6) shows that this velocity results as a function of the undeformed position \underline{r}_0 of the material point and the time t , i. e. the velocity, eq. (2.6), is given at the undeformed interface.

It has already been said that the undisturbed fluid velocity \underline{u}^0 is the velocity, in a laminar (case I) or a turbulent (case II) boundary layer along the rigid wall. Thus \underline{u}^0 has to vanish at the undeformed position of the interface

$$(2.7) \quad \underline{u}_0^0 = \underline{u}^0(\underline{r}_0, t) = \sigma.$$

The disturbed velocity at the deformed interface is

$$(2.8) \quad \begin{aligned} &\underline{u}^1(\underline{r}_0 + \epsilon \underline{v}^1 + O(\epsilon^2), t) + \epsilon \underline{u}^1(\underline{r}_0 + \epsilon \underline{v}^1 + O(\epsilon^2), t) + O(\epsilon^2) \\ &= \underline{u}^1(\underline{r}_0, t) + \epsilon \{ (\underline{v}^1 \cdot \nabla) \underline{u}^0 \}_0 + \underline{u}_0^1 \} + O(\epsilon^2) \\ &= \epsilon \{ (\underline{v}^1 \cdot \nabla) \underline{u}^0 \}_0 + \underline{u}_0^1 \} + O(\epsilon^2), \end{aligned}$$

where the additional subscript \cdot indicates quantities at the undeformed interface, i. e. at $z = 0$. ∇ is the symbol for the gradient. The first coupling condition eq. (2.2) requires eq. (2.6) and eq. (2.8) to be equal. This results in

$$(2.9) \quad \underline{u}_0^1 = \frac{\partial \underline{v}^1}{\partial t} - [(\underline{v}^1 \cdot \nabla) \underline{u}^0]_0,$$

which is the boundary condition for the velocity disturbances \bar{u} . Eq. (2.7) states that the undisturbed velocity field \bar{u} vanishes at the undeformed interface, i.e. at $z = 0$ for all x and y , hence, also

$$(2.10) \quad \frac{\partial \bar{u}_x}{\partial x} = \frac{\partial \bar{u}_y}{\partial y} = \sigma.$$

Thus eq. (2.9) may be simplified:

$$(2.11) \quad \bar{u}_x = \frac{\partial \bar{u}_x}{\partial t} - \bar{v}_y \left(\frac{\partial \bar{u}_x}{\partial z} \right).$$

The first term on the right hand side arises naturally. The second term has occasionally been left out in earlier theories. It arises because the undisturbed velocity field has non-zero value at the disturbed position of the interface, which has to be compensated for by an additional disturbance velocity. According to its derivation eq. (2.11) also applies in the case of an active wall, where $\varepsilon \bar{v}_y$ is prescribed by some mechanism, or even in the case of a wavy rigid wall, provided only the amplitudes are small enough.

The next step has to consider the force boundary conditions eq. (2.3): $\langle \tau^{ik} \rangle n_k = \sigma$. First the unit normal vector on the deformed interface has to be determined. Eq. (2.5) is a description of the deformed interface. $\underline{r}_0 = (r^1, \sigma)$ may also be regarded as surface parameters. Differentiation of eq. (2.5) with respect to \underline{r}_0 renders two independent tangent vectors for the interface, from which the normal vector \underline{n} follows:

$$(2.12) \quad \left. \begin{aligned} n^k &= -\varepsilon \partial^k \bar{v}_y \\ n^3 &= 1 \end{aligned} \right\} + \sigma(\varepsilon^2)$$

The coupling force exerted by the flow on the compliant wall (which is the negative of the force exerted by the compliant wall on the flow) then is:

$$(2.13) \quad \begin{aligned} t^i &= \tau^{ik} n_k \\ &= \left\{ \bar{t}^{ik} (\underline{r}_0 + \varepsilon \bar{\underline{v}}_y + \sigma(\varepsilon^2), t) + \varepsilon \bar{t}^{ik} \bar{r}_k + \varepsilon \bar{\underline{v}}_y + \sigma(\varepsilon^2), t \right\} + \\ &\quad + \left\{ -\varepsilon \partial_k \bar{v}_y \right\} \\ &\quad + \left\{ \bar{t}^{ik} (\underline{r}_0 + \varepsilon \bar{\underline{v}}_y + \sigma(\varepsilon^2), t) + \varepsilon \bar{t}^{ik} (\underline{r}_0 + \varepsilon \bar{\underline{v}}_y + \sigma(\varepsilon^2), t) \right\} + \sigma(\varepsilon^2), \end{aligned}$$

which on proper expansion yields:

$$(2.14) \quad \bar{t}^i = \bar{t}_0^i$$

and for the first order

$$(2.15) \quad \bar{t}^i = -\bar{t}_0^k \partial_k \bar{v}_y + \bar{v}_y (\partial_k \bar{t}_0^k) + \bar{t}_0^i.$$

Besides the coupling force eq. (2.14 + 15) the power flow between fluid flow and compliant wall is of interest. This is obtained as the product of the coupling force and the wall velocity:

$$(2.16) \quad L = t^i u_i$$

where, as above, $t^i = \tau^{ik} n_k$. Thus when, without restriction of generality, the normal \underline{n} is taken to be the outer normal for the compliant wall, L will be the power flowing from the fluid into the wall or the negative of the power flowing from the wall into the fluid.

In the present context one is only interested in the power flow to the first order in the small parameter ε :

$$(2.17) \quad L = \bar{t}_0^i \bar{u}_{0i} + \varepsilon \left\{ \bar{t}_0^i \bar{u}_{1i} + \bar{t}_1^i \bar{u}_{0i} \right\} + \sigma(\varepsilon^2),$$

with \bar{t}_0^i and \bar{t}_1^i taken from eq. (2.14) and eq. (2.15) respectively. According to eq. (2.7) $\bar{u}_x = \sigma$ and \bar{u}_y follows from eq. (2.11) with the result

$$(2.18) \quad L = \varepsilon \bar{t}_0^i \left\{ \frac{\partial \bar{v}_y}{\partial t} - \bar{v}_y \left(\frac{\partial \bar{u}_x}{\partial z} \right) \right\} + \sigma(\varepsilon^2).$$

The lowest order term is zero. This is just a restatement of the fact, that the rigid ($z = 0$) plate does not drain any power from the flow.

This is typical for the situation in a wind or water tunnel, where the turbulent boundary layer (over a rigid wall) obtains its energy from the mean flow, which in turn is driven by the pumps or propellers of the tunnel. The situation is different for a body propelled at constant speed through a fluid otherwise at rest. The propellant mechanism on board the body has to be supplied with power which is lost to the flow, especially to the turbulent boundary layer around the body, as was discussed in the first section above. Here one is concerned with the change of this power due to the presence of compliant walls. This change in power is given by the first order (in ϵ) term eq. (2.18). The following arguments apply whether the basic situation is that of the wind (or water) tunnel or that of the selfpropelled body.

In the case of the stability of a stationary laminar boundary layer over a compliant wall the undisturbed flow (indicated here by the superscript (0)) is just that stationary laminar boundary layer. Thus all zero order quantities are dependent of time, while the disturbances (indicated here by the superscript (1)) will vanish on the temporal average: $\overline{u_0^{(1)}} = 0$. The time average of the first order (in ϵ) power flow from the fluid to the wall, given in eq. (2.18), turns out to be zero. A net power flow may be expected from the second order terms, neglected in eq. (2.18). These are

$$(2.19) \quad \overline{L} = \overline{t^{(1)} u_{0,1}^{(1)}} + \overline{t^{(1)} u_{0,1}^{(1)}} + \overline{t^{(1)} u_{0,1}^{(1)}}.$$

The first term again is zero because of $\overline{u_0^{(1)}} = 0$. The last term contains the second order velocity disturbances $u_{0,1}^{(1)}$, which are not computed in a theory restricting to first order disturbances. However $\overline{u_0^{(1)}}$ will again vanish on the temporal average and as $\overline{t^{(1)}}$ is independent of time this means, that the last term in eq. (2.19) vanishes on the average. Thus, with $\overline{\quad}$ indicating temporal averaging, one obtains

$$(2.20) \quad \overline{L} = \epsilon^2 \overline{t^{(1)} u_{0,1}^{(1)}} + O(\epsilon^2)$$

for the net power flow from the fluid to the wall. There is no net first order (in ϵ) power flow, but the net second order power flow may be computed from first order quantities alone, as indicated by eq. (2.20).

The situation is quite different in the case of the turbulent boundary layer influenced by a compliant wall. Here the undisturbed flow and thus the first order forces are quantities fluctuating in time. Of course $\overline{u_0} = 0$ still applies as this is a consequence of the hard wall condition encountered in the lowest order. Again one has $\overline{u_0} = 0$. But as $\overline{t^{(1)}}$ and $\overline{u_0^{(1)}}$ are both quantities fluctuating in time one expects

$$(2.21) \quad \overline{L^{(1)}} = \overline{t^{(1)} u_{0,1}^{(1)}}$$

to be different from zero, at least under conditions when the compliant wall introduces a suitable phase shift between $\overline{t^{(1)}} = \overline{t^{(1)}}$ (see eq. (2.14) above) and $\overline{u_0^{(1)}}$.

As will be discussed in a little more detail below the compliant wall turns out to have little or no influence on the stability of the stationary laminar boundary layer, while it is expected that suitable compliant walls may favourably influence the turbulent boundary layer, although this point is far from being clarified. One is tempted to connect these findings with the fact that there is no first order net power flow in the case of the stationary laminar boundary layer while there may be such a power flow in the case of the turbulent boundary layer.

It has been discussed in the first section that any argument on drag reduction derived from energy considerations must be regarded with some caution. However this discussion was with reference to the total power flow over all of the compliant wall, while here we are concerned with the local power flow. Thus one may imagine a wall which drains energy from the flow at one location, returning this energy to the flow at some other location, with the transfer affected by wave propagation.

On the other hand one could argue that the instantaneous rather than the net, i. e. time average, power flow is of importance. Thus one may imagine a wall which drains energy from the wall at one location, stores it for some time and then returns it to the flow at the same location. One may also imagine a combination of the energy-storage mechanism with the energy-transfer-through-wave-propagation mechanism.

Above two cases had been differentiated, case I: stability of a stationary laminar boundary layer over a compliant wall, and case II: a fully turbulent boundary layer influenced by a compliant wall. In both cases a linearization has been used to simplify the problem. The linearization of the coupling conditions between fluid flow and compliant wall could be carried out for both cases in common. From now on, however, the different physical mechanisms have to be taken into account.

2.2 The Stability Problem In this section the problem of linear stability of a stationary laminar boundary layer over a compliant wall will be discussed in a little more detail. This discussion will be based on the paper by T. Brooke Benjamin [2] which covers the essential points. A more comprehensive review of papers on this topic may be found in J. N. Hefner [3] elsewhere in this book.

The rigid wall linear stability theory superimposes the unperturbed stationary laminar boundary layer flow with small disturbances and investigates whether these disturbances are, spatially or temporally, amplified or damped. It is especially asked under what conditions neutral disturbances, which are

neither amplified nor damped, can exist. Instability is regarded as an essential prerequisite of turbulence. Introducing the compliant wall merely replaces one set of linear and homogeneous boundary conditions for the flow disturbances at the wall, valid in the rigid wall case, by another set of such boundary conditions, while the decay conditions for the flow disturbances at large distances from the wall and the differential equation, governing the flow disturbances, the Orr-Sommerfeld equation (see below), remain valid. Thus a large part of the results of the rigid wall case remains valid for the compliant wall case.

Certain simplification of the rigid wall theory will also be taken over. These simplifications are as follows. The unperturbed flow is assumed to be plane. Its weak dependence on the streamwise coordinate x is suppressed together with the w -velocity component normal to the wall. Thus the unperturbed flow is approximately characterized by the u -velocity component, i. e. the nondimensional profile $U(z)$, and the Reynolds number $Re = U_\infty \delta^*/\nu$ (U_∞ = constant upstream velocity, δ^* = displacement thickness, ν = kinematic viscosity). Again the x -dependence of the displacement thickness is suppressed. Under current conditions (zero pressure gradient, semiinfinite flat plate) $U(z)$ will be the Blasius profile. Suppressing the x -dependence of the unperturbed flow can be interpreted as confining the stability investigation to a finite section of the boundary layer, long enough to accommodate several wave lengths of the flow perturbation and short enough to disregard streamwise changes in the unperturbed flow. Reynolds numbers Re are local Reynolds numbers corresponding to certain distances downstream from the plate edge. The critical Reynolds number (see below) then corresponds to a critical distance from the plate edge. This marks the point of indifference, referred to above, from which onward the boundary layer becomes unstable at least with respect to certain perturbations.

In addition to the essential condition of small amplitude the disturbances are also assumed to be plane. The case of three-dimensional disturbances, depending on the spanwise coordinate y and having a non-zero v -component of velocity, may by a simple transformation (Squire's theorem) be reduced to the two-dimensional or plane case. It should be noted, however, that Squire's theorem breaks down in the presence of compliant walls that are anisotropic in planes $z = \text{const.}$, i. e. show different properties in the streamwise as in the spanwise direction. From the fact that the unperturbed flow $U(z)$ depends on z only it follows that flow perturbations of the form $\hat{u} = \hat{u}(z) \exp(i\alpha(x - ct))$, $\hat{v} = -i\alpha \hat{\psi}(z) \exp(i\alpha(x - ct))$, $\hat{\psi} = \hat{\psi}(z) \exp(i\alpha(x - ct))$ a disturbance stream function and $\hat{v}' = d\hat{\psi}/dz$ and similarly for the perturbation pressure may be assumed. α has the general meaning of a wave number, αc that of a frequency and c that of a velocity of wave propagation. The imaginary parts of α and αc are respectively responsible for spatial and temporal damping or amplification. It is not obvious from the start that α and αc may be prescribed independently. In fact, it will turn out that they are coupled through an eigenvalue condition.

The perturbed flow, the sum of unperturbed flow and flow perturbation, is inserted into the flow equations, i. e. the Navier-Stokes equations and the condition for incompressibility. After linearization with respect to the small perturbation amplitudes the resulting set of equations may be reduced to a single equation for $\hat{\psi}(z)$ alone, which is the Orr-Sommerfeld equation:

$$(2.22) \quad W(\hat{\psi}'''' - \alpha^2 \hat{\psi}) - W' \hat{\psi}' = \frac{i}{\alpha Re} (\hat{\psi}'''' - 2\alpha^2 \hat{\psi}'' + \alpha^4 \hat{\psi}),$$

where $W = U(z) - c$, and $W' = dW/dz$, etc. The terms on the right hand side result from the viscous terms of the Navier-Stokes equations. At large distances from the wall the perturbations are to decay. Boundary conditions at the wall will be discussed below.

Confining attention to the case of neutral disturbances of a given profile $U(z)$ one can either prescribe a real wave number α and ask for those combinations Re, c where the imaginary part of c is zero (neutral stability) or prescribe a real propagation velocity c and ask for the combinations Re, α with $\text{Im } \alpha = 0$ ($\text{Im } \alpha$ = imaginary part of α). This results in the wellknown curves of neutral stability in the (Re, α) -plane or (Re, c) -plane, see Fig. 2. There are no exact solutions known for the Orr-Sommerfeld equation (2.22) in the case of the Blasius profile (nor in most other cases). However one knows that the critical Reynolds number is large:

$\alpha Re \gg 1$. Thus one may try the inviscid Orr-Sommerfeld or Rayleigh equation, obtained from eq. (2.22) by replacing the right hand side with zero. Let $\varphi(z)$ be that solution of the Rayleigh equation which decays at infinity, where W is constant and thus solutions will be combinations of $e^{\alpha z}$ and $e^{-\alpha z}$. The critical point $z = z_c$, where $U(z_c) = c$ and thus $W(z_c) = 0$ and which according to a general theorem always lies within the boundary layer, is a singular point of the Rayleigh equation. φ has a logarithmic singularity there. The correct branch of the complex logarithm is determined by regarding viscosity in a layer of thickness $\sim (\alpha Re)^{-1/2}$ around the critical point.

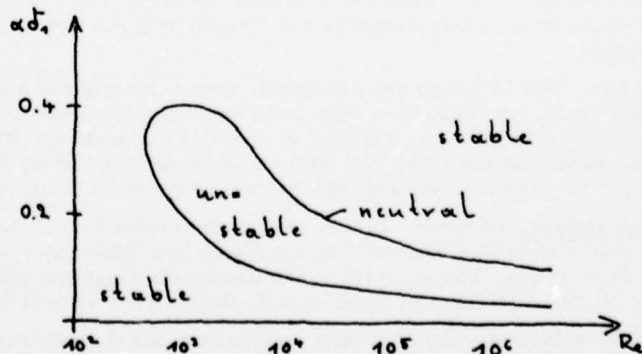


Fig. 2

φ also becomes singular at the wall, where it is unable to meet the two independent boundary conditions of vanishing normal and tangential velocity. Again viscosity has to be taken into account in a wall friction layer of thickness $\sim (\alpha Re)^{-\frac{1}{2}}$. This results in a second solution $f(z)$ which is essentially zero outside the wall friction layer. The general solution then is $\hat{\varphi}(z) = A\varphi(z) + Bf(z)$. On imposing the rigid wall boundary conditions $\hat{\varphi}_0 = A\varphi_0 + Bf_0 = \hat{\varphi}'_0 = A\varphi'_0 + Bf'_0 = 0$ (subscript 0 for values at the wall $z=0$) it becomes obvious that a nontrivial solution exists only when

$$(2.23) \quad \frac{f_0}{f'_0} = \frac{\varphi_0}{\varphi'_0}.$$

The inviscid solution φ is a function of α and c only, independent of the Reynolds number. After multiplication by $-U_0 c$ the left hand side may be written as a function of $\gamma = (\alpha Re U_0)^{\frac{1}{2}} \cdot \frac{c}{U_0}$ only such that eq. (2.23) has the general form

$$(2.24) \quad F(\gamma) = E(\alpha, c),$$

which admits simple numerical/graphical determination of the eigen-values c for given Re and α .

Introducing the compliant wall only affects the boundary conditions at the wall: $\hat{\varphi}_0 = \hat{\varphi}'_0 = \sigma$ will no longer apply. Before the compliant wall boundary conditions are discussed a few words on the unperturbed state of the compliant wall are necessary. The unperturbed fluid stresses will be constant at the unperturbed interface. According to eq. (2.14) unperturbed stresses are continuous there. Thus, in its unperturbed state the compliant material will be under the influence of constant stresses resulting, except for edge zones, in linear displacements. This state has above been used as a reference state by putting the unperturbed displacements equal to zero: $\hat{v}'_0 = \sigma$. In an experiment, however, one may well have to take into account the effects of, e.g., the static pressure on the compliant wall.

According to eq. (2.15) the perturbed forces

$$(2.25) \quad \hat{t}^{(1)}_i = (\partial_\alpha \frac{\hat{t}^{(0)}_{i3}}{c})_0 \hat{v}^{(1)}_0 - \frac{\hat{t}^{(0)}_{i3}}{c} \partial_\alpha \hat{v}^{(1)}_0 + \frac{\hat{t}^{(1)}_{i3}}{c}$$

have to be continuous at the wall ($z=0$). It has just been recalled that the unperturbed stresses $\frac{\hat{t}^{(0)}_{i3}}{c}$ are continuous. The same applies to the displacements \hat{v} and their tangential derivatives. Thus the terms $-\frac{\hat{t}^{(0)}_{i3}}{c} \partial_\alpha \hat{v}^{(1)}_0$ in eq. (2.25) are continuous by definition. The same applies to the terms $\partial_\alpha \frac{\hat{t}^{(1)}_{i3}}{c} \hat{v}^{(1)}_0$. Thus eq. (2.25) requires continuity of

$$(2.26) \quad \frac{\hat{t}^{(1)}_{i3}}{c} + \hat{v}^{(1)}_0 \left(\frac{\partial \hat{t}^{(1)}_{i3}}{\partial z} \right)_0.$$

In the flow $\frac{\hat{t}^{(0)}_{13}}{c} = \frac{1}{Re} U'$ and thus $\left(\frac{\partial \hat{t}^{(0)}_{13}}{\partial z} \right)_0 = \frac{1}{Re} U''_0$ and $\frac{\hat{t}^{(0)}_{23}}{c} = -p = \text{const.}$ (in the approximate x -independent representation of the unperturbed flow) and thus $\left(\frac{\partial \hat{t}^{(0)}_{23}}{\partial z} \right)_0 = 0$. Unperturbed stresses in the compliant wall are constant. Thus in the wall the second term in eq. (2.26) is zero. With subscripts F and C denoting stress perturbations at the wall for fluid and compliant wall respectively one has

$$(2.27) \quad \begin{aligned} \frac{\hat{t}^{(1)}_{13}}{c} &= \frac{\hat{t}^{(1)}_{13}}{c_F} + \frac{1}{Re} U''_0 \hat{v}^{(1)}_0 \\ \frac{\hat{t}^{(1)}_{23}}{c} &= \frac{\hat{t}^{(1)}_{23}}{c_F} \end{aligned}$$

The displacement disturbances $\hat{v}^{(1)}$ in the compliant wall are governed by a linear and homogeneous equation. For a single wave number frequency component the displacement disturbances at the wall will therefore depend linearly on the prescribed stresses there:

$$(2.28) \quad \begin{aligned} \hat{v}^{(1)}_0 &= Y_{11} \left\{ \frac{\hat{t}^{(1)}_{13}}{c_F} + \frac{1}{Re} U''_0 \hat{v}^{(1)}_0 \right\} + Y_{12} \frac{\hat{t}^{(1)}_{23}}{c_F} \\ \hat{v}^{(1)}_0 &= Y_{21} \left\{ \frac{\hat{t}^{(1)}_{13}}{c_F} + \frac{1}{Re} U''_0 \hat{v}^{(1)}_0 \right\} + Y_{22} \frac{\hat{t}^{(1)}_{23}}{c_F} \end{aligned}$$

Through the coupling conditions the displacements also appear on the right hand side.

The quantities Y , depending on wave number α and propagation velocity c , form an admittance tensor. It is usually assumed that the compliant wall is infinitely stiff in tangential direction and does not yield to tangential stresses $Y_{11} = Y_{12} = Y_{21} = 0$. Only $Y_{22} = Y(\alpha, c)$ remains and eq. (2.28) reads:

$$(2.29) \quad \begin{aligned} \hat{v}^{(1)}_0 &= \sigma \\ \hat{v}^{(1)}_0 &= -Y \hat{p}_0 \end{aligned}$$

where $\hat{u}_z' = -\hat{p}_z'$, \hat{p}' the perturbation pressure in the fluid, has been used. Eq. (2. 29) may now be used to eliminate \hat{u}_z' from the boundary conditions for the flow velocity disturbances eq. (2. 11) with the result

$$(2. 30) \quad \begin{aligned} \hat{u}_z' &\equiv \hat{\psi}'(z) e^{i\alpha(x-ct)} = Y U_0' \hat{p}_z' \\ \hat{u}_z' &\equiv -i\alpha \hat{\psi}'(z) e^{i\alpha(x-ct)} = i\alpha Y c \hat{p}_z'. \end{aligned}$$

This is the boundary condition used by Brooke Benjamin. The derivation shows that this condition is valid only under a number of assumptions. The wall properties only enter via the remaining admittance component Y . The pressure \hat{p}_z' has the form $\hat{p}_z' = \hat{p}_z e^{i\alpha(x-ct)}$ where to a good approximation $\hat{p}_z = U_0' A \varphi_z + c A \varphi_z'$ and φ is the inviscid solution of the Orr-Sommerfeld equation (see above). Thus the boundary conditions eq. (2. 30) render

$$(2. 31) \quad \begin{aligned} \hat{\psi}' &\equiv A \varphi_z' + B f_z' = Y U_0' (U_0' A \varphi_z + c A \varphi_z') \\ \hat{\psi} &\equiv A \varphi_z + B f_z = -Y c (U_0' A \varphi_z + c A \varphi_z'). \end{aligned}$$

Thus in the compliant wall case the eigenvalue condition

$$(2. 32) \quad F(\gamma) = \frac{E + Y U_0' c (E - 1)}{1 + Y U_0' c (E - 1)}$$

is obtained. Again the left hand side depends on $\gamma = (\alpha R_e U_0')^{\frac{1}{2}} c U_0'^{-1}$ only, while the right hand side is independent of the Reynolds number R_e . (2. 29) shows that the wall remains at rest when $Y = 0$. This is the rigid wall limit. In that limit eq. (2. 24) is recovered from eq. (2. 32).

It is convenient to put eq. (2. 32) into the alternative form

$$(2. 33) \quad \tilde{F}(\gamma) \equiv \frac{1}{1 - F(\gamma)} = \frac{1}{1 - E} - Y U_0' c.$$

Besides modifying neutral Tollmien-Schlichting waves of the rigid wall case the presence of the compliant wall, i. e. the presence of Y in eq. (2. 33) may lead to other neutral waves, which are absent in the rigid wall limit.

Following Brooke Benjamin the first case considered will be the case of non-dissipative compliant walls, i. e. walls described by real Y . For small enough frequencies αc , when the static deformation limit is approached, any positive pressure in the flow will tend to deflect the compliant wall downwards ($\hat{u}_z' < 0$). Eq. (2. 29) shows that this requires positive admittance Y in this limit αc small. The wall then is stiffness controlled. For larger frequencies Y^{-1} may have a zero and become negative beyond, when the wall is mass controlled. Zeros of Y^{-1} describe free waves in the compliant wall: $\hat{u}_z' \neq 0$ although $\hat{p}_z' = 0$ (see eq. (2. 29)). For large enough wave numbers $Y \sim \alpha^{-2}$, at least for non-dispersive systems. For small enough α , i. e. for large wave lengths, when the load \hat{p}_z' becomes nearly (spatially) constant over all of the wall, Y has to approach a finite limit, depending on the compressibility of the wall material. In between Y will assume a maximum.

Asymptotic solution of the Orr-Sommerfeld equation shows, that at least approximately

$$(2. 34) \quad \frac{1}{1 - E(\alpha, c)} = H(c) + \frac{U_0' c}{\alpha (1 - c)^2}.$$

Thus, when γ, α, c is a solution of eq. (2. 33) in the rigid wall limit $Y = 0$, γ, α, c will be a solution of eq. (2. 33) for a compliant wall $Y = Y(\alpha, c) \neq 0$, when

$$(2. 35) \quad \frac{-U_0' c}{\alpha (1 - c)^2} + \frac{U_0' c}{\alpha (1 - c)^2} - Y U_0' c = 0,$$

or, when α is determined from

$$(2. 36) \quad \alpha \left\{ 1 - Y(\alpha, c) \alpha (1 - c)^2 \right\}^{-1} = \alpha_R.$$

One had $\gamma = (\alpha R_e U_0')^{\frac{1}{2}} c U_0'^{-1}$. Hence any pair of values γ, c determine a value of the product αR_e . Thus in changing from the rigid wall α_R, R_e, c (and $\gamma = (\alpha_R R_e U_0')^{\frac{1}{2}} c U_0'^{-1}$) to the compliant wall α, R_e, c (and $\gamma = (\alpha R_e U_0')^{\frac{1}{2}} c U_0'^{-1}$) the product αR_e remains the same

$$(2. 37) \quad \alpha_R R_e = \alpha R_e$$

with α from eq. (2. 36).

Thus introducing the compliant wall results in a shift of the points of the neutral curve in the (Re, α) -plane (see Fig. 2) along hyperbolae, the amount and direction of shift being determined by the magnitude and sign of Y . For $Y > 0$ one has $\alpha < \alpha_R$ and therefore $Re > Re_R$, i.e. stabilization. For $Y < 0$ one has $\alpha > \alpha_R$ and therefore $Re < Re_R$, i.e. destabilization. For values of wave number α and wave velocity c near zeros of Y^{-1} , i.e. near resonance, very large negative values of Y may occur, leading to $\alpha \gg \alpha_R$, and hence $Re \approx 0$. This means that the boundary layer is completely destabilized. There are "unstable" wave numbers α at all Reynolds numbers Re .

It thus is obvious, that for a non-dissipative compliant wall to be an effective stabilizing device, the velocity of free waves in the wall should be larger than the velocities of the relevant Tollmien-Schlichting waves.

It was argued above that for small enough wave numbers α , Y will assume a maximum $Y = Y_m$. Obviously the stabilizing effect of the compliant wall will essentially be controlled by this maximum. In the vicinity of this maximum one has for non-dispersive walls.

$$(2.38) \quad Y_m(c) = \frac{Y_m(\sigma)}{1 - \frac{c^2}{c_1^2}},$$

where c_1 is the velocity of free waves in the wall. According to the above it is safe to assume that this wave velocity is of the order of the potential flow speed outside the boundary layer: $c_1 \approx 1$. One may also assume $\alpha Y_m(\sigma) \approx 1$. In the Blasius profile Tollmien-Schlichting waves of a wave velocity $c = 0.41$ are the first to become unstable at a critical Reynolds number of $Re = 420$. For these values eq. (2.36) renders

$$(2.39) \quad \frac{\alpha}{\alpha_R} = 1 - \frac{(1 - 0.41)^2}{1 - (0.41)^2} = 0.58$$

and therefore from eq. (2.37)

$$(2.40) \quad Re_{crit} = \frac{\alpha_R}{\alpha} Re_{R,crit} = 1.72 Re_{R,crit}.$$

Thus a compliant wall with these properties may increase the critical Reynolds number by a factor of 1.72. As $Re = \frac{U_\infty}{\nu} \delta_1(\omega) \sim \sqrt{x}$ this corresponds to an increase in the distance of the point of indifference from the leading edge of the plate by a factor of $(1.72)^2 \approx 3$.

Next the influence of a purely dissipative wall on Tollmien-Schlichting waves is considered. In this case $Y = i Y_i$ is purely imaginary. In a passive dissipative wall energy is always lost due to dissipation, requiring $Y_i > 0$. Again one can find solutions in the presence of $Y \neq 0$ of eq. (2.33) from rigid wall solutions of eq. (2.33) with $Y = 0$ by suitably changing α and c and using Re to keep γ unchanged. The imaginary part of $(1 - E)^{-1}$ is proportional to c , with a positive constant of proportionality. Thus the presence of the compliant wall will shift the velocities of neutral waves to higher values c . A slight increase in the wave number α is necessary to keep the real part of $(1 - E)^{-1} Y U_\infty$ balanced. For $\gamma = \text{const.}$ $Re \sim \alpha^{-1} c^{-3}$ and thus the critical Reynolds number is drastically decrease as c is increased due to the presence of the compliant wall.

Thus dissipative effects in the compliant wall have a strong destabilizing effect on Tollmien-Schlichting waves. Although the effects of real wall admittance Y (non-dissipative wall) and imaginary wall admittance $i Y_i$ (purely dissipative wall) do not add linearly, one may expect the destabilizing effects of wall dissipation to offset stabilizing effects of the real part of Y . Thus in order to stabilize Tollmien-Schlichting waves the wall should only have small dissipation in addition to the properties discussed above.

In addition to its influence on Tollmien-Schlichting waves the wall compliance gives rise to two other types of instability waves.

The first type is analogous to Kelvin-Helmholtz instability waves on free shear layers. This is essentially a nonviscous, potential flow effect. A potential flow over a wavy wall develops negative pressure over the peaks ($\vec{v}_1 > \sigma$) of the wall wave and positive pressure over the valleys ($\vec{v}_1 < \sigma$), thus tending to amplify or support the wave. These pressures are of the order of the dynamic pressure. Thus if U_∞ is large enough these pressures will balance or even outweigh any elastic restoring forces. The wave then will grow. Dissipation in the wall will only introduce a slight phase shift between the pressure in the flow and the wall wave such that energy is supplied to the wall at a sufficient rate to balance dissipative losses in the wall.

A second type of additional instability waves consists in free waves in the wall, modified by the presence of the flow, and essentially stabilized by wall dissipation. For the discussion of this type of instability the reader is referred to Brooke Benjamin [2].

In conclusion Brooke Benjamin suggests that a stabilizing compliant wall should have the following properties. It should be sufficiently stiff to avoid Kelvin-Helmholtz instability. For any Reynolds number Re the velocity $c_1(\alpha)$ of free waves in the wall at the wave number α for which Tollmien-Schlichting waves are most amplified should be just larger than the wave velocity of these Tollmien-Schlichting waves. The choice of internal damping in the wall is critical. A certain amount of damping is required to suppress modified free surface waves. On the other hand, to large damping may destabilize Tollmien-Schlichting waves.

Brooke Benjamin conjectures that these conditions may have been met in the tests conducted by Kramer.

2.3 The Turbulence Problem Two essentially different approaches to the problem of compliant walls for drag reduction purposes had been recognized above: the problem of the linear stability of a stationary laminar boundary layer over a compliant wall (case I) discussed in the preceding section and the problem of the influence of a compliant wall on the fully developed turbulent boundary layer (case II).

In the first case the rigid wall reference case is fairly well understood and many of its results could be taken over. This is quite different in the second case, where the rigid wall reference case, the turbulent boundary layer flow over a rigid wall, is far from being clarified. Thus case II is by far the more complicated.

It has already been discussed, that in both cases an asymptotic expansion with respect to a suitable small parameter ϵ is employed in all known cases. For theories dealing with the compliant wall/turbulence interaction problem this is often only implied by an approximate treatment of the coupling conditions between the compliant wall and the turbulent boundary layer flow.

In the stability problem (case I) ϵ was the small amplitude of disturbances imposed on the boundary layer. The limiting case $\epsilon = 0$ was that of the stationary laminar boundary layer along a rigid wall.

It has already been noted that in the turbulent interaction problem (case II) ϵ is the inverse of the relatively large non-dimensional stiffness of the compliant wall material. For a purely elastic wall the dimensional stresses $\rho \cdot u_{\alpha}^i \tau^{ik}$ are homogeneous functions of the strains γ^{ik} only, strains being dimensionless by definition. The value of this function must of course have the dimension of a stress. Thus the function may be written as the product of a typical elastic constant of the dimension of a stress, such as the shear modulus G , and a dimensionless function $F^{ik}(\gamma_{em})$ of the strains, having the order of magnitude 1: $\rho \cdot u_{\alpha}^i \tau^{ik} = G F^{ik}(\gamma_{em})$. After dividing by G and observing $\frac{\rho \cdot u_{\alpha}^i}{G} = \epsilon \ll 1$ (see eq. (2.1)) one obtains

$$(2.39) \quad \epsilon \tau^{ik} = F^{ik}(\gamma_{em}).$$

Proper expansion of strains and stresses yields in the lowest order

$$(2.40) \quad \sigma = F^{ik}(\gamma_{em}^{(0)}).$$

Thus $\gamma_{em}^{(0)} = 0$, leading to a vanishing displacement field $\underline{v} = 0$.

To the first order eq. (2.39) then yields

$$(2.41) \quad \tau^{ik} = E^{ikem} \gamma_{em}^{(1)},$$

where E^{ikem} are the wellknown elastic moduli, in the most general case 21 independent quantities, in the case of full isotropy 2 independent quantities (of which one has been absorbed into the expansion parameter ϵ).

The compliant wall remains at rest in the lowest order in ϵ . The lowest order or undisturbed flow then is the turbulent boundary layer flow along the wall at rest or the rigid wall.

The force coupling conditions in the lowest order eq. (2.14) then say that the zero order elastic stresses in the wall have values at the undeformed interface $z = 0$ which are prescribed by the undisturbed flow. According to eq. (2.41) therefore the first order or disturbance motion of the wall has to be computed from a problem of linear elasticity theory with prescribed stresses at $z = 0$, prescribed by the undisturbed flow. The solution of this problem will then, via eq. (2.11), render the velocity boundary conditions (at $z = 0$) for the flow disturbances. Essentially the same considerations apply to visco-elastic compliant walls, where eq. (2.39) is replaced by an appropriate visco-elastic law, containing typical decay times in addition to the elastic moduli.

Thus the flow disturbances have to be determined from the linearized flow equations, i. e. Navier-Stokes and continuity equations with a decay condition at large distances $z \rightarrow \infty$ from the wall and prescribed values of the velocity disturbances at the wall $z = 0$:

$$(2.42) \quad \left. \begin{aligned} \frac{\partial \underline{u}}{\partial t} + \nabla \cdot \underline{p} - \frac{1}{R} \Delta \underline{u} &= \underline{q} \\ \nabla \cdot \underline{u} &= 0 \end{aligned} \right\} \quad z \geq 0, \quad |\underline{r}| < \infty, \quad |t| < \infty.$$

Here $\underline{q} = -(\underline{u} \cdot \nabla) \underline{u} - (\underline{u} \cdot \nabla) \underline{u}$ is an abbreviation for the linearized convection terms.

In eq. (2.42) the Navier-Stokes equations have been written in a somewhat unfamiliar form, collecting all purely linear terms on the left hand side, while the linearized (originally nonlinear) convection terms have been transferred to the right hand side. The reason for this is the fact that the convection terms, although linearized, essentially prevent an analytical solution of the mathematical problem for the flow disturbances \underline{u} , \underline{p} , eq. (2.42) plus boundary conditions.

Therefore, approximate theories have been proposed in which eq. (2.42) is used with the right hand side q replaced by zero. The problem then is easily solved and information on the disturbances of wall stresses may be extracted, in the hope of estimating drag reduction due to the wall compliance. As a justification for dropping q altogether it is sometimes said that q vanishes at the wall and will therefore be negligible in a vicinity of the wall, e. g. in the viscous sublayer. However, while $q = 0$ at a rigid wall it will be different from zero at a compliant wall. Furthermore, on confining to the viscous sublayer one loses the decay condition at large distances from the wall. It is difficult to see what boundary conditions are applicable at the outer edge of the viscous sublayer.

Therefore, the present author [4] has suggested a theory in which the linearized convection terms are at least approximately retained. This theory will be reviewed here in a little more detail. For a more comprehensive review of theories on the compliant wall/turbulent boundary layer interaction problem the reader is again referred to J. N. Hefner [3], elsewhere in this book.

In the context of drag reduction the changes in the wall stresses, especially the wall shear stresses, due to the wall compliance, i. e. the wall stress disturbances \hat{u}_w' , are of particular interest. Therefore the focus will be on these quantities.

One could use prescribed wall stress disturbances \hat{u}_w' as additional boundary conditions at the wall to replace the decay condition for the flow disturbances at large distances $z \rightarrow \infty$ from the wall: given the wall velocity disturbances \hat{u}_w' and the wall stress disturbances \hat{u}_w' , then from eq. (2.42) the flow disturbances are uniquely determined. This fact will be used below.

It has already been mentioned that eq. (2.42) with q replaced by zero is easily solved. E. g., the solution can be obtained by Fourier transformation with respect to the variables r_0 in the wall plane and the time t . This renders a linear ordinary differential equation in z with constant coefficients, which is solved by a linear combination of exponential functions $e^{-\gamma z}$ with $\gamma = \gamma_1 = k$ and $\gamma = \gamma_2 = k \sqrt{1 - i R_e \frac{\omega}{k^2}}$ where k is the wave number in the wall plane, $k = |k|$, and ω is the radian frequency and the condition $R_e \gamma \geq 0$ ($R_e \dots$ = real part of \dots) takes care of the decay condition for $z \rightarrow \infty$. Similarly, eq. (2.42) may be solved without difficulties if q were a given inhomogeneity. Solving directly for the wall stress disturbances one obtains:

$$(2.43) \quad \hat{u}_w' = \iint [G' \hat{u}' + \int H' q' dz] d^2 r' dt',$$

where G' and H' result from a Green's function type solution of eq. (2.42) with q replaced by zero, to be determined by the Fourier transformation procedure outlined above. They depend on the differences $(r_0 - r_0', t - t')$ of observation point (r_0, t) and source point (r_0', t') only. H' in addition depends on z . Hence the integral over (r_0', t') in eq. (2.43) is a convolution integral, a point that is of importance below.

Now, in the present problem q is not a given inhomogeneity of eq. (2.42). Rather it depends on the unknown flow disturbances \hat{u}' . It has been said above that \hat{u}' is uniquely determined by the wall velocity disturbances \hat{u}_w' and the wall stress disturbances \hat{u}_w' . Thus eq. (2.43) turns out to be an integral equation for the unknown wall stress disturbances \hat{u}_w' .

It should be noted that this integral equation is exact (except for the linearization in ϵ). However, before any quantitative information can be obtained from this equation it is necessary to make a simplifying approximation.

To this end a single Fourier component of eq. (2.43) at wave number k and frequency ω is considered. It has been noted above that the integral with respect to r_0' and t' on the right hand side of eq. (2.43) is a convolution integral between G' and \hat{u}' and H' and q respectively. Its Fourier transform will therefore simply be the product of the Fourier components of G' and \hat{u}' and H' and q respectively. The second term, involving q , then is of the form

$$(2.44) \quad \int \hat{H}' \hat{q}' dz,$$

with the superscript $\hat{}$ denoting Fourier transforms. Now, as stated above, \hat{H}' is a linear combination of exponential terms $e^{-\gamma z}$ with $\gamma = \gamma_1 = k$ and $\gamma = \gamma_2 = k \sqrt{1 - i R_e \frac{\omega}{k^2}}$.

As q and thus \hat{q} will decay for large z essential contribution to the integral eq. (2.44) will come from a region close to the wall where $\sigma \ll z \ll \delta^{-1}$. It may be argued that q is approximately constant in this region. In that case the following approximation holds

$$(2.45) \quad \int \hat{H}' \hat{q}' dz \approx \int \hat{H}' dz \cdot \hat{q}_0$$

where \hat{q}_0 again is the value of \hat{q} at the wall.

The approximation eq. (2.45) is the essential simplification of the present analysis. It would not hold if q were to grow to a maximum at a certain distance from the wall and then decay. However, such a behaviour of q is not to be expected. It should be noted that the approximation of eq. (2.45) constitutes the first step in a systematic series of approximations.

With this approximation eq. (2. 44) is replaced by

$$(2. 46) \quad \tau_{0,1}^{(1)} = \iint [G_{1e}^{(1)} \tilde{u}_e^{(1)} + \int H_{1e}^{(1)} dz \cdot q_e^{(1)}] d^2 r_0' dt',$$

where $q_e^{(1)}$ is easily determined and turns out to depend only on the unperturbed flow and the prescribed disturbance velocities at the wall $\tilde{u}_e^{(1)}$. Thus, the above approximation renders an explicit representation of the wall stress disturbances $\tau_{0,1}^{(1)}$ in terms of the unperturbed flow and the wall velocity disturbances $\tilde{u}_e^{(1)}$.

In the context of drag reduction one is primarily interested in the temporal mean (denoted by $\overline{\quad}$) of the streamwise shear component: $\overline{\tau_{0,1}^{(1)}}$. One obtains from eq. (2. 46):

$$(2. 47) \quad \overline{\tau_{0,1}^{(1)}} = - \frac{\rho_0}{2\pi} \int \frac{(x-x')(r_0-r_0')}{|r_0-r_0'|^3} \overline{\tilde{u}_e^{(1)} \tau_{0,1}^{(1)}} d^2 r_0'.$$

As discussed above the wall velocity disturbances $\tilde{u}_e^{(1)}$ may be expressed by the unperturbed wall stresses $\tau_{0,1}^{(1)}$ through a wall admittance, describing the properties of the compliant wall. Thus the wall stress disturbances $\tau_{0,1}^{(1)}$ depend on the properties of the compliant wall through a wall admittance and correlations of the unperturbed stresses. These correlations have to be estimated from measured data.

From eq. (2. 47) one estimates for fluids of approximately the same density as the wall material and for a simple elastic layer on a solid foundation a reduction in wall shear stresses in the order of 10 %. In [4] a similar reduction in drag has been inferred from this result. However, it is the change in total coupling force $\tau_{0,1}^{(1)}$, eq. (2. 15), that is responsible for a change in drag. This change in coupling force contains additional terms in addition to the change in shear stress. It is difficult to estimate the contributions of these additional terms. Thus the conclusions given in [4] are somewhat doubtful.

3. Conclusion In this review the aim was not so much to give a broad over-view over all or most of the theoretical papers on drag reduction by compliant walls.

Rather the attempt has been made to familiarize the reader with typical difficulties met in such theoretical work and the necessary assumptions, simplifications and approximations to overcome these difficulties by reviewing two papers in a little more detail: one paper, dealing with the problem of stability of a stationary laminar boundary layer over a compliant wall, and a second paper, dealing with the turbulent boundary layer/compliant wall interaction problem. These papers, especially in the second case, are not representative of all theoretical work in this field.

One purpose of theory is to determine those properties of compliant walls most promising for drag reduction purposes. It is then the problem of the experimenter to manufacture and test such walls.

A second purpose of theory is to point out gaps in understanding which may be filled by experiment. In this context it is of interest to note that most theoretical approaches treat the compliant wall as constituting a small disturbance of the rigid wall reference case, i. e. the laminar or turbulent boundary layer flow along the rigid wall. It turns out that a certain knowledge of the rigid wall reference case, such as wall stress correlations, together with a wall admittance is sufficient for an estimate of drag reduction.

Emphasis has been put on a general discussion of the coupling conditions between fluid flow and compliant wall, as it seems that these are sometimes treated with a certain negligence.

No general statement on the possibilities of drag reduction by compliant walls can be made as these crucially depend on the wall properties. However, further research efforts seem to be justified.

4. References

- [1] M. O. Kramer: Boundary Layer Stabilization by Distributed Damping, J. Aeron. Sc. 24 (1957), pp. 459-460;
- [2] T. Brooke Benjamin: Effects of a Flexible Boundary on Hydrodynamic Stability, J. Fluid 9 (1960), pp. 513-532;
- [3] J. N. Hefner: to be published in this book;
- [4] G. Zimmermann: Interaction between a Turbulent Boundary Layer and a Flexible Wall, Report 10 a/1974, Max-Planck-Institut für Strömungsforschung, Göttingen, Germany.

ON THE PROBLEM OF DRAG REDUCTION BY MEANS OF COMPLIANT WALLS

Dr. A. Dinkelacker
Max-Planck-Institut für Strömungsforschung
Böttingerstr. 4-8
D 3400 Göttingen, Germany

SUMMARY

Drag reduction with the help of compliant coatings would be of great interest for technical applications as well as for research in turbulence. At present, however, there is to the author's knowledge no single experiment on drag reduction by means of compliant walls which has been successfully repeated by a second investigator. Therefore the basic requirement of reproducibility seems to be not yet fulfilled. This does not imply that drag reduction with the help of compliant walls is impossible or that reported results are wrong, it only indicates that the problem has to be regarded as being in an uncertain state. In the present paper some of the difficulties arising from experiments with compliant walls are discussed and recommendations for further studies are given. Investigations of turbulent wall pressure fluctuations are reported which are believed to be helpful for a better understanding of interactions between the flow and compliant walls.

1. THE PROBLEM

In fluid mechanics, boundary surfaces are usually treated as "rigid" surfaces. Such rigid surfaces can be realized to a good degree of approximation by bodies out of wood or metal and in theoretical work the concept of rigid surfaces leads to clearly defined simple boundary conditions. In nature, however, flow bounding surfaces often are not rigid but show some sort of movability. A few examples may demonstrate this: Wind going over the sea, over the tree-tops of a wood or over the blades of a corn field; flow of blood in veins; flow along the bodies of fish and birds. It is evident that flow along a movable surface cannot be exactly the same as flow along a rigid body. The question is, under which conditions the differences become significant.

In 1936 Gray¹ discussed the problem of propulsion of the dolphin and came to the statement of what later often has been called the Dolphin-Paradox. In Gray's own words: "If the resistance of an actively swimming dolphin is equal to that of a rigid model towed at the same speed, the muscles must be capable of generating energy at a rate at least seven times greater than that of other types of mammalian muscle ... If the flow of water past the body of a dolphin is free from turbulence, the horse-power developed per pound of muscle agrees closely with that of other types of mammalian muscle". The statement of Gray shows that the problem of drag of "non rigid" bodies was formulated already in 1936. To a broader discussion, however, it came only after Kramer had published his first paper² on "Boundary Layer Stabilization by Distributed Damping" in 1957, which was followed by three more papers^{3, 4, 5} by the same author under the same title. Kramer^{3, 4, 5} reports on experiments in which parts of streamlined bodies (typical length 2.5 m) were coated with a thin coating (typical thickness 3 mm) of specially designed rubber with oil-filled interspaces. The drag of bodies coated in this way is reported to be considerable smaller than that of smooth rigid bodies of the same shape. Drag reductions up to 60 % were reported. Kramer interprets the results as meaning that the coatings damp out small disturbances in the boundary layer and lead to laminar flow in regions in which otherwise turbulence would occur. Figure 1 (from Ref. 3) shows a sketch of one of the coatings used and Figure 2 (from Ref. 3) shows a typical set of results. As can be seen for three coatings (curves B, C and D in Fig. 2) and for different Reynolds Numbers (which means here different towing speeds of the bodies) drag coefficients are reported which lie between fully laminar and fully turbulent flow and which are considerably lower than those of the rigid reference model (curve A in Fig. 2). Coatings with such qualities of course would be of great interest for technical applications. It may be mentioned that Kramer constructed his coatings in connection with studies of the skin of dolphins^{6, 7}.

Following Kramer's publications, investigations on the problem of flow along flexible walls were started at many research institutes, including investigations on stability of laminar flow in the presence of flexible walls as well as investigations on the question whether wall flexibility can influence developed turbulence. Surveys on these experimental and theoretical investigations have been given by Brooke Benjamin⁸ in 1964 and more recently by Zimmermann⁹ and by Bushnell, Hefner and Ash¹⁰ (compare also papers No. 7 and No. 9 in this volume). While the theoretical work led to some positive results (compare e.g. Ref. 8) the situation with the experimental work is, that there is - to the author's knowledge - no single experiment on drag reduction by means of flexible walls which has been successfully repeated by a second investigator. So the basic requirement of reproducibility is not yet fulfilled. Of course, this does not imply that drag reduction by means of flexible walls is impossible or that reported positive results are wrong, it only indicates that the problem has to be regarded as being in an uncertain state.

Looking for reasons for this situation, the following considerations may be of some value:

(1) While "rigid" is a clearly defined quality, "flexible" (or movable, or compliant) is not just the "other case" but an enormous variety of qualities. An example may illustrate this: Assumed that a flexible wall

could be characterized by three independent parameters - this is certainly not yet a full description - and assumed that each of these parameters could take 10 significant stages, one would have thousand different sorts of flexible walls as compared to one sort of rigid wall. (2) Turbulent boundary layer flows along rigid walls are already complicated phenomena - much of which are not fully understood - so if these flows are combined with "flexibility" the problem is even more complicated. (3) Experiments with flexible walls suffer from many inherent experimental difficulties. (4) Bushnell, Hefner and Ash¹⁰ have shown in their review that several of the published "positive" results can be attributed to evaluation or measuring errors. Taking these considerations together it is not too astonishing that the problem is not yet solved. For further investigations, however, one should take the difficulties of the problem into account.

The aim of this paper is to give some suggestions for planning further work. In order to do this in section 2 some experiments with flexible walls are reported whereby special reference is given to difficulties which can occur in connection with flexible-wall investigations. In section 3 a report on some investigations on turbulent wall pressure fluctuations is given. Such investigations might lead to a better insight into the processes of interactions between flows and flexible walls.

Before starting with details it might be useful to give a classification of flexible walls. Table 1 shows such a classification. Case 3 in this table which is denoted as "passive" flexible wall is the case which is normally discussed in the context of drag reduction by compliant walls. In this case the wall movements are caused by the flow and it is hoped that these wall movements influence the flow. Cases 4 and 5 characterize actively moved flexible walls. In these cases the energy to move the walls is supplied from outside the flow. In case 4 also control of the wall movements occurs from outside the flow, in case 5 this movements can be controlled with the help of a sensor and a feed-back system by the flow itself. In this case the walls can react controlled on selected processes in the flow. Experiments with active walls can be expensive; they have, however, the advantage that the wall movements are comparatively simple and the problem of "flexibility" is widely excluded from the experiment. So active flexible walls may well be useful for further research. Application of active flexible walls for drag reduction at present looks strange, but if the concept would work, it might well be that solutions for technical realization could be found. Cases 1 and 2 show rigid walls. Case 1 is understood as the normal, hydraulically smooth rigid wall which is used in many technical applications and which is in the context of flexible wall investigations used as the reference case. The reason that an additional case "modified rigid wall" has been included in Table 1 is that the author is not sure that "hydraulically smooth" is a fully sufficient description - if one is interested in details - of flow bounding smooth rigid surfaces. The experimental results of W. D. Beasley reported by Hefner and Bushnell in Figure 22 of paper No. 1 of this volume can demonstrate what could be meant by a "modified rigid surface". Here application of a thin foil - with negligible flexibility - led to drastic changes in drag. So before discussing effects of flexibility one certainly needs clear results on the drag of rigid wall used as references.




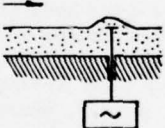
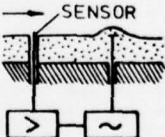
CASE NO.	
	1 SMOOTH RIGID WALL
	2 MODIFIED RIGID WALL
	3 PASSIVE FLEXIBLE WALL
	4 ACTIVE FLEXIBLE WALL
	5 FLOW CONTROLLED ACTIVE FLEXIBLE WALL

Table 1

2. SOME DIFFICULTIES WITH COMPLIANT WALL EXPERIMENTS

In the following a few compliant wall experiments briefly will be reported, whereby special reference is given to difficulties which can occur in performance or evaluation of such experiments. The examples are taken mainly from experiments performed in Göttingen and in Southampton.

2.1 Mechanical Stability

Figure 3 (from Ref. 11) shows the arrangement used for flexible wall investigations performed in Southampton. Water flows through a vertically suspended pipe of 5.08 cm inner diameter. Flow through flexible tube sections is compared with flow through rigid tube sections. Figure 4 (from Ref. 11) shows a flexible tube section as used in the beginning of this investigation. As can be seen in this figure the flexible tube forms wrinkles at the downstream tube end and under the action of increased flow velocity these wrinkles tend to develop into bulges. In this way the tubes usually have been destroyed within seconds.

This difficulty of overall instability has been overcome by gluing a layer of porous foam between the inner flexible tube and the outer rigid tube. The interspaces in the porous foam could be filled with liquid. Figure 5 (from Ref. 11) shows such an improved flexible tube construction. Such effects of instability of the flexible coatings have to be taken into account when flexible wall experiments are to be performed.

2.2 Evaluation of Pipe-Flow Experiments

As flow through a pipe is generally connected with pressure drop along the pipe, experiments with flexible pipes suffer principally from the fact, that differences in static pressure occurring along the pipe may cause changes in the diameter of the pipes. Bushnell, Hefner and Ash¹⁰ have pointed out that such changes could have led to errors in evaluation of drag measurements in flexible pipes (compare section 5.2 of paper No. 9 in this volume). To some extent, similar difficulties have been encountered with the experiments performed with flexible tube sections of the type shown in Figure 5. As the inner diameter of these tubes depends on the volume of the liquid filled into the interspace between the inner flexible and the outer rigid tube, measurements with different filling volumes have been performed. Figure 6 (from Ref. 11) shows results of such measurements. The abscissa in Figure 6 is the volume V of water filled into the interspace behind the flexible tube, the ordinate is the normalized pressure drop along the test section, i.e. the ratio of the pressure drop along the flexible tube to that along a rigid reference tube. As can be seen the pressure drop remains constant in a wide range of volumes V and is about 50 % lower than that measured along the rigid tube. This result could be interpreted as drag reduction. However, these measurements were not fully reproducible and with certain volumes V the pressure drop even became "negative" (compare $V = 38$ ccm in Fig. 6), which, of course, makes the interpretation as drag reduction impossible. A more detailed investigation of these effects then has shown, that with the flexible tubes the axial-symmetry of the flow in the tubes was not fully maintained - and this led to difficulties with the interpretation of the measured wall pressure and to inconclusive results with respect to drag reduction. This example shows that even small changes in the shape of flexible coatings can lead to misleading evaluations.

It may be mentioned here, that Carstensen¹² has done similar experiments with water flow in pipes. The insides of his tubes partly have been coated with a "sound-soft" foam-rubber coating. Carstensen compared turbulence levels in these coated tubes with turbulence levels in rigid tubes and found quite interesting differences. However, again he could not fully maintain constant inner diameter of the flexibly coated tubes and so the interpretation of his results is not fully conclusive. Figure 7 (from Ref. 12) shows some of Carstensen's results.

One way to overcome these difficulties with different static pressure along flexible pipes could be to build the experimental arrangements so that the frictional pressure drop just is cancelled by pressure increase because of gravity. Arrangements with variable inclination of the pipes could be helpful for such experiments.

2.3 Influence of Small Steps

If flexible coatings are arranged in an experimental device this leads usually to small steps at the joints between rigid and flexible surface elements. In the investigation reported in Ref. 11 it has been shown that even very small steps under certain circumstances can lead to comparably strong changes in the flow. Such changes easily can make evaluation of flexible wall experiments inconclusive.

2.4 Influence of Sound Fields

It is well-known that sound fields under certain circumstances can have an influence on flow configurations. If one compares flow over flexible walls with flow over rigid walls it may be of importance to take acoustical effects into account because the acoustical boundary conditions usually also depend on the wall flexibility. In the experiments reported in Ref. 11 such effects have been observed.

It may be of interest to report here briefly some experiments of Mechel and Schilz¹³. They used a loudspeaker in a wind-tunnel to generate a soundfield at the leading edge of a flat plate. The influence of the sound on the development of the turbulent boundary layer along the plate was investigated. Figures 8 to 11 (from Ref. 13) show the arrangement and some of the results. As can be seen from Figure 9 the growth of the velocity fluctuations along the plate is strongly influenced by the soundfield. Remarkable is that application of "high" sound frequencies leads to decreases of velocity fluctuations. Figures 10 and 11 show some details. With respect to drag reduction it seems to be possible that under certain conditions influence of sound successfully could be applied. In two later papers^{14, 15} Schilz has investigated such effects in more detail.

2.5 Experiments with Nonisotropic Elasticity and Effects of Aging of Coatings

Großkreutz¹⁶ has developed an interesting concept for influencing turbulence with the help of flexible walls. His basic idea is to build flexible walls the surface motions of which are always so that an outward movement of a wall element is automatically combined with a downstream movement of the same

element and vice versa. Figure 12 (from Ref. 17) shows the principle and Figure 13 (from Ref. 17) shows a cross section through a rubber plate which has such nonisotropic elastic qualities. With the help of such flexible plates boundary conditions can be achieved which always have a positive uv-correlation. It was hoped that in this way drag reduction could be achieved. The experiments have been performed in a water tunnel. Figures 14 and 15 (from Ref. 17) show some of the results. As can be seen from Figure 14 the mean velocity profiles obtained with flexible and rigid plates show some differences. The calculated change in the momentum thickness can be interpreted as a drag reduction of 5 %. However, such drag reductions were only found in a limited range of flow velocities and the results were not quite reproducible. As can be seen from Figure 15 tests performed 6 weeks later with the same compliant plate showed increased drag as compared with the rigid reference plate. This example shows that changes of the elastic qualities of flexible coatings because of aging may play an important role.

2.6 Observation of Movements of the Wall

For theoretical evaluation of flexible wall experiments a detailed knowledge on the actually occurring surface movements of a flexible coating is rather necessary. There are several means to measure the surface movements, e.g. with capacitive probes from the rear side of the flexible coating or with optical means through the flow. Figure 16 (from Ref. 16) shows a sketch of a Schlieren-method which has been developed by Viering and Meier¹⁸ for the measurement of angular displacements of the surface of a flexible plate. Figure 17 (from Ref. 16) shows a set of results gained with this method at a flexible plate in the water tunnel used by Großkreutz. This figure shows how the frequency components and the angular amplitudes of the wall oscillations increase with increasing flow velocity. This example demonstrates that with comparatively simple means information on flexible wall movements can be gained.

2.7 Surmounting the Stability Border

In pipe flow at Reynolds-Numbers higher than 2300 turbulence usually occurs. But it is well-known that with smooth inflow conditions the laminar flow regime can be maintained up to considerable higher Reynolds-Numbers. Similar effects can be observed in flow investigations with flexible surfaces and here this effect could lead to evaluation errors. Figure 18 (from Ref. 19) shows an example. In an experiment performed by J. Meseth in Göttingen water was led through commercially available vertically suspended rubber tubes. The inner tube diameter, the flux through the tubes and the pressure drop along the tubes have been measured. As it was necessary to keep the tube ends in a fixed position small metal blocks of weights of a few hundred grammes have been fixed at the downstream tube end. As can be seen from Figure 18 it was found that the friction factor λ depends systematically from the weight G of these small metal blocks. At first it was thought that a flexible wall effect had been found - some similar looking effects had been observed earlier by the author²⁰ - but more detailed investigations have shown that the "straightness" of the tubes is a critical factor for transition to turbulence. The higher the weight G , the straighter the flexible tube and the later the transition. This example shows again, that one has to be rather careful when interpreting flexible wall experiments.

2.8 An Experiment to Repeat Measurements of Kramer

In view of the lack of reproducible results an experiment has been started in co-operation with M.O. Kramer to repeat some of Kramer's measurements. For this experiment Kramer supplied a coated body which he had used for the experiments reported in Ref. 21. With this body experiments have been performed in the Ammersee in Bavaria. Details of these experiments are reported in Ref. 22. A pity is, that these promising looking attempt had to be stopped without conclusive results because the flexible coating of the body had suffered damage during the experiments and no second test body was available.

3. INVESTIGATION OF TURBULENT WALL PRESSURE FLUCTUATIONS

As has been shown in the previous section several investigations with flexible coatings remained inconclusive with respect to the question of drag reduction. In our opinion one reason for the difficulties encountered in experiments with compliant walls is that one does not have enough knowledge of the mechanisms in a turbulent boundary layer along a rigid wall and especially that one does not have enough knowledge of pressure fluctuations beneath a turbulent boundary layer. Such pressure fluctuations certainly play an important role in the problem of interactions between turbulent flows and compliant walls. So, we have started to investigate turbulent wall pressure fluctuations in more detail. Usually, wall pressure fluctuations are measured with the help of microphones built flat into one of the flow bounding walls. Such measurements, however, give only the pressure fluctuations at one point on the wall or if several microphones are used at a few points. Emmerling, Meier and Dinkelacker^{23,24} have developed an optical method which allows the investigation of the instantaneous structure of the wall pressure field under a turbulent boundary layer. The main component of this method is a pressure transducer consisting of several hundred small elastic membranes, the displacements of which are recorded by interferometric means with a high-speed camera. As the amplitudes of the transducer membrane movements are only a small fraction (order of 0.01) of the thickness of the viscous sublayer no influence of these movements on the flow is expected. With other words: The wall can be regarded as a rigid wall. In appendix A of this paper

the method is explained and examples of measurements in a wind-tunnel are presented. The measurements show the development and convection of pressure patterns of a wide range of sizes (from larger than one boundary layer thickness δ down to 0.1δ) and with a wide range of convection velocities (from about $0.9 U_\infty$ down to about $0.2 U_\infty$, where U_∞ is the flow velocity outside the boundary layer).

These investigations are not yet in a state, such that conclusions with respect to flexible wall investigations could be drawn. It might be of interest, however, to mention the fact, that fairly small pressure patterns with fairly high amplitudes have been found which are convected downstream sometimes over fairly wide distances. Examples of such patterns can be seen from Figures 10 and 11 in Appendix A. Measurements with very small electromechanical pressure transducers confirmed the existence of these small high amplitude patterns. Figure 19 (from Ref. 23) shows results of such measurements. As can be seen from Figure 19 the RMS-values of turbulent wall pressure fluctuations increase when the microphone diameters d become smaller than about $100 \nu/u_\tau$ (ν = kinematic viscosity, u_τ = shear velocity) and this increase continues right down to the smallest transducers used, which had a diameter $d = 15 \nu/u_\tau$. This increase of RMS-values shows that the small pressure patterns have dimensions of the same order as the thickness of the viscous sublayer and that they have fairly high amplitudes. It is believed that these small patterns play an important role for the mixing process in the boundary layer and they might well be also of importance with respect to interactions between flow and flexible walls.

4. CONCLUSIONS AND RECOMMENDATIONS

1. Some of our experiments led to results which can be interpreted as drag reduction by means of flexible coatings, but in all cases there are possible alternative explanations. Our experiments therefore are not conclusive with respect to the question of drag reduction.

2. The investigations of pressure fluctuations beneath turbulent boundary layers show interesting details of the pressure fields, especially the convection of pressure patterns having a wide range of sizes and convection velocities. It is hoped that these investigations will lead to a better understanding of the processes in turbulent boundary layers with rigid as well as with flexible walls.

3. Study of the literature led to the result, that there is - to the author's knowledge - no single experiment on drag reduction by means of compliant walls which has been successfully repeated by a second investigator. As long as the basic requirement of reproducibility is not fulfilled, the whole topic must be regarded as being in an uncertain state.

4. In spite of this uncertainty the question under which conditions wall movability has a significant influence on boundary layer flow and on drag seems to be worthwhile further investigation.

5. For planning further investigation in this field the following can be suggested:

- a) Further experimental and theoretical work should be aimed mainly toward improved basic understanding of the processes. Successful application of compliant coatings for drag reduction without such understanding can hardly be expected.
- b) If further research work is planned, the complexity of the problem should be taken into account. Experiments should contain:
 - detailed measurements of the flow properties,
 - detailed measurements of the wall properties,
 - detailed measurements of the wall movements,
 - careful elimination of possible disturbing effects,
 - a thorough investigation of the reference case with rigid walls.
- c) Close contact between theoretical and experimental work should be maintained.
- d) The question of reproducibility of results should receive the necessary attention.

REFERENCES

- ¹ Gray, J.: Studies in Animal Locomotion. VI The Propulsive Powers of the Dolphin. J. exp. Biol. 13 (1936), pp. 192.
- ² Kramer, M.O.: Boundary-Layer Stabilization by Distributed Damping. J. Aero. Sci. 24 (1957), pp. 459.
- ³ Kramer, M.O.: Boundary-Layer Stabilization by Distributed Damping. J. Aero Space Sc. 27 (1960), p. 69.
- ⁴ Kramer, M.O.: Boundary-Layer Stabilization by Distributed Damping. Am. Soc. Nav. Eng. J. (Febr. 1960) pp. 25.
- ⁵ Kramer, M.O.: Boundary-Layer Stabilization by Distributed Damping. Nav. Eng. J. (May 1962), pp. 341.
- ⁶ Kramer, M.O.: The Dolphin's Secret. The New Scientist 7 (May 1960), pp. 1118.

- ⁷ Kramer, M.O.: Hydrodynamics of the Dolphin. *Advances in Hydrosience* 2 (1965), pp. 111.
- ⁸ Brooke Benjamin, T.: Fluid Flow with Flexible Boundaries. *Proc. 11th Intern. Congr. Appl. Mech. Munich 1964*. Edited by H. Görtler, Springer Berlin, Heidelberg, New York (1966) pp. 109.
- ⁹ Zimmermann, G.: Wechselwirkungen zwischen turbulenten Wandgrenzschichten und flexiblen Wänden. Max-Planck-Institut für Strömungsforschung, Göttingen, Bericht 10/1974.
- ¹⁰ Bushnell, D.M.; Hefner, J.N.; and Ash, R.L.: Effect of Compliant Wall Motion on Turbulent Boundary Layers. Lecture given at IUTAM Symposium on Structure of Turbulence and Drag Reduction, Washington, June 1976 (compare paper No. 9 of this volume).
- ¹¹ Dinkelacker, A.: Preliminary Experiments on the Influence of Flexible Walls on Boundary Layer Turbulence. *J. Sound Vib.* 4 (1966), pp. 187.
- ¹² Carstensen, H.R.: Über den Einfluß einer schallweichen Wand auf die turbulente Rohrströmung. *Acustica* 18 (1967), pp. 1.
- ¹³ Mechel, F. und Schilz, W.: Untersuchungen zur akustischen Beeinflussung der Strömungsgrenzschicht in Luft. *Acustica* 14 (1964), pp. 325.
- ¹⁴ Schilz, W.: Untersuchungen über den Einfluß biegeformiger Wandschwingungen auf die Entwicklung der Strömungsgrenzschicht. *Acustica* 15 (1965), pp. 6.
- ¹⁵ Schilz, W.: Experimentelle Untersuchungen zur akustischen Beeinflussung der Strömungsgrenzschicht in Luft. *Acustica* 16 (1965/66), pp. 208.
- ¹⁶ Großkreutz, R.: Wechselwirkungen zwischen turbulenten Grenzschichten und weichen Wänden. Mitteilungen aus dem Max-Planck-Institut für Strömungsforschung und der Aerodynamischen Versuchsanstalt, Göttingen, Nr. 53 (1971) (also Navships Translation No. 1320).
- ¹⁷ Großkreutz, R.: An Attempt to Control Boundary Layer Turbulence with Nonisotropic Compliant walls. *University Sci. J.* 1, pp. 65 (Univ. of Dar es Salam, 1975) (short english version of Ref. 16).
- ¹⁸ Viering, K.M. und Meier, G.E.A.: Zweidimensionales Schlierenverfahren zur Bestimmung der Neigungswinkel bewegter Flächen. Max-Planck-Institut für Strömungsforschung, Göttingen, Bericht 10/1972.
- ¹⁹ Dinkelacker, A. und Müller, E.-A.: Strömungsakustische Untersuchungen turbulenter Wasserströmungen im Hinblick auf Geräuschminderung. Max-Planck-Institut für Strömungsforschung, Göttingen, Bericht 110/1973.
- ²⁰ Dinkelacker, A.: Measurements and Observations on Flow Noise in Water-Filled Plastic Tubes. *Acustica* 12 (1962), pp. 341.
- ²¹ Kramer, M.O.: Die Widerstandsverminderung schneller Unterwasserkörper mittels künstlicher Delphinhaut. *Jahrbuch d. Deutschen Gesellschaft für Luft- und Raumfahrt (DGLR)* 1969, pp. 102.
- ²² Dinkelacker, A.: Bericht über einen Versuch zur Wiederholung von Kramers Messungen zur Widerstandsverminderung schneller Unterwasserkörper mittels künstlicher Delphinhaut. Max-Planck-Institut für Strömungsforschung, Göttingen, Bericht 2/1971.
- ²³ Emmerling, R.: Die momentane Struktur des Wanddruckes einer turbulenten Grenzschichtströmung. Mitteilungen aus dem Max-Planck-Institut für Strömungsforschung und der Aerodynamischen Versuchsanstalt, Göttingen, Nr. 56 (1973). [English translation: Max-Planck-Institut für Strömungsforschung, Göttingen, Bericht 9/1973.]
- ²⁴ Emmerling, R.; Meier, G.E.A. und Dinkelacker, A.: Investigation of the Instantaneous Structure of the Wall Pressure under a Turbulent Boundary Layer Flow. NATO-AGARD Conference Proceedings No. 131 on "Noise Mechanisms", pp. 24-1, London: Technical Editing and Reproduction, Ltd., March 1974.

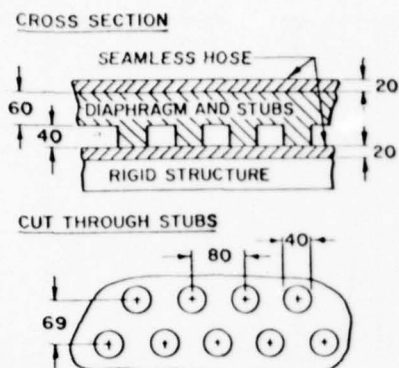


Figure 1 Ducted rubber coating (from Ref. 3, dimensions in 1/1000 of an in.)

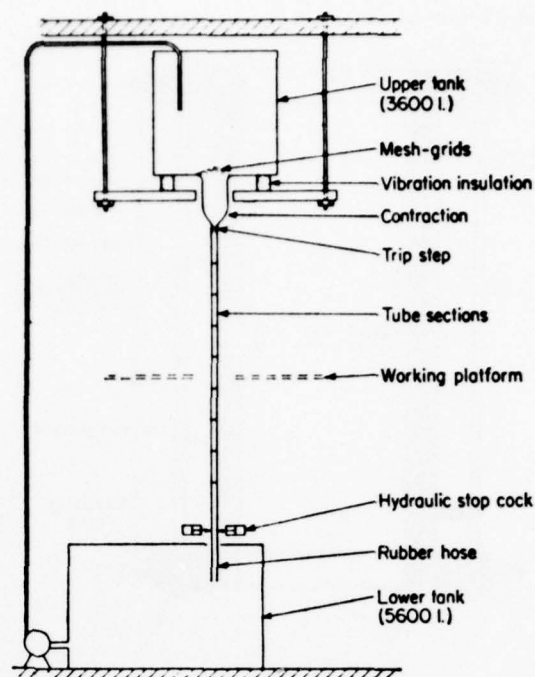


Figure 3 Arrangement for pipe flow investigation (from Ref. 11)

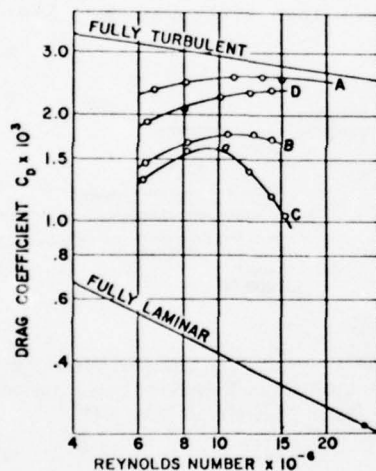


Figure 2 The drag coefficient of various models as a function of the Reynolds Number (from Ref. 3). Curve A is the rigid reference model, and Curves B, C, and D are fully coated models with a stiffness of the coating on the cylindrical section (B = 1,600 lbs. per cu. in., C = 800 lbs. per cu. in., and D = 600 lbs. per cu. in.)

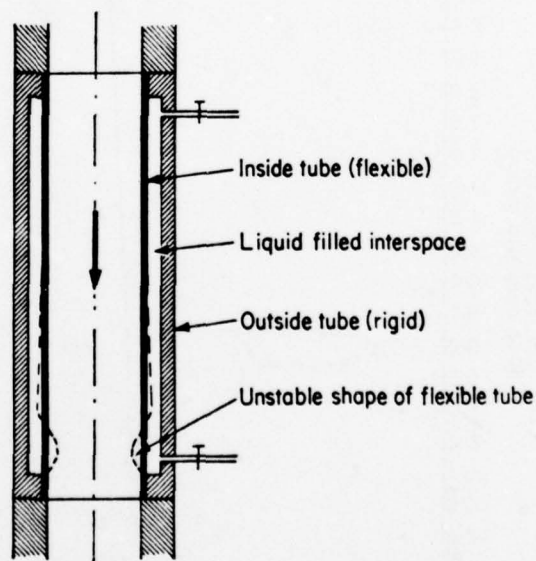


Figure 4 Flexible tube section, showing instability (from Ref. 11)

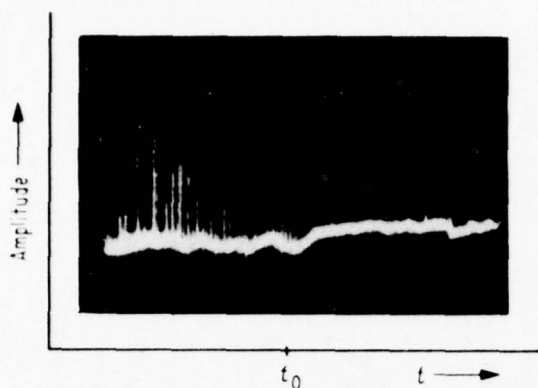


Figure 10 Suppression of turbulence by sound (from Ref. 13, ordinate: hot wire signal, abscissa: time, whereby at time $t = t_0$ sound was switched in).

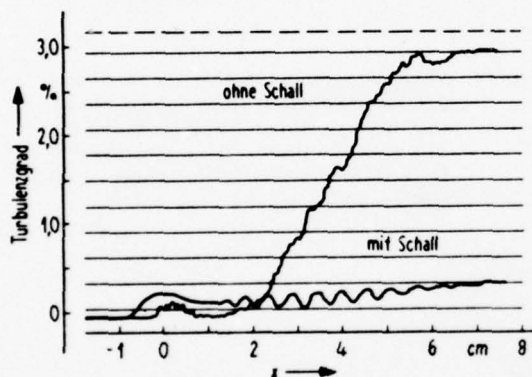


Figure 11 Suppression of turbulence by sound (from Ref. 13, $x = 0$ is leading edge of plate, distance of hot wire probe 0.5 mm from plate, ohne Schall = without sound, mit Schall = with sound of 4 kHz).

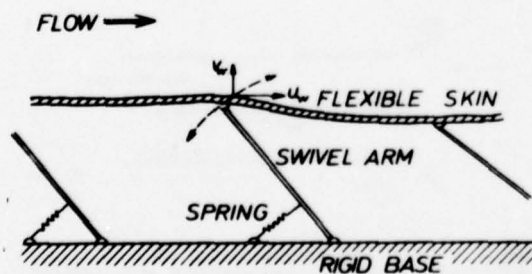


Figure 12 Sketch of a compliant wall with restricted surface mobility, illustrating the principle proposed to ensure positively correlated surface motion $u_w \cdot v_w > 0$ (from Ref. 17).

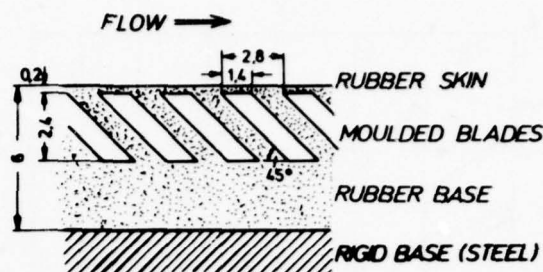


Figure 13 Cross-section of a small part of compliant coating with nonisotropic elasticity (dimensions in millimeters, from Ref. 17).

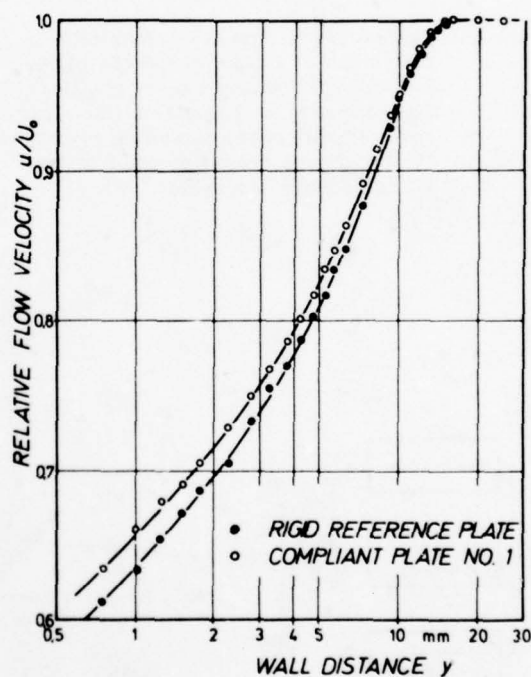


Figure 14 Normalized velocity profiles of flow over a compliant plate and over a rigid reference plate (from Ref. 17).

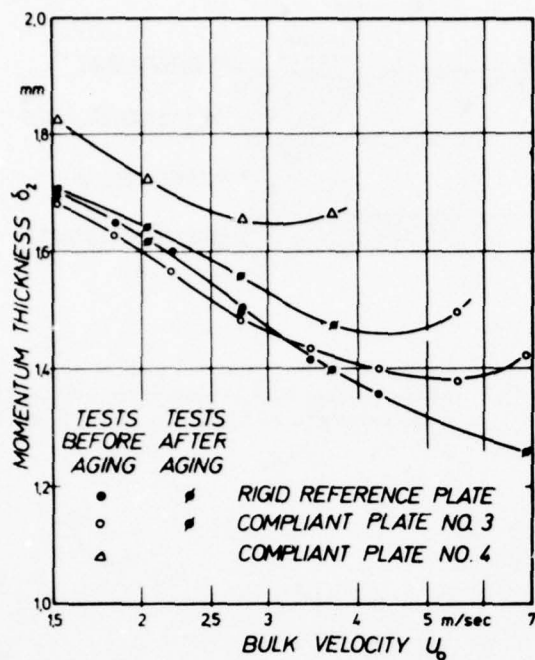


Figure 15 Momentum thickness of compliant plates and of a rigid reference plate as calculated from velocity profiles. The decrease in momentum thickness obtained with fresh compliant plates is lost after 6 weeks of aging of the silicon rubber (from Ref. 17).

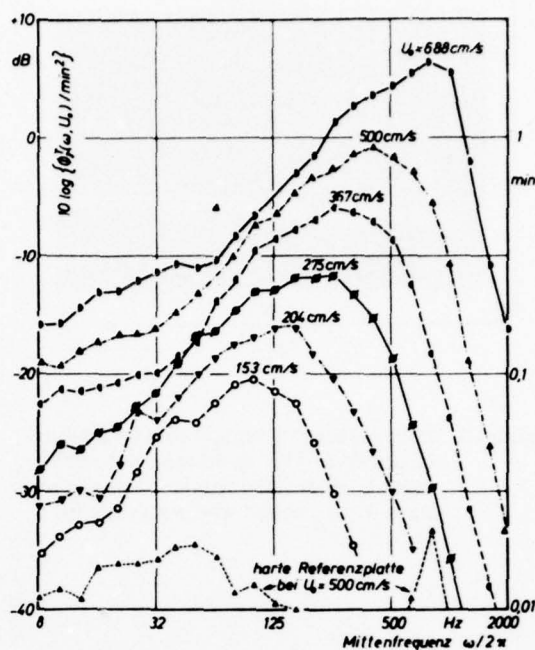


Figure 17 Frequency spectra (1/3-octave bands) of flow induced angular oscillations of a small mirror fixed on the surface of a flexible plate (from Ref. 16; U_0 = flow velocity of the water outside the boundary layer).

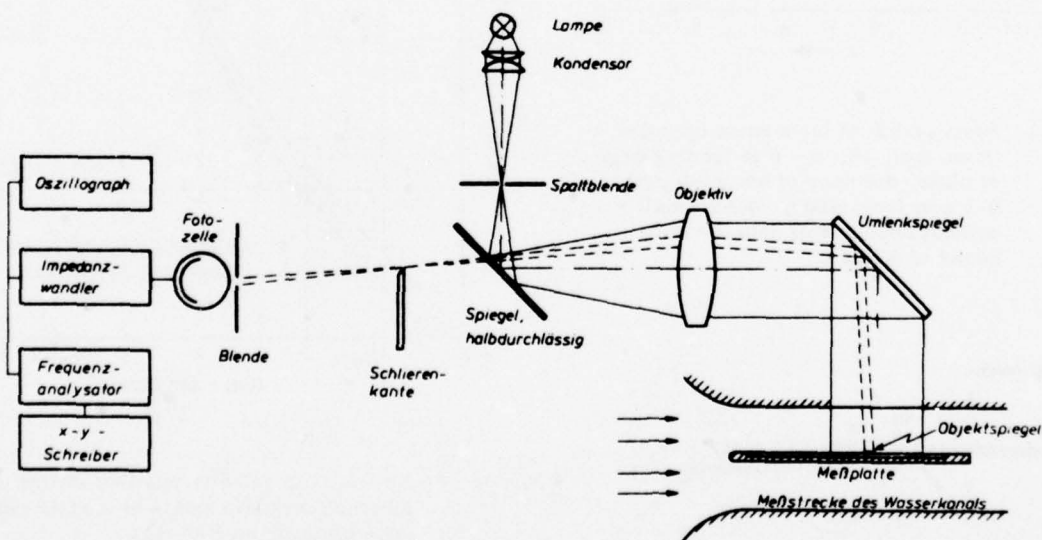


Figure 16 Sketch of a Schlieren arrangement for the measurement of surface oscillations of a flexible plate in a water tunnel (from Ref. 16; at the surface of the flexible plate a small mirror is fixed).

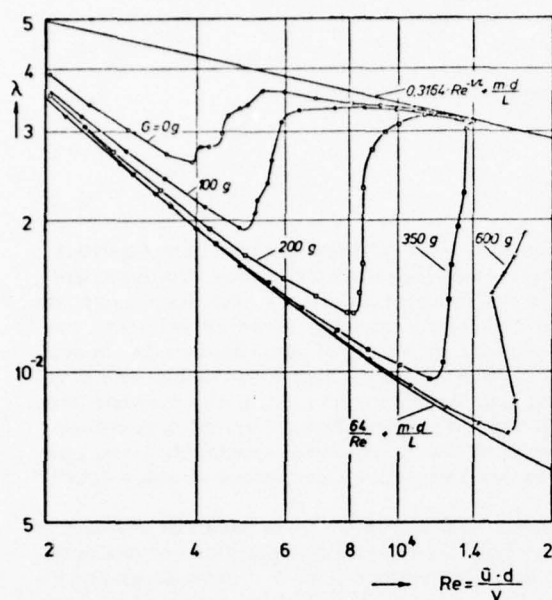


Figure 18 Friction factor of a vertically suspended rubber tube (from Ref. 19; tube length $L = 3.9$ m, inner tube diameter $d = 6$ mm. \bar{u} = mean velocity in the tube, m = correction factor for tube inlet flow (compare: E. Bender: Druckverlust bei laminarer Strömung im Rohreinlauf. Chem. Ing. Tech. 41 (1969) pp. 682), G = weight of metal block at downstream tube end, controlling straightness of the tube).

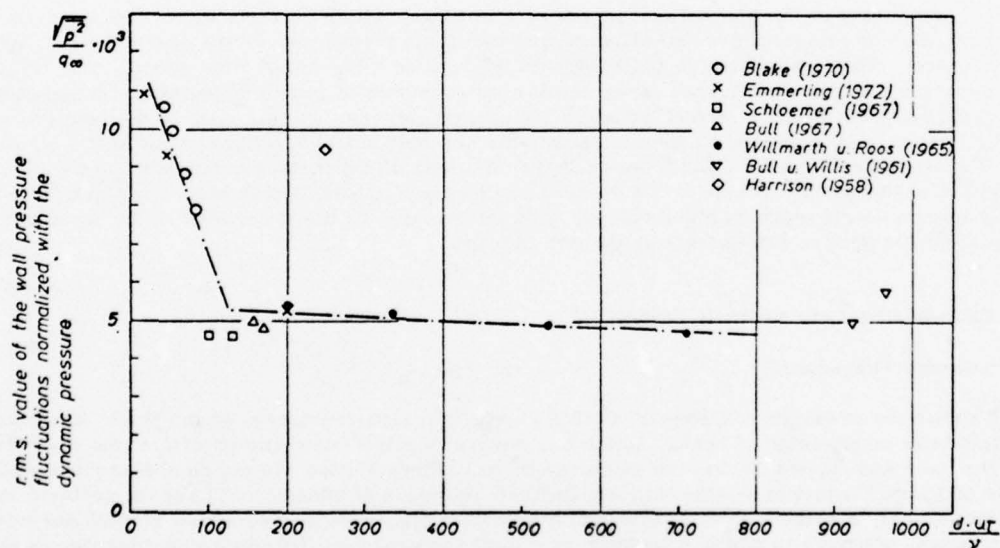


Figure 19 Dependence of the normalized RMS-values of turbulent wall pressure fluctuations on the factor $d \cdot u_{\tau} / \nu$ (from Ref. 23; d = transducer diameter, u_{τ} = shear velocity, ν = kinematic viscosity, q_{∞} = dynamic pressure outside the boundary).

APPENDIX

INVESTIGATION OF PRESSURE FLUCTUATIONS BENEATH A TURBULENT BOUNDARY LAYER
BY MEANS OF AN OPTICAL METHOD*

A. Dinkelacker, M. Hessel, G.E.A. Meier, G. Schewe
Max-Planck-Institut für Strömungsforschung, Göttingen

I. INTRODUCTION

During recent years in Göttingen, as well as in Southampton, several experimental investigations with flow over compliant walls have been performed. These include three investigations with turbulent pipe flow¹⁻³, one with turbulent flow over a flat plate⁴ and one in which an attempt was made to repeat an experiment of Kramer with a rising body technique⁵. For different reasons, these experiments remained inconclusive with respect to the question of drag reduction by means of compliant walls. In our opinion one reason for the difficulties encountered in experiments with compliant walls is that one does not have enough knowledge of the mechanisms in a turbulent boundary layer and especially that one does not have enough knowledge of pressure fluctuations beneath a turbulent boundary layer. Such pressure fluctuations certainly play an important role in the problem of interactions between turbulent flows and compliant walls. So, we have started to investigate turbulent wall pressure fluctuations in some detail.

Usually, wall pressure fluctuations are measured with the help of microphones built flat into one of the flow bounding walls. Such measurements, however, give only the pressure fluctuations at one point on the wall or if several microphones are used at a few points. Emmerling et al.^{6,7} have developed a new optical method which allows the investigation of the wall pressure field and of its temporal changes. In the following, the method and the experimental arrangements are briefly explained and some results of experiments performed in a low speed wind-tunnel are reported.

II. THE METHOD

The main component of the method is a pressure transducer which consists of several hundred small elastic membranes. The membranes are silvered and the whole transducer forms one mirror of a Michelson-interferometer. This transducer is built flat into the wall of a low speed wind-tunnel. The turbulent pressure fluctuations in the wind-tunnel cause small displacements of the membranes and these displacements are recorded with the interferometer and a high speed camera. No influence of the membrane movements on the flow is to be expected as the displacements are only small fractions of the viscous sublayer thickness. The films are evaluated and from each frame a map of the instantaneous pressure distribution over the field of observation (here 50 mm x 30 mm) can be constructed. These maps, which are comparable to the well-known isobaric maps in meteorology, give information on the processes in the turbulent boundary layer without the need to introduce a probe into the flow.

III. THE EXPERIMENTAL ARRANGEMENTS

A. The Pressure Transducer

Fig. 1 shows the pressure transducer. A thin elastic foil (approximately 35 μ m thick) is stretched across a rigid base constructed of brass, which has several hundred small holes of 2.5 mm diameter. The surface of the base was lapped so that the deviation from flatness across the entire surface was reduced to the order of 1 μ m. On this base, the thin foil is fixed by means of adhesive. The main problem in producing the transducer is obtaining a thin foil with a low elasticity modulus and with a smooth surface and uniform thickness, accurate to within a fraction of a light wave-length. This extreme accuracy is necessary because, otherwise even without flow, a dense interference fringe pattern would appear. The foils used here were made of silicone rubber and silvered with the help of a vacuum coating device (for details see Ref. 6). The pressure transducer was fixed in a metal ring and together with this ring mounted flush in the wall of the wind-tunnel. Small holes were drilled in the ring to allow for pressure equalization between the wind-tunnel and the chamber behind the membranes.

Static calibration of the transducer was done by applying a static pressure difference to the membranes. Fig. 2 shows that the number of interference fringes (usually concentric rings) occurring on a membrane is very nearly proportional to the static pressure applied. Changes in the fringe pattern of about 0.25 fringes (corresponding to about 1 μ bar) can be evaluated. Dynamic calibration was accomplished with a loudspeaker and two calibrated microphones. Fig. 3 shows the frequency response of one transducer membrane. It should be noted that this relatively flat frequency response was only achieved after placing

* Oral version was presented by A. Dinkelacker at IUTAM Symposium "Structure of Turbulence and Drag Reduction" Washington DC, 7.-12.6.1976. The paper is scheduled for publication in the Proceedings of the IUTAM Symposium as a supplement to an issue of The Physics of Fluids.

a damping layer (silk cloth) at the rearside of the base plate (compare Fig. 1). Without this damping the membranes showed a sharp resonance peak at about 1 kHz. The equality of the different transducer membranes was checked with the help of the interferometer. In fact, the membranes of the transducer used here showed rather low inequalities.

The spatial resolution of the transducer is determined by the diameter of the individual membranes which was $d = 2.5$ mm here. With the flow used this diameter corresponds to 0.08δ or to $57 \nu / u_\tau$ where δ is the boundary layer thickness, ν is the kinematic viscosity, and u_τ is the shear velocity. Under certain circumstances one can draw conclusions even on pressure patterns which are smaller than the transducer. These evaluations, however, in which details of the shape of the fringe pattern, e.g., "S" shape, are taken into account only give qualitative results. An additional problem encountered was that the thin rubber foils lose their tension after periods of a month or so. For this reason, before each run, the static calibration of the membranes had to be repeated.

B. The Wind-Tunnel

The arrangement is shown in Fig. 4. The test section of the wind-tunnel has a cross section of 200 mm x 100 mm and a length of 2.4 m. In the inlet of the tunnel two sets of drinking straws were arranged as flow smoothing devices. The flow is driven by suction and controlled by a sonic nozzle. Great care was taken to reduce noise and vibrations in the whole arrangement. The tunnel is of heavy construction with walls of cast aluminium about 20 mm thick. All the parts lying within the dotted lines shown in Fig. 4 are rigidly connected and elastically suspended on springs. The fundamental frequency of this system is less than 1 Hz. Furthermore, the sonic nozzle was especially designed in order to produce low noise levels. The outside casing of the nozzle is constructed with double walls. A sound absorber is mounted downstream of the nozzle (absorber B in Fig. 4). In principle, a sonic nozzle does not radiate sound upstream, but, in practice, it still produces some noise in the upstream direction (flow noise in the convergent area, transmission in the flow boundary layer, transmission in the walls of the nozzle). To eliminate these influences the sonic nozzle is connected to the test section only with a soft rubber gasket and a specially designed sound absorber (absorber A in Fig. 4). Noise in the laboratory is also reduced as far as possible.

The coordinate system is chosen so that the origin lies in the middle of the transducer surface. The positive x axis points in the flow direction, the positive y axis is normal to the transducer and the z axis points along the wall in the spanwise direction forming a right-handed system with the other axes.

C. The Optical Apparatus

The arrangement of the optical apparatus is also shown in Fig. 4. The individual parts of the interferometer are mounted on a stable steel frame. A 100-W super pressure mercury lamp serves as the light source. Passing through an iris, an interference filter ($\lambda = 0.547 \mu\text{m}$) and a collimator (100 mm diameter), the light reaches the beam splitter and from there it goes partly to the pressure transducer and partly to the reference mirror. As can be seen in Fig. 4, one interferometer beam passes through the turbulent flow twice. Since the refractive index of air is dependent upon density, sufficiently large pressure fluctuations in the flow can change the optical path of the beam. This could lead to errors in the evaluation of the membrane displacement. It can be shown, however, that at a flow velocity of 8.5 m/sec, these disturbances are negligibly small. Photographs of the interference patterns were taken with a high-speed camera (Fastax WF-4m). The frame rate at any point on the film can be determined with the aid of timing marks (1 milli second) on the edge of the film.

D. The Flow

For the experiment reported here the sonic nozzle was adjusted so that the centerline velocity in the tunnel at the position of the transducer was $U_\infty = 8.5$ m/sec. In this case the flow was the "tunnel inlet flow" type with boundaries becoming turbulent immediately after the drinking straws (see Fig. 4). Characteristic qualities of the flow used in this investigation are shown in Figs. 5 to 8. For the position of the pressure transducer the following parameters are obtained: Centerline velocity $U_\infty = 8.5$ m/sec, dynamic pressure $q_\infty = 420 \mu\text{bar}$, shear velocity $u_\tau = 0.34$ m/sec, sublayer length scale $\nu / u_\tau = 44 \mu\text{m}$, boundary layer thickness $\delta = 30$ mm, momentum thickness $\theta = 3.5$ mm, Reynolds number $Re_\theta = 2 \times 10^3$, displacement thickness $\delta^* = 4.6$ mm, pressure gradient $dp/dx = -53 \mu\text{bar per meter}$ or $0.006 q_\infty$ over the length of the transducer observation field.

E. Film Evaluation

Fig. 9 shows one individual frame from a film which was taken at a framing speed of about 7000 frames per second. The field of observation is about 50 mm x 30 mm and contains patterns of about 200 small circular membranes. With the help of the calibration curve (Fig. 2) and with the help of a so-called base fringe pattern, the amplitude and the direction of the membrane displacement can be determined. The base fringe pattern is produced by turning the reference mirror of the interferometer in such a way that with no pressure difference at the membranes (i.e., with no flow in the tunnel) approximately two interference

fringes, extending in the lengthwise direction, appear on each membrane. For the evaluation, it is necessary to determine the difference between the instantaneous fringe pattern on a membrane and the base fringe pattern of the same membrane. This part of the evaluation makes the evaluation process rather difficult and time consuming and up to now has made automatic film evaluation unsuccessful. As one can see in Fig. 9 some of the fringes have an S shape which indicated a local pressure gradient on the membrane. Absolute evaluation in this case is difficult because both the calibration curve and the frequency response curve are only valid for symmetric displacements of the membranes.

The evaluated pressure readings can be represented and processed in different ways. One way is to plot pressure maps as shown in Fig. 10. In these maps the small crosses show the positions of the individual membranes. The lines are isobaric lines connecting points of equal pressure. (The corners in the isobaric lines have no physical significance, they are just a consequence of the plotting process.) Solid lines are lines of overpressure and zero pressure. Dashed lines are lines of underpressure. Zero pressure is defined so that the average over the 198 membranes of each map is zero. The pressure differences between adjacent lines in Fig. 10 correspond to 0.5 fringes ($= 1.75 \mu\text{bar}$ or $0.0042 q_{\infty}$).

Two more questions seem to be of importance with respect to the confidence one can have in the pressures evaluated. The first question is whether the movements of the transducer membranes influence the adjacent flow. It is assumed that this is not the case, because the membrane displacements are very small compared with the dimensions of the viscous sublayer (e.g., 6 fringes correspond to a membrane displacement of $y = 1.64 \mu\text{m}$ or $y^+ = 0.04$). The second question is whether the high frequency parts of the fluctuations are represented properly. If one compares the frequency spectrum measured with the help of the microphone (Fig. 8) and the frequency response curve of the membranes (Fig. 3), it can be concluded that no serious difficulties arise, because the maximum of the electrically measured frequency spectrum is at about 100 Hz and the membranes operate with constant sensitivity up to about 700 Hz.

IV. RESULTS

With the method and experimental arrangements described in the previous sections one can achieve insight into a pressure field beneath a turbulent boundary layer. The evaluation of the fringe patterns, however, is at the present stage still a rather lengthy process. At present we are still evaluating and processing results of a film taken by Emmerling in 1972. As of now, 208 consecutive frames of this film have been evaluated containing about 40 000 pressure readings. Some examples from this material will be reported in the following text. The examples show clearly that the method works. Furthermore, it is believed that the reported examples are not just arbitrary events in the investigated flow, but that they are typical for turbulent boundary layers. The proof, however, that this is so still has to be established, as the number of observations is still rather small. For this reason, the results reported here have to be regarded as preliminary.

Fig. 10 shows 20 consecutive pressure maps. These maps contain the information of frame Nos. 58 to 96 out of the above-mentioned film whereby for brevity only every second map is printed. The time difference between consecutive maps is $\Delta t = 0.28$ milliseconds or $\Delta t^+ = 2$, if made nondimensional with ν/u_{τ}^2 . The flow direction is from left to right. The flow velocity and all other data are as reported in Sec. III D.

Fig. 11 shows the spatial pressure distribution of one row of the transducer membranes for 208 temporal consecutive frames of the same film (9th row, frame Nos. 1 to 208). The row consists of 17 membranes lying in the flow direction one behind the other. Some of the represented curves therefore are "cross cuts" through the fields represented in Fig. 10. The time difference between consecutive curves in Fig. 11 is one half that in the previous figures, i.e., $\Delta t = 0.14$ milliseconds or $\Delta t^+ = 1$.

In Fig. 11 one can easily recognize the downstream convection of some pressure patterns. Since it is not always clear what should be regarded as a "pattern" we will explain for each example separately what is meant by the word pattern. Usually, individual patterns can be followed over distances of about half the length of the observation field. In some cases, however, one can follow individual patterns through the whole field of observation from the first to the last membrane.

The first example (pattern A) is a structure of this type. Pattern A (in Fig. 11 drawn in ink with heavy solid lines) consists of an area of overpressure followed by an area of underpressure. The pattern enters the observation field in frame No. 26 and can be followed until it leaves the observation field in frame No. 89. The convection velocity of this pattern (characterized by the zero between its two parts) is found to be $U_c = 0.76 U_{\infty}$. The extensions of pattern A are of the order of 0.5δ . Furthermore, one can see that the lengthwise extension of the overpressure area of the pattern is increasing with time [e.g., in frame No. 30 the overpressure area of the pattern has a lengthwise extension of 2 membrane distances ($= 6 \text{ mm}$) while in frame No. 70 the same extension has grown to 4 membrane distances ($= 12 \text{ mm}$)]. In the Fig. 10 pattern A can also be observed. In the pressure maps (maps 58 to 80) a few isobars of this pattern are drawn in ink [for the overpressure part of the pattern the $+3.5 \mu\text{bar}$ line and the $+7.0 \mu\text{bar}$ line (both heavy solid lines) for the underpressure part the $-3.5 \mu\text{bar}$ line and the $-7.0 \mu\text{bar}$ line (both heavy dotted lines)]. In addition to the convection effect in these maps the extensions of the pattern can clearly be seen. The fact that the pattern is observed throughout the field of observation means that this structure exists over a length of at least 1.6δ or $1100 \nu/u_{\tau}$.

The second example (pattern B) is again an area of overpressure followed by an area of underpressure. (In frame Nos. 49 and 60 of Fig. 11 pattern B is marked with heavy dotted lines.) As can be seen from Fig. 11 and also from Fig. 10 the extensions of pattern B are only of the order of two membrane distances and the lifetime is rather short (the pattern can be recognized in Fig. 11 from frame 49 to frame 62). Furthermore, one can see that pattern B reaches a rather high pressure amplitude and shows large pressure gradients. In frame No. 61 (Fig. 11) the overpressure of pattern B is $17 \mu\text{bar}$ ($= 0.04 q_\infty$). Two frames later the pattern has disappeared. For the spatial gradient, a maximum $dp/dx = 25 \mu\text{bar}$ over a distance of 3 mm is found. Recalculated this would be $0.60 q_\infty$ over a distance of δ . Another interesting fact is that this pattern hardly changes its position while it is observed. Evaluating its shift (from frame 49 to frame 62 it shifts only by 3 mm) a convection velocity as low as $U_c = 0.2 U_\infty$ is found. The low convection velocity, the small extensions, and the short lifetime of pattern B suggest that pattern B is related to a local flow process of short duration occurring rather close to the wall.

The third example shows the convection of a large area of underpressure (pattern C). In Fig. 10 this area is shaded. The boundaries are zero pressure lines. As can be seen, with increasing frame number, the shaded area moves to the right, i.e., in the flow direction. In the lengthwise direction, the area has an extension of the order of the boundary layer thickness δ and in the spanwise direction the extension must be even larger than δ . (This can be concluded because beginning in frame 80 pattern B touches both lengthwise boundaries of the observation field, these boundaries are at a distance of 30 mm which is equal to δ). The convection velocity of pattern C is about $U_c = 0.85 U_\infty$. In the maps one can observe how the underpressure area as it travels sometimes joins with or separates from other areas of underpressure (compare maps No. 66 and 68) or overtakes smaller, slower moving areas of overpressure which then become peninsulae or islands in the underpressure area. The lifetime of pattern C is evidently considerably larger than the time of its stay in the observation field. The fact that the whole underpressure area is inclined at an angle of about 45° to the flow direction is not believed to be typical. In other evaluations different angles have been obtained. The large extensions of pattern C, the high convection velocity and the long lifetime suggest that this pattern might be related to a large scale flow process occurring in a region of the boundary layer which is farther away from the wall.

V. SPECULATIONS CONCERNING THE FLOW FIELDS

From the information given in the previous section one can speculate what sort of flows could have generated these pressure patterns. In Fig. 12 a fairly simple model is given in which flow in curved streamtubes is related to nearby pressure fields. According to this model the large scale underpressure area (pattern C) could be related to a spatially extended flow with streamlines bent towards the wall [see Fig. 12(a)]. The medium scale pressure pattern (pattern A) in which an area of overpressure is followed by an area of underpressure could be related to flow with doubly curved streamlines as shown in Fig. 12(c). Pattern B with its very low convection velocity ($U_c = 0.2 U_\infty$), could also be related to flow with doubly curved streamlines, but occurring very close to the wall [see Fig. 12(d)].

The ideas given in this last section are at present only speculations. However, some numerical calculations performed by Schumann^{8,9}, in which turbulent channel flow is simulated with the help of a computer, show pressure fields which are, to some extent, similar to the pressure fields presented in Sec. IV and show flow fields which are to some extent similar to the speculative flow patterns given in this section. Furthermore, it seems to be possible to connect the ideas given here to visual observations of flow fields as given, e.g., by Nychas, et al.¹⁰ or by Falco¹¹.

VI. CONCLUDING REMARKS

- a) The examples show that the method works, and that it is possible to gain, with this method, detailed information on the pressure field beneath a turbulent boundary layer without the need to introduce a probe into the flow.
- b) Large scale pressure patterns are observed which have lengthwise extensions of the order of the boundary layer thickness δ and spanwise extensions larger than δ . Convection velocities of these patterns up to $0.9 U_\infty$ are found.
- c) Smaller scale pressure patterns are observed which have sometimes extensions right down to the resolution limits of the transducer (0.08δ or $57 \nu/u_\tau$). The downstream movements of these patterns sometimes can be followed over the whole field of observation which is 1.6δ or $1100 \nu/u_\tau$. Convection velocities of these patterns were observed down to $0.2 U_\infty$.
- d) The proof that the observed structures are typical for turbulent boundary layers is not yet established. Therefore the results have to be regarded as preliminary.
- e) Further efforts are now directed toward the following aims: (1) Continuation and improvement of film evaluation. (2) Development of models for the generation of the observed pressure patterns. (3) Examination of these models with the help of conventional techniques (hot wires, electromechanical pressure transducers, computer analysis). (4) Establishment of the connections between the observations

made with this method and the large set of data on turbulent wall pressure fluctuations gained with electro-mechanical transducers as summarized by Willmarth¹². (5) Finally it is hoped to return to the question of how compliant coatings could influence turbulent boundary layer flow.

REFERENCES

- ¹ Dinkelacker, A.: Measurements and Observations on Flow Noise in Water-Filled Plastic Tubes. *Acustica* 12, 341 (1962).
- ² Dinkelacker, A.: Preliminary Experiments on the Influence of Flexible Walls on Boundary Layer Turbulence. *J. Sound Vib.* 4, 187 (1966).
- ³ Carstensen, H.R.: Über den Einfluß einer schallweichen Wand auf die turbulente Rohrströmung. *Acustica* 18, 1 (1967).
- ⁴ Großkreutz, R.: Wechselwirkungen zwischen turbulenten Grenzschichten und weichen Wänden. *Mitteilungen aus dem Max-Planck-Institut für Strömungsforschung und der Aerodynamischen Versuchsanstalt Göttingen*, Nr. 53 (1971), [Navships Translation No. 1320, and in a short version: *University Sci. J.* 1, 65 (Univ. of Dar es Salam, 1975)].
- ⁵ Dinkelacker, A.: Bericht über einen Versuch zur Wiederholung von Kramers Messungen zur Widerstandsverminderung schneller Unterwasserkörper mittels künstlicher Delphinhaut. *Max-Planck-Institut für Strömungsforschung, Göttingen*, Bericht Nr. 2 (1971).
- ⁶ Emmerling, R.: Die momentane Struktur des Wanddruckes einer turbulenten Grenzschichtströmung. *Mitteilungen aus dem Max-Planck-Institut für Strömungsforschung und der Aerodynamischen Versuchsanstalt, Göttingen*, Nr. 56 (1973), [English translation: *Max-Planck-Institut für Strömungsforschung, Göttingen*, Bericht Nr. 9 (1973)].
- ⁷ Emmerling, R.; Meier, G.E.A.; and Dinkelacker, A.: Investigation of the Instantaneous Structure of the Wall Pressure under a Turbulent Boundary Layer Flow. *NATO-AGARD Conference Proceedings No. 131 on "Noise Mechanisms"* p. 24-1, London: Technical Editing and Reproduction, Ltd., March 1974.
- ⁸ Schumann, U.: Subgrid Scale Model for Finite Difference Simulations of Turbulent Flows in Plane Channels and Annuli. *J. Comput. Phys.* 18, 376 (1975).
- ⁹ Schumann, U.: (private communication).
- ¹⁰ Nychas, S.G.; Hershey, H.C.; and Brodkey, R.S.: A Visual Study of Turbulent Shear Flow. *J. Fluid Mech.* 61, 513 (1973).
- ¹¹ Falco, R.E.: Some Comments on Turbulent Boundary Layer Structure Insert from the Movements of a Passive Contaminant. *AIAA Paper No. 74-99* (1974).
- ¹² Willmarth, W.W.: Pressure Fluctuations beneath Turbulent Boundary Layers. *Annual Review of Fluid Mechanics*, edited by M. Van Dyke, W.G. Vincenti, and J.V. Wehausen (*Annual Rev. Inc. Palo Alto, California*, 1975) Vol. 7, p. 13.

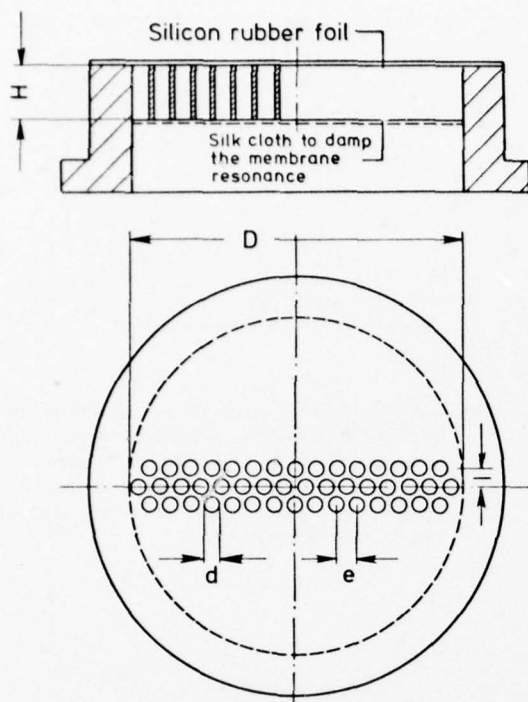


Figure 1 Pressure transducer ($D = 97$ mm, $H = 6$ mm, $d = 2.5$ mm, $e = 3$ mm, $l = 2.6$ mm).

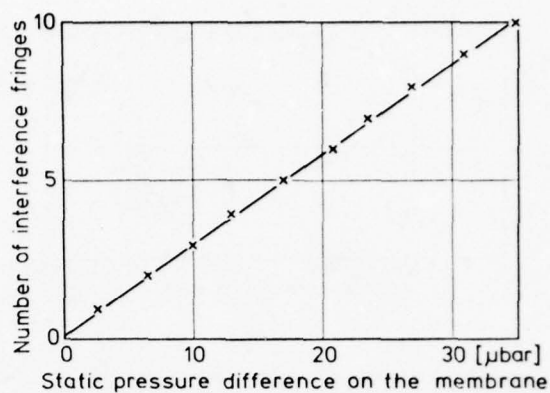


Figure 2 Calibration curve for the membranes (light wave length $\lambda = 0.547 \mu\text{m}$).

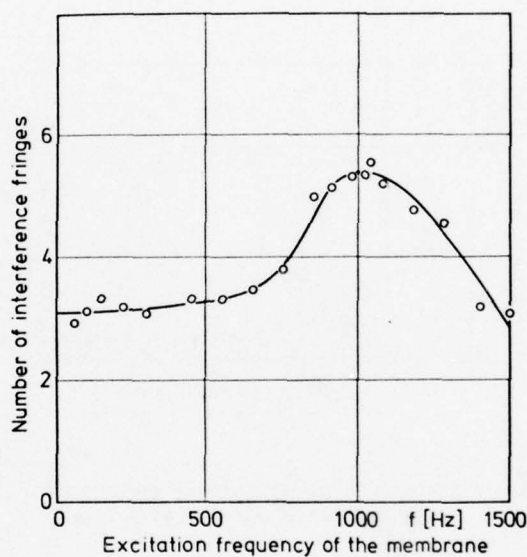


Figure 3 Frequency response of the membranes (transducer with silk cloth for damping).

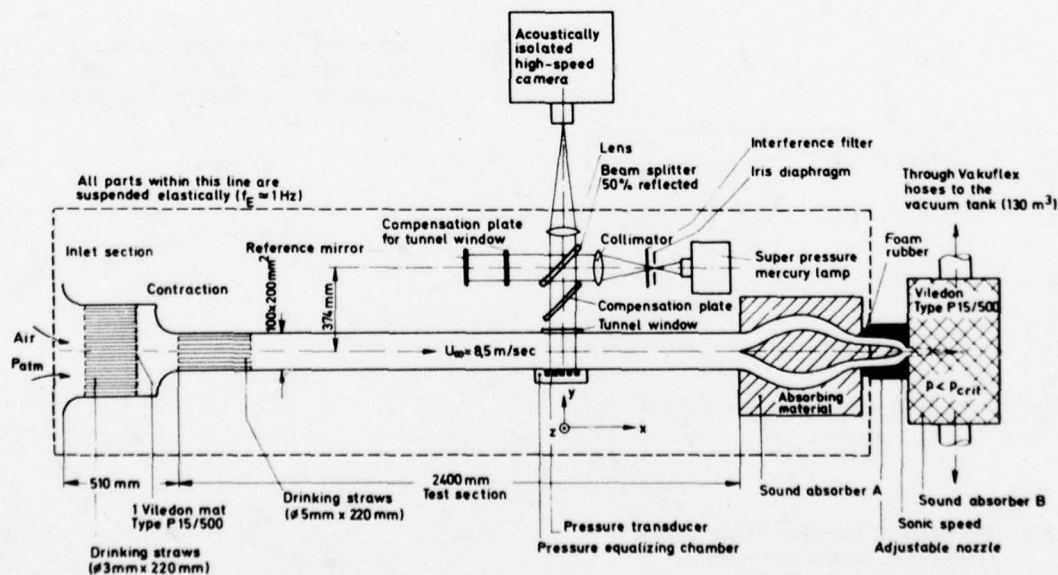


Figure 4 Experimental facility.

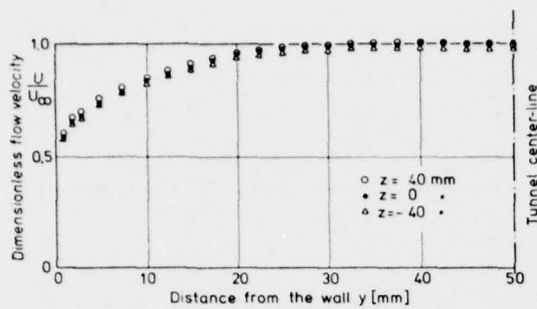


Figure 5 Velocity distributions in the test section of the wind-tunnel (measured with a Pitot tube at $x = -150$ mm, $U_\infty = 8.3$ m/sec).

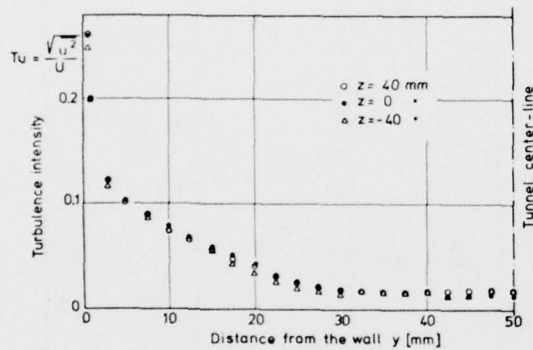


Figure 6 Dimensionless velocity distribution (recalculated values from Fig. 5).

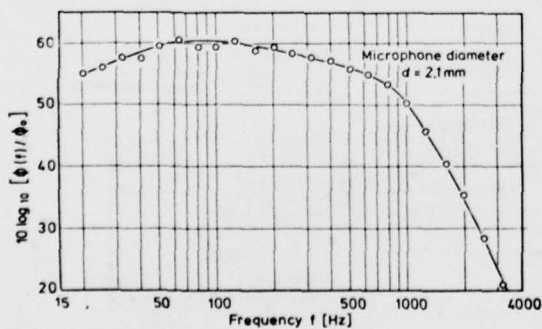


Figure 7 Turbulence intensity distribution (measured with a hot wire at $x = -150$ mm, $U_\infty = 8.3$ m/sec).

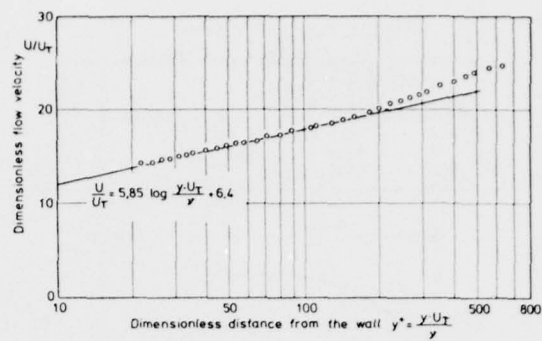


Figure 8 Spectral density of wall pressure fluctuations relative to a reference spectral density ϕ_0 of $(2 \times 10^{-4} \mu \text{ bar})^2/\text{Hertz}$. (Measured with a microphone mounted flush in the tunnel wall at the position of the optical transducer.)



Figure 9 Interference fringe pattern of one frame of a film taken with $U_\infty = 8.5$ m and a frame rate of 7000 frames per second.

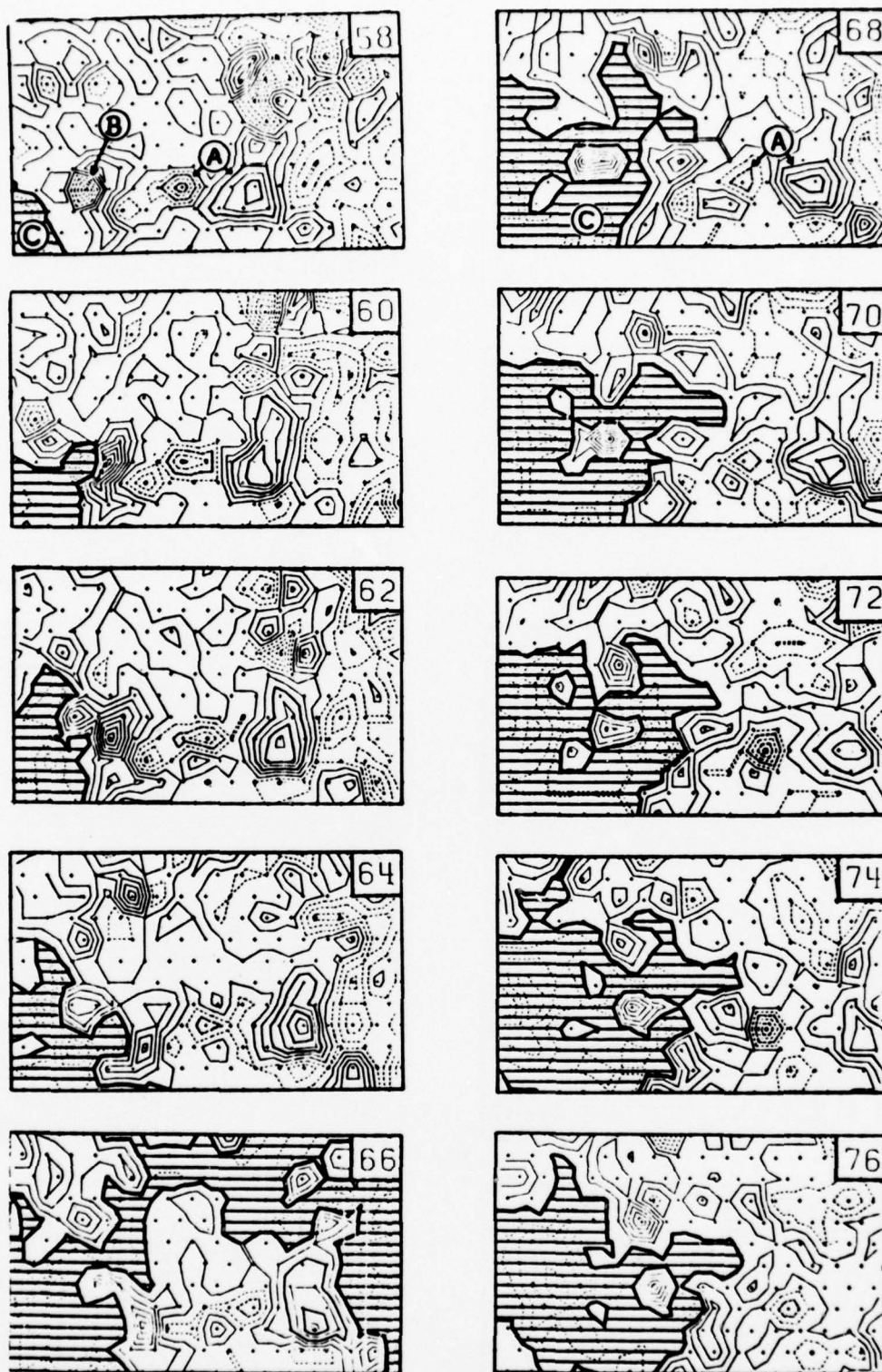
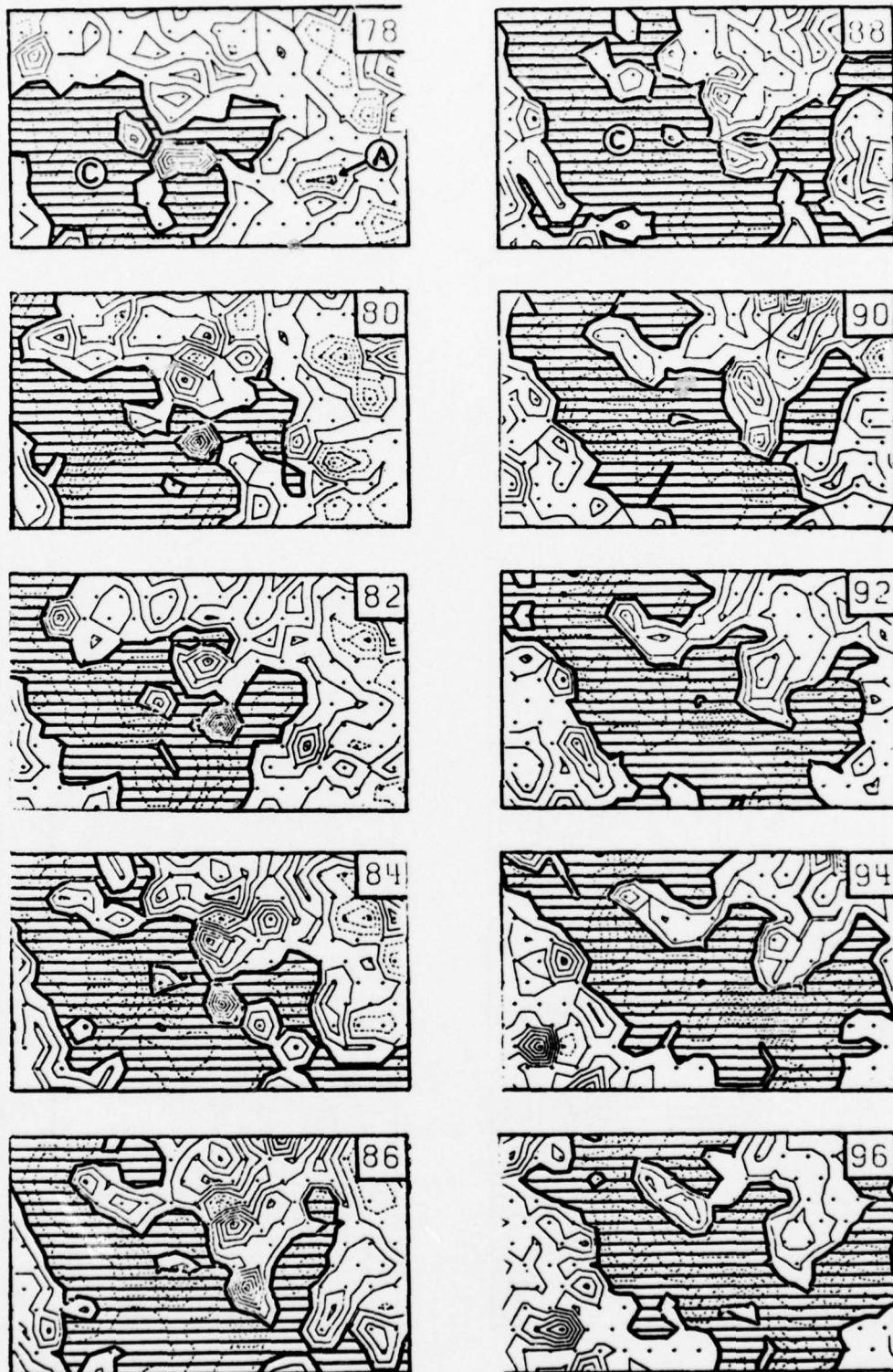


Figure 10 Sequence of consecutive pressure distributions. (Flow from left to right, flow velocity $U_{\infty} = 8.5$ m/sec, time between consecutive maps $\Delta t = 0.28$ msec, field of observation 50 mm x 30 mm.)



Continuation of Figure 10

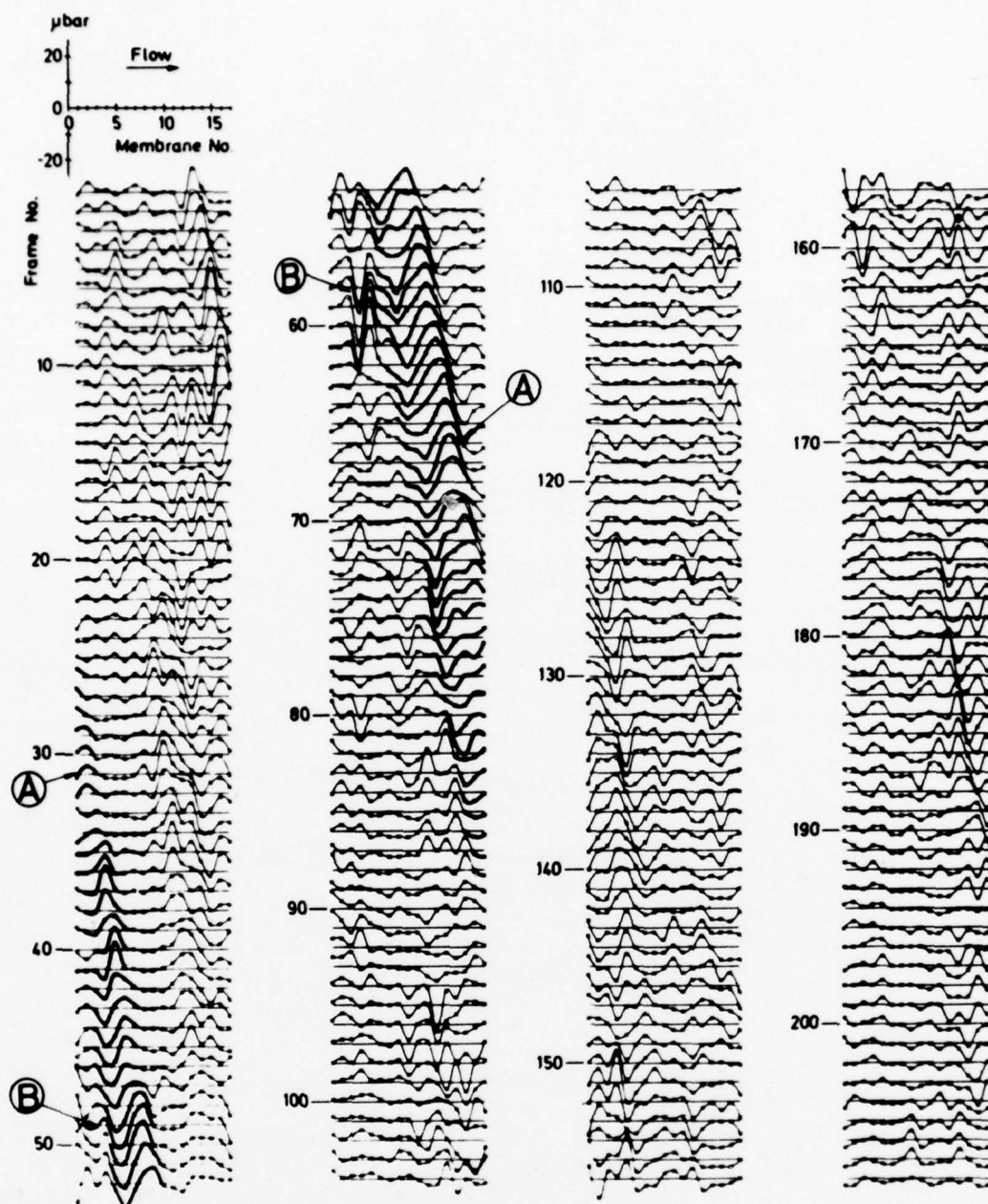


Figure 11 Sequence of consecutive pressure distributions along one row of 17 membranes lying in flow direction one behind the other. (Flow from left to right, flow velocity $U_{\infty} = 8.5$ m/sec, time between consecutive maps $\Delta t = 0.14$ msec).



Figure 12 Relation between bent streamtubes and nearby pressures (+ = overpressure, - = underpressure).

EFFECT OF COMPLIANT WALL MOTION ON TURBULENT BOUNDARY LAYERS

Dennis M. Bushnell* and Jerry N. Hefner**
 NASA Langley Research Center
 Hampton, Virginia 23665
 U.S.A.

and

Robert L. Ash†
 Old Dominion University
 Norfolk, Virginia 23508
 U.S.A.

SUMMARY

A critical analysis of available compliant wall data which indicated drag reduction under turbulent boundary layers. Detailed structural dynamic calculations suggest the surfaces responded in a resonant, rather than compliant, manner. Alternate explanations are given for drag reductions observed in two classes of experiments (1) flexible pipe flows and (2) water-backed membranes in air. Analysis indicates the wall motion for the remaining data is typified by short wave lengths in agreement with the requirement of a possible compliant wall drag reduction mechanism recently suggested by Langley.

NOTATION

A^+	Van Driest wall damping constant
C_f	Skin-friction coefficient
D	Tube diameter
k	Roughness height
K	Prandtl wall slope
L	Tube length
N_x	Axial tension load
P	Pressure
q_∞	Free-stream dynamic pressure
R_e	Reynolds number
R_{LC}	Lower critical Reynolds number
R_o	Undeformed tube radius
S_t	Strouhal number; $S_t = \omega \delta / U_\infty$
T	Applied tension
u	Local velocity component in x-direction
u_τ	Friction velocity; $u_\tau = U_\infty (C_f/2)^{1/2}$
U_∞	Free-stream velocity
v	Local velocity component in x-direction
V	Mean pipe flow velocity
w	Radial tube displacement
W	Wall vibration response amplitude

x	Streamwise coordinate
x^+, y^+	Spatial coordinates in wall-coordinate units $x^+ = xu_\tau/\nu$
y	Vertical coordinate

Greek Symbols

γ_o	Pressure gradient
δ	Boundary-layer thickness
δ^*	Displacement thickness
Δ	A difference
ζ	Vertical surface displacement
λ	Friction factor
ρ	Density
μ	Dynamic viscosity
ν	Kinematic viscosity
τ	Shear stress
ω	Radian frequency

Subscripts

o	Reference value
w	Wall

Superscripts

$+$	Wall coordinate units based on u_τ
$'$	Fluctuation component
$-$	Time average

* Head, Fluid Mechanics Branch, High-Speed Aerodynamics Division.

** Special Assistant, Fluid Mechanics Branch, High-Speed Aerodynamics Division.

† Professor, Old Dominion University.

1. INTRODUCTION

The current energy shortage places additional emphasis upon research to increase the efficiency of transportation, including aircraft.¹ Since, for long-haul aircraft, the viscous drag is approximately 40-50% of the total drag, any sizable decrease in turbulent skin friction translates directly into an appreciable fuel saving. Reference 2 provides a discussion of various techniques for reducing viscous drag, as well as drag due to lift. A more detailed review of various C_f reduction approaches³ concluded that five techniques (laminar flow control, slot injection, particle injection, polymers, and compliant skins) were worthy of further detailed research.

The laminar flow control (LFC) technology is quite mature, and most of the important remaining problems are in the practical areas of maintainability and reliability. Further research is, however, still required for optimization of suction rate and distribution. Skin-friction reduction due to injection of low momentum air near the wall (slot or porous injection) can definitely cause large local C_f reductions⁴ but recent studies⁵ have shown that, as one might expect, the penalties for collecting and ducting the slot air outweigh the expected drag reduction benefits on aircraft; therefore, this method is presently suitable only for local regions where excess air, perhaps from an LFC system, might be available. Particle injection can also provide a drag reduction,⁶ but applying this technique to aircraft (particularly considering the various anti-pollution regulations) is not currently feasible. Polymer injection produced large C_f reductions⁷⁻¹⁰ but the effect is limited to liquids.

The remaining technique, compliant walls, is the subject of the present critical review. Blick¹¹ discussed the field, with primary emphasis upon the University of Oklahoma research. The Introduction sections of References 12, 13, and 14 provide fairly up-to-date synopses.

The purpose of the present paper is to investigate the entire subject for both the transitional and the turbulent flow cases and discuss possible correlations between computed wall motion and observed drag reduction. The paper also presents alternate explanations for "drag reductions" observed in several cases reported in the literature.

Considering the demonstrated success with LFC on the X-21 aircraft,¹⁵ one might reasonably ask why anything further (another drag reduction technique) is needed for aircraft. There are two responses. First, LFC has thus far been applied on wings, and not fuselages. On the present wide-body transports, approximately one-half of the surface area is on the fuselage. Since the fuselage boundary layer is relatively thick and generally has small pressure gradients, it may be much more suitable for applying compliant walls rather than for LFC (although there has been no concentrated effort to apply LFC to the fuselage). The second and more serious comment concerns the high-altitude operating conditions necessary for LFC. The low unit Reynolds numbers required for a successful LFC system (primarily dictated by roughness and radiated noise from the fuselage) are only available at altitudes above 35,000 feet and, ideally, over 40,000 feet. However, most operational flights (and 60% of aircraft fuel) are for stage lengths less than 1500 miles and, therefore, considerable fuel is burned at altitudes below the levels required for LFC. The application of LFC is optimal for high-altitude, long-range aircraft but something else (perhaps compliant walls) is needed for the considerable traffic in the shorter stage length, lower-altitude cases. With these considerations, and because there does not seem to be any other potentially viable viscous drag reduction scheme, compliant wall research should obviously be pursued until the potential for drag reduction under turbulent boundary layers is either conclusively proved or disproved.

The current state of compliant wall technology can best be described as confusing and inadequate. Although the mechanism for altering the drag must be connected with the flow induced wall motion, to the present authors' knowledge, except for some recent attempts at Langley, only the study by Grosskreutz¹⁶ measured wall motion for either successful, or unsuccessful, compliant wall experiments. Extensive wall motion measurements must be made, particularly in cases where drag reduction is obtained, before any theoretical approach to the problem (or derived design methodology) can be reasonably validated. The problem is obviously one of fluid-structural dynamic interaction, and yet the structural side has been somewhat ignored by the experimenters. Another confusing issue is the various options available for eventual application to aircraft, that is, (1) delaying/stretching out transition versus reducing C_f in fully turbulent flow and (2) use of truly compliant (flow perturbation following) walls versus resonant (excited eigenmode) walls. Also, theoretical research indicated that compliant walls with low damping were required for flow stabilization, whereas practical applications and experiments necessarily utilize resonant walls with appreciable damping. Studies are available for practical application of the transition-retarding option.¹⁷

An additional use for compliant walls is reduction of turbulent boundary-layer noise. Both analytical¹⁸ and experimental^{19,20} work are available, but this option has not yet received extensive study. Reference 12 discusses the possible application of compliant walls for drag reduction in other modes of transportation besides aircraft.

Compliant wall research evidently originated from consideration of the drag of dolphins.²¹⁻²⁵ However, the possible presence of such walls on dolphins is problematical. In an article in *Scientific American*,²¹ Sir James Gray surmised, based upon the observed 22 mph speed of dolphins and their (then) known physiological propulsion efficiency, that the dolphin must have some means of producing extensive regions of laminar flow (although it was not mentioned, lower drag can obviously also be due to considerably reduced transitional/turbulent drag levels as well as to more extensive regions of laminar flow). Kramer,²² in 1961, published a suggestion as to how extensive regions of laminar flow might be produced on the dolphin. He based his suggestion, which he termed "distributed flow damping" or compliant walls, upon detailed examination of porpoise skin. He found that the skin is quite pliable and contains a considerable quantity of absorbed water. His initial tests (starting in 1956) of man-made coatings simulating porpoise skin did indeed yield lower drag in sea water. In a later paper,²² Kramer estimated that the porpoise could obtain up to a 40% drag reduction just due to the favorable pressure gradient influence on transition Reynolds number (body shaping); he further concludes that an additional drag reduction is necessary to explain the porpoise speed and again advances the compliant skin concept as a method for stabilizing the boundary-layer fluctuations by supplying distributed damping. However, tests conducted

by Lang et al.^{24,25} indicate that, while the porpoise can indeed reach high speeds (on the order of 22 knots), the animal does so only for relatively short time periods and this may be accomplished by running the muscles into "oxygen deficit." Lang's studies of porpoises observed during relatively controlled but "open water" tests yielded drag coefficients in approximate agreement with fully turbulent predictions during high-speed coasting (where the drag coefficient may be determined more accurately than, but may not be a true representation of, the propulsive case).

Therefore, whether the porpoise uses a compliant skin still seems to be somewhat a matter of contention, but an important result of this line of inquiry is the drag reduction obtained by Kramer on periodic "porpoise-like" skins where, evidently, the wall motion induced in the surface by the boundary-layer disturbance field caused a lower drag. It is not entirely clear from Kramer's results whether the lower drag is a result of (a) delaying transition, (b) reducing the intensity of bursts in the transitional region, or (c) reducing the turbulent skin friction. The present authors conjecture that at least the latter two effects ((b) and (c)) may have occurred. As a footnote to the porpoise skin discussion, there is available a hydrophilic coating for use on boats. The surface of this coating evidently becomes somewhat similar to a compliant wall when water saturated. Some details concerning the coating are available in Reference 11. The coating was tested both in the laboratory²⁶ and on ships.²⁷ Some drag reduction is observed, but the mechanism involved has not been studied and the reduction is evidently not large.

The present critical review first considers briefly the structural dynamics and flow stability areas. The major portion of the paper concerns the theory and experiments for compliant walls under turbulent boundary layers.

2. STRUCTURAL DYNAMIC CONSIDERATIONS FOR COMPLIANT WALLS

The compliant wall problem is one of fluid-structural dynamic interaction. Considerable structural dynamics and fluid-structural interaction research is available^{28,29} but many compliant wall experimenters have not used this technology to design their walls. Although this may be stating it somewhat strongly, the usual approach seems to have been, "this feels soft, let's try it."

The problem is not straightforward. The walls are exposed to a relatively wide-band spectral loading and the formulation must include the influence of wall motion-induced aerodynamic forces. The prime variables are multitudinous and include: (a) flow parameters such as speed, Reynolds number, boundary-layer thickness, and state (laminar, transitional, or turbulent), pressure gradient and flow medium (air or water, etc.); (b) structural configuration (vertical and/or horizontal layers, two or three dimensions, with or without pretensioned members) and the possibility of nonlinear effects such as caused by membranes backed with small air gaps; and (c) material property parameters such as density, modulus, damping, degree of anisotropy, and the possible variation of these properties with temperature, vibration frequency, and aging. Given a set of flow parameters and a stable of available materials, the type of structure is dictated by the surface response desired.

For the case of a simple two-dimensional convected surface wave, the fundamental wall motion parameters are wave length, wave amplitude, and wave speed or frequency. However, since the structure is continuous, the surfaces will, in general, react over a whole range of amplitudes, wave speeds, and wave lengths. In addition, since the forcing field is three-dimensional, the induced motion could also be three-dimensional, depending upon the degree of "compliance." It is also possible that favorable alteration of the turbulence field demands the presence of unsymmetric surface waves having particular wall curvature or pressure gradient distributions.

Some attempts have been made^{12,13,30-33} to utilize structural dynamics technology, of varying sophistication, to design compliant walls according to various assumed aerodynamic (or disturbance damping/alteration) criteria. One such criterion ("roughness" effect) is quite obvious from difficulties encountered in the experiments. The amplitude of the motion must be kept low enough to avoid causing a "roughness" effect which would increase, rather than decrease, the drag. The occurrence of static divergence conditions (large standing waves) have been commonly observed in compliant wall experiments³⁴⁻³⁶ at high flow speeds and generally lead to drag increases. For application to the turbulent case, one could use the common roughness height rule of thumb of $k^+ \leq 6$ to determine an allowable wave amplitude, where k^+ equals the wave or roughness height in usual law of the wall coordinates. For most turbulent flows, this limits the maximum wave height to less than 0.5 mm. However, except for the static divergence case, the Langley experience is that it is quite difficult, for airflows, to excite practical walls to amplitudes even the order of 0.02 mm (based upon both surface amplitude measurements and structural dynamic calculations).

There is another design criterion which is probably correct — the waves must move or at least have fairly high frequency. Most experiments with fixed wavy walls³⁷ (and the zero wave speed results of Ref. 38) used wave amplitudes which exceed the roughness criterion just mentioned and thus measured increases in drag. Reference 38 indicates a fixed wavy wall has a pressure drag due to the phase shift between the surface contour and the wave-induced pressure field. Unpublished experiments at Langley with fixed waves smaller than those of Reference 38 indicated, within an accuracy of $\pm 3\%$, no net change in drag for low-speed turbulent flow. These latter data seem to suggest that drag reduction requires moving or relatively high-frequency waves. Aerodynamic design criteria which might be used for compliant walls is discussed more fully in the theoretical sections of this paper.

One basic structural dynamics consideration that should be emphasized is the difference between the "compliant" walls dictated by stability theory^{39,40} and the usual flexible walls employed in experiments. The successful compliant wall, according to stability theory, has extremely small damping and modulus of elasticity and can therefore respond, with little phase lag, to the wall forcing function produced by the flow disturbance field. However, such surfaces are practically impossible to construct. Therefore, the experimental data are taken with structures which are not optimal in the stability theory sense, but are actually "resonant surfaces" in that the flow-disturbance forcing function excites wall vibration modes.

Compliant wall experiments must, practically speaking, be conducted using resonant walls. The design of structures to provide the desired wall motion is complex and requires design techniques based on aerodynamic wall motion criteria obtained either from wall motion measurements during successful experiments or from rather sophisticated theory.

3. INFLUENCE OF WALL MOTION ON STABILITY/TRANSITION

Although the major purpose of the present paper concerns the influence of wall motion upon the drag in turbulent boundary layers, in this section a brief review of the laminar/transitional results (which are primarily theoretical) is provided for later theoretical application in the turbulent case. In particular, the turbulent wall "burst" formation and preburst flow may involve a relatively brief region (brief in time and space) where stability theory applies in the near wall region. Influencing this portion of the flow may be sufficient to break the "feedback loop" which allows the turbulence to be self-sustaining. (See also Ref. 40, section on "Effects of Flexible Boundaries on Turbulent Flows.")

3.1 "Conventional Compliant" Walls

Pelt⁴¹ reviewed the various approaches to the stability theory of compliant walls through approximately 1964, including the results of Benjamin,⁴² Landahl,³⁹ Betchov,⁴³ Boggs and Tokita,⁴⁴ Hains and Price,⁴⁵ Nonweiler,⁴⁶ and Linebarger.⁴⁷ Theoretical research since the Pelt review comprises further work by Benjamin,⁴⁸ (including an excellent summary paper⁴⁰), Landahl,⁴⁹ Kaplan,⁵⁰ Takematsu,⁵¹ Burden,⁵² and Amfilokhiyev et al.⁵³ From the number of authors cited, this has obviously been a popular problem, with most of the work accomplished in the early sixties (primarily due to the stimulus of Kramer's results^{22,23}). However, attempts to experimentally validate the theoretical calculations generally used either resonant surfaces, which do not correspond to the theoretical assumptions employed, or active walls.⁵⁴ In fact, Landahl⁴⁹ concludes that the Kramer surfaces were so far removed from the conditions necessary for stabilization according to the theory that the Kramer drag reduction must be due to a favorable modulation of the later stages of transition or turbulent portions of the body.

Burden⁵² suggests the following "compliant" wall characteristics as necessary for stabilization of oscillations in the early stages of transitional flow (see also Kaplan⁵⁰): (a) wall density the order of the fluid density (obviously out of the question for air); (b) shear modulus the order of the fluid dynamic pressure; (c) small wall dissipation; and (d) impervious wall. He further states, in agreement with earlier authors, that too much flexibility, or too much dissipation will allow the growth of instabilities not otherwise found in the zero-pressure-gradient rigid wall case. The definitive review of research in this area is that of Benjamin.⁴⁰ It should be noted that all of these approaches used "steady-state" stability theory in the sense that the wall motion was not allowed to "back react" upon the assumed mean profile. For moderate to large wall displacements, the surface motion induces a traveling pressure signal³⁸ which can modulate the "mean profile" and this invalidates a key assumption in the conventional stability theory approach to compliant walls. The relaxation of this assumption is discussed in a subsequent section of the paper.

Although Wehrmann⁵⁴ had to use an "active" or driven wall to simulate the "compliant" surface assumed in the theories, he was able to show experimentally that, depending upon the phase between the driven wall wave and the Tollmien-Schlichting wave generated by a vibrating ribbon, large reductions in velocity fluctuation intensity could be obtained. The largest reduction occurred near the wall.

In summary, there is a large body of theoretical research (which is probably correct, judging by the available checks on rigid wall stability theory and the results of Ref. 54) which suggests that certain types of compliant walls can (a) increase the lower critical Reynolds number, and (b) reduce the spatial and temporal amplification rates of unstable waves. The problem, particularly for the air case, is that the walls required to produce these effects evidently cannot be constructed with current technology. Consequently, we have a possible drag reduction effect of highly compliant walls which, while intriguing, is probably not practical, especially for airflows.

3.2 Stability With Resonant Walls

The Kramer surfaces²² are obviously more resonant than compliant due to their large damping. In the present review, we treat the Kramer data^{22,55-57} as primarily indicating an alteration of the transitional and turbulent burst frequency/structure rather than a delay of the onset of transition, because of the amount and slope of the drag reduction obtained with the surface at large Reynolds numbers (up to 15×10^6).²² Therefore, the detailed discussion of the Kramer data is deferred until the section on turbulent experiments.

There is essentially no applicable theory for the influence of resonant (excited structural eigenvalue, fairly wide-band motion, random phase) walls on transition except perhaps for piecewise application of the fairly large, and recent, effort on stability in modulated or periodic boundary-layer flows. These latter efforts (theory and available experiments) are discussed in the next section since they were developed primarily for active or driven oscillations (wall or stream); the present discussion focuses on passive walls.

An experimental study was conducted at MIT⁵⁸ to simulate a compliant wall by a series of streamwise-connected Helmholtz resonators. "The vertical motions of plugs of air adjacent to the flow was intended to model the oscillations of a flexible membrane." These experimental results indicate earlier (increased instability), rather than retarded transition primarily because of the fairly large size and discrete nature of the surface perturbations. Attempts to duplicate Kramer's work by delaying transition in ground facilities during the early sixties were also unsuccessful.^{59,60}

The major investigations on the influence of resonant surfaces on stability were conducted by V. V. Babenko. This work included porpoise skin studies⁶¹ and experimental stability investigations using a wide variety of surfaces.⁶²⁻⁶⁴ These studies concentrated quite heavily upon the characterization of the structural dynamic parameters for the surfaces tested. The experimental results indicate that for compliant surfaces the wave number corresponding to initial loss of stability was larger than for rigid surfaces.

Measurements of neutral stability curves provided Reynolds numbers for the "loss of stability" ("lower critical Reynolds number") for wide variations in surface design and material parameters. Variables include surface material, damping, density, modulus, and tension (for those surfaces using membranes).

The data indicate significant changes in critical Reynolds number occurred for resonant walls, with measured values both above and below the conventional Blasius value, depending upon the surface parameters. On the basis of the Babenko results, it seems that not only compliant walls but resonant walls as well can favorably alter the stability boundaries of laminar flows. Considerably more experimental and theoretical research is required in this area, but the results may have eventual practical application, particularly for water flows, where one can build resonant walls over a wide range of wall motion parameters (e.g., frequency, amplitude, wave speed, spectra). This research further suggests that Kramer's assertions that he delayed transition with his fairly high damping surfaces may be correct. As a final note to this section, there are also the data of Karplus,⁶⁵ who measured a decrease in Reynolds number for transition, and a lengthening of the transition region itself; the results are of a preliminary nature.

3.3 Stability of Periodic Boundary Layers

As already stated, the modulation produced by a resonant wall can be sufficient to significantly alter the effective "mean velocity profile" under investigation. There are two effects: one is the obvious influence of alternately increasing and decreasing, through profile modification, the disturbance amplification rate, so that the integrated amplitude ratio may be greater (or less) depending upon the amplitude, frequency, and wave speed of the imposed oscillation. The second influence involves the timewise dynamics of the modulated boundary layer in that the application of ordinary stability theory in a quasi-steady sense is not sufficient and one must include time derivatives of the mean profile parameters in the theory. It is the present authors' contention that this timewise modulation of the mean flow and the subsequent influence upon stability may be the key to further theoretical understanding of the experimental results obtained using resonant walls — for both laminar and turbulent flows.

Several types of modulations are possible. The free-stream (or wall) velocity can be varied primarily in the in-plane or stream direction.⁶⁶ This imposes a cyclic variation which diffuses in a viscous manner through the profile. On the other hand, one can impose a pressure gradient modulation upon the flow, in which case the entire profile is modified. This pressure modulation can be imposed either upon the flow as a whole (i.e., vary the imposed pressure drop in a Poiseuille flow with time) or can be generated locally at the wall by the use of traveling surface waves. This latter method probably occurs for the resonant or active wall case.¹³

As noted earlier, the rigid wavy wall does not seem to produce a favorable effect, one needs moving surface waves, or at least stationary, nodal time-dependent surface motion. The stability theory calculation for a rigid wavy wall (with "parallel" flow assumption⁶⁷), indicates a destabilization effect.

There are two recent, and quite excellent, reviews in this area of stability for modulated viscous flows, References 68 and 69, the latter being an outgrowth of work in References 70-72. These reviews are highly recommended by the present authors as entry points for this relatively new, and quite exciting, technology. It appears to be important to account for the true time-dependent nature of the complete problem; a quasi-steady stability analysis of the modulated flow⁷³ is not sufficient in many cases. For instance, if one examines a flow containing an inflection point during some portion of the cycle, this instantaneous profile will generally have a reduced lower critical Reynolds number compared to the unmodulated profile. The initial reaction is to brand the modulation as destabilizing, since, somewhere in the cycle, the lower critical Reynolds number is reduced. Such a conclusion could be erroneous. A more satisfactory approach (but incorrect for high frequencies) is to use the quasi-steady analysis to generate local amplification rates and then integrate these over complete cycles of the modulation.⁶⁹ For stabilization, the trick seems to involve using modulations which are not so large that they trigger enormous amplification during part of a cycle. Therefore, one needs small to moderate amplitude modulations but not so small as to have little or no measurable effect upon the flow — a problem with resonant surfaces in airflows where an extremely low wall modulus is required to produce any reasonable surface amplitude. Another requirement for stabilization, although this varies with the particular type of flow,⁶⁸ is a relatively high-frequency modulation. Theoretical papers of particular interest include References 74 and 75. Some of the limited experimental backup data (using active or driven disturbances) are given in References 76-79.

In summary, the results of both theoretical and experimental studies in time-modulated flows indicate that it may be possible to stabilize boundary-layer flows using low to moderate amplitude/relatively high-frequency oscillations. In the compliant wall case these oscillations, in the form of pressure modulations due to traveling surface waves, could result from the use of resonant walls. Further research is obviously needed to determine whether these indications are correct or not.

4. THEORETICAL C_f REDUCTION MECHANISMS FOR TURBULENT FLOWS WITH MOVING WALLS

Based upon References 80 and 81, it is probable that the turbulent drag reduction mechanisms to be discussed in this section are also applicable to the later (turbulent burst) stage of transition and therefore one or more of these mechanisms could cause a stretchout and reduction of drag for the transition region as well as a turbulent skin-friction reduction. This postulation is further bolstered by the common sensitivity of transitional and turbulent flow regions to changes in boundary conditions (other than wall motion) such as pressure gradient, wall suction/blowing, and longitudinal curvature.

The influence of wall modulation upon shear flows is part of the general problem of the behavior of turbulent flows subjected to periodic disturbances. This question is investigated in some detail in References 82 and 83, but the perturbation amplitudes are relatively small, and the studies do not consider the possibility of altering the basic turbulent structure via this approach. Experimental attempts to introduce substantial periodic disturbances into turbulent wall layers (other than by wall motion) are documented in References 84 and 85. Reference 84 describes the influence of large (up to 34%) narrow-band fluctuations in free-stream velocity at Strouhal numbers less than 1 (based on boundary-layer thickness and free-stream velocity). This is a low frequency in terms of the modulations required by unsteady

stability (as described in the previous section). No appreciable alteration of the turbulence structure was observed. In Reference 85, a turbulent boundary layer was subjected to an imposed sound field over a wide frequency range. The experimental trends observed are in agreement with the unsteady stability theory results in that high-frequency sound caused a reduction in surface heating and lower-frequency sound caused an increase. However, the effects are not large, only the order of 4%.

This experiment, along with the compliant wall burst modulation theory and interpretations of compliant wall data (both described later in this paper) as well as the unsteady stability theory, indicate that a reduction in the turbulence transport rate requires a high-frequency modulation (of moderate amplitude). The present authors suggest that future experiments in the area of turbulence control for wall flows concentrate on the high-frequency range to prove or disprove this evidentiary material.

4.1 Sublayer Models

Direct Coupling. A simple sublayer approach to the compliant wall problem is given in Reference 12. The boundary-layer momentum equation very near the wall is:

$$\frac{\partial u}{\partial t} + u \frac{\partial u}{\partial x} + v \frac{\partial u}{\partial y} = \nu \frac{\partial^2 u}{\partial y^2}$$

assumptions:

- (a) $\frac{\partial p}{\partial x} = 0$
- (b) $\frac{\partial u}{\partial y} = \frac{\tau}{\mu} = \text{constant}$
- (c) Surface motion $\zeta(x, t) \approx \text{periodic function}$

The solution of the momentum equation with these assumptions is:

$$u(x, y, t) = (y - \zeta) \frac{\tau}{\mu}$$

$$v(x, y, t) = \frac{\partial \zeta}{\partial t} + (y - \zeta) - \frac{\partial \zeta}{\partial x}$$

and

$$\tau_w = \mu \left(\frac{\partial u}{\partial y} + \frac{\partial v}{\partial x} \right) = \tau \left(1 - \frac{\partial \zeta}{\partial x} \right)^2 + \mu \frac{\partial^2 \zeta}{\partial x \partial t}$$

therefore:

$$\bar{\tau}_w = \tau \left(1 - \left(\frac{\partial \zeta}{\partial x} \right)^2 \right)$$

Since $\left(\frac{\partial \zeta}{\partial x} \right)^2$ must be positive, a shear stress at the wall lower than the conventional level is again indicated. However, this simple approach does not include the influence of the pressure gradient induced by the wall motion, and if one includes the contribution of the normal stresses for the portion of the cycle when the wave is no longer parallel to the original wall the actual drag is increased.

Analysis of J. E. Ffowcs-Williams. Ffowcs-Williams⁸⁶ uses the assumption of two-dimensional disturbances and linearized (sublayer) equations to derive an expression for shear stress near a compliant membrane. From examination of this expression, he concludes that moving waves in a surface with low wave speed can produce a region of "negative Reynolds stress" which could "starve the turbulent eddies" and "may lead to a reduction in the turbulent level." Therefore, for a shear stress decrease, this approach seems to indicate the use of surfaces designed to generate low-speed waves (less than $\approx 0.8U_\infty$, the convection speed of the gross wall pressure fluctuations). The approach of Blich⁸⁷ is quite similar.

The Sublayer Approach of Semenov. Semenov⁸⁸ provides an alternate sublayer type analysis, using equations similar to those of Sternberg.⁸⁹ He predicts that the Reynolds stress could decrease, or increase, depending upon the characteristics of the surface motion, and is careful to point out the importance of the surface wave phase angle. Comparisons between the predictions of Reference 88 and the data of Reference 90 (shown in Fig. 3 of Ref. 88) indicate quite reasonable agreement for the change in Reynolds stress as a function of frequency due to a resonant wall. Both hot-wire data⁹⁰ and theory give a reduction due to the wall motion at low frequency (region of "energy containing eddies") and an increase for higher frequencies. To the present authors' knowledge, the theory has not yet been extensively applied, evidently due to the lack of the necessary empirical input for cases other than Reference 90. The approach probably could be used in parametric studies to "predict" the type of surface motion necessary for drag reduction (and thus provide design "data" for experimental surfaces).

A Mixing Length Approach. Amfilokhiyev⁹¹ assumes that the elasticity of a surface (wall motion) reduces the "Prandtl wall slope" ($K \approx 0.4$ for rigid walls) and indicates skin-friction values as a function of the assumed decrease in K . This approach does not agree with the data of Reference 90, where K was still ≈ 0.4 in the drag reduction case. In Reference 90 the sublayer thickness was increased, thereby indicating, in terms of mixing length turbulence closure, an increase in the Van Driest wall damping constant A^+ .

Analysis of Zimmermann.¹⁴ Considers the surface motion as a small disturbance to the basic turbulent flow, which is assumed known in detail. Further assumptions include low damping in the surface and small thickness, an approach to the surface dynamics which is similar to that used in the conventional stability theory of "compliant walls." The Navier-Stokes equations are then linearized using the small disturbance assumption and solved by a Green's function approach. He uses measured pressure-velocity correlation data from rigid walls to estimate the change in shear stress due to the flexible surface and predicts only a small reduction for air, but a measurable ($\approx 5\%$) reduction for water where the coupling is greater between the fluid and flexible wall.

$u'v'$ at Surface. Hueristic arguments concerning the possibility of producing an altered Reynolds stress condition simply due to the u' and v' associated with the surface motion itself are available in References 92 and 93.

4.2 Drag Reduction Mechanisms Based Upon Turbulent Burst Modulation

The "sublayer" theoretical approaches just described for the problem of the wall motion effect upon turbulence were based upon traditional modeling of sublayer flow and the use of Reynolds averaging. Analysis of the more recent research on the detailed structure of wall turbulence, particularly the flow visualization and conditional sampling data, yields an alternate theoretical approach,¹³ based upon the possible modulation of the preburst flow. The implications from the detailed data on rigid walls are first summarized briefly and then the possible modification of the turbulence production process using higher-frequency wall motion is discussed.

Coherent Structures and a Possible Feedback Mechanism for Turbulent Wall Flows. There is considerable evidence that a "quasi-ordered" or "coherent" series of fluid dynamic events are responsible for the production of turbulence in wall flows. These events occur randomly in time and space and originate in the near wall ($y^+ < 100$) region. Several excellent reviews are available which analyze and summarize this relatively recent information,⁹⁴⁻⁹⁶ especially Reference 97. Reference 81 attempts to model turbulent flows using this information. Stated briefly, a low-speed "streak" occurs very near the wall; this streak undergoes retardation with increases in time and space with a "burst" or eruption of the low-speed fluid occurring for the more severe retardations. This burst and subsequent "sweep" provides the bulk of the Reynolds stress and turbulence production. The flow between events and the preburst retardation region is relatively "quiescent" (low $u'v'$). This latter statement is important for theoretical calculations of these events, because in order to reproduce the retardation one should not use the "fully developed" or time-averaged Reynolds stress level in the flow, but instead a rather small fraction of that level. There is still considerable controversy as to the relationship between the retardation and the burst or ejection. Many authors suggest that the (retardation-influenced) preburst profile undergoes an instability growth/amplification in a fashion similar to the "burst formation" in transitional flows. Landahl (see Section 7 of Ref. 80) suggests that the burst may be due to space-time focusing of instability waves, leading to the observed catastrophic growth. However, both experiment and theory indicate the existence of a highly inflected retarded profile (inflection point at $y^+ \approx 25$, Fig. 31 of Ref. 97) as the required preburst condition. (In Landahl's theory, the inflection is a necessary, but not sufficient, condition.) This near wall turbulence production, through discrete bursts, bears remarkable resemblance to the earlier theories.⁹⁸⁻⁹⁹

A logical question is, what sets up the requisite preburst profile, why does the profile become retarded? It has long been known (Ref. 100 and others) that the larger scale, more intense portion of the wall pressure spectrum has a convection speed the order of 0.7 to $0.8U_\infty$ and appears to originate at $y^+ > 100$. There is evidence^{97,101-102} that the retardation is caused by this portion of the wall pressure field, which, in turn, is probably due to the growth and interaction of "old bursts" produced upstream. In fact, Burton⁹⁴ measured a strong correlation between the occurrence of a burst and the imposition on the wall flow of a large moving adverse pressure gradient signal with magnitude the order of three times the rms wall pressure intensity. This adverse pressure gradient was followed by a favorable gradient, perhaps at least partially responsible for the "sweep" portion of the event cycle. It should be noted that recent evidence appears to show more high-frequency energy in the wall pressure fluctuation spectra than was originally indicated, perhaps associated with the burst process (see Fig. 9 of Ref. 97 and Ref. 103). However, the burst initiation seems to involve the lower-frequency portion of the spectrum. It should be noted that not all "outer-flow imposed," low-frequency wall pressure fluctuations produce bursts. Evidently only the large amplitude, long-lasting pulses can cause sufficient retardation to produce the necessary preburst conditions. Preliminary quasi-steady retarded near wall calculations, using low levels of Reynolds stress and the burst-producing pressure pulses measured by Burton,⁹⁴ indicate that the pressure gradients involved are sufficient to cause severe retardation of the near wall flow.¹³ The recognition of the low Reynolds stress condition of the preburst flow is critically important to the success of such calculations. Further, much more detailed and complete calculations of the preburst flow (with and without resonant wall motion) are currently underway by Orszag in collaboration with NASA Langley.

Therefore, there exists a possible "feedback" mechanism in which older bursts, which have grown and migrated up to the law of the wall and outer portions of the boundary layer, interact and produce a pressure field which contains pulses of sufficient duration and amplitude to induce new bursts in the near wall flow. This near wall region contains a high level of background turbulence but fairly low levels of $u'v'$ during the nonburst periods.

It is interesting that an effort to artificially induce bursts using a stationary pressure pulse¹⁰⁴ did not seem to alter the characteristic burst frequency of a turbulent wall flow.

Burst Modulation Due to Wall Motion. One approach to a theory of drag reduction due to wall motion is to postulate that certain types of surface motion can alter or interrupt some portion of the feedback process just described. The portion of the process most available for alteration by wall motion is the preburst, near wall retardation region. Other drag reducing procedures, such as the injection of polymers, may alter this or some other part of the feedback loop.

Reference 13 suggests that the moving surface waves associated with a resonant wall can produce a modulation of the preburst retarded flow. The details of this modulation are a function of the wave length, wave speed (or frequency) and amplitude of the surface motion; however, for short, steep traveling waves the wall motion can produce a modulated pressure gradient (modified for viscous effects and wave speed as per the Kendall³⁸ data), alternately positive and negative. This modulation is superimposed upon the adverse gradient signal which normally triggers the bursts. The suggestion¹³ is that this modulation, if it has high frequency and moderate amplitude (see the section on stability theory for periodic flows), can delay the burst formation. Considering the expected stabilizing influence of the "following" favorable gradient portion of the outer flow generated signal, only a small delay may be sufficient to completely obviate the burst. Longer waves ($\Delta x^+ > 500$) would presumably trigger as many extra bursts (due to the long adverse gradient portion of the wave) as the number of bursts eliminated by the stabilizing influence of the favorable gradient part of the wave train. An alternate approach to a similar mechanism is to analyze the preburst flow using the breakdown mechanism of Landahl.^{105,106}

The burst alteration mechanism just described is only a suggestion; further, more detailed calculations and experiments are necessary to either prove, or disprove, this approach. However, it is known that small surface waves can alter much larger scales of turbulence in the atmosphere over a sea surface^{107,108} and the high-frequency surface motion dictated by the mechanism is in general agreement with wall motions computed for successful drag reduction experiments (next section of report). Detailed calculations using this burst modulation model are underway.

5. CRITICAL ANALYSIS OF RESONANT WALL EXPERIMENTS UNDER TURBULENT BOUNDARY LAYERS

In this section we attempt to examine the available data with the following two questions in mind:

(1) Is there another possible (and defensible), explanation for the "drag reduction" observed? and (2) for the successful cases which survive the filter of question 1, what is the computed wall motion? is it high or low frequency (Strouhal number much greater than, or less than, one)? We also mention, for completeness, some of the experiments on drag over "resonant water waves" in air and the "unsuccessful" compliant wall experiments, which are discussed first.

5.1 "Unsuccessful" (Small Reduction, No Change of C_f Increase) Experiments

It should be noted beforehand that this class of experiments has not received the detailed study by the present authors which it perhaps deserves. We have spent most of our efforts trying to understand the successful experiments, in an attempt to infer the type of wall motion responsible for the observed drag reduction (if no other cause for the reduction other than wall motion input could be found). On the basis of the theoretical and experimental results thus far, it is reasonable to conjecture that a favorable influence (reduction) on C_f , if indeed such a thing can occur, is probably only possible over a relatively narrow range of wall motion conditions. Without an attempt to control, measure, or widely vary the wall motion, hitting the correct combination in an experiment is a pure happenstance. Nevertheless, there are a few obvious comments which can be made concerning these "unsuccessful" studies.

Ritter and Porteous¹⁰⁹ (1965). This water experiment used the original Kramer surface material (periodic, "studded" rubber — discussed in considerable detail in a later section of the report). A pertinent comment from Reference 110 on these data is that the free-stream turbulence level was probably too high to constitute a valid test of the laminarizing properties of the surface. The speed was limited due to the formation of local blisters in the coating at high dynamic pressure. Skin friction was estimated from measured values of momentum thickness, a procedure which is not always sufficiently accurate.¹² Problems with the fairing at the leading edge of the coating caused premature transition.

What is fascinating about these data is (1) the use of a periodic surface (spatially repeated substructure, although the modulus of the rubber may have been somewhat high considering the reduced speed range of the tests) and (2) the data on Figure 5 of Reference 109 which indicate that drag levels at various distances back along the body have a premature turbulentlike variation with Reynolds number, and this distribution is below the developed turbulent level. The amount of this "drag reduction" is greater farther forward on the body, but due to the later transition on the rigid body (better surface finish) the compliant wall drag levels are generally above the rigid case (and therefore the authors of Ref. 109 did not consider the data as indicating a drag reduction). The present authors strongly suggest that the fact that these compliant data, obtained using a periodic surface, have a turbulentlike variation with Reynolds number (but at a lower C_f level) may be highly significant. Based on the discussion in the paper thus far, a single stub spacing would not be expected to work well over a wide Reynolds number range, and also the well-known peak in P'_w/q_∞ associated with the end of transition may help explain the apparent variation of performance with body distance. This experiment should probably be redone, with more complete instrumentation, to higher speeds, and using a series of periodic surfaces designed over a range of wave length, wave amplitude, and wave speed (or frequency).

Ritter/Messum¹¹¹ (1964). This is a continuation of the research of Reference 109, but using small flat plates rather than cylindrical bodies. Again, the stream turbulence levels were quite high, and Kramer's studded coatings were used. The data, taken only for turbulent boundary-layer flow on six different skins, exhibit considerable scatter but two types of skins gave a drag reduction. One skin showed a consistent 7-14% drag reduction, again exhibiting a variation with Reynolds number parallel to, but below, the rigid turbulent case. A second skin gave a drag reduction (7-15%) except at high speed where standing waves (roughness) may have occurred.

Laufer and Maestrello¹¹² (1963). From Reference 113, one of the problems in this experiment was the possible reflection of flow-induced surface waves from the downstream end of the channel. Periodic surfaces were used (in some of the tests). A further difficulty in this experiment is that air (rather than water) was used as the test medium. Therefore, the velocity of the flow must be considerably higher to provide a level of wall pressure fluctuation (forcing function) necessary to excite the fairly stiff surfaces used. However, when the flow speed is increased, the frequency requirements which the surface waves must meet also increase and therefore a very careful surface structural design effort is needed. The Langley experience with the design of periodic surfaces for airflows shows that one can get reasonable amplitudes with

long wave length (low frequency), but as one tries to increase the frequency of the surface response the amplitude of the motion is considerably reduced, even using very low modulus materials. The periodic surface design problem for airflows is not straightforward. The general conclusion from Reference 112 is that the surfaces used were too rigid, except for one case, and in that case the duct cross section changed, due to the pressure loading on the flexible surface, thus invalidating the results.

Smith¹¹⁴ (1963). This is a pipe flow experiment using a nonperiodic (gel-coated) surface and diesel fuel as the test fluid. Only drag increases were measured, and these were ascribed to the roughness of the gel coating. For the higher Reynolds number data, long wave instabilities may have occurred, giving increased roughness. There are several other pipe experiments besides Reference 114, but these gave substantial drag reductions and therefore the discussion of the main portion of the pipe data is postponed until the next major section of the report.

Dinkelacker^{115,116} (1966). This is one of the most carefully conducted of the compliant surface tests. Water was the test medium and the facility was a "pipe inlet flow." In particular, Dinkelacker attempted to determine, for his experiments (a) the repeatability of the rigid tube data, (b) influence of small steps in the tube walls (found to be significant), and (c) possible occurrence/effect of organ pipe acoustic modes, along with studies of other possible influences upon his experimental results. In his own words,¹¹⁵ "The main outcome of this investigation was the establishment of a detailed picture of the difficulties which may occur in experiments with flexible walls." Some results of the study seemed to indicate a reduction in drag.

Taneda/Honji¹¹⁷ (1967). This study measured drag on towed flat plates in water, using nonperiodic surfaces. The drag of the flexible surface covered plates was generally greater than the rigid ones (due perhaps to early transition). Also, the turbulent levels for the flexible data were generally equal to, or greater than, the rigid levels.

Mattout¹¹⁸⁻¹²⁰ (1971). A fairly detailed study using both resonant and active (driven) walls in water. For the driven wall case, a 25% drag reduction and a thrust¹²¹ is obtained. For the flexible wall, only a 7% reduction was observed. For the driven wall case, the waves were quite long (4.2 to 50 cm) compared to the boundary-layer thickness which was on the order of 2 cm. The passive walls were membrane covered foams, which are not really periodic surfaces for the relatively small pore size used. Mattout invested considerable effort in determining the modulus of his passive surfaces and used both PVC and mylar membranes. Prime variables included membrane tension and flow velocity. Figure 39 of Reference 119 provides a thumbnail review of the compliant wall results up to 1970.

Grosskreutz^{16,93,122-123} (1971). This was an attempt to build nonisotropic effects into the wall and is one of the very few studies with wall motion data. The basic concept was to "preload" the surface so that the surface motion always produced a positive correlation of Reynolds stress, that is, u and v at the surface were either both positive or both negative. Therefore the surfaces (which were periodic due to the discrete preloading used) directly "controlled" the Reynolds stress at the wall. The tests were conducted in water, and the surfaces used are somewhat similar to Kramer's (see Fig. 2 of Ref. 93) except that the "periodicity length" is greater than in the Kramer case. Grosskreutz measured a reduction in momentum thickness on one of the surfaces for the low velocity (low unit Reynolds number) cases. The present authors speculate that there is a possibility that the favorable low unit Reynolds number results may have been due to thicker sublayers where the periodic spacing used was closer to the wave lengths required for burst modulation.

Hansen/Hunston³⁴ (1973). These experiments were run on a rotating disk in water using layered (non-periodic) surfaces. There is insufficient conditional sampling data for the three-dimensional boundary layers on rotating disks to determine the type of wave lengths and three-dimensional wave forms which might be required for burst modulation. The results of the experiment³⁴ were null in that no drag reduction occurred. At high speeds, where static divergence waves formed, the drag increased. One should probably stay with zero pressure gradient, two-dimensional, turbulent flows for testing of wall motion effects and prove/disprove the case for drag reduction there, before considering three-dimensional and pressure gradients effects.

Kawamata et al.¹²⁴ (1974). This study used a floating element model on the wall of a water tunnel. Material properties such as damping coefficient and stiffness are given for several of the surfaces used, which were fairly thick rubber or neoprene membranes backed by either air or olive oil. Due to the non-periodicity of the surfaces, the wave lengths were probably quite large. The authors claim large drag reductions, but there are more drag increase data than drag reduction. The most worrisome point is that sizable reductions are observed in the fully laminar case, indicating perhaps possible problems with accuracy using the floating element balance (flow/pressure gradients in the gap, etc.) or other experimental problems. These experiments should be carefully analyzed and perhaps repeated.

McAlister and Wynn¹²⁵ (1974). This was an attempt to confirm the results of Blick et al. at the University of Oklahoma (Refs. 126-132, 90, 36, reviewed in Ref. 11). In the next section of the report the present authors suggest, based upon recent Langley analysis and experimental results, a possible alternative explanation for the "drag reductions" observed during the Oklahoma liquid-backed membrane tests. This alternate explanation may account for the difficulty which McAlister and Wynn and also Lissaman and Harris³⁵ experienced in reproducing the liquid-backed Oklahoma results. McAlister and Wynn used an airfoil type model mounted on flexures for direct force measurements and tested in air. There may be an absolute accuracy problem in these experiments associated with the combination of pressure and skin-friction drag sensed by the load cells and the percentage of overall surface area covered with compliant surface. The flexible surfaces used were layered and nonperiodic and were probably too stiff to respond well to the relatively low dynamic pressure of the airflow. No drag reduction was observed.

In summary, even though labeled "unsuccessful," several of these studies did observe some drag reduction ($\approx 5-15\%$) particularly for conditions conducive to small wave length, steep waves (low unit Reynolds number, water flow, periodic surfaces with small cell size).

5.2 Flexible Pipe Experiments

Successful drag reduction experiments with turbulent flows in flexible pipes have been reported by Pelt,⁴¹ Teslo and his coworkers,^{133,134} and Klinzing et al.¹³⁵ All of these investigators have reported significant reductions in the pressure drop for a flexible pipe when compared to a rigid pipe. However, these data should be questioned because of the extreme sensitivity of pressure drop to changes in diameter. A theoretical model is discussed here which indicates significant drag reductions can be attributed directly to changes in tube shape rather than a compliant effect (see also Ref. 136 for possible effects of geometry change).

Hydrostatic displacement of the tubes employed in Pelt's experiments has been studied in some detail.¹³⁷ Although that analysis does not apply directly here, an important result was that, for the materials and geometry employed in Pelt's experiments, the radial tube displacement, $w(x)$, could be well approximated by

$$w(x) = \frac{R_o}{\alpha} [R_o P(x) - \nu_T N_x(x)]$$

for axial (x) locations away from the ends. In this equation, R_o is the tube radius, P is the local fluid pressure, ν_T is Poisson's ratio, N_x is the axial load, and α is a constant given by:

$$\alpha = E \delta_T \left[1 + \frac{\delta_T^2}{12 R_o^2 (1 - \nu_T^2)} \right]$$

where E is Young's modulus for the tube and δ_T is the tube thickness. The tube was modeled as a shell, and the influence of end conditions on the tube deformation was restricted to very small regions in the vicinity of each end (less than two diameters). These approximations are also valid for the flexible tube employed by Teslo et al.^{133,134} By assuming quasi-parallel flow, the tube deformation can be coupled with the flow-induced pressure drop in a straightforward manner.

Assuming the rigid pipe friction factor, λ can be employed locally for the flexible pipe (quasi-parallel flow) and that γ varies with Reynolds number, Re according to

$$\lambda = C R_e^{-\beta} = 0.3164 R_e^{-1/4}$$

which is related to the local pressure gradient by:

$$\frac{dP}{dx} = \frac{\lambda}{D} \frac{1}{2} \rho V^2$$

where D is the local pipe diameter, ρ is the fluid density, and V is the local mean velocity, the local pressure gradient can be developed as a function of diameter. If γ_o is the rigid pipe, fully developed pressure gradient, given by:

$$-\gamma_o = \frac{dP}{dx}_{\text{rigid}} = -\frac{\lambda_o}{D_o} \frac{1}{2} \rho V_o^2$$

it can be incorporated in the last equation along with the conservation of mass requirement:

$$VD^2 = V_o D_o^2$$

to write:

$$\frac{dP}{dx} = -\gamma_o \left(\frac{D_o}{D} \right)^{5-\beta}$$

Furthermore, the local diameter is given by:

$$D(x) = D_o + 2w = D_o \left[1 + \frac{R_o P(x) - \nu_T N_x}{\alpha} \right]$$

and the axial load, N_x is related to the applied tension, T and local fluid pressure, $P(x)$ by:

$$N_x = T + \frac{R_o}{2} P(x)$$

when the pressure at the end of the tube ($x = L$) is zero. Combining the last three equations

$$\frac{dP}{dx} = \frac{-\gamma_o}{1 - \frac{\nu}{\alpha} T + \frac{R_o}{\alpha} \left[1 - \left(\frac{\nu}{2} \right) P \right]^{5-\beta}}$$

which can be integrated between $x = 0$ and L to yield:

$$\left[1 - \frac{\nu}{\alpha} T + \frac{R_0}{\alpha} \left(1 - \frac{\nu}{2}\right) P_0\right]^{6-\beta} = \left(1 - \frac{\nu}{\alpha} T\right)^{6-\beta} + \frac{R_0 (6-\beta) \left(1 - \frac{\nu}{2}\right) \gamma_0 L}{\alpha}$$

or

$$P_0 = \frac{\alpha}{R_0 \left(1 - \frac{\nu}{2}\right)} \left[\left(1 - \frac{\nu}{\alpha} T\right)^{6-\beta} + \frac{(6-\beta) \left(1 - \frac{\nu}{2}\right) \gamma_0 R_0 L}{\alpha} \right]^{\frac{1}{6-\beta}} - \left(1 - \frac{\nu}{\alpha} T\right)$$

where P_0 is the pressure at $x = 0$, which in this case corresponds to the estimated pressure drop.

Using the flexible pipe data in Table I, the pressure drop has been calculated from this last equation for various Reynolds numbers and is shown in Figure 1. Since the effect of gravity (which was important in Pelt's⁴¹ vertical flow experiments) has been ignored, the calculated pressure drops cannot agree with Pelt's measurements — particularly at low Reynolds numbers where hydrostatic effects dominate. However, at Reynolds numbers of 50,000, the calculated pressure drop agrees with the measured data to within about 10% in all cases except for fygon tubing where the theoretical prediction was about 30% lower than the measured value.

The close agreement between theory and experiment may be fortuitous because end effects and visco-elastic effects have not been considered. End conditions would generally increase the pressure drop whereas visco-elastic creep would likely result in diametral increases and subsequent reductions in pressure drop. The latter effect may be responsible for the 25% drag reduction reported in Teslo et al.^{133,134} Teslo and Filipchuk¹³⁴ note a 3% increase in diameter occurred in their experiments, which is not predicted by the current theory. A 3% increase in diameter will cause a 15% reduction in pressure drop. Conversely, a 25% reduction can be caused by a 5% change in diameter which may be within the uncertainty of their measurements. Although the present investigation cannot show positively that the data of Teslo et al. are a result of pipe deformations, it appears very likely that creep may have occurred during those tests.

5.3 Reevaluation of Compliant Wall Experiments in Air With Water Substrates

A large portion of the successful compliant wall air data (which indicate drag reductions to 50%) were obtained at the University of Oklahoma during the years of 1966 through 1969.¹²⁶⁻¹³² A reevaluation of the Oklahoma experiments with water substrates (most of the data) was conducted at NASA Langley Research Center and is presented in Reference 138.

The Oklahoma experiments, conducted on compliant surfaces in air at subsonic speeds with foam and/or fluid substrates, measured directly the skin-friction drag on floating panel models which were mounted flush with the tunnel floor. The models, shown schematically in Figure 2, were mounted on a long, vertical, single-column beam. Weights were attached to the upstream portion of the models to counterbalance bending moments caused by the surface skin friction. This arrangement permitted very low drag forces to be measured on the compliant model panels (e.g., forces as small as 1/2% of the hard plate drag could be detected).

The models for Reference 127 had a compliant surface 63.8 cm long by 18.1 cm wide, whereas the model surface for Reference 128 was 38.1 cm long by 24.1 cm wide. Various fluid substrates with different viscosities (i.e., air, water, and solutions of water and Polyox) were explored in the investigation of Reference 127 which was conducted at a free-stream velocity of 11.6 m/sec. Skin-friction drag reductions up to 50% were reported for these tests. Reference 128 explored the effects of free-stream velocity (i.e., $U_\infty \approx 5.2 - 67.1$ m/sec) on the compliant wall drag reduction for porous polyurethane foam substrates (some of which were saturated with water), and drag reductions up to 38% were achieved. Both investigations used thin polyvinyl chloride (PVC) sheets, either 0.0064 cm or 0.0089 cm thick, for the compliant wall skins.

The following reevaluation of the Oklahoma water-backed membrane tests stems from thus-far unsuccessful attempts at NASA Langley Research Center to experimentally verify the University of Oklahoma experiments. As noted previously, References 35 and 125 were also unable to reproduce the liquid-backed Oklahoma experiments. No drag reductions were obtained in unpublished Langley experiments conducted in a small subsonic wind tunnel on floating panel compliant wall models with liquid substrates. The size of the models tested, the fluid substrates, and the flow conditions were similar to those reported in References 127 and 128, and are summarized in Table II. The major difference between the Langley experiments and those at the University of Oklahoma was the method of obtaining the direct skin-friction drag measurements. Whereas the University of Oklahoma experiments used the single-column, cantilever-beam type of arrangement, the Langley experiments supported the floating panels by thin wires attached to each of the four corners of the test panels outside the airstream (see Fig. 3). The drag force was then obtained by determining the amount of weight necessary to null the test plate to the original wind-off position.

In the Langley attempts to duplicate the University of Oklahoma experiments, small standing waves were measured on the compliant surface as the free-stream velocity was increased from 15 m/sec to 30 m/sec. These waves resembled sine waves with half of the wave protruding over the upstream portion of the model and the other half of the wave being recessed over the downstream end of the model. Reference 128 and private communications with Dr. Edward F. Blick of the University of Oklahoma acknowledged the existence of small standing waves in the Oklahoma tests at certain free-stream velocities. It is concluded that this information, coupled with the results of the Langley drag reduction experiments, suggest that standing waves in the University of Oklahoma experiments could have caused a shift in the model center of gravity and this shift may have created a bending moment on their single-column balance that was interpreted as a reduction in the skin-friction drag.

Reference 138 analytically determined the amplitude of a simple sine wave necessary to produce a center-of-gravity shift and resulting bending moment large enough to account for an apparent 40% reduction in skin-friction drag on a single-beam balance. The assumed wave shape is shown in Figure 2. Based on a

hard plate average skin-friction coefficient of 0.00389 for the tests of Reference 127, the apparent drag reduction was approximately 1.9 grams. For the balance moment arm of 85.7 cm in the University of Oklahoma tests, this apparent drag reduction could have generated a bending moment of 1.63 gm-m. The maximum amplitude of a sine wave necessary to shift the model center of gravity upstream and to create this bending moment was only 0.013 cm (assuming that the compliant wall skin was always in contact with the water substrate). As Reference 138 points out, surface motion this small would obviously be very difficult to detect with the unaided eye and could probably have been overlooked.

To check the analytically determined magnitude of the possible surface deflections, Reference 138 presents measured surface deflections for the Langley experiments of Figure 3 on a compliant wall model with 0.0064-cm-thick PVC skin stretched over a water-filled cavity. The tests were representative of those reported in Reference 127. The model had a compliant surface 66.0 cm long by 20.3 cm wide and was tested at a free-stream velocity of 16.2 m/sec. Uniform tension (≈ 3.5 N/m) was applied laterally and longitudinally to the compliant wall membrane with a vacuum-tensioning device. During the Langley drag reduction tests, the tension was actually varied over a wide range, and no drag reduction was observed. The value of 3.5 N/m for tension applies to the data runs for surface deformation measurements. An optical system, developed by L. M. Weinstein at NASA Langley, was used to measure the compliant wall surface deflections. The system used two photo detectors, 1.37 cm apart, driven on a track over the full length of the model surface. Each photo detector measured the instantaneous surface angle over a spot 0.13 cm in diameter to within 0.002 of a degree. However, for the data of Reference 139, only one detector was used to obtain a time-average surface angle. The original wind-off and then the wind-on surface angles were measured, and the differences between the two were integrated to obtain the flow induced change in surface position.

The surface position measurements of Reference 138 on the PVC compliant skin model with water-filled substrate are presented in Figure 4 for three longitudinal pressure gradients. Pressure gradients of these magnitudes were found in References 127 and 128. Reference 127 modified the upper tunnel wall in an attempt to eliminate or reduce the gradients, whereas Reference 128 "corrected" the drag measurements by calculating the bending moment induced by action of the "measured" variation in the surface pressures on the edges of the balance. In the study of Reference 138, the gradients were obtained by moving the tunnel sidewalls ± 0.318 cm from the mean zero pressure gradient position. These changes produced a 1.1% variation in the stream velocity with a 2.2% variation in static pressure. The corresponding changes in the static pressure (Δp) over the 76.2-cm-long model was approximately ± 3.4 N/m².

Reference 138 showed the large effect of only small pressure gradients on the formation of standing waves on the compliant wall surface (see Fig. 4). For the nearly zero pressure gradient, the surface protruded outward by approximately 0.009 cm. The positive gradient created a bulge over the upstream portion of the model, whereas the negative gradient caused the bulge to shift to the downstream portion of the surface. The model fairing plate around the compliant surface caused the surface to dip over the first 7.6-16.5 cm for all three gradients; the surface dipped over the last 23 cm for the zero and slightly positive gradients.

The water volume under each of the three waves in Figure 4 was integrated in the study of Reference 138 to determine the bending moment caused by the transfer of the water mass. The slightly positive gradient shifted the center of gravity upstream of the model center line and generated a 3-gm-m bending moment. The near zero and negative pressure gradients shifted the model center of gravity downstream of the model center line and generated 0.1 gm-m and 3.3 gm-m bending moments, respectively. As Reference 138 showed, these bending moments in each situation would be sufficient to significantly alter the drag reductions reported in References 127 and 128 and, hence, compromise the validity of the data (e.g., the 3-gm-m bending moment for the positive gradient could have indicated an apparent 70% "drag reduction"). A further problem with tests of this type is that, from the Langley experiments, the balance reading is quite sensitive to even small air leaks in the enclosure surrounding the tunnel and balance system. An excellent seal is mandatory for accurate data.

Structural Dynamics Analysis of Water-Backed Membranes. Having suggested that drag reduction did not occur for airflow over water-backed membranes, it is of interest to determine whether their characteristic surface response is in agreement with the arguments thus far which indicate that high-frequency surfaces are necessary for drag reduction. The influence of water backing on membrane surface motion has been studied by Blick⁸⁷ and Ash and Balasubramanian.³² Those analyses are similar, but the somewhat more detailed calculations of Ash and Balasubramanian³² are extended in the present work. Details of their calculations are given in Reference 32 and only the salient features of the model are discussed here.

Membrane motion has been assumed driven by three pressure force contributions — a direct turbulent wall pressure field and two reaction pressure fields induced by wall motion. The turbulent wall pressure was assumed to obey Taylor's "frozen pattern" hypothesis so that individual wave number pressure contributions could be analyzed one at a time. The turbulent wall pressure spectrum was modeled using Bull's¹³⁹ data, but modified for very low frequencies (Strouhal numbers, $\frac{\omega \delta^*}{U_\infty}$, below 0.05) by assuming the spectrum level fell off with the fourth power of wave number $\left(\frac{U_\infty}{\omega}\right)$. A potential flow model was employed to estimate the induced pressure field resulting from membrane motions over the water backing, and a wave equation could be solved to estimate the induced pressure on the turbulent air boundary-layer side of the membrane when wave velocities were different from the flow velocity.

Membrane deflection was developed using a normal mode expansion approach. Subsequently, surface motion calculations were obtained for individual turbulent wall pressure frequency contributions, which included the two induced pressure effects, and a spectrum of expected surface motion values was generated from the compilation of those frequencies. Calculation results are shown in Figure 5 for a typical case corresponding to the Langley data. It is obvious from these results that the surface motion is at quite low frequency, having very little motion at frequencies larger than the Strouhal number one level. This indicates that surface wave lengths are larger than the boundary-layer thickness and therefore more than an order of magnitude larger than values necessary for drag reduction according to the "burst modulation" mechanism described herein. Therefore, the null result (no drag reduction) on these surfaces is, in a sense, somewhat encouraging as far as verification of this theory is concerned.

5.4 High Frequency/Periodic Surfaces

The turbulence modification model (modulation of preburst flow) discussed previously requires short wave length, high-frequency surface motions for effective compliant wall interaction. Since that motion does not normally occur on structural panels, it is important to determine whether such motion could have been present during previously reported highly successful experiments. Three sets of such experiments cannot, at this point, be dismissed by alternate explanations: (1) Kramer's experiments⁵⁵⁻⁵⁷ in water, (2) Walters⁹⁰ experiments in air, and (3) the experiment of Fischer et al.¹² at low temperature (on the order of 0° C) in air. Aside from being in air, the experiments of Walters⁹⁰ and Fischer et al.¹² have marked similarities and will be discussed first.

In these experiments in air, both investigators employed thin rectangular membrane surfaces stretched over a soft elastic substrate. Walters⁹⁰ employed a thin polyvinyl chloride skin stretched over a porous polyurethane foam, while Fischer et al.¹² used a mylar skin stretched over a sticky, gelatinous layer of polyvinyl chloride plastisol. It should be noted that even though these substrates were structurally soft, both were very rigid from the standpoint of the available turbulent pressure forces. Walters⁹⁰ found that no drag reduction occurred when the membrane skin was attached to the substrate by means of a spray adhesive, but drag reduction did occur when the membrane simply rested against the substrate. Fischer et al.¹² apparently achieved significant drag reduction only when the wind-tunnel temperature was near 0° C. Recalling that the substrate employed by Fischer was naturally sticky, and noting further that a 20° C temperature drop would result in significant thermal contraction of the substrate, it is likely that the substrate pulled away from the mylar skin during the successful test. Both experiments suggest strongly that the substrate does not act effectively as a continuous spring during successful tests. Rather, those data indicate that the substrate may act intermittently to alter the motion of a conventional membrane. Specifically, if the membrane is separated from the substrate by a thin air gap, as shown in Figure 6, it is likely that the substrate functions as a "wavelength chopper." That is, by interfering with the downward displacement of long wave length fundamental membrane vibration modes, the substrate can act to drive the membrane into short wave length higher harmonic vibration modes. That possibility has been examined by Ash et al.¹³ and Ash and Balasubramanian³² and their results can be extended here.

The equations governing the motion of a membrane over a thin air gap are, in their simplest form, nonlinear.¹³ However, they can be analyzed using conventional finite-difference techniques. Because of the nonlinearity, it was very desirable to determine the dynamic surface motion under conditions of a simulated, nonfrozen, turbulent wall pressure loading. Details of the turbulence simulation are discussed briefly by Ash and Balasubramanian³² and simulated surface motion histories are also shown.

Again referring to Figure 6, the membrane substrate system employed by Fischer et al.¹² could change from (1) an integral system of a membrane attached to a continuous elastic spring, to (2) a membrane separated from its substrate by a thin gap, and finally (3) to a membrane over a cavity which is deep enough to eliminate contact between the membrane and substrate. Those three configurations have been subjected to the same simulated turbulent wall pressure to show the influence of those structural changes on the response amplitude spectra and are shown in Figure 7. It can be seen that the integral system produces a smoother, lower amplitude response, whereas the narrow air gap case yields a higher frequency motion.

Recently, unpublished experiments have been performed at Langley in which attempts were made to control the thin air gap behind a membrane in a low-speed airflow. The major finding of those tests was that a specified gap cannot be maintained beneath a membrane with any reasonable tolerance over a large surface. (Small localized "bubbles" did, however, occur and produced drag reductions of 10-15%.) That work is continuing, but alternate methods for producing short wave length, high-frequency surface motion are being examined. The most direct method for producing short wave-length motion is to employ a ribbed periodic substructure beneath a thin skin. The rib spacing can be used to control the surface wave length and frequency. However, analysis has shown that in the low-speed, turbulent, air boundary layers currently available for testing, reasonable amplitudes of surface motion cannot be achieved. That would not be the case in water and, since Kramer's⁵⁵ original model designs employed the types of periodic structures just suggested, a reexamination of his experiments is appropriate.

A cross section of one of Kramer's⁵⁵ successful compliant surfaces is shown in Figure 8, where the structural elements are periodic, that is, repeated with the same dimensions. If one assumes that Kramer achieved his drag reduction beneath a fully turbulent boundary layer, the reported average skin-friction coefficients can be used to estimate a turbulent wave length, λ^+ , ($\lambda^+ = \lambda u_\tau / \nu$) for the compliant surface. The variation of λ^+ was found to be between 200 and 500 over the velocity range (7 to 18 m/sec) of his successful tests.

It has been rather commonplace to discount Kramer's results, for many reasons. First, because the tests were performed by towing test models behind a motor boat in Long Beach Harbor, it has been reasoned that the tests may not have been as closely controlled as most laboratory facility experiments. Kramer acknowledges that his experiments were affected by the season (experiments in summer were less encouraging than at other times of the year) and attempts to duplicate his results in towing tanks⁵⁹ and water tunnels¹⁰⁹ were unsuccessful or inconclusive.

The structural dynamics response of Kramer's model has been recently examined at Langley assuming interaction with a fully turbulent boundary layer. For a two-dimensional model of the configuration shown in Figure 8, an approximately equivalent spring-dashpot (also shown) has been used to study the system, employing the method of space harmonics.²⁹ A frozen turbulence pattern was assumed with the same spectrum employed in the water-backed membrane analysis. The spectrum of surface motion is displayed in Figure 9 for the test conditions just mentioned and it is observed that significant high-frequency motion can be developed by that surface — adding further support to a high-frequency requirement and, by inference, the turbulence modification explanation.

To conclude this section, there is sufficient evidence in support of the turbulent burst modulation theory for compliant wall drag reduction to merit further investigation of high-frequency surfaces. Furthermore, surface motion measurements during successful tests are crucially needed, as are reliable numerical predictions of expected surface motion for a particular design (which also must be verified by experimental data). To date, the surface design concepts shown in Figure 10 have been examined on the basis of high-frequency surface motion potential. Of these concepts, only the membrane over the thin air gap and the periodic structures are considered promising at this time for significant modification of low-speed turbulent air boundary layers.

5.5 Air-Sea Interface as a Problem of Wall Motion Influence Upon Turbulence

As a final note on the influence of wall motion on wall turbulence structure, we discuss briefly the air-sea interface problem. As already mentioned, References 107 and 108 indicate that the suppression of small (capillary) waves on the ocean surface can alter much larger scales of turbulence in the atmosphere above the surface. In the absence of capillary waves, the air boundary layer appears to lose coherence with the ocean waves. The usual influence of the large ocean waves on skin friction is to increase drag¹⁴⁰ (evidently due to a roughness effect for traveling waves,¹⁴¹ and also zero wave speed case³⁷). Although there is still controversy, the wind generated waves on this "resonant surface" (air-sea interface) can evidently become large enough to separate the airflow between waves.¹⁴² Nevertheless, the present authors suggest that the information on the air-sea interface problem can at least be used to indicate regions in the "three space" of wave length, wave speed, and wave amplitude (normalized in law of the wall coordinates) which one should stay away from (drag increasing) in the design of resonant walls.

6. CONCLUDING REMARKS

In this paper we have reviewed, briefly, the following subjects pertinent to the use of walls with moving surface waves for drag reduction:

- (a) The need, in aeronautics, for drag reduction research using moving walls under turbulent boundary layers.
- (b) Simple structural dynamic considerations which indicate that practical walls must be of the "resonant" type and also periodic for control of wave length.
- (c) The influence of wall motion upon boundary-layer stability for highly compliant and also resonant walls and the stability of periodic flows. Recent Soviet experimental research indicates that resonant walls can also influence transition.
- (d) Theoretical models of the drag reduction mechanism for moving walls under turbulent boundary layers. The current best strategy, in the opinion of the present authors, is to investigate further an approach based upon modulation of the preburst flow. This modulation may result in delay of burst formation and the subsequent elimination of a reasonable percentage of the total number of bursts. This mechanism requires considerable further research but does provide a crude guideline for future experiments (small wave length, steep wave high-frequency surfaces).
- (e) A critical analysis of the available compliant wall data (resonant walls under turbulent boundary layers) — indicates that the best performance has been obtained using high-frequency response surfaces. Alternate explanations (other than alteration of the turbulence structure) are given for the drag reductions observed in pipe flows and also for liquid-backed membranes in air.

As a suggestion, further experiments should be conducted in water using both periodic and active (driven) surfaces, but over a much wider range of wave length than used in past experiments, particularly at the low end (smaller wave lengths). Due to the low dynamic pressures associated with air tests for velocities much less than transonic, subsequent air tests should concentrate initially on driven surfaces, especially with small wave length. All experiments should measure surface motion and, if a drag reduction is observed, the influence of the wall motion upon the bursting process should be determined. Also, redundant drag measurements should be mandatory.

The purpose of the active wall experiments is to provide a controlled experiment to determine what type of wall motion (wave speed, length, amplitude, etc.) is required to produce a drag reduction. These criteria can then be used to design passive surfaces which will work (or we will find out that such surfaces cannot be designed using today's technology and therefore a substantial supporting materials/structures research effort is needed).

7. REFERENCES

- ¹Nagel, A. L.; Alford, W. J., Jr.; and Dugan, J. F., Jr.: Future Long-Range Transports — Prospects for Improved Fuel Efficiency. AIAA Paper No. 75-316 presented at AIAA 11th Annual Meeting and Technical Display, Washington, D.C., February 24-26, 1975.
- ²Bower, R. E.: Opportunities for Aerodynamic Drag Reduction. NASA/University Conference on Aeronautics "The Future of Aeronautics," University of Kansas, Lawrence, Kansas, October 23-24, 1974, NASA CR-142559.
- ³Fischer, Michael C.; and Ash, Robert L.: A General Review of Concepts for Reducing Skin Friction, Including Recommendations for Future Studies. NASA TM X-2894, March 1974.
- ⁴Beckwith, Ivan E.; and Bushnell, Dennis M.: Calculation by a Finite-Difference Method of Supersonic Turbulent Boundary Layers With Tangential Slot Injection. NASA TN D-6221, April 1971.
- ⁵Marino, A.; Economos, C.; and Howard, F. G.: Evaluation of Viscous Drag Reduction Schemes for Subsonic Transports. NASA CR-132718, ATL TR 216, 1975.
- ⁶Pfeffer, Robert; and Rossetti, Salvatore J.: Experimental Determination of Pressure Drop and Flow Characteristics of Dilute Gas-Solid Suspensions. NASA CR-1894, August 1971.

- ⁷Lumley, J. L.: Drag Reduction in Turbulent Flow by Polymer Additives. *J. Polymer Sci. Macromolecular Reviews*, Vol. 7, 263-290 (1973).
- ⁸Bark, F. H.; Hinch, E. J.; and Landahl, M. T.: Drag Reduction in Turbulent Flow Due to Additives. A Report on Euromech 52. *J. Fluid Mechanics* (1975), Vol. 68, Part 1, pp. 129-138.
- ⁹Granville, Paul S.: Progress in Frictional Drag Reduction Summer 1974 to Summer 1975. Naval Ship Research and Development Center Report SPD 569-03, November 1975.
- ¹⁰Wood, Albert D.: International Conference on Drag Reduction. Office of Naval Research, London, England, Report AD/A-006 784, December 1975.
- ¹¹Blick, E. F.: Skin Friction Drag Reduction by Compliant Coatings. International Conference on Drag Reduction, September 4-6, 1974.
- ¹²Fischer, M. C.; Weinstein, L. M.; Bushnell, D. M.; and Ash, R. L.: Compliant Wall-Turbulent Skin-Friction Reduction Research. AIAA Paper No. 75-833 presented at the AIAA Eighth Fluid and Plasma Dynamics Conference, Hartford, Connecticut, June 16-18, 1975.
- ¹³Ash, R. L.; Bushnell, D. M.; Weinstein, L. M.; and Balasubramanian, R.: Compliant Wall Surface Motion and Its Effect on the Structure of a Turbulent Boundary Layer. Fourth Biennial Symposium on Turbulence in Liquids, September 1975, University of Missouri, Rolla.
- ¹⁴Zimmermann, G.: Interaction Between a Turbulent Boundary Layer and a Flexible Wall. Report 10a/1974, Max-Planck-Institut für Stromungsforschung, Göttingen.
- ¹⁵Antonatos, P. P.: Laminar Flow Control — Concepts and Applications. *Astronautics and Aeronautics*, July 1966, pp. 32-36.
- ¹⁶Grosskreutz, R.: Interaction Between Turbulent Boundary Layers and Compliant Walls. (Wechselwirkungen Zwischen Turbulenten Grenzschichten und Weichen Wänden.) Max-Planck-Institut für Stromungsforschung, 1971.
- ¹⁷Gyorgyfalvy, Dezso: The Possibilities of Drag Reduction by the Use of Flexible Skin. AIAA Paper No. 66-430, presented at Fourth Aerospace Sciences Meeting, Los Angeles, California, June 27-29, 1966.
- ¹⁸Pan, Y. S.: Noise Radiation From Turbulent Flows Over Compliant Surfaces. AIAA Paper No. 75-507, presented at AIAA Second Aero-Acoustics Conference, Hampton, Virginia, March 24-26, 1975.
- ¹⁹Von Winkel, W. A.; and Barger, J. E.: Evaluation of a Boundary Layer Stabilization Coating. *J. Acoust. Soc. Amer.* 33, p. 836 (1961).
- ²⁰Nisewanger, C. R.: Low Noise and Drag Measurements of Vehicle With Compliant Coating. NAVWEPS Report 8518, NOTS TP-3510, July 1964.
- ²¹Gray, Sir James: How Fishes Swim. *Scientific American*, p. 29, August 1957.
- ²²Kramer, Max O.: The Dolphins' Secret. *A.S.N.E. Journal*, February 1961, pp. 103-107.
- ²³Kramer, Max O.: Hydrodynamics of the Dolphin. *Advances in Hydrosience*, Vol. 2, 1965, pp. 111-130.
- ²⁴Lang, Thomas G.; and Pryor, Karen: Hydrodynamic Performance of Porpoises (*stenella attenuata*). *Science*, Vol. 152, April 1966, pp. 531-533.
- ²⁵Lang, T. G.: Speed, Power, and Drag Measurements of Dolphins and Porpoises. Symposium on Swimming and Flying in Nature, California Institute of Technology, Pasadena, California, July 1974.
- ²⁶Pemberton, T. Michael: An Evaluation of the Resistance Characteristics of Hydron Paint Using Models 4125 and 4667-1. N.S.R.D.C. Test and Evaluation Report No. P-351-H-01, September 1969.
- ²⁷Van Londen, A. M.: A Study on the Importance of the Ship's Hull Condition. National Bureau of Standards Special Publication, Proceedings of the Third International Congress on Marine Corrosion and Fouling, held October 2-6, 1972, Gaithersburg, Maryland.
- ²⁸"Flow-Induced Structural Vibrations," IUTAM-IAHR Symposium Karlsruhe (Germany) August 14-16, 1972, Edited by Eduard Naudascher, Springer-Verlag.
- ²⁹Mead, D. J.; and Pujara, K. K.: Space-Harmonic Analysis of Periodically Supported Beams; Response to Convected Random Loading. *Journal of Sound and Vibration*, Vol. 14, No. 4, pp. 525-541, 1971.
- ³⁰Kerkman, E. F.; and Kerwin, E. M., Jr.: Unified Approach to the Technology of Thin Compliant Coatings. Volume II. Coating Models: Relation of Coating Geometric Configuration and Material Properties to Coating Acoustic Properties. Bolt Beranek and Newman, Inc., Report No. 2374, June 1972.
- ³¹Tokita, N.; and Boggs, F. W.: Final Report on Theoretical Study of Compliant Coatings to Achieve Drag Reduction on Underwater Vehicles. United States Rubber Company, Research and Development Department Research Center, Wayne, New Jersey, March 1962.
- ³²Ash, Robert L.; and Balasubramanian, R.: Resonance Phenomena Due to Turbulent Boundary Layer Excitation. Preprint 2726, presented at ASCE National Water Resources and Ocean Engineering Convention, San Diego, California, April 5-8, 1976.

33. Kramer, M. O.: Material Requirements for Boundary-Layer Stabilizing Coatings — Water Application. The Rand Corporation, Memorandum RM-3018-PR, August 1962.
34. Hansen, R. J.; and Hunston, D. L.: An Experimental Study of Turbulent Flows Over Compliant Surfaces. *Journal of Sound and Vibration* (1974), pp. 1-13.
35. Lissaman, P. B. S.; and Harris, Gordon L.: Turbulent Skin Friction on Compliant Surfaces. AIAA Paper No. 69-164 presented at AIAA Seventh Aerospace Sciences Meeting, New York, New York, January 20-22, 1969.
36. Blick, Edward F.; Walters, Robert R.; Smith, Roger; and Chu, Humphrey: Compliant Coating Skin Friction Experiments. AIAA Paper No. 69-165, presented at AIAA Seventh Aerospace Sciences Meeting, New York, New York, January 20-22, 1969.
37. Cancelli, C.; and Vatta, F.: Experimental Investigation of the Coefficient of Friction in the Turbulent Flow of an Incompressible Fluid in the Presence of an Undulated Wall. NASA TT F-16,525, August 1975. *Accademia della Scienze, Classe di Scienze Fisiche, Matematiche Naturali, Memorie No. 20*, 1974, pp. 1-20.
38. Kendall, James M.: The Turbulent Boundary Layer Over a Wall With Progressive Surface Waves. *J. Fluid Mech.*, 1970, Vol. 41, Part 2, pp. 259-281.
39. Landahl, Marten T.: On the Stability of a Laminar Incompressible Boundary Layer Over a Flexible Surface. *J. Fluid Mech.*, 13, November 1961, pp. 609-632.
40. Benjamin, T. B.: Fluid Flow With Flexible Boundaries. *Applied Mechanics, Proceedings of the 11th International Congress of Applied Mechanics, Munich, Germany, 1964*, pp. 109-128.
41. Pelt, R. J.: A Preliminary Investigation of Surface Damping Effects on Fluid Flow Through Flexible Tubes. University of Pittsburgh, Ph. D. Thesis, 1964.
42. Benjamin, T. Brooke: Effects of a Flexible Boundary on Hydrodynamic Stability. *J. Fluid Mechanics*, September 1960, pp. 513-532.
43. Betchov, R.: Simplified Analysis of Boundary-Layer Oscillations. Douglas Aircraft Company Report, No. ES-29174, p. 1, 1959.
44. Boggs, F. W.; and Tokita, N.: A Theory of the Stability of Laminar Flow Along Compliant Plates. Paper presented at the Third Symposium on Naval Hydrodynamics, Scheveningen, Holland, Vol. 3, p. 451, 1960.
45. Hains, F. D.; and Price, J. F.: Effect of a Flexible Wall on the Stability of Poiseuille Flow. *The Physics of Fluids*, Vol. 5, No. 3, March 1962, pp. 365-369.
46. Nonweiler, T.: Qualitative Solutions of the Stability Equation for a Boundary Layer in Contact With Various Forms of Flexible Surfaces. A.R.C. Report, No. 22, p. 670, 1961.
47. Linebarger, John H.: On the Stability of a Laminar Boundary Layer Over a Flexible Surface in a Compressible Fluid. M.S. Thesis, Massachusetts Institute of Technology, June 1961.
48. Benjamin, T. Brooke: The Threefold Classification of Unstable Disturbances in Flexible Surfaces Bounding Inviscid Flows. *J. Fluid Mechanics*, Vol. 16, 1963, pp. 436-450.
49. Landahl, Marten T.: On the Stability of a Laminar Incompressible Boundary Layer Over a Flexible Surface. *J. Fluid Mechanics*, 13, 1963, pp. 609-632.
50. Kaplan, Richard E.: The Stability of Laminar Incompressible Boundary Layers in the Presence of Compliant Boundaries. Massachusetts Institute of Technology, Report ASRL TR 116-1, June 1964, pp. 1-179.
51. Takematsu, Masaki: Stability of a Laminar Flow Along a Flexible Boundary. Kyushu University, Research Institute for Applied Mechanics, Reports, Vol. 16, No. 53, 1968, pp. 109-120.
52. Burden, Harvey W.: The Effect of Wall Porosity on the Stability of Parallel Flows Over Compliant Boundaries. University of Pennsylvania, Requirements for the Degree of Doctor of Philosophy, 1969.
53. Amfilokhiyev, V. B.; Droblennov, V. V.; and Zavorokhina, A. S.: Increase of Small Disturbances in the Boundary Layer on an Elastic Surface. NASA TT F-14,855, *Zhurnal Prikladnoi Mekhaniki i Tekhnicheskoy fiziki*, March-April 1972, pp. 137-139.
54. Wehrmann, O. H.: Tollmien-Schlichting Waves Under the Influence of a Flexible Wall. *Physics of Fluids*, Vol. 8, July 1965, pp. 1389-1390.
55. Kramer, Max O.: Boundary Layer Stabilization by Distributed Damping. *A.S.N.E. Journal*, February 1960, pp. 25-34.
56. Kramer, Max O.: Boundary Layer Stabilization by Distributed Damping. *Naval Engineers Journal*, May 1962, pp. 341-348.
57. Kramer, Max O.: Die Widerstandsverminderung Schneller Unterwasserkörper Mittels Künstlicher Delphinhaut. (The Drag Reduction of Fast Underwater Bodies With the Aid of an Artificial Dolphin Skin.) 1969 Yearbook of the German Society of Aeronautics and Astronautics, pp. 102-110.

- ⁵⁸Rhines, Peter B.; and Mollo-Christensen, Erik L.: Boundary Layer Oscillations Over a Resonant Surface. The Physics of Fluids, Vol. 10, No. 5, May 1967, pp. 916-926.
- ⁵⁹Puryear, F. W.: Boundary Layer Control-Drag Reduction by Use of Compliant Coatings. David Taylor Model Basin, Hydromech. Lab., Res. and Devel. Report 1668, 1962.
- ⁶⁰Galway, R. D.: An Investigation Into the Possibility of Laminar Boundary Layer Stabilization Using Flexible Surfaces. M.S. Thesis, Dept. Aero. Eng., Queens University, Belfast, Ireland, 1963.
- ⁶¹Babenko, V. V.: Part IV. Skin Cover Structure. Principal Characteristics of Flexible Coverings and Similarity Criteria. Bionika, No. 5, 1971, Kiev.
- ⁶²Babenko, V. V.: Technique for Determining the Mechanical Properties of Flexible Coatings and a Basis for the Selection of Their Design. NASA TT F-16,392. (Translation of: "Metodika opredeleniya mekhanicheskikh svoystv i obosnovaniye vybora konstruktsii gibkikh pokrytiy," Bionika, No. 7, 1973, pp. 71-29.)
- ⁶³Babenko, V. V.; and Kozlov, L. F.: Experimental Investigation of Hydrodynamic Stability at Rigid and Elastic-Damping Surfaces. (Eksperimental'noe issledovanie gidrodinamicheskoi ustoychivosti na zhestkoi i uprugodempfiruiushchikh poverkhnostiakh.) Akademiia Nauk SSSR, Izvestiia Mekhanika Zhidkosti i Gaza, January-February 1973, pp. 122-127.
- ⁶⁴Babenko, V. V.: Experimental Investigation of Hydrodynamic Stability for Flows Past Simple Membrane Surfaces. (Eksperimental'noe issledovanie gidrodinamicheskoi estoichivosti pri obtekanii prostykh membrannykh poverkhnostei.) Akademiia Nauk Ukrainsoi SSR, Gidromekhanika, No. 24, 1973, pp. 3-11.
- ⁶⁵Karplus, Henry B.: Turbulent Flow Transition Near Solid and Flexible Boundaries. IIT Research Institute, Chicago, Illinois, Report No. IITRI 1205-4, March 1963.
- ⁶⁶Kestin, J.; Maeder, P. F.; and Wang, H. E.: On Boundary Layers Associated With Oscillating Streams. Appl. Sci. Res., Section A, Vol. 10, April 1960, pp. 1-22.
- ⁶⁷Levchenko, V. Ya; and Solov'ev, A. S.: Boundary Layer Stability on a Wave-Periodic Surface. (Novosibirsk, Translated from Izvestiya Akademii Nauk SSSR.) Mekhanika Zhidkosti i Gaza, No. 6, pp. 11-16, 1972.
- ⁶⁸Davis, Stephen H.: The Stability of Time-Periodic Flows. Annual Review of Fluid Mechanics, Vol. 8, 1976, Annual Reviews Incorporated, Palo Alto, California, pp. 57-74.
- ⁶⁹Loehrke, R. I.; Morkovin, M. V.; and Fejer, A. A.: Review — Transition in Nonreversing Oscillating Boundary Layers. Journal of Fluids Engineering, December 1975, pp. 534-549.
- ⁷⁰Obremski, H. J.; and Fejer, A. A.: Transition in Oscillating Boundary Layer Flows. J. Fluid Mechanics, 1967, Vol. 29, Part 1, pp. 93-111.
- ⁷¹Obremski, Henry J.; and Morkovin, Mark V.: Application of a Quasi-Steady Stability Model to Periodic Boundary-Layer Flows. AIAA Journal, Vol. 7, No. 7, July 1969, pp. 1298-1301.
- ⁷²Loehrke, R. I.; Morkovin, M. V.; and Fejer, A. A.: New Insights on Transition in Oscillating Boundary Layers. AFOSR Scientific Report, AFOSR 70-1586TR. Presented at the Fluid Dynamics Symposium, August 25-27, 1970, at McMaster University, Hamilton, Ontario, Canada.
- ⁷³Kobashi, Y.; Hayakawa, M.; and Nakagawa, K.: Development of Disturbances in Unsteady Boundary Layers. Proc. Symp. Unsteady Aerodynamics, sponsored by USAF-AFOSR and University of Arizona, 1975.
- ⁷⁴Von Kerczek, Christian; and Davis, Stephen H.: Linear Stability Theory of Oscillatory Stokes Layers. J. Fluid Mech., 1974, Vol. 62, Part 4, pp. 753-773.
- ⁷⁵Grosch, Chester E.; and Salwen, Harold: The Stability of Steady and Time-Dependent Plane Poiseuille Flow. J. Fluid Mech., 1968, Vol. 34, Part 1, pp. 177-205.
- ⁷⁶Sergeev, S. I.: Fluid Oscillations in Pipes at Moderate Reynolds Numbers. Fluid Dynamics, Vol. 1, No. 1 (Mekhanika Zhidkosti i Gaza, Vol. 1, No. 1, pp. 168-170, 1966).
- ⁷⁷Finucane, R. G.; and Kelly, R. E.: Onset of Instability in a Fluid Layer Heated Sinusoidally From Below. Int. J. Heat Mass Transfer, Vol. 19, pp. 71-85, Pergamon Press, 1976.
- ⁷⁸Donnelly, R. J.: Experiments on the Stability of Viscous Flow Between Rotating Cylinders. III. Enhancement of Stability by Modulation. Proc. R. Soc. A281, 130-139, 1964.
- ⁷⁹Donnelly, R. J.; Reif, F.; and Suhl, H.: Enhancement of Hydrodynamic Stability by Modulation. Physical Review Letters, Vol. 9, No. 9, November 1962, pp. 363-365.
- ⁸⁰Landahl, M. T.: Drag Reduction by Polymer Addition. Proceedings of the 13th International Congress of Theoretical and Applied Mechanics. Moscow University, August 21-26, 1972. Eds. E. Becker and G. K. Mikhailov.
- ⁸¹Loudenback, L. D.; and Abbott, D. E.: Time-Dependent Turbulent Wall Layers in a Nominally Steady Flow. School of Mechanical Engineering, Purdue University Technical Report CFM TR-73-1, 1973.
- ⁸²Davis, Russ E.: Perturbed Turbulent Flow, Eddy Viscosity and the Generation of Turbulent Stresses. J. Fluid Mech., 1974, Vol. 63, Part 4, pp. 673-693.

- ⁸³Hussain, A.; and Reynolds, W. D.: The Mechanics of an Organized Wave in Turbulent Shear Flow. Part 3, J. Fluid Mech., 54, 263, 1972.
- ⁸⁴Karlsson, Sture K. F.: An Unsteady Turbulent Boundary Layer. J. Fluid Mech., Vol. 5, Part 4, May 1959, pp. 622-636.
- ⁸⁵Gougat, P.: External Sound Field Effect on a Turbulent Layer. NASA TT F-15,852. Translation of "influence d'un champ acoustique exterieur sur une couche limite turbulente," Centre National de la Recherche Scientifique, Meudon, France, Lab. d'Aerothermique, Rept. 70-8, September 1970, 51 pp.
- ⁸⁶Ffowcs-Williams, J. E.: Reynolds Stress Near a Flexible Surface Responding to Unsteady Air Flow. Bolt Beranek and Newman Inc., Report No. 1138, June 1964, pp. 1-22.
- ⁸⁷Blick, Edward F.: The Theory of Skin Friction Reduction by a Compliant Coating in a Turbulent Boundary Layer. University of Oklahoma. Reprinted from: Viscous Drag Reduction, Plenum Press, 1969, pp. 409-425.
- ⁸⁸Semenov, B. N.: Interaction of an Elastic Boundary With the Viscous Sublayer of a Turbulent Boundary Layer. NASA TT F-14,391. Translation of "O vzaimodeystvii elastichnoy granitsy a vyazkim plosloyem turbulentnogo pogrannichnogo sloya," Zhurnal Prikladnoy Mekhaniki i Tekhnicheskoy Fiziki, May-June 1971, No. 3, pp. 58-62.
- ⁸⁹Sternberg, J.: A Theory for the Viscous Sublayer of a Turbulent Flow. J. Fluid Mech., Vol. 13, No. 2, 1962.
- ⁹⁰Walters, Robert R.: Turbulent Boundary Layer Characteristics of Flow Over a Compliant Surface. The University of Oklahoma, Ph. D. Thesis, 1969.
- ⁹¹Amfilokhiyev, V. B.: Turbulent Flows With Elastic Boundaries. NASA TT F-14,601. (Translation of "Turbulentnyye techeniya s uprugimi granitsami," IN: Gidrodinamicheskiye voprosy bioniki Hydrodynamic Problems of Bionics), Edited by S. A. Shalayeva, Kiev, "Naukova Dumka" Press, No. 3, 1969, pp. 46-53.
- ⁹²Ash, Robert L.: On the Theory of Compliant Wall Drag Reduction in Turbulent Boundary Layers. NASA CR-2387, April 1974.
- ⁹³Grosskreutz, R.: An Attempt to Control Boundary Layer Turbulence With Nonisotropic Compliant Walls. University Science Journal (Dares Salaam Univ.) 1 (1) 1975, pp. 65-74.
- ⁹⁴Burton, Thomas E.; and Leehey, Patrick: The Connection Between Intermittent Turbulent Activity Near the Wall of a Turbulent Boundary Layer With Pressure Fluctuations at the Wall. Degree of Doctor of Science Thesis, Massachusetts Institute of Technology, February 1974.
- ⁹⁵Offen, G. R.; and Kline, S. J.: A Proposed Model of the Bursting Process in Turbulent Boundary Layers. J. Fluid Mech., Vol. 70, Part 2, 1975, pp. 209-228.
- ⁹⁶Laufer, John: New Trends in Experimental Turbulence Research. Annual Review of Fluid Mechanics, Vol. 7, 1975, pp. 307-326.
- ⁹⁷Willmarth, W. W.: Structure of Turbulence in Boundary Layers. Advances in Applied Mechanics, Vol. 15, 1975.
- ⁹⁸Einstein, H. A.; and Li, Huon: Shear Transmission From a Turbulent Flow to Its Viscous Boundary Sub-Layer. Heat Transfer and Fluid Mechanics Inst., Chapter XIII, June 23-25, 1955, pp. 1-16.
- ⁹⁹Black, Thomas J.: Some Practical Applications of a New Theory of Wall Turbulence. Heat Transfer and Fluid Mechanics Inst., 1966, pp. 366-386.
- ¹⁰⁰Willmarth, W. W.: Space-Time Correlations and Spectra of Wall Pressure in a Turbulent Boundary Layer. NASA Memo 3-17-59W, March 1959.
- ¹⁰¹Cliff, William C.; and Sandborn, Virgil A.: Correlation Between the Outer Flow and the Turbulent Production in a Boundary Layer. NASA TM X-64935, May 1975.
- ¹⁰²Blackwelder, Ron; and Kovaszny, Leslie S. G.: Large Scale Motion of a Turbulent Boundary Layer With a Zero and a Favorable Pressure Gradient. Interim Technical Report, DA-31-124-ARO-D-313, July 1970.
- ¹⁰³Bull, M. K.; and Thomas, A. S. W.: High Frequency Wall-Pressure Fluctuations in Turbulent Boundary Layers. Phys. of Fluids, Vol. 19, No. 4, April 1976, pp. 597-599.
- ¹⁰⁴Blackwelder, R. F.; and Woo, H. H. W.: Pressure Perturbation of a Turbulent Boundary Layer. The Physics of Fluids, Vol. 17, No. 3, March 1974, pp. 515-519.
- ¹⁰⁵Landahl, Marten T.: Wave Mechanics of Breakdown. J. Fluid Mechanics, Vol. 56, 1972, p. 775.
- ¹⁰⁶Bark, Fritz H.: On the Wave Structure of Turbulent Boundary Layers With Application to Drag Reduction. TRITA-MEK-74-01, The Royal Institute of Technology, Department of Mechanics, S-100 44 Stockholm 70, Sweden, 1974.
- ¹⁰⁷Barger, William R.; Garrett, William D.; Mollo-Christensen, Erik L.; and Ruggles, Kenneth W.: Effects of an Artificial Sea Slick Upon the Atmosphere and the Ocean. J. of Applied Meteorology, Vol. 9, 1970, pp. 396-400.

- 108 Mollo-Christensen, Erik: Intermittency in Large-Scale Turbulent Flows. Annual Review of Fluid Mechanics, Vol. 5, 1973, pp. 101-118.
- 109 Ritter, H.; and Porteous, J. S.: Water Tunnel Measurements of Skin Friction on a Compliant Coating. ARL, Teddington, Middlesex, A.R.L./N3/G/HY/9/7, June 1965.
- 110 Private Communication with Max O. Kramer, 1976.
- 111 Ritter, H.; and Messum, L. T.: Water Tunnel Measurements of Turbulent Skin Friction on Six Different Compliant Surfaces of 1-Ft. Length. ARL, Teddington, Middlesex, A.R.L./N1/G/NY/9/7, June 1964.
- 112 Laufer, J.; and Maestrello, L.: The Turbulent Boundary Layer Over a Flexible Surface. The Boeing Co., Document No. DY-9708, October 1963.
- 113 Private Communication with Lucio Maestrello, 1976.
- 114 Smith, Larry LaCross: An Experiment on Turbulent Flow in a Pipe With a Flexible Wall. M.S. Thesis, University of Washington, 1963.
- 115 Dinkelacker, A.: Preliminary Experiments on the Influence of Flexible Walls on Boundary Layer Turbulence. J. Sound and Vib., 4 (2), 1966, 187-214.
- 116 Dinkelacker, A.: Preliminary Experiments on the Influence of Flexible Walls on Boundary Layer Turbulence. DLR FB 66-78, Deutsche Luft- und Raumfahrt Forschungsbericht 66-78.
- 117 Taneda, Sadatoshi; and Honji, Hiroyuki: The Skin-Friction Drag on Flat Plates Coated With Flexible Material. Reports of Research Institute for Applied Mechanics, Kyushu University, Vol. XV, No. 49, 1967.
- 118 Mattout, R.: Reduction de trainee par parois souples (Reduction of Drag by Flexible Walls), Association Technique Maritime et Aeronautique, Bulletin No. 72, pp. 207-227, 1972.
- 119 Mattout, R.: Etude Experimentale En Tunnel Hydrodynamique De La Reduction De Trainee Par L'Utilisation De Parois Souples Passives. Mesures Globales. (Experimental Study in a Water Tunnel of Drag Reduction by the Use of Stationary Flexible Walls. Summary of Results.) Societe Bertin & Cie, RM/FC-FA-Le, December 1971.
- 120 Mattout, R.; and Cottenceau, B.: Etude Experimentale De Une Paroi Souple Activee en Tunnel Hydrodynamique. Mesures Globales. (Experimental Study of a Waving Flexible Wall in a Water Tunnel: Summary of Results.) Societe Bertin & Cie, Note technique No. 71-CI-09, RM/VBA - Le 23 Mars 1972.
- 121 Botman, M.: Propulsion by Undulating Plates. AIAA Paper No. 64-461, Presented at First AIAA Annual Meeting, Washington, D.C., June 29-July 2, 1964.
- 122 Grosskreutz, R.: Interaction Between Turbulent Boundary Layers and Compliant Walls. (Wechselwirkungen zwischen turbulenten Grenzschichten und weichen Wanden.) Max-Planck-Institut fur Stromungsforschung, 1971.
- 123 Grosskreutz, R.: Navships Translation No. 1320 — Interaction Between Turbulent Boundary Layers and Compliant Walls. (Wechselwirkungen zwischen turbulenten Grenzschichten und weichen Wanden.) Mitteilungen aus dem Max-Planck-Institut fur Stromungsforschung und der Aerodynamischen Versuchsanstalt, Nr. 53, Gottingen, 1971.
- 124 Kawamata, Shin; Kato, Toyofumi; Matsumura, Yoshihiko; and Sato, Tomohiro: Experimental Research on the Possibility of Reducing the Drag Acting on a Flexible Plate. Theoretical and Applied Mechanics, University of Tokyo Press, Vol. 21, 1973, pp. 507-518.
- 125 McAlister, Kenneth W.; and Wynn, Thom M.: Experimental Evaluation of Compliant Surfaces at Low Speeds. NASA TM X-3119, October 1974.
- 126 Blick, Edward F.; and Walters, Robert R.: Turbulent Boundary-Layer Characteristics of Compliant Surfaces. J. of Aircraft, Vol. 5, No. 1, January-February 1968, pp. 11-16.
- 127 Looney, William R.; and Blick, Edward F.: Skin-Friction Coefficients of Compliant Surfaces in Turbulent Flow. J. of Spacecraft, Vol. 3, No. 10, October 1966, pp. 1562-1564.
- 128 Chu, Humphrey H.; and Blick, Edward F.: Compliant Surface Drag as a Function of Speed. J. of Spacecraft, Vol. 6, No. 6, June 1969, pp. 763-764.
- 129 Looney, William R.: Skin Friction Coefficients of Compliant Surfaces in Turbulent Flow. M.E. Thesis, University of Oklahoma, 1966.
- 130 Fisher, Donald H.; and Blick, Edward F.: Turbulent Damping by Flabby Skins. J. of Aircraft, Vol. 3, No. 2, 1966, pp. 163-164.
- 131 Blick, Edward F.: Skin Friction Drag Reduction by Compliant Coatings. USARO Final Report, DA-31-124-AGROD-349, May 1974.
- 132 Chu, Humphrey H.: Drag Characteristics for a Compliant Surface Airfoil. Doctor of Philosophy Thesis, University of Oklahoma, 1971.

- ¹³³ Teslo, A. P.; and Zhoga, V. A.: Some Results of Experimental Investigations of Turbulent Flow in Flexible Pipes — Selected articles from the Russian-language journal *Gidromekhanika*, No. 24, 1973, Kiev in "Turbulent Flow in Flexible Pipes and Ramjet Engines," JPRS 60785, December 1973.
- ¹³⁴ Teslo, A. P.; and Filipchuk, V. Ye: Influence of a Compliant Surface on the Characteristics of Turbulent Flow. Translation of *Gidromekhanika*, No. 29, 1974, pp. 45-50. NASA TT F-16, 555.
- ¹³⁵ Klinzing, G. E.; Kubovcik, R. J.; and Marmo, J. F.: Frictional Losses in Foam-Damped Flexible Tubes. *I&EC Process Design and Development*, Vol. 8, No. 1, January 1969, pp. 112-114.
- ¹³⁶ Ivlev, U. P.: Investigation of the Characteristics of Turbulent Air Flow in a Channel With Elastic Walls. (Issledovanie kharakteristik turbulentnogo potoka vozdukha v kanale s uprugimi stenkami.) *Bionika*, No. 6, 1972, pp. 39-41.
- ¹³⁷ Ash, Robert L.: Flexible Pipe Deformations Resulting From Applied Tension and Pressure Gradients. Old Dominion University Technical Report 76-T1, March 1976.
- ¹³⁸ Hefner, Jerry N.; and Weinstein, Leonard M.: Re-examination of Compliant Wall Experiments in Air With Water Substrates. *AIAA J. of Spacecraft and Rockets*, Vol. 13, No. 8, August 1976, pp. 502-503.
- ¹³⁹ Bull, M. K.: Wall-Pressure Fluctuations Associated With Subsonic Turbulent Boundary Layer Flow. *J. Fluid Mechanics*, Vol. 28, 1967, pp. 719-754.
- ¹⁴⁰ Stewart, Robert H.: Laboratory Studies of the Velocity Field Over Deep-Water Waves. *J. Fluid Mechanics*, Vol. 42, Part 4, 1970, pp. 733-754.
- ¹⁴¹ Plate, E. J.; and Hidy, G. M.: Laboratory Study of Air Flowing Over a Smooth Surface Onto Small Water Waves. *J. of Geophysical Research*, Vol. 72, No. 18, September 1967, pp. 4627-4641.
- ¹⁴² Chang, P. C.; Plate, E. J.; and Hidy, G. M.: Turbulent Air Flow Over the Dominant Component of Wind-Generated Water Waves. *J. Fluid Mechanics*, Vol. 47, Part 1, 1971, pp. 183-208.

ACKNOWLEDGMENT

The authors would like to thank Mr. Ramakrishnan Balasubramanian for his contribution to this work.

TABLE I. FLEXIBLE PIPE DATA

Pipe material	Thick rubber (a)	Thin rubber (a)	Tygon (a)	Texin (a)	Polyethylene (b)
L, m	2.79	2.79	2.79	2.79	2.80
R ₀ , mm	4.8	4.8	4.8	4.0	25.0
δ_T , mm	5.6	3.6	1.6	.8	.16
E, N/cm ²	140	70	250	1000	15,000
v_T	0.49	0.49	0.45	0.45	0.45
T*, N/cm	5.2	2.4	3.8	3.3	NA
$\Delta P_{\text{measured}}, \frac{N}{cm^2}$	18.1	12.8	18.6	22.0	0.110
P ₀ (T = 0), $\frac{N}{cm^2}$	20.3	12.2	13.4	24.8	.128
$\Delta P_{\text{rigid}}, \frac{N}{cm^2}$	24.7	18.0	18.0	31.1	.128

(a) Data from Pelt (Ref. 41).

(b) Data from Teslo and Zhoga (Ref. 133).

*Tension estimation based on reported elongation.

TABLE II. COMPARISON OF LANGLEY RESEARCH CENTER AND UNIVERSITY OF OKLAHOMA
EXPERIMENTS IN AIR WITH WATER SUBSTRATES

		University of Oklahoma	
		Looney/Blick	Chu/Blick
Stream velocity	9-30 m/sec	11.6 m/sec	5-67 m/sec
Model surface			
Length	66 cm	63.8 cm	38.1 cm
Width	20.3 cm	18.1 cm	24.1 cm
Depth	1.27 cm	.79 cm	1.27 cm
Membrane			
Material	PVC	PVC	PVC
Thickness	0.0064 cm	0.0064 & 0.0089 cm	0.0064 cm
Longitudinal tension	3.5 N/m	4-111.7 N/m	55.3 N/m
Lateral tension	3.5 N/m	1.9-55.5 N/m	53.6 N/m

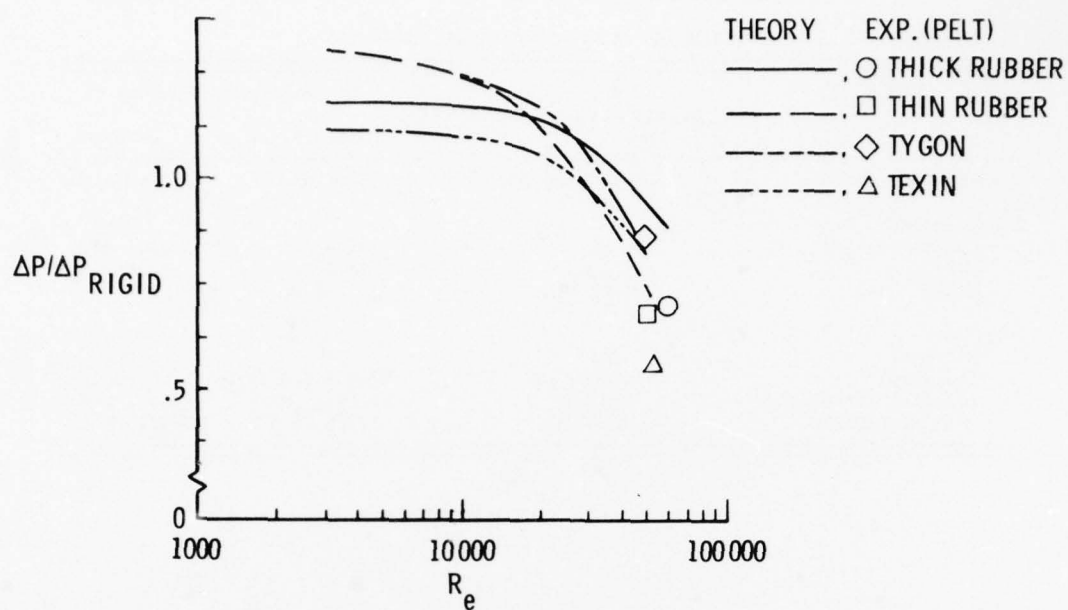


Figure 1. Variation of flexible pipe pressure drop with Reynolds number.

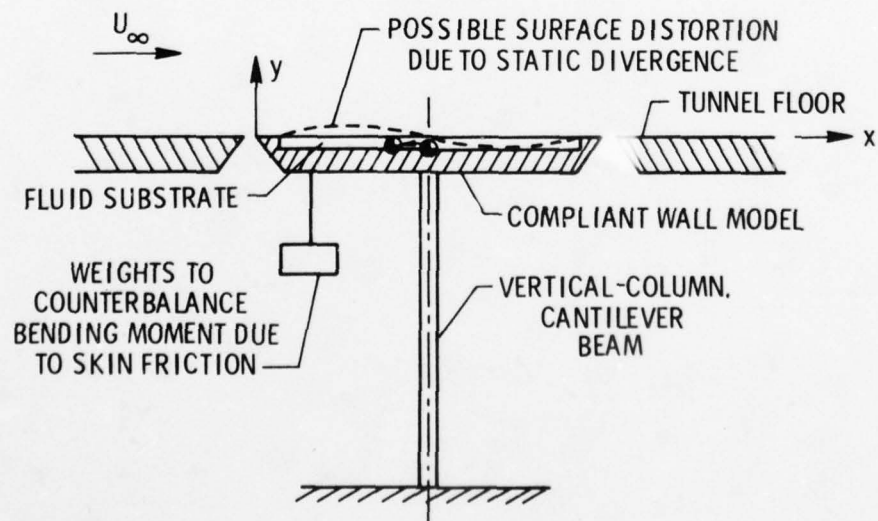


Figure 2. Typical University of Oklahoma experiment.

LaRC ATTEMPTED REDO OF TYPICAL UNIVERSITY OF OKLAHOMA EXPERIMENT

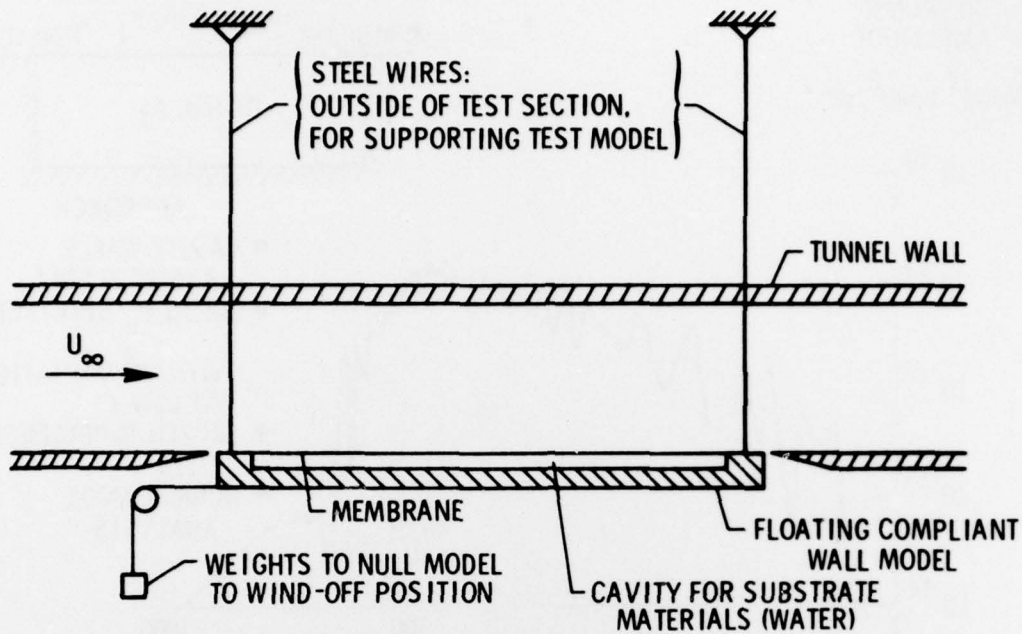


Figure 3. Airflow over water-backed membranes. Langley attempted redo of typical University of Oklahoma experiments.

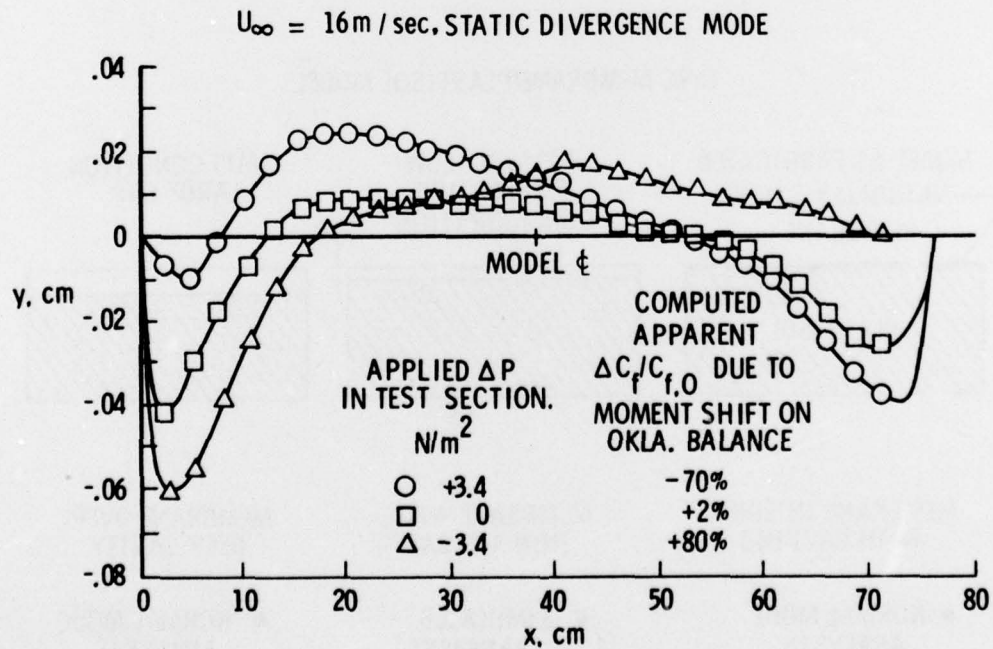


Figure 4. Surface position measurements for compliant surface with water substrate in Langley experiments. $U_{\infty} = 16 \text{ m/sec. static divergence mode.}$

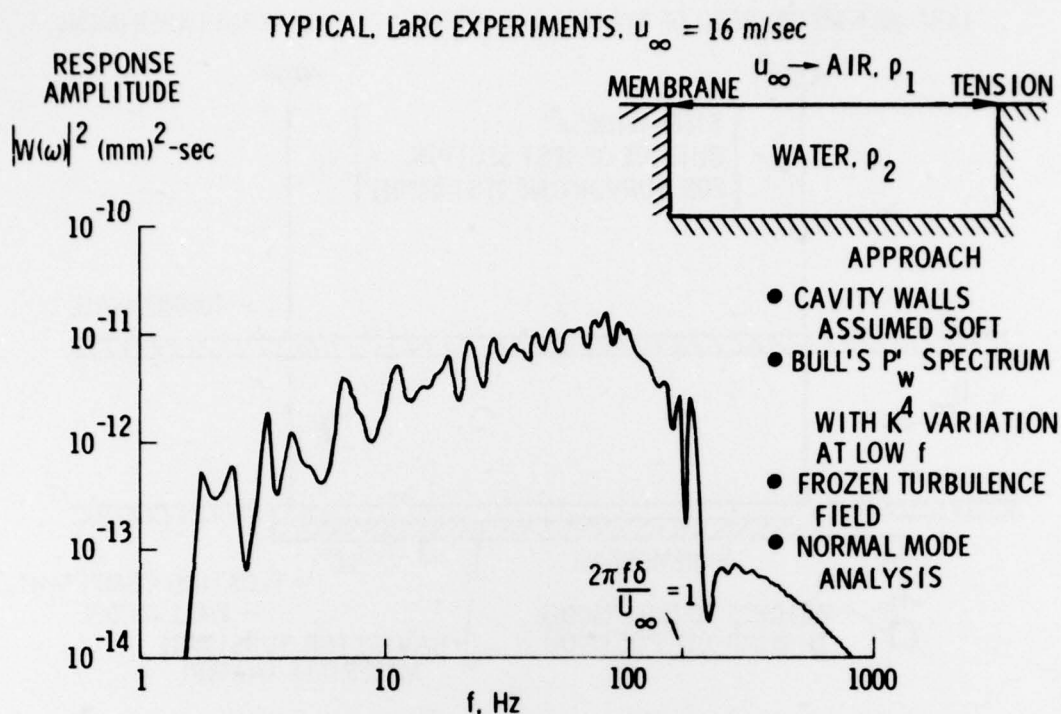


Figure 5. Predicted surface motion of water-backed membranes. Typical Langley experiments, $U_{\infty} = 16$ m/sec.

LaRC MEMBRANE/PLASTISOL MODEL

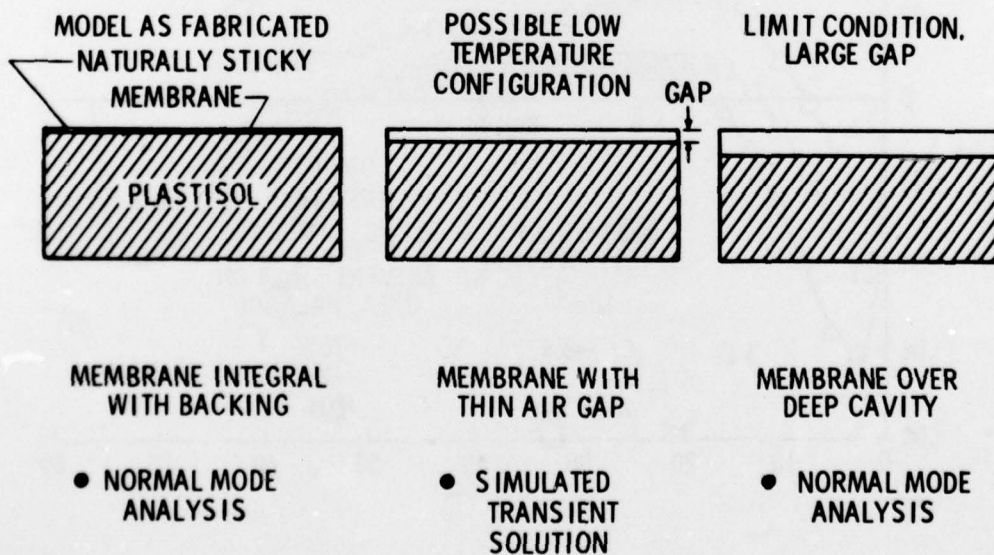


Figure 6. Possible geometric configurations. Langley membrane/Plastisol model.

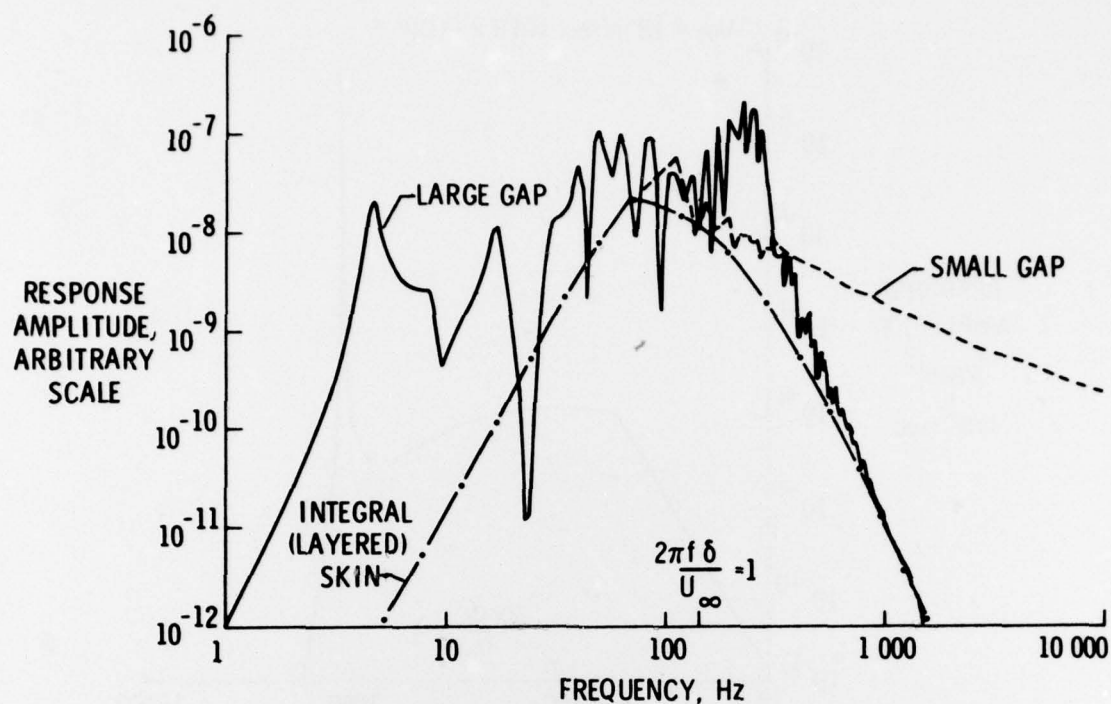


Figure 7. Predicted response of Langley membrane/Plastisol model.

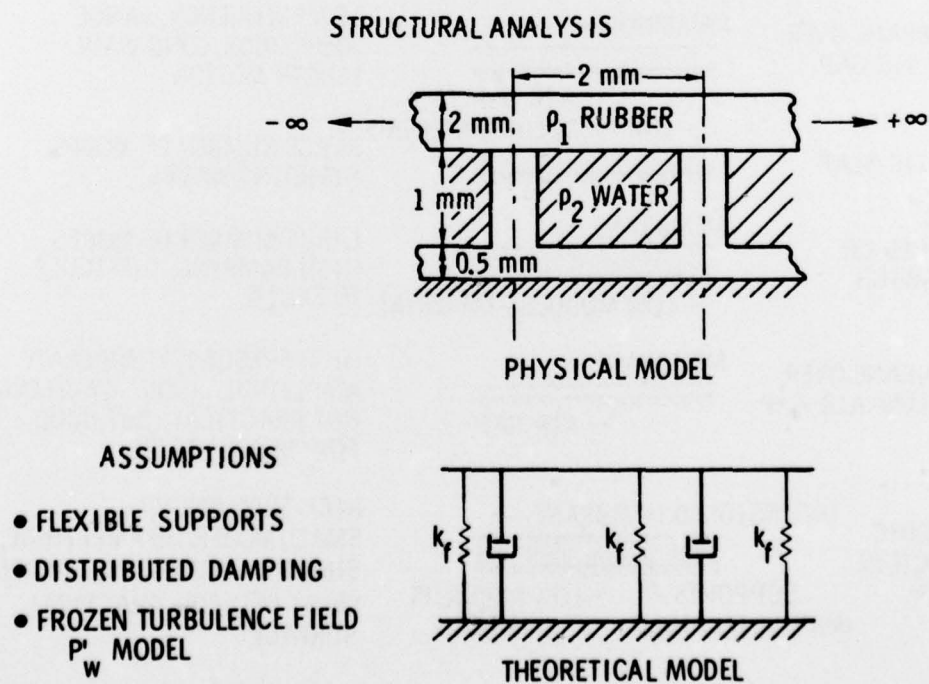


Figure 8. Predicted surface motion — Kramer's periodic structure.

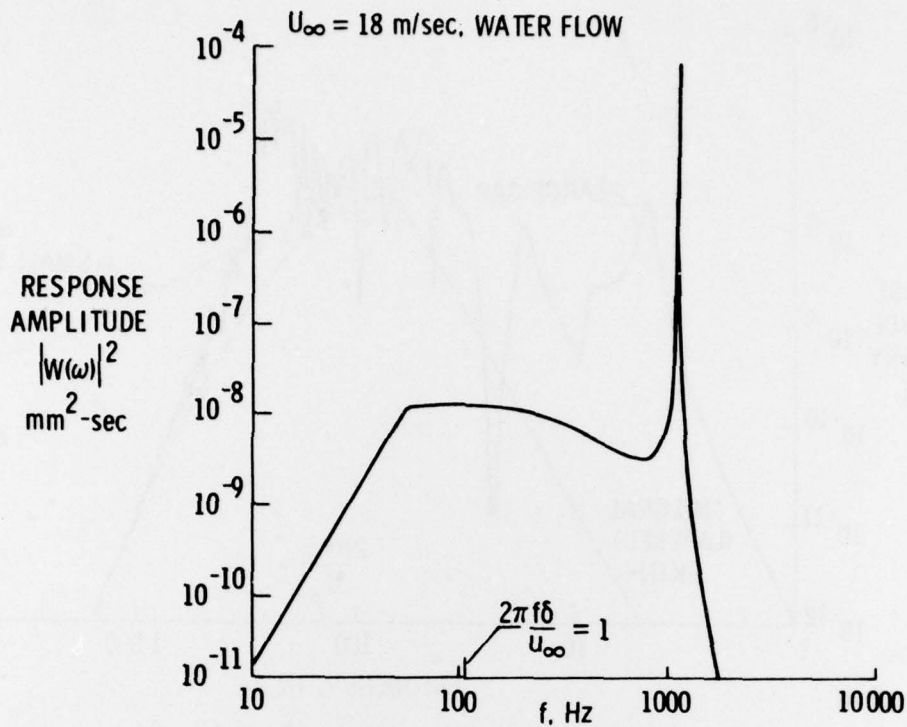


Figure 9. Steady-state response of Kramer stubbed periodic surface. $U_{\infty} = 18$ m/sec, water flow.

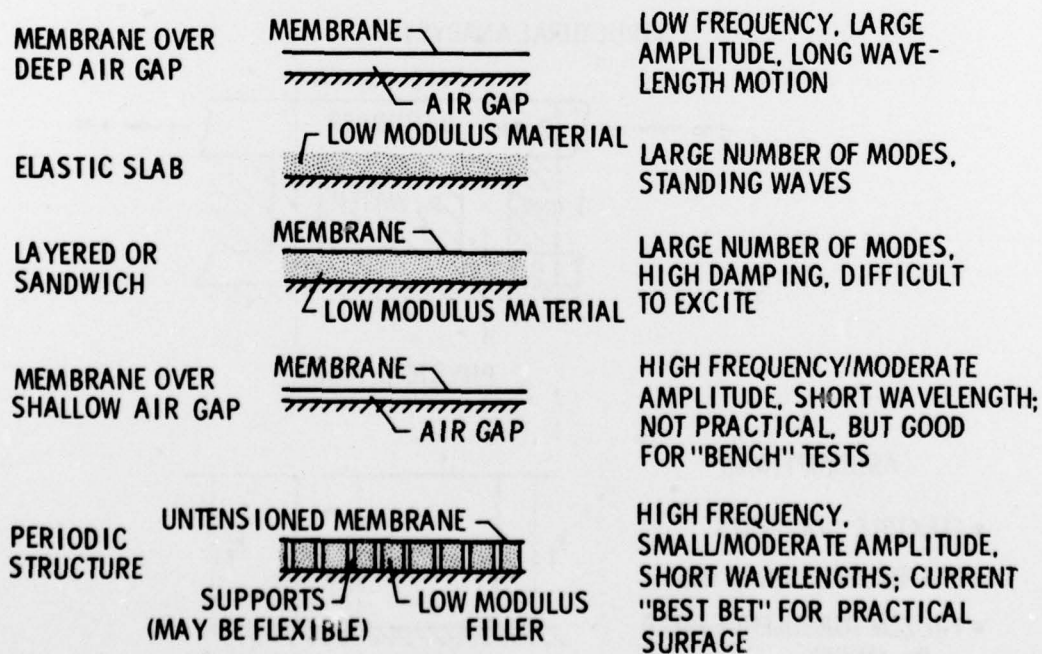


Figure 10. Resonant compliant wall structural concepts.

REPORT DOCUMENTATION PAGE												
1. Recipient's Reference	2. Originator's Reference AGARD-R-654	3. Further Reference ISBN 92-835-1247-2	4. Security Classification of Document UNCLASSIFIED									
5. Originator	Advisory Group for Aerospace Research and Development North Atlantic Treaty Organization 7 rue Ancelle, 92200 Neuilly sur Seine, France											
6. Title	SPECIAL COURSE ON CONCEPTS FOR DRAG REDUCTION											
7. Presented at	an AGARD Special Course at the von Karman Institute, Rhode-St-Genese, Belgium, 28 March - 1 April 1977.											
8. Author(s)	Various		9. Date June 1977									
10. Author's Address	Various		11. Pages 300									
12. Distribution Statement	This document is distributed in accordance with AGARD policies and regulations, which are outlined on the Outside Back Covers of all AGARD publications.											
13. Keywords/Descriptors	<table border="0"> <tr> <td>Aerodynamic drag</td> <td>Wave drag</td> <td>Performance</td> </tr> <tr> <td>Skin friction</td> <td>Diffusers</td> <td>Aircraft engines</td> </tr> <tr> <td>Boundary layer control</td> <td>Ducts</td> <td></td> </tr> </table>			Aerodynamic drag	Wave drag	Performance	Skin friction	Diffusers	Aircraft engines	Boundary layer control	Ducts	
Aerodynamic drag	Wave drag	Performance										
Skin friction	Diffusers	Aircraft engines										
Boundary layer control	Ducts											
14. Abstract	<p>A growing research effort is being mounted in a number of countries into investigations of ideas for drag reduction, some novel and some that were looked at in the past but were not then pursued to the point of application because the economic 'facts of life' were different from and less pressing than they are now. These ideas include means for reducing skin friction drag (e.g. compliant walls, boundary layer control, etc.), induced drag (e.g. winglets), interference drag, transonic shock wave drag (supercritical wings) and supersonic wave drag. In addition the internal aerodynamics of ducting, especially diffusers is receiving attention to improve the performance of engines.</p> <p>Already this research effort is bearing fruit and it was thought by the AGARD Fluid Dynamics Panel and the Von Karman Institute that the time was opportune to provide a Special Lecture Course devoted to this work and its potential for the future. The organisers of the course were fortunate in persuading outstanding experts in this field in the USA and in Europe to contribute to the Course.</p>											

<p>AGARD Report No.654 Advisory Group for Aerospace Research and Development, NATO SPECIAL COURSE ON CONCEPTS FOR DRAG REDUCTION Published June 1977 300 pages</p> <p>A growing research effort is being mounted in a number of countries into investigations of ideas for drag reduction, some novel and some that were looked at in the past but were not then pursued to the point of application because the economic 'facts of life' were different from and less pressing than they are now.</p> <p>P.T.O.</p>	<p>AGARD-R-654</p> <p>Aerodynamic drag Skin friction Boundary layer control Wave drag Diffusers Ducts Performance Aircraft engines</p>	<p>AGARD-R-654</p> <p>Aerodynamic drag Skin friction Boundary layer control Wave drag Diffusers Ducts Performance Aircraft engines</p>
<p>AGARD Report No.654 Advisory Group for Aerospace Research and Development, NATO SPECIAL COURSE ON CONCEPTS FOR DRAG REDUCTION Published June 1977 300 pages</p> <p>A growing research effort is being mounted in a number of countries into investigations of ideas for drag reduction, some novel and some that were looked at in the past but were not then pursued to the point of application because the economic 'facts of life' were different from and less pressing than they are now.</p> <p>P.T.O.</p>	<p>AGARD-R-654</p> <p>Aerodynamic drag Skin friction Boundary layer control Wave drag Diffusers Ducts Performance Aircraft engines</p>	<p>AGARD-R-654</p> <p>Aerodynamic drag Skin friction Boundary layer control Wave drag Diffusers Ducts Performance Aircraft engines</p>

<p>These ideas include means for reducing skin friction drag (e.g. compliant walls, boundary layer control, etc.), induced drag (e.g. winglets), interference drag, transonic shock wave drag (supercritical wings) and supersonic wave drag. In addition the internal aerodynamics of ducting, especially diffusers is receiving attention to improve the performance of engines.</p> <p>Already this research effort is bearing fruit and it was thought by the AGARD Fluid Dynamics Panel and the Von Karman Institute that the time was opportune to provide a Special Lecture Course devoted to this work and its potential for the future. The organisers of the course were fortunate in persuading outstanding experts in this field in the USA and in Europe to contribute to the Course.</p> <p>The material assembled in this book was prepared under the combined sponsorship of the Fluid Dynamics Panel, the von Karman Institute and the Consultant and Exchange Program of AGARD and was presented as an AGARD Special Course at the von Karman Institute, Rhode-St-Genese, Belgium on 28 March – 1 April 1977.</p> <p>ISBN 92-835-1247-2</p>	<p>These ideas include means for reducing skin friction drag (e.g. compliant walls, boundary layer control, etc.), induced drag (e.g. winglets), interference drag, transonic shock wave drag (supercritical wings) and supersonic wave drag. In addition the internal aerodynamics of ducting, especially diffusers is receiving attention to improve the performance of engines.</p> <p>Already this research effort is bearing fruit and it was thought by the AGARD Fluid Dynamics Panel and the Von Karman Institute that the time was opportune to provide a Special Lecture Course devoted to this work and its potential for the future. The organisers of the course were fortunate in persuading outstanding experts in this field in the USA and in Europe to contribute to the Course.</p> <p>The material assembled in this book was prepared under the combined sponsorship of the Fluid Dynamics Panel, the von Karman Institute and the Consultant and Exchange Program of AGARD and was presented as an AGARD Special Course at the von Karman Institute, Rhode-St-Genese, Belgium on 28 March – 1 April 1977.</p> <p>ISBN 92-835-1247-2</p>
<p>These ideas include means for reducing skin friction drag (e.g. compliant walls, boundary layer control, etc.), induced drag (e.g. winglets), interference drag, transonic shock wave drag (supercritical wings) and supersonic wave drag. In addition the internal aerodynamics of ducting, especially diffusers is receiving attention to improve the performance of engines.</p> <p>Already this research effort is bearing fruit and it was thought by the AGARD Fluid Dynamics Panel and the Von Karman Institute that the time was opportune to provide a Special Lecture Course devoted to this work and its potential for the future. The organisers of the course were fortunate in persuading outstanding experts in this field in the USA and in Europe to contribute to the Course.</p> <p>The material assembled in this book was prepared under the combined sponsorship of the Fluid Dynamics Panel, the von Karman Institute and the Consultant and Exchange Program of AGARD and was presented as an AGARD Special Course at the von Karman Institute, Rhode-St-Genese, Belgium on 28 March – 1 April 1977.</p> <p>ISBN 92-835-1247-2</p>	<p>These ideas include means for reducing skin friction drag (e.g. compliant walls, boundary layer control, etc.), induced drag (e.g. winglets), interference drag, transonic shock wave drag (supercritical wings) and supersonic wave drag. In addition the internal aerodynamics of ducting, especially diffusers is receiving attention to improve the performance of engines.</p> <p>Already this research effort is bearing fruit and it was thought by the AGARD Fluid Dynamics Panel and the Von Karman Institute that the time was opportune to provide a Special Lecture Course devoted to this work and its potential for the future. The organisers of the course were fortunate in persuading outstanding experts in this field in the USA and in Europe to contribute to the Course.</p> <p>The material assembled in this book was prepared under the combined sponsorship of the Fluid Dynamics Panel, the von Karman Institute and the Consultant and Exchange Program of AGARD and was presented as an AGARD Special Course at the von Karman Institute, Rhode-St-Genese, Belgium on 28 March – 1 April 1977.</p> <p>ISBN 92-835-1247-2</p>